Integrated Exploration, Geothermal Modelling and Techno-Economic Resource Assessment of the Crystalline Basement in the Northern Upper Rhine Graben

Dissertation

Doctoral thesis submitted in fulfillment of the requirements for the degree of doctor rerum naturalium (Dr. rer. nat.)

TECHNISCHE UNIVERSITÄT DARMSTADT

at the
Department of Material and Earth Sciences,
Technical University of Darmstadt

Submitted by
Matthis Frey, M.Sc.

Supervisor Prof. Dr. Ingo Sass
Co-supervisor Dr. Philippe Calcagno

Darmstadt, March 2023

Author: Matthis Frey
Title: Integrated Exploration, Geothermal Modelling and Techno-Economic Resource Assessment of the Crystalline Basement in the Northern Upper Rhine Graben
Place: Darmstadt, Technical University of Darmstadt
Date of the defence: 30.06.2023

This document is made available by TUprints,
E-Publishing Service of the TU Darmstadt:
https://tuprints.ulb.tu-darmstadt.de
tuprints@ulb.tu-darmstadt.de

Year of publication on TUprints: 2023

Board of examiners

First assessor: Prof. Dr. Ingo Sass

Second assessor: Dr. Philippe Calcagno

Examiner: Prof. Dr. Eva Schill

Examiner: Prof. Dr. Andreas Henk

Technical University of Darmstadt

Institute of Applied Geosciences

Schnittspahnstraße 9

64287 Darmstadt

Germany

Declaration

I hereby declare that the presented dissertation is based on original research and is the result of my own work. I certify that this dissertation contains no material which has been accepted for the award of any other degree in my name, in any university or other tertiary institution and, to the best of my knowledge and belief, contains no material previously published or written by another person, except where due reference has been made in the text.

_____ _____

Place, Date Signature

Synopsis (english)

The climate crisis is already causing significant humanitarian and economic impacts that will intensify in the future if global greenhouse gas emissions are not immediately reduced. Under the Climate Protection Act, Germany is therefore obliged to achieve net carbon neutrality by 2045. To meet this ambitious target, a far-reaching transformation of the energy sector is necessary, with imports of fossil fuels being replaced by domestic renewable energy production. In addition to established energy sources, deep geothermal energy, as a low-emission, base-load capable, local and scalable solution, will likely become a cornerstone of energy supply in the upcoming decades. The crystalline basement offers the greatest geothermal potential, which could be exploited through so-called enhanced geothermal systems (EGS). Particularly favorable conditions for geothermal utilization exist in the Upper Rhine Graben (URG), where compared to other regions in Germany higher reservoir temperatures and permeabilities are observed. To date, however, deep geothermal energy occupies only a small niche due to the comparatively high costs and risks associated with drilling, development, and operation of geothermal power plants. In addition, geological uncertainties in the basement are particularly large, as it has been insufficiently explored by the hydrocarbon industry and previous geothermal research projects. This thesis aims to quantify and reduce these uncertainties to promote geothermal development in the northern URG. A comprehensive lithological, petrophysical and structural reservoir characterization is carried out by combining geological and geophysical techniques on multiple scales. All relevant data are integrated into a 3D geothermal model that enables a regional resource assessment for the basement.

In the northern ORG, geologic modeling of the basement faces significant challenges because well data from the basement are very sparse and 3D seismic data are often not openly available. Therefore, gravity and magnetic data were additionally considered in a stochastic joint inversion that provided new insights into the structure and composition of the basement while also quantifying model uncertainties. The inversion demonstrates that the geologic units of the graben shoulders can be traced below the sedimentary filling. Comparison of the inverted petrophysical properties with existing databases and newly collected susceptibility measurements yielded a map of the predicted basement lithology in the northern URG. Accordingly, most areas are dominated by granitoids, which tend to have higher permeability than shales and gneisses and thus are preferred targets of geothermal drilling. In contrast, a predominantly metamorphic basement can be assumed in the Saxothuringian Zone and at the northwestern rift margin.

The developed 3D basement model and inversion results were key input for a techno-economic resource assessment, which furthermore incorporated data from thermal and geomechanical models, operating geothermal power plants, and financial aspects of geothermal utilization. Calculation of resources at the regional scale was based on the widely used volumetric 'heat in place' method, whereby model uncertainties were quantified by means of Monte Carlo simulation. The recoverable heat along large-scale fault zones, considered as preferential fluid pathways, was estimated as a function of the slip and dilation tendency in the recent stress field. The economically exploitable part of the resources (reserves) was subsequently investigated by a sensitivity analysis of relevant parameters. The assessment reveals that the basement in the URG is characterized by a vast resource base, of which between 8 and 16 PWh are potentially recoverable with current EGS technologies. This could sustainably provide a significant fraction of the heat and power supply in the northern URG. About 65% of the

resources were economically recoverable at market conditions in January 2022. In view of the enormous increases in energy prices resulting from the war in Ukraine, the share is now likely higher. A comparison of the calculated resources with the socio-economic-environmental conditions for geothermal utilization at the surface shows a high level of correlation, especially in the densely populated areas around Mannheim and Darmstadt.

As groundwater flow in the crystalline basement is mainly controlled by open fractures, accurate knowledge of the natural fracture network is essential for the planning, development and operation of geothermal power plants. Image logs from deep boreholes provide the most meaningful information on fracture properties, but these are very rare and often inaccessible in the URG. A comprehensive structural outcrop analog study was conducted to compensate for the lack of borehole data. The Tromm Granite in the southern Odenwald was selected as the study area as it is both a suitable analog for the granitoid reservoirs in the northern URG and a potential site for the upcoming GeoLaB project. Here, lineament analyses and lidar surveys in abandoned quarries were combined, resulting in a multiscale description of the basement's fracture network. Discrete fracture network (DFN) models were then developed based on the obtained properties to estimate the permeability under assumed reservoir conditions. While the Tromm Granite is overall intensely fractured and the network is well connected, the density and orientation of fractures is strongly influenced by nearby fault zones. Fractures cluster roughly in the N-S direction, parallel to σ_{Hmax}, resulting in an order of magnitude higher permeability than in the E-W direction.

The structural investigations were complemented by geophysical surveys, designed to map and characterize the buried faults in the Tromm Granite. As in the regional modelling, potential field methods (terrestrial gravimetry and aeromagnetics) were applied and additionally the radon activity concentration was measured along one profile. The gravity data show rather broad anomalies, which cannot be assigned to single faults, but rather to zones of increased fault and fracture density. Inversion of the gravity data indicated a fracture related porosity of up to 9% along the pluton margins. The drone-based aeromagnetic survey, conversely, allows a more detailed mapping of the fault network. After filtering, the dataset revealed a complex network of linear anomalies that are interpreted as altered fault zones with increased reactivation potential, thus representing preferred fluid pathways.

In conclusion, the crystalline basement is an attractive target for deep geothermal exploitation in the northern URG due to the vast resource base. As part of the dissertation, a new detailed geothermal 3D model and a regional map of the resources have been developed, providing politicians, investors, and project engineers with a more reliable basis for decision-making. Furthermore, the understanding of the fracture network properties and thus of the hydraulic properties in the northern URG was improved. Nevertheless, significant uncertainties remain at the local scale that can only be eliminated through targeted exploration measures and coupled numerical modelling. Besides, the risk of noticeable induced seismicity persists, which is a major obstacle to the exploitation of deep geothermal energy. Great hope therefore lies in the development of new safe stimulation techniques for EGS reservoirs, which will be advanced in particular within the framework of the upcoming GeoLaB project.

Synopsis (deutsch)

Die Klimakrise zeigt bereits heute erhebliche humanitäre und wirtschaftliche Auswirkungen, die sich in Zukunft noch verstärken werden, wenn die globalen Treibhausgasemissionen nicht schnellstens minimiert werden. Gemäß dem Klimaschutzgesetz ist Deutschland daher verpflichtet, bis 2045 klimaneutral zu werden. Um dieses ehrgeizige Ziel zu erreichen, ist ein tiefgreifender Umbau des Energiesektors notwendig, bei dem Importe fossiler Energieträger durch heimische erneuerbare Energieerzeugung ersetzt werden. Neben den etablierten Energiequellen wie Wind, Sonne, Wasser und Biomasse wird die Tiefengeothermie als emissionsarme, grundlastfähige, lokale und skalierbare Anwendung in den kommenden Jahrzehnten vermutlich zu einem Eckpfeiler der Energieversorgung aufsteigen. Das größte geothermische Potenzial bietet das kristalline Grundgebirge, das durch sogenannte Enhanced Geothermal Systems (EGS) erschlossen werden könnte. Besonders günstige Voraussetzungen für die geothermische Nutzung bestehen im Oberrheingraben (ORG), wo die Reservoirtemperaturen und -permeabilitäten im Vergleich zu anderen Regionen Deutschlands generell erhöht sind. Aufgrund der relativ hohen Kosten und Risiken, die mit Bohrung, Erschließung und Betrieb von Geothermiekraftwerken verbunden sind, nimmt die Tiefengeothermie bisher jedoch nur eine kleine Nische ein. Zudem sind die geologischen Unsicherheiten im Grundgebirge besonders groß, da dieses durch die Kohlenwasserstoffindustrie und vorangegangene geothermische Forschungsprojekte nur unzureichend erkundet wurde. Ziel dieser Arbeit ist es, diese Unsicherheiten im nördlichen ORG zu quantifizieren und zu reduzieren, um die geothermische Entwicklung in der Region voranzutreiben. Es erfolgt eine umfassende lithologische, petrophysikalische und strukturelle Reservoircharakterisierung durch die Kombination strukturgeologischer und geophysikalischer Ansätze auf multiplen Skalen. Alle verfügbaren Daten werden in ein 3D Modell integriert, das eine regionale Ressourcenbewertung für das Grundgebirge ermöglicht.

Im nördlichen ORG steht die geologische Modellierung des Grundgebirges vor großen Herausforderungen, da nur sehr wenige Bohrlochdaten aus dem Grundgebirge existieren und 3D-seismische Daten häufig nicht offen zugänglich sind. Daher wurden zusätzlich Schwere- und Magnetikdaten in einer gemeinsamen stochastischen Inversion berücksichtigt, die neue Einblicke in die Struktur und Zusammensetzung des Grundgebirges liefert und gleichzeitig die Modellunsicherheiten quantifiziert. Die Inversion zeigt, dass die geologischen Einheiten der Grabenschultern unterhalb der sedimentären Füllung nachverfolgt werden können. Durch einen Vergleich der invertierten petrophysikalischen Eigenschaften mit bestehenden Datenbanken und neu erhobenen Suszeptibilitätsmessungen konnte eine Karte der voraussichtlichen Grundgebirgslithologie im nördlichen ORG erstellt werden. Demnach werden die meisten Gebiete von Granitoiden dominiert, die tendenziell eine höhere Permeabilität als Schiefer und Gneise aufweisen und somit bevorzugte Ziele geothermischer Bohrungen darstellen. Im Saxothuringikum und am nordwestlichen Grabenrand kann dagegen von einem überwiegend metamorphen Grundgebirge ausgegangen werden.

Das entwickelte 3D-Grundgebirgsmodell und die Inversionsergebnisse waren der zentrale Bestandteil einer technisch-ökonomischen Ressourcenbewertung, in die zudem Daten aus thermischen und geomechanischen Modellen, aus dem Betrieb geothermischer Kraftwerke und aus finanziellen Aspekten der geothermischen Nutzung einflossen. Die Berechnung der Ressourcen auf regionaler Ebene beruht auf der etablierten volumetrischen "heat in place"-Methode, wobei Modellunsicherheiten mittels Monte-Carlo-Simulation quantifiziert wurden.

Die gewinnbare Wärme entlang großräumiger Störungszonen, die als bevorzugte Fluidpfade gelten, wurde als Funktion der sogenannten Slip und Dilatation Tendency im rezenten Spannungsfeld abgeschätzt. Der wirtschaftlich nutzbare Teil der Ressourcen (Reserven) wurde anschließend durch eine Sensitivitätsanalyse der relevanten Parameter untersucht. Die Bewertung zeigt, dass das Grundgebirge im ORG über enorme geothermische Ressourcen verfügt, von denen zwischen 8 und 16 PWh mit den derzeitigen EGS-Technologien potenziell gewinnbar sind. Damit könnte ein erheblicher Teil der Wärme- und Stromversorgung im nördlichen ORG nachhaltig gesichert werden. Rund 65% der Ressourcen sind zu Marktbedingungen im Januar 2022 wirtschaftlich förderbar. Angesichts der enormen Energiepreissteigerungen infolge des Krieges in der Ukraine dürfte der Anteil inzwischen sogar höher sein. Ein Vergleich der berechneten Ressourcen mit den sozioökonomisch-ökologischen Bedingungen für die geothermische Nutzung an der Oberfläche zeigt eine hohe Übereinstimmung, insbesondere in den dicht besiedelten Gebieten um Mannheim und Darmstadt.

Da der Grundwasserfluss im kristallinen Grundgebirge hauptsächlich durch offene Klüfte gesteuert wird, ist die genaue Kenntnis des natürlichen Kluftnetzwerkes für die Planung, die Entwicklung und den Betrieb geothermischer Kraftwerke unerlässlich. Die aussagekräftigsten Informationen über die Klufteigenschaften liefern Image Logs aus Tiefbohrungen, die im ORG jedoch sehr selten und oft nicht zugänglich sind. Um den Mangel an Bohrlochdaten zu kompensieren, wurde eine umfassende strukturelle Aufschlussanalogstudie durchgeführt. Der Tromm Granit im südlichen Odenwald wurde als Untersuchungsgebiet ausgewählt, da dieser zum einen ein geeignetes Analogon für die granitoiden Reservoire im nördlichen ORG darstellt und zum anderen ein potentieller Standort für das kommende GeoLaB Projekt ist. Hier wurden Lineamentanalysen und Lidar-Untersuchungen in fünf aufgelassenen Steinbrüchen kombiniert, womit eine multiskalige Beschreibung des Kluftnetzes des Grundgebirges erreicht wurde. Auf der Grundlage der gewonnenen Eigenschaften wurden daraufhin diskrete Kluftnetzwerkmodelle (DFN) entwickelt, um die Durchlässigkeit des Grundgebirges unter angenommenen Lagerstättenbedingungen abzuschätzen. Das Kluftnetzwerk im Tromm Granit zeigt sich als generell stark geklüftet und gut verbunden, wobei die Dichte und Orientierung von Klüften durch nahegelegene Störungszonen beeinflusst werden. Klüfte clustern in N-S Richtung, also etwa parallel zu σ_{Hmax}, sodass die Reservoirpermeabilität etwa eine Größenordnung höher ist als in O-W Richtung.

Die strukturgeologischen Untersuchungen wurden durch geophysikalische Messungen ergänzt, mit denen die überdeckten Störungen im Tromm Granit kartiert und charakterisiert wurden. Wie bei der regionalen Modellierung kamen auch dabei wieder Potenzialfeldmethoden (terrestrische Gravimetrie und Aeromagnetik) zum Einsatz und zusätzlich wurde die Radonaktivitätskonzentration entlang eines Profils gemessen. Die Schwerefelddaten zeigen eher breite Anomalien, die nicht einzelnen Verwerfungen, sondern Zonen mit erhöhter Störungs- und Kluftdichte zugeordnet werden können. Die Inversion der Schweredaten deutet auf eine Kluftporosität von bis zu 9 % entlang der Plutonränder hin. Die drohnengestützte aeromagnetische Vermessung ermöglicht im Vergleich eine detailliertere Kartierung des Störungsnetzwerkes. Nach der Filterung zeigt der Datensatz ein komplexes Netzwerk von linearen Anomalien, die als alterierte Störungszonen mit erhöhtem Reaktivierungspotenzial interpretiert werden und somit mögliche Fluidwegsamkeiten darstellen.

Abschließend ist festzustellen, dass das kristalline Grundgebirge aufgrund der großen Ressourcenbasis ein attraktiver Zielhorizont der Tiefengeothermie im nördlichen ORG darstellt.

Im Rahmen der Dissertation wurden ein neues detailliertes geologisches Modell und eine regionale Ressourcenkarte entwickelt, die PolitikerInnen, InvestorInnen und ProjektingenieurInnen eine zuverlässigere Entscheidungsgrundlage bieten. Zudem wurde das Verständnis der Kluftnetzwerkeigenschaften und damit der hydraulischen Eigenschaften im nördlichen ORG verbessert. Dennoch verbleiben erhebliche Unsicherheiten auf der lokalen Skala, die nur durch gezielte Erkundungsmaßnahmen und gekoppelte numerische Modellierung reduziert werden können. Zudem besteht weiterhin das Risiko spürbarer induzierten Seismizität während der Entwicklung und des Betriebes des Kraftwerkes, die ein großes Hindernis für den Ausbau der Tiefengeothermie darstellt. Große Hoffnung liegt daher in der Entwicklung neuer sicherer Stimulationstechniken für EGS-Reservoire, die insbesondere im Rahmen des anstehenden GeoLaB-Projekts vorangetrieben werden sollen.

Preface

This doctoral thesis was prepared at the Institute of Applied Geosciences of the Technical University of Darmstadt in cooperation with BRGM (Bureau de Recherches Géologiques et Minières) between 2020 and 2023. The research was funded by the Interreg NWE program (grant no. NWE892) through the "Roll-out of Deep Geothermal Energy in North-West Europe project" (DGE-ROLLOUT, https://www.nweurope.eu/DGE-Rollout). DGE-ROLLOUT directly follows up on the previous projects Hessen 3D (1.0 and 2.0) and GeORG (geopotential of the deeper subsurface in the Upper Rhine Graben). By implementing additional datasets and advanced modelling techniques, the geological model of the northern Upper Rhine Graben could be harmonized and substantially refined. Main objectives of the presented thesis were the multiscale lithological, petrophysical, and structural characterization as well as the integrated modelling of the crystalline basement in this region. This allowed a more accurate assessment of geothermal resources, providing investors, policymakers and project developers with a reliable basis for decision-making. The work is closely linked to the dissertation of Jeroen van der Vaart, who focused his investigations on the hydrothermal potentials in the Upper Rhine Graben and applied advanced techniques to quantify model uncertainties.

This thesis is written in a cumulative form, which includes five peer-reviewed publications, given in the chapters 2 to 6. Note that the order of publications is based on their content, not publication date. The chapters contain the unchanged content of the original publication.

Chapter 2

Frey, M., Bär, K., Stober. I., Reinecker, J., van der Vaart, J., & Sass, I. (2022). Assessment of deep geothermal research and development in the Upper Rhine Graben. Geothermal Energy, 10(18). https://doi.org/10.1186/s40517-022-00226-2.

This chapter presents a comprehensive literature review of the geological setting in the URG and previous research efforts with respect to geothermal energy utilization. Nine potential geothermal reservoir horizons were identified and described in detail with respect to their lithological, structural, thermal, hydraulic, hydrochemical, petrophysical, and seismic properties. In addition, all previously implemented deep geothermal projects in the URG are reviewed followed by a discussion of the lessons learned. Finally, an overview of publicly available geological 3D models of the Upper Rhine Graben is given. Thus, the review paper lays the foundation of all research activities in the DGE-ROLLOUT project and future comparable projects.

Matthis Frey conducted most of the literature review, especially with respect to the geologic description of the reservoir horizons, prepared the figures, and wrote most of the manuscript. Kristian Bär supported Matthis Frey with the conceptualization and drafted the petrophysical rock characterization chapter. Ingrid Stober contributed to the chapters on hydraulic and hydrochemical reservoir characterization. John Reinecker prepared the chapters on the structural geologic setting and recent stress field. Jeroen van der Vaart added the aspects of uncertainty modelling to the discussion. Ingo Sass and the other co-authors reviewed the manuscript and approved the final version.

Chapter 3

Frey, M., Weinert, S., Bär, K., van der Vaart, J., Dezayes, C., Calcagno, P., & Sass, I. (2021). Integrated 3D geological modelling of the northern Upper Rhine Graben by joint inversion of gravimetry and magnetic data. Tectonophysics, 813, 228927. https://doi.org/10.1016/j.tecto.2021.228927.

Chapter 3 covers the integrated 3D modelling of the crystalline basement in the northern Upper Rhine Graben. First, the Hessen 3D and GeORG models were merged and harmonized. The model was then improved by joint inversion of gravity and magnetic data, which provided new insights into the structure and composition of the basement. For a realistic model parameterization, existing petrophysical databases were consulted and additionally over 430 measurements of the magnetic susceptibility were performed on representative rock samples. The inversion yielded on the one hand the 3D geometry of the basement units including uncertainties and on the other hand detailed information about the petrophysical properties. This allowed an interpretation of the basement lithology below the sedimentary cover.

Matthis Frey performed the petrophysical measurements, processed the data, carried out the modelling and inversion, visualized the results, and wrote the manuscript. Sebastian Weinert assisted Matthis Frey with the 3D modelling and model parameterization. Kristian Bär gave support in the conceptualization of the study. Jeroen van der Vaart contributed by providing his modelling expertise. Chrystel Dezayes and Philippe Calcagno provided the modelling software and engaged in the discussion of the methods and results. Ingo Sass and Kristian Bär supervised the research. All co-authors reviewed the manuscript and approved the final version.

Chapter 4

Frey, M., van der Vaart, J., Bär, K., Bossennec, C., Calcagno, P., Dezayes, C., & Sass, I. (2023). Techno-Economic Assessment of Geothermal Resources in the Variscan Basement of the Northern Upper Rhine Graben. Natural Resources Research, 32. https://doi.org/10.1007/s11053-022-10138-4.

In this chapter, a quantitative resource assessment for the basement in the northern Upper Rhine Graben is presented based on the inversion results and additional datasets. Emphasis was placed on the potentials linked to large-scale fault zones, which are generally considered as fluid conduits in the basement. Model uncertainties were quantified through Monte Carlo simulation. A sensitivity analysis was subsequently performed to examine the impact of selected factors on the levelized costs of energy as well as geothermal reserves. By comparing the calculated resources with the socio-economic-environmental potential at the surface, favorable sites for geothermal drilling were indicated. The combination of geological, technical, economic, and societal aspects of geothermal exploitation in the applied approach provides stakeholders with a useful basis for decision-making.

Matthis Frey carried out the geothermal modelling and resource assessment, visualized the results, and wrote the manuscript. The study was designed by Matthis Frey, Kristian Bär, and Jeroen van der Vaart. Claire Bossennec, Chrystel Dezayes, Philippe Calcagno, and Ingo Sass contributed to the discussion of the applied methods and results. Ingo Sass and Kristian Bär supervised the research. All co-authors reviewed the manuscript and approved the final version.

Chapter 5

Frey, M., Bossennec, C., Seib, L., Bär, K., Schill, E., & Sass, I. (2022). Interdisciplinary fracture network characterization in the crystalline basement: a case study from the Southern Odenwald, SW Germany. Solid Earth, 13(6), 935-955. https://doi.org/10.5194/se-13-935-2022.

Chapter 5 comprises an interdisciplinary outcrop analog study of the fracture network in the basement in the southern Odenwald. The gained insights into the structural framework of the basement helped to overcome the lack of data from deep wells in the Upper Rhine Graben. Lidar surveys of quarry walls were combined with lineament analysis to obtain a multiscale description of the fracture network. This information was direct input for a Discrete Fracture Network (DFN) modelling, with the purpose to estimate the basement permeability under assumed reservoir conditions. A refined mapping and characterization of potentially permeable fractures and faults was furthermore carried out by measuring gravity and radon anomalies. Based on the findings, recommendations for reservoir development in the northern Upper Rhine Graben are presented.

Matthis Frey performed the data analysis and visualization and wrote the original draft. Claire Bossennec gave support in the design of the study, the fieldwork, and the processing of the structural data. Lukas Seib also contributed to the data acquisition and performed the DFN modelling. Eva Schill provided the gravimeter and participated in the design of the gravimetric survey. The work was supervised by Kristian Bär and Ingo Sass. All co-authors reviewed the manuscript and approved the final version.

Chapter 6

Frey, M., Bossennec, C., & Sass, I. (2023). Mapping buried fault zones in a granitic pluton using aeromagnetic data. Pure and Applied Geophysics, 180, 2241–2255. https://doi.org/10.1007/s00024-023-03258-2.

This chapter follows up on the interdisciplinary outcrop analog study in chapter 5, with a stronger focus on the exploration for GeoLaB. The results of a drone-based aeromagnetic survey in the southern Odenwald are presented. Different signal filters were compared using a synthetic model and were then applied to the field data. The filtered anomalies reveal a large number of magnetic lineaments, which are interpreted as faults and whose distribution partially correlates with the reactivation potential. The aeromagnetic data consequently provides a high-resolution map of potentially permeable faults in the study area.

Matthis Frey performed the analysis and visualization of the aeromagnetic data and wrote the manuscript. The survey was conceptualized by Matthis Frey and Claire Bossennec. Ingo Sass supervised the research. Both co-authors reviewed the manuscript and approved the final version.

In addition to the above-mentioned first-author publications, Matthis Frey contributed to the following peer-reviewed articles during his time as a PhD researcher:

Bossennec, C., Frey, M., Seib, L., Bär, K., & Sass, I. (2021). Multiscale Characterisation of Fracture Patterns of a Crystalline Reservoir Analogue. Geosciences, 11(9), 371. https://doi.org/10.3390/geosciences11090371.

Bossennec, C., Seib, L., Frey, M., van der Vaart, J., & Sass, I. (2022). Structural Architecture and Permeability Patterns of Crystalline Reservoir Rocks in the Northern Upper Rhine Graben: Insights from Surface Analogues of the Odenwald. Energies, 15(4), 1310. https://doi.org/10.3390/en15041310.

Seib, L., Welsch, B., Bossennec, C., Frey, M., & Sass, I. (2022). Finite element simulation of permeable fault influence on a medium deep borehole thermal energy storage system. Geothermal Energy, 10(1), 1-21. https://doi.org/10.1186/s40517-022-00224-4.

van der Vaart, J., Bär, K., Frey, M., Reinecker, J., & Sass, I. (2021). Quantifying model uncertainty of a geothermal 3D model of the Cenozoic deposits in the northern Upper Rhine Graben, Germany. Zeitschrift der Deutschen Gesellschaft für Geowissenschaften, 172(3), 365-379. https://doi.org/10.1127/zdgg/2021/0286.

Finally, the research was presented at various national and international conferences and workshops (Note that only first-author contributions are listed below):

Frey, M., Weinert, S., Bär, K., van der Vaart, J., Dezayes, C., Calcagno, P., Schill, E., & Sass, I. (2020). Verbesserte Modellierung des nördlichen Oberrheingrabens durch Joint Inversion von Schwere- und Magnetikdaten. In Der Digital Geothermie Kongress, 9–13 November 2020.

Frey, M., Weinert, S., Bär, K., van der Vaart, J., Dezayes, C., Calcagno, P., & Sass, I. (2021). 3D Modelling of the Northern Upper Rhine Graben Crystalline Basement by Joint Inversion of Gravity and Magnetic Data. In EGU General Assembly Conference Abstracts, 19-30 April 2021. https://doi.org/10.5194/egusphere-egu21-477.

Frey, M., Bossennec, C., Bär, K., & Sass, I. (2021). Multiscale and -disciplinary Investigation of the Fracture Network in the Odenwald Crystalline Complex, Germany. In Jahrestagung der Deutschen Geophysikalischen Gesellschaft, 1-5 March 2021, Kiel/online.

Frey, M., Bossennec, C., Seib, L., Bär, K., & Sass, I. (2021). Structural and Geophysical Characterisation of the Crystalline Basement in the Northern Upper Rhine Graben. In European Geothermal Workshop, 23-24 September 2021, Karlsruhe/online.

Frey, M., van der Vaart, J., Bär, K., Bossennec, C., Seib, L., Calcagno, P., Dezayes, C., & Sass, I. (2022). Towards a Techno-Economic Geothermal Resource Assessment of the Northern Upper Rhine Graben Crystalline Basement. In Proceedings of the European Geothermal Congress, 17-21 October 2022, Berlin.

Acknowledgements

First of all, I would like to thank my main supervisor Prof. Dr. Ingo Sass for his valuable support of my research. In many interesting discussions, he gave me important advice and opened my eyes to a variety of research approaches. Thereby I was able to develop my skill set immensely and to raise the quality of this thesis to a much higher level. At the same time, he gave me enough freedom in my work, so that I could also pursue my own ideas and conceptions.

I would also like to express my gratitude to Dr. Chrystel Dezayes and Dr. Philippe Calcagno who co-supervised this thesis. They gave me access to the essential modelling software (GeoModeller) in a very uncomplicated manner. In several stimulating discussions, they provided me with important suggestions, which led to a considerable improvement of the publications.

I thank the two other members of the examination board, Prof. Dr. Eva Schill and Prof. Dr. Andreas Henk. Eva Schill allowed me access to the gravimeter and we had several helpful discussions, especially about the geophysical data acquisition and analysis in this thesis. Andreas Henk provided me with the lidar scanner, which allowed me to acquire a comprehensive dataset on the fracture network in the crystalline basement.

My special thanks go to Dr. Kristian Bär, who has supported me continuously in my research, even long after he had left the TU Darmstadt. He contributed significantly to the conceptualization of the modelling and other investigations. For all problems, he was able to propose reasonable solutions to me. In addition, his numerous contacts in industry and research proved to be helpful.

I am grateful to Jeroen van der Vaart, with whom I worked most closely in the DGE Rollout project. He shared with me his years of experience in geological modelling and introduced me in particular to the topic of uncertainty analysis. We had countless technical but also private conversations over the last three years, without which the time would have been much less enjoyable.

I would like to thank Dr. Claire Bossennec for her continuous support, especially with regard to the structural and geophysical investigations. She introduced me to the topic of characterizing fracture networks in crystalline reservoirs and outcrops. The fieldwork together with her was definitely a highlight of this PhD project.

Moreover, I am grateful to Lukas Seib for his support during our geophysical field campaigns in the Odenwald and for taking over the DFN modelling.

I thank Sebastian Weinert, who introduced me to the crystalline basement in the Upper Rhine Graben in the early phase of my work. His PhD project was closely related to my topic, therefore I benefited immensely from his expertise.

I would also like to thank the other members of the Applied Geothermal Science and Technology group for the pleasant working atmosphere and many interesting discussions. My special thanks go to Simone Roß-Krichbaum, who always reliably fulfilled all administrative tasks even in the difficult times of the COVID-19 pandemic. Furthermore, I would like to thank Leandra Weydt for her support in the preparation of this thesis.

For their valuable contribution to the review paper, which is part of this thesis, I would like to thank Prof. Dr. Ingrid Stober and Dr. John Reinecker.

I am grateful to Dr. Heiner Menzel for sharing his profound experience with the economic aspects of geothermal power generation.

Essential geological and geophysical data were kindly provided by the Leibniz Institute for Applied Geophysics (LIAG), the Hessian State Office for Nature Conservation, Environment and Geology (HLNUG), the Bureau de recherches géologiques et minières (BRGM), the Hessian Administration for Land Management and Geoinformation (HVBG), the Rhineland-Palatinate State Office for Surveying and Geographic Information (LVermGeo) and the Baden-Württemberg State Survey Office (LGL). In addition, the Institut für Steinkonservierung in Mainz gave me access to their extensive rock collection.

Petrel was kindly provided by Schlumberger for this research.

I thank TERREMYS for the acquisition and basic processing of the aeromagnetic dataset.

The research was funded by the Interreg NWE Program through the Roll-out of Deep Geothermal Energy in North-West Europe (DGE-ROLLOUT Project, www.nweurope.eu/DGE-Rollout). The Interreg NWE Program is part of the European Cohesion Policy and is financed by the European Regional Development Fund (ERDF).

Finally, I would like to thank my family and especially my partner Kiki for her continuous practical and emotional support during the three years of my PhD project.

List of Figures

List of Tables

Index of Abbreviations and Symbols

Abbreviations:

ATES	Aquifer thermal energy storage
BB	Borehole breakouts
BG	Bresse Graben
BO	Böllstein Odenwald
CLGS	Closed-loop geothermal systems
CHP	Combined heat and power
CSGC	Central Schwarzwald Gneiss Complex
DEKORP	German Continental Reflection Seismic Program
DEM	Digital elevation model
DFN	Discrete fracture network model
DHN	District heating network
DIFT	Drilling induced tensile fractures
DST	Drill-stem test
ECRIS	European Cenozoic Rift System
EGS	Enhanced/engineered geothermal system
EM	Electromagnetic methods
EMBF	Eastern main boundary fault
EPM	Equivalent porous medium
EU-SPI	European Social Progress Index
FC	Frankenstein Complex
FGZ	Flaser-Granitoid Zone
FIT	Formation integrity tests
FMS	Earthquake focal mechanisms
GDP	Gross domestic product
GeoLaB	Geothermal underground research laboratory
GNSS	Global navigation satellite system
GPS	Global Positioning System
HDI	Human Development Index
HDR	Hot Dry Rock
HG	Heidelberg Granite
HLNUG	Hessisches Landesamt für Naturschutz, Umwelt und Geologie
HVBG	Hessian Administration for Soil Management and Geoinformation
HWR	Hot Wet Rock
LG	Limagne Graben
LGL	Landesamt für Geoinformation und Landentwicklung Baden-Württemberg
LIAG	Leibniz-Institut für Angewandte Geophysik
LIDAR	Light detection and ranging
LOT	Leak-off tests
LRG	Lower Rhine Graben
LVermGeo	Landesamts für Vermessung und Geobasisinformation Rheinland-Pfalz
MB	Mainz Basin
MCMC	Markov Chain Monte Carlo
MD-BHE	Medium-deep borehole heat exchangers
MGCH	Mid-Germany Crystalline High

MNZ	Moldanubian Zone
NPZ	Northern Phyllite Zone
NUTS	Nomenclature of Territorial Units for Statistics
ORC	Organic Rankine Cycle
OZ	Otzberg Shear Zone
REV	Representative elementary volume
RHZ	Rhenohercynian Zone
RMS	Root mean square
RTP	Reduction to the pole
SA	Schollenagglomerat
SBG	Southern Bergstraesser Granitoids
SH	Sprendlinger Horst
SNB	Saar-Nahe Basin
SRTM	Shuttle Radar Topography Mission
SSGC	Southern Schwarzwald Gneiss Complex
STZ	Saxothuringian Zone
TAB	Office of Technology Assessment at the German Bundestag
TDS	Total of dissolved solids
TG	Tromm Granite
TVD	True vertical depth
UAV	Unmanned aerial vehicle
URG	Upper Rhine Graben
VSP	Vertical seismic profiling
WMBF	Western Main Boundary Fault
WP	Weschnitz Pluton

Formula Symbols

ASA	[nT/m]	Analytical signal amplitude
cL	[-]	Number of connections per fracture
c_{invest}	[€]	Investment costs
$c_{O\&M}$	[€]	Operation and maintenance costs
d	[%]	Discount rate
$E_{gross/net}$	[J, Wh]	Net/gross electricity production
F	[nT]	Magnetic field
$FSED$	[-]	Fast sigmoid function
h_{full}	[h]	Full load hours
k	[m²]	Permeability
$LCOE$	[€/kWh]	Levelized cost of energy/electricity
$LCOH$	[€/kWh]	Levelized cost of heat
$L(m)$	[-]	Model likelihood
$NTHG$	[-]	Normalized total horizontal gradient
r	[€]	Revenues
R	[%]	Recovery factor
$P10$	[m^{-1}]	Linear fracture frequency
$P20$	[m^{-2}]	Areal fracture density
$P21$	[m^{-1}]	Areal fracture intensity

Q_{total}	[j, Wh]	Geothermal resource base
Q_{rec}	[j, Wh]	Geothermal resources (technically recoverable heat)
t	[s, h, yr]	Time step
t_{life}	[yr]	Project lifetime
T_d	[-]	Dilation tendency
T_s	[-]	Slip tendency
T_r	[°C]	Reservoir temperature
T_{fl}	[°C]	Fluid temperature
T_0	[°C]	Reference temperature
TDR	[rad]	Tilt derivative
TDX	[rad]	Normalized horizontal tilt derivative
THG	[nT/m]	Total horizontal gradient
V	[m³]	Reservoir volume
VDR	[nT/m]	Vertical derivative
x, y, z	[m]	Spatial coordinates
Θ	[rad]	Theta map
ρ	[kg/m³]	Density
$\sigma_{1/2/3}$	[N/m³]	Principle stresses
σ_{Hmax}	[N/m³]	Maximum horizontal stress
σ_{hmin}	[N/m³]	Minimum horizontal stress
Φ	[%]	Porosity
χ	[-]	Magnetic susceptibility
$\eta_{gross/net}$	[-]	Gross/net system efficiency

Table of Contents

1. Introduction

Man-made climate change is without a doubt the greatest challenge facing the international community over the coming decades (IPCC 2022a). In the medium to long term, vast stretches of land around the world will become uninhabitable, be it due to persistent droughts, successive sea level rise or widespread destruction of ecosystems. This is expected to result in massive refugee flows especially from developing countries (Biermann and Boas 2008; Farbotko and Lazrus 2012; Lister 2014), which will potentially lead to severe geopolitical conflicts. In addition, an increase of extreme weather events, such as the devastating floods in the Ahr Valley in 2021, is already evident, causing significant economic damage. In Germany alone, the estimated costs arising from extreme weather amounted to at least 80 billion euros between 2018 and 2021 (Trenczek et al. 2022).

To limit the harmful effects of climate change, 195 countries committed under the Paris Agreement to keep global warming well below 2 °C compared to pre-industrial times (United Nations 2015). The Climate Protection Act, which was once again tightened in 2021, defines the legal framework in Germany for achieving this goal (Bundesregierung 2021a). Accordingly, at least 65% of yearly greenhouse gas emissions compared to 1990 must be saved by 2030 and 88% by 2040. Net carbon neutrality should be reached no later than 2045. Fig. 1.1 shows the development of the German greenhouse gas emissions from 1990 to 2021, clearly indicating that the climate targets will be missed by a wide margin if the current downward trend is maintained.

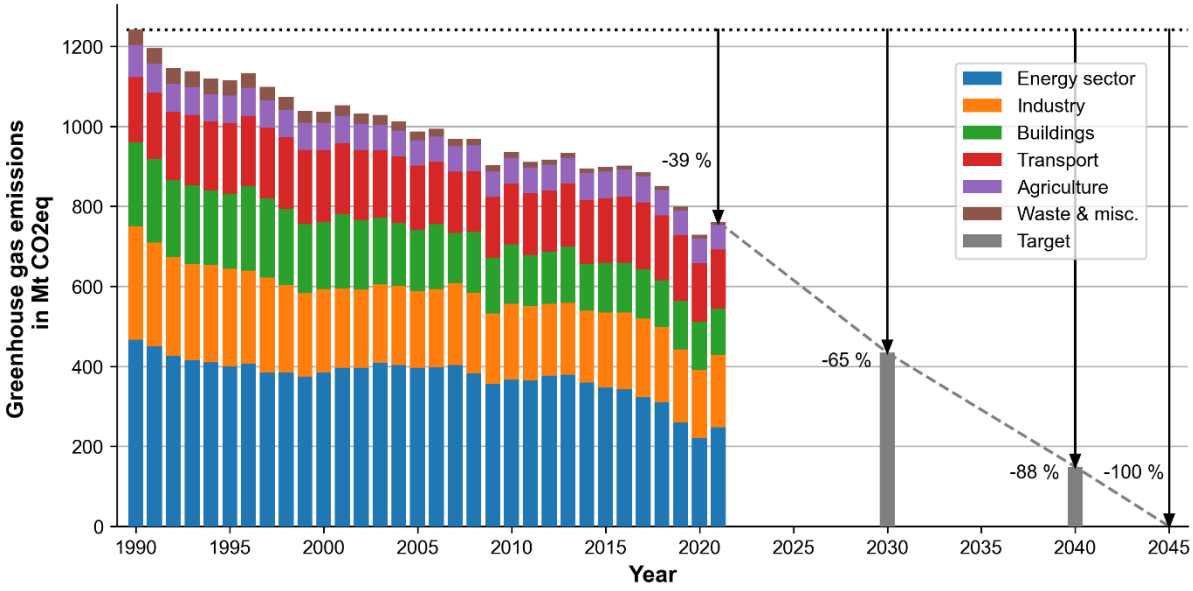

Figure 1.1: Development of greenhouse gas emissions in Germany from 1990 to 2021 split by sectors including emission targets until 2045 (Bundesregierung 2021a; UBA 2022b). Note that the current downward trend is not sufficient to reach the climate goals.

The Climate Protection Plan 2050 sets out the strategies for reaching the ambitious targets (BMU 2016). Essential components of lowering emissions include energetic modernization of buildings, the introduction of more efficient industrial processes, and the electrification of the traffic. Even more important, however, is the rapid transition of the energy supply from fossil fuels to renewable energies. In this context, the public debate usually focusses on electricity generation, around 47% of which was already secured by renewable energies in Germany at

the beginning of 2022 (Destatis 2022b). Yet, electricity accounts for only about 1/5 of the final energy consumption. The share of renewable energies in transportation and heating, by contrast, has stagnated at less than 20% for years (AEE 2020). Thus, substantial efforts are still required in these sectors to achieve zero greenhouse gas emissions by 2045.

Apart from climate change, the current geopolitical situation illustrates that excessive dependence on fossil fuel imports can lead to serious economic consequences. The price of gas already reached a long-term high at the end of 2021 (Destatis 2022a), since global production capacity had not been ramped up again following the COVID-19 pandemic. The situation further escalated with the war in Ukraine, when Russia significantly restricted gas deliveries to the European Union in response to the Western sanctions. Consequently, gas prices increased four- to fivefold compared to early 2021 (DIE ZEIT 2023), and supply security for households and industry were threatened. At the same time, the inflation rate rose to a historic high of 10.4 % (October 2022) in Germany (Destatis 2022c), which in the worst case could drive the economy into a recession. Reliable predictions of fuel prices are unavailable at the moment, making considerable investments in renewable energies all the more critical. The expansion of domestic renewable energy generation would create a favorable strategic position, as the national energy market becomes much less susceptible to external influences (Liutak et al. 2021).

Currently, German efforts concentrate on the development of wind and solar power plants (UBA 2022a; Bundesregierung 2021b), as these technologies have been long established and are comparatively inexpensive. However, the weather-dependent and seasonal fluctuations of these energy sources are a major drawback (Lund and Münster 2003; Spiecker and Weber 2014; Tani et al. 2014). Especially in the case of solar-thermal energy, there is a significant seasonal mismatch between production and demand, which requires the construction of huge storage capacities (Tian and Zhao 2013). Given these challenges, the subsurface will play a key role in the energy transition by enabling both large-scale energy storage (e.g., in the form of heat or hydrogen) and heat production (Sanner et al. 2003; Huenges et al. 2013; Chamorro et al. 2014; Bär et al. 2015; Tarkowski 2019). In addition, the extraction of lithium and rare earths from geothermal brines (Saevarsdottir et al. 2014) as well as the sequestration of CO_2 in suitable geological formations (Benson and Cole 2008) will make an essential contribution to climate protection.

As a baseload capable, renewable and local energy source, deep geothermal energy offers huge potentials to accelerate climate protection (Bauer 2014). Hot groundwater is extracted from 400 m to several kilometers deep reservoirs either for direct use, power generation, or combined heat and power (CHP) production. Depending on the natural hydraulic properties, a formation is classified as hydrothermal or petrothermal system. Hydrothermal reservoirs are aquifers mostly in sedimentary or volcanic units that allow high production rates without any stimulation. Petrothermal systems, on the other hand, are characterized by low natural permeability, which applies to the crystalline basement or strongly cemented sedimentary rocks. To make the stored heat usable, artificial reservoirs referred to as Enhanced or Engineered Geothermal Systems (EGS) are created using hydromechanical, chemical or thermal stimulation techniques (Tester et al. 2006; Huenges 2016; Olasolo et al. 2016). A comprehensive overview of the EGS technology is given in subchapter 1.2.

Although the technically usable geothermal resources exceed the total energy demand by several orders of magnitude, especially in the crystalline basement, deep geothermal energy

accounts for far less than one percent of the German energy mix (Fig. 1.2). Currently, 42 commercial deep geothermal plants are operating in Germany, which together supply about 44 MW of electricity and 354 MW of heat (Bundesverband Geothermie 2022). Considerably higher capacities are already installed in countries with high enthalpy resources (e.g. Iceland, Japan, USA, Turkey, Italy) (Ren21 2018). One reason for this slow development is the low awareness in public and politics of the opportunities presented by geothermal energy. Besides, high upfront costs and high risk of geothermal drilling in complex geological settings often discourage private investors. Therefore, a detailed multiscale and interdisciplinary characterization of the potential target horizons is required to bring risks down to an acceptable level and to provide stakeholders with a reliable basis for decision-making.

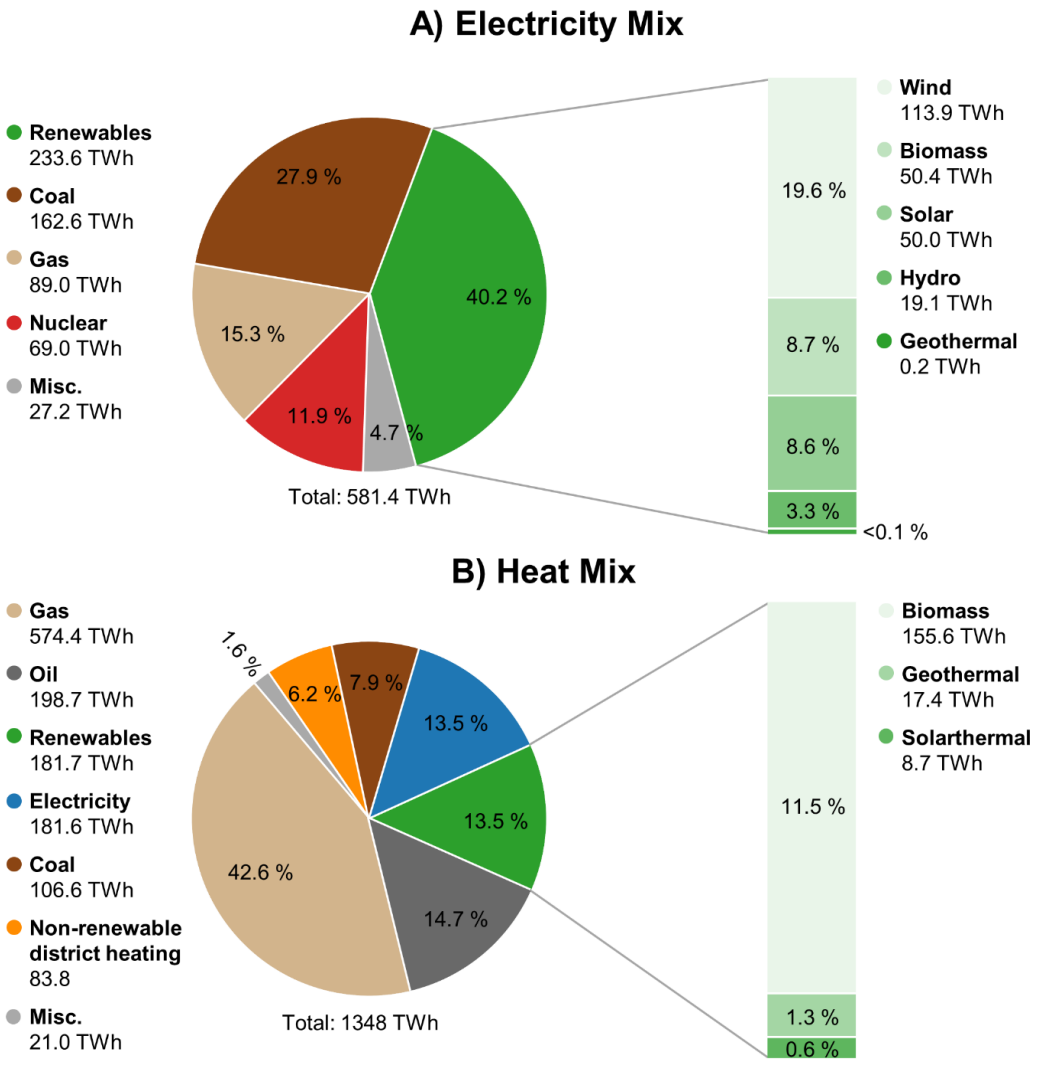

Figure 1.2: Energy mix in Germany according to AEE (2022): (A) electricity mix in 2021; (B) heat mix in 2020. Note that geothermal heat production in (B) combines both deep and shallow sources. The share of geothermal energy could be significantly increased by large-scale exploitation of the crystalline basement through Enhanced Geothermal Systems.

1.1. Geothermal Regime in the Upper Rhine Graben

Geothermal resources are heterogeneously distributed depending on the thermal and hydraulic properties of the available geological formations. In Germany, three major regions with

increased potential for deep geothermal utilization have been identified in the past (Fig. 1.3) (Agemar et al. 2010): the North German Basin, the South German Molasse Basin, and the Upper Rhine Graben (URG). The latter exhibits an exceptionally high geothermal gradient of locally more than 100 °C/km (e.g. Schellschmidt and Clauser 1996) and is therefore of particular interest for research and industry.

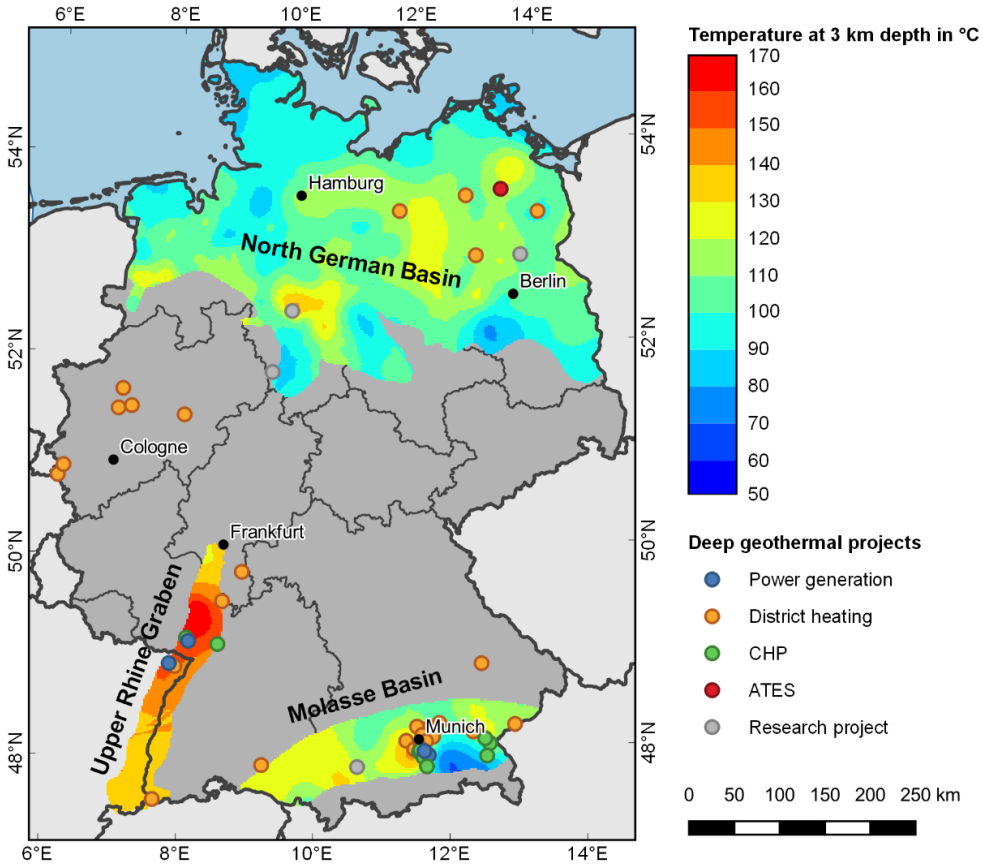

Figure 1.3: Overview of the three main regions for deep geothermal utilization in Germany. The reservoir temperatures at 3 km depth were drawn from the model of Agemar et al. (2012). In addition, all operating deep geothermal plants are marked (Bundesverband Geothermie 2022). CHP – Combined Heat and Power, ATES – Aquifer Thermal Energy Storage.

The URG is an approximately 300 km long and 30-40 km wide passive rift that roughly extends from the Jura Mountains in the south to the Rhenish Massif in the north (Fig. 1.4). To the east, the rift is bounded by the Odenwald and the Black Forest, and to the west by the Palatinate and the Vosges. The URG represents the central segment of the transcontinental European Cenozoic Rift System (ECRIS) (Ziegler 1992; Ziegler 1994; Dèzes et al. 2004), which formed from the Eocene onward as a consequence of the changing lithospheric stress regime in the Alpine foreland. Northward compressional movements of the Alpine orogen initiated east-west oriented crustal extension, starting initially in the southern section and gradually shifting northward (Ziegler et al. 1995; Ziegler and Dèzes 2005). Major pre-existing discontinuities in the crust that developed during the Variscan orogeny, Permo-Carboniferous, and Mesozoic were likely reactivated and thereby significantly influenced the orientation and position of the URG (Schumacher 2002; Edel et al. 2007; Grimmer et al. 2017). During the main extensional phase, the surface subsided by up to 4 km along numerous roughly N-S-directed faults within the rift valley, while the rift shoulders were isostatically uplifted (Villemin et al. 1986; Villemin and Coletta 1990). During the Lower Miocene, a counterclockwise rotation of main horizontal stresses resulted in a transtensive to transpressive reactivation of the existing normal faults

(Illies 1978; Buchner 1981; Schumacher 2002; Behrmann et al. 2003). This led to laterally varying subsidence rates and increased the segmentation and pronounced asymmetry of the URG. The Cenozoic graben was successively filled with heterogeneous fluviatile, marine, and limnetic deposits (Grimm 2005; Grimm et al. 2011). Crustal extension was furthermore accompanied by repeated volcanism, of which the Kaiserstuhl is the prime example. A comprehensive tectonic and geologic description of the URG is given in Chapter 2.

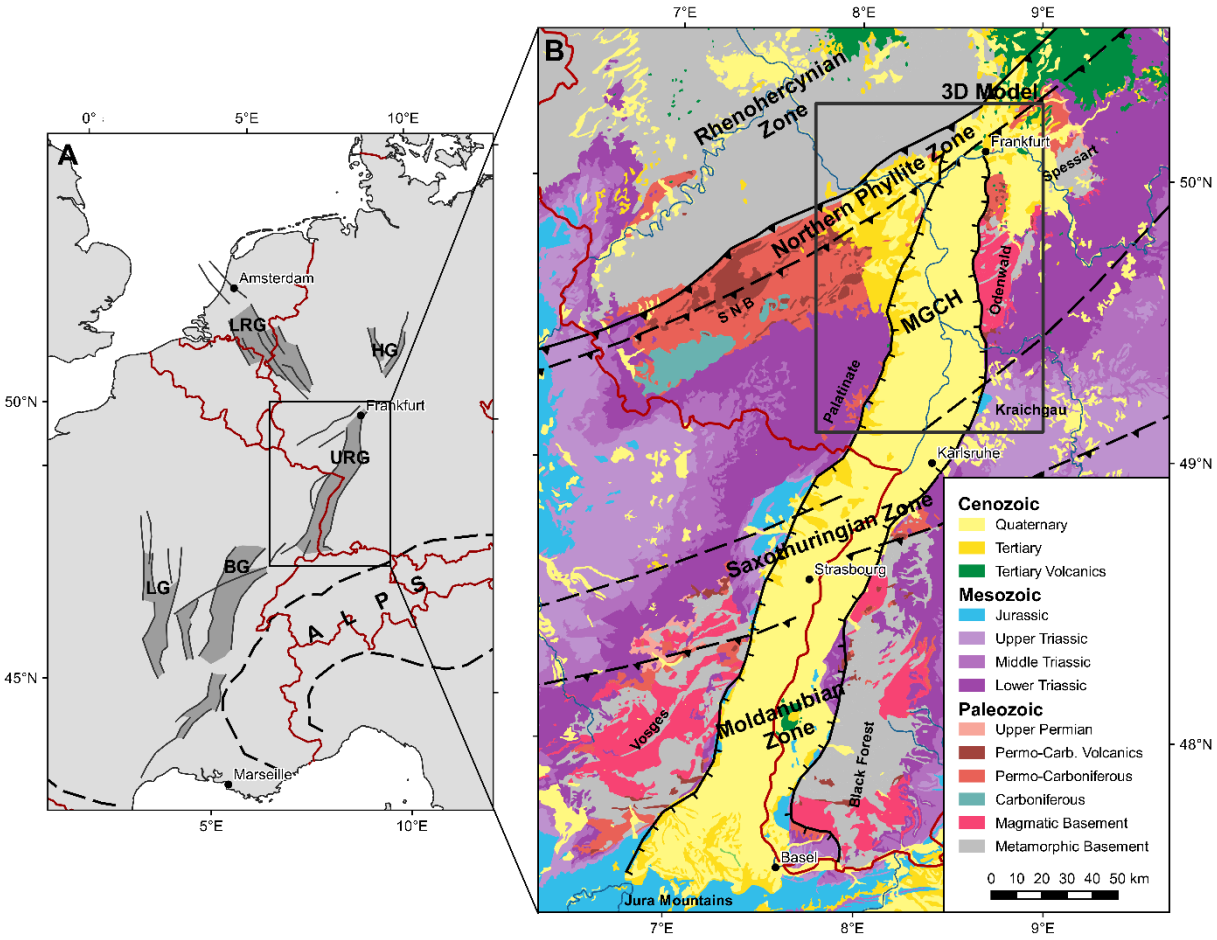

Figure 1.4: (A) Regional overview of the European Cenozoic Rift System (adapted from Ziegler and Dèzes 2005) and (B) geological map of the Upper Rhine Graben including main tectonic boundaries between the Variscan basement units (modified after BGR 2016). BG – Bresse Graben, HG – Hessian grabens, LG – Limagne Graben, LRG – Lower Rhine Graben, MGCH – Mid-German Crystalline High, SNB – Saar-Nahe Basin, URG – Upper Rhine Graben

As a still active extensional area, the URG is assigned to the convection-dominated geothermal play type, where large-scale faults primarily control the heat transport (Moeck 2014). Localized temperature anomalies are thus mainly a consequence of the upwelling and downwelling of fluids along permeable fault zones. Radiogenic heat production in the crystalline basement enhanced heat flux from the Earth's mantle through the thinned crust, and thermal blanketing beneath the thick Cenozoic sediments further contribute to the high temperature gradient (Freymark et al. 2017).

The balneological use of geothermal brines at the URG margins can be traced back to Roman times, e.g. in Wiesbaden (Umweltamt Wiesbaden 2011). First attempts to exploit the hydrothermal resources for district heating and power generation were made in Bruchsal, Bühl, and Cronenbourg in the late 1970s as a reaction to the oil crisis (Bertleff et al. 1988). This was followed by the European EGS project in Soultz-sous-Forêts (Dezayes et al. 2005), which

substantially contributed to the understanding of artificial reservoirs in crystalline rocks. Today, seven deep geothermal plants are in operation in the URG, providing a total of 50 MW of heat and 10 MW of electricity (Bundesverband Geothermie 2022). The planning and implementation of additional power plants in the region has recently received a significant boost in connection with lithium extraction from geothermal brine (Saevarsdottir et al. 2014) and the emerging of so-called Advanced (closed-loop) Geothermal Systems (van Horn et al. 2020).

Potentially exploitable horizons have been identified and comprehensively characterized as part of numerous research projects in the URG (Sauer and Munck 1979; Dornstadter et al. 1999; Stober and Jodocy 2009; Sass et al. 2011; Bär 2012; GeORG Projektteam 2013; Bär et al. 2021). Among the nine suitable geologic units (chapter 2), the crystalline (Variscan) basement generally exhibits the highest reservoir temperatures. In addition, the URG basement is intensely faulted and fractured due to the complex deformation history, which leads to a naturally elevated permeability compared to other German regions. A report from the Office of Technology Assessment at the German Bundestag (TAB) revealed that the basement accounts for the bulk (about 95%) of the overall geothermal resources (Paschen et al. 2003). Accordingly, the technical potential for electricity generation is about 17 PWh, almost 35 times the annual electricity demand of Germany. However, unlike the Tertiary formations, the basement has been explored to a much lesser extent by the hydrocarbon industry using wells and reflection seismic profiles. This thesis additionally integrates potential field data (chapter 3) as well as analog studies (chapters 5 & 6) into the characterization of the reservoir. This provides new insights into the structure and composition of the basement while reducing geological uncertainties.

1.2. Fundamentals of Enhanced Geothermal Systems

Huenges (2016) defines EGS as "geothermal reservoirs that enable economic use of low-permeability, conductive rock by creating fluid communication in originally low-permeability rock through hydraulic, thermal, or chemical stimulation methods or advanced well configurations". While there is still certain controversy on the exact definition and physical processes underlying EGS (e.g. Li et al. 2022), it is important to note that it always refers to artificially created or enhanced reservoirs in petrothermal or hydrothermal systems. To date, this technology faces significant difficulties, such as induced seismicity, uncertain geological conditions, and high drilling costs, which is why only a small percentage of its vast potential has been tapped. Nevertheless, starting with the first project at Fenton Hill (New Mexico) in the 1970s, a steep learning curve is evident, and large-scale commercial application seems feasible in the near future.

This subchapter summarizes the fundamentals of the EGS technology that are directly related to reservoir development and operation in the crystalline basement. First, the hydraulic properties of the basement are reviewed, and the influence of fault zones and the fracture network is discussed. Then a detailed description of the possible stimulation measures and the related physical process is given, followed by an overview of the historical development of EGS with special focus on projects in the URG. Finally, the remaining challenges and tasks are outlined.

1.2.1. Hydraulic Properties of the Crystalline Basement

Permeability is a main controlling factor for the productivity of geothermal wells and consequently the economic viability of the power plant. Comprehensive insight into the hydraulic properties of the natural reservoir is therefore crucial for the design of the well path and stimulation measures. Traditionally, the basement was regarded as impermeable or low-permeable ($< 10^{-16}$ m²). But in fact, permeability varies by up to 15 orders of magnitude (Achtziger-Zupančič et al. 2017) depending on geologic formation, depth, orientation, stress field, fracture network, etc. Over the last decades, several thousand permeability measurements have been carried out in the crystalline basement worldwide using different measurement techniques in boreholes (pump tests, packer tests, Lugeon/WD tests, drill stem tests, flow meter logs) and tunnels (pressure test, discrete tunnel inflow analysis). The theoretical background of the most common hydraulic tests is summarized in Kruseman and Ridder (1990). In addition, permeability was indirectly determined by means of thermo-hydraulic modelling and observations of induced seismicity. The obtained properties may therefore be significantly biased depending on the selected method. Most in situ measurements were taken from a few hundred meters depth, whereas data are very sparse below 2 to 3 km depth.

It has been repeatedly shown that the permeability of the basement declines exponentially with depth as potential fluid pathways are successively closed by the increasing overburden and cementation. Empirical equations depicting this trend have been published, for example, by Manning and Ingebritsen (1999), Shmonov et al. (2003), Stober and Bucher (2007), and Achtziger-Zupančič et al. (2017). Fig. 1.5 shows a compilation of these permeability-depth curves. In general, a high level of agreement is apparent, especially at greater depth. A comparison with individual measurements from selected site reveals that the natural range of values is in fact much greater than suggested by the permeability trends. Permeability varies by up to 10 orders of magnitude near the surface and by 5 to 7 orders of magnitude at several kilometers depth (Achtziger-Zupančič et al. 2017).

Apart from the depth dependence of permeability, Achtziger-Zupančič et al. (2017) observed a significant correlation with the current seismo-tectonic activity as well as the long-term tectono-geological history on the global scale. At the regional scale, Stober and Bucher (1999) additionally identified a strong dependence on the lithology. They performed hydraulic tests in the Black Forest showing that the permeability of gneisses is on average two orders of magnitude smaller than that of granites. The might be explained by the foliation within the metamorphic rocks, which on the one hand creates a pronounced permeability anisotropy and on the other hand accelerates the resealing of fractures.

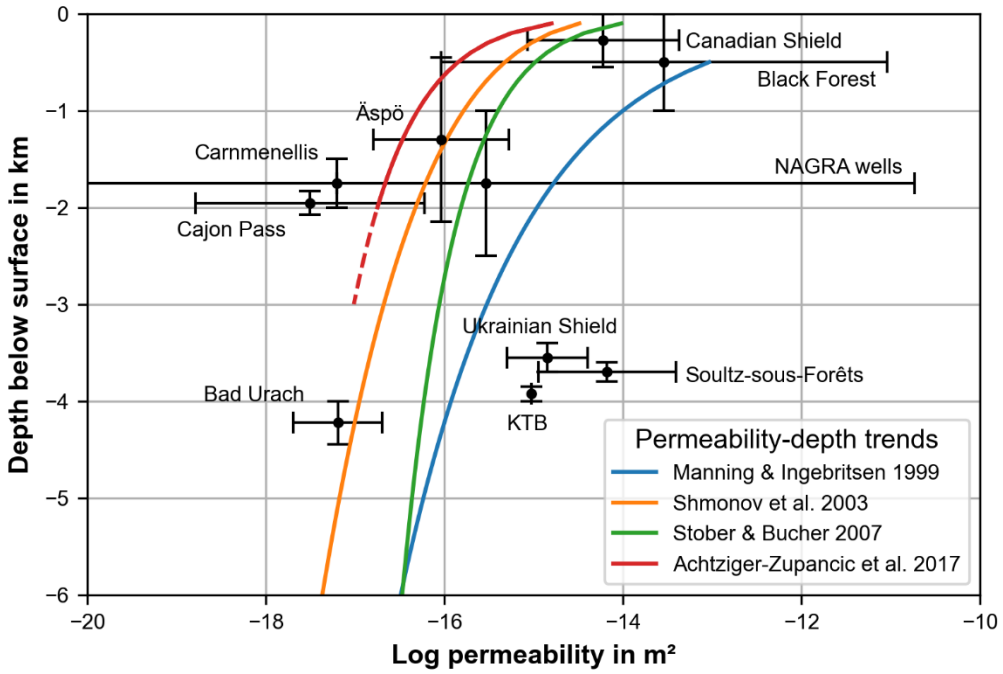

Figure 1.5: Comparison of four permeability-depth-relationships for the crystalline basement. Measured permeability ranges are given for selected test sites (modified after Stober and Bucher 2007 and references therein).

The permeability of the rock matrix is usually very low in the basement ($<10^{-18}$ m²) (e.g. Bär et al. 2020), meaning that fluid flow is almost exclusively controlled by hydraulically active fractures and faults. In general, tensile fractures (joints, fissures) and shear fractures are distinguished (Fossen 2016). Tensile failure occurs when the effective minimum principal stress exceeds the tensile strength of the rock. This may be caused by cooling of magma, sharp increase in pore pressure, or exhumation of deep rock. Tensile fractures are always oriented perpendicular to σ_3 and parallel to σ_1. Shear fractures, on the other hand, form at an angle of 20 to 30 ° to σ_1 when the shear stress exceeds the shear strength of the formation. They are the most common type of brittle deformation. The characteristics of the fracture network depend on the depth, lithology, tectonic history, and stress field.

In turn, reservoir permeability is affected by various fracture network properties, such as the density, length distribution, orientation, connectivity, and hydraulic opening of the fractures (Long and Witherspoon 1985; Koudina et al. 1998; Mahmoodpour et al. 2022). The latter influences the hydraulic reservoir properties most, since it is related to permeability via a cubic law for fractures with relatively low roughness (Oda 1985). However, it is particularly difficult to accurately determine the hydraulic aperture using borehole logs. Measured values from core analyses and analog outcrop studies are also not representative of reservoir conditions at larger depth. The aperture can instead be modeled as a function of the shear and normal stress along the fracture plane (Barton et al. 1995; Vermilye and Scholz 1995; Bisdom et al. 2017). Accordingly, fractures perpendicular to σ_3 or with a high shear to normal stress ratio tend to have the largest opening.

Laboratory measurements are generally not suitable to assess the bulk permeability of the reservoir since the representative elemental volume (REV) is violated. Integration of in situ hydraulic test data is thus critical for the determination of reliable permeability values.

Faults are macroscopic discontinuities with significant shear displacements ranging from a few centimeters to several kilometers. They typically consist of a fault core, where most of the slip is accumulated, and the damage zone, which has a significantly increased fracture density compared to the undisturbed host rock (Evans et al. 1997). The fracture density often decreases exponentially with distance from the fault core. As a first approximation, the width of core and damage zone scales with the total slip (Torabi and Berg 2011). At fault linkages, bends or terminations, the structural architecture may be much more complex (Fig. 1.6). The fault zone can therefore also consist of several cores and damage zones as well as multiple subsidiary faults (Faulkner et al. 2010; Fletcher et al. 2020). In addition, faults may be segmented along strike or down dip, resulting in an overall complicated mechanical and hydraulic behavior (Bense et al. 2013). Depending on lithology, deformation history, and confining pressure, the core consists of breccias, fine-grained gouge, or cataclasites (Sibson 1977). These rocks may accelerate or impede fluid flow, mainly as a function of phyllosilicate content (Faulkner et al. 2010). In general, the core of inactive faults is considered to be a cross-fault fluid barrier, whereas in active fault zones fluid pathways can be kept open by continuous deformation. The damage zone, on the other hand, is seen as an along-fault conduit in which fluid flow is channeled due to the increased fracture density. Scibek (2020) compiled worldwide permeability measurements on fault-related rocks of different lithologies. In plutonic rocks, the bulk permeability of the fault zone averages about 10^{-13} m², but with variations of nine orders of magnitude. In comparison, the average permeability of the fault core is only about 10^{-17} m². Caine et al. (1996) concluded that the hydraulic character of the fault zone is mainly determined by the ratio between the damage zone and the core thickness.

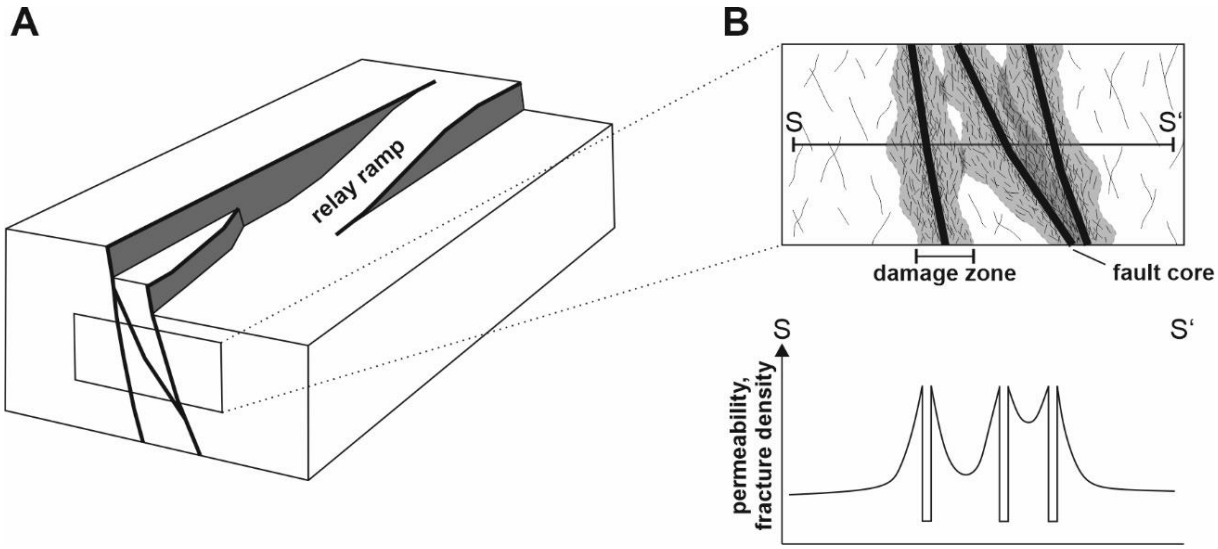

Figure 1.6: Typically structural setting in extensional domains such as the URG (modified after Bense et al., 2013). (A) Interference of normal faults, leading to the development of relay ramps. (B) Detailed view of fault and fracture network and qualitative permeability profile crossing the protolith, damage zone and fault core.

The complex structural situation in URG is the result of a multi-phase evolution (e.g. Schumacher 2002). The geologic sequence is fragmented by a high density of oblique normal faults with offsets ranging from tens of meters to several kilometers. In the later development of the URG, these fault zones were often reactivated by strike-slip deformation. Because of this repeated deformation over extended time periods, the basement exhibits a high fracture density. In addition, the current transtensive stress regime tends to keep the existing fractures open, which likely yields more favorable hydraulic properties for EGS projects than in mainly undeformed or compressive regions (Ziagos et al. 2013). However, due to the small number of

boreholes that penetrate the basement in this region, an assessment of the actual fracture network properties is only possible at a local scale (e.g., at Soultz-sous-Forêts) or in outcrop analogs. Given the lack of in situ test data, this thesis applies a set of non-invasive exploration methods as well as Discrete Fracture Network (DFN) modelling to further constrain the hydraulic properties of the basement in the northern URG and to define potentially permeable zones.

1.2.2. Reservoir Enhancement

As described above, the basement permeability is usually insufficient for direct utilization of geothermal resources, even in the influence area of major fault zones. The reason for this is that under reservoir conditions, most fractures are closed due to high overburden or hydrothermal mineralization. The few hydraulically active fractures moreover rarely connect to a conductive network. Wells may also be poorly connected to the reservoir, resulting in high pressure drop and low productivity. In addition, permeability can be progressively reduced due to scaling during operation. To develop a viable reservoir, targeted stimulation of the crystalline rock is therefore necessary (Schulte et al. 2010), which either opens new fractures or improves the permeability of the existing fracture network. A distinction is made between hydraulic, chemical, and thermal stimulations, most of which were developed by the oil and gas industry and have been adapted for geothermal purposes. The techniques can be applied either individually or in combination, depending on the specifications of the reservoir.

Hydraulic stimulation is the most commonly used method for reservoir development and enhancement in the crystalline basement (Huenges 2016). To date, it is the only technique that can significantly increase the permeability in a distance of several hundred meters to kilometers from the wellbore. The stimulation is based on massive water injections with downhole pressures of up to 50 MPa. This results in the opening of fractures, which can be explained by two basic mechanisms (McClure and Horne 2014; Gischig and Preisig 2015): hydraulic fracturing and hydraulic shearing. Hydraulic fracturing describes the tensile failure of the rock due to the pore pressure increase. This leads to the formation of new tensile fractures and is mainly applied in tight hydrocarbon reservoirs. Proppants can be added to create fractures with larger apertures and to keep the fractures permanently open (Barati and Liang 2014). Hydraulic shearing, in contrast, induces shear displacements along pre-existing fractures. This is the predominant process in naturally fractured reservoirs, such as the crystalline basement. Natural fractures are always characterized by a rough and irregular surface. During shear replacement, this leads to the so-called self-propping effect (Jeffrey et al. 2010), whereby the fractures become permanently open. Fluid additives or packers may be used to stimulate only certain well sections and to control the reservoir growth (Mégel et al. 2006; Yakeley et al. 2007). Induced seismicity is nearly inevitable with hydraulic stimulation (Zang et al. 2014), but the maximum magnitude of earthquakes can potentially be kept below a predefined threshold by controlling injection pressure and cyclic treatment (see a detailed discussion below). Hofmann et al. (2021) recently demonstrated in Iceland that a mild stimulation treatment can effectively increase reservoir permeability while retaining the magnitude of induced seismic events well below the perceptual level.

Chemical stimulation is a long-established method that has been used in oil wells since the end of the 19th century (Portier et al. 2007). It mainly involves acid injection into the reservoir at

a moderate pressure to remove skin damage caused by the drilling or to dissolve hydrothermal mineralization in fractures (Morris et al. 1984; Portier et al. 2009). Besides, scaling that accumulates after months and years of operation can be removed. Hydrochloric acid and hydrofluoric acid are mostly used in the stimulation, which typically consists of pre-, main-, post-flush. Particularly good results are achieved in carbonate rocks, where acidification leads to artificial karstification (Xie et al. 2005). But chemical stimulation of the matrix as well as the fracture network yields also good results in crystalline rocks (Schulz et al. 2022; Portier et al. 2009). Unlike hydraulic stimulation, however, mainly the near-wellbore permeability is enhanced (Rose et al. 2007). Acidization is ideally implemented before hydraulic stimulation to reduce the pressure drop, thus making the massive water injection as effective as possible. A combination of chemical and hydraulic stimulation is another option to enable deep penetration of the chemicals into the reservoir.

Thermal stimulation describes the injection of cold water into a hot reservoir with moderate injection rates, limiting the well head pressure to 1 to 6 MPa (Siratovich et al. 2011). As with chemical stimulation, this primarily enhances the near-well reservoir and the connection of the well to the reservoir. Rapid cooling of the reservoir causes contraction of the rock, reducing the effective stress (Ghassemi et al. 2007; Zhou et al. 2009). This either opens existing fractures or creates new ones. In addition, debris or mineral deposits from open fractures are removed. Thermal stimulation is more effective the greater the temperature difference between the reservoir and the injection fluid. For this reason, with a few exceptions (e.g. in Rittershoffen), this procedure is used in high-enthalpy systems (Tulinius et al. 2000). But it should be mentioned that in all EGS reservoirs thermal stresses occur as a co-effect of hydraulic stimulation and long-term circulation (Grant et al. 2013). Consequently, reservoir productivity often improves over long time scales, if no significant scaling occurs.

1.2.3. History of EGS Projects

EGS technologies now looks back on a five-decade long history (Breede et al. 2013). The first project, led by Los Alamos National Laboratory, was undertaken at Fenton Hill (New Mexico) in the 1970s (Cummings and Morris 1979; Tester et al. 1989; Brown 1997). Drilling operations began in 1974, followed by various stimulations and hydraulic tests until operations were finally suspended in 2000. Originally referred to as Hot Dry Rock (HDR) method, the plan was to apply techniques from the oil and gas industry to develop an artificial heat exchanger in crystalline rock (Potter et al. 1974). Specifically, hydraulic fracturing was intended to create large, penny-shaped tensile fractures that would then serve as hydraulic connections between production and injection wells (Fig. 1.7). However, one of the key findings from Fenton Hill was that the natural fracture network played a much larger role in reservoir development than anticipated (Tester et al. 2006). Rather than creating artificial tensile fractures, shear deformation was induced along existing fractures. Therefore, the original HDR strategy was abandoned and the Hot Wet Rock (HWR) and EGS concepts were developed.

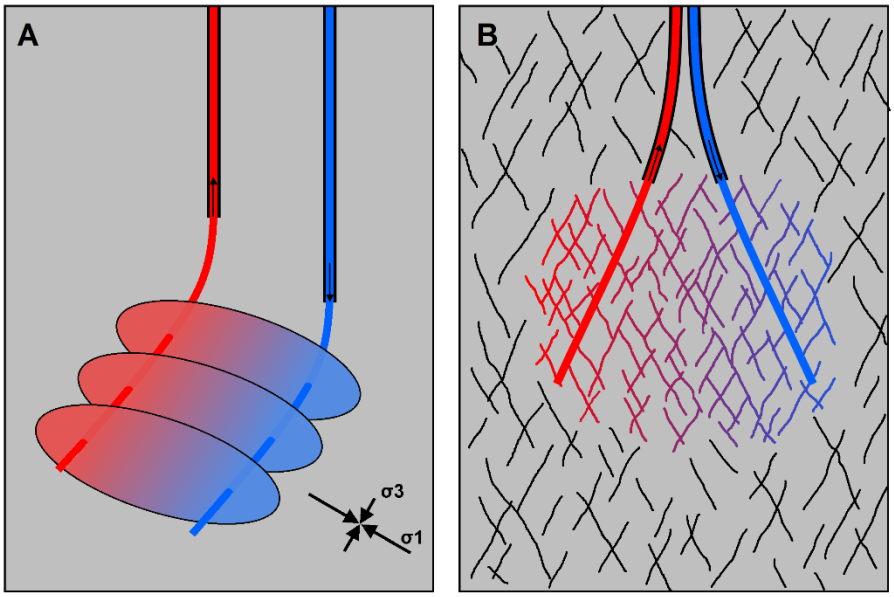

Figure 1.7: Comparison of the original Hot Dry Rock concept (A) with the current understanding of Enhanced Geothermal Systems (B).

Building on the findings of Fenton Hill, further attempts to create a viable reservoir in the basement followed in the UK (Rosemanowes), Japan (Hijiori and Ogachi) and Australia (Cooper Basin). The first EGS project of commercial size was developed in European collaboration at Soultz-sous-Forets (France) starting in 1987. Numerous stimulations and hydraulic tests provided detailed insights into hydrothermal and hydromechanical processes in the deep crystalline rocks, which contributed significantly to the progress of the EGS technology. From the 2000s onward, the number of purely commercial projects gradually increased, resulting in more than 50 existing EGS reservoirs worldwide in 2022. Still, the share of EGS technology in the total energy supply has been small so far, mainly due to the technical challenges involved in the reservoir development (Ren21 2018). It is therefore particularly important to learn from the difficulties encountered in previous projects. The EGS projects targeting the crystalline basement in the URG are described in detail below.

Soultz-sous-Forêts

Since the late 1980s, the recovery of heat from the crystalline basement using HDR/EGS technologies has been tested in Soultz-sous-Forêts (Alsace) (Gérard and Kappelmeyer 1987; Dezayes et al. 2005; Cuenot et al. 2008; Genter et al. 2010), involving research teams from France, Germany, the UK, Switzerland, Sweden, Italy, the USA, and Japan. The abandoned Pechelbronn oil field was selected as a suitable site because the geological sequence was already well explored and the geothermal gradient near the surface reached over 100 °C/km in this area. The first well GPK1 was drilled in 1987 to a depth of about 2 km and encountered the granitic basement at 1.4 km below surface. Instead of the expected reservoir temperature of 200 °C, only 140 °C was measured at the base, which was attributed to dominant convective heat transport between 1.5 and 3.5 km depth. The well was initially stimulated between 1.4 and 2.0 km depth in 1991 and deepened to 3.6 km in 1992. High flow rate stimulations and hydraulic testing between 2.85 and 3.6 km followed in 1993 and 94. In 1995, the GKP2 well was drilled to a depth of approximately 3.9 km, and further stimulation resulted in a good

connection with GKP1. Circulation tests in the produced reservoir yielded a thermal output of about 10 MW.

After the successful realization of the doublet, an economically sustainable operation of the geothermal plant was aimed at by constructing a triplet at greater depth. Starting in 1997, GPK2 was therefore once again deepened, and between 2001 and 2004, GPK3 as well as GPK4 were drilled to a depth of approx. 5 km. Multiple hydraulic stimulations with high flow rates and well pressures up to 18 MPa created a well-connected reservoir with temperatures around 200 °C in the reservoir. In the following years, numerous hydraulic tests and long-term cyclic experiments were carried out. A research power plant was then constructed in 2008, which was replaced in 2016 by a new commercial power plant with an electrical output of 1.7 MW.

Well logs, acoustic emissions and modelling demonstrated that fluid flow in the deep reservoir is dominated by natural fractures (Genter and Traineau 1996; Sausse and Genter 2005; Ledésert et al. 2010). Particularly high permeabilities are present in fractures that strike 160°, which are approximately parallel to the maximum horizontal stress (Dorbath et al. 2010). Hydraulic stimulation and long-term circulation resulted in significant improvements in hydraulic yield, with improvement factors of up to 50 (Schill et al. 2017). At the same time, fluid injections also resulted in a significant number of induced seismic events. In the 3.0 to 3.5 km deep reservoir, the maximum magnitude was 1.9, just below the perceptual threshold. The largest seismic event in the 5 km deep reservoir had a magnitude of 2.9 (Baisch et al. 2010) but did not cause any structural damage.

Landau

The geothermal power plant in Landau was developed by Geo x GmbH in the western URG starting in 2004 (Teza et al. 2008; Baumgärtner et al. 2013a). In contrast to previous EGS projects, not only the crystalline basement but multiple reservoir horizons were tapped simultaneously to minimize exploration risks and achieve economic productivity. The first well, Gt La1, was drilled in 2005 to a depth of approximately 3.3 km and targeted the three reservoir horizons Buntsandstein, Rotliegend (Permo-Carboniferous), and granitic basement. A hydraulic test revealed sufficient productivity, as a highly permeable fault was penetrated by the well path. The second well, Gt La2, was drilled to a depth of 3.34 km in 2006, but showed too low productivity, which required targeted hydraulic stimulation. Injection was carried out at 190 l/s at a maximum wellhead pressure of about 13.5 MPa and resulted in a significant increase in injectivity. During the subsequent hydraulic test phase, hydraulic properties of the borehole were further improved. The Organic Rankine Cycle (ORC) power plant started operation in 2007 with a nominal electrical capacity of 3.8 MW. No significant induced seismicity was detected during the stimulation and circulation tests. However, increased seismic activity occurred during operation from 2008 onwards, reaching its maximum in August 2009 with a magnitude of 2.6 (Grünthal 2014). Moreover, surface uplift of up to 3.5 cm occurred around the power plant in 2013, which was caused by a leakage in the casing at a depth of about 450 m (Heimlich et al. 2015).

Basel

The Deep Heat Mining Project developed by Geopower Basel AG was intended to be one of the first fully commercial EGS projects in crystalline rocks (Ladner et al. 2008; Häring et al. 2008). The plan was to operate a CHP plant using deep brines with a temperature of up to 200 °C. The site is located in the southernmost part of the URG, between the Jura Mountains and the Black Forest. Here, the region's strongest historic earthquake with an estimated magnitude between 6.7 and 7.1 took place in 1356 (Fäh et al. 2009). The first well was drilled in 2006 to a maximum depth of 5 km, intersecting about 2.4 km of sediments and 2.6 km of granitic basement. Hydraulic stimulation was conducted in the lower 400 m of the well with a maximum wellhead pressure exceeding 30 MPa. Originally planned for 21 days, the stimulation had to be stopped after 6 days due to a magnitude 2.6 earthquake (Deichmann and Giardini 2009). Within hours after shut-in, a magnitude 3.4 event occurred. In the following weeks, the activity only slowly decreased and three more earthquakes with magnitudes greater than 3 were recorded. The induced seismicity did not cause any structural damage, but the public acceptance was permanently impaired. After a risk analysis, it was finally decided to abandon the project and to close the well in 2011. As a result, the pressure at the wellhead rose again, causing a renewed increase in seismicity (Wiemer et al. 2017).

Insheim

Following the example of the power plant in Landau, the Pfalzwerke geofuture GmbH developed a geothermal power plant 5 km to the south in Insheim (Baumgärtner et al. 2013a; Baumgärtner et al. 2013b). Again, a multi-horizon approach was chosen, in which the reservoir horizons Keuper, Muschelkalk, Buntsandstein, Rotliegend, and basement were tapped. The two wells, GTI 1 and GTI 2, were drilled to a depth of 3.8 km in 2008 and 2009, targeting a single fault zone. The wells exhibited contrasting hydraulic properties despite the similar geological setting. Since GTI 1 suffered from insufficient productivity, a stepwise hydraulic stimulation with a maximum wellhead pressure of about 9 MPa was applied. This measure caused increased seismic activity with a maximum magnitude of 2.3 (Grünthal 2014). Since the well productivity was not significantly improved, an additional sidetrack was drilled in 2010. The ORC power plant with an electrical output of 4 MW started operation at the end of 2012.

Rittershoffen

The geothermal power plant at Rittershoffen, 5 km southeast of Soultz, was developed by ÉS-Géothermie to supply heat to a biorefinery, located 15 km from the drill site (Baujard et al. 2017; Mouchot et al. 2018; Duringer et al. 2019). The two wells were drilled between 2012 and 2014 into a local N-S trending fault zone where a high density of near vertical fractures was encountered. The wells penetrate the Cenozoic, Mesozoic, and Permian sediments before reaching the crystalline basement at 2.15 km depth. Target for geothermal utilization was the interface between sediments and basement, which exhibits favorable hydraulic properties due to hydrothermal alteration and paleo-weathering. The path of the first well GRT-1 is almost vertical, therefore only one permeable fracture was intersected, resulting in a too low productivity. By applying thermal, chemical, and hydraulic stimulation, an improvement by a factor of 5 could be achieved. Several induced earthquakes occurred a few days after fluid

injection, during which the overpressure in the borehole reached up to 3 MPa. However, the maximum magnitude of 1.6 was below the predefined threshold (Maurer et al. 2020). The well path of GRT-2 was deviated, which led to a much better connection of the wellbore to the natural fracture network and made stimulation obsolete. The power plant with a thermal capacity of 24 MW was finally commissioned in 2016.

Vendenheim and Illkirch

Based on the experience gained in Soultz and Rittershoffen, several geothermal power plants for power and heat supply were planned and developed in the greater Strasbourg area (Boissavy et al. 2019). The most advanced was the GEOVEN project in Vendenheim. As of 2017, the two deviated wells VDH-GT1 and VDH-GT2 were drilled to a depth of 5 km, where a temperature of about 200 °C was encountered. The granitic basement was reached at 4.6 km. After hydraulic testing in 2019 and 2020, several earthquakes with magnitudes greater than 3 were recorded (Schmittbuhl et al. 2021). The highest magnitude of 3.6 marked the strongest induced event associated with geothermal work in the URG to date. Consequently, the project has been suspended indefinitely. In Illkirch, 15 km to the south, the GIL-1 well was drilled in 2018 to a depth of 3400, where a temperature of 150 °C was reached. After the seismic events in Vendenheim, this project was also stopped.

1.2.4. Lessons Learned and Remaining Challenges

Five decades of EGS research and development resulted in a comprehensive knowledge base of the underlying physical processes and significant improvements of the applied technologies (Tester et al. 2006). Considerable progress has been made in drilling techniques by adapting them to the high-temperature conditions in deep geothermal reservoirs. It is now standard practice to drill deviated wells into the crystalline basement with adequately high accuracy, which is essential for targeted reservoir development. Similarly, sensors and logging tools have been developed that can withstand high temperatures, allowing accurate analysis and monitoring of the wellbore. However, a major obstacle to the widespread implementation of EGS power plants are the still very high costs of drilling, amounting to up to 70 % of the total investment (Lukawski et al. 2014; Bloomfield and Laney 2005). Although they are expected to fall in the next years with the expansion of geothermal energy, this cannot be reliably predicted. One way to save costs in the greenfield is to first drill exploration wells with a smaller diameter (slimholes) to prove the resources and only then start with drilling the production and injection wells (Kruszewski et al. 2017).

One of the most important findings from the early EGS projects was that the natural fracture network has a substantially stronger influence on reservoir development and fluid circulation in the basement than previously assumed (Ito 2003; Rutledge and Phillips 2003; Tester et al. 2006; Jeffrey et al. 2010; Jung 2013). The initial approach of creating large tensile fractures in the basement by water injection (pure opening mode) had therefore to be abandoned. Instead, shear activation of advantageously oriented, pre-existing fractures seems to predominate during hydraulic stimulation (pure shear mode). This is supported by the abundance of induced seismicity and observations from wells in which the fluid flow almost exclusively occurs along natural fractures. Jung (2013) and McClure and Horne (2014), however, argue that both

processes play a role in the stimulation of crystalline rocks (mixed-mechanics mode), which leads to the formation of a complex fracture network. According to them, tensile fractures are opened at the tips of shear fractures, which terminate again at the closest pre-existing fracture. In summary, the thermo-hydro-mechanical processes involved in the hydraulic stimulation are not fully understood up to now. Fracture formation and growth therefore need to be studied in more detail in in-situ experiments, e.g. in the upcoming GeoLaB project (Schätzler et al. 2020), to enable better prediction of reservoir development and hydraulic properties in the future.

By using the currently available technologies, it is already possible to create an artificial reservoir in the basement which sustains the enhanced permeability and can be utilized for electricity production and district heat supply. For economic operation of EGS power plants, it is desirable to develop the largest possible reservoir volume, while at the same time achieving sufficient production rates. If the distance between the production and injection wells is too far, there is a risk of a poorly or not at all connected reservoir. If the distance is too small, thermo-hydraulic short-circuiting between the wells may occur (Schulte et al. 2010). Hence, the well path and completion must be planned thoroughly to meet the requirements. The open-hole section should be designed in such a way that it penetrates a large number of potentially permeable fractures. These are primarily oriented parallel to σ_{Hmax} (~160° in the URG (Reiter et al. 2016)) and steeply dipping, so horizontal boreholes perpendicular to σ_{hmin} are most appropriate. However, the local structural setting must always be considered, as larger fault zones will affect fracture network properties and stress conditions. It is also recommended to initially only drill and stimulate one well (Tester et al. 2006). Based on the recorded micro-seismic activity during and after stimulation, the second well can then be accurately planned to ensure hydraulic connectivity between the producer and the injector. Sequential stimulations with packers are promising tools for creating a highly branched fracture network.

Induced seismicity remains arguably the biggest challenge in the construction of EGS power plants (Cornet et al. 1997; Majer et al. 2007; Evans et al. 2012). In the URG alone, three projects (Basel, Vendenheim, Illkirch) were terminated due to the occurrence of induced earthquakes with magnitudes over 3 (Deichmann and Giardini 2009; Schmittbuhl et al. 2021), after several million euros had already been invested in the drillings. At other sites, induced seismicity led to considerable resistance among the population, despite the fact that structural damages were rarely caused (Grünthal 2014). The strongest stimulation-induced earthquake to date with an estimated magnitude of 5.5 was recorded in Pohang (South Korea) on November 15, 2017 (Kim et al. 2018; Ellsworth et al. 2019). Water injections with a maximum wellhead pressure of around 89 MPa (almost three times as much as was reached in the Basel 1 well) led to the seismic activation of a previously unknown fault zone.

As mentioned above, induced seismicity is inherent to hydraulic stimulation, as instant shear displacements are caused along fractures (Zang et al. 2014). However, it is crucial to limit the maximum magnitude to the perceptible threshold (usually around magnitude 2) and to implement a traffic light system to ensure compliance (Mignan et al. 2017). Simplified physical models suggest that the risk of strong seismic events increases with rising injection pressure. In reality, the relationship between the maximum size and the injection pressure is more complex (Evans et al. 2012). The size of induced earthquakes depends also considerably on the natural seismicity level, the stress conditions and the local structural setting. Accordingly, seismic hazard assessments should be a key component of the exploration phase. Furthermore, the cyclic or soft treatment of the reservoir seems to reduce the risk of strong induced earthquakes

(Zang et al. 2013; Hofmann et al. 2021), but there is still a considerable need for more adequate stimulation techniques.

1.3. Aim and Scope of the Thesis

This cumulative thesis was prepared as part of the Interreg project DGE-Rollout, aiming to promote deep geothermal energy as a climate and environmentally friendly energy source in northwestern Europe. The Technical University of Darmstadt has undertaken the mapping of geothermal resources in the northern URG, defined here as the region north of Karlsruhe. The northern URG was only partially addressed by the previous geothermal research projects GeORG and Hessen 3D (Sass et al. 2011; GeORG Projektteam 2013; Bär et al. 2021). As a result, there are significant inconsistencies in the overlapping areas of the models that require harmonization. This thesis focuses specifically on the crystalline basement, which hosts the largest geothermal resources but has been greatly simplified in the existing geological models. Despite the enormous potential, little is known so far about the thermal, structural, lithologic, petrophysical, and hydraulic properties of the reservoirs below the thick sedimentary cover. Accordingly, available assessments (e.g., Paschen et al. 2003) provide merely rough estimates of the usable resources in the basement.

The main objective of the work was to develop an integrated 3D geothermal model and to comprehensively characterize the lithology, petrophysics, and structure of the basement at multiple scales. On that basis, the EGS potential for power and heat generation in the northern URG was quantified. The results allow for selection of favorable drilling targets and improved well path planning, reducing the previously described risks of EGS projects, such as insufficient productivity and perceptible induced seismicity during development and operation. By additionally assessing societal aspects of geothermal utilization, both policy makers and investors are provided with a reliable basis for decision-making. The results are moreover valuable for technical planners, who can use them in the early project phase as input for detailed modelling and the design of targeted exploration measures. At the same time, part of the research serves as pre-exploration to find suitable sites for the upcoming GeoLaB project in the Odenwald.

More specifically, the following tasks are covered in the thesis:

- Comprehensive review of approximately 500 relevant literature sources to identify and characterize potentially usable geothermal reservoir horizons in the URG (chapter 2)
- Development of a parameterized 3D basement model of the northern URG by integrating all available geological and geophysical data (chapter 3)
- Techno-Economic resource assessment for the crystalline basement to identify preferred targets for geothermal drilling (chapter 4)
- Structural and hydraulic characterization of the basement by outcrop analog studies in the southern Odenwald (chapter 5)
- Complementation of the structural investigations by geophysical (terrestrial gravimetry, aeromagnetics, radon) surveys to identify potentially permeable fault zones (chapters 5 and 6)

2. Assessment of Deep Geothermal Research and Development in the Upper Rhine Graben

This chapter includes the peer-reviewed review article with same title that was published in the journal Geothermal Energy (Springer Nature) on the 29 September 2022. The content is unchanged.

A comprehensive literature review of the deep geothermal situation in the Upper Rhine Graben is presented and the results of nearly a century of geological research in this region are summarized. Nine potential geothermal reservoir horizons were identified and described in detail with respect to their lithological, structural, thermal, hydraulic, hydrochemical, petrophysical, and seismic properties. In addition, all previously implemented deep geothermal projects in the URG are reviewed followed by a discussion of learned lessons. Finally, an overview of all freely available geological 3D models of the Upper Rhine Graben is given. The review paper thus lays the foundation of all research activities in DGE-ROLLOUT and following comparable projects.

Reference:

Frey, M., Weinert, S., Bär, K., van der Vaart, J., Dezayes, C., Calcagno, P., & Sass, I. (2021). Assessment of deep geothermal research and development in the Upper Rhine Graben. Geothermal Energy, 10(18). https://doi.org/10.1186/s40517-022-00226-2.

Frey *et al. Geothermal Energy* (2022) 10:18
https://doi.org/10.1186/s40517-022-00226-2

Geothermal Energy

REVIEW Open Access

Assessment of deep geothermal research and development in the Upper Rhine Graben

Matthis Frey[1*], Kristian Bär[2], Ingrid Stober[3], John Reinecker[2], Jeroen van der Vaart[1] and Ingo Sass[1,4]

*Correspondence:
frey@geo.tu-darmstadt.de

[1] Institute of Applied Geosciences, Department of Geothermal Science and Technology, Technical University of Darmstadt, Schnittspahnstraße 9, 64287 Darmstadt, Germany
[2] GeoThermal Engineering GmbH, An Der Raumfabrik 33C, 76227 Karlsruhe, Germany
[3] Institute of Earth and Environmental Sciences, University of Freiburg, Albertstr. 23b, D-79104 Freiburg, Germany
[4] GFZ German Research Centre for Geosciences, Section 4.8: Geoenergy, Telegrafenberg, 14473 Potsdam, Germany

Abstract

Deep geothermal energy represents a key element of future renewable energy production due to its base load capability and the almost inexhaustible resource base. Especially with regard to heat supply, this technology offers a huge potential for carbon saving. One of the main targets of geothermal projects in Central Europe is the Upper Rhine Graben, which exhibits elevated subsurface temperatures and reservoirs with favorable hydraulic properties. Several decades of intensive research in the region resulted in a comprehensive understanding of the geological situation. This review study summarizes the findings relevant to deep geothermal projects and thus provides a useful working and decision-making basis for stakeholders. A total of nine geological units have been identified that are suitable for deep geothermal exploitation, comprising the crystalline basement, various sandstone formations and Mesozoic carbonates. An extensive lithostratigraphic, structural, geochemical, hydraulic and petrophysical characterization is given for each of these potential reservoirs. This paper furthermore provides an overview of the available data and geological as well as temperature models.

Keywords: Upper Rhine Graben, Geothermal energy, Renewable energies, Reservoir characterization, Open data

Introduction

The Upper Rhine Graben (URG) is a major target for deep geothermal exploration in Central Europe due to the highly elevated geothermal gradient of locally more than 100 K/km (e.g., Soultz-sous-Forêts) (Schellschmidt and Clauser 1996; Pribnow and Schellschmidt 2000; Agemar et al. 2012; Baillieux et al. 2013) and the abundance of large fault zone providing potential fluid pathways (Bächler et al. 2003; Guillou-Frottier et al. 2013; Duwiquet et al. 2021). According to Kock and Kaltschmitt (2012), the technical potential for deep geothermal utilization in the URG sums up to 186 TWh/a, which is approximately 5% of the annual primary energy demand of Germany (AG Energiebilanzen 2021). A number of suitable reservoir horizons have been identified and characterized in the course of numerous research projects over the last decades and the hydro- as well as petrothermal potentials have been determined in local or regional studies (Commission of the European Communities 1979; Hurter and Schellschmidt

2003; Kohl et al. 2005; Agemar et al. 2022; Sass et al. 2011; Arndt 2012; GeORG Projektteam 2013; Stober and Bucher 2015; Bär et al. 2016; Aretz et al. 2016).

Exploration in the URG started with the first discoveries of oil-bearing sandstones at Merkwiller-Pechelbronn (Böcker 2015; Reinhold et al. 2016). In the twentieth century, large-scale hydrocarbon exploration was conducted, reaching its peak between the 1950s and 1980s. By 1989, more than 440 exploration wells and 550 production wells had been drilled and a dense network of 2D reflection seismic profiles with a total length of more than 5000 km had been shot (Durst 1991; Jodocy and Stober 2008). This extensive data basis allows detailed investigations on the structural setting, lithological properties, stratigraphy as well as petrophysical, chemical and thermal properties of the Cenozoic horizons. Conventional exploration data (seismic and well data) resolving the Mesozoic, Permo-Carboniferous and crystalline basement structures, on the other hand, remained sparse, resulting in high model uncertainties with respect to these horizons (Frey et al. 2021b).

The exploration for deep geothermal resources in the URG came into focus during the energy crisis in the 1970s. First geothermal wells drilled are Bühl 1 (1979), Cronenbourg GCR-1 (1980) and Bruchsal GB-BR1 and GB-BR2 (1983/84) with more or less success (Bertleff et al. 1988; Pauwels et al. 1993; Meixner et al. 2014). In the late 1980s, the European EGS (Enhanced Geothermal Systems) project was launched in Soultz-sous-Forêts (France, central URG) with the aim of extracting heat from fractured granitic rock as a new power source (Gérard and Kappelmeyer 1987; Dezayes et al. 2005a). Between 1987 and 2004, a total of 5 research wells (GPK1-4 and EPS1) with a maximum depth of partly more than 5000 m were drilled to obtain a comprehensive understanding of the hydrothermal circulation in deep geothermal reservoirs (Dezayes et al. 2005b; Genter et al. 2010). Several hydraulic, chemical stimulations and long-term circulation tests were carried out to increase and monitor the permeability of the fracture network between the wells (Evans et al. 2005; Portier et al. 2009; Schill et al. 2017). To date, Soultz is still one of the most important model sites for EGS systems worldwide and provides an extremely valuable reference for the design of such projects (Genter et al. 2010). After the Renewable Energy Sources Act came into force in 2000, the development of the geothermal sector was further accelerated, leading to the realization of several additional projects in the last two decades (Baumgärtner et al. 2013; Baujard et al. 2017; Reinecker et al. 2019). At present, there are six active deep geothermal heat and/or power plants in the URG. Additionally, thermal waters for balneological purposes are extracted at numerous locations, especially along the main border faults, but as well in the graben center (e.g., Baden-Baden, Bad Krozingen, Bad Bellingen, Freiburg, Weinheim). Nevertheless, the technical potential is currently exploited only to a very small extent (Paschen et al. 2003; Kock and Kaltschmitt 2012), which can be attributed to various reasons. The complex geology and tectonic activity pose considerable risks during the drilling operation and reservoir development. But difficulties with the legal framework (e.g., mining law) or lack of public acceptance represent also serious problems.

In this review, a detailed geological description of the main horizons and tectonic structures suitable for deep geothermal exploitation in the URG region is presented. They have been identified based on the expected reservoir temperature and the hydraulic permeability of the formation or fault zone. In addition, this study summarized all

available data regarding the relevant hydrogeological, hydraulic, hydrochemical and petrophysical properties of each reservoir unit. Subsequently, a review of the structural setting, the stress field, natural seismicity, available temperature data, the geothermal projects and the existing 3D models in the URG is provided herein. This article is intended to serve as a comprehensive information basis and decision support. However, for each site additional specific exploration measures may be required, as the geological conditions in the URG are due to its complex tectonic setting laterally highly variable. Additionally, the conditions at surface and societal challenges (e.g., infrastructure, public acceptance) play a key role and may pose significant risks to the projects, but are only briefly discussed here.

Geological setting

The URG is the central part of the European Cenozoic Rift System (ECRIS), which consists of several interlinked tectonic rifts, extending from the Mediterranean to the North Sea (Fig. 1) (Illies and Fuchs 1974; Prodehl et al. 1992, 1995; Ziegler 1992, 1994; Ziegler and Dèzes 2005; Dèzes et al. 2004; McCann 2008). The main strike direction of the approximately 300 km long and 30 to 40 km wide URG is NNE–SSW in the southern and central part and roughly N–S in the northern part. The structure is bounded to the north by the Rhenish Massif, the Hesse Depression and the Vogelsberg, to the south by the Swiss Jura Mountains and at the graben shoulders by the Black Forest, the Vosges, the Odenwald and the Palatinate. Well-founded concepts about the paleogeographic

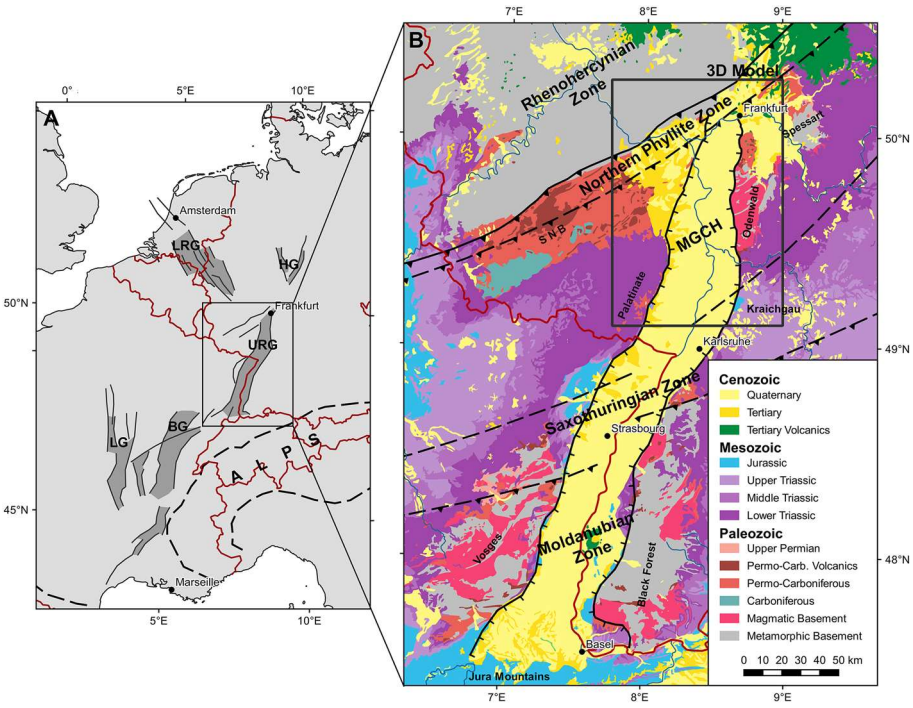

Fig. 1 **A** Simplified map of the European Cenozoic Rift System (adapted from Ziegler and Dèzes 2005), dark grey areas represent rift-related sediment basins. *BG* Bresse Graben, *HG* Hessian grabens, *LG* Limagne Graben, *LRG* Lower Rhine Graben, *MGCH* Mid-German Crystalline High, *SNB* Saar-Nahe Basin, *URG* Upper Rhine Graben. **B** Geological map of the URG including the main stratigraphic units (adapted from BGR 2016)

and tectonic development as well as the lithology, structure, facies, stratigraphy, diagenesis and metamorphism of the individual horizons were established inter alia by Andres and Schad (1959), Straub (1962), Sauer (1962), Rothe and Sauer (1967), Illies and Mueller (1970), Villemin et al. (1986), Villemin and Coletta (1990), Sissingh (1998), Michon and Merle (2000), Gaupp and Nickel (2001), Behrmann et al. (2003), Behrmann et al. (2005), Reinhold et al. (2016) and Perner (2018). In the following, an overview about the Phanerozoic evolution of the URG region is given. A summary of the lithostratigraphic sequence in the URG is shown in Fig. 2.

Variscan orogeny

The basement in the URG region represents primarily the structure of the Variscan fold belt that was first defined by Suess (1926) and Kossmat (1927). Comprehensive descriptions and discussions of the Variscan Orogeny are, for example, given in Behr et al. (1984), Franke (1989), Dallmeyer et al. (1995), Oncken (1997), Franke (2000), Matte (2003), Kroner et al. (2008) and Zeh and Gerdes (2010).

Prior to the continental collision between the Silurian and Lower Devonian, the vast Rheic Ocean, located to the south of Laurussia, was subducted northwards (Nance et al. 2010). This led to a drift of the Armorican Terrane Assemblage, consisting of several microplates including Franconia, Saxothuringia and Moldanubia, towards Laurussia (Crowley et al. 2000). These terranes disintegrated from the northern margin of Gondwana during the Cambrian and Ordovician (Kemnitz et al. 2002) and typically consist of Neoproterozoic crust, overlain by a Neoproterozoic to Lower Carboniferous passive margin sequence and intruded by subduction-related magmatic complexes.

Back-arc extension resulted in the opening of the Rhenohercynian Basin during the Lower Devonian (Fig. 3) (Stets and Schäfer 2011; Franke et al. 2017). At first, mainly siliciclastic and carbonate shelf sediments were deposited, but with increasing extension during the middle Devonian also oceanic crust was formed in the deeper parts of the basin (Franke 1995b; Belka and Narkiewicz 2008). According to Zeh and Gerdes (2010), the subduction direction of the Rheic Ocean changed to the south in the Upper Devonian resulting in a new magmatic arc, known as the Mid-German Crystalline High (MGCH) (Reischmann and Anthes 1996; Anthes and Reischmann 2001). The prior island arc between the Rheic Ocean and the Rhenohercynian Basin was then partially underplated beneath the MGCH (Oncken 1997; Oncken et al. 1999). Further to the south, the Saxothuringian Basin was subducted underneath Moldanubia, which resulted in widespread magmatic activity, e.g., indicated by granitic intrusions in the Black Forest and Vosges (Okrusch et al. 1995; Skrzypek et al. 2014).

The final closure of the oceanic basins took place in the Lower Carboniferous and was followed by the collision of Laurussia with the Armorican Terrane Assemblage and Gondwana in Visean and Namurian times (Eckelmann et al. 2014). As a result, the individual microplates were juxtaposed and the sedimentary sequences of the marine basins and continental margins were partly thrust onto the crystalline basement (Behr and Heinrichs 1987; Hegner et al. 2001; Kroner et al. 2008; McCann et al. 2008). The degree of metamorphism varies significantly across the fold belt (Oncken et al. 1995; Okrusch 1995). While the Rhenohercynian Zone and Saxothuringian Basin show only a low-grade overprint, the MGCH shows typical medium- to high-grade regional

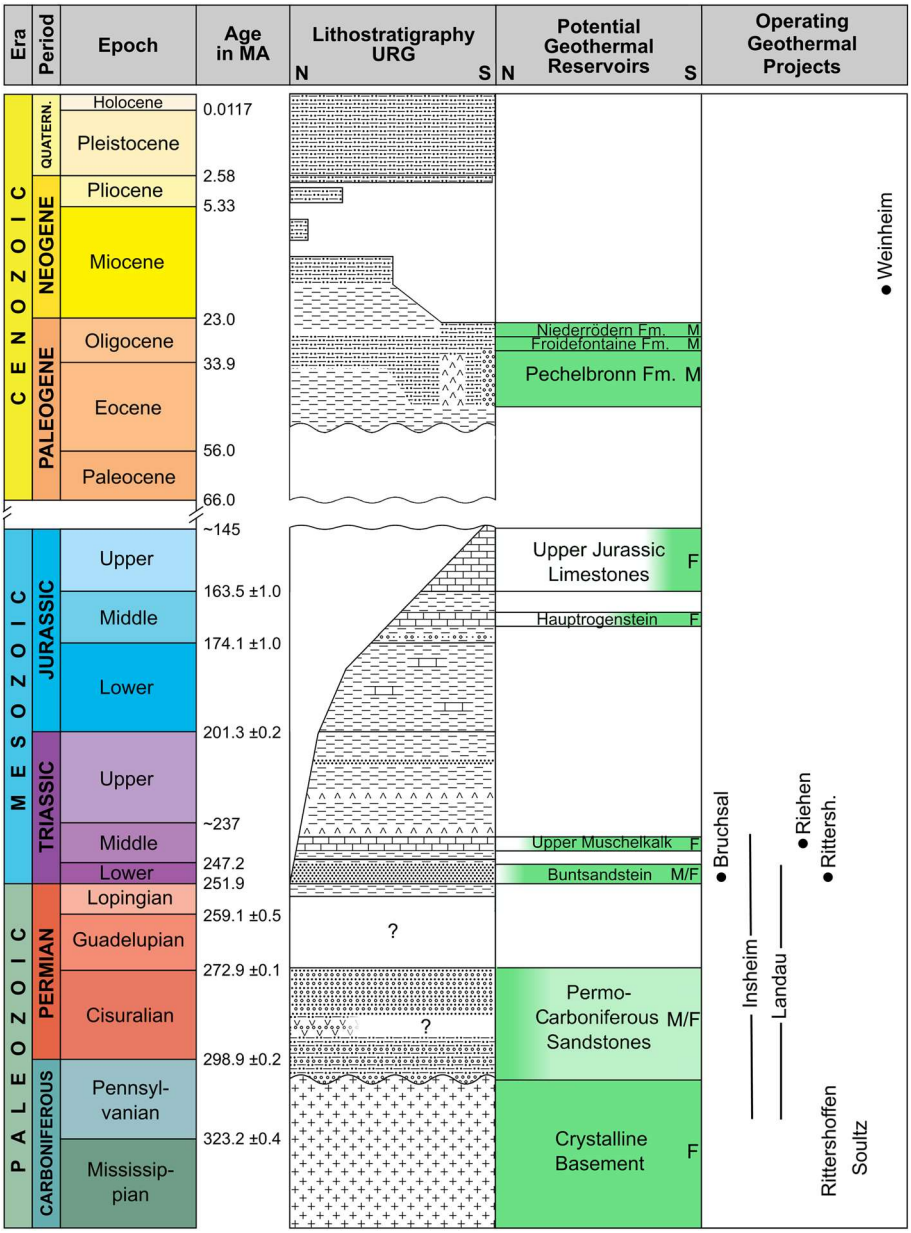

Fig. 2 Lithostratigraphic sequence in the Upper Rhine Graben with the potential geothermal reservoir units (modified after GeORG Projektteam (2013) and Deutsche Stratigraphische Kommission (2016)). It is indicated whether the fluid flow in the reservoir horizon is dominated by fractures (F) or matrix (M). For a detailed visualization of the Tertiary succession, see also Fig. 9. The regional importance of each horizon is indicated by the color gradient

metamorphic conditions. In contrast, the metamorphism was temperature-dominated in the Moldanubian Zone, indicated by partial melting.

Permo-Carboniferous and Mesozoic sediment basins

At the end of the Variscan Orogeny in the Upper Carboniferous, a rapid collapse of the orogen occurred and several NE–SW striking intramontane molasse basins (Figs. 3 and 4a), such as the Saar-Nahe Basin, the Hessian Depression, the Vosges-Kraichgau Basin

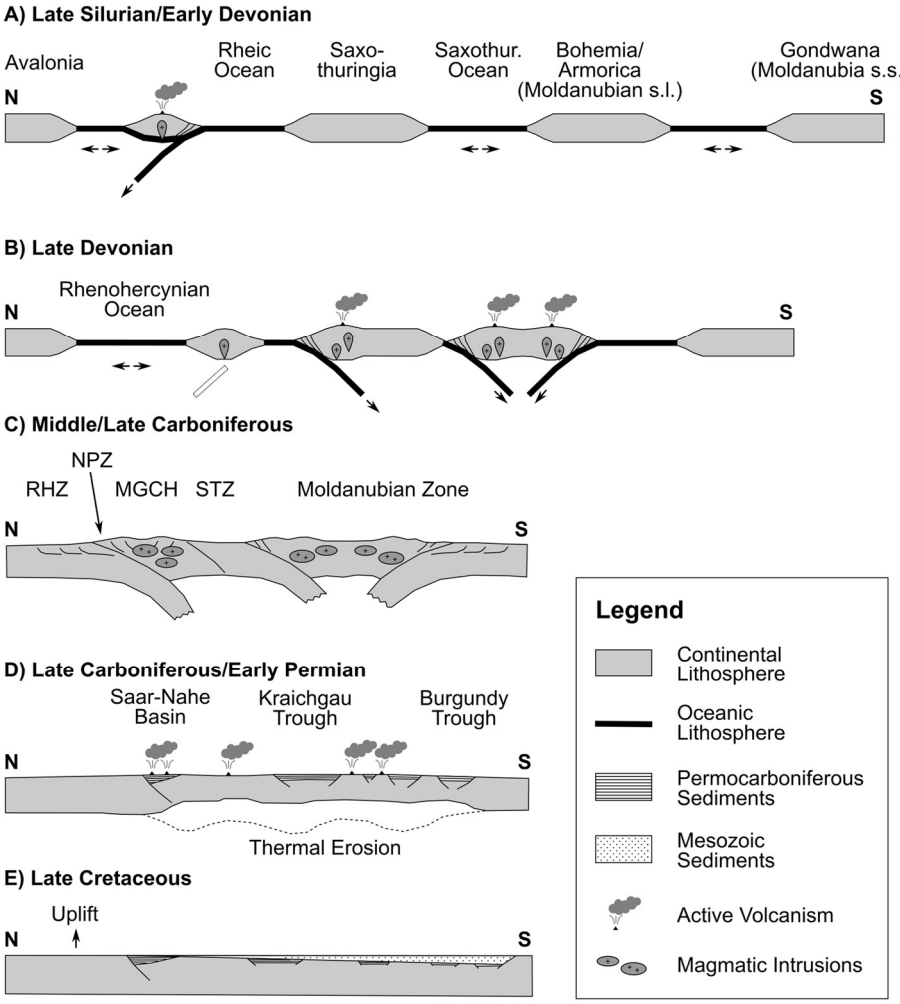

Fig. 3 Plate tectonic evolution of the lithosphere in the Upper Rhine Graben region from the Upper Silurian until Upper Carboniferous (adapted from Franke (2000) and Zeh and Gerdes (2010)). *MGCH* Mid-German Crystalline High, *NPZ* Northern Phyllite Zone, *RHZ* Rhenohercynian Zone, *STZ* Saxothuringian Zone

and the Burgundy Basin, formed along pre-existing Variscan fault zones (Henk 1993; Weber 1995b; Stollhofen 1998; Schumacher 2002; Schäfer 2011). The erosion of the surrounding mountain ranges produced large quantities of clastic sediments that were deposited in these isolated basins, reaching a maximum thickness of up to 10 km in the Saar-Nahe Basin (Henk 1992). The Permo-Carboniferous succession is in the lower part dominated by fluvial–lacustrine conglomerates, sandstones and claystones. Later, the sedimentation was increasingly controlled by aeolian transport, indicating an arid environment (Schäfer 1989; Schäfer and Korsch 1998; Stollhofen 1998; Aretz et al. 2016). Furthermore, rifting in the Lower Permian was accompanied by widespread mantle-driven volcanic activity mostly between 300 and 290 Ma, which shows a mafic to felsic composition (von Seckendorff et al. 2004; von Seckendorff 2012). In the Upper Permian (Fig. 4b), no evaporite cycles were deposited in the URG area, but the Zechstein is characterized by marginal facies deposits with a high proportion of fine-clastic sediments (Hug and Vero 2008).

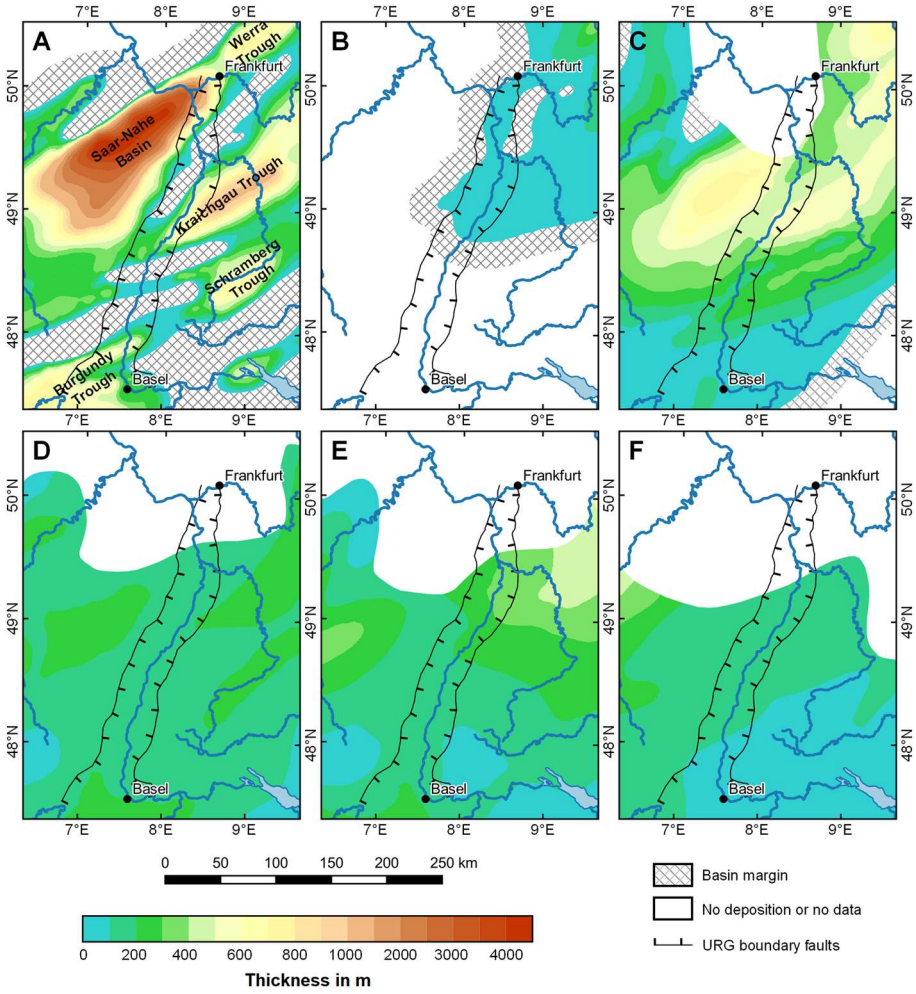

Fig. 4 Paleogeographic situation in the URG region (modified after Boigk and Schöneich 1974). Reconstructed sediment thickness after deposition for **A** the Permo-Carboniferous, **B** the Upper Permian (Zechstein), **C** the Lower Triassic (Buntsandstein), **D** the Middle Triassic (Muschelkalk), **E** the Upper Triassic (Keuper) and **F** the Lower Jurassic (Lias)

The subsequent Triassic is divided into the three independent lithostratigraphic groups Buntsandstein, Muschelkalk and Keuper in the Germanic Basin (Boigk and Schöneich 1974; Schröder 1982; Aigner and Bachmann 1992; Feist-Burkhardt et al. 2008). After the regression of the Zechstein Sea at the end of the Permian, continental facies were again predominantly deposited (Scholze et al. 2017). In comparison to the Permo-Carboniferous, sedimentation of the Buntsandstein (Fig. 4c) was no longer limited to the isolated Variscan sub-basins (Backhaus 1974; Feist-Burkhardt et al. 2008; Lepper et al. 2014), but the highest thickness was still reached in the Saar-Nahe Basin and the Kraichgau Depression (Boigk and Schöneich 1974).

During the Middle Triassic a wide-ranging transgression occurred (Fig. 4d), leading to the development of the Germanic Basin into a marginal sea of the Tethys Ocean (Szulc 2000; Götz and Gast 2010; McKie 2017). Deep and shallow marine areas were spatially separated by the Variscan orogen, with seaways existing along tectonic depressions. The intramontane basins and especially the Burgundy Trough still represented major

depocenters during this time, but sedimentation occurred on a broad scale in the whole Germanic Basin (Boigk and Schöneich 1974). During the deposition of the Muschelkalk, several transgression and regression cycles took place, which are documented as alternating deposits of evaporites including halite, shallow-marine carbonates and deep-water carbonates (Schwarz 1975; Hagdorn 1999; Götz 2004). The Keuper sequence (Fig. 4e) shows an alternation of clastic sediments with evaporites, indicating a frequent change between continental and shallow marine conditions (Vecsei and Duringer 2003; Barnasch 2010; Franz et al. 2018). Similarly, cycles of arid and humid climate conditions are documented in the succession. Large delta regions are typical for this period, which have a predominant sediment transport in southwestern directions.

In the Lower Jurassic (Fig. 4f), southern Germany became part of the epicontinental shelf by a renewed transgression of the Peri-Tethys (Pienkowski et al. 2008; Barth et al. 2018). Under these conditions, mainly black shales and clays were deposited. In the Middle Jurassic, an alternating deposition of sandstone, clays and especially oolithic limestones is recorded in the URG. Deposits from the Upper Jurassic are preserved in the URG only up to the Oxfordian. During the Cretaceous, large uplift movements occurred along the Rhenish Massif, which led to considerable erosion of the Mesozoic and partly the Paleozoic sediments in the northern URG (Pflug 1982). For this reason, the stratigraphic horizons below the Tertiary sediments become steadily older from south to north.

Cenozoic graben formation

The URG formed as a result of the changing lithospheric stress field in the foreland of the Alpine Orogeny and can therefore be classified as a passive rift. It is likely that pre-existing NNE–SSW striking Variscan, Permo-Carboniferous and Mesozoic discontinuities, shear or fault zones, were reactivated (Edel et al. 2007; Grimmer et al. 2017). The plate tectonic relationships and the deformation of the Alpine foreland on a lithosphere scale are presented, e.g., in Ziegler et al. (1995), Sissingh (1998), Dèzes et al. (2004), Cloetingh et al. (2005) and Ziegler and Dèzes (2005).

The Cenozoic changes in the Central European stress regime led to an extension of the lithosphere parallel to the orogenic belt and to an uplift of the mantle in the URG region. During the development of the URG, the regional stress field was repeatedly redirected (Buchner 1981; Schumacher 2002; Behrmann et al. 2003; Dèzes et al. 2004) (Fig. 5), resulting in reactivation of faults and changes of the fault movement direction. This led to variable subsidence and uplift rates and to local displacements of the deposition centers. Two main phases of graben development are generally distinguished (Illies 1978; Hüttner 1991; Schwarz 2006), an initial mostly extensional phase from Eocene to Lower Miocene and a later transtensional to transpressional phase from Miocene to Quaternary. A detailed paleogeographic reconstruction of the URG from Eocene to Pliocene is given in Berger et al. (2005).

The formation of the URG was initiated by an acceleration of the northward directed compressional movement of the Alpine Orogen that resulted in an E–W oriented crustal extension of the foreland in the Middle to Upper Eocene (Villemin et al. 1986; Ziegler et al. 1995; Dèzes et al. 2004). During this period, lacustrine clays and siltstones were deposited in locally confined basins, accompanied by a period of

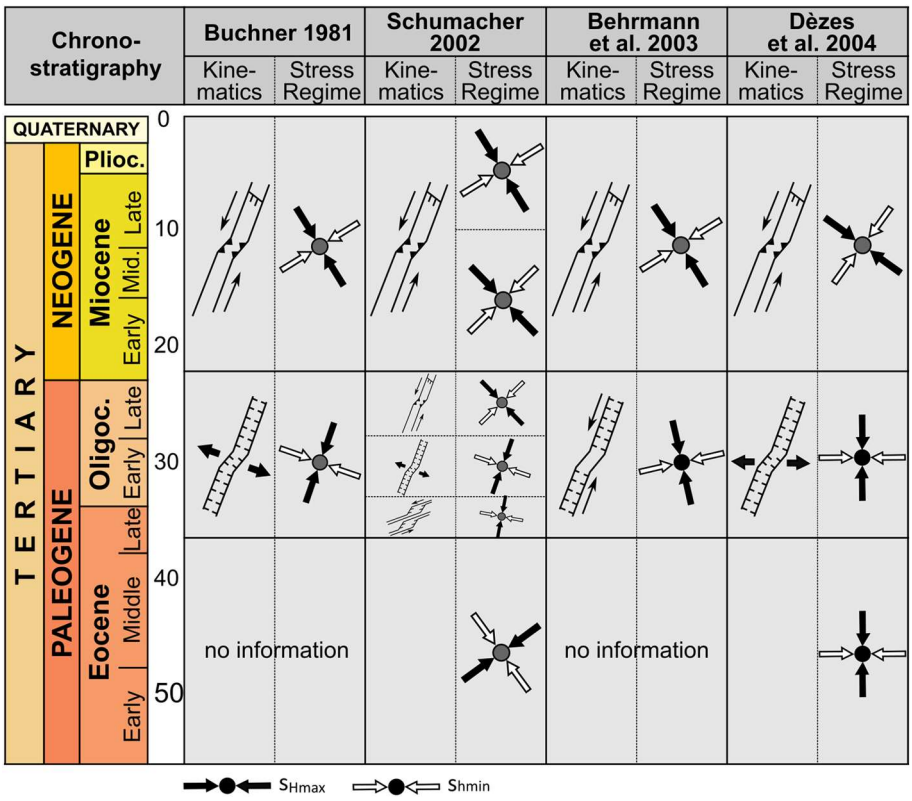

Fig. 5 Different models of the Cenozoic evolution of the URG (compiled by Schwarz et al. 2006)

increased volcanic activity at the graben shoulders (Lippolt et al. 1974; Illies 1977). By the Upper Eocene (Priabonium), two depositional centers had formed in the southern URG, the Mulhouse and Strasbourg Basins, whose extent reflected the location of the Permo-Carboniferous molasse basins of the Variscan Orogen (Pflug 1982).

In the Lower Oligocene (Rupelian), the strongest rifting phase occurred, which covered the entire graben and led to the deposition of the thick Pechelbronn and Froidefontaine Formations (Gaupp and Nickel 2001; Derer et al. 2003; Grimm 2005). For this period, a main direction of the deformation between WSW–ENE and WNW–ESE was determined (Fig. 5). With increasing subsidence, two and locally three marine transgressions with connections to the North German Basin and the South German Molasse Basin took place (Meier and Eisbacher 1991; Berger et al. 2005; Rousse et al. 2012). During the Upper Oligocene (Chattian), the extension came to a halt in the southern URG, and the depositional center was successively shifted northwards (Illies and Fuchs 1974).

The further development of the URG is influenced by an anti-clockwise rotation of S_{Hmax} that resulted in a reactivation of the faults in a sinistral strike–slip sense, with S_{hmin} oriented in SW–NE direction (Buchmann and Connolly 2007). This was caused by an abrupt decrease in the convergence between Europe and Africa during the Lower Miocene (Rosenbaum et al. 2002). The southern URG was affected by strong uplift, which is documented by a pronounced erosional unconformity and a hiatus from the Lower Miocene to Pliocene. Between 18 and 15 Ma, volcanic activity

reached its peak at the Kaiserstuhl (Wagner 1976). Conversely, the northern URG was characterized by high subsidence rates, which led to continuous sedimentation until the Quaternary.

Structural geology, recent stress field and seismicity

Structural geology

The complex and multiphase Cenozoic graben evolution resulted in a cross-sectional asymmetry with either the Eastern Main Boundary Fault (EMBF) or the Western Main Boundary Fault (WMBF) being more prominent. Graben formation-related subsidence shifted gradually from south to north (Illies 1978; Derer et al. 2005; Grimm 2005; Hinsken et al. 2007) resulting also in an asymmetry along strike of the graben structure (Fig. 6). Oblique normal faulting dominates the structural inventory within the Tertiary sedimentary infill of the URG, directly linked to the graben evolution. The graben main border faults as well as major faults parallel to the graben strike have a considerable share of sinistral strike–slip component not directly visible in seismic sections. 3D seismics are needed to restore and interpret the detailed structural inventory and fault kinetics on regional to local scale (e.g., Reinhold et al. 2016).

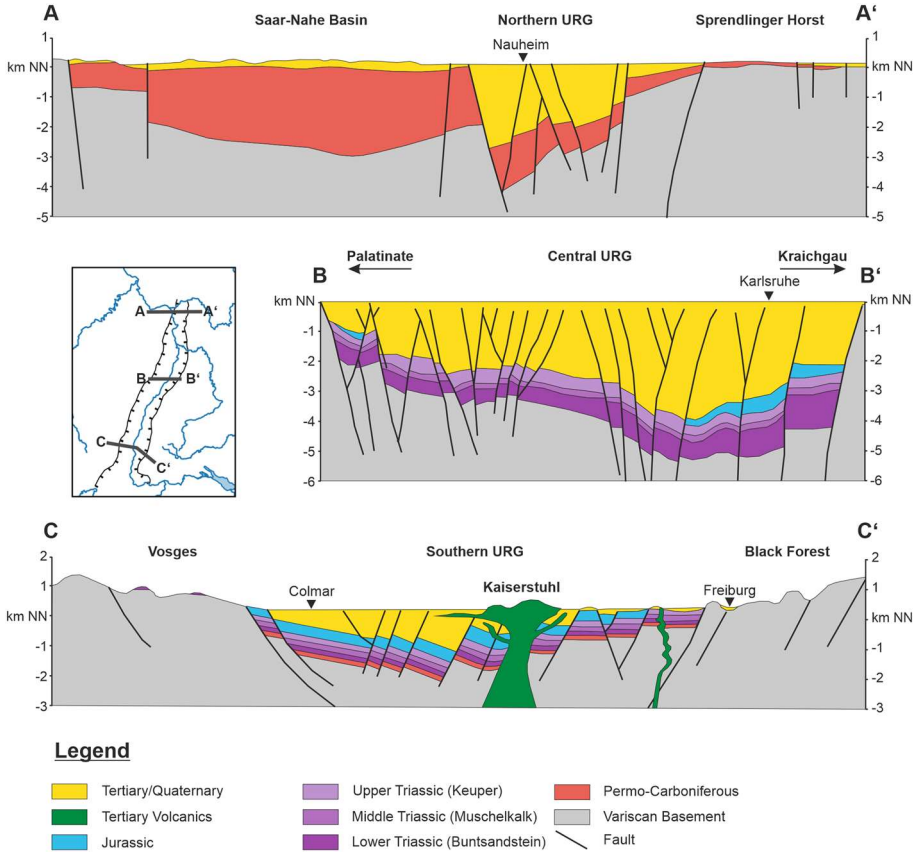

Fig. 6 Three geological cross sections through the northern (AA'), central (BB') and southern URG (CC') (modified after Arndt 2012; GeORG Projektteam 2013; LGRB 2022)

Prior to the URG development, the Variscan basement as well as the Permo-Mesozoic sedimentary cover have been faulted by NW–SE and NNE–SSW striking faults (e.g., Grimmer et al. 2017) of which some have been reactivated during Tertiary evolution. Mapping of faults within the Variscan crystalline basement using 2D or 3D seismics is often not possible with confidence as seismic reflectors are missing. Instead faults clearly visible in Permo-Mesozoic successions may be traced down into the crystalline basement wherever possible. However, faults within the crystalline basement and the overlaying Permo-Mesozoic succession form the main targets for deep geothermal exploration. All major projects in the URG so far target larger scale fault structures in this succession (Dezayes et al. 2005a; Teza et al. 2008; Baumgärtner et al. 2013; Duringer et al. 2019).

Fault zones with a vertical displacement of several 100 m to over 1000 m can promote or inhibit fluid transport through the rock depending on their internal structure, activity and orientation in the regional stress field (Barton et al. 1995; Caine et al. 1996; Evans et al. 1997; Gudmundsson et al. 2001; Meixner et al. 2014). The fault core, consisting mostly of fault gouges, fault breccias, clay smear and mineralizations, represents a potential barrier to fluid transport in inactive fault zones (Morrow et al. 1984). In active fault zones, however, flow paths can be formed or kept open in this unit by constantly re-breaking fractures, i.e., by earthquakes, that have been cemented in the meantime by upwelling thermal waters, thus increasing permeability (Stober and Bucher 2015; Agemar et al. 2017; Guillou-Frottier et al. 2020). Increased permeability is to be expected in the highly fractured damage zones (Caine et al. 1996; Faulkner et al. 2010) adjacent to both sides of the fault core. Permeability here is mainly dependent on fracture density, mean fracture lengths, degree of cross-linking of fractures and the mean fracture (fault) orientation within the respective local stress field (Jafari and Babadagli 2011). Fractures mechanically tend to be open when perpendicular to σ3 (mode I: opening, dilation) or with a high ratio of shear stress in the fracture plane to normal stress acting on the fracture plane. With the analytical modeling of slip (T_s) and dilation tendency (T_d) of fault zones, the spatial distribution of potentially 'open' or hydraulically conducting areas can be visualized (Morris et al. 1996; Ferrill and Morris 2003). However, due to mineralization along fractures and the complex geometry of the fault zone, the permeability structure within and along the fault zone is in detail more complex and may vary significantly laterally and with depth as well as between different geological units (Sausse and Genter 2005; Ledésert et al. 2010; Dezayes et al. 2010; Meller and Ledésert 2017). Open conduits may localize hydraulic flow along fractures and where fractures (or faults) are intersecting.

Present-day stress field

Knowledge on in situ stress is important to understand subsurface fluid flow controlled by fracture systems and to prevent wellbore stability problems. Information on the in situ stress state in the URG are mainly derived from earthquake focal mechanisms (FMS) and borehole data such as borehole breakouts (BO), drilling induced tensile fractures (DITF) and leak-off tests (LOT) (see Heidbach et al. (2016) for a detailed description on stress indicators and Reiter et al. (2016) for a detailed description of the WSM database in Germany and adjacent areas). Furthermore, an overview of the orientation

and magnitudes of the regional stress field is provided by the 3D numerical modeling of Ahlers et al. (2021).

Published stress studies at Soultz (Rummel and Baumgärtner 1991; Cuenot et al. 2006; Cornet et al. 2007; Dorbath et al. 2010), Bruchsal (Meixner et al. 2014), Rittershoffen (Azzola et al. 2019) and Basel (Valley and Evans 2009, 2019) have analyzed BO and DITF occurrence in detail and have proposed vertical stress profiles incorporating density logs for calculating vertical stress (i.e., overburden) as well as LOT and formation integrity tests (FIT) for minimum horizontal stress (S_h) magnitude estimation. Magnitude of maximum horizontal stress (S_H) has been estimated using the hypothesis of a frictional limit of optimally oriented faults (Zoback et al. 2003). Formation pressures are found to be hydrostatic with static water table close to ground surface.

The stress regime in the URG is derived by regional FMS studies (Ahorner 1983; Bonjer et al. 1984; Plenefisch and Bonjer 1997; Cuenot et al. 2006; Ritter et al. 2009; Homuth et al. 2014) and varies between strike–slip and normal faulting. Indications for thrust faulting are sparse and most probably reflect local inversion tectonics (e.g., Illies and Greiner 1979). Figure 7 displays the orientation of S_H as documented in the WSM database and recently published studies. In addition, unpublished stress reports from drilling projects throughout the URG reveal essentially the same, roughly N–S to NW–SE oriented S_H orientation. Local perturbations of the stress field result mainly from mechanically weak and active fault zones including URG border faults. Valley (2007), for example, reported a strong localized rotation of the maximum horizontal stress component linked to the occurrence of a large-scale permeable fault at Soultz-sous-Forêts. Perturbation may be significant over short distances and should be kept in mind when defining potential target zones and planning drilling projects.

Natural seismicity

Seismicity, whether natural or induced, poses a significant risk to deep geothermal projects. For this reason, a detailed study of historic events is essential to assess the seismic hazard. A detailed discussion of the induced seismicity related to geothermal projects is given in chapter 7. The tectonically active URG is marked by increased seismicity compared to adjacent regions in Central Europe (e.g., Grünthal et al. 2018), but in contrast to other continental rift valley systems, such as the East African Rift, events in access of magnitude of 3 are rare. In the European seismic hazard map of Giardini et al. (2014), the hazard to the URG is indicated as moderate with a 10% probability of exceeding a peak ground acceleration of 0.2 g in a 50-year interval.

The strongest historically documented event is the 1356 Basel earthquake with an estimated local magnitude of 6.7 to 7.1 (Fäh et al. 2009) which caused severe destruction to the city. Meghraoui et al. (2001) determined a mean recurrence interval of 1500 to 2500 years for seismic events of this size. The strongest recent earthquake with a local magnitude of about 5.4 occurred in Waldkirch near Freiburg in 2005 (Schwarz et al. 2006), but no damages were caused. The largest documented event in the northern URG was recorded in Worms in February 1952 and had a local magnitude of 4.7 (Leydecker 2011). This earthquake marks the onset of a seismic sequence that shows a southward migration of the hypocenters. In September and October 1952, two events

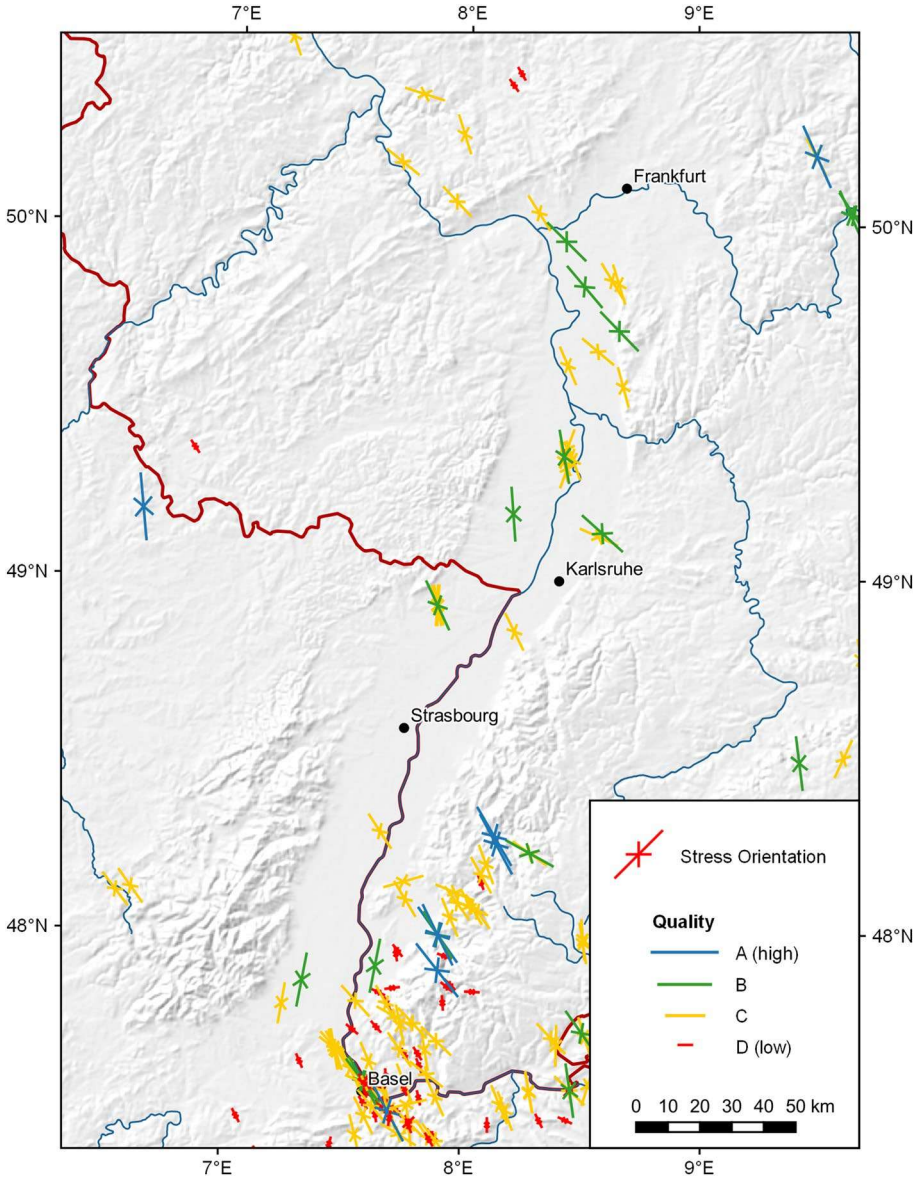

Fig. 7 Stress orientation map of the URG region (adapted from Reiter et al. 2016). The quality of stress measurements is indicated by the length of the symbol

of comparable magnitude followed between Landau and Wissenbourg and Wissenbourg and Haguenau, respectively (Doubre et al. 2021).

The URG exhibits significant lateral variations in the number and size of seismic events (Fig. 8) (Bonjer et al. 1984; Bonjer 1997; Homuth et al. 2014; Henrion et al. 2020). The largest cluster of epicenters is located south of Strasbourg, which according to Barth et al. (2015) can be explained by an increase of tectonic stresses related to convergence in the Alpine Orogen and the steep topography in this area. The central URG section between the Palatinate and Kraichgau is a seismically quiet zone, whereas seismicity increases again to the north. Barth et al. (2015) identified four sections of varying b-values (ranging from 0.83 to 1.42) in the URG. These differences can most likely be attributed to the local segmentation of the fault systems. In areas with relatively small-scale

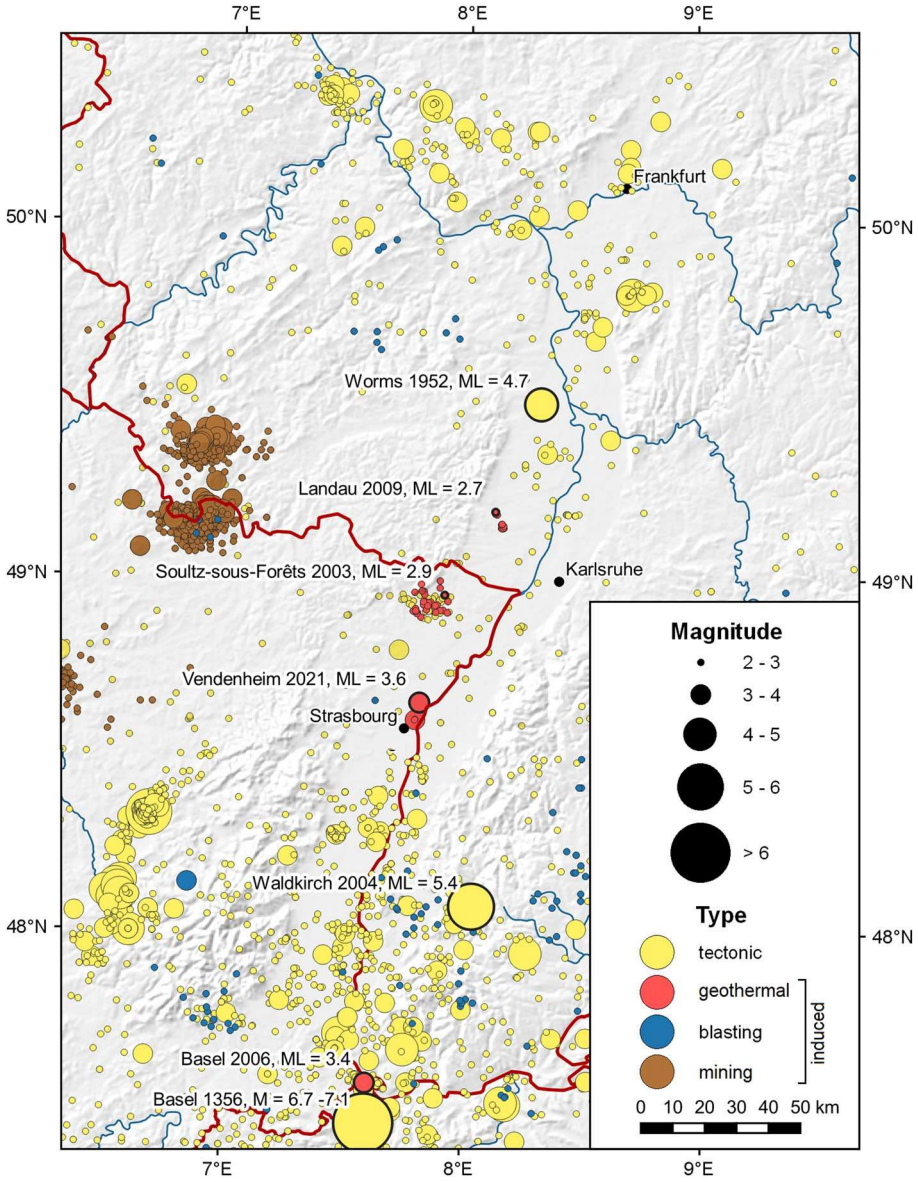

Fig. 8 Earthquakes with a local magnitude larger than 2 for the years between 1900 and 2021 observed in the wider region of the Upper Rhine Graben (data source: BGR (2021)). The 1356 Basel event is also included as the largest known earthquake in the region. Natural and induced events are distinguished

geological structures, e.g., between Mulhouse and Freiburg, accumulation of large tectonic stresses is limited, resulting in a smaller number of strong earthquakes. In general, the location of epicenters correlates well with larger fault zones, but the main border faults do not seem to be distinctly active (Grünthal et al. 2018).

Like the size of earthquake, the focal depth is also subject to variations across the URG region (Bonjer 1997; Edel et al. 2006). In the URG, earthquakes are observed in the upper crust down to depths of 13 to 16 km. The seismogenic zone is thinnest above the Moho uplift close to the Kaiserstuhl. Below the Black Forest and the Jura Mountains, the maximum focal depth increases to 20 km. N- to NNE-striking normal faulting and steep NNW- to WNW-striking strike–slip faulting are the predominant focal mechanisms

(Ahorner and Schneider 1974; Plenefisch and Bonjer 1997; Deichmann and Ernst 2006; Ritter et al. 2009; Grimmer et al. 2017). Thrust events occur rarely, hence the URG represents an overall transtensional regime.

Crustal temperature field

A significant increase in subsurface temperatures can be observed almost throughout the entire URG, with the highest geothermal gradients of up to 100 K/km being measured in the areas of Soultz-sous Forêts and Landau (Pribnow and Schellschmidt 2000; Agemar et al. 2012; Baillieux et al. 2013). The region represents a classical non-magmatic convection-dominated and fault-controlled geothermal play system (Moeck 2014) in an extensional domain. Fluid flow and effective heat transport are predominant along active fault zones bearing high fracture permeability. Upwelling of deep groundwater is hence the main reason for localized thermal anomalies.

Besides, several factors are influencing the crustal temperature field on a broader scale, resulting in a complex pattern of conductive and convective elements. Due to the Cenozoic rifting activities, the URG shows a considerable thinning of the crust and lithospheric mantle of up to 25% (Brun et al. 1992). This leads to a regional increase in the heat flux compared to the rest of Central Europe. Additionally, the radiogenic heat production of the crust is a major heat source controlled mainly by the thickness, structure and composition of the Variscan basement (Freymark et al. 2017). Different thermal properties of the Mesozoic and Tertiary sediments cause furthermore spatial variations in the conductive heat transport. Especially thermal insulation ('thermal blanketing effect') by thick clay-rich sediments results in increased geothermal gradients within the Tertiary formations (Zhang 1993; Wangen 1995; Freymark et al. 2019). A reversed effect occurs within salt deposits, such as the Weinstetter Diapir (Esslinger 1968). These are characterized by a particularly high thermal conductivity, which leads to a local chimney effect with high temperatures at the top and relatively low temperatures at the base of the salt structure.

Temperature measurements have been performed in c. 1000 wells throughout the URG so far, most of which are collected in the Geophysics Information System (FIS Geophysik) of the LIAG (Kühne 2006). Different measuring techniques were applied, resulting in significant quality variations. The most reliable results are provided by undisturbed temperature logs, where the thermal field reached equilibrium after drilling. However, disturbed temperature logs or bottom-hole temperature measurements are also common. In addition, temperature data were acquired in production tests and hydrochemical analyses. It is therefore necessary to correct disturbed temperature measurements before they are implemented in a model (Hermanrud et al. 1990; Schulz and Schellschmidt 1991; Agemar 2022). Moreover, it is recommended to weight the data according to their quality (Agemar et al. 2012; Rühaak 2015).

To create a comprehensive temperature model of the URG based on the measurements, geostatic interpolation is often applied. The most common method is kriging, which accounts for the closeness, redundancy and spatial continuity of the data. This has been used for example by Agemar et al. (2012) for the whole of Germany (Fig. 9), by Arndt et al. (2011) and Rühaak (2015) for Hesse and by the GeORG Projektteam (2013) for the central and southern URG. However, the disadvantage is that

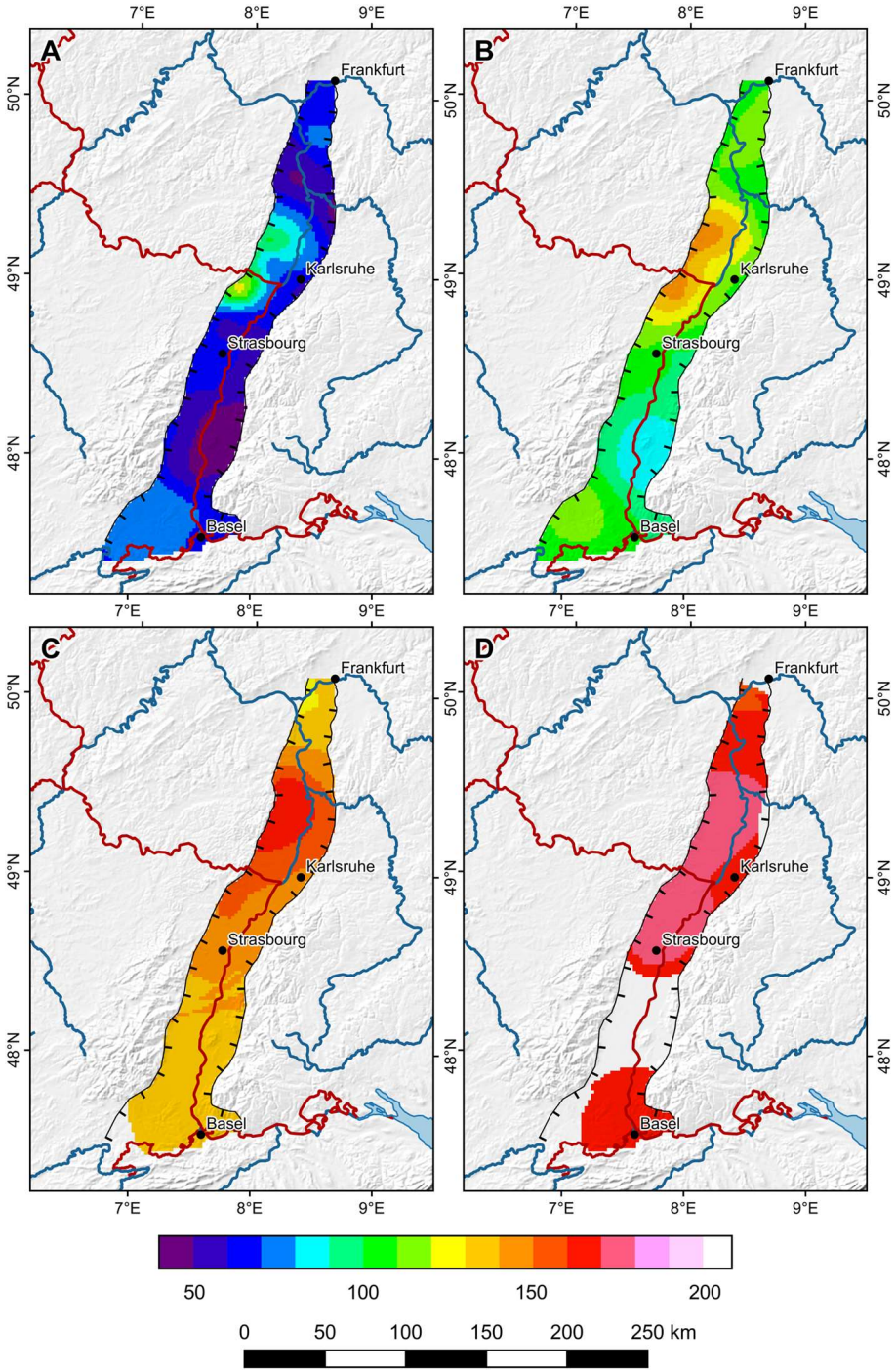

Fig. 9 Depth slices through the temperature model of Agemar et al. (2012) at **A** 1000 m, **B** 2000 m, **C** 3000 m and **D** 4000 m below sea level

discontinuities in the geological structure or the rock properties are not included in the interpolation, which can lead to an incorrect estimate of the subsurface temperatures. Furthermore, the results of the interpolation are uncertain in areas of low data density and for depths greater than about 2 km. Alternatively, the 3D temperature

distribution can also be calculated by numerical simulation (GeORG Projektteam 2013; Guillou-Frottier et al. 2013; Freymark et al. 2019, 2017, 2016; Koltzer et al. 2019). As shown by validation of these examples by measured temperatures, the mismatch for regional models can be kept below 20 °C with proper parametrization and carefully selected boundary conditions. A better fit is up to now not possible for regional-scale models due to the complex geometry of the faults acting as vertical and horizontal conduits, the variability of the other governing rock properties and due to the computational limits of most numerical simulation tools. However, numerical simulation of the subsurface temperature field can provide more accurate results especially on the local scale, where based on sufficiently accurate exploration data (3D seismics, reference wells) detailed models can be developed (Bär et al. 2021). To summarize, for regional scale assessment of the temperature field geostatistical interpolation is currently the primary method while numerical simulation has a much better potential for accurate temperature prediction at field scale.

Geothermal reservoir horizons

The investigation of deep geothermal potentials in the URG began already in the 1970s with the "Geothermische Synthese" (Sauer and Munck 1979). Since then, numerous studies have been carried out to characterize the subsurface and in particular the potential of geothermal target horizons (Dornstadter et al. 1999; Bär 2008, 2012; Stober and Jodocy 2009; GeORG Projektteam 2013; Bär et al. 2016; Frey et al. 2021a, 2021b). Based on that, in total nine geological units were identified, which show sufficient temperature, thickness and hydraulic permeability for the exploitation of heat at levels of more than 90 °C. In the following, these horizons are described with regard to their lithological properties and spatial distribution. Figure 2 summarizes the respective reservoir horizons and indicates the individual importance for deep geothermal projects in the URG.

Due to consolidation of the sediments with reduced porosity and permeability compared to their outcropping analogues, deep geothermal exploitation of intact rocks comes with a high risk of not reaching sufficient flow rates. For this reason, hydraulically active fault zones cross-cutting the geothermal reservoir horizons are usually targeted, which can exhibit significantly higher permeabilities and therefore allow high flow rates. In addition, as vertical conduits, they may be associated with natural upwelling of hot groundwater, resulting in increased geothermal gradients. Exceptions to this are to some extent the Mesozoic carbonates (Muschelkalk-Keuper, Hauptrogenstein and Upper Jurassic Limestones), which are locally karstified and thus sufficiently permeable. In addition, high permeabilities may also be reached in the coarse-grained initial as well as marginal facies of the graben filling (e.g., Pechelbronn Formation) and the double-porosity horizon of the Lower and Middle Buntsandstein.

Crystalline basement

According to the definition of the Variscan Orogenic Belt by Kossmat (1927), the crystalline basement of the URG is divided from north to south into the Rhenohercynian Zone, the Northern Phyllite Zone, the Mid-German Crystalline High (MGCH), the Saxothuringian Zone and the Moldanubian Zone. In deep geothermal exploration and research, interest in the crystalline basement is high, as it holds an almost inexhaustible potential

due to the favorable temperatures and large potential reservoir volume. In addition, it is the main source of radiogenic heat production (Vilà et al. 2010) and thus influences the thermal state of the crust to a considerable extent. Along the URG, the basement is already successfully used by the four power plants in Landau, Insheim, Rittershoffen and Soultz-sous-Forêts for electricity and heat generation (Vidal and Genter 2018) and was also the target of the abandoned projects in Basel and Vendenheim. Target reservoirs are generally related to large fault zones, where the fractured rocks show elevated natural permeability. However, for an economic operation of a geothermal system, hydraulic and chemical stimulation is necessary in most cases to increase the connectivity and permeability of the fracture network. A detailed description of the hydraulic, hydrochemical and petrophysical properties is given in chapter 6 for the main basement lithologies.

The limited availability of structural geologic information on the subsurface beneath sedimentary formations poses a significant challenge to the exploration, modeling and utilization of the basement. There is a total of 20 deep boreholes in the URG, which penetrate the top basement, whereas most of them are connected to the geothermal projects mentioned above. Figure 10 shows the location of these wells including the main rock type that was encountered. Likewise, the basement in the URG was surveyed by only a few large-scale seismic profiles, such as the DEKORP 9N and 9S lines. The latter was recently reprocessed and reinterpreted as part of the Hessen 3D 2.0 project (Homuth et al. 2021a, 2021b). The resolution and penetration depth of old seismic campaigns are usually not sufficient, but faults in shallower horizons may be traced into the basement. Crystalline outcrops at the graben shoulders, e.g., in the Black Forest, the Vosges, the Odenwald, the Palatinate or the Taunus, allow detailed investigations of petrophysical and thermal rock properties as well as the structural framework (Weinert et al. 2020; Bossennec et al. 2021; Frey et al. 2022). In addition, gravimetric and magnetic data sets (Rotstein et al. 2006; Edel and Schulmann 2009; Baillieux et al. 2014; Edel et al. 2018; Frey et al. 2021b) are suitable to study the structures, composition and properties of the basement beneath the sedimentary cover. These data sets are available in sufficiently high resolution for regional-scale models throughout the entire URG region.

Rhenohercynian and Northern Phyllite Zone

The Rhenohercynian and Northern Phyllite Zone are located at the northernmost rim of the URG (Blundell et al. 1992; Brun et al. 1992; Franke 2000). They make up only a small part of the region's basement and are therefore of rather subordinate importance for the deep geothermal power and heat production. But especially at the southern margin of the Taunus, there are several thermal springs (e.g., in Wiesbaden, Bad Nauheim, Bad Soden) related to large faults within these zones, which are used for balneological purposes (e.g., Loges et al. 2012).

The Rhenohercynian Belt is exposed in the Rhenish Massif (Taunus and Hunsrück) as well as in the Harz Mountains and Cornwall (Franke 1995b). The zone is mainly characterized by clastic shelf sediments, which were deposited from the Silurian onwards at the southern continental margin of Laurussia on top of Cadomian paragneisses (Molzahn et al. 1998; Franke 1995a). The unit further consists of subordinate reef carbonates, pelagic sediments, mid-ocean ridge basalts, and felsic volcanics (Huckriede et al. 2004; Stets and Schäfer 2011; Grösser and Dörr 1986; Floyd 1995). During the main

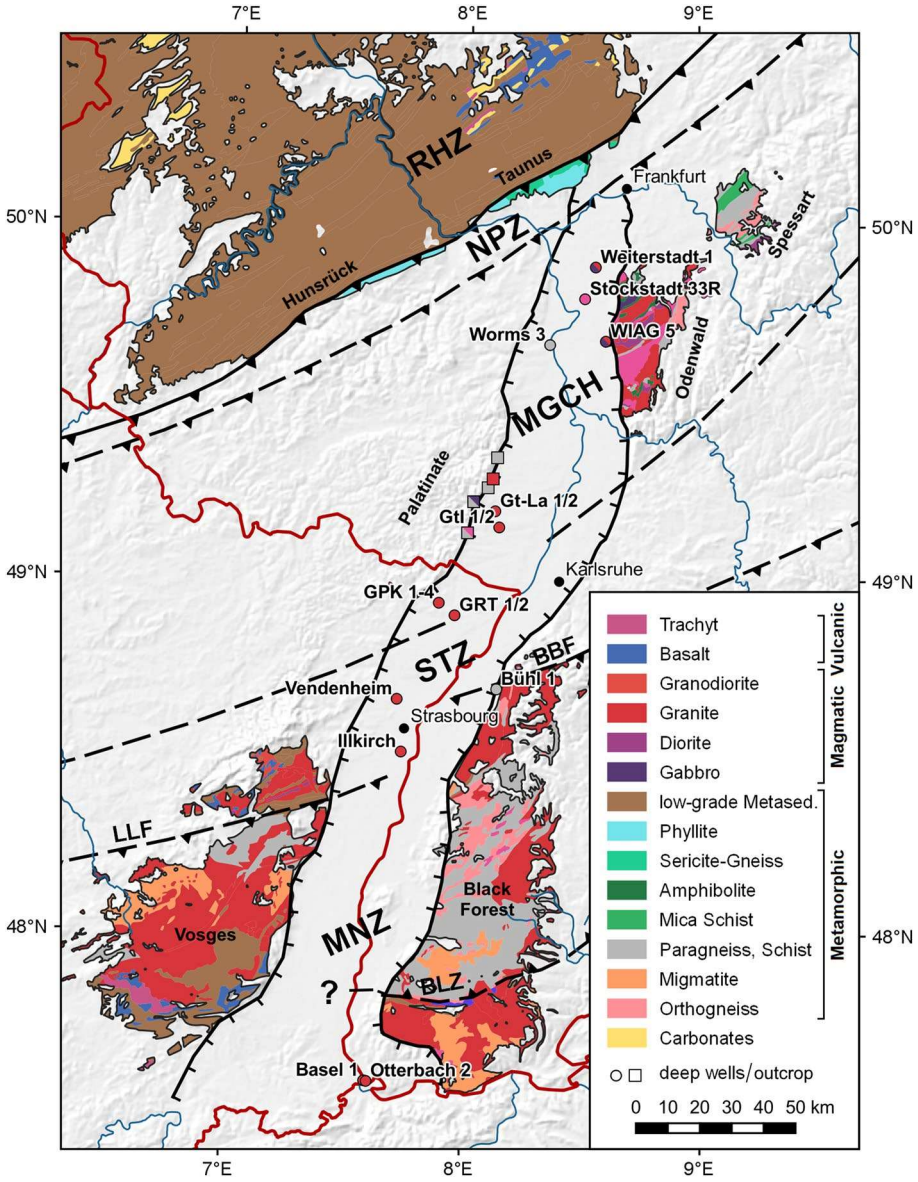

Fig. 10 Map of the Variscan basement outcrops around the URG (adapted from BGR 2016) including the location of deep boreholes that intersect the top basement. *BBF* Baden-Baden Zone, *BLZ* Badenweiler-Lenzkirch Zone, *LLF* Lalaye-Lubine Fault Zone, *MGCH* Mid-German Crystalline High, *MNZ* Moldanubian Zone, *NPZ* Northern Phyllite Zone, *RHZ* Rhenohercynian Zone, *STZ* Saxothuringian Zone

collision phase in the Carboniferous, far-reaching thrust sheets of marine sediments were established in the northern foreland of Variscan Orogeny (Edel and Weber 1995; Oncken et al. 1999), which show mainly low- to very low-grade metamorphic overprint (Doublier et al. 2012).

The Northern Phyllite Zone is a narrow belt on the plate boundary between Laurussia and the Armorican Terrain Assemblage. This zone is exposed at the southern Taunus and Hunsrück (Klügel 1997), but mostly covered by post-Variscan sediments. It is a heterogeneous tectonic mélange of 60 to 70% sedimentary rocks and 30 to 40% volcanic rocks (Klügel et al. 1994; Anderle et al. 1995). The Northern Phyllite was predominantly

overprinted by pressure-dominated greenschist facies metamorphism (Massonne 1995), which is intermediate between the P-/T-conditions in the Rhenohercynian Zone and the MGCH.

Mid-German Crystalline High

The MGCH is the deeply exposed basement of the northern active continental margin of the Armorican Terrain Assemblage, which consists mostly of plutonic rocks related to the southward subduction of the Rheic Ocean and Rhenohercynian Basin during the Carboniferous (Hirschmann 1995; Oncken 1997; Franke 2000). In addition, remnants of the Lower Paleozoic host rocks and earlier volcanic arc-related plutons with high-grade metamorphic overprint are found in this zone (Altenberger and Besch 1993; Zeh and Gerdes 2010).

The largest outcrop of the MGCH is the Odenwald at the northeastern shoulder of the URG, which is devided into the metamorphic Böllsteiner Odenwald in the east and the predominantly igneous Bergsträßer Odenwald in the west (Stein 2001). The latter is subdivided from north to south into the subunits Frankenstein Complex, Flaser-Granitoid Zone and Southern Granites/Granodiorites. From north to south, the plutons become gradually younger (from around 360 Ma in the north (Kirsch et al. 1988) to 325 Ma in the south (Kreuzer and Harre 1975; Anthes and Reischmann 2001)) and the SiO_2 increases (Okrusch et al. 1995). The westernmost exposure of the MGCH is situated in the Palatinate at the northwestern margin of the URG (Flöttmann and Oncken 1992). In contrast to the Odenwald, there are only a few local outcrops with the largest one in Albersweiler. At this location, orthogneisses derived from 369 ± 5 Ma old magmatic protoliths are predominant, that are vertically intercalated by metabasites (Frenzel 1971; Okrusch et al. 1995; Anthes and Reischmann 1997). Besides, granitoid intrusions with an age of about 340 Ma as well as metapelite and metagreywacke are found in the Palatinate basement (e.g., in Waldhambach).

Apart from surface outcrops, insights are derived from samples of several deep boreholes of the hydrocarbon and geothermal industries that penetrated the top MGCH in the URG (Fig. 10). The exploration wells Stockstadt 33R, Weiterstadt 1 and Wiag Hessen 5 reached mainly granitoids and subordinate amphibolites in depths between 2180 and 2490 m (Marell 1989; Lippolt et al. 1990; Müller 1996). In the well Worms 3 located about 20 km westbound in the graben, a cataclastic zone is intersected at 2170 m depth which is composed of strongly fractured gneisses, pegmatites and isolated granitoids. A mostly granitic basement was moreover encountered in the geothermal wells west of the Rhine River, Soultz-sous Forêts, Rittershoffen, Landau, Insheim, Vendenheim and Illkirch. However, it is still unsettled how far south the MGCH actually extends in this area. The Saar 1 well in the Saar-Nahe Basin is the westernmost borehole of the MGCH. Here, the deformed granitic basement was encountered under about 5.6-km-thick Carboniferous sediments (Weber 1995b).

Saxothuringian Zone

The Saxothuringian Zone or Saxothuringian Basin is located to the south of the MGCH. This unit is largely covered by sedimentary formations in the URG, leaving the course of the tectonic boundary unknown. However, geophysical data provide insights about

the lateral extent of the zone (Behr and Heinrichs 1987; Edel and Fluck 1989; Rotstein et al. 2006; Edel and Schulmann 2009; Frey et al. 2021b). The largest outcrop of the Saxothuringian Zone is situated in eastern Germany in the Thuringian Forest, the Fichtel Mountains and the Ore Mountains (Franke 1995c). There are two main facies types: the (para-)autochthonous Thuringian Facies is characterized by a sequence of Lower Paleozoic shelf sediments overlying the Precambrian gneiss basement of the Armorican Terrane Assemblage (Bankwitz and Bankwitz 1990; Behr et al. 1994; Falk et al. 1995). The autochthon is overlain by the allochthonous Bavarian Facies, which is a stack of tectonic nappes with varying metamorphic overprint (Behr et al. 1982; Martin 2003; Bahlburg et al. 2010). This unit consists of Upper Devonian to Lower Carboniferous deep marine deposits and intraplate volcanic as well as distal flysch in the uppermost part.

It is mostly unresolved how the Saxothuringian Zone continues to the west. Traditionally, the northern margins of the Vosges and the Black Forest are seen as outcrops of this unit (Kossmat 1927). The northern Vosges and the northern Black Forest (the so-called Baden-Baden Zone) are lithologically and structurally very heterogeneous, comprising gneisses intercalated with amphibolites, mica schist and quartzites as well as low-grade sedimentary and volcanic rocks, that are intruded by granites (e.g., Wickert et al. 1990).

Moldanubian Zone

The Moldanubian Zone is the southernmost unit of the Variscan basement in central Europe (Kossmat 1927; Franke 2000; Ziegler and Dèzes 2005). It is a heterogeneous and highly overprinted assemblage of Gondwana derived terranes that were juxtaposed during the Variscan Orogeny. Major outcrops of this zone are located in the Massif Central, in the Bohemian Massif as well as in the Vosges and Black Forest along the southern margin of the URG (Lardeaux et al. 2014).

The Moldanubian part of the Black Forest (Schwarzwald in German) is dominated by large gneiss complexes in the center and south (Central Schwarzwald Gneiss Complex (CSGC) and Southern Schwarzwald Gneiss Complex (SSGC)) (Eisbacher et al. 1989; Chen et al. 2000; McCann et al. 2008). CSGC and SSGC are further subdivided into a series of nappes consisting of Lower Paleozoic meta-granitoids and meta-sediments (Geyer et al. 2011). Large granitic plutons intruded at the boundaries of these nappes between 334 and 332 Ma (Schaltegger 2000). As in the Black Forest, the Vosges Mountains are divided into a northern, presumably Saxothuringian part and a central and southern Moldanubian part (McCann et al. 2008). The central Vosges consist of high-grade metamorphic zones that were intruded by large granitoid plutons in the Mid-Carboniferous. Granulites, migmatitic gneisses and meta-sediments are predominant in this region (Lardeaux et al. 2014). In general, the central Vosges show great similarities with the CSGC, but are shifted relatively southwards by about 30 km. The southern Vosges are a locally confined extensional basin (Eisbacher et al. 1989), filled with a Upper Devonian to Lower Carboniferous marine sequence of shales and greywackes, partly intruded by basalts and rhyolites (Schaltegger 2000).

In total three deep boreholes reached the Moldanubian basement in the URG. The geothermal well Bühl 1 encountered gneiss close to the eastern boarder fault. In the southernmost URG, the two wells Basel 1 and Otterbach 2 intersected a granitic basement.

Permo-Carboniferous

From the Westfalian onwards, Permo-Carboniferous (Rotliegend, r) sediments were deposited in numerous SE–NW oriented intramontane basins (Henk 1993; Weber 1995b; Schäfer and Korsch 1998; Scheck-Wenderoth et al. 2008). A thickness that allows an economic geothermal exploitation is only known from the northern URG (Sass et al. 2011; Arndt 2012; Bär 2012), whereas the extent and thickness of additional basins in the middle and southern URG is largely unknown and not confirmed by any deep wells (Rupf and Nitsch 2008). The largest exposure of the Permo-Carboniferous is located in the Saar-Nahe Basin (Schäfer 1989). Smaller outcrops can be found at the Sprendlinger Horst (Marell 1989), the Wetterau (Kowalczyk 2001) and in several location in the Vosges and Black Forest (e.g., near Baden-Baden where the thermal spas are fed by hot groundwater from this horizon or in the Badenweiler-Lenzkirch-Zone). The outcrops in the Saar-Nahe Basin and the Sprendlinger Horst and Wetterau can be correlated by several deep wells (Weiterstadt 1, Stockstadt 33R, Gimbsheim 2, Worms 3 and Trebur GT1) in the northern URG and show several suitable reservoir rock horizons (Bär 2012; Boy et al. 2012; Aretz et al. 2016). Accordingly, the highest thickness of presumably more than 2000 m is reached in the area west of Groß-Gerau.

In the Saar-Nahe Basin, the Permo-Carboniferous is divided into the lower Glan and upper Nahe Subgroups (Schäfer 2005; Deutsche Stratigraphische Kommission 2016). The former, also known as the pre-volcanic syn-rift phase, is further divided into the Kusel, Lebach and Tholey Layers (Stapf 1990) and consists of fine-to-coarse clastic sediments, which are occasionally interlayered by carbonates. The Nahe Subgroup comprises the volcanic syn-rift phase and the post-rift phase. Increased volcanic activity between 300 and 290 Ma led to the deposition of the up to 1100 m thick Donnersberg formation, which comprises basaltic-to-rhyolitic lava flows, tuffs and pyroclastics alternate with fluviatile and playa-like sediments (Stollhofen 1994; Stollhofen and Stanistreet 1994). During the post-rift phase mainly aeolian and playa-like sand-, silt- and claystones were deposited in a very hot-dry climate, known as the Standenbühl and Kreuznach formations (Aretz et al. 2016). Significant alluvial deposits of coarse clastics were simultaneously deposited at the basin margins in the Wadern formation. At the Sprendlinger Horst, sedimentation began during the active volcanic syn-rift phase (Marell 1989; Müller 1996). Here, however, alluvial fans as well as meandering and intertwined river systems are predominant.

The strong lithologic heterogeneity, both temporally and spatially, of the Permo-Carboniferous makes a general statement about the suitability of specific horizons for deep geothermal use very challenging. Broadly speaking, the coarse-grained fluviatile, aeolian and volcanoclastic sediments have higher permeabilities than the fine-grained lacustrine and playa deposits. However, because of the limited number of wells drilled into the Permo-Carboniferous of the URG, a detailed reservoir characterization can in most areas and especially to the south only be performed with larger uncertainties so far. The matrix of the sedimentary rocks is usually cemented, thus large-scale fault zones are again the main target of exploration as potential fluid pathways.

Buntsandstein

At the base of the Mesozoic, the Buntsandstein (s) was deposited in the Germanic Basin, which is dominated by terrigenous siliciclastic sediments (Backhaus 1974; Valeton 1953; Klapperer 2009; Meisel 1995). During the Lower Triassic, the depositional environment was similar to in the Permo-Carboniferous, with the Variscan Orogen still being the main sediment source (Paul et al. 2008). However, the deposition was not limited to the SW–NE trending molasse basins anymore but took place throughout the whole Germanic basin (Doebl and Olbrecht 1974; Ziegler 1990). The fluvio-lacustrine succession is therefore generally more homogeneous. Large outcrops of the Buntsandstein can be found across the entire URG area, but especially in the Palatinate, Buntsandstein Odenwald and Kraichgau (Fig. 1).

The lithostratigraphic unit is subdivided into the Lower, Middle and Upper Buntsandstein (Röhling et al. 2016). In the southern Germanic Basin, the Lower Buntsandstein comprises the Gelnhausen and Salmünster Sequences (Fazies 1966). The boundary to the fine-grained deposits of the Upper Zechstein is marked by boulder-bearing coarse sandstones, also known as Eck Formation. This horizon is overlain by fine and medium sandstones interlayered by clay and silt (Paul 1982). Towards the south, the grain size is steadily increasing, and the sediments are less sorted, which indicates a shorter transport distance. In the Middle Buntsandstein, the Volprihausen, Detfurth, Hardegsen and Solling Sequences are distinguished, which represent a cyclic sequence of fine- to coarse-grained clastic sediments (Dersch-Hansmann and Hug 2004). The Upper Buntsandstein is characterized by a gradual decrease in grain size. Fine and medium sandstones (Plattensandstein Formation) are overlain by silt and clay, referred to as Rötton Formation (Backhaus and Heim 1995).

In the URG, the thickness of the Buntsandstein increases continuously from about 65 m near Basel to 500 m in Karlsruhe. In a deep borehole in the Kraichgau, 539 m of Buntsandstein were intersected (Jodocy and Stober 2010a). North of Karlsruhe, a gradual thinning to a maximum of 300 m can be observed, caused by pre-Tertiary uplift of the Rhenish Shield and associated erosion processes (e.g., Sissingh 1998). The Buntsandstein is a double-porosity reservoir, where the main contribution to flow is provided by the fracture network (Haffen et al. 2012; Bossennec et al. 2021). In sandstone layers, the permeability of the rock matrix (e.g., measured on cores from oil and gas wells) is still comparatively high even at depths of more than 3 km, therefore contributing to the well productivity in addition to the fracture network (Bär 2012). However, the necessary data to quantify the respective contribution to fluid flow are currently missing, since hydraulic test data in deep wells always provide an integral value for the permeability. One possibility to determine the matrix permeability under reservoir conditions would be, e.g., drill stem tests in open borehole sections without hydraulically active fractures. In contrast to the coarse-grained layers, the clay-rich layers, mainly in the Upper Buntsandstein, exhibit overall low permeabilities.

Upper Muschelkalk

After the widespread transgression of the Tethys Ocean during the Middle Triassic, limestones, claystones and evaporites were predominantly deposited (Szulc 2000; Feist-Burkhardt et al. 2008; Götz and Gast 2010). The Upper Muschelkalk aquifer

(kuL/mo), which also includes the upper part of the Middle Muschelkalk and lowermost Keuper, is suitable for deep geothermal utilization (Wicke 2009; Stober and Bucher 2015). This lithostratigraphic unit consists mainly of banked lime- and dolostones, reflecting a full marine sedimentary environment. These rocks often contain larger amounts of trochites and oolites that lead to a high primary porosity. Furthermore, they are intensely fractured and karstified at fault zones. The Upper Muschelkalk is exposed on a large scale in the Kraichgau, where the highest thickness of more than 100 m is reached. In contrast, the thickness ranges from about 50 to 100 m in the central and southern URG (Boigk and Schöneich 1974; Jodocy and Stober 2010b; GeORG Projektteam 2013). In the north, the unit is thinned or not present at all, because, like the Buntsandstein, these rocks were eroded by Cretaceous uplift.

Jurassic carbonates

During the Middle Jurassic, the so-called Burgundy Carbonate Platform, in their sedimentary environment and extent comparable to today's Bahama Banks, developed in Central Europe (e.g., Brigaud et al. 2014). In the eastern part of this platform, mainly shallow marine carbonates were deposited in the Middle and Upper Mid-Jurassic (Dogger, jm), which are referred to as Hauptrogenstein (bjHR) (Ernst 1991; Gonzalez and Wetzel 1996; Pienkowski et al. 2008; Köster 2010). This formation consists of cross-bedded oolite-limestones and is bounded by clay and marl horizons. The deposits are interlayered by clay, marl and bioclastic horizons. Large outcrops of the Hauptrogenstein are located in the Swiss Jura Mountains and the eastern part of France. In the URG, it is present south of Hagenau and is exposed along the main graben faults at the Black Forest and the Vosges. The thickness increases continuously towards the south and reaches its maximum of about 120 to 140 m near Mulhouse (Jodocy and Stober 2010a, 2010b; GeORG Projektteam 2013).

Beside the Hauptrogenstein, also the Upper Jurassic carbonates (jo) represent potential targets for deep geothermal projects. This horizon is preserved only south of Mulhouse and consists of grey limestones interlayer with marlstones. The maximum thickness of about 100 m is reached at the southern URG margin. Like the Upper Muschelkalk, the Jurassic carbonates are often characterized by a comparatively large pore volume and a high fracture density. Moreover, they are usually karstified close to large fault zones, potentially allowing economic flow rates in geothermal wells (Stober and Bucher 2015).

Tertiary graben fill

The Tertiary (t) fill of the URG was intensively investigated by the hydrocarbon exploration, resulting in a large number of deep wells and seismic lines. Based on this, detailed characterization of the lithostratigraphic units was developed by various authors (Straub 1962; Doebl 1967, 1979; Rothe and Sauer 1967; Illies and Mueller 1970; Sauer and Munck 1979; Illies and Fuchs 1974; Doebl and Olbrecht 1974; Teichmüller 1979; Clauser and Villinger 1990; Durst 1991; Gaupp and Nickel 2001; Derer et al. 2003; Hurter and Schellschmidt 2003; Grimm 2005; Grimm et al. 2011; Jodocy and Stober 2011; GeORG Projektteam 2013; Reinhold et al. 2016; Hintze et al. 2018). It should be noted, however,

that the stratigraphic classification of the individual horizons has been regularly adapted over the last decades. Consequently, there are in many cases different names for identical geological units, which makes for example the correlation of formations between

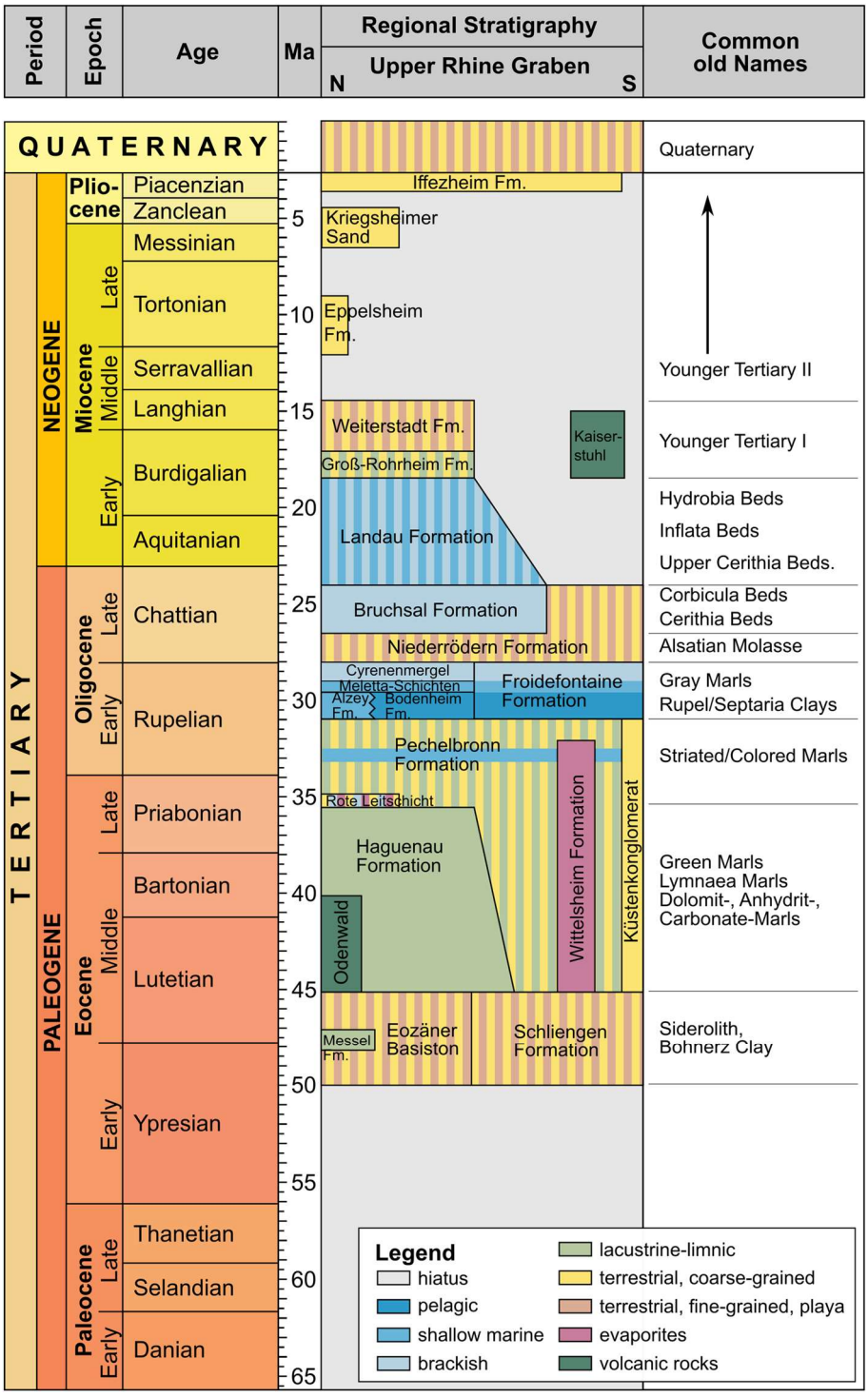

Fig. 11 Extract from the stratigraphic table of Germany, Tertiary lithostratigraphy of the URG (Deutsche Stratigraphische Kommission 2016)

wells sometimes challenging. In the following, we refer to the current nomenclature according to the German Stratigraphic Table (Fig. 11).

In the central and northern URG, the Cenozoic graben filling is usually characterized by a thickness of 1 to more than 3 km. Especially in local depositional centers, such as the Rastatt depression and the Heidelberg Trough ("Heidelberger Loch"), large amounts of Quaternary and Tertiary sediments were deposited. The highest thickness of more than 3300 m is reached between Heidelberg and Worms (Doebl and Olbrecht 1974), up to 2 km of which were deposited during the Miocene and Pliocene. In the southern URG, thick Tertiary sediments are limited to restricted basins, like the Hartheim Basin or the Kehl Basin (Jodocy and Stober 2010b). Particularly low sediment thicknesses are reached in the area of the so-called Rhenish Hauptschwelle north of the Kaiserstuhl.

The Cenozoic sediments of the URG contain partly high amounts of pelitic components, which are unfavorable for the utilization of geothermal resources due to their low permeability. Clay minerals also pose challenges for deep drilling operations, as they tend to fill cavities by swelling processes (Löschan et al. 2017). Furthermore, in fault and fracture zones, hydraulic contact can be interrupted by the accumulation of pelites or clay-smear development (Morrow et al. 1984; Jolley et al. 2007; Faulkner et al. 2010). The targets of geothermal exploration in the URG are therefore mainly medium- and coarse-grained horizons, which exhibit sufficiently high permeability and temperature. The Pechelbronn Formation seems to be most suitable in this context, particularly in the northern URG (Hintze et al. 2018; Stricker et al. 2020). In addition, the Niederrödern Formation and the Meletta Beds of the Froidefontaine Formation may also be a target for deep geothermal projects and underground thermal energy storages (UTES). Please note that the syn-sedimentary tectonics caused strong lateral changes of the depositional conditions and thus limit lateral reservoir amalgamation and hydraulic connectivity. Especially in the marginal areas and internal highs, considerable facies changes occur.

Pechelbronn Formation

The Pechelbronn Formation, also known as Pechelbronner Schichten or Pechelbronn Group, comprises syn-rift sediments of the Upper Eocene to Lower Oligocene that occur almost throughout the entire URG (Derer et al. 2003; Gaupp and Nickel 2001; Grimm 2005; Hintze et al. 2018). Due to the locally high oil content within this unit, it has been intensively studied since the nineteenth century. The Pechelbronn Formation generally overlies the Hagenau or Schliengen Formations in the southern and central URG (Grimm 2005). In the northern part, pre-tertiary rocks or Eocene base clays are located at the lower boundary. The top is marked by the onset of marine clays of the Bodenheim Formation (old name: Rupelton). The sequence can be divided into the Lower, Middle and Upper Pechelbronn Formation based on litho- and biostratigraphic characteristics. The Lower and Upper Pechelbronn Formation are characterized by fluvio-lacustrine conditions, which led to the formation of an alternation of colorful to gray, dolomitic marlstones with siltstones, sandstones and conglomerates. Coarser sedimentary rocks are mainly located in former channel structures. In subsidence centers like the Rastatt Basin, fine-clastic sediments are predominant (GeORG Projektteam 2013). The deposition of the Middle Pechelbronn Formation took place under brackish-marine conditions

after a transgression during the Uppermost Eocene (Doebl 1967). In the graben center, deep marine basins formed, in which grey to brown clay marl stones and subordinately fine sandstone layers and lenses were deposited. Due to the high proportion of pelites, the middle Pechelbronn Formation is rather unsuitable for geothermal utilization.

The Pechelbronn Formation is interlocked with the so-called Küstenkonglomerat (= costal conglomerate) Layer towards the URG margin (Geyer et al. 2011). This horizon consists of coarse sandstones and conglomerates of former alluvial and debris compartments or channels, containing boulders with diameters of locally more than 0.5 m. In the southern section of the Graben, the Haguenau and Pechelbronn Formations are moreover intercalated with halite sequences of up to 200 m thickness and several hundred meters thick marl stones, which are summarized under the term Wittelsheim Formation. The thickness of the Pechelbronn Formation ranges from a few meters in the Mainz Basin to 810 m in the Hagsfeld I well east of Karlsruhe (Doebl 1967). On average, the sediments are about 200 to 400 m thick (GeORG Projektteam 2013).

Froidefontaine Formation

The Lower Oligocene Froidefontaine Formation, also called Froidefontaine Subgroup or Grey Marl Formation, occurs throughout the whole URG (Grimm 2005). It is located on top of the Pechelbronn Formation and is overlain by the Niederrödern Formation. This subgroup is further divided into the Alzey and Bodenheim Formations, the Meletta Beds and the Cyrena Marl. The last two are sometimes also referred to as the Karlsruhe Formation. The Alzey Formation represents marine coastal facies, accordingly, it consists of mostly yellow sandstones and conglomerates (Grimm et al. 2000; Grimm 2005). At the same time, the basin facies of the Bodenheim Formation was deposited, which is characterized by alternating dark claystones and marl deposits. Alzey and Bodenheim Formation are overlain by the laminated, blue to grey clay- and marlstones of the Meletta Beds. In these, the proportion of carbonate-bearing sandstones increases continuously towards the top. The Froidefontaine Formation is completed by the Cyrene Marl, which consists mainly of colorful marlstones that contain thin layers of fine sandstones. The total thickness of the sequence ranges usually from 250 to 400 m, but locally up to 1250 m are reached (GeORG Projektteam 2013).

Niederrödern Formation

The Niederrödern Formation, which deposited during the Upper Oligocene, occurs also in the entire URG (Grimm et al. 2011). It overlays concordantly the Froidefontaine Formation. At the upper boundary, it is overlain by the Bruchsal Formation and south of Karlsruhe by unconsolidated tertiary sediments. The sequence consists of a colorful alternation of limnic marl and claystones with intercalated sandstones and siltstones. Especially in the upper half, sand horizons can be found that might be suitable for the deep geothermal exploration. The sequence is laterally variable and shows intercalations of carbonate banks, sulfate nodules and marginal conglomerates. The Niederrödern Formation is on average about 200 to 400 m thick. Locally, however, a thickness of up to 1 km is reached (GeORG Projektteam 2013; van der Vaart et al. 2021).

Reservoir characterization

Geohydrological and hydrochemical properties

Hydrogeological and hydrochemical data from laboratory investigations of drill cores from several hundred wells—mostly oil and gas drillings—within deep siliciclastic, carbonate and crystalline reservoirs of the URG area in France, Switzerland and Germany and their respective outcrop analogues have been compiled, examined, validated and analyzed with the aim to characterize fluid, rock and reservoir properties. This chapter compiles furthermore assessed, validated and analyzed hydrogeological and hydrochemical data from about 200 deep wells in different reservoirs in the URG and adjacent regions. Solely in situ testing data are presented from tests in single reservoirs; data from tests hydraulically connecting different reservoir formations with each other are excluded herein. The data have been collected from wellbores of some hundred to more than 3500 m depth. Bottom hole temperatures range from 60–160 ˚C. The prominent hard-rock reservoirs in the URG include sandstone, carbonate rock, a mixed lithology reservoir and the crystalline basement. Petrophysical properties were compiled from studies on cores from deep oil and gas as well as geothermal wells, as well as from outcrop analogue studies on the main reservoir horizons exposed in the Eastern and Western Graben shoulders.

Hydrogeological properties

Deeply buried sedimentary formations may contain and conduct water. Consequently, some formations at several km depths can behave as reservoirs, particularly limestones and sandstones. However, most of the subcritical liquid H_2O in fractured continental crust resides in the fracture pore space of the crystalline basement, which was only investigated during some local studies in the URG (e.g., Soultz, Rittershoffen and Basel). Thus, a compilation of hydraulic well test data in crystalline rocks of the Black Forest and from deep wells in northern Switzerland is introduced here. Data measured before stimulation in up to 5 km deep geothermal wells in the URG are included. For the influence of stimulation on the hydraulic properties, see e.g., Schill et al. (2017), Reinecker et al. (2019) and Stober et al. (2022).

The key data on the hydraulic conductivity of the reservoir formation of the reservoir are typically obtained from hydraulic well tests. The well yield depends not exclusively on the hydraulic properties of the reservoir formation (mainly hydraulic conductivity, storage coefficient) but to some degree also on the hydraulic properties of the wellbore itself (skin, wellbore storage), which were taken into account (Stober 1996). Hydraulic well tests also provide water samples for hydrochemical investigations and isotope studies.

A large number of hydraulic tests were completed in the different fractured and/or karstified deep reservoirs of the URG. Oil and gas industry tested most boreholes hydraulically several times within the same stratigraphic horizon. So, the results could be verified, and implausible results were rejected. Concept, approach and realization of most of the tests were dictated by the needs of the oil and gas industry. Tests included drill stem tests (DST), slug-tests and pumping-tests depending on the specific requirements. Most of these tests were typically of short duration and were performed in

relatively narrow packer-isolated test-sections. In contrast, tests in hydrothermal or geothermal wells were conducted over significantly longer time periods in longer borehole sections. Stober and Jodocy (2009) give general information on test realization and chosen evaluation methods. The straightforward evaluation of these hydraulic tests results in a value for the transmissivity (T [m^2/s]). The hydraulic conductivity (K [m/s]) can be retrieved from the transmissivity and the thickness of the tested formation (H [m]) as K = T/H assuming a homogeneous and isotropic tested formation.

The examined geothermal reservoir formations are characterized by relatively high hydraulic conductivity reflecting the active tectonic setting of the rift valley and its fractured and karstified reservoirs (Fig. 12).

The highest hydraulic conductivity with a median value of about $K = 1 \cdot 10^{-6}$ m/s is derived from the double porous (fractured and karstified) limestone reservoir of the Upper Muschelkalk (kuL/mo) and the lowest median value from the double porous Hauptrogenstein (bjHR) reservoir ($K = 6 \cdot 10^{-8}$ m/s). Five locations in the Buntsandstein (s) revealed high hydraulic conductivity, three wells provided low to very low conductivity (median: $K = 2.4 \cdot 10^{-7}$ m/s). The Buntsandstein typically is fractured with few fractures per meter, however, the fractures have relatively increased apertures ranging from approximately 1 to 10 mm (measured on cores) (Bossennec 2019). In addition to the fracture network, the hydraulic of the Buntsandstein is influenced by the matrix permeability, which depends strongly on the degree of diagenesis.

Figure 12 illustrates typical ranges of K, which indicate different flow-behaviors of the reservoirs. The two limestone reservoirs (Hauptrogenstein and Muschelkalk) are narrowly fractured, whereas in the Buntsandstein reservoir the distance between single water conducting fractures is much wider. Thus, it has to be considered that the test-length, especially for tests of the oil and gas industry, was too short in the Buntsandstein reservoir to fulfill always the criterions of an representative elementary volume (REV)

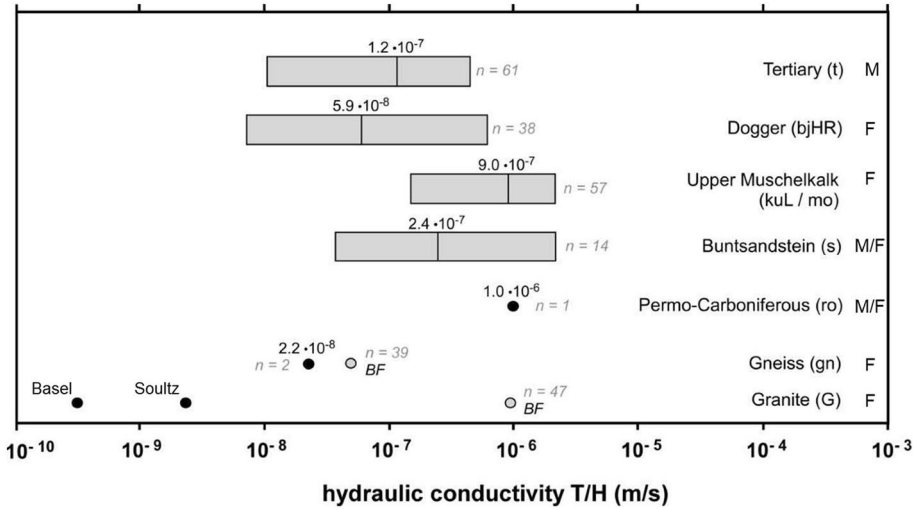

Fig. 12 Hydraulic conductivity of different deep reservoirs in the Upper Rhine Graben presented as boxplot; shown are the median values (*n* number of different boreholes, *BF* data of Black Forest and deep wells in N-Switzerland). It is indicated whether the fluid flow in the reservoir horizon is dominated by fractures (F) or matrix (M)

(Bear 1979) for fractured reservoirs and might only be representative for the rock matrix. The Tertiary (t) sediments (Fig. 12) on the other hand comprise hydraulic conductivity data of several hydraulically independent sedimentary strata (also compare Stober and Jodocy 2009). The retrieved hydraulic properties may not represent a single reservoir but several layers with heterogeneous properties. The vertical and lateral connectivity of permeable layers within the Tertiary strata can differ significantly from one location to another depending on the sedimentary environment and subsidence to accommodation space ratio.

In most reservoirs, the measured hydraulic conductivities show no regional variations or trend. The data also reveal that hydraulic conductivity decreases only marginally with depth in each of the reservoirs (Stober and Bucher 2015), probably a result of the young and still active tectonics in the Graben leading to intensified joint and fissure production rate or reactivation and thus to increased hydraulic conductivity even at greater depth. The data also clearly show that the Upper Muschelkalk- and Buntsandstein reservoir (with the exception of a few outliers) have the highest hydraulic conductivity, which might allow cross formations advective flow of thermal waters.

The crystalline basement is poorly investigated in the URG, since hydraulic data are only available from the deep wells of the Soultz-sous-Forêts geothermal project, while most other projects produce water from additional reservoirs on top of the crystalline (Vidal and Genter 2018; Reinecker et al. 2019). Thus, Fig. 12 presents additional hydraulic data of crystalline basement rocks from the Black Forest and deep wells in northern Switzerland (Stober 1996). Generally, hydraulic conductivity of the crystalline basement varies over several orders of magnitude. Some volumes of the continental crust are essentially impervious; other areas are highly conductive and (Stober and Bucher 2007) may hydraulically behave like near surface reservoirs (Ingebritsen and Manning 1999; Manning and Ingebritsen 1999; Scibek 2020; Achtziger-Zupančič et al. 2017; Stober et al. 2022). Deep geothermal wells in the URG often revealed a surprisingly high hydraulic conductivity at the top of the crystalline basement, e.g., at the former Paleozoic land surface. However, granite seems to be more permeable than gneiss (Fig. 12). The observed nearly depth-independent conductivity structure of the sediments in the Rhine Rift Valley is in marked contrast to the significant conductivity decrease with depth observed in the crystalline basement of the Black Forest (Stober and Bucher 2007).

Hydrochemical properties

Generally, the chemical data of water samples presented here are old data from archives reported from samples collected during production tests performed by the oil and gas industry. The original, tested and sampled boreholes are closed now, so that resampling is not possible anymore. A few recently collected samples from thermal spas and geothermal wells have been added to the data set. A total of more than 200 water analyses have been compiled (Pauwels et al. 1993; He et al. 1999; Stober and Jodocy 2009; Stober and Bucher 2015; Sanjuan et al. 2016; Stober et al. 2022). In some wells several samples had been taken from the same formation. So, on the one hand the hydrochemical data could be verified and implausible analyses could be rejected and on the other hand the best analyses for further investigations could be used, onsidering standard criteria given, e.g., in Hölting and Coldewey (2009).

The composition of the fluids from all four investigated reservoirs show systematic variations with increasing TDS corresponding to increasing depth (Fig. 13). The chemical composition of water from shallow sedimentary formations (< 800 m depth) typically reflects the mineral inventory of the sediments:

- Tertiary sedimentary formations: Ca-HCO_3 water, controlled by sediments with carbonate components. Locally SO_4 is enriched probably because of the occurrence of gypsum/anhydrite in some strata.
- Hauptrogenstein: Ca-HCO_3 water, related to fractured, karstified limestone (calcite)
- Upper Muschelkalk: Ca-SO_4-HCO_3 water, due to fractured, karstified limestone, containing gypsum/anhydrite-bearing strata beneath the reservoir (Middle Muschelkalk).
- Buntsandstein: Ca-HCO_3 waters with elevated SO_4 concentration, resulting from gypsum lenses in the fractured sandstone, locally cemented with calcite and abundant calcite veins.

Also, near-surface conditions such as recharge rate and REDOX conditions control the water composition. It is therefore not surprising that water residing in limestone reservoirs is strongly influenced by the carbonate minerals present in the rock (Fig. 13).

Deep thermal groundwater in the URG is always highly mineralized (Pauwels et al. 1993), with the total of dissolved solids (TDS) typically exceeding 5 g/kg in groundwaters below 800 m depth. TDS furthermore drastically increases with depth in all investigated reservoirs. The highest overall TDS-value of 300 g/kg is observed in brines from the Hauptrogenstein. In the Buntsandstein brine, the highest TDS is 127 g/kg, in Upper Muschelkalk 79 g/kg and in the Tertiary strata 240 g/kg. Na-Cl brines are the dominant chemical character irrespective of the rock forming minerals (Fig. 13) and the salinity of thermal waters in sedimentary formations is most commonly higher than in seawater (35 g/kg) (Stober and Bucher 2015), reflecting worldwide observations (Carpenter 1978; Grasby and Betcher 2002; Karro et al. 2004; Kharaka and Hanor 2004).

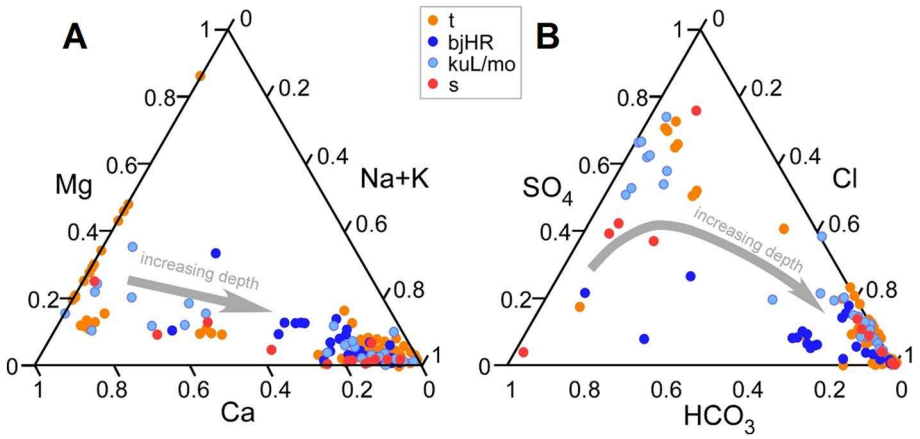

Fig. 13 **A** cations and **B** anions in different reservoirs of the URG (t—Tertiary, bjHR—Hauptrogenstein, kuL/mo—Upper Muschelkalk, s—Bundsandstein). With increasing depth, the main water components are Na and Cl

In the URG, the sulphate (SO_4) concentration first increases with TDS and becomes the dominant anion in some waters. At very high TDS, the SO_4 concentration relatively decreases in favor of Cl. Bicarbonate (HCO_3) is typically higher concentrated than sulphate in shallow, low TDS water. With depth and increasing TDS (increasing Cl concentration) also the SO_4 concentration increases and strongly outweighs HCO_3. Almost all deep high Cl (high TDS) water exhibits a higher concentration in SO_4 than in HCO_3. Thus, in all deep URG-reservoirs, the fluids evolve to a Na-Cl dominated brine, independent of the rock composition and the minerals of the reservoir rocks (Fig. 13).

Despite the very high salinity of brines in the URG, deep groundwaters within the Graben are still below saturation with respect to halite. However, waters reach saturation with respect to various minerals including calcite and quartz at much lower concentrations. Saturation of the water with some low-solubility minerals controls the composition of the fluid at depth. Since solubility depends on temperature and pressure, the water composition changes during flow along pressure and temperature gradients, that is during up- or downward flow or during uplift (decompression) or burial of the rock masses. The solubility changes may leave mineral precipitates (scales) on fracture surfaces or may cause dissolution corrosion on mineral surfaces. All deep waters of all reservoirs are saturated with respect to calcite. Calcium is increasing with increasing TDS and depth, whereas HCO_3 is decreasing as a consequence of the inverse concentration of Ca and carbonate at equilibrium with calcite ($CaCO_3$ solid $\Leftrightarrow Ca^{2+} + {CO_3}^{2-}$). All deep waters are moreover saturated with respect to dolomite, quartz and barite (Parkhurst and Appelo 1999). Thus, the waters have a certain scaling potential if pumped and used in geothermal energy applications as already proven for Soultz, Bruchsal, Insheim and other operating projects.

Buntsandstein water (e.g., in Cronenbourg and Bruchsal) is rich in strontium and lithium (> 0.1 g/kg) and arsenic may reach several 10^{-3} g/kg. Similar strontium- and lithium-concentrations were only measured in several crystalline basement and Tertiary wells (Sanjuan et al. 2016; Drüppel et al. 2020).

Water from a number of wells in Buntsandstein, Upper Muschelkalk and Hauptrogenstein showed CO_2-gas concentrations of more than 1 g/kg, while in the Tertiary sediments most CO_2-gas concentrations are on the order of several 0.1 g/kg. Generally, in all reservoirs the H_2S concentrations are low, often below detection limit.

The origin of salinity and major water components in deep sedimentary URG-reservoirs and in the crystalline basement was in detail investigated by Stober and Bucher (2015). Chloride can apart from external sources (fossil seawater, halite deposits) be found in the crystal lattice of minerals, in fluid inclusions and along grain boundaries. In magmatic rocks of the Black Forest chloride and lithium are typically found in biotite (Drüppel et al. 2020). During alteration, Cl and Li are (among others) removed from the solid into the fluid phase. Both elements behave rather conservatively, leading to enrichment in water. The high TDS of deep crystalline basement waters is not a consequence of prolonged acid–base reaction of water with the primary unstable minerals of the basement rocks, but rather the mechanism of zeolite formation from feldspar that generates saline neutral waters. Zeolitization does not affect pH and chemically binds free H_2O into the structure of a framework silicate, increasing passively the TDS of the remaining water (Stober and Bucher 2004; Brady et al. 2019). Zeolites have been

observed and mineralogically analyzed in drill cores from the Black Forest (Walenta 1992). Similar observations were, for example made in the Gotthard Massif (Zangerl et al. 2006; Weisenberger 2009). In addition, the formation of zeolites as hydrothermal transformation products has also been demonstrated in laboratory experiments under reservoir conditions (Schmidt et al. 2017, 2018, 2019).

Based on profound hydrochemical indicators (like Cl/Br, (Na + K)/Cl) and additional hydrochemical and geochemical indications (e.g., geothermometry), precipitation of specific minerals in cores (Vidal et al. 2018; Drüppel et al. 2020), on enhanced temperatures in the URG and temperature profiles in deep wells (e.g., Vidal et al. 2017), on heat flow anomalies (e.g., Clauser 1989) and on numerical modeling (Person and Garven 1992; Freymark et al. 2019; Koltzer et al. 2019) it is known that there are areas with (even recent) ascending thermal brines from deeper into shallower parts of the crystalline basement and in the central URG into the Buntsandstein and even in higher formations. The strong topography (Black Forest, Vosges Mountains) in combination with the fault-bound vertical fluid pathways induces fluid flow over long distances not only from the graben shoulders to the center, but also from south to the north within the graben. The deep hydrothermal flow system is both topography (Tóth 1978) and buoyancy driven and the upwelling water is focused and channeled along zones of higher permeability (faults, fractures, etc.). Upwelling waters with enhanced temperature and TDS, with significant amounts of Na, Cl, etc., are typically found in the foot hills or valleys of these mountains as thermal springs (Stober et al. 1999) and along major faults within the crystalline and in deep sedimentary layers in the URG as shown in the conceptual sketch in Fig. 14a.

Thus, the salinity of the Buntsandstein brine seems to be at least partly influenced by upwelling water from the crystalline basement. This assumption is supported by temperature profiles, barite precipitation, and numerical simulations, among others. In contrast, Sanjuan et al. (2016) argue, based on the Na/Li ratio and Sr isotopy, that fluids discharged from the crystalline basement mainly originate from the Buntsandstein. In any case, mixing of fluids from these two reservoirs is to be expected, depending on the local circulation system. Further upwelling of hot water from the Buntsandstein preferentially along fractures and fault systems is possible, especially in the halite-rich Middle Muschelkalk, thus leading to high salinity in the Upper Muschelkalk reservoir (Fig. 14a). Since particularly the Lower Jurassic (in addition to parts of the Keuper and Middle Jurassic) is very compartmentalized, circulation in the upper system (Hauptrogenstein, Tertiary sediments) is more or less separated and decoupled from the lower system (Crystalline basement, Buntsandstein, Upper Muschelkalk) (Stober and Bucher 2015). In the Tertiary sediments, the high salinity is mainly caused by dissolution of halite present in some of the Tertiary layers. Saline water in Tertiary sediments may possibly migrate into the Hauptrogenstein. However, fluid circulation from the lower into the upper system seems merely possible in areas with huge vertical displacement within the Graben, e.g., along prominent graben/horst-structures. Near the rim of the Graben the waters seem to be hydrochemically influenced by adjacent layers, being in line with the findings of the modeling of the temperature field by Clauser (1989), Person and Garven (1992), Rühaak et al. (2014) and (Freymark et al. 2019). Nevertheless, a systematic temperature trend with colder values at the two rims of the Graben and higher ones more in

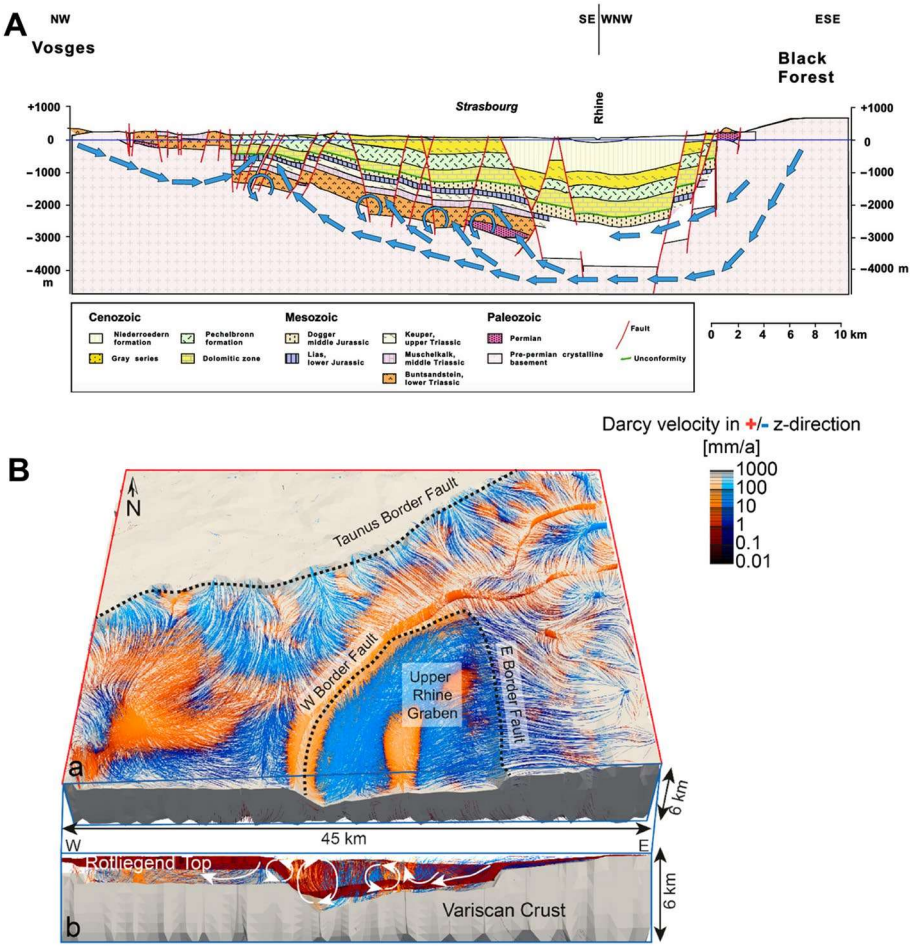

Fig. 14 **A** Schematic illustration of deep topography driven, hydrothermal flow systems with upwelling of saline water in the central URG (Stober and Bucher 2015), blue arrows showing the generalized fluid pathways within the basement and lower situated sedimentary horizons; **B** 3D visualization of simulated streamlines in the northern URG (Koltzer et al. 2019). The color code shows in red Darcy velocities in the positive z-direction (upflow) and in blue in the negative z-direction (downflow). With velocities from black over dark colors to light colors into white. **a** Streamlines above the Variscan crust in a block in South-West Hesse; **b** profile perpendicular to the Upper Rhine Graben with streamlines in Cenozoic and Rotliegend sediments. White arrows highlight the simulated fluid circulation in the URG

the center of the Graben is not visible in the temperature model of Agemar et al. (2013), which might also be a result of spatial data distribution and the interpolation approach.

Conceptual 2D profiles (as in Fig. 14a) can only describe to some degree the hydraulic processes in a complex system such as the URG, where small-scale changes in groundwater flow regime are expected. Therefore, attempts have been made in the past, e.g., by Koltzer et al. (2019), to refine the picture using 3D numerical modeling (Fig. 14b). The results suggest that the URG is characterized by a large number of locally confined convection cells tied to hydraulically active fault zones, an observation which matches very well with known geothermal anomalies present in the URG mainly along major graben internal faults. However, also this approach can only represent a limited geologic complexity (e.g., number of faults, spatial variation of hydraulic properties) with regard to the computational effort and data availability. For

this reason, the exact paths of fluid flow throughout the URG remain uncertain until new data are collected and combined in complex integrated models as proposed by Bär et al. (2021a).

Petrophysical properties

To assess and review the petrophysical properties of the sedimentary and basement reservoirs in various depths of the URG (Fig. 15), published data were compiled and structured following the guidelines of P^3—the PetroPhysical Property Database (Bär et al. 2020). Therefore, the data compiled and presented here only stem from lab measurements on core samples and not from any kind of borehole geophysical logging. Borehole geophysical logs in the URG are usually confidential and in most cases too old to determine the relevant petrophysical properties directly. Since petrophysical data from actual samples of reservoir depth is very sparse due to the high costs of drilling cores and often also confidential, results from various outcrop analogue investigations (mostly active and abandoned quarries) performed around the URG were included as well. An exception for data and core availability are the research wells of Soultz-sous-Forêts, where multiple investigations were performed both on logs as well as on drill cores.

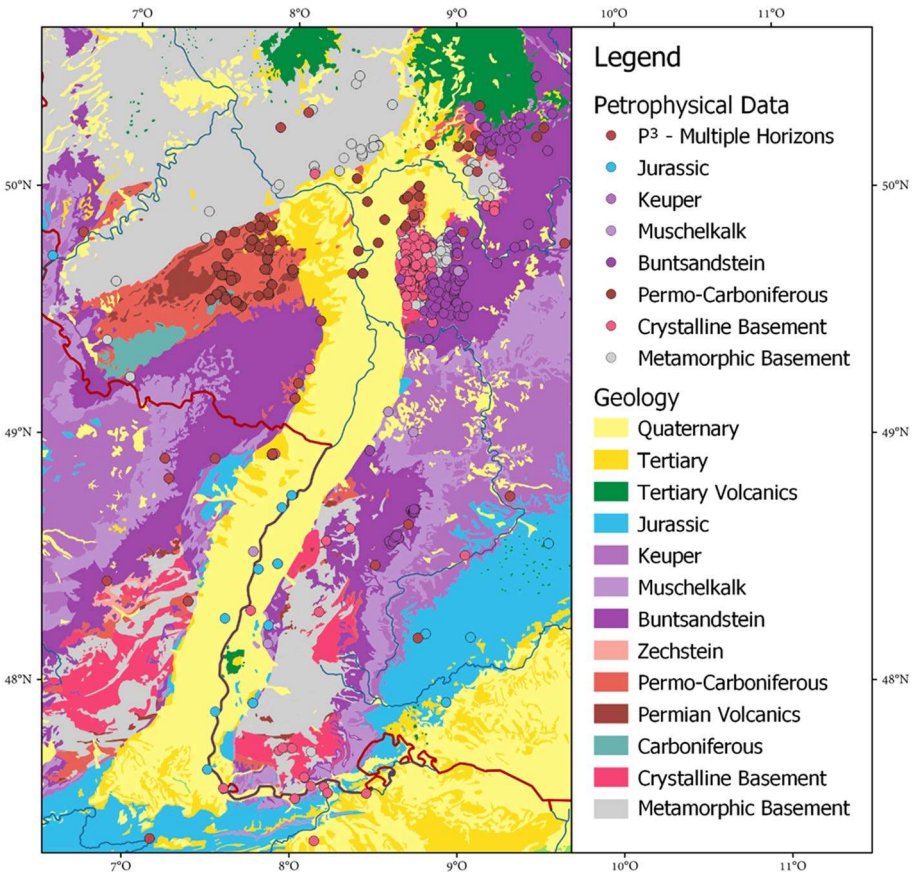

Fig. 15 Location of datapoints with petrophysical property data measured on samples from drill cores or outcrop analogues of the deep geothermal reservoir units of the Upper Rhine Graben

Overall, more than 19,000 single or averaged measurement values were compiled. Data evaluation was performed for each reservoir formations and for the main lithologies of the crystalline and metamorphic basement. Naturally, for such a large and diverse dataset, documentation of the original sources is very heterogeneous and of different quality, resulting in the need to compare and statistically assess results of single measurements together with mean values of multiple measurements of the same rock type.

Data availability also differs quite a lot depending on the particular properties to be assessed. While density, porosity and permeability are most abundant as well as thermal conductivity, data for other properties like specific heat capacity and thermal diffusivity are rather sparse. Direct measurements of mechanical rock properties like p-and s-wave velocities, Poisson ratio, uniaxial compressive strength, shear strength, cohesion, angle of internal friction are very rare and restricted to cores from less than three wells and only a couple of outcrop analogues. Mechanical rock properties are thus not yet included in the compilation here and need to be investigated in more detail in the future.

Depth trends and influence of alteration and weathering were not assessed in detail due to the heterogeneity of the dataset but are well known and investigated for the crystalline basement (Ledésert et al. 1999; Surma and Geraud 2003; Griffiths et al. 2016) and its weathering zone at the top and strongly hydrothermally altered sections as well as for the Buntsandstein, where hydrothermal bleaching is well known to reduce primary porosity and intrinsic permeability of the rock matrix (Gaupp et al. 1998; Haffen et al. 2013, 2015; Bossennec et al. 2021). For the Permo-Carboniferous, a thorough comparison of reservoir and outcrop analogue samples is presented by Aretz et al. (2016), where it is shown that the depositional facies plays an important role on the preservation of primary porosity at reservoir depth. Heap et al. (2017) and Kushnir et al. (2018a) investigated the influence of paleo-weathering on Soultz core samples of the Buntsandstein, Permo-Carboniferous and the crystalline basement and showed the positive influence of the associated processes on the reservoir properties.

As presented in Figs. 16 and 17 all reservoirs and reservoir lithologies show a large data spread reflecting the internal heterogeneity of the reservoirs with a wide range of different rock types (e.g., pelites to coarse sandstones; gabbro to granite, meta-pelites to quartzites). For the plutonic basement rocks, granites and granodiorites exhibit the best petrophysical properties for geothermal utilization. They both have considerably high thermal conductivities and thermal diffusivities and according to Vilà et al. (2010) also the highest internal radiogenic heat production. Additionally, from outcrop analogue investigation, strongly increased effective porosities and intrinsic permeabilities are known, resulting mainly from weathering effects and hydrothermal alteration. A more detailed statistic assessment is for example presented in Weinert et al. (2020) for the crystalline basement of the northern URG. For the less dominant metamorphic basement rocks, the gneiss and quartzites show the best thermal properties, but lowest porosities and intrinsic or apparent permeabilities. The hydraulic rock properties are seemingly better for meta-volcanics and meta-pelites, while still completely insufficient to provide the flow rates needed for geothermal utilization.

The Paleo- to Cenozoic reservoir units of the sedimentary units of the URG also cover a large spread of rock properties. The Tertiary, Buntsandstein, Zechstein and Permo-Carboniferous reservoir rocks have porosities, which are interesting for deep geothermal

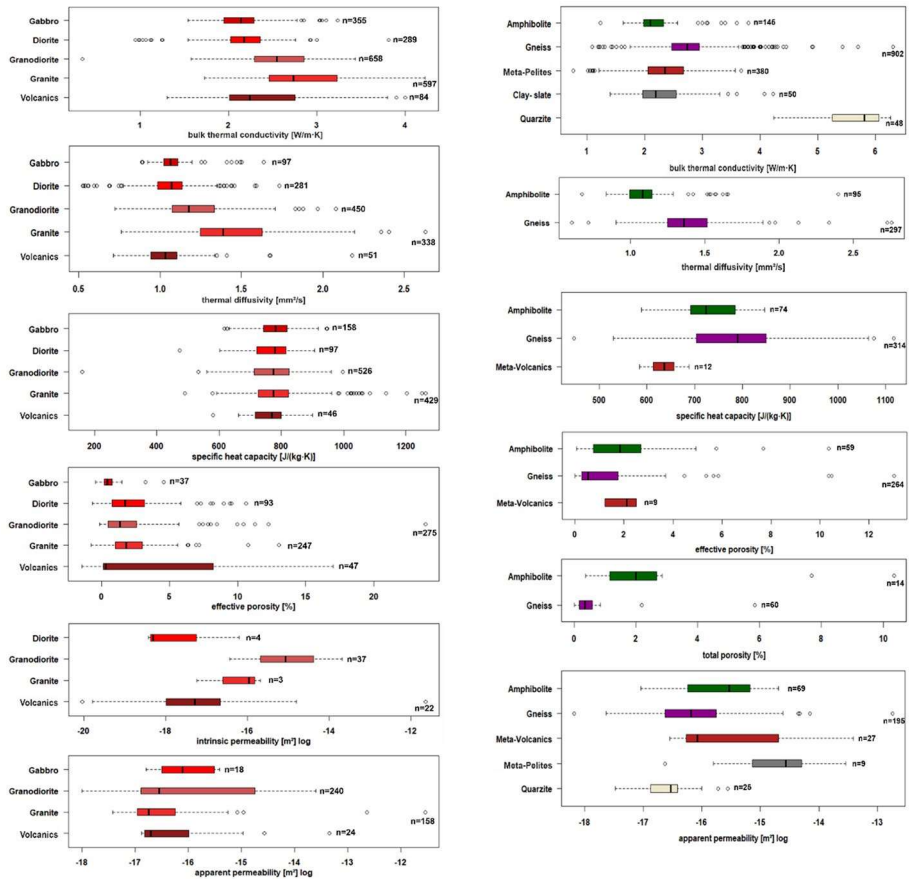

Fig. 16 Petrophysical properties (thermal conductivity, thermal diffusivity, specific heat capacity, effective and/or total porosity and intrinsic and/or apparent permeability) of different lithologies of the basement reservoirs in the Upper Rhine Graben from outcrop analogue and deep drill core investigations presented as box-whisker plots; shown are the average, Q25, Q75 and minimum and maximum values (n – number of data points per property and lithology). Data compiled from (Wenk and Wenk 1969; Kappelmeyer and Haenel 1974; Schärli and Kohl 2002; Surma 2003; Stober and Bucher 2007; Pei 2009; Kraus 2009; Faridfar 2010; Kläske 2010; Klumbach 2010; Vilà et al. 2010; Hoffmann 2011, 2015; Welsch 2011; Bär 2012; GeORG Projektteam 2013; Maire 2014; Hückel and Kappelmeyer 1966; Orendt 2014; Wiesner 2014; Weber 2014; Aretz et al. 2016; Lambert 2016; Schintgen 2016; Vogel 2016; Schäffer et al. 2018; Weinert et al. 2021)

utilization concerning their heat storage potential. The Jurassic, Keuper and Muschelkalk reservoir rocks have significant lower effective porosities and thus can mainly be classified as fracture-flow or karstified reservoirs. This observation is proven by the intrinsic or apparent permeabilities of the different reservoir rocks. Here, the Tertiary, Buntsandstein, Zechstein and Permo-Carboniferous have average values of more than $5{\cdot}10^{-15}$ m^2, which can be sufficient for deep geothermal utilization even if the contribution of the fracture network is not considered.

The petrophysical properties of the Tertiary succession is described in more detail, by e.g., Gaupp and Nickel (2001), Jodocy and Stober (2011), GeORG Projektteam (2013), Reinhold et al. (2016), Hintze et al. (2018), Stricker et al. (2020) and Bär et al. (2021b).

The petrophysical properties of the Buntsandstein as a double-porosity reservoir is well described by Bär (2012), Haffen et al. (2012), Haffen et al. (2015) and Bossennec et al. (2021).

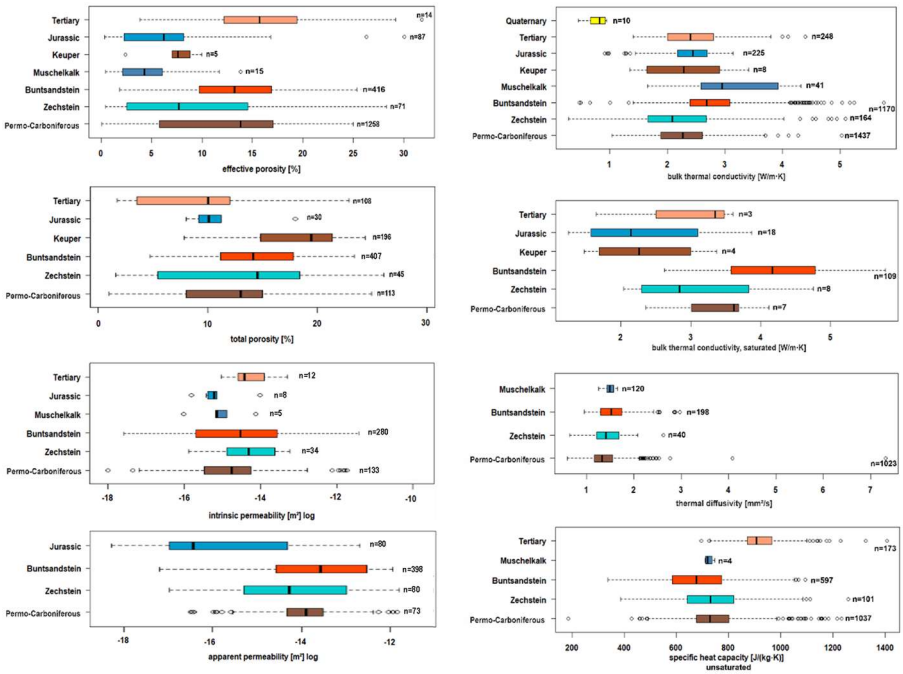

Fig. 17 Petrophysical properties (effective and total porosity, intrinsic and apparent permeability, thermal conductivity (dry and saturated), thermal diffusivity and specific heat capacity, of the different sedimentary reservoirs in the Upper Rhine Graben from outcrop analogue and deep drill core investigations presented as box-whisker plots; shown are the average, Q25, Q75 and minimum and maximum values (*n* number of data points per property and reservoir). Data compiled from (Leu et al. 1999; Mack 2007; Schumann 2008; Gu 2010; Klumbach 2010; Vilà et al. 2010; Hesse 2011; Jodocy and Stober 2011; Nehler 2011; Schubert 2011; Welsch 2011; Bär 2012; GeORG Projektteam 2013; Schöpflin 2013; Homuth 2014; Jensen 2014; Müller 2014; Weber 2014; Betten 2015; El Dakak 2015; Esteban et al. 2015; Sandkühler 2015; Aretz et al. 2016; Schintgen 2016; Heap et al. 2017; Kushnir et al. 2018b; Schäffer et al. 2018)

The petrophysical properties of the Permo-Carboniferous are described by e.g., Aretz et al. (2016), Gu et al. (2017), Molenaar et al. (2015), Reinecker et al. (2015) and Heap et al. (2017).

Geothermal projects

For centuries, deep thermal groundwaters have been used for balneological purposes along the margin of the URG starting with the Romans. Since the beginning of the twentieth century, this application has been further expanded by the drilling of numerous shallow or middle deep wells (Fig. 18). The large-scale exploration of deep geothermal resources for the generation of heat and electrical power began in the late 1970s and 1980s with the projects in Bühl, Cronenbourg and Bruchsal (Table 1).

This first phase was followed by the extensive European EGS (Enhanced Geothermal Systems) project at Soultz-sous-Forêts, which to date has provided extremely valuable insights into the hydraulic, mechanical and chemical properties of fractured reservoirs and the potential for economic exploitation. At this location in total 5 deep wells (GPK1-4 and EPS1), partly with a depth of more than 5 km, were drilled between 1987 and 2004 (Genter and Traineau 1996; Dezayes et al. 2005b; Baujard et al. 2017). Multiple hydraulic and chemical stimulation experiments were conducted, some of which

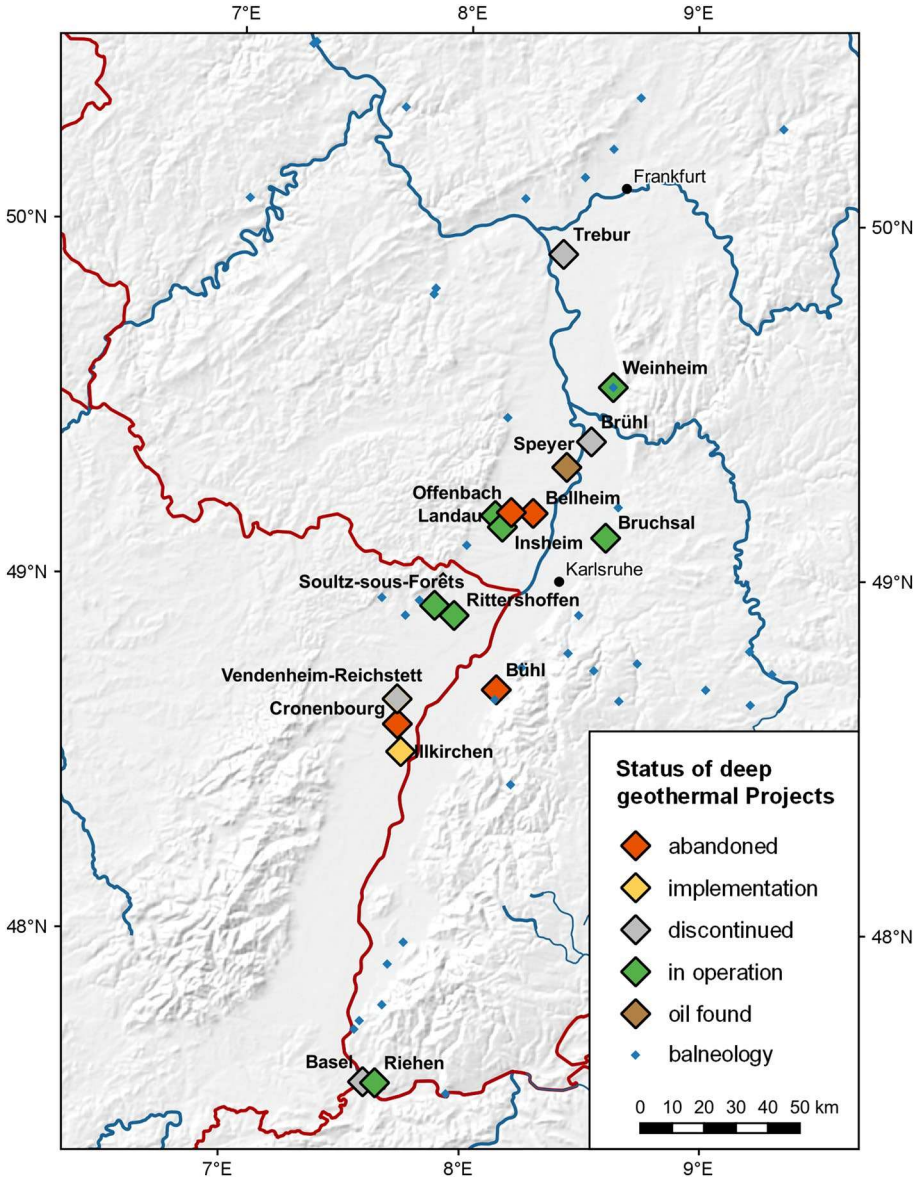

Fig. 18 Overview of the geothermal projects in the URG and their current status (adapted from Agemar et al. 2010). The geothermal wells in Weinheim are used for balneological and heating purposes, but the project has an exceptional position because a doublet was implemented here instead of a single production well

significantly improved the permeability of the fractured reservoir (Evans et al. 2005; Portier et al. 2009; Schill et al. 2017). Subsequently, the hydraulic properties of the subsurface were then investigated through long-term circulation tests.

Further successful projects were realized in Riehen, Landau, Weinheim, Insheim and Rittershoffen. Two additional projects near Strasbourg, Vendenheim and Illkirch, were in development until all operations were halted by political decisions after induced seismic events in Vendenheim. Besides, many projects are currently being planned, but will not be discussed here in detail. By 2020, geothermal power plants with a total capacity of about 50 MWth and 10 MWel have been installed in the URG, which is only a minor fraction of the total technical potential (Paschen et al. 2003; Kock and Kaltschmitt 2012).

Table 1 Summary of the major deep geothermal projects with drilled wells in the URG in 2020

Project location	Status	Target reservoir	Number of wells	Year of drilling	Max. depth TVD [m]	Max. temp [°C]	Power generation [MW]		References
							Thermal	Electrical	
Basel	Discontinued	Basement	1	2006	4992	190	–	–	Häring et al. (2008), Ladner et al. (2008)
Bellheim	Abandoned	Muschelkalk	1	2005–2006	2606	–	–	–	Internal reports
Bruchsal	In operation	Buntsandstein, Rotliegend	2	1983–1985	2542	123	5.5	0.55	Bertleff et al. (1988), Rettenmaier et al. (2013), Herzberger et al. (2010)
Brühl	Discontinued	Buntsandstein	1	2012–2013	3281	153	–	–	Reinecker et al. (2015)
Bühl	Abandoned	Dogger, Keuper, Basement	1	1979–1980	2699	120	–	–	Bertleff et al. (1988), Pauwels et al. (1993)
Cronenbourg	Abandoned	Buntsandstein	1	1980	2870	140	–	–	Housse (1984), Pauwels et al. (1993), Vidal and Genter (2018)
Illkirch	In implementation	Basement	1	2018–2019	3400	150	–	–	https://www.geothermie-illkirch.es.fr/le-projet/
Insheim	In operation	Muschelkalk to Basement	2	2008 -2010	3750	165	–	4.8	Baumgärtner et al. (2013)
Landau	In operation	Buntsandstein to Basement	2	2005–2006	3256	159	6	3.8	Teza et al. (2008), Schindler et al. (2010)
Offenbach a. d. Queich	Discontinued	Muschelkalk, Buntsandstein	1	2004	2732	–	–	–	Internal reports
Riehen	In operation	Muschelkalk	2	1988	1550	65	5.25	–	Bertleff et al. (1988), Hauber (1993), Mégel and Rybach (2000), Klingler (2010)
Rittershoffen	In operation	Buntsandstein, Basement	2	2012, 2014	2750	170	24	–	Baujard et al. (2017), Mouchot et al. (2018), Duringer et al. (2019)
Soultz-sous Forêts	In operation	Basement	3 + 2	1987–2003	5260	170	-	1.7	Dezayes et al (2005a), Cuenot et al. (2008), Schill et al. (2017), etc.

Table 1 (continued)

Project location	Status	Target reservoir	Number of wells	Year of drilling	Max. depth TVD [m]	Max. temp [°C]	Power generation [MW]		References
							Thermal	Electrical	
Speyer	Oil found	Buntsandstein, Rotliegend	1	2004	?	?	–	–	Internal reports
Trebur	Discontinued	Rotliegend	1	2016	3697	–	–	–	Internal reports
Vendenheim	Discontinued	Basement	2	2017–2019	5393 MD	200	–	–	Boissavy et al. (2019), Sanjuan et al. (2021), Schmittbuhl et al. (2021)
Weinheim	In operation	Hydrobia Beds (Tertiary)	2	2006	1145	65	?	–	Internal reports

Wells for mainly balneological purposes are not included, except for the project in Weinheim where a geothermal doublet was installed

In total, seven realized deep geothermal projects have not been successful in the URG so far due to a variety of technical and political reasons. First of all, induced seismicity, in particular during the enhancement of geothermal systems, but also during operation of the power plant, poses a major risk to these projects (e.g., Majer et al. 2007). The main reason for the seismic activity is the increase in pore pressure due to the reinjection of large volumes of water into the fractured reservoir. This reduces friction along joints and fault zones, which can lead to shear failure if the natural stress state is already critical. The resulting earthquakes are usually of magnitudes less than 2 and thus rarely perceptible. Cornet et al. (1997) could furthermore show for Soultz-sous-Forêts that most of the slip during injection is actually aseismic. Nevertheless, larger events have been detected at various sites in the URG: Basel ($M_L = 3.4$), Landau ($M_L = 2.7$), Insheim ($M_L = 2.4$), Soultz-sous-Forêts ($M_L = 2.9$) and Vendenheim ($M_L = 3.6$) (Deichmann and Giardini 2009; Dorbath et al. 2010; Leydecker 2008; Evans et al. 2012; Schmittbuhl et al. 2021; BGR 2021). In Basel and Vendenheim, seismic activity even led to the complete stop of the projects. Based on these experiences, different methods have been developed to reduce the pore pressure during reinjection. One option is the further decrease of the temperature of the re-injection fluid, which causes the rock to contract and consequently the fracture to open. Alternatively, chemicals can be added to the injection fluid to dissolve mineral precipitates on the joint and fault planes, resulting in increased hydraulic permeability (Portier et al. 2009). Other possibilities to minimize the seismic risk are geomechanical modeling in advance (e.g., Rathnaweera et al. 2020), i.e., to optimize the drilling path and to limit the injection flow rate and pressure and to monitor seismicity before and during drilling, stimulation and production to predict the reaction of the subsurface.

In other projects like Bühl, Bellheim, Cronenbourg, Offenbach a.d. Queich and Trebur, technical problems, insufficient permeability or not reaching the target horizon were the reason for unsuccessful projects. Here it became evident that a detailed

geological and geophysical exploration is essential for the success of deep geothermal projects (Reinecker et al. 2019; Bär et al. 2021a). Especially for the localization of the targeted fault zones, the use of existing or acquisition of new 3D seismic data sets and of data form old oil/gas wells is highly recommended, as they provide a much better spatial resolution than 2D seismic profiles (e.g., Reinhold et al. 2016). Nevertheless, the classical input data (seismic and borehole data) provide only limited information about the hydraulic conditions in targeted aquifers and faults. Integration of secondary geophysical data offer additional insight to characterize the reservoir (e.g., Frey et al. 2021b). Electromagnetic methods (magnetotelluric or controlled source EM, Volpi et al. 2003; Newman et al. 2008; Darnet et al. 2020), for example, can be used to identify high saline fluid flow in the subsurface. Likewise, gravimetric measurements can reveal zones of increased fracture porosity (Guglielmetti et al. 2013; Baillieux et al. 2014; Frey et al. 2022).

Finally, public acceptance is critical to the success of any deep geothermal power plant. The project in Brühl, for example, was stopped in response to poor public acceptance, even though drilling the first well has been successful and a very high flow rate was achieved during a first pumping and injection test (Reinecker et al. 2015). It has been shown that public opinion and knowledge regarding this energy form as well as the perception of potential risks can vary greatly between different locations (Chavot et al. 2019). Chavot et al. (2018) distinguish between "locally anchored" projects, where experiences with geothermal use are already existing and an intensive dialogue takes place, and "unbound" projects, where site selection is purely based on political-economic factors. The latter have a much higher risk of failure, as they are disconnected from local needs. Consequently, it is essential to involve the public in the planning of geothermal projects at an early stage and to communicate the benefits but also the possible risks in a transparent way (Meller et al. 2018). The support of local politicians can have a particularly positive effect on acceptance.

One good example of a transparent communication policy was the one implemented in the Trebur project (https://www.risiko-dialog.ch/projekt/dialoggeo/). The project developers started a public information campaign directly with the first steps of the project and formed a public stakeholder forum (Bürgerbeirat). They developed an own scientific and technical assessment of the project and a list of recommendations and requirements, the project developers declared themselves to fulfill. Additionally, the public information campaign included a detailed project website and six public information workshops, where regional and international experts where invited to present all associated risks and benefits to the public.

To conclude, with every drilling the risk of failure decreases because the technical challenges and the complex geological structure (van der Vaart et al. 2021) become more known. Moreover, as the risks become increasingly controllable and awareness of geothermal energy grows, public acceptance can be expected to improve in the future.

3D models

In the last two decades, a variety of geological 3D models of the URG serving different purposes has been developed. Some of these models cover the whole rift valley, whereas others focus on local structures, e.g., in the area of Soultz-sous-Forêts. Additionally, a lot

of 2D sections reaching the basement rocks through the URG exist and are implemented in GeotIS (Agemar et al. 2010). For a better overview, a selection of models is shown in Fig. 19.

The so far most detailed regional-scale models for geothermal potential assessment were developed during the GeORG (GeORG Projektteam 2013) and Hessen 3D (1.0 and 2.0) (Sass et al. 2011; Arndt et al. 2011; Bär 2012; Bär et al. 2016, 2021b) projects. The first covers the central and southern, the latter the northernmost part of the URG and they include the main geothermal reservoir horizons in the respective region. Modeling of the horizons was mostly based on the available borehole and reflection seismic data

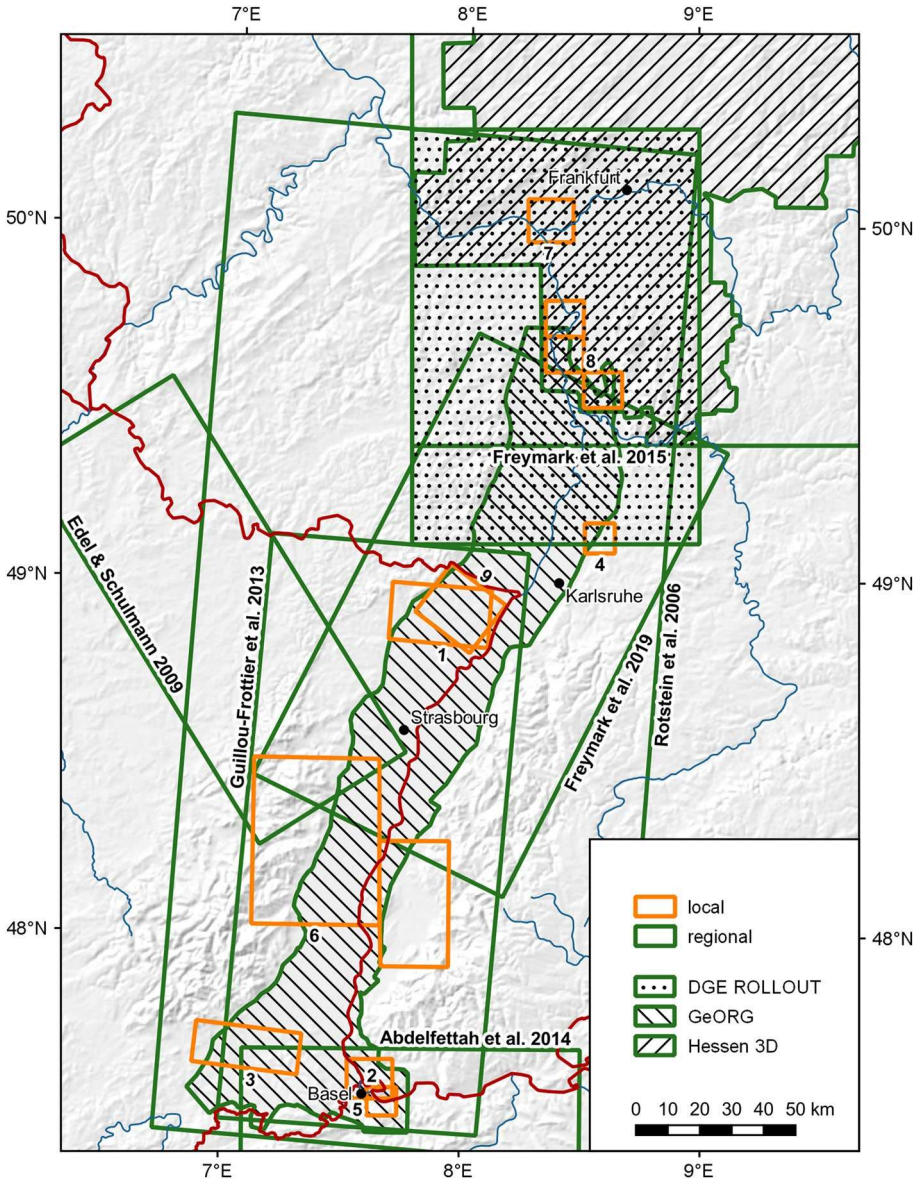

Fig. 19 Selection of published 3D geological models in the URG region. 1 = Dezayes et al. (2011), 2 = Spottke et al. (2005), 3 = Le Carlier de Veslud et al. (2005), 4 & 5 = Meixner et al. (2016), 6 = Bertrand et al. (2005), 7 = Deckert et al. (2017), 8 = Wächter et al. (2018), 9 = Abdelfettah et al. (2020). Note that the Freymark et al. (2020) model area is larger than the map section shown here

(for an overview of the available data see e.g., FIS Geophysik: www.fis-geophysik.de, GeotIS: www.geotis.de, GEORG-Portal: www.geopotenziale.org,). Afterward, the models were parameterized with temperature, hydrogeological and petrophysical data to quantify the deep geothermal potential. Within the framework of the EU-NW-Interreg project DGE-Rollout, these models are being merged and the potential estimation will be carried out again using also newly collected data (Frey et al. 2021b) and uncertainty modeling techniques (van der Vaart et al. 2021). Additional potential assessments on a regional scale in the URG have been performed by e.g., Dornstadter et al. (1999) and Paschen et al. (2003).

Since the classical input data, such as boreholes and 2D and 3D seismics, are not evenly distributed in the URG and only cover certain depth ranges, gravity and magnetic data were additionally used in several models. Particularly noteworthy are the regional studies by Rotstein et al. (2006), Edel and Schulmann (2009), Freymark et al. (2017) and Frey et al. (2021a). The potential field data are often applied to map crustal-scale structures. However, in the case of high-resolution surveys, also near-surface features, for example fault networks (e.g., Deckert et al. 2017; Abdelfettah et al. 2020) or even petrophysical properties can be explored (Frey et al. 2021b). By applying frequency filters to the observed potential fields, information about specific depth ranges can be obtained (pseudo-tomography, Baillieux et al. (2014)).

The numerous deep-reaching fault zones in the URG represent hydraulic pathways for hydrothermal fluids, which significantly increases the influence of convective heat transport. Both up- and downflow of the groundwater can be observed, leading to the formation of locally distinct temperature anomalies, e.g., in Soultz-sous Forêts or Landau. To further investigate this factor, comprehensive 3D groundwater flow models have been developed (Freymark et al. 2019; Guillou-Frottier et al. 2013; Koltzer et al. 2019; Les Landes et al. 2019). These showed a general flow direction from the graben flanks towards the center and from south to north, following the topographic gradient. Moreover, pronounced upflows occur mainly at the central graben axis, where the Rhine river represents the lowest hydraulic head.

Finally, it should be mentioned that a variety of local models exist that aim to explore specific reservoirs or target areas (Bertrand et al. 2005; Spottke et al. 2005; Cornu et al. 2007; Sausse et al. 2010; Dezayes et al. 2011; Lehne et al. 2013; Meixner et al. 2016; Deckert et al. 2017). In most cases, borehole and reflection seismic data served as primary input data, in some cases also gravity data as well as earthquake tomography and hypocenter locations were integrated.

Discussion

Future of geothermal energy in the URG

In the medium to long term, man-made climate change will have a severe impact on all aspects of life through a rise in mean temperatures, an increase in extreme weather events and a rising sea level. To mitigate the consequences of this process, 195 nations committed themselves in the Paris Climate Agreement to limit global warming to well below 2 °C (United Nations 2015). In order to achieve this goal, a rapid reduction of greenhouse emissions is inevitable. Geothermal energy can make an important contribution, since greenhouse gas emissions per unit of energy are

one to two orders of magnitude smaller than for fossil fuels (Lacirignola and Blanc 2013; Douziech et al. 2021). In recent years, the share of renewable energy forms in Germany's electricity production has increased to over 50% in 2020, mainly due to the expansion of wind and solar energy (Frauenhofer ISE 2021). In contrast, the proportion of renewables in the heat supply, which accounts for about half of Germany's energy consumption, stagnates at about 15% (BMWK 2021), leaving a large potential for savings in this sector. This could be enhanced through the large-scale development of deep geothermal power and heating plants, as the technical potential of geothermal energy considerably exceeds the demand in Germany (e.g., Jain et al. 2015).

The URG offers a unique framework of high population densities with several large cities (Frankfurt, Mainz, Wiesbaden, Mannheim, Heidelberg, Strasbourg, Karlsruhe, Basel, Freiburg, etc.), well-established district heating networks and large geothermal resources. Thus, the potential to use deep geothermal energy for the decarbonization of the heating sector is extraordinarily high. The combination of deep geothermal heat generation with medium-deep seasonal heat storage, especially in urban areas with existing district heating networks, allows the inclusion of other renewable energy heat sources. Excess heat can be stored in the summer and extracted again in the winter, when demand is much higher. By doing this, the peak loads can be met more easily by renewable sources without the need of additional fossil fuel or expensive hydrogen boilers. One possible implementation type is the use aquifers in medium depth especially in the Tertiary (aquifer thermal energy storage—ATES, e.g., Dickinson et al. 2009; Fleuchaus et al. 2018, 2021). Here, horizons which have been used in the past for oil and gas production or storage have suitable properties and usually a sufficient impermeable cap-rock to be used for ATES systems even at high temperatures of more than 120 °C (Stricker et al. 2020). Furthermore, deep and hot thermal underground storage is gaining a certain interest and upcoming projects have been reported already (Banks et al. 2021).

So far, deep geothermal energy occupies a rather small niche in the total heat and power supply, because of the comparatively high investment costs and risks. However, modern drilling methods are expected to become more affordable in the near future, which will make this technology much more attractive to investors. Upscaling of geothermal power plants by drilling multiple wells from one drill pad and wells with multilaterals allow to increase the inflow at lower relative costs and thereby ensures economic reservoir operation.

Coproduction and extraction of lithium (or other mineral resources contained in the thermal water) adds a significant economic value and can help to make deep geothermal energy economic without any subsidies in the very near future (e.g., Saevarsdottir et al. 2014). Similarly, the hydrocarbon reservoirs of the URG offer potentials for co-production of heat and oil, which would optimize the use of natural resources (e.g., Ziabakhsh-Ganji et al. 2018). In addition, unsuccessful or exhausted oil and gas wells can be geothermally exploited, e.g., by retrofitting deep borehole heat exchangers (van Horn et al. 2020).

Data availability and uncertainties

To successfully plan and realize any geothermal project accurate knowledge of the subsurface conditions is key. Nowadays, 3D geological models of the concession areas are developed as standard, which are used for potential assessment, planning of well paths or the numerical simulation of reservoir behavior during development and operation. For the URG, a large variety of datasets and models are already available, as presented above. However, it must be considered that all data are subject to some errors. They create uncertainties in models, which can significantly elevate the risk of project failure (Witter et al. 2019). Commonly, three types of errors are distinguished in geological modeling (Cox 1982; Mann 1993): all input datasets are affected by inaccuracies inherent to each individual measurement, which are referred to as Type 1 errors. For example, errors arise with respect to the well path due to wireline stretching or due to precision and accuracy limits of the measurement. On the other hand, seismic interpretation commonly suffers from errors of migration and velocity uncertainty, cumulating in a depth conversion error. Each of these errors need to be analyzed individually to understand and account for them in the final model. While this error is usually small for well data, variations in the velocity model might produce errors of more than 100 m in seismic profiles or cubes. Type 2 errors are associated with the inter- and extrapolation between available data points. Depending on the interpolation method, vastly different results can be obtained, especially where the data density is low. Geostatistical methods such as kriging have been developed to account for the uncertainties (Chilès et al. 2004). Type 3 errors stem from our lack of knowledge and inability to model nature accurately. A typical example is the existence of a fault between two wells, which could not be detected with the available data (e.g., wells and 2D seismic) so far. Here, a 3D seismic survey may close this gap of knowledge considerably and allow for a much better prediction of the fault position, fault type and detailed geometry and orientation in the recent stress field. Type 1 and 2 errors can be quantitatively described as probability density functions and be included in a stochastic uncertainty modeling, whereas type 3 errors are considered as purely qualitative components (Mann 1993).

Within the URG, the presented data and models are subject to all 3 types of errors to varying degrees, as they are based on different source datasets with different levels of accessibility. Depending on whether commercial or open-access data are used, the quality and density may vary substantially. Secondly, when only interpreted data like well markers are available, commonly it cannot be verified or checked for quality against the source. The limited access to source data leads to a significant reduction in the model reliability. Indeed, spatial uncertainties on the vertical position of horizons have been reported with standard deviations of nearly 130 m for the potential Tertiary geothermal reservoirs in the northern URG (van der Vaart et al. 2021). For the older reservoir units, uncertainties are most likely much higher, as the depth is considerably greater, input data sparser and data suitability (e.g., target horizon of seismic exploration) is not always given. However, this situation is subject to change with the new geological data law (Geologiedatengesetz, (Bücker 2021)) which has come into effect in 2021. This law requires geological surveys, institutions and companies to make their data publicly available within 5–10 years after acquisition completion through the respective state authorities, depending on data source and purpose. This should allow for a better understanding

of the subsurface and a reduction of uncertainties. Indeed, Perner (2018) shows a deviation of 30 m between 3D seismic and well data near Stockstadt in the northern part of the URG, indicating unpublished data could decrease errors in many of the public models.

Evaluation of geothermal reservoirs in the URG

For the URG, a total of nine horizons were identified that are suitable for deep geothermal exploitation due to their favorable thermal–hydraulic properties. The question remains which of these reservoirs is locally the most promising considering the local project context, the financial framework conditions and the planned type of utilization. In the following, the pros and cons of the different reservoir horizons will be discussed based on the data presented here and the experiences of past projects.

The crystalline basement presents an attractive target horizon for deep geothermal applications because it is usually is the deepest potential reservoir and thus has the highest reservoir temperatures. Additionally, due to its longest tectonic history it has both several fracture sets and a comparable high fracture density, which are prone to reactivation by recent tectonic events. The large-scale fault zones as targeted in Soultz and Rittershoffen proved to locally act as hydraulic conduits making them primary targets for geothermal exploitation. On the other hand, large-scale fault zones can also lead to the development of high fault core thicknesses with significant hydrothermal alteration and mineral precipitation, decreasing horizontal permeabilities orthogonal to the fault strike direction. However, the likelihood of permeable faults or fractures in the vicinity of large-scale fault zones is significantly increased if the fault has been recently active and has a preferential orientation in the present stress field (high slip- and dilation tendencies). Especially the upper, hydrothermally altered part of the basement, where additional secondary porosity was developed during alteration exhibits a higher hydraulic conductivity than the unaltered basement, where permeability is only controlled by the fracture network. As shown in chapter 6.1 the hydraulic properties of the basement strongly depend on the predominant rock type. Granites, for example, have on average about 1 to 2 magnitudes higher hydraulic conductivities than gneisses (Stober and Bucher 2007). Therefore, crystalline basement reservoirs are more suitable targets where granitic lithologies are predominant compared to metamorphic rock types. Using geophysical exploration data as presented by Frey et al. (2021b) are therefore key to identify suitable areas before selecting a drill site, especially since the lithologic composition of the basement is still subject to large uncertainties in most parts of the URG due to the low density of wells reaching the basement. The encountered natural permeability of the basement is usually not sufficient for an economic operation of a power plant, thus measures to enhance the geothermal reservoir are necessary. The hydraulic stimulation, as well as the regular geothermal operation, of crystalline rocks often induces seismicity, which, in severe cases, led to the termination of a geothermal project (e.g., Basel in 2006/2007 or Vendenheim in 2020/2021). Worldwide research activities (e.g., Grimsel Rock Laboratory, Bedretto Tunnel Laboratory, Äspö, GeoLAB) are currently and in future scientifically addressing this problem at various scales of investigation (Bossart et al. 1991; Schill et al. 2016; Zimmermann et al. 2019; Hertrich et al. 2021), so new stimulation procedures and techniques are in development to enhance the understanding of

hydro- or thermomechanical interactions and can provide the basis to reduce or mitigate induced seismicity in the future. In addition, improved geomechanical models will help to select the most appropriate borehole path, or paths in case of wells with multilateral reservoir completion. In any project, seismic monitoring is required to start well ahead before drilling and accompany testing, stimulation and operation together with a pre-defined reaction plan approved by the respective authorities to mitigate induced seismicity. Another measure to mitigate induced seismicity during reservoir development is chemical stimulation or 'acid cleaning', which has proven to be effective in several projects in the URG (e.g., Soultz, Vendenheim, Rittershoffen).

The Permo-Carboniferous and Triassic sandstones are to be expected in almost the entire URG with varying thicknesses. While the Permo-Carboniferous heterogeneous fine-to-coarse siliciclastic and volcanic rocks are mainly present in the position of SW–NE-striking molasse basins of the Variscan Orogen, the Triassic sandstones are limited in their northern extent by pre-Tertiary erosion roughly at the position of Worms-Bensheim. Again, high reservoir temperatures are usually encountered, allowing for both heat and power production throughout the entire URG. As a result of the strong compaction and cementation, the sandstone matrix shows a permeability one or two orders lower than the permeability created by the connected fracture network (e.g., Bär 2012). Matrix permeability is often additionally reduced by hydrothermal alteration (sandstone bleaching) associated to long-term hydraulically active fault zones further reducing the primary porosity by secondary precipitations (Gaupp et al. 1998). Fluid flow thus occurs mainly along fractures and faults. Based on outcrop analogue studies in the Odenwald and the Palatinate it can be concluded, that compared to the basement, the fracture density is often lower (e.g., Gottschalk 2010), resulting in highly variable lateral hydraulic properties. In the vicinity of faults, very high hydraulic conductivities can be achieved (e.g., in Brühl 1, Reinecker et al. 2019). In order to minimize the exploration risk, drilling inclined wells respecting the fault and fracture set orientation and recent in situ stress field is recommended, which significantly increases the probability of intersecting hydraulically active steeply dipping fault zones and fracture sets. Hydraulic stimulation of the sandstones is associated with reduced seismic risks, since the rock strength is smaller than that of the crystalline basement and part of the pore pressure increase by injection is resulting in poroelastic response of the rock matrix. But inducing seismicity is still possible, especially when faults are targeted that extend into the basement where a pore pressure increase is mainly restricted to the fault zone itself. Additionally, chemical stimulation is a useful reservoir stimulation technique, in particular if carbonatic fracture mineralization has been proven by core or cutting analysis. In these cases, both mineralized fractures and fault zones can be treated and even the connectivity to the rock matrix can be increased (Wiedemann 2021).

The strongly fractured and karstified Upper Muschelkalk features the highest hydraulic conductivity of all investigated units in the URG and thus represents a very interesting reservoir for deep geothermal projects. However, the degree of karstification is highly variable from one to another location. A borehole might easily miss karst cavities and only encounter unkarstified rock. Additionally, the Upper Muschelkalk is only present in the central and southern URG with a thickness of usually less than 100 m which might locally be insufficient to achieve sustainable economic flow

rates. Furthermore, karstification poses an additional risk to drilling operations and well stability during drilling, testing and operation which needs to be accounted for. Similarly, high permeabilities are expected in the karstified Jurassic carbonates, which are limited to the southern URG and are also limited in thickness. Here as well as for the Upper Muschelkalk, karstification is usually fault-bound, while the tectonic block between the faults only show a very limited degree of karstification and thus comparatively lower hydraulic conductivities.

The Cenozoic infill of the URG includes at least three formations with coarse-grained clastic sediments of sufficient thickness that may allow deep geothermal exploitation. Due to the shallower depth, power production might not be feasible with the obtained reservoir temperatures, whereas heat production or seasonal heat storage are promising utilizations. So far, only the installed doublet in Weinheim uses Tertiary sandstones for geothermal heat production. From the oil and gas industry, an extensive dataset including numerous wells, core investigations and seismic lines exists, which can significantly minimize exploration costs and risks (Hintze et al. 2018; Van der Vaart et al. 2021). In contrast to the deeper reservoirs, the matrix permeability of the coarse-grained clastic Tertiary sediments of the Pechelbronn Formation, the Froidefontaine Formation and the Niederrödern Formation could allow for sufficient flow rates in geothermal wells. The frequently occurring interlayering by clay and silt horizons may have a negative effect on conductivity, especially along fault zones, where clay smear effects might seal the fault. Of particular interest are the Tertiary marginal facies along the eastern and western boundary fault of the URG, which often have a much higher share of coarse-grained sediments and a much higher lateral reservoir connectivity compared to the clay dominated basinal facies along the graben axis.

In summary, all geological units suitable as deep geothermal reservoirs in the URG have been identified with certain pros and cons. The approach of exploiting multiple reservoirs with one well, e.g., Landau, Insheim, Illkirch and Rittershoffen, also appears to be an adequate method for increasing the flow rates. In the past, the goal was in many cases to drill as deep as possible in order to obtain maximum temperatures produced at wellhead. However, convective heat transport along recently active fault zones in the URG leads to a significant increase in the geothermal gradient (up to more than 10 K/100 m) above the convection cells. In these areas, adequate reservoir temperatures may prevail even at shallow depths. In contrast, in the convection-dominated interval, the geothermal gradient is usually very small (e.g., Soultz-sous-Forêts), meaning that greater well depths do not result in a significant increase in heat production. Note that convection can also lead to negative temperature anomalies when dense near-surface groundwater is transported downwards along faults. In areas of the URG that are less influenced by active fault zones, conductive heat transport dominates, with gradients between about 3 and 6 K/100 m. Thus, the aim of exploration should be primarily to identify the reservoirs in areas of positive geothermal anomalies in the vicinity of the above-mentioned fault zones (Bär et al. 2021). High-temperature heat pumps can be used if necessary to raise the temperature level, especially in the combined utilization of deep geothermal reservoirs and medium deep reservoirs for seasonal heat storage.

Conclusions

In this review, a comprehensive overview of the geological and geothermal situation of the URG is given. The region exhibits an overall very high potential for deep geothermal utilization. Nine potential reservoir horizons have been identified and were characterized with respect to their distribution and thickness, lithology, structural geology, hydrochemistry, hydraulics and petrophysics. These include the crystalline basement, the Permo-Carboniferous sandstones, the Buntsandstein, the Upper Muschelkalk, the Hauptrogenstein, the Upper Jurassic Limestones, the Pechelbronn Formation, the Froidefontaine Formation and the Niederrödern Formation, showing suitable temperatures and permeabilities depending on the location. However, as a result of the multistage tectonic and diagenetic evolution and hydrothermal alteration, complex reservoirs with double porosity (fracture-matrix, fracture-karstification) have formed. The strong heterogeneity of relevant properties between and within geologic units remains therefore a key challenge in defining the exploration and drilling target.

The abundant, hydraulically active fault zones in the URG can serve as major fluid conduits and thus also contribute significantly to the development of temperature anomalies in the subsurface. Compared to the intact rock matrix, large-scale faults often show significantly increased permeabilities, making them preferred targets for geothermal projects. In this context, the location of fault planes in the ambient stress field may be used as a proxy for permeability (slip and dilatation tendency). That said, mineral precipitation, particularly in the fault core, can also act as a natural fluid barrier. In order to reduce exploration risks as much as possible, new comprehensive exploration concepts combining different methods (3D seismics, electromagnetic methods, gravimetry, magnetics, hydrochemistry, gradient wells, slim hole exploration wells) are required. This includes also rigorous statistical modeling of uncertainties that takes into account the intrinsic errors of individual measurements.

In addition to geological uncertainties, economic aspects of course play a crucial role in the realization of geothermal projects. Upscaling power plants through multiwell systems and multilateral drilling can help to save costs and thus increase economic efficiency. Besides, co-production of lithium presents an additional revenue stream that could enable economic power and heat production even without subsidies. Apart from the classical deep geothermal system for power and heat supply, the URG offers a high potential for seasonal heat storage via ATES, which can compensate the mismatch between production and demand of heat at the surface.

Abbreviations

ATES	Aquifer thermal energy storage
BO	Borehole breakouts (BO)
CSGC	Central Schwarzwald Gneiss Complex
DST	Drill stem tests
ECRIS	European Cenozoic Rift System
EGS	Enhanced geothermal system
EM	Electromagnetic methods
EMBF	Eastern Main Boundary Fault
FMS	Earthquake focal mechanisms
LOT	Leak-off tests
DIFT	Drilling-induced tensile fractures
MGCH	Mid-Germany Crystalline High
REV	Representative elementary volume
SSGC	Southern Schwarzwald Gneiss Complex

TDS	Total dissolved solids
Td	Dilation tendency
Ts	Slip tendency
URG	Upper Rhine Graben
WMBF	Western Main Boundary Fault

Acknowledgements
We acknowledge support by the Deutsche Forschungsgemeinschaft (DFG—German Research Foundation) and the Open Access Publishing Fund of Technical University of Darmstadt.

Author contributions
MF: conception, analysis and interpretation of data, drafting and revision of the text; KB: conception, analysis and interpretation of data, drafting and revision of the text; IS: analysis and interpretation of data, drafting and revision of the text; JR: analysis and interpretation of data, drafting and revision of the text; JV: drafting and revision of the text; IS: revision of the text. All authors read and approved the final manuscript.

Funding
Open Access funding enabled and organized by Projekt DEAL. This study was funded by the Interreg NWE Program through the Roll-out of Deep Geothermal Energy in North-West Europe (DGEROLLOUT) Project www.nweurope.eu/DGE-Rollout). The Interreg NWE Program is part of the European Cohesion Policy and is financed by the European Regional Development Fund (ERDF).

Availability of data and materials
A large quantity of research data were presented in this review, most of which are freely available. The respective studies have been cited accordingly. Detailed information on the individual datasets is provided in the main text.

Declarations

Competing interests
We have no conflicts of interest to disclose.

Received: 16 February 2022 Accepted: 17 August 2022
Published online: 29 September 2022

References

Abdelfettah Y, Hinderer J, Calvo M, Dalmais E, Maurer V, Genter A. Using highly accurate land gravity and 3D geologic modeling to discriminate potential geothermal areas: application to the Upper Rhine Graben. France GEOPHYSICS. 2020;85(2):G35–56.
Achtziger-Zupančič P, Loew S, Mariéthoz G. A new global database to improve predictions of permeability distribution in crystalline rocks at site scale. J Geophys Res. 2017;122(5):3513–39. https://doi.org/10.1002/2017JB014106.
AG Energiebilanzen. Energieverbrauch in Deutschland im Jahr 2021; 2022. https://ag-\.de/wp-content/uploads/2022/04/AGEB_Jahresbericht2021_20220524_dt_Web.pdf. Accessed 29 Aug 2022.
Agemar T. Bottom hole temperature correction based on empirical correlation. Geothermics. 2022;99: 102296. https://doi.org/10.1016/j.geothermics.2021.102296.
Agemar T, Schellschmidt R, Schulz R. Subsurface temperature distribution of Germany. Geothermics. 2012;44:65–77. https://doi.org/10.1016/j.geothermics.2012.07.002.
Agemar T, Brunken J, Jodocy M, Schellschmidt R, Schulz R, Stober I. Untergrundtemperaturen in Baden-Württemberg. ZDGG. 2013;164(1):49–62. https://doi.org/10.1127/1860-1804/2013/0010.
Agemar T, Hese F, Moeck I, Stober I. Kriterienkatalog für die Erfassung tiefreichender Störungen und ihrer geothermischen Nutzbarkeit in Deutschland. ZDGG. 2017;168(2):285–300. https://doi.org/10.1127/zdgg/2017/0084.
Agemar T, Alten JA, Ganz B, Kuder J, Kühne K, Schumacher S, Schulz R. GeotIS–das Geothermische Informationssystem für Deutschland. In: Der Geothermiekongress, 17–19 November 2010, Karlsruhe, Germany; 2010. https://www.geothermie.de/fileadmin/useruploads/aktuelles/Geothermiekongress/2010/Programmuebersicht_DGK_2010_1009_2.pdf. Accessed 29 August 2022.
Ahlers S, Henk A, Hergert T, Reiter K, Müller B, Röckel L, et al. 3D crustal stress state of Germany according to a data-calibrated geomechanical model. Solid Earth. 2021;12(8):1777–99. https://doi.org/10.5194/se-12-1777-2021.
Ahorner L. Historical seismicity and present-day microearthquake activity of the Rhenish Massif, Central Europe. In: Fuchs K, Gehlen K, Mälzer H, Murawski H, Semmel A, editors. Plateau uplift: the rhenish shield—a case history. Berlin: Springer, Berlin Heidelberg; 1983. p. 198–221 (**10.1007/978-3-642-69219-2_27**).
Ahorner L, Schneider G. Herdmechanismen von Erdbeben im Oberrheingraben und in seinen Randgebirgen. In: Illies JH, Fuchs K, editors. Approaches to taphrogenesis. Stuttgart: Schweizerbart; 1974. p. 104–17.
Aigner T, Bachmann GH. Sequence-stratigraphic framework of the German Triassic. Sed Geol. 1992;80(1–2):115–35. https://doi.org/10.1016/0037-0738(92)90035-P.
Altenberger U, Besch T. The Böllstein Odenwald: evidence for pre- to early Variscan plate convergence in the Central European variscides. Int J Earth Sci. 1993;82(3):475–88. https://doi.org/10.1007/BF00212411.
Anderle H-J, Franke W, Schwab M. III.C.1 stratigraphy. In: Dallmeyer RD, Franke W, Weber K, editors. Pre-Permian geology of Central and Eastern Europe. Berlin: Springer, Berlin Heidelberg; 1995. p. 99–107.
Andres J, Schad A. Seismische Kartierung von Bruchzonen im mittleren und nördlichen Teil des Oberrheintalgrabens und deren Bedeutung für die Ölansammlung. Erdöl Und Kohle. 1959;5:323–34.

Anthes G, Reischmann T. New 207Pb/206Pb single zircon evaporation ages from the central part of the Mid German Crystalline Rise. Terra Nostra. 1997;97(5):10.
Anthes G, Reischmann T. Timing of granitoid magmatism in the eastern mid-German crystalline rise. J Geodyn. 2001;31(2):119–43. https://doi.org/10.1016/S0264-3707(00)00024-7.
Aretz A, Bär K, Götz AE, Sass I. Outcrop analogue study of Permocarboniferous geothermal sandstone reservoir formations (northern Upper Rhine Graben, Germany): impact of mineral content, depositional environment and diagenesis on petrophysical properties. Int J Earth Sci. 2016;105(5):1431–52. https://doi.org/10.1007/s00531-015-1263-2.
Arndt D, Bär K, Fritsche J-G, Sass I, Hoppe A. 3D structural model of the Federal State of Hesse (Germany) for geopotential evaluation. ZDGG. 2011;162(4):353–69. https://doi.org/10.1127/1860-1804/2011/0162-0353.
Arndt D. Geological structural modelling of Hesse to determine geopotentials (Geologische Strukturmodellierung von Hessen zur Bestimmung von Geopotenzialen) [PhD thesis]: Technische Universität Darmstadt; 2012.
Azzola J, Valley B, Schmittbuhl J, Genter A. Stress characterization and temporal evolution of borehole failure at the Rittershoffen geothermal project. Solid Earth. 2019;10(4):1155–80. https://doi.org/10.5194/se-10-1155-2019.
Bächler D, Kohl T, Rybach L. Impact of graben-parallel faults on hydrothermal convection−–Rhine Graben case study. Phys Chem Earth. 2003;28:431–41. https://doi.org/10.1016/S1474-7065(03)00063-9.
Backhaus E. Limnische und fluviatile Sedimentation im südwestdeutschen Buntsandstein. Int J Earth Sci. 1974;63(3):925–42. https://doi.org/10.1007/BF01821318.
Backhaus E, Heim D. Die fluvio-lakustrine Fazies des Übergangsbereichs Plattensandstein/Rötquarzit (Oberer Buntsandstein) im mittleren Odenwald unter besonderer Berücksichtigung der Violetten Zone. Geol Jb Hessen. 1995;123:49–68.
Bahlburg H, Vervoort JD, DuFrane SA. Plate tectonic significance of Middle Cambrian and Ordovician siliciclastic rocks of the Bavarian Facies, Armorican Terrane Assemblage, Germany—U-Pb and Hf isotope evidence from detrital zircons. Gondwana Res. 2010;17(2–3):223–35. https://doi.org/10.1016/j.gr.2009.11.007.
Baillieux P, Schill E, Edel JB, Mauri G. Localization of temperature anomalies in the Upper Rhine Graben: insights from geophysics and neotectonic activity. Int Geol Rev. 2013;55(14):1744–62. https://doi.org/10.1080/00206814.2013.794914.
Baillieux P, Schill E, Abdelfettah Y, Dezayes C. Possible natural fluid pathways from gravity pseudo-tomography in the geothermal fields of Northern Alsace (Upper Rhine Graben). Geotherm Energy. 2014. https://doi.org/10.1186/s40517-014-0016-y.
Banks J, Poulette S, Grimmer J, Bauer F, Schill E. Geochemical changes associated with high-temperature heat storage at intermediate depth: thermodynamic equilibrium models for the deepstor site in the Upper Rhine Graben, Germany. Energies. 2021;14(19):6089. https://doi.org/10.3390/en14196089.
Bankwitz E, Bankwitz P. Lower Paleozoic series at the southern margin of the Central German Crystalline Zone. Terranes in the circum-Atlantic Paleozoic orogens.(Abstr vol, unpubl). 1990.
Bär K, Hintze M, Weinert S, Sippel J, Freymark J, Scheck-Wenderoth M, Sass I. Das Verbundprojekt Hessen 3D 20. Geotherm Energie. 2016;3(85):24–5.
Bär K, Reinsch T, Bott J. The PetroPhysical Property Database (P^3)—a global compilation of lab-measured rock properties. Earth Syst Sci Data. 2020;12(4):2485–515. https://doi.org/10.5194/essd-12-2485-2020.
Bär K, Reinecker J, Bott J, Cacace M, Frey M, van der Vaart J, et al. Integrated Exploration Strategy 'ConvEx' to detect Hydrothermal Convection in the Subsurface. In: World Geothermal Congress 2020; April - October 2021a; Reykjavik, Iceland; 2021a.
Bär K, Schäffer R, Weinert S, Sass I. Schlussbericht Verbundprojekt „Hessen 3D 2.0": 3D-Modell der geothermischen Tiefenpotenziale von Hessen: Technical University of Darmstadt; 2021b.
Bär K. 3D-Modellierung des tiefengeothermischen Potenzials des nördlichen Oberrheingrabens und Untersuchung der geothermischen Eigenschaften des Rotliegend [Diplomathesis]: Technical University Of Darmstadt; 2008.
Bär K. Assessment of the deep geothermal potentials of Hessen (Untersuchung der tiefengeothermischen Potenziale von Hessen) [PhD thesis]: Technische Universität Darmstadt; 2012.
Barnasch J. Der Keuper im Westteil des Zentraleuropäischen Beckens (Deutschland, Niederlande, England, Dänemark): diskontinuierliche Sedimentation, Litho-, Zyklo- Und Sequenzstratigraphie. SDGG. 2010;71:7–169. https://doi.org/10.1127/sdgg/71/2010/7.
Barth A, Ritter J, Wenzel F. Spatial variations of earthquake occurrence and coseismic deformation in the Upper Rhine Graben, Central Europe. Tectonophysics. 2015;651–652:172–85. https://doi.org/10.1016/j.tecto.2015.04.004.
Barth G, Franz M, Heunisch C, Ernst W, Zimmermann J, Wolfgramm M. Marine and terrestrial sedimentation across the T-J transition in the North German Basin. Palaeogeogr Palaeoclimatol Palaeoecol. 2018;489:74–94. https://doi.org/10.1016/j.palaeo.2017.09.029.
Barton CA, Zoback MD, Moos D. Fluid flow along potentially active faults in crystalline rock. Geology. 1995;23(8):683. https://doi.org/10.1130/0091-7613(1995)023%3c0683:FFAPAF%3e2.3.CO;2.
Baujard C, Genter A, Dalmais E, Maurer V, Hehn R, Rosillette R, et al. Hydrothermal characterization of wells GRT-1 and GRT-2 in Rittershoffen, France: implications on the understanding of natural flow systems in the Rhine graben. Geothermics. 2017;65:255–68. https://doi.org/10.1016/j.geothermics.2016.11.001.
Baumgärtner J, Teza D, Wahl G. Gewinnung geothermischer Energie durch Entwicklung und Zirkulation eines Störungssystems im Kristallin und deren mikroseismische Überwachung am Beispiel des Geothermieprojektes Insheim (Internal Report No. 0325158): Bestec GmbH; 2013.
Baumgärtner J, Kölbel T, Mergner H, Schlagermann P, Hettkamp T, Teza D, Lerch C. Betriebserfahrungen mit den Geothermiekraftwerken Landau, Insheim und Bruchsal. BBR Fachmagazine fur Brunnen und Leitungsbau. 2013:48–57.
Bear J. Hydraulics of groundwater. New York: McGraw-Hill Book Comp; 1979.
Behr HJ, Heinrichs T. Geological interpretation of DEKORP 2-S: a deep seismic reflection profile across the Saxothuringian and possible implications for the Late Variscan structural evolution of Central Europe. Tectonophysics. 1987;142(2–4):173–202. https://doi.org/10.1016/0040-1951(87)90122-3.
Behr H-J, Engel W, Franke W. Variscan wildflysch and nappe tectonics in the Saxothuringian Zone (Northeast Bavaria, West Germany). Am J Sci. 1982;282(9):1438–70. https://doi.org/10.2475/ajs.282.9.1438.

Behr H-J, Engel W, Franke W, Giese P, Weber K. The Variscan Belt in Central Europe: main structures, geodynamic implications, open questions. Tectonophysics. 1984;109(1–2):15–40. https://doi.org/10.1016/0040-1951(84)90168-9.
Behr H-J, Dürbaum H-J, Bankwitz P, Bankwitz E, Benek R, Berger H-J, et al. Crustal structure of the Saxothuringian Zone: Results of the deep seismic profile MVE-90 (East). Z Geol Wiss. 1994;22(6):647–770.
Behrmann JH, Hermann O, Horstmann M, Tanner DC, Bertrand G. Anatomy and kinematics of oblique continental rifting revealed: a three-dimensional case study of the southeast Upper Rhine graben (Germany). Bulletin. 2003;87(7):1105–21. https://doi.org/10.1306/02180300153.
Behrmann JH, Ziegler PA, Schmid SM, Heck B, Granet M. The EUCOR-URGENT Project. Int J Earth Sci. 2005;94(4):505–6. https://doi.org/10.1007/s00531-005-0513-0.
Belka Z, Narkiewicz M. Devonian. In: McCann T, editor. The Geology of Central Europe: Volume 1: Precambrian and Palaeozoic. London: Geological Society of London; 2008. p. 383–410.
Berger J-P, Reichenbacher B, Becker D, Grimm M, Grimm K, Picot L, et al. Paleogeography of the Upper Rhine Graben (URG) and the Swiss Molasse Basin (SMB) from Eocene to Pliocene. Int J Earth Sci. 2005;94(4):697–710. https://doi.org/10.1007/s00531-005-0475-2.
Bertleff B, Joachim H, Koziorowski G, Leiber J, Ohmert W, Prestel R, et al. Ergebnisse der Hydrogeothermiebohrungen in Baden-Württemberg. GLAB. 1988;30:27–116.
Bertrand G, Horstmann M, Hermann O, Behrmann JH. Retrodeformation of the southern Upper Rhine Graben: new insights on continental oblique rifting. Quatern Sci Rev. 2005;24(3–4):345–52. https://doi.org/10.1016/j.quascirev.2004.07.011.
Betten I. 3D-Laserscanning, DFN-Modellierung und Aufschlussaufnahme im Rotliegend des östlichen Saar-Nahe-Beckens [Masterthesis]. Darmstadt: Technische Universität Darmstadt; 2015.
BGR. Geologische Karte der Bundesrepublik Deutschland 1 : 1 000 000 (GK1000); 2016.
BGR. Der Geodatendienst für Erdbeben in Deutschland - GERSEIS. 2021. https://www.bgr.bund.de/DE/Themen/Erdbeben-Gefaehrdungsanalysen/Seismologie/Seismologie/GERSEIS/gerseis_node.html. Accessed 12 Dec 2021.
Blundell DJ, Freeman R, Mueller S, Button S. A continent revealed: the European Geotraverse, structure and dynamic evolution. Cambridge: Cambridge University Press; 1992.
BMWK. Energiedaten: Gesamtausgabe. Bundesministerium für Wirtschaft und Klimaschutz; 2022. https://www.bmwk.de/Redaktion/DE/Artikel/Energie/energiedaten-gesamtausgabe.html. Accessed 29 August 2022.
Böcker J. Petroleum system and thermal history of the Upper Rhine Graben - Implications from organic geochemical analyses, oil-source rock correlations and numerical modelling [PhD thesis]: RWTH Aachen; 2015.
Boigk H, Schöneich H. The Rhinegraben: geologic history and neotectonic activity—Perm, Trias und älterer Jura im Bereich der südlichen Mittelmeer-Mjösen-Zone und des Rheingrabens. In: Illies JH, Fuchs K, editors. Approaches to Taphrogenesis. Stuttgart: Schweizerbart; 1974. p. 60–72.
Boissavy C, Henry L, Genter A, Pomart A, Rocher P, Schmidlé-Bloch V. Geothermal Energy Use, Country Update for France. In: European Geothermal Congress; 11.-14. June; Den Haag; 2019.
Bonjer K-P. Seismicity pattern and style of seismic faulting at the eastern borderfault of the southern Rhine Graben. Tectonophysics. 1997;275(1–3):41–69. https://doi.org/10.1016/S0040-1951(97)00015-2.
Bonjer K-P, Gelbke C, Gilg B, Rouland D, Mayer-Rosa D, Massinon B. Seismicity and dynamics of the Upper Rhinegraben. J Geophys. 1984;55(1):1–12.
Bossart P, Mazurek M, Hellmuth KH, Siitari-Kauppi M, Schneebeli M. Grimsel Test Site: Structural geology and water flow-paths in the migration shear-zone: Nationale Genossenschaft fuer die Lagerung Radioaktiver Abfaelle (NAGRA); 1991. https://www.nagra.ch/de/technical-report-91-12. Accessed 29 Aug 2022.
Bossennec C, Géraud Y, Böcker J, Klug B, Mattioni L, Bertrand L, Moretti I. Characterisation of fluid flow conditions and paths in the Buntsandstein Gp. sandstones reservoirs. Upper Rhine Graben BSGF. 2021;192:35. https://doi.org/10.1051/bsgf/2021027.
Bossennec C, Géraud Y, Böcker J, Klug B, Mattioni L, Sizun J-P, et al. Evolution of diagenetic conditions and burial history in Buntsandstein Gp. fractured sandstones (Upper Rhine Graben) from in-situ δ18O of quartz and 40Ar/39Ar geochronology of K-feldspar overgrowths. Int J Earth Sci. 2021;110(8):2779–802. https://doi.org/10.1007/s00531-021-02080-2.
Bossennec C, Frey M, Seib L, Bär K, Sass I. Multiscale characterisation of fracture patterns of a crystalline reservoir analogue. Geosciences. 2021. https://doi.org/10.3390/geosciences11090371.
Bossennec C. Evolution of transfer properties of sandstones by diagenesis and deformation : Case study on Buntsandstein Gp. sandstones, Upper Rhine Graben: Évolution des propriétés de transfert des grès par diagénèse et déformation : application aux formations du Buntsandstein Gp., Graben du Rhin: Université de Lorraine; 2019.
Boy JA, Haneke J, Kowalczyk G, Lorenz V, Schindler T, Thum H. Rotliegend im Saar-Nahe-Becken, am Taunus-Südrand und im nördlichen Oberrheingraben. SDGG. 2012;61:254–377. https://doi.org/10.1127/sdgg/61/2012/254.
Brady P, Lopez C, Sassani D. Granite hydrolysis to form deep brines. Energies. 2019;12(11):2180. https://doi.org/10.3390/en12112180.
Brigaud B, Vincent B, Carpentier C, Robin C, Guillocheau F, Yven B, Huret E. Growth and demise of the Jurassic carbonate platform in the intracratonic Paris Basin (France): interplay of climate change, eustasy and tectonics. Mar Pet Geol. 2014;53:3–29. https://doi.org/10.1016/j.marpetgeo.2013.09.008.
Brun JP, Gutscher M-A. Deep crustal structure of the Rhine Graben from dekorp-ecors seismic reflection data: a summary. Tectonophysics. 1992;208(1–3):139–47. https://doi.org/10.1016/0040-1951(92)90340-C.
Buchmann TJ, Connolly PT. Contemporary kinematics of the Upper Rhine Graben: a 3D finite element approach. Global Planet Change. 2007;58(1–4):287–309. https://doi.org/10.1016/j.gloplacha.2007.02.012.
Buchner F. Rhinegraben: Horizontal stylolites indicating stress regimes of earlier stages of rifting. Tectonophysics. 1981;73(1–3):113–8. https://doi.org/10.1016/0040-1951(81)90178-5.
Bücker C. Das Geologiedatengesetz GeolDG—was ist neu? Geotherm Energie. 2021;99:28–30.
Caine JS, Evans JP, Forster CB. Fault zone architecture and permeability structure. Geology. 1996;24(11):1025. https://doi.org/10.1130/0091-7613(1996)024%3c1025:FZAAPS%3e2.3.CO;2.

Carpenter AB. Origin and chemical evolution of brines in sedimentary basins. In: SPE Annual Fall Technical Conference and Exhibition; October 1978; Houston, Texas. OnePetro: OnePetro; 1978. https://doi.org/10.2118/7504-MS.
Chavot P, Heimlich C, Masseran A, Serrano Y, Zoungrana J, Bodin C. Social shaping of deep geothermal projects in Alsace: politics, stakeholder attitudes and local democracy. Geotherm Energy. 2018. https://doi.org/10.1186/s40517-018-0111-6.
Chavot P, Masseran A, Bodin C, Heimlich C, Serrano Y, Zoungrana J. Public perception of geothermal projects in Alsace: between energy transition and territorial rooting. In: European Geothermal Congress; 11.-14. June; Den Haag; 2019.
Chen F, Hegner E, Todt W. Zircon ages and Nd isotopic and chemical compositions of orthogneisses from the Black Forest, Germany: evidence for a Cambrian magmatic arc. Int J Earth Sci. 2000;88(4):791–802. https://doi.org/10.1007/s005310050306.
Chilès J, Aug C, Guillen A, Lees T. Modelling the Geometry of Geological Units and its Uncertainty in 3D From Structural Data: The Potential-Field Method. In: Orebody Modelling and Strategic Mine Planning; 22 - 24 November; Perth; 2004. p. 313–320.
Clauser C. Conductive and convective heat flow components in the Rheingraben and implications for the deep permeability distribution. In: Beck AE, editor. Hydrogeological regimes and their subsurface thermal effects. Washington: DC; 1989. p. 59–64.
Clauser C, Villinger H. Analysis of conductive and convective heat transfer in a sedimentary basin, demonstrated for the Rheingraben. Geophys J Int. 1990;100(3):393–414. https://doi.org/10.1111/j.1365-246X.1990.tb00693.x.
Cloetingh S, Ziegler PA, Beekman F, Andriessen PAM, Hardebol N, Dèzes P. Intraplate deformation and 3D rheological structure of the Rhine Rift System and adjacent areas of the northern Alpine foreland. Int J Earth Sci. 2005;94(4):758–78. https://doi.org/10.1007/s00531-005-0502-3.
Commission of the European Communities. Geothermische Synthese des Oberrheingrabens. BRGM Alsace & Geologisches Landesamt Baden-Württemberg; 1979. https://lgrbwissen.lgrbbw.de/geothermische-synthese-des-oberrheingrabens-bestandsaufnahme. Accessed 29 Aug 2022.
Cornet FH, Helm J, Poitrenaud H, Etchecopar A. Seismic and aseismic slips induced by large-scale fluid injections. Pure Appl Geophys. 1997;150:563–83. https://doi.org/10.1007/978-3-0348-8814-1_12.
Cornet FH, Bérard T, Bourouis S. How close to failure is a granite rock mass at a 5km depth? Int J Rock Mech Min Sci. 2007;44(1):47–66. https://doi.org/10.1016/j.ijrmms.2006.04.008.
Cornu T, Cardozo GL, Cloetingh S, Beekman F. A structural model from local earthquake tomography: application to present-day tectonics of the Upper Rhine Graben. Global Planet Change. 2007;58(1–4):270–86. https://doi.org/10.1016/j.gloplacha.2007.03.008.
Coward MP. Structural and tectonic setting of the Permo-Triassic basins of northwest Europe. Geol Soc Spec Publ. 1995;91(1):7–39. https://doi.org/10.1144/GSL.SP.1995.091.01.02.
Cox LA. Artifactual uncertainty in risk analysis. Risk Anal. 1982;2(3):121–35. https://doi.org/10.1111/j.1539-6924.1982.tb01375.x.
Crowley QG, Floyd PA, Winchester JA, Franke W, Holland JG. Early Palaeozoic rift-related magmatism in Variscan Europe: fragmentation of the Armorican Terrane Assemblage. Terra Nova. 2000;12(4):171–80. https://doi.org/10.1046/j.1365-3121.2000.00290.x.
Cuenot N, Charléty J, Dorbath L, Haessler H. Faulting mechanisms and stress regime at the European HDR site of Soultz-sous-Forêts, France. Geothermics. 2006;35(5–6):561–75. https://doi.org/10.1016/j.geothermics.2006.11.007.
Cuenot N, Faucher J-P, Fritsch D, Genter A, Szablinski D. The European EGS project at Soultz-sous-Forêts: From extensive exploration to power production. In: 2008 IEEE Power & Energy Society General Meeting; 7/20/2008 - 7/24/2008; Pittsburgh, PA. Pittsburgh, Pa.: IEEE: IEEE; 2008. p. 1–8. https://doi.org/10.1109/PES.2008.4596680.
Dallmeyer RD, Franke W, Weber K, editors. Pre-Permian Geology of Central and Eastern Europe. Berlin: Springer, Berlin Heidelberg; 1995.
Darnet M, Wawrzyniak P, Coppo N, Nielsson S, Schill E, Fridleifsson G. Monitoring geothermal reservoir developments with the Controlled-Source Electro-Magnetic method—a calibration study on the Reykjanes geothermal field. J Volcanol Geoth Res. 2020;391: 106437. https://doi.org/10.1016/j.jvolgeores.2018.08.015.
Deckert H, Bauer W, Abe S, Horowitz F, Schneider U. Geophysical greenfield exploration in the permo-carboniferous Saar-Nahe basin—the Wiesbaden Geothermal Project, Germany. Geophys Prospect. 2017. https://doi.org/10.1111/1365-2478.12598.
Deichmann N, Ernst J. Earthquake focal mechanisms of the induced seismicity in 2006 and 2007 below Basel (Switzerland). Swiss J Geosci. 2009. https://doi.org/10.1007/s00015-009-1336-y.
Deichmann N, Giardini D. Earthquakes induced by the stimulation of an enhanced geothermal system below Basel (Switzerland). Seismol Res Lett. 2009;80(5):784–98. https://doi.org/10.1785/gssrl.80.5.784.
Derer C, Kosinowski M, Luterbacher HP, Schäfer A, Süß MP. Sedimentary response to tectonics in extensional basins: the Pechelbronn Beds (Late Eocene to early Oligocene) in the northern Upper Rhine Graben, Germany. Geological Society, London, Special Publications. 2003;208(1):55–69. https://doi.org/10.1144/GSL.SP.2003.208.01.03.
Derer CE, Schumacher ME, Schäfer A. The northern Upper Rhine Graben: basin geometry and early syn-rift tectono-sedimentary evolution. Int J Earth Sci. 2005;94(4):640–56. https://doi.org/10.1007/s00531-005-0515-y.
Dersch-Hansmann M, Hug N. Oberer und Mittlerer Buntsandstein im Untergrund des Dieburger Beckens. Geologisches Jahrbuch Hessen. 2004;131:81–95.
Deutsche Stratigraphische Kommission. Stratigraphische Tabelle von Deutschland 2016: Potsdam (Deutsches GeoForschungsZentrum); 2016. ISBN 978-3-9816597-7-1. https://gfzpublic.gfzpotsdam.de/pubman/item/item_2524907. Accessed 29 Aug 2022.
Dezayes C, Genter A, Valley B. Structure of the low permeable naturally fractured geothermal reservoir at Soultz. CR Geosci. 2010;342(7–8):517–30. https://doi.org/10.1016/j.crte.2009.10.002.
Dezayes C, Gentier S, Genter A. Deep Geothermal Energy in Western Europe: The Soultz-Project: Final Report. BRGM; 2005a. http://infoterre.brgm.fr/rapports/RP-54227-FR.pdf. Accessed 29 Aug 2022.

Dezayes C, Chevremont P, Tourlière B, Homeier G, Genter A. Geological study of the GPK4 HFR borehole and correlation with the GPK3 borehole (Soultz-sous-Forêts, France). BRGM; 2005b. http://infoterre.brgm.fr/rapports/RP-53697-FR.pdf. Accessed 29 Aug 2022.
Dezayes C, Beccaletto L, Oliviero G, Baillieux P, Capar L, Schill E. 3-D Visualization of a Fractured Geothermal Field: The Example of the EGS Soultz Site (Northern Upper Rhine Graben, France). In: Stanford University, ed. Thirty-Sixth Workshop on Geothermal Reservoir Engineering; 31. January—2. February; Stanford, California; 2011.
Dèzes P, Schmid SM, Ziegler PA. Evolution of the European Cenozoic Rift System: interaction of the Alpine and Pyrenean orogens with their foreland lithosphere. Tectonophysics. 2004;389(1–2):1–33. https://doi.org/10.1016/j.tecto.2004.06.011.
Dickinson JS, Buik N, Matthews MC, Snijders A. Aquifer thermal energy storage: theoretical and operational analysis. Géotechnique. 2009;59(3):249–60. https://doi.org/10.1680/geot.2009.59.3.249.
Doebl F. The Tertiary and Pleistocene sediments of the northern and central part of the Upper Rhinegraben. Abh Geol Landesamts Baden-Württemb. 1967;6:48–54.
Doebl F. Die tertiären und quartären Sedimente des südlichen Rheingrabens. In: Illies JH, Mueller S, editors. Graben problems. Stuttgart: Schweizerbart; 1970. p. 56–66.
Doebl F, Olbrecht W. An isobath map of the Tertiary base in the Rhinegraben. In: Illies JH, Fuchs K, editors. Approaches to Taphrogenesis. Stuttgart: Schweizerbart; 1974. p. 71–2.
Doebl F. Zur Geologie und Geothermik im mittleren Oberrheingraben. Fortschr. Geol. Rheinld. u. Westf. 1979;27:1–17.
Dorbath L, Evans K, Cuenot N, Valley B, Charléty J, Frogneux M. The stress field at Soultz-sous-Forêts from focal mechanisms of induced seismic events: Cases of the wells GPK2 and GPK3. CR Geosci. 2010;342(7–8):600–6. https://doi.org/10.1016/j.crte.2009.12.003.
Dornstadter J, Kappelmeyer O, Welter M. The geothermal potential in the Upper Rhine Graben valley. In: European Geothermal Conference Basel 1999; 28.-30. September; Basel, Switzerland; 1999.
Doublier MP, Potel S, Franke W, Roache T. Very low-grade metamorphism of Rheno-Hercynian allochthons (Variscides, Germany): facts and tectonic consequences. Int J Earth Sci. 2012;101(5):1229–52. https://doi.org/10.1007/s00531-011-0718-3.
Doubre C, Meghraoui M, Masson F, Lambotte S, Jund H, Bès de Berc M, Grunberg M. Seismotectonics in Northeastern France and neighboring regions. Comptes Rendus Géosci. 2021;353(S1):153–85. https://doi.org/10.5802/crgeos.80.
Douziech M, Tosti L, Ferrara N, Parisi ML, Pérez-López P, Ravier G. Applying harmonised geothermal life cycle assessment guidelines to the rittershoffen geothermal heat plant. Energies. 2021;14(13):3820. https://doi.org/10.3390/en14133820.
Drüppel K, Stober I, Grimmer JC, Mertz-Kraus R. Experimental alteration of granitic rocks: implications for the evolution of geothermal brines in the Upper Rhine Graben, Germany. Geothermics. 2020;88: 101903. https://doi.org/10.1016/j.geothermics.2020.101903.
Duringer P, Aichholzer C, Orciani S, Genter A. The complete lithostratigraphic section of the geothermal wells in Rittershoffen (Upper Rhine Graben, eastern France): a key for future geothermal wells. BSGF. 2019;190:13. https://doi.org/10.1051/bsgf/2019012.
Durst H. Aspects of exploration history and structural style in the Rhine graben area. Generation, accumulation and production of Europe's hydrocarbons. Eur Assoc Petrol Geosci Spec Publ. 1991;1:247–61.
Duwiquet H, Guillou-Frottier L, Arbaret L, Bellanger M, Guillon T, Heap MJ. Crustal Fault Zones (CFZ) as geothermal power systems: a preliminary 3D THM model constrained by a multidisciplinary approach. Geofluids. 2021;2021:1–24. https://doi.org/10.1155/2021/8855632.
Eckelmann K, Nesbor H-D, Königshof P, Linnemann U, Hofmann M, Lange J-M, Sagawe A. Plate interactions of Laurussia and Gondwana during the formation of Pangaea—constraints from U-Pb LA–SF–ICP–MS detrital zircon ages of Devonian and Early Carboniferous siliciclastics of the Rhenohercynian zone Central European Variscides. Gondwana Res. 2014;25(4):1484–500. https://doi.org/10.1016/j.gr.2013.05.018.
Edel JB, Fluck P. The upper Rhenish Shield basement (Vosges, Upper Rhinegraben and Schwarzwald): main structural features deduced from magnetic, gravimetric and geological data. Tectonophysics. 1989;169(4):303–16. https://doi.org/10.1016/0040-1951(89)90093-0.
Edel JB, Schulmann K. Geophysical constraints and model of the "Saxothuringian and Rhenohercynian subductions - magmatic arc system" in NE France and SW Germany. Bull Soc Geol Fr. 2009;180:545–58. https://doi.org/10.2113/gssgfbull.180.6.545.
Edel JB, Weber K. Cadomian terranes, wrench faulting and thrusting in the central Europe Variscides: geophysical and geological evidence. Int J Earth Sci. 1995. https://doi.org/10.1007/BF00260450.
Edel J-B, Whitechurch H, Diraison M. Seismicity wedge beneath the Upper Rhine Graben due to backwards Alpine push? Tectonophysics. 2006;428(1–4):49–64. https://doi.org/10.1016/j.tecto.2006.08.009.
Edel JB, Schulmann K, Rotstein Y. The Variscan tectonic inheritance of the Upper Rhine Graben: evidence of reactivations in the Lias, Late Eocene-Oligocene up to the recent. Int J Earth Sci. 2007;96(2):305–25. https://doi.org/10.1007/s00531-006-0092-8.
Edel JB, Maurer V, Dalmais E, Genter A, Richard A, Letourneau O, Hehn R. Structure and nature of the Palaeozoic basement based on magnetic, gravimetric and seismic investigations in the central Upper Rhinegraben. Geothermal Energy. 2018;6(1):13. https://doi.org/10.1186/s40517-018-0099-y.
Eisbacher GH, Lüschen E, Wickert F. Crustal-scale thrusting and extension in the Hercynian Schwarzwald and Vosges, central Europe. Tectonics. 1989;8(1):1–21. https://doi.org/10.1029/TC008i001p00001.
El Dakak W. Influence of Temporal Variation of Water Saturation on Shallow Geothermal Systems Using Numerical Modeling [Masterthesis]: TU Darmstadt; 2015.
Ernst M. Lithostratigraphische und fazielle Untersuchungen des Hauptrogensteins (Bajocium) im SE-Oberrheingraben. Jahresberichte und Mitteilungen des Oberrheinischen Geologischen Vereins. 1991:311–82. https://doi.org/10.1127/jmogv/73/1991/311.
Esslinger G. Rezente Bodenbewegungen über dem Salinar des südlichen Oberrheingrabens [PhD thesis]: TU Berlin; 1968.

Esteban L, Pimienta L, Sarout J, Piane CD, Haffen S, Geraud Y, Timms NE. Study cases of thermal conductivity prediction from P-wave velocity and porosity. Geothermics. 2015;53:255–69. https://doi.org/10.1016/j.geothermics.2014.06.003.

Evans JP, Forster CB, Goddard JV. Permeability of fault-related rocks, and implications for hydraulic structure of fault zones. J Struct Geol. 1997;19(11):1393–404. https://doi.org/10.1016/S0191-8141(97)00057-6.

Evans KF, Genter A, Sausse J. Permeability creation and damage due to massive fluid injections into granite at 3.5 km at Soultz: 1. Borehole observations. J Geophys Res. 2005. https://doi.org/10.1029/2004JB003168.

Evans K, Zappone A, Kraft T, Deichmann N, Moia F. A survey of the induced seismic responses to fluid injection in geothermal and CO2 reservoirs in Europe. Geothermics. 2012;41:30–54. https://doi.org/10.1016/j.geothermics.2011.08.002.

Fäh D, Gisler M, Jaggi B, Kästli P, Lutz T, Masciadri V, et al. The 1356 Basel earthquake: an interdisciplinary revision. Geophys J Int. 2009;178(1):351–74. https://doi.org/10.1111/j.1365-246X.2009.04130.x.

Falk F, Franke W, Kurze M. Stratigraphy. In: Dallmeyer RD, Franke W, Weber K, editors. Pre-Permian Geology of Central and Eastern Europe. Berlin: Springer, Berlin Heidelberg; 1995. p. 221–34.

Faridfar N. Untersuchung und Bewertung der geothermischen Eigenschaften der Gesteine der Noerdlichen Pyllitzone, Vordertaunus [Bachelorthesis]: TU Darmstadt; Goethe Universität Frankfurt am Main; 2010.

Faulkner DR, Jackson C, Lunn RJ, Schlische RW, Shipton ZK, Wibberley C, Withjack MO. A review of recent developments concerning the structure, mechanics and fluid flow properties of fault zones. J Struct Geol. 2010;32(11):1557–75. https://doi.org/10.1016/j.jsg.2010.06.009.

Fazies DG, Paläogeographie und Genese des unteren Buntsandsteins norddeutscher Auffassung im südlichen Beckenbereich. Notizbl. hess. L.-Amt Bodenforsch. 1966;94:132–57.

Fei L, Niu J, Linsel A, Hinderer M, Scheuvens D, Petschick R. Rock alteration at the post-Variscan nonconformity: implications for Carboniferous-Permian surface weathering versus burial diagenesis and paleoclimate evaluation. Solid Earth. 2021;12:1165–84. https://doi.org/10.5194/se-2020-221.

Feist-Burkhardt S, Götz A, Szulc J, Borkhataria R, Geluk M, Haas J, et al. Triassic. In: McCann T, editor., et al., The geology of Central Europe: Volume 2: Mesozoic and Cenozoic. London: Geological Society of London; 2008. p. 749–821.

Ferrill DA, Morris AP. Dilational normal faults. J Struct Geol. 2003;25(2):183–96. https://doi.org/10.1016/S0191-8141(02)00029-9.

Fleuchaus P, Godschalk B, Stober I, Blum P. Worldwide application of aquifer thermal energy storage—a review. Renew Sustain Energy Rev. 2018;94:861–76. https://doi.org/10.1016/j.rser.2018.06.057.

Fleuchaus P, Schüppler S, Stemmle R, Menberg K, Blum P. Aquiferspeicher in Deutschland. Grundwasser. 2021;26(2):123–34. https://doi.org/10.1007/s00767-021-00478-y.

Flöttmann T, Oncken O. Contraints on the evolution of the Mid German Crystalline Rise—a study of outcrops west of the river Rhine. Geol Rundsch. 1992;82(2):515–43. https://doi.org/10.1007/bf01828613.

Floyd PA. Igneous Activity. In: Dallmeyer RD, Franke W, Weber K, editors. Pre-Permian Geology of Central and Eastern Europe. Berlin: Springer, Berlin Heidelberg; 1995. p. 59–81.

Franke W. Tectonostratigraphic units in the Variscan belt of central Europe. Geol Soc Am Bull. 1989;230:67–90. https://doi.org/10.1130/SPE230-p67.

Franke W. III.B.1 Stratigraphy. In: Dallmeyer RD, Franke W, Weber K, editors. Pre-Permian Geology of Central and Eastern Europe. Berlin: Springer, Berlin Heidelberg; 1995a. p. 33–49.

Franke W. Rhenohercynian foldbelt: autochthon and nonmetamorphic units—stratigraphy. In: Dallmeyer RD, Franke W, Weber K, editors. Pre-Permian Geology of Central and Eastern Europe. Berlin: Springer, Berlin Heidelberg; 1995b. p. 33–49.

Franke W. Saxothuringian Basin. In: Dallmeyer RD, Franke W, Weber K, editors. Pre-Permian Geology of Central and Eastern Europe. Berlin: Springer, Berlin Heidelberg; 1995c. p. 217–8.

Franke W. The mid-European segment of the Variscides: tectonostratigraphic units, terrane boundaries and plate tectonic evolution. Geol Soc Spec Publ. 2000;179:35–61. https://doi.org/10.1144/GSL.SP.2000.179.01.05.

Franke W, Cocks LRM, Torsvik TH. The Palaeozoic Variscan oceans revisited. Gondwana Res. 2017;48:257–84. https://doi.org/10.1016/j.gr.2017.03.005.

Franz M, Bachmann GH, Barnasch J, Heunisch C, Röhling H-G. Der Keuper in der Stratigraphischen Tabelle von Deutschland 2016 – kontinuierliche Sedimentation in der norddeutschen Beckenfazies (Variante B). ZDGG. 2018;169(2):203–24. https://doi.org/10.1127/zdgg/2018/0114.

Frauenhofer ISE. Öffentliche Nettostromerzeugung in Deutschland im Jahr 2020. Fraunhofer-Institut für Solare Energiesysteme ISE. 2021. https://www.energy-charts.info/downloads/Stromerzeugung_2020_1.pdf. Accessed 29 Aug 2022.

Frenzel G. Die Mineralparagenese der Albersweiler Lamprophyre. Neues J Mineral Abh. 1971;115:164–91.

Frey M, Weinert S, Bär K, van der Vaart J, Dezayes C, Calcagno P, Sass I. Integrated 3D geological modelling of the northern Upper Rhine Graben by joint inversion of gravimetry and magnetic data. Tectonophysics. 2021b;813: 228927. https://doi.org/10.1016/j.tecto.2021.228927.

Frey M, Bossennec C, Seib L, Bär K, Schill E, Sass I. Interdisciplinary fracture network characterization in the crystalline basement: a case study from the Southern Odenwald, SW Germany. Solid Earth. 2022;13(6):935–55. https://doi.org/10.5194/se-13-935-2022.

Frey M, Weinert S, Bär K, van der Vaart J, Dezayes C, Calcagno P, Sass I. 3D Geological Model of the Crystalline Basement in the Northern Upper Rhine Graben Region. Technical University Of Darmstadt; 2021a. https://doi.org/10.48328/tudatalib-417.2.

Freymark J, Sippel J, Scheck-Wenderoth M, Bär K, Stiller M, Fritsche J-G, Kracht M. The deep thermal field of the Upper Rhine Graben. Tectonophysics. 2017;694:114–29. https://doi.org/10.1016/j.tecto.2016.11.013.

Freymark J, Bott J, Cacace M, Ziegler M, Scheck-Wenderoth M. Influence of the main border faults on the 3D hydraulic field of the Central Upper Rhine Graben. Geofluids. 2019;2019:1–21. https://doi.org/10.1155/2019/7520714.

Freymark J, Sippel J, Scheck-Wenderoth M, Bär K, Stiller M, Fritsche J-G, Kracht M. The thermal field of the Upper Rhine Graben – Temperature predictions based on a 3D model. In: European Geothermal Congress; 19.-23. September; Strasbourg, France; 2016.
Freymark J, Bott J, Scheck-Wenderoth M, Bär K, Stiller M, Fritsche J-G, et al. 3D-URG: 3D gravity constrained structural model of the Upper Rhine Graben; 2020. https://doi.org/10.5880/GFZ.4.5.2020.004.
Fritsche R, Rüter H. Seismizität. In: Bauer MJ, editor. Handbuch Tiefe Geothermie: Prospektion, Exploration, Realisierung, Nutzung. Berlin: Springer Spektrum; 2014. p. 397–427.
Gaupp R, Clauer N, Bauer A, Eynatten H von, Baaske U, Mezger J. Untersuchung des Einflusses von Diagenese im Bereich von Störungen anhand von Oberflächenaufschlüssen – Buntsandstein westlich der Rheingraben-Randstörung zwischen Bad Bergzabern und Leistadt / Bad Drükheim: Bericht zur Piotstudie 10/97 bis 5/98: Friedrich-Schiller-Universität Jena; CNRS Strasbourg; 1998.
Gaupp R, Nickel B. Die Pechelbronn-Schichten im Raum Eich-Stockstadt (Nördlicher Oberrheingra-ben; Blatt 6216 Gernsheim). Geol Jb Hessen. 2001;128:19–27.
Genter A, Traineau H. Analysis of macroscopic fractures in granite in the HDR geothermal well EPS-1, Soultz-sous-Fore^ts, France. J Volcanol Geoth Res. 1996;72(1–2):121–41. https://doi.org/10.1016/0377-0273(95)00070-4.
Genter A, Evans K, Cuenot N, Fritsch D, Sanjuan B. Contribution of the exploration of deep crystalline fractured reservoir of Soultz to the knowledge of enhanced geothermal systems (EGS). CR Geosci. 2010;342(7–8):502–16. https://doi.org/10.1016/j.crte.2010.01.006.
GeORG Projektteam. Geopotenziale des tieferen Untergrundes im Oberrheingraben: Fachlich-Technischer Abschlussbericht des INTERREG-Projekts GeORG; 2013. https://www.geopotenziale.org/products/fta?lang=1. Accessed 29 Aug 2022.
Gérard A, Kappelmeyer O. The Soultz-sous-Forêts project. Geothermics. 1987;16(4):393–9. https://doi.org/10.1016/0375-6505(87)90018-6.
Geyer G, Elicki O, Fatka O, Zylinska A. Cambrian. In: McCann T, editor. The Geology of Central Europe: Volume 1: Precambrian and Palaeozoic. London: Geological Society of London; 2008. p. 155–202.
Geyer OF, Gwinner MP, Simon T. Geologie von Baden-Württemberg. 5th ed. Stuttgart: Schweizerbart; 2011.
Giardini D, Wössner J, Danciu L. Mapping Europe's Seismic hazard. Eos Trans AGU. 2014;95(29):261–2. https://doi.org/10.1002/2014EO290001.
Gonzalez R. Response of shallow-marine carbonate facies to third-order and high-frequency sea-level fluctuations: Hauptrogenstein Formation, northern Switzerland. Sed Geol. 1996;102(1–2):111–30. https://doi.org/10.1016/0037-0738(95)00059-3.
Gonzalez R, Wetzel A. Stratigraphy and paleogeography of the Hauptrogenstein and Klingnau Formations (middle Bajocian to late Bathonian), northern Switzerland. Eclogae Geol Helv. 1996. https://doi.org/10.5169/seals-167921.
Gottschalk K. Oberflächenanaloge zu geothermischen Reservoiren im mittleren Oberrheingraben - Kristallin, Rotliegend und Buntsandstein im südlichen Pfälzerwald [Diplomathesis]: Universität Freiburg i. Br.; 2010.
Götz AE, Gast S. Basin evolution of the Anisian Peri-Tethys: implications from conodont assemblages of Lower Muschelkalk key sections (Central Europe). ZDGG. 2010;161(1):39–49. https://doi.org/10.1127/1860-1804/2010/0161-0039.
Götz AE. Zyklen und Sequezen im Unteren Muschelkalk des Germanischen Beckens. Hallesches Jb. Geowiss. 2004;Beih. 18:91–8.
Grasby SE, Betcher RN. Regional hydrogeochemistry of the carbonate rock aquifer, southern Manitoba. Can J Earth Sci. 2002;39(7):1053–63. https://doi.org/10.1139/E02-021.
Griffiths L, Heap MJ, Wang F, Daval D, Gilg HA, Baud P, et al. Geothermal implications for fracture-filling hydrothermal precipitation. Geothermics. 2016;64:235–45. https://doi.org/10.1016/j.geothermics.2016.06.006.
Grimm MC. Beiträge zur Lithostratigraphie des Paläogens und Neogens im Oberrheingebiet (Oberrheingraben, Mainzer Becken, Hanauer Becken). Geol JB Hessen. 2005;132:79–112.
Grimm KI, Grimm MC, Schindler T. Lithostratigraphic subdivision of the Rupelian and Chattian in the Mainz Basin. Germany Njgpa. 2000;218(3):343–97. https://doi.org/10.1127/njgpa/218/2000/343.
Grimm MC, Wielandt-Schuster U, Hottenrott M, Radtke G, Berger J-P, Ellwanger D, et al. Oberrheingraben (Tertiär des Oberrheingrabens). SDGG. 2011;75:57–132. https://doi.org/10.1127/sdgg/75/2011/57.
Grimmer JC, Ritter JRR, Eisbacher GH, Fielitz W. The Late Variscan control on the location and asymmetry of the Upper Rhine Graben. Int J Earth Sci. 2017;106(3):827–53. https://doi.org/10.1007/s00531-016-1336-x.
Grösser J, Dörr W. MOR-type basalts of the Eastern Rhenish Massif. NJGPM. 1986;1986(12):705–22. https://doi.org/10.1127/njgpm/1986/1986/705.
Grünthal G, Stromeyer D, Bosse C, Cotton F, Bindi D. The probabilistic seismic hazard assessment of Germany—version 2016, considering the range of epistemic uncertainties and aleatory variability. Bull Earthquake Eng. 2018;16(10):4339–95. https://doi.org/10.1007/s10518-018-0315-y.
Gu Y, Rühaak W, Bär K, Sass I. Using seismic data to estimate the spatial distribution of rock thermal conductivity at reservoir scale. Geothermics. 2017;66:61–72. https://doi.org/10.1016/j.geothermics.2016.11.007.
Gu Y. Calculations of the Optimized Design for an Existing Multifunction Building with Borehole Heat Exchangers [Masterthesis]: TU Darmstadt; 2010.
Gudmundsson A, Berg SS, Lyslo KB, Skurtveit E. Fracture networks and fluid transport in active fault zones. J Struct Geol. 2001;23(2–3):343–53. https://doi.org/10.1016/S0191-8141(00)00100-0.
Guglielmetti L, Comina C, Abdelfettah Y, Schill E, Mandrone G. Integration of 3D geological modeling and gravity surveys for geothermal prospection in an Alpine region. Tectonophysics. 2013;608:1025–36. https://doi.org/10.1016/j.tecto.2013.07.012.
Guillou-Frottier L, Carrè C, Bourgine B, Bouchot V, Genter A. Structure of hydrothermal convection in the Upper Rhine Graben as inferred from corrected temperature data and basin-scale numerical models. J Volcanol Geoth Res. 2013;256:29–49. https://doi.org/10.1016/j.jvolgeores.2013.02.008.
Guillou-Frottier L, Duwiquet H, Launay G, Taillefer A, Roche V, Link G. On the morphology and amplitude of 2D and 3D thermal anomalies induced by buoyancy-driven flow within and around fault zones. Solid Earth. 2020;11(4):1571–95. https://doi.org/10.5194/se-11-1571-2020.

Haffen S, Geraud Y, Diraison M, Dezayes C. Determination of fluid-flow zones in a geothermal sandstone reservoir using thermal conductivity and temperature logs. Geothermics. 2013;46:32–41. https://doi.org/10.1016/j.geothermics.2012.11.001.
Haffen S, Géraud Y, Diraison M, Dezayes C. Determining majors fluid-flow zones in a geothermal sandstone reservoir from thermal conductivity and temperature logs. In: EGU General Assembly; 2012. p. 9043.
Haffen S, Géraud Y, Diraison M. Geothermal, structural and petrophysical characteristics of Buntsandstein sandstone reservoir (Upper Rhine Graben, France). In: World Geothermal Congress; 19.-24. April; Melbourne, Australia; 2015.
Hagdorn H. Triassic Muschelkalk of Central Europe. In: Hess H, Ausich WI, Brett CE, Simms MJ, editors. Fossil crinoids. Cambridge: Cambridge University Press; 1999. p. 164–76.
Hann HP, Chen F, Zedler H, Frisch W, Loeschke J. The Rand Granite in the southern Schwarzwald and its geodynamic significance in the Variscan belt of SW Germany. Int J Earth Sci. 2003;92(6):821–42. https://doi.org/10.1007/s00531-003-0361-8.
Häring MO, Schanz U, Ladner F, Dyer BC. Characterisation of the Basel 1 enhanced geothermal system. Geothermics. 2008;37(5):469–95. https://doi.org/10.1016/j.geothermics.2008.06.002.
Hauber L. Der südliche Rheingraben und seine geothermische Situation. Bulletin der Vereinigung Schweiz. Petroleum-Geologen und -Ingenieure. 1993. doi:https://doi.org/10.5169/seals-216879.
He K, Stober I, Bucher K. Chemical evolution of thermal waters from limestone aquifers of the Southern Upper Rhine Valley. Appl Geochem. 1999;14(2):223–35. https://doi.org/10.1016/S0883-2927(98)00046-8.
Heap MJ, Kushnir ARL, Gilg HA, Wadsworth FB, Reuschlé T, Baud P. Microstructural and petrophysical properties of the Permo-Triassic sandstones (Buntsandstein) from the Soultz-sous-Forêts geothermal site (France). Geotherm Energy. 2017. https://doi.org/10.1186/s40517-017-0085-9.
Hegner E, Chen F, Hann H. Chronology of basin closure and thrusting in the internal zone of the Variscan belt in the Schwarzwald, Germany: evidence from zircon ages, trace element geochemistry, and Nd isotopic data. Tectonophysics. 2001;332(1–2):169–84. https://doi.org/10.1016/S0040-1951(00)00254-7.
Heidbach O, Rajabi M, Reiter K, Ziegler M, WSM Team. World Stress Map Database Release 2016; 2016. https://doi.org/10.5880/WSM.2016.001.
Henk A. Mächtigkeit und Alter der erodierten Sedimente im Saar-Nahe-Becken (SW-Deutschland). Int J Earth Sci. 1992;81(2):323–31. https://doi.org/10.1007/BF01828601.
Henk A. Late orogenic Basin evolution in the Variscan internides: the Saar-Nahe Basin, southwest Germany. Tectonophysics. 1993;223(3–4):273–90. https://doi.org/10.1016/0040-1951(93)90141-6.
Henk A. Late-Orogenic Burial and Exhumation at a Major Variscan Suture Zone. In: Oncken O, editor. Basement Tectonics 11 Europe and Other Regions. Dordrecht: Springer; 1996.
Henrion E, Masson F, Doubre C, Ulrich P, Meghraoui M. Present-day deformation in the Upper Rhine Graben from GNSS data. Geophys J Int. 2020;223(1):599–611. https://doi.org/10.1093/gji/ggaa320.
Hermanrud C, Cao S, Lerche I. Estimates of virgin rock temperature derived from BHT measurements: bias and error. Geophysics. 1990;55(7):924–31. https://doi.org/10.1190/1.1442908.
Hertrich M, Brixel B, Broeker T, et al. Characterization, Hydraulic Stimulation, and Fluid Circulation Experiments in the Bedretto Underground Laboratory for Geosciences and Geoenergies. In: 55th US Rock Mechanics/Geomechanics Symposium; 2021.
Herzberger P, Münch W, Kölbel T, Bruchmann U, Schlagermann P, Hötzl H, et al. The Geothermal Power Plant Bruchsal. In: World Geothermal Congress 2010; 25–29 April; Bali, Indonesia; 2010.
Hess JC, Schmidt G. Zur Altersstellung der Kataklasite im Bereich der Otzberg-Zone, Odenwald. Geol JB Hessen. 1989;117:69–77.
Hesse J. Untersuchung des geothermischen Potenzials der effusiven Vulkanite der permischen Donnersberg-Formation [Bachelorthesis]: TU Darmstadt; 2011.
Hinsken S, Ustaszewski K, Wetzel A. Graben width controlling syn-rift sedimentation: the Palaeogene southern Upper Rhine Graben as an example. Int J Earth Sci. 2007;96(6):979–1002. https://doi.org/10.1007/s00531-006-0162-y.
Hintze M, Plasse B, Bär K, Sass I. Preliminary studies for an integrated assessment of the hydrothermal potential of the Pechelbronn Group in the northern Upper Rhine Graben. Adv Geosci. 2018;45:251–8. https://doi.org/10.5194/adgeo-45-251-2018.
Hirschmann G. IV.B Lithological Characteristics. In: Dallmeyer RD, Franke W, Weber K, editors. Pre-Permian Geology of Central and Eastern Europe. Berlin: Springer, Berlin Heidelberg; 1995. p. 155–63.
Hoffmann H. Bestimmung von geothermischen Kennwerten an Gesteinen des Kellerwaldes [Bachelorthesis]: TU Darmstadt; Goethe Universität Frankfurt am Main; 2011.
Hoffmann H. Petrophysikalische Eigenschaften der Mitteldeutschen Kristallinschwelle im Bereich des Oberrheingrabens [Masterthesis]: TU Darmstadt; 2015.
Hölting B, Coldewey WG. Hydrogeologie: Einführung in die allgemeine und angewandte Hydrogeologie; 90 Tabellen. 7th ed. Heidelberg: Spektrum Akad. Verl; 2009.
Homuth B, Rümpker G, Deckert H, Kracht M. Seismicity of the northern Upper Rhine Graben—constraints on the present-day stress field from focal mechanisms. Tectonophysics. 2014;632:8–20. https://doi.org/10.1016/j.tecto.2014.05.037.
Homuth B, Stiller M, Schmidt B. Reprocessed deep seismic reflection profile DEKORP 1988–9N across the Northern Upper Rhine Graben. Southwest Germany. 2021a. https://doi.org/10.5880/GFZ.DEKORP-9N.002.
Homuth B, Bär K, Weinert S, Sass I. Reprocessing of the hessian DEKORP seismic profiles. In: DGG, ed. 81. Jahrestagung der Deutschen Geophysikalischen Gesellschaft; 01.-05. March 2021b; Kiel; 2021b. p. 182.
Homuth S. Aufschlussanalogstudie zur Charakterisierung oberjurassischer geothermischer Karbonatreservoire im Molassebecken [PhD thesis]. Darmstadt: Technische Universität Darmstadt; 2014.
Housse B-A. Reconnaisance du potentiel géothermique du Buntsadnstein à Strasbourg-Cronenbourg. Géothermie Actualités. 1984;1:36–41.
Hückel B, Kappelmeyer O. Geothermische untersuchungen im saarkarbon. ZDGG_ALT. 1966;117(1):280–311.

Huckriede H, Wemmer K, Ahrendt H. Palaeogeography and tectonic structure of allochthonous units in the German part of the Rheno-Hercynian Belt (Central European Variscides). Int J Earth Sci. 2004;93(3):414–31. https://doi.org/10.1007/s00531-004-0397-4.
Hug N, Vero G. Ein vollständiges Zechsteinprofil im südlichen Odenwald: die hydrogeologische Erkundungsbohrung Langenthal BK2/05. Geol JB Hessen. 2008;135:25–45.
Hug N. Sedimentgenese und Paläogeographie des höheren Zechstein bis zur Basis des Buntsandstein in der Hessischen Senke. Hessisches Landesamt für Umwelt; 2004.
Hurter S, Schellschmidt R. Atlas of geothermal resources in Europe. Geothermics. 2003;32(4–6):779–87. https://doi.org/10.1016/S0375-6505(03)00070-1.
Hüttner R. Bau und Entwicklung des Oberrheingrabens. Ein Überblick mit historischer Rückschau. Geol Jahrbuch. 1991;48:17–42.
Illies JH, Mueller S, editors. Graben problems. Stuttgart: Schweizerbart; 1970.
Illies JH, Fuchs K, editors. Approaches to Taphrogenesis. Stuttgart: Schweizerbart; 1974.
Illies JH. Ancient and recent rifting in the Rhinegraben. Geol En Mijnbouw. 1977;56(4):329–50.
Illies JH. Two Stages Rheingraben Rifting. In: Ramberg IB, Neumann ER, editors. Tectonics and geophysics of continental rifts. Dordrecht: D. Reidel Publ. Comp; 1978. p. 63–71.
Illies JH, Greiner G. Holocene movements and state of stress in the rhinegraben rift system. Dev Geotecton. 1979;13:349–59. https://doi.org/10.1016/B978-0-444-41783-1.50057-X.
Ingebritsen SE, Manning CE. Geological implications of a permeability-depth curve for the continental crust. Geology. 1999;27(12):1107. https://doi.org/10.1130/0091-7613(1999)027%3c1107:GIOAPD%3e2.3.CO;2.
Jafari A, Babadagli T. Effective fracture network permeability of geothermal reservoirs. Geothermics. 2011;40(1):25–38. https://doi.org/10.1016/j.geothermics.2010.10.003.
Jain C, Vogt C, Clauser C. Maximum potential for geothermal power in Germany based on engineered geothermal systems. Geotherm Energy. 2015. https://doi.org/10.1186/s40517-015-0033-5.
Jensen B. Geothermische Untersuchung des Hauptrogenstein im suedlichen Oberrheingraben [Bachelorsthesis]: TU Darmstadt; 2014.
Jodocy M, Stober I. Development of an internet based geothermal information system for Germany-region Baden-Wuerttemberg; Aufbau eines geothermischen Informationssystems fuer Deutschland-Landesteil Baden-Wuerttemberg. Erdoel Erdgas Kohle. 2008;124.
Jodocy M, Stober I. Geologisch-geothermische Tiefenprofile für den baden-württembergischen Teil des nördlichen und mittleren Oberrheingrabens. Erdöl Erdgas Kohle. 2010a;126(2):68–76.
Jodocy M, Stober I. Geologisch-geothermische Tiefenprofile für den südlichen Teil des Oberrheingrabens in Baden-Württemberg. Z Geol Wiss. 2010b;38(1):3–25.
Jodocy M, Stober I. Porositäten und Permeabilitäten im Oberrheingraben und südwestdeutschen Molassebecken. Erdöl Erdgas Kohle. 2011;127(1):20–7.
Jolley SJ, Dijk H, Lamens JH, Fisher QJ, Manzocchi T, Eikmans H, Huang Y. Faulting and fault sealing in production simulation models: Brent Province, northern North Sea. Pet Geosci. 2007;13(4):321–40. https://doi.org/10.1144/1354-079306-733.
Kappelmeyer O, Haenel R. Geothermics with special reference to application. Berlin: Gebrueder Borntraeger; 1974.
Karro E, Marandi A, Vaikme R. The origin of increased salinity in the Cambrian-Vendian aquifer system on the Kopli Peninsula, northern Estonia. Hydrogeol J. 2004. https://doi.org/10.1007/s10040-004-0339-z.
Kemnitz H, Romer RL, Oncken O. Gondwana break-up and the northern margin of the Saxothuringian belt (Variscides of Central Europe). Int J Earth Sci. 2002;91(2):246–59. https://doi.org/10.1007/s005310100209.
Kharaka YK, Hanor JS. Deep fluids in the continents: I. Sedimentary basins. In: Drever JI, ed. Surface and Groundwater, Weathering, and Soils. Treatise on Geochemistr. Elsevier Pergamon; 2003. p. 499–540. https://doi.org/10.1016/B0-08-043751-6/05085-4.
Kirsch H, Kober B, Lippolt HJ. Age of intrusion and rapid cooling of the Frankenstein gabbro (Odenwald, SW-Germany) evidenced by40Ar/39Ar and single-zircon207Pb/206Pb measurements. Int J Earth Sci. 1988;77(3):693–711. https://doi.org/10.1007/BF01830178.
Klapperer S. Zur Fazies des Buntsandsteins im Odenwald und nördlichen Oberrheingraben [Diplomathesis]: Universität Jena; 2009.
Kläske U. Bestimmung des geothermischen Potenzials des Kristallinen Odenwaldes [Bachelorthesis]: TU Darmstadt; 2010.
Klingler P. Charakterisierung des Geothermischen Reservoirs Riehen: 3D-Struktur und Tracer-Test [Masterthesis]. Neuchâtel: Université de Neuchâtel; 2010.
Klügel T, Ahrendt H, Oncken O, Käfer N, Schäfer F, Weiss B. Age and Provenance of the Sediments and the Detritus of the Northern Phyllite Zone (South Taunus). ZDGG_ALT. 1994;145(1):172–91. https://doi.org/10.1127/zdgg/145/1994/172.
Klügel T. Geometrie und Kinematik einer variszischen Plattengrenze: der Südrand des Rhenoherzynikums im Taunus. Hessisches Landesamt für Bodenforschung; 1997. ISBN: 3895318035.
Klumbach S. Petrophysical properties of geothermal reservoir rocks in the Upper Rhine Graben from surface outcrops [Masterthesis]: Albert-Ludwigs-Universität Freiburg; 2010.
Knaust D. Invertebrate trace fossils and ichnodiversity in shallow-marine carbonates of the German Middle Triassic (Muschelkalk). SEPM Special Publication. 2006;88:223–40.
Kock N, Kaltschmitt M. Geothermisch erschließbare Niedertemperaturwärmesenken in Deutschland—identifikation und Quantifizierung. Z Energiewirtsch. 2012;36(3):191–203. https://doi.org/10.1007/s12398-012-0079-z.
Kohl T, Signorelli S, Engelhardt I, Berthoud NA, Sellami S, Rybach L. Development of a regional geothermal resource atlas. J Geophys Eng. 2005;2(4):372–85. https://doi.org/10.1088/1742-2132/2/4/S11.
Koltzer N, Scheck-Wenderoth M, Bott J, Cacace M, Frick M, Sass I, et al. The effects of regional fluid flow on deep temperatures (Hesse, Germany). Energies. 2019;12(11):2081. https://doi.org/10.3390/en12112081.
Kossmat F. Gliederung des varistischen Gebirgsbaues. Abh Sächsischen Geol Landesamts. 1927;1:1–39.

Köster MH. Mikrofazies, Diagenese und Geochemie des Hauptrogensteins aus dem Pfirter Jura [PhD Thesis]: Freie Universität Berlin; 2010.
Kowalczyk G. Permokarbon des Sprendlinger Horstes und der westlichen Wetterau (Exkursion I am 20. April 2001). JBER_OBERRH. 2001;83:211–36. https://doi.org/10.1127/jmogv/83/2001/211.
Kraus E. 3D Modellierung des tiefengeothermischen Potentials und der Petrologie des westlichen Taunus, Rheinisches Schiefergebirge [Diplomathesis]: TU Darmstadt; 2009.
Krawczyk CM, McCann T, Cocks L, England R, McBride J, Wybraniec S. Caledonian tectonics. In: McCann T, editor. The Geology of Central Europe: Volume 1: Precambrian and Palaeozoic. London: Geological Society of London; 2008. p. 303–82.
Kreuzer H, Harre W. K/Ar-Altersbestimmungen an Hornblenden und Biotiten des Kristallinen Odenwalds. In: Amstutz GC, Meisl S, Nickel E, eds. Mineralien und Gesteine im Odenwald. Heidelberg; 1975. p. 70–78. https://hdl.handle.net/10013/epic.42772. Accessed 29 Aug 2022.
Krohe A. Structural evolution of intermediate-crustal rocks in a strike-slip and extensional setting (Variscan Odenwald, SW Germany): differential upward transport of metamorphic complexes and changing deformation mechanisms. Tectonophysics. 1992;205(4):357–86. https://doi.org/10.1016/0040-1951(92)90443-A.
Krohe A, Willner AP. IV.C.2 The Odenwald Crystalline Complex. In: Dallmeyer RD, Franke W, Weber K, editors. Pre-Permian Geology of Central and Eastern Europe. Berlin: Springer, Berlin Heidelberg; 1995. p. 182–5.
Kroner U, Mansy JL, Mazur S, Aleksandrowski P, Hann HP, Huckriede H. Variscan tectonics. In: McCann T, editor. The Geology of Central Europe: Volume 1: Precambrian and Palaeozoic. London: Geological Society of London; 2008. p. 599–664.
Kühne K. Das Fachinformationssystem Geophysik und seine Nutzung über das Internet. GIS. 2006;57:227–31.
Kushnir AR, Heap MJ, Baud P. Assessing the role of fractures on the permeability of the Permo-Triassic sandstones at the Soultz-sous-Forêts (France) geothermal site. Geothermics. 2018a;74:181–9. https://doi.org/10.1016/j.geothermics.2018.03.009.
Kushnir ARL, Heap MJ, Baud P, Gilg HA, Reuschlé T, Lerouge C, et al. Characterizing the physical properties of rocks from the Paleozoic to Permo-Triassic transition in the Upper Rhine Graben. Geotherm Energy. 2018b. https://doi.org/10.1186/s40517-018-0103-6.
Lacirignola M, Blanc I. Environmental analysis of practical design options for enhanced geothermal systems (EGS) through life-cycle assessment. Renew Energy. 2013;50:901–14. https://doi.org/10.1016/j.renene.2012.08.005.
Ladner F, Schanz U, Häring MO. Deep-Heat-Mining-Projekt Basel-Erste Erkenntnisse bei der Entwicklung eines Enhanced Geothermal System (EGS). Bull Für Angew Geol. 2008;13:41–54. https://doi.org/10.5169/seals-226675.
Lambert AD. Bestimmung der petrophysikalischen und felsmechanischen Kennwerte des Tromm-und Weschnitz-Plutons, Odenwald, Deutschland [Bachelorthesis]: TU Darmstadt; 2016.
Lardeaux JM, Schulmann K, Faure M, Janoušek V, Lexa O, Skrzypek E, et al. The Moldanubian Zone in the French Massif Central, Vosges/Schwarzwald and Bohemian Massif revisited: differences and similarities. Geol Soc Spec Publ. 2014;405(1):7–44. https://doi.org/10.1144/SP405.14.
Le Carlier de Veslud C, Bourgeois O, Diraison M, Ford M. 3D stratigraphic and structural synthesis of the Dannemarie basin (Upper Rhine Graben). Bull Soci Géol Fr. 2005;176(5):433–42. https://doi.org/10.2113/176.5.433.
Ledésert B, Berger G, Meunier A, Genter A, Bouchet A. Diagenetic-type reactions related to hydrothermal alteration in the Soultz-sous-Forêts granite. France Ejm. 1999;11(4):731–42. https://doi.org/10.1127/ejm/11/4/0731.
Ledésert B, Hebert R, Genter A, Bartier D, Clauer N, Grall C. Fractures, hydrothermal alterations and permeability in the Soultz Enhanced Geothermal System. CR Geosci. 2010;342(7–8):607–15. https://doi.org/10.1016/j.crte.2009.09.011.
Lehne RJ, Hoselmann C, Heggemann H, Budde H, Hoppe A. Geological 3D modelling in the densely populated metropolitan area Frankfurt/Rhine-Main. ZDGG. 2013. https://doi.org/10.1127/1860-1804/2013/0051.
Lepper J, Rambow D, Röhling H-G. Lithostratigraphy of the Buntsandstein in Germany. SDGG. 2014;69:69–149. https://doi.org/10.1127/sdgg/69/2014/69.
Les Landes AA, Guillon T, Peter-Borie M, Blaisonneau A, Rachez X, Gentier S. Locating geothermal resources: insights from 3D stress and flow models at the upper Rhine graben scale. Geofluids. 2019;2019:1–24. https://doi.org/10.1155/2019/8494539.
Leu W, Keller B, Matter A, Schärli U, Rybach L. Geothermische Eigenschaften Schweizer Molassebecken (Tiefenbereich 0–500m). Bern: Bundesamt für Energie; 1999.
Leydecker G. Erdbebenkatalog für Deutschland mit Randgebieten für die Jahre 800 bis 2008. Schweizerbart; 2011. ISBN 978-3-510-95989-1.
LGRB. Querschnitt durch den Oberrheingraben auf Höhe des Kaiserstuhls. 2022. https://lgrbwissen.lgrb-bw.de/geotourismus/aufschluesse/oberrhein-hochrheingebiet/vulkanite-am-kaiserstuhl. Accessed 3 Jun 2022.
Lippolt HJ, Todt WA, Horn P. Apparent potassium-argon ages of Lower Tertiary Rhine Graben volcanics. In: Illies JH, Fuchs K, editors. Approaches to Taphrogenesis. Stuttgart: Schweizerbart; 1974. p. 213–21.
Lippolt HJ, Kirsch H, Plein E. Karbonische und permische Vulkanite aus dem Untergrund des nördlichen Oberrheingrabens: Art, Altersbestimmung und Konsequenz. JBER_OBERRH. 1990;72:227–42. https://doi.org/10.1127/jmogv/72/1990/227.
Loeschke J, Güldenpfennig M, Hann HP, Sawatzki G. The Zone of Badenweiler-Lenzkirch (Black Forest): A Variscan suture zone. ZDGG_ALT. 1998;149(2):197–212. https://doi.org/10.1127/zdgg/149/1998/197.
Loges A, Wagner T, Kirnbauer T, Göb S, Bau M, Berner Z, Markl G. Source and origin of active and fossil thermal spring systems, northern Upper Rhine Graben, Germany. Appl Geochem. 2012;27(6):1153–69. https://doi.org/10.1016/j.apgeochem.2012.02.024.
Löschan G, Emmerich K, Reinhold C, Reinecker J. Clay mineralogy of Tertiary formations in the northern Upper Rhine Graben – New insights from geothermal and hydrocarbon exploration. ZDGG. 2017;168(2):233–44. https://doi.org/10.1127/zdgg/2017/0083.
Mack C. Geothermische Untersuchungen in Calw [Diplomathesis]: TU Darmstadt; 2007.

Madritsch H, Kounov A, Schmid SM, Fabbri O. Multiple fault reactivations within the intra-continental Rhine-Bresse Transfer Zone (La Serre Horst, eastern France). Tectonophysics. 2009;471(3–4):297–318. https://doi.org/10.1016/j.tecto.2009.02.044.
Maire R. Investigation of thermo-physical and mechanical parameters of crystalline geothermal reservoir rocks of the Upper Rhine Graben (Germany) [Masterthesis]: LaSalle Beauvais; TU Darmstadt; 2014.
Majer EL, Baria R, Stark M, Oates S, Bommer J, Smith B, Asanuma H. Induced seismicity associated with Enhanced Geothermal Systems. Geothermics. 2007;36(3):185–222. https://doi.org/10.1016/j.geothermics.2007.03.003.
Mann JC. Uncertainty in geology. Computers in geology—25 years of progress. Oxford: Oxford University Press; 1993. p. 241–54.
Manning CE, Ingebritsen SE. Permeability of the continental crust: implications of geothermal data and metamorphic systems. Rev Geophys. 1999;37(1):127–50. https://doi.org/10.1029/1998RG900002.
Marell D. Das Rotliegende zwischen Odenwald und Taunus. Hessisches Landesamt für Bodenforschung; 1989.
Martin U. The Early Palaeozoic Break-up of Northern Gondwana: Sedimentology, Physical Volcanology and Geochemistry of a Submarine Volcanic Complex in the Bavarian Facies Association, Saxothuringian Basin, Germany. Gondwana Res. 2003;6(4):839–58. https://doi.org/10.1016/S1342-937X(05)71029-7.
Massonne HJ. Metamorphic evolution. In: Dallmeyer RD, Franke W, Weber K, editors. Pre-Permian geology of Central and Eastern Europe. Berlin: Springer, Berlin Heidelberg; 1995. p. 132–7.
Matte P. The Variscan collage and orogeny (480–290 Ma) and the tectonic definition of the Armorica microplate: a review. Terra Nova. 2003;13(2):122–8. https://doi.org/10.1046/j.1365-3121.2001.00327.x.
McCann T, Skompski S, Poty E, Dusar M, Vozarova A, Schneider J, et al. Carboniferous. In: McCann T, editor., et al., The geology of central Europe: Volume 1: Precambrian and Palaeozoic. London: Geological Society of London; 2008. p. 410–530.
McCann T, editor. The Geology of Central Europe: Volume 1: Precambrian and Palaeozoic. London: Geological Society of London; 2008.
McKerrow WS, MacNiocaill C, Dewey JF. The Caledonian Orogeny redefined. J Geol Soc. 2000;157(6):1149–54.
McKie T. Paleogeographic evolution of latest Permian and Triassic salt basins in Northwest Europe. In: Soto JI, Flinch J, Tari G, editors. Permo-triassic salt provinces of Europe, North Africa and the atlantic margins: tectonics and hydrocarbon potential. Saint Louis: Elsevier Science; 2017. p. 159–73 (**10.1016/B978-0-12-809417-4.00008-2**).
Mégel T, Rybach L. Production Capacity and Systainability of Geothermal Doublets. In: World Geothermal Congress 2000; 28. May, 10. June; Kyushu - Tohoku, Japan; 2000.
Meghraoui M, Delouis B, Ferry M, Giardini D, Huggenberger P, Spottke I, Granet M. Active normal faulting in the upper Rhine graben and paleoseismic identification of the 1356 Basel earthquake. Science. 2001;293(5537):2070–3. https://doi.org/10.1126/science.1010618.
Meier L, Eisbacher GH. Crustal kinematics and deep structure of the northern Rhine Graben, Germany. Tectonics. 1991;10(3):621–30. https://doi.org/10.1029/91TC00142.
Meisel M. Petrographie, Fazies und Diagenese des Buntsandsteinreservoirs am Oberrhein [Diplomathesis]: Universität Jena; 2009.
Meisl S. III.C.3 Igneous Activity. In: Dallmeyer RD, Franke W, Weber K, editors. Pre-Permian geology of Central and Eastern Europe. Berlin: Springer, Berlin Heidelberg; 1995. p. 118–31.
Meixner J, Schill E, Gaucher E, Kohl T. Inferring the in situ stress regime in deep sediments: an example from the Bruchsal geothermal site. Geotherm Energy. 2014. https://doi.org/10.1186/s40517-014-0007-z.
Meixner J, Schill E, Grimmer JC, Gaucher E, Kohl T, Klingler P. Structural control of geothermal reservoirs in extensional tectonic settings: an example from the Upper Rhine Graben. J Struct Geol. 2016;82:1–15. https://doi.org/10.1016/j.jsg.2015.11.003.
Meller C, Ledésert B. Is there a link between mineralogy, petrophysics, and the hydraulic and seismic behaviors of the Soultz-sous-Forêts granite during stimulation? A review and reinterpretation of petro-hydromechanical data toward a better understanding of induced seismicity. J Geophys Res. 2017;122(12):9755–74. https://doi.org/10.1002/2017JB014648.
Meller C, Schill E, Bremer J, Kolditz O, Bleicher A, Benighaus C, et al. Acceptability of geothermal installations: a geoethical concept for GeoLaB. Geothermics. 2018;73:133–45. https://doi.org/10.1016/j.geothermics.2017.07.008.
Michon L, Merle O. Crustal structures of the Rhinegraben and the Massif Central grabens: an experimental approach. Tectonics. 2000;19(5):896–904. https://doi.org/10.1029/2000TC900015.
Moeck IS. Catalog of geothermal play types based on geologic controls. Renew Sustain Energy Rev. 2014;37:867–82. https://doi.org/10.1016/j.rser.2014.05.032.
Molenaar N, Felder M, Bär K, Götz AE. What classic greywacke (litharenite) can reveal about feldspar diagenesis: an example from Permian Rotliegend sandstone in Hessen, Germany. Sed Geol. 2015;326:79–93. https://doi.org/10.1016/j.sedgeo.2015.07.002.
Molzahn M, Anthes G, Reischmann T. Single zircon Pb/Pb age geochronology and isotope systematics of the Rhenohercynian basement. Terra Nostra. 1998;98(1):67–8.
Morris A, Ferrill DA, Brent HD. Slip-tendency analysis and fault reactivation. Geology. 1996;24(3):275. https://doi.org/10.1130/0091-7613(1996)024%3c0275:STAAFR%3e2.3.CO;2.
Morrow CA, Shi LQ, Byerlee JD. Permeability of fault gouge under confining pressure and shear stress. J Geophys Res. 1984;89(B5):3193–200. https://doi.org/10.1029/JB089iB05p03193.
Mouchot J, Genter A, Cuenot N, Scheiber J, Seibel O, Bosia C, Ravier G. First Year of Operation from EGS geothermal Plants in Alsace, France: Scaling Issues. In: Stanford University, ed. 43rd Workshop on Geothermal Reservoir Engineering; 12.-14. February; Stanford, California; 2018.
Müller H. Das Permokarbon im nördlichen Oberrheingraben: Paläogeographische und strukturelle Entwicklung des permokarbonen Saar-Nahe-Beckens im nördlichen Oberrheingraben. Wiesbaden: Hess. Landesamt für Bodenforschung; 1996.
Müller D. Investigation on the spatial variability of petrophysical parameters of sandstone (Buntsandstein) in the Spessart, Germany [Bachelorthesis]: TU Darmstadt; 2014.

Nance RD, Gutiérrez-Alonso G, Keppie JD, Linnemann U, Murphy JB, Quesada C, et al. Evolution of the Rheic Ocean. Gondwana Res. 2010;17(2–3):194–222. https://doi.org/10.1016/j.gr.2009.08.001.
Nehler M. Geothermische Untersuchungen des Zechsteins im Raum Sontra [Bachelorthesis]: TU Darmstadt; 2011.
Newman GA, Gasperikova E, Hoversten GM, Wannamaker PE. Three-dimensional magnetotelluric characterization of the Coso geothermal field. Geothermics. 2008;37(4):369–99. https://doi.org/10.1016/j.geothermics.2008.02.006.
Nickel E. Geologische Position und Petrogenese des kristallinen Odenwaldes. In: Amstutz GC, Meisl S, Nickel E, eds. Mineralien und Gesteine im Odenwald. Heidelberg; 1975. p. 1–25.
Okrusch M. Metamorphic evolution. In: Dallmeyer RD, Franke W, Weber K, editors. Pre-Permian geology of Central and Eastern Europe. Berlin: Springer, Berlin Heidelberg; 1995. p. 201–13.
Okrusch M, Schubert W, Nasir S. IV.D igneous activity (Pre- to Early Variscan Magmatism). In: Dallmeyer RD, Franke W, Weber K, editors. Pre-Permian geology of Central and Eastern Europe. Berlin: Springer, Berlin Heidelberg; 1995. p. 190–200.
Oncken O. III.B.2 Structure. In: Dallmeyer RD, Franke W, Weber K, editors. Pre-Permian geology of Central and Eastern Europe. Berlin: Springer, Berlin Heidelberg; 1995. p. 50–8.
Oncken O. Transformation of a magmatic arc and an orogenic root during oblique collision and it's consequences for the evolution of the European Variscides (Mid-German Crystalline Rise). Geol Rundsch. 1997;86(1):2–20. https://doi.org/10.1007/s005310050118.
Oncken O, Massonne HJ, Schwab M. III.B.4 metamorphic evolution. In: Dallmeyer RD, Franke W, Weber K, editors. Pre-Permian Geology of Central and Eastern Europe. Berlin: Springer, Berlin Heidelberg; 1995. p. 82–6.
Oncken O, von Winterfeld C, Dittmar U. Accretion of a rifted passive margin: the Late Paleozoic Rhenohercynian fold and thrust belt (Middle European Variscides). Tectonics. 1999;18(1):75–91. https://doi.org/10.1029/98TC02763.
Orendt R. Geothermisches Potenzial im Erlaubnisfeld Südtaunus [Diplomathesis]: TU Darmstadt; 2014.
Parkhurst DL, Appelo CA. User's guide to PHREEQC (Version 2): a computer program for speciation, batch-reaction, one-dimensional transport, and inverse geochemical calculations. WRIR. 1999;99(4259):312. https://doi.org/10.3133/wri994259.
Paschen H, Ortel D, Grünwald R. Möglichkeiten geothermischer Stromerzeugung in Deutschland: Sachstandsbericht: Büro für Technikfolgen-Abschätzung beim Deutschen Bundestag (TAB); 2003.
Paul J. Untere Buntsandstein des Germanischen Beckens. Int J Earth Sci. 1982;71(3):795–811. https://doi.org/10.1007/BF01821104.
Paul J, Wemmer K, Ahrendt H. Provenance of siliciclastic sediments (Permian to Jurassic) in the Central European Basin. ZDGG. 2008;159(4):641–50. https://doi.org/10.1127/1860-1804/2008/0159-0641.
Pauwels H, Fouillac C, Fouillac A-M. Chemistry and isotopes of deep geothermal saline fluids in the Upper Rhine Graben: Origin of compounds and water-rock interactions. Geochim Cosmochim Acta. 1993;57(12):2737–49. https://doi.org/10.1016/0016-7037(93)90387-C.
Pei L. Analysis of initiation and propagation of hydraulically induced fracture [Masterthesis]: TU Darmstadt; 2009.
Perner MJ. Evolution of Palaeoenvironment, Kerogen Composition and Thermal History in the Cenozoic of the Northern Upper Rhine Graben, SW-Germany [PhD thesis]: Universität Heidelberg; 2018.
Person M, Garven G. Hydrologie constraints on petroleum generation within continental rift basins: theory and application to the Rhine graben. Bulletin. 1992;76(4):468–88. https://doi.org/10.1306/BDFF883A-1718-11D7-8645000102C1865D.
Pflug R. Bau und Entwicklung des Oberrheingrabens. Darmstadt: Wissenschaftl; 1982.
Pienkowski G, Schudack ME, Bosak P, Enay R, Feldman-Olszewska A, Golonka J, et al. Jurassic. In: McCann T, editor., et al., The geology of central Europe: volume 2: Mesozoic and Cenozoic. London: Geological Society of London; 2008. p. 823–922.
Plenefisch T, Bonjer K-P. The stress field in the Rhine Graben area inferred from earthquake focal mechanisms and estimation of frictional parameters. Tectonophysics. 1997;275(1–3):71–97. https://doi.org/10.1016/S0040-1951(97)00016-4.
Portier S, Vuataz F-D, Nami P, Sanjuan B, Gérard A. Chemical stimulation techniques for geothermal wells: experiments on the three-well EGS system at Soultz-sous-Forêts. France. Geothermics. 2009;38(4):349–59. https://doi.org/10.1016/j.geothermics.2009.07.001.
Pribnow D, Schellschmidt R. Thermal tracking of upper crustal fluid flow in the Rhine graben. Geophys Res Lett. 2000;27(13):1957–60. https://doi.org/10.1029/2000GL008494.
Prodehl C, Mueller S, Haak V. The European Cenozoic rift system. In: Olsen KH, editor. Continental rifts: evolution, structure, tectonics. Amsterdam: Elsevier; 1995. p. 133–212 (**10.1016/S0419-0254(06)80012-1**).
Prodehl C, St. Mueller, Glahn A, Gutscher M, Haak V. Lithospheric cross sections of the European Cenozoic rift system. Tectonophysics. 1992;208(1–3):113–38. https://doi.org/10.1016/0040-1951(92)9033-8.
Rathnaweera TD, Wu W, Ji Y, Gamage RP. Understanding injection-induced seismicity in enhanced geothermal systems: From the coupled thermo-hydro-mechanical-chemical process to anthropogenic earthquake prediction. Earth Sci Rev. 2020;205: 103182. https://doi.org/10.1016/j.earscirev.2020.103182.
Reinecker J, Bauer JF, Bechstädt T, Drews T, Filomena M, Grobe R, et al. Verbundprojekt AuGE: Aufschlussanalogstudien und ihre Anwendbarkeit in der geothermischen Exploration—Entwicklung von Methoden zur Ermittlung von Permeabilitäten und Transmissivitäten aus Reservoir-Informationen des Oberrheingrabens. AUGE—Outcrop analogue studies in geothermal exploration: Schlussbericht Teilprojekt A; 2015.
Reinecker J, Hochschild T, Kraml M, Löschan G, Kreuter H. Experiences and challenges in geothermal exploration in the Upper Rhine Graben. In: European Geothermal Congress; 11.-14. June; Den Haag; 2019.
Reinhold C, Schwarz M, Bruss D, Heesbeen B, Perner M, Suana M. The Northern Upper Rhine Graben: re-dawn of a mature petroleum province? Swiss Bull Angew Geol. 2016;21(2):35–56. https://doi.org/10.5169/seals-658196.
Reischmann T, Anthes G. Geochronology of the mid-German crystalline rise west of the River Rhine. Geol Rundsch. 1996;85(4):761–74. https://doi.org/10.1007/BF02440109.
Reischmann T, Anthes G, Jaeckel P, Altenberger U. Age and origin of the Böllsteiner Odenwald. Mineral Petrol. 2001;72(1–3):29–44. https://doi.org/10.1007/s007100170025.

Reiter K, Heidbach O, Müller B, Reinecker J, Röckl T, Reiter K, et al. Stress Map Germany 2016 2016. https://doi.org/10.5880/WSM.Germany2016_en.
Reith S, Kölbel T, Schlagermann P, Pellizzone A, Allansdottir A. Public acceptance of geothermal electricity production: GEOELEC. EnBW Energie Baden-Württemberg AG, University of Milan & University of Sienna. 2013. http://www.geoelec.eu/wp-content/uploads/2014/03/D-4.4-GEOELEC-report-on-public-acceptance.pdf. Accessed 29 Aug 2022.
Rettenmaier D, Gaucher E, Ghergut J, Huttenloch P, Kohl T, Meixner J, et al. LOGRO—Langzeitbetrieb und Optimierung eines Geothermiekraftwerks in einem geklüftetporösen Reservoir im Oberrheingraben: Schlussbericht; 2013. https://www.tib.eu/de/suchen/id/TIBKAT:77165135X/Langzeitbetrieb-und-Optimierung-eines-Geothermiekraftwerks?cHash=9ba6621535f847902833cef0522ee635. Accessed 29 Aug 2022.
Ritter JRR, Wagner M, Bonjer K-P, Schmidt B. The 2005 Heidelberg and Speyer earthquakes and their relationship to active tectonics in the central Upper Rhine Graben. Int J Earth Sci. 2009;98(3):697–705. https://doi.org/10.1007/s00531-007-0284-x.
Robardet M. The Armorica 'microplate': fact or fiction? Critical review of the concept and contradictory palaeobiogeographical data. Palaeogeogr Palaeoclimatol Palaeoecol. 2003;195(1–2):125–48. https://doi.org/10.1016/S0031-0182(03)00305-5.
Röhling H-G, Lepper J, Diehl M, Dittrich D, Freudenberger W, Friedlein V, et al. Der Buntsandstein in der Stratigraphischen Tabelle von Deutschland 2016. ZDGG. 2018;169(2):151–80. https://doi.org/10.1127/zdgg/2018/0132.
Rosenbaum G, Lister GS, Duboz C. Relative motions of Africa, Iberia and Europe during Alpine orogeny. Tectonophysics. 2002;359(1–2):117–29. https://doi.org/10.1016/S0040-1951(02)00442-0.
Rothe JP, Sauer K. The Rhinegraben Progress Report 1967. Geologisches Landesamt Baden-Württemberg; 1967.
Rotstein Y, Edel JB, Gabriel G, Boulanger D, Schaming M, Munschy M. Insight into the structure of the Upper Rhine Graben and its basement from a new compilation of Bouguer Gravity. Tectonophysics. 2006;425(1–4):55–70. https://doi.org/10.1016/j.tecto.2006.07.002.
Rousse S, Duringer P, Stapf KRG. An exceptional rocky shore preserved during Oligocene (Late Rupelian) transgression in the Upper Rhine Graben (Mainz Basin, Germany). Geol J. 2012;47(4):388–408. https://doi.org/10.1002/gj.1349.
Rühaak W. 3-D interpolation of subsurface temperature data with measurement error using kriging. Environ Earth Sci. 2015;73(4):1893–900. https://doi.org/10.1007/s12665-014-3554-5.
Rühaak W, Bär K, Sass I. Combining numerical modeling with geostatistical interpolation for an improved reservoir exploration. Energy Proc. 2014;59:315–22. https://doi.org/10.1016/j.egypro.2014.10.383.
Rummel F, Baumgärtner J. Hydraulic fracturing stress measurements in the GPK1 borehole, Soultz sous Forêts. Geotherm Sci Technol. 1991;3(1–4):119–48.
Rupf I, Nitsch E. Das geologische Landesmodell von Baden-Württemberg: Datengrundlagen technische Umsetzung und erste geologische Ergebnisse. Landesamt für Geologie Rohstoffe und Bergbau Baden-Württemberg; 2008. https://produkte.lgrb-bw.de/docPool/c623_data.pdf. Accessed 29 Aug 2022.
Saevarsdottir G, Tao P, Stefansson H, Harvey W. Potential use of geothermal energy sources for the production of lithium-ion batteries. Renew Energy. 2014;61:17–22. https://doi.org/10.1016/j.renene.2012.04.028.
Sandkühler L. Untersuchung des Einflusses der Wassersättigung auf die thermophysikalischen Eigenschaften von Kernproben der Bohrungen Aura und Rosenthal [Bachelorthesis]: TU Darmstadt; 2015.
Sanjuan B, Millot R, Innocent C, Dezayes C, Scheiber J, Brach M. Major geochemical characteristics of geothermal brines from the Upper Rhine Graben granitic basement with constraints on temperature and circulation. Chem Geol. 2016;428:27–47. https://doi.org/10.1016/j.chemgeo.2016.02.021.
Sanjuan B, Négrel G, Le Lous M, Poulmarch E, Gal F, Damy PC. Main Geochemical Characteristics of the Deep Geothermal Brine at Vendenheim (Alsace, France) with Constraints on Temperature and Fluid Circulation. In: World Geothermal Congress 2020; April - October 2021; Reykjavik, Iceland; 2021.
Sass I, Hoppe A, Arndt D, Bär K. Forschungs-und Entwicklungsprojekt 3D Modell der Geothermischen Tiefenpotenziale von Hessen. Abschlussbericht: TU Darmstadt; 2011.
Sauer K, Munck F. Geothermische Synthese des Oberrheingrabens (Bestandsaufnahme): Geologisches Landesamt Baden-Württemberg; 1979.
Sauer K. Erdöl am Oberrhein. Ein Heidelberger Kolloquium. Abhandlungen des Geologischen Landesamtes Baden-Württemberg; 1962;4:1–136.
Sausse J, Genter A. Types of permeable fractures in granite. Geol Soc Spec Publ. 2005;240(1):1–14.
Sausse J, Dezayes C, Dorbath L, Genter A, Place J. 3D model of fracture zones at Soultz-sous-Forêts based on geological data, image logs, induced microseismicity and vertical seismic profiles. CR Geosci. 2010;342(7–8):531–45. https://doi.org/10.1016/j.crte.2010.01.011.
Schäfer A. Variscan molasse in the Saar-Nahe Basin (W-Germany), Upper Carboniferous and Lower Permian. Int J Earth Sci. 1989;78(2):499–524. https://doi.org/10.1007/BF01776188.
Schäfer A. Sedimentologisch-numerisch begrundeter stratigraphischer Standard fur das Permo-Karbon des Saar-Nahe-Beckens. Cour Forsch-Inst Senckenberg. 2005;254:369–94.
Schäfer A. Tectonics and sedimentation in the continental strike-slip Saar-Nahe Basin (Carboniferous-Permian, West Germany). ZDGG. 2011;162(2):127–55. https://doi.org/10.1127/1860-1804/2011/0162-0127.
Schäfer A, Korsch RJ. Formation and sediment fill of the Saar-Nahe Basin (Permo-Carboniferous, Germany). Zeitschrift Deutschen Geol Gesellschaft. 1998;149(2):233–69. https://doi.org/10.1127/zdgg/149/1998/233.
Schäffer R, Bär K, Sass I. Multimethod exploration of the hydrothermal reservoir in Bad Soden-Salmünster, Germany. ZDGG. 2018;169(3):311–33. https://doi.org/10.1127/zdgg/2018/0147.
Schälicke W. Die Otzberg-Zone. In: Amstutz GC, Meisl S, Nickel E, eds. Mineralien und Gesteine im Odenwald. Heidelberg; 1975. p. 47–59.
Schaltegger U. U–Pb geochronology of the Southern Black Forest Batholith (Central Variscan Belt): timing of exhumation and granite emplacement. Int J Earth Sci. 2000;88(4):814–28. https://doi.org/10.1007/s005310050308.
Schärli U, Kohl T. Archivierung und Kompilation geothermischer Daten der Schweiz und angrenzender Gebiete. Schweizerische Geophysikalische Kommission; 2002.

Scheck-Wenderoth M, Krzywiec P, Zühlke R, Maystrenko Y, Froitzheim N. Permian to Cretaceous tectonics of Central Europe. In: McCann T, editor. The geology of central Europe: volume 1: Precambrian and Palaeozoic. London: Geological Society of London; 2008. p. 999–1030.
Schellschmidt R, Clauser C. The thermal regime of the Upper Rhine Graben and the anomaly at Soultz. Z Angew Geol. 1996;42(1):40–4.
Schill E, Meixner J, Meller C, Grimm M, Grimmer JC, Stober I, Kohl T. Criteria and geological setting for the generic geothermal underground research laboratory, GEOLAB. Geotherm Energy. 2016. https://doi.org/10.1186/s40517-016-0049-5.
Schill E, Genter A, Cuenot N, Kohl T. Hydraulic performance history at the Soultz EGS reservoirs from stimulation and long-term circulation tests. Geothermics. 2017;70:110–24. https://doi.org/10.1016/j.geothermics.2017.06.003.
Schindler M, Baumgärtner J, Gandy T, Hauffe P, Hettkamp T, Menzel H, et al. Successful Hydraulic Stimulation Techniques for Electric Power Production in the Upper Rhine Graben, Central Europe. In: World Geothermal Congress 2010; 25–29 April; Bali, Indonesia; 2010.
Schintgen TV. The Geothermal Potential of Luxembourg: Geological and thermal exploration for deep geothermal reservoirs in Luxembourg and the surroundings [PhD thesis]: Universität Potsdam; 2016.
Schmidt RB, Bucher K, Drüppel K, Stober I. Experimental interaction of hydrothermal Na-Cl solution with fracture surfaces of geothermal reservoir sandstone of the Upper Rhine Graben. Appl Geochem. 2017;81:36–52. https://doi.org/10.1016/j.apgeochem.2017.03.010.
Schmidt RB, Bucher K, Stober I. Experiments on granite alteration under geothermal reservoir conditions and the initiation of fracture evolution. EJM. 2018;30(5):899–916. https://doi.org/10.1127/ejm/2018/0030-2771.
Schmidt RB, Göttlicher J, Stober I. Experiments on sandstone alteration under geothermal reservoir conditions and the formation of zeolites. EJM. 2019;31(5–6):929–44. https://doi.org/10.1127/ejm/2019/0031-2870.
Schmittbuhl J, Lambotte S, Lengliné O, Grunberg M, Jund H, Vergne J, et al. Induced and triggered seismicity below the city of Strasbourg, France from November 2019 to January 2021. Comptes Rendus Géosci. 2021;353(S1):1–24. https://doi.org/10.5802/crgeos.71.
Scholze F, Wang X, Kirscher U, Kraft J, Schneider JW, Götz AE, et al. A multistratigraphic approach to pinpoint the Permian-Triassic boundary in continental deposits: the Zechstein-Lower Buntsandstein transition in Germany. Global Planet Change. 2017;152:129–51. https://doi.org/10.1016/j.gloplacha.2017.03.004.
Schöpflin S. Determination of Rockmechanical Properties of the Palatinate Forest's Buntsandstein [Master thesis]: Albert-Ludwigs-Universität Freiburg; 2013.
Schröder B. Entwicklung des Sedimentbeckens und Stratigraphie der klassischen Germanischen Trias. Int J Earth Sci. 1982;71(3):783–94. https://doi.org/10.1007/BF01821103.
Schubert KO. Geothermische Untersuchungen des Buntsandsteins des Odenwaldes [Bachelorthesis]: TU Darmstadt; Goethe Universitaet Frankfurt am Main; 2011.
Schulz R, Schellschmidt R. Das Temperaturfeld im südlichen Oberrheingraben. Geol Jb E. 1991;48:153–65.
Schumacher ME. Upper Rhine Graben: role of preexisting structures during rift evolution. Tectonics. 2002. https://doi.org/10.1029/2001TC900022.
Schumann A. GIS basierte Erdwaermepotenzialkarte Spielberg und Wart [Diplomathesis]: TU Darmstadt; 2008.
Schwarz H-U, editor. Sedimentary structures and facies analysis of shallow marine carbonates. Stuttgart: Schweizerbart; 1975.
Schwarz M, Henk A. Evolution and structure of the Upper Rhine Graben: insights from three-dimensional thermomechanical modelling. Int J Earth Sci. 2005;94(4):732–50. https://doi.org/10.1007/s00531-004-0451-2.
Schwarz J, Abrahamczyk L, Amstein S, Kaufmann C, Langhammer T. Das Waldkirch-Erdbeben (Baden-Württemberg) vom 5. Dezember 2004. Bautechnik. 2006;83(3):202–8. https://doi.org/10.1002/bate.200610020.
Schwarz M. Evolution und Struktur des Oberrheingrabens - quantitative Einblicke mit Hilfe dreidimen-sionaler thermomechanischer Modellrechnungen [PhD thesis]. Freiburg i. Br.: University of Freiburg; 2006.
Scibek J. Multidisciplinary database of permeability of fault zones and surrounding protolith rocks at world-wide sites. Sci Data. 2020;7(1):95. https://doi.org/10.1038/s41597-020-0435-5.
Signorelli S, Kohl T. Technischer Bericht 08–03: Vorschlag geologischer Standortgebiete für das SMA- und das HAA-Lager: Nagra; 2008.
Sissingh W. Comparative Tertiary stratigraphy of the Rhine Graben, Bresse Graben and Molasse Basin: correlation of Alpine foreland events. Tectonophysics. 1998;300(1–4):249–84. https://doi.org/10.1016/S0040-1951(98)00243-1.
Skrzypek E, Schulmann K, Edel JB. Palaeozoic evolution of the Variscan Vosges Mountains. Geol Soc Spec Publ. 2014;405(1):45–75. https://doi.org/10.1144/SP405.8.
Smith DB. Rapid marine transgressions and regressions of the Upper Permian Zechstein Sea. J Geol Soc. 1979;136(2):155–6. https://doi.org/10.1144/gsjgs.136.2.0155.
Spottke I, Zechner E, Huggenberger P. The southeastern border of the Upper Rhine Graben: a 3D geological model and its importance for tectonics and groundwater flow. Int J Earth Sci. 2005;94(4):580–93. https://doi.org/10.1007/s00531-005-0501-4.
Stapf KRG. Einführung lithostratigraphischer Formationsnamen im Rotliegend des Saar-Nahe-Beckens (SW-Deutschland). Mitteilungen Der POLLICHIA. 1990;77:111–24.
Stein E. The geology of the Odenwald Crystalline Complex. Mineral Petrol. 2001;72(1–3):7–28. https://doi.org/10.1007/s007100170024.
Stets J, Schäfer A. The Lower Devonian Rhenohercynian Rift - 20 Ma of sedimentation and tectonics (Rhenish Massif, W-Germany). ZDGG. 2011;162(2):93–115. https://doi.org/10.1127/1860-1804/2011/0162-0093.
Stober I. Researchers study conductivity of crystalline rock in proposed radioactive waste site. Eos Trans AGU. 1996;77(10):93. https://doi.org/10.1029/96EO00062.
Stober I, Bucher K. Fluid sinks within the earth's crust. Geofluids. 2004;4(2):143–51. https://doi.org/10.1111/j.1468-8115.2004.00078.x.

Stober I, Bucher K. Hydraulic properties of the crystalline basement. Hydrogeol J. 2007;15(2):213–24. https://doi.org/10.1007/s10040-006-0094-4.
Stober I, Bucher K. Hydraulic and hydrochemical properties of deep sedimentary reservoirs of the Upper Rhine Graben, Europe. Geofluids. 2015;15(3):464–82. https://doi.org/10.1111/gfl.12122.
Stober I, Jodocy M. Characteristics of geothermal reservoirs in the Upper Rhine Graben of Baden-Württemberg and France. Grundwasser. 2009;14(2):127–37.
Stober I, Richter A, Brost E, Bucher K. The Ohlsbach plume—discharge of deep saline water from the crystalline basement of the Black Forest, Germany. Hydrogeol J. 1999;7(3):273–83. https://doi.org/10.1007/s100400050201.
Stober I, Ladner F, Hofer M, Bucher K. The deep Basel-1 geothermal well: an attempt assessing the predrilling hydraulic and hydrochemical conditions in the basement of the Upper Rhine Graben. Swiss J Geosci. 2022. https://doi.org/10.1186/s00015-021-00403-8.
Stollhofen H. Vulkaniklastika und Siliziklastika des basalen Oberrotliegend im Saar-Nahe-Becken (SW-Deutschland). Terminologie Ablagerungsprozesse Mainzer Geowissenschaftliche Mitteilungen. 1994;23:95–138.
Stollhofen H. Facies architecture variations and seismogenic structures in the Carboniferous-Permian Saar–Nahe Basin (SW Germany): evidence for extension-related transfer fault activity. Sed Geol. 1998;119(1–2):47–83. https://doi.org/10.1016/S0037-0738(98)00040-2.
Stollhofen H, Stanistreet IG. Interaction between bimodal volcanism, fluvial sedimentation and basin development in the Permo-Carboniferous Saar-Nahe Basin (south-west Germany). Basin Res. 1994;6(4):245–67. https://doi.org/10.1111/j.1365-2117.1994.tb00088.x.
Straub EW. Die Erdöl- und Erdgaslagerstätten in Hessen und Rheinhessen. Abh Geol Landesam Baden-Württem. 1962;4:123–36.
Stricker K, Grimmer JC, Egert R, Bremer J, Korzani MG, Schill E, Kohl T. The potential of depleted oil reservoirs for high-temperature storage systems. Energies. 2020;13(24):6510. https://doi.org/10.3390/en13246510.
Suess FE. Intrusion-und Wandertektonik im variszischen Grundgebirge. Berlin: Gebr. Bornträger; 1926.
Surma F, Geraud Y. Porosity and Thermal Conductivity of the Soultz-sous-Forêts Granite. In: Kümpel H-J, editor. Thermo-hydro-mechanical coupling in fractured rock. Basel: Birkhäuser; 2003. p. 1125–36.
Surma F. Determination de la porosite des zones endommagees autour des failles et rle de l'etat du materiau sur les proprietes d'echange fluides-roches: mineralogie, structures de porosite, caracteristiques mecaniques [PhD thesis]. Strasbourg, France: Universite Louis Pasteu; 2003.
Szulc J. Middle Triassic evolution of the northern Peri-Tethys area as influenced by early opening of the Tethys Ocean. Ann Soc Geol Pol. 2000;70(1):1–48.
Teichmüller M. Zur geothermischen Geschichte des Oberrhein-Grabens. Zusammenfassung und Auswertung eines Symposiums. 1979.
Teza D, Menzel H, Baumgärtner J. Multihorizontansatz zur Erschließung ökonomisch relevanter Fließraten am Beispiel des Geothermieprojektes Landau: Schlussbericht; 2008.
Tischendorf G, Förster H-J, Frischbutter A, Kramer W, Schmidt W, Werner CD. Igneous activity. In: Dallmeyer RD, Franke W, Weber K, editors. Pre-Permian geology of central and eastern Europe. Berlin: Springer, Berlin Heidelberg; 1995. p. 249–59.
Tóth J. Gravity-induced cross-formational flow of formation fluids, red earth region, Alberta, Canada: Analysis, patterns, and evolution. Water Resour Res. 1978;14(5):805–43. https://doi.org/10.1029/WR014i005p00805.
United Nations, editor. Paris Agreement; 2015.
Valeton I. Petrographie des süddeutschen Hauptbuntsandsteins. Heidelberger Beitr Mineral Petrogr. 1953;3(5):335–79.
Valley B, Evans KF. Stress orientation to 5 km depth in the basement below Basel (Switzerland) from borehole failure analysis. Swiss J Geosci. 2009. https://doi.org/10.1007/s00015-009-1335-z.
Valley B, Evans KF. Stress magnitudes in the Basel enhanced geothermal system. Int J Rock Mech Min Sci. 2019;118:1–20. https://doi.org/10.1016/j.ijrmms.2019.03.008.
Valley BC. The relation between natural fracturing and stress heterogeneities in deep-seated crystalline rocks at Soultz-sous-Forêts (France) [PhD Thesis]: ETH Zurich; 2007.
van der Vaart J, Bär K, Frey M, Reinecker J, Sass I. Quantifying model uncertainty of a geothermal 3D model of the Cenozoic deposits in the northern Upper Rhine Graben, Germany. ZDGG. 2021. https://doi.org/10.1127/zdgg/2021/0286.
van Horn A, Amaya A, Higgins B, Muir J, Scherer J, Pilko R, Ross M. New opportunities and applications for closed-loop geothermal energy systems. GRC Transact. 2020;44:1123–43.
Vecsei A, Duringer P. Sequence stratigraphy of Middle Triassic carbonates and terrigenous deposits (Muschelkalk and Lower Keuper) in the SW Germanic Basin: maximum flooding versus maximum depth in intracratonic basins. Sed Geol. 2003;160(1–3):81–105. https://doi.org/10.1016/S0037-0738(02)00337-8.
Vecsei A, Rauscher R, Hohage K. Palynology of the marine Middle Triassic in the SW Germanic Basin (Upper Muschelkalk, Luxembourg): evidence for an important latest Anisian-early Ladinian sea-level lowstand. Paläontol Z. 2003;77(1):195–202. https://doi.org/10.1007/BF03004568.
Vidal J, Genter A. Overview of naturally permeable fractured reservoirs in the central and southern Upper Rhine Graben: Insights from geothermal wells. Geothermics. 2018;74:57–73. https://doi.org/10.1016/j.geothermics.2018.02.003.
Vidal J, Genter A, Chopin F. Permeable fracture zones in the hard rocks of the geothermal reservoir at Rittershoffen. France J Geophys Res. 2017;122(7):4864–87. https://doi.org/10.1002/2017JB014331.
Vidal J, Patrier P, Genter A, Beaufort D, Dezayes C, Glaas C, et al. Clay minerals related to the circulation of geothermal fluids in boreholes at Rittershoffen (Alsace, France). J Volcanol Geoth Res. 2018;349:192–204. https://doi.org/10.1016/j.jvolgeores.2017.10.019.

Vilà M, Fernández M, Jiménez-Munt I. Radiogenic heat production variability of some common lithological groups and its significance to lithospheric thermal modeling. Tectonophysics. 2010;490(3–4):152–64. https://doi.org/10.1016/j.tecto.2010.05.003.
Villemin T, Alvarez F, Angelier J. The Rhinegraben: extension, subsidence and shoulder uplift. Tectonophysics. 1986;128(1–2):47–59. https://doi.org/10.1016/0040-1951(86)90307-0.
Villemin T, Coletta B. Subsidence in the Rhine Graben: a new compilation of borehole data. In: ICL-WG-3. Symp.; 1990.
Vogel BC. Petrophysikalische und felsmechanische Untersuchung kristalliner Gesteine des Weschnitz-Plutons [Bachelorthesis]: TU Darmstadt; 2016.
Volpi G, Manzella A, Fiordelisi A. Investigation of geothermal structures by magnetotellurics (MT): an example from the Mt Amiata area, Italy. Geothermics. 2003;32(2):131–45. https://doi.org/10.1016/S0375-6505(03)00016-6.
von Seckendorff V. Der Magmatismus in und zwischen den spätvariscischen permokarbonen Sedimentbecken in Deutschland. SDGG. 2012;61:743–860. https://doi.org/10.1127/sdgg/61/2012/743.
von Seckendorff V, Arz C, Lorenz V. Magmatism of the late Variscan intermontane Saar-Nahe Basin (Germany): a review. Geol Soc Spec Publ. 2004;223(1):361–91. https://doi.org/10.1144/GSL.SP.2004.223.01.16.
Wächter J, Lehné R, Prein A, Hoselmann C, Schüth C. Zusammenführung von Bohrschichtinformationen zur bundesländerübergreifenden 3D-Modellierung im nördlichen Oberrheingraben. Grundwasser. 2018;23(4):337–46. https://doi.org/10.1007/s00767-018-0400-9.
Wagner GA. Fission track dating on apatite and sphene from the subvolcanics of the Kaiserstuhl (Germany). Neues Jahrbuch fuer Geologie und Palaeontologie: Monatshefte; 1976. p. 389–93.
Walenta K. Die Mineralien des Schwarzwaldes und ihre Fundstellen. München: Weise; 1992.
Wangen M. The blanketing effect in sedimentary basins. Basin Res. 1995;7(4):283–98. https://doi.org/10.1111/j.1365-2117.1995.tb00118.x.
Weber K. IV.C.1 The spessart crystalline complex. In: Dallmeyer RD, Franke W, Weber K, editors. Pre-Permian geology of Central and Eastern Europe. Berlin: Springer, Berlin Heidelberg; 1995a. p. 167–73.
Weber K. IV.C.3 The Saar-Nahe Basin. In: Dallmeyer RD, Franke W, Weber K, editors. Pre-Permian geology of Central and Eastern Europe. Berlin: Springer; 1995b. p. 182–5.
Weber JN. Geothermische Aufschlussanalyse des Steinbruches Mainzer Berg, oestlich von Darmstadt [Bachelorthesis]: TU Darmstadt; 2014.
Weinert S, Bär K, Sass I. Database of petrophysical properties of the Mid-German Crystalline Rise. Earth Syst Sci Data. 2021;13(3):1441–59. https://doi.org/10.5194/essd-13-1441-2021.
Weinert S, Bär K, Sass I. Petrophysical properties of the mid-german crystalline high: a database for Bavarian, Hessian, Rhineland-Palatinate and Thuringian Outcrops; 2020. doi:https://doi.org/10.25534/tudatalib-278.
Weisenberger T. Zeolites in fissures of crystalline basement rocks [PhD Thesis]: Albert-Ludwigs-Universität Freiburg im Breisgau; 2009.
Welsch B. Geothermische Untersuchungen an ausgewählten Standorten der Schwäbischen Alb [Bachelorthesis]: TU Darmstadt; 2011.
Wenk H-R, Wenk E. Physical constants of Alpine rocks: density, porosity, specific heat, thermal diffusivity and conductivity. Kümmerly und Frey: Leemann; 1969.
Wicke H. Faziesabhängigkeit geothermischer Kennwerte am Beispiel des Oberen Muschelkalk (Crailsheim, Baden-Württemberg) [Diplomathesis]: TU Darmstadt; 2009.
Wickert F, Altherr R, Deutsch M. Polyphase Variscan tectonics and metamorphism along a segment of the Saxothuringian-Moldanubian boundary: the Baden-Baden Zone, northern Schwarzwald (FRG). Geol Rundsch. 1990;79(3):627–47. https://doi.org/10.1007/BF01879206.
Wiedemann T. Autoklav und Thermotriaxialversuche zur Untersuchung des Einflusses von Fluid Gesteins Wechselwirkungen auf die Permeabilität [Master thesis]: Technical University Of Darmstadt; 2021.
Wiesner P. Modellierung einer mitteltiefen Erdwaermesonde zur Heiz-Grundlastabdeckung des Taunusgymnasiums Koenigstein [Masterthesis]: TU Darmstadt; 2014.
Will TM, Lee S-H, Schmädicke E, Frimmel HE, Okrusch M. Variscan terrane boundaries in the Odenwald-Spessart basement, Mid-German Crystalline Zone: new evidence from ocean ridge, intraplate and arc-derived metabasaltic rocks. Lithos. 2015;220–223:23–42. https://doi.org/10.1016/j.lithos.2015.01.018.
Witter JB, Trainor-Guitton WJ, Siler DL. Uncertainty and risk evaluation during the exploration stage of geothermal development: a review. Geothermics. 2019;78:233–42. https://doi.org/10.1016/j.geothermics.2018.12.011.
Zangerl C, Loew S, Eberhardt E. Structure, geometry and formation of brittle discontinuities in anisotropic crystalline rocks of the Central Gotthard Massif. Switzerland Eclogae Geol Helv. 2006;99(2):271–90. https://doi.org/10.1007/s00015-006-1190-0.
Zeh A, Gerdes A. Baltica- and Gondwana-derived sediments in the mid-german crystalline rise (Central Europe): implications for the closure of the Rheic ocean. Gondwana Res. 2010;17(2–3):254–63. https://doi.org/10.1016/j.gr.2009.08.004.
Zhang YK. The thermal blanketing effect of sediments on the rate and amount of subsidence in sedimentary basins formed by extension. Tectonophysics. 1993;218(4):297–308. https://doi.org/10.1016/0040-1951(93)90320-J.
Ziabakhsh-Ganji Z, Nick HM, Donselaar ME, Bruhn DF. Synergy potential for oil and geothermal energy exploitation. Appl Energy. 2018;212:1433–47. https://doi.org/10.1016/j.apenergy.2017.12.113.
Ziegler PA. Geological atlas of western and central Europe 1990. 2nd ed. The Hague: Shell Internationale Petroleum Maatschappij BV; 1990.
Ziegler PA. European Cenozoic rift system. Tectonophysics. 1992;208(1–3):91–111. https://doi.org/10.1016/0040-1951(92)90338-7.
Ziegler PA. Cenozoic rift system of Western and Central-Europe-an overview. Geol Mijnbouw. 1994;73(2–4):99–127.
Ziegler PA, Dèzes P. Evolution of the lithosphere in the area of the Rhine Rift system. Int J Earth Sci. 2005;94(4):594–614. https://doi.org/10.1007/s00531-005-0474-3.

Ziegler PA, Cloetingh S, van Wees J-D. Dynamics of intra-plate compressional deformation: the Alpine foreland and other examples. Tectonophysics. 1995;252(1–4):7–59. https://doi.org/10.1016/0040-1951(95)00102-6.
Zimmermann G, Zang A, Stephansson O, Klee G, Semiková H. Permeability enhancement and fracture development of hydraulic in situ experiments in the Äspö hard rock laboratory, Sweden. Rock Mech Rock Eng. 2019;52(2):495–515. https://doi.org/10.1007/s00603-018-1499-9.
Zoback MD, Barton CA, Brudy M, Castillo DA, Finkbeiner T, Grollimund BR, et al. Determination of stress orientation and magnitude in deep wells. Int J Rock Mech Min Sci. 2003;40(7–8):1049–76. https://doi.org/10.1016/j.ijrmms.2003.07.001.

Publisher's Note

3. Integrated 3D Geological Modelling of the Northern Upper Rhine Graben by Joint Inversion of Gravimetry and Magnetic Data

This chapter includes the peer-reviewed research article with same title that was published in the journal Tectonophysics (Elsevier) on the 20 August 2021. The content is unchanged and copyright protected.

The integrated 3D modelling of the crystalline basement in the northern Upper Rhine Graben is presented. First, the Hessen 3D and GeORG models were combined and harmonized. The model was then improved by joint inversion of gravity and magnetic data, which provided new insights into the structure and composition of the basement. For a realistic model parameterization, existing petrophysical databases were consulted and additionally over 430 measurements of the magnetic susceptibility were performed on relevant rock samples. The inversion yielded on the one hand the 3D geometry of the basement units including uncertainties and on the other hand detailed information about the petrophysical properties. This allowed an interpretation of the basement lithology below the sedimentary cover, which is essential for the site selection of geothermal drilling.

Reference:

Frey, M., Weinert, S., Bär, K., van der Vaart, J., Dezayes, C., Calcagno, P., & Sass, I. (2021). Integrated 3D geological modelling of the northern Upper Rhine Graben by joint inversion of gravimetry and magnetic data. Tectonophysics, 813, 228927. https://doi.org/10.1016/j.tecto.2021.228927 .

Tectonophysics 813 (2021) 228927

Contents lists available at ScienceDirect

Tectonophysics

journal homepage: www.elsevier.com/locate/tecto

Integrated 3D geological modelling of the northern Upper Rhine Graben by joint inversion of gravimetry and magnetic data

Matthis Frey [a,*], Sebastian Weinert [a,b], Kristian Bär [a], Jeroen van der Vaart [a], Chrystel Dezayes [c], Philippe Calcagno [c], Ingo Sass [a,b]

[a] Technical University of Darmstadt, Institute of Applied Geosciences, Department of Geothermal Science and Technology, Schnittspahnstraße 9, 64287 Darmstadt, Germany
[b] Darmstadt Graduate School of Excellence Energy Science and Engineering, Otto-Berndt-Straße 3, 64287 Darmstadt, Germany
[c] BRGM, 3, avenue Claude Guillemin, BP36009, 45060 Orléans cedex, France

ARTICLE INFO

Keywords:
Upper Rhine Graben
Joint inversion
Gravity
Magnetics
3D modelling
Petrophysics

ABSTRACT

The crystalline basement of the Upper Rhine Graben is a major target for deep geothermal exploration due to the generally high reservoir temperatures and the increased radiogenic heat production. The geothermal potential is strongly dependent on the lithology because mainly the thermal but also the hydraulic properties are affected by the rock type. For this reason, the so far most detailed 3D model of the basement in the northern Upper Rhine Graben was developed based on existing structural models, in particular the Hesse 3D 2.0 and GeORG models. Since only a few boreholes fully penetrate the thick sediment cover, additional magnetic and gravity data provided valuable information on the geometry of the deep horizons. To interpret the Bouguer anomalies reasonably with respect to the crystalline basement, the regional gravity field and sedimentary effect were subtracted from the observed data. In comparison to the commonly applied deterministic modelling approaches, a stochastic joint inversion of the gravity and magnetic anomalies was performed that utilizes the principles of a Monte-Carlo-Markov-Chain simulation. For an appropriate attribution of the model units, existing petrophysical databases of the region have been used and in addition, the magnetic susceptibility of more than 430 rock samples was measured. High-resolution voxel models of the density and susceptibility distribution were generated as a result of the inversion, which allow conclusions about the crustal composition under the sedimentary formations. An interpretative map of the basement geology, derived from the inversion results, is presented.

1. Introduction

The Upper Rhine Graben (URG), with its elevated geothermal gradient of locally more than 100 °C/km (Agemar et al., 2012), is one of the main targets for geothermal research and exploitation in Central Europe. Besides the sedimentary horizons, the crystalline basement is due to the favorable temperatures attractive for deep geothermal projects in this region (e.g. Jain et al., 2015). Currently, the power plants in Landau, Insheim, Rittershoffen and Soultz-sous-Forêts, use inter alia the top basement for heat or heat and power co-generation. On top of that, several other projects throughout the entire URG are in planning or under development. The deep geothermal potential of crystalline reservoirs depends on a number of parameters, which are primarily controlled by the respective lithology. First, the thermal structure of the crust in the URG is, in addition to the shallow Moho depth and the deep fluid circulation patterns along large-scale fault zones (Bächler et al., 2003), directly related to the radiogenic heat production of the basement (Jaupart et al., 2016; Lachenbruch, 1970; Mareschal and Jaupart, 2013). While the highest values are measured in granites due to the increased concentration of radioactive elements, the heat production of mafic rocks is on average almost one magnitude smaller (Vilà et al., 2010). Likewise, the thermal conductivity of granites is by a factor of 1.3 higher than in gabbros (Weinert et al., 2020a). Moreover, also the hydraulic conductivity of the basement is strongly influenced by the lithology. Stober and Bucher (2007) could show from hydraulic test data in the Black Forest that granites have on average 2 magnitudes higher natural permeabilities than gneisses. This observation can be attributed, on the one hand, to the significant permeability anisotropy due to layered mica minerals in gneisses and, on the other hand, to the preferred fracturing along those layers with an increased tendency of

* Corresponding author.
E-mail address: frey@geo.tu-darmstadt.de (M. Frey).

https://doi.org/10.1016/j.tecto.2021.228927
Received 15 December 2020; Received in revised form 6 May 2021; Accepted 11 May 2021
Available online 13 May 2021

reclosing. In summary, felsic intrusions represent the preferred targets for deep geothermal wells, whereas mafic and metamorphic rocks have less advantageous thermal and hydraulic properties.

In the URG, knowledge about the basement structure and composition beneath the sedimentary cover is limited due to the scarcity of very deep wells reaching crystalline rocks and crustal-scale seismic profiles such as the DEKORP 9 N line. (Brun et al., 1992; Meier and Eisbacher, 1991; Meissner and Bortfeld, 1990). Key information is therefore mainly provided by the crystalline outcrops at the graben borders, which for example allow the conduction of analogue studies (Bär, 2012; Dezayes et al., 2021; Weinert et al., 2020a; Welsch et al., 2014). Additional constraints are given by gravity and magnetic data that are available throughout the whole area. In the past decades, several attempts have already been made to model the crystalline basement based on the available data and to determine its properties more precisely. In this context, the work of Edel and Fluck (1989), Rousset et al. (1993), Rotstein et al. (2006), Edel and Schulmann (2009), Baillieux et al. (2013), Freymark et al. (2015), Freymark et al. (2017), Edel et al. (2018) and Weinert et al. (2021), in prep. should be mentioned. In contrast to these studies, a joint inversion of gravity and magnetic data was performed, that has already been successfully applied in other regions (Frey and Ebbing, 2020; Gallardo and Thebaud, 2012; Kamm et al., 2015). Compared to time-consuming forward modelling, this approach automatically generates complex petrophysical models that are moreover easily reproducible. From these, the basement lithology can be deduced, which will enable more reliable estimates of geothermal potentials in the future.

Inversions are widely used in the geosciences to infer the distribution of petrophysical properties in the subsurface from physical parameters measured at the surface, such as the arrival times of seismic waves, the acceleration of gravity or the magnetic field strength (Bosch and McGaughey, 2001; Li and Oldenburg, 1996, 1998). From this, information about geological structures can be derived. With advancing computer capacity, calculation-intensive stochastic inversions, like the Monte-Carlo-Markov-Chain method, have become increasingly important in the last 2 to 3 decades (Bosch et al., 2006; Mosegaard and Tarantola, 1995). A major advantage of this method compared to deterministic modelling is that a collection of possible solutions is generated, allowing a statistical analysis to compute, for example, model uncertainties. To obtain reliable inversion results, comprehensive information on the petrophysical properties of the model units is required. Therefore, more than 430 rock samples were analyzed with regard to their magnetic susceptibility. Information on the rock density was taken from existing databases (Bär et al., 2020; Weinert et al., 2020b).

2. Geological setting

2.1. Tectonics

The URG represents the central part of the European Cenozoic Rift System (ECRIS) (Fig. 1), which consists of several tectonic grabens extending over more than 1200 km from the Mediterranean to the North

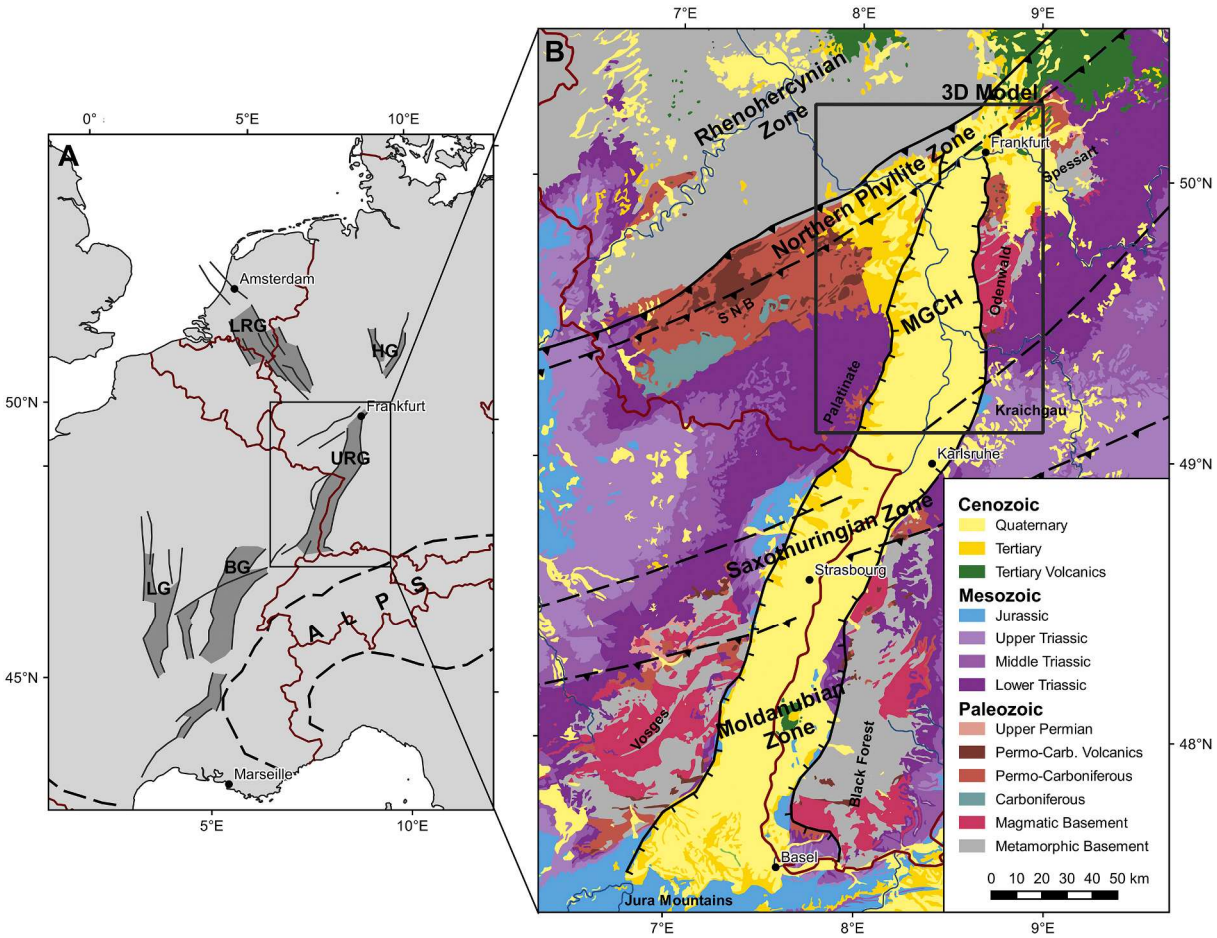

Fig. 1. Overview of the study area: (A) simplified map of the European Cenozoic Rift System (modified after Ziegler and Dèzes, 2005), dark gray areas represent rift-related sediment basins; (B) geological map of the URG including boundaries of the Variscan basement units. The black box shows the location of the 3D model. BG = Bresse Graben, HG = Hessian Grabens, LG = Limagne Graben, LRG = Lower Rhine Graben, MGCH = Mid-German Crystalline High, SNB = Saar-Nahe Basin, URG = Upper Rhine Graben. (For interpretation of the references to color in this figure legend, the reader is referred to the web version of this article.)

Sea (Dèzes et al., 2004; Ziegler, 1992; Ziegler and Dèzes, 2005). The northern URG region has a complex geological structure due to its changeful plate tectonic history from the Early Paleozoic to present (Dallmeyer et al., 1995; McCann, 2008a, 2008b; Ziegler, 1990). The opening of this passive continental rift started in the late Eocene as a reaction to the changing lithospheric stress field in the alpine foreland (Behrmann et al., 2003; Buchner, 1981; Villemin and Bergerat, 1987). Both location and orientation of the URG are largely controlled by reactivation of major fault and shear zones in the basement that were already established during the Variscan orogeny (Edel et al., 2007; Grimmer et al., 2017; Schumacher, 2002).

The crystalline basement in the URG comprises units of the northern side of the Variscan orogenic belt that formed due to the convergence of Laurussia and Gondwana in the Middle Paleozoic (Behr et al., 1984; Franke, 2000; Giese, 1995; Kroner et al., 2008; Zeh and Gerdes, 2010). The paleogeographic environment between these major continents was characterized by various micro terranes and marine basins, also known as Armorican Terrane Assemblage, which had been separated from the northern margin of Gondwana since the Cambrian (Crowley et al., 2000; Franke et al., 2017; Kemnitz et al., 2002). Accordingly, the Variscan mountain range shows strong changes in age, lithology and metamorphic grade mainly perpendicular but also parallel to the main strike direction of NE-SW (Okrusch, 1995; Oncken, 1995). The subduction of the oceanic basins as a result of the advancing convergence led to the formation of extensive volcanic arcs in the Devonian and Carboniferous, exposed e.g. in the Odenwald, Black Forest and Vosges (Okrusch et al., 1995; Stein, 2001; Timmermann, 2008). The complete closure of the oceans was followed by the main collision phase in Visean and Namurian times during which the individual terranes were juxtaposed and pronounced continental thrusts were established along the oceanic sutures (McCann et al., 2008; Oncken et al., 1999; Skrzypek et al., 2014).

Shortly after this collision phase, the regional stress field was reoriented towards an extensional/transtensional regime, resulting in a rapid collapse of the Variscides and opening of numerous NE-SW striking intramontane basins, such as the Saar-Nahe Basin (Henk, 1993a, 1993b; Scheck-Wenderoth et al., 2008; Weber, 1995a). These were filled with erosional debris from the surrounding mountain ranges, reaching a cumulative thickness of up to 10 km (Henk, 1992; Schäfer, 1989, 2011). In addition, the rifting was accompanied by widespread felsic to mafic volcanism at the Carboniferous-Permian boundary (von Seckendorff et al., 2004). In the Mesozoic, sedimentation was no longer limited to these basins. The Triassic and Jurassic sediments document continuous changes in the depositional environment caused by eustatic sea-level fluctuations in the adjacent Arctic and Tethys Oceans (Feist-Burkhardt et al., 2008). During the Upper Jurassic and Cretaceous, especially the northern URG region was affected by minor volcanism (Böcker, 2015; Martha et al., 2014) and uplift movements, which led to partial erosion of the sediments (Sittler, 1969, 1992). Consequently, the age of the youngest Mesozoic formations increases continuously from south to north, with no more Mesozoic formation preserved in the northernmost part of the URG.

The Cenozoic formation of the URG is usually divided into two main phases (Behrmann et al., 2003; Buchner, 1981; Dèzes et al., 2004; Villemin et al., 1986). During the first phase from the Late Eocene to the Early Miocene, most of the crustal extension took place. In this period, the main horizontal stress direction S_H was roughly NNE-SSW. In the second phase from the Miocene to the present, the stress field was reoriented with S_H mainly trending in NW-SE direction, leading to sinistral reactivation of faults zones parallel to the main graben axis (Buchmann and Connolly, 2007; Homuth et al., 2014). While a transtensional regime in the northern URG led to subsidence of the sedimentary basin, the southern part was affected by transpression (Illies and Greiner, 1979; Rotstein and Schaming, 2011). Latter caused uplift in the Middle and Late Miocene, resulting in erosion or non-deposition of sediments and thus in a hiatus of about 10 Ma (Geyer et al., 2011; Grimmer et al., 2017). All sedimentary units as well as the Variscan basement in this region are affected by intensive faulting with vertical offsets between fault blocks of partly several hundred meters. The total horizontal extension ranges from about 5 to 8 km and the total vertical offset reaches up to 4 km (Grimmer et al., 2017; Meier and Eisbacher, 1991).

Based on analysis of gravity and magnetic data as well as field observations at the graben margins, the existence of a NNE-striking crustal-scale shear zone in the crystalline basement of the URG has been postulated, which may have already developed during the juxtaposition of Variscan terranes in the Visean (Edel et al., 2007; Edel and Weber, 1995; Schumacher, 2002). According to the authors, this sinistral transform system had a considerable impact on past and recent deformation in the URG due to multiple reactivations. Thus far, however, the shear zone has not been detected in any boreholes, meaning that no definite statements can be made about its exact location, geometry and structure.

2.2. Pre-Permian crystalline basement

A first definition of the Variscan basement in Central Europe was developed by Suess (1926) and Kossmat (1927) and has been continuously expanded since then. The following main units can be distinguished from north to south: Rhenohercynian Zone, Northern Phyllite Zone, Mid-German Crystalline High (MGCH), Saxothuringian Zone and Moldanubian Zone (Figs. 1 and 2). In the northern URG, the MGCH makes up the largest part of the basement. It is traditionally seen as the deeply exposed northern active margin of the Armorican Terrain Assemblage, that formed between the Late Devonian and Mid-Carboniferous as a result of the southward subduction of the Rheic and Rhenohercynian Oceans (Hirschmann, 1995; Zeh and Gerdes, 2010).

The largest and hence most important outcrop of the MGCH in the URG region is the crystalline Odenwald (Fig. 2), which is usually divided into the eastern, metamorphic Böllstein Odenwald and the western, mainly plutonic Bergsträßer Odenwald (Krohe and Willner, 1995; Stein, 2001). Both units are separated by the Otzberg Zone, a crustal-scale sinistral strike-slip fault. The Böllstein Odenwald consists of a granitic and granodioritic orthogneiss core, surrounded by metapelitic schists. According to Reischmann et al. (2001), the age of the protoliths is 405 ± 3 Ma, thus presumably representing relics of a Silurian/Early Devonian magmatic arc (Altenberger and Besch, 1993). Due to the great lithological similarities, the Spessart is most likely the northeastern extension of the Böllstein Odenwald (Weber, 1995b). The Bergsträßer Odenwald consists mainly of mafic to felsic plutonic rocks, that are intruded into Early Paleozoic metasediments, the so-called 'Schieferzüge' (Krohe, 1991, 1992). This unit is again subdivided into the Frankenstein Complex, the Flasergranitoid Zone and the Southern Plutons, each separated by large strike-slip fault zones. The first two units have a very heterogeneous structure due to numerous local intrusions. The southern Bergsträßer Odenwald, in comparison, is dominated by large and homogeneous plutons (Weschnitz, Tromm, Heidelberg pluton). From north to south, the age of the intrusions is continuously decreasing from about 360 Ma in the Frankenstein Complex to about 325 Ma in the Heidelberg area (Kirsch et al., 1988; Kreuzer and Harre, 1975). Likewise, the rock composition is rather mafic in the north and becomes felsic towards the south (Laue et al., 1990; Okrusch et al., 1995). The Bergsträßer Odenwald is hence interpreted as a transition zone from an island arc to an active continental margin (Altherr et al., 1999).

In the Palatinate west of the URG, surface exposures of the MCGH are very limited (Flöttmann and Oncken, 1992; Laue and Reischmann, 1994). The largest outcrop is located in Albersweiler, where orthogneisses derived from 369 ± 5 Ma old magmatic protoliths are strongly intercalated with metamorphosed mafic dykes (Stellrecht, 1971; Anthes and Reischmann, 1997). In the nearby Waldhambach quarry, granodiorite is predominant alongside amphibolite and gneiss. Metagreywackes and metapelites were found at several locations, e.g. in Burrweiler,

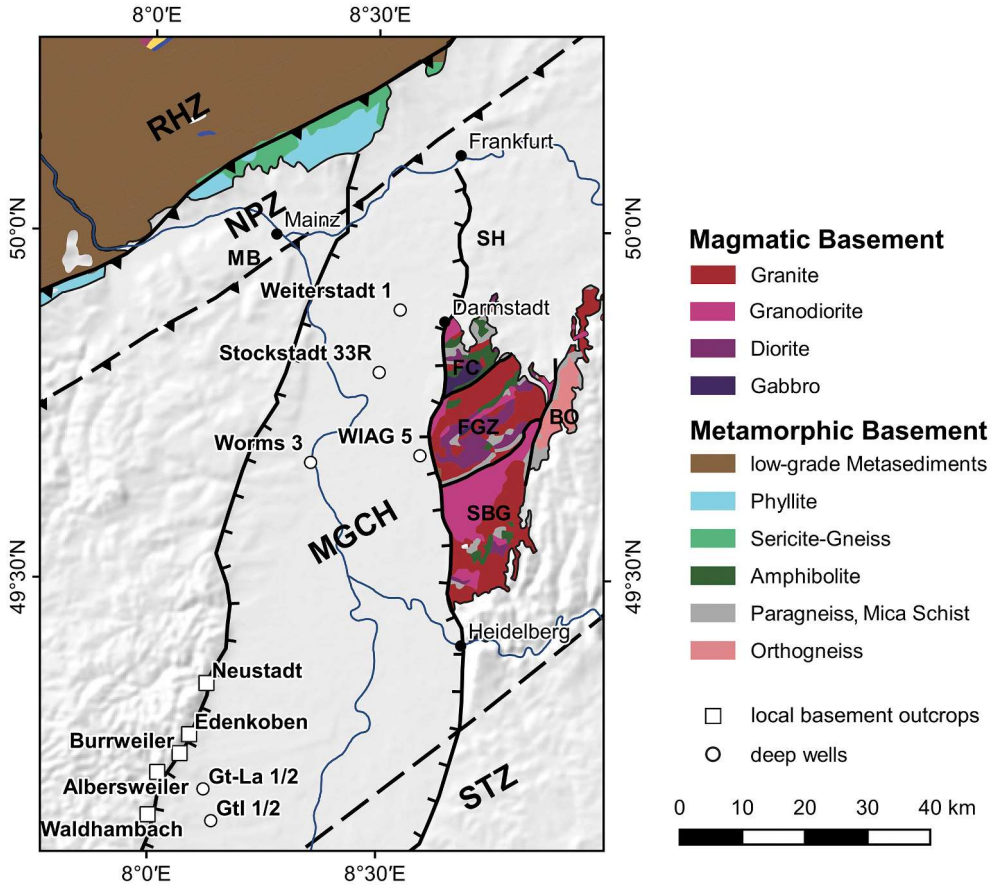

Fig. 2. Generalized map illustrating the basement outcrops in the northern URG region including the available wells intersecting the basement. BO = Böllstein Odenwald, FC = Frankenstein Complex, FGZ = Flaser-Granitoid Zone, MB = Mainz Basin, MGCH = Mid-German Crystalline High, NPZ = Northern Phyllite Zone, RHZ = Rhenohercynian Zone, SBG = Southern Bergsträßer Granitoids, SH = Sprendlinger Horst, STZ = Saxothuringian Zone.

Neustadt and Weiler. Granitoid intrusions with an age of about 340 Ma are present in the Schwarzbach valley, the Kaiserbach valley and Edenkoben (Frenzel, 1971). Apart from the above-mentioned outcrops, only a few deep boreholes penetrate the basement in the northern URG (Bär, 2012). Granitoids are predominant at most locations and additionally, amphibolites were drilled in the wells Weiterstadt 1 and WIAG Hessen 5. In the well Worms 3, the basement consists of fractured gneisses and cataclasites that might be related to the adjacent Worms Fault Zone within the URG.

In the north, the MGCH borders the Northern Phyllite Zone, which is exposed in the southern Taunus and Hunsrück (Anderle et al., 1995; Klügel, 1997). This zone comprises a tectonic mélange of about $^{2}/_{3}$ sedimentary and $^{1}/_{3}$ volcanic rocks that were overprinted by pressure-dominated greenschist-facies conditions. The boundary between the two units is a major continental thrust, but the exact location is still unknown due to the complete sedimentary cover. Xenoliths from the Vogelsberg can be assigned to both the Northern Phyllite Zone and the MGCH, allowing to trace the tectonic contact beneath the Miocene volcanics (Martha et al., 2014).

In the south, the MGCH transitions into the Saxothuringian Zone, which crops out in the northern Black Forest and Vosges (McCann et al., 2008). This zone comprises a metamorphosed, early Paleozoic shelf sequence that overlies a Neoproterozoic gneiss basement. The style of the boundary between MGCH and Saxothuringia is still under debate, but the location can be inferred from the gravity anomalies (Edel and Fluck, 1989; Giese, 1995), as the latter is characterized by a distinct high density.

2.3. Post-Variscan sediments

The sedimentary cover and especially the Cenozoic infill of the northern URG was, in contrast to the crystalline basement, well studied by the extensive hydrocarbon exploration since the 1950s (Reinhold et al., 2016; Boigk, 1981). An overview of the distribution and lithological properties of the most important horizons is given in the following.

The Permo-Carboniferous is overlying the crystalline basement of the northern URG on a large area. It mainly consists of erosional debris from the Variscan mountain chain and intercalated volcanics, which were deposited in several NE-SW oriented transtensional basins, like the Saar-Nahe Basin, the Hessian Basin or the Kraichgau Trough (Aretz et al., 2016; Henk, 1993b; Schäfer, 1989; Weber, 1995a). Close to the Hunsrück border fault, these deposits reach their maximum thickness of more than 6.5 km. The Saar-Nahe Basin continues to the northeast under the Cenozoic cover of the northern URG up to the Sprendlinger Horst (Molenaar et al., 2015; Müller, 1996), but the thickness is much smaller here (Marell, 1989). The volcanic formations consist of rhyolite, andesite and basalt, which occur in form of dikes and lava flows (Hertle, 2003; Stollhofen, 1998). They are heterogeneously distributed in the URG region and an accurate 3D representation is difficult due to the poor well data availability.

The Buntsandstein mainly consists of clastic sedimentary rocks, which reflect the terrestrial conditions in the Lower Triassic. This succession is dominated by uniform red-brown or light gray sandstone sequences with alternating fine- and coarse-grained layers (Backhaus, 1974). The Buntsandstein is exposed over a large area in the Palatinate

and eastern Odenwald (Backhaus, 1975; Backhaus and Heim, 1995; Backhaus and Schwarz, 2003; Dachroth, 1988). In the URG, however, the horizon is only found approximately south of Worms at a depth of more than 2.5 km and has a maximum thickness of about 500 m (Bär, 2012; Boigk and Schöneich, 1974). Younger Triassic sediments only occur south of Heidelberg and their total thickness is usually less than 500 m (Sokol et al., 2013). The Muschelkalk consists of marine limestones and dolostones, documenting a full marine sedimentary environment. In contrast, the Keuper, is dominated by claystones and sandstones, which are interbedded by evaporite layers.

With the opening of the URG in the Eocene, an important sedimentary basin was again established, in which marl, sandstones, carbonates, and evaporites were alternatingly deposited (Doebl, 1967; Sissingh, 1998). The sedimentary conditions were predominantly limnic or brackish, but at least two marine transgressions are also documented. Almost in the entire northern URG, the Cenozoic graben infill has a thickness of more than 2000 m. The highest thickness of 3300 m is reached close to the eastern margin between Worms and Heidelberg (Doebl and Olbrecht, 1974).

3. Material and methods

3.1. Data

3.1.1. Geological information

The initial 3D model of the northern URG was mainly developed by compiling existing structural models (Fig. 3). In the inner part of the graben as well as in the remaining area of Hesse, the detailed models of the Interreg GeORG and Hessen 3D (1.0 and 2.0) projects were used (Arndt, 2012; Bär et al., 2016; Sokol et al., 2013; Weinert et al., 2021, in prep.), which are based on 2D reflection seismic data, borehole data, geological profiles and isopach maps. At the southern border of Hesse, where the study areas of these projects partly overlap, the depth of specific horizons can deviate by several hundred meters. In order to harmonize these different results, also the recently reprocessed and reinterpreted DEKORP 9 N line was incorporated (Bär et al., 2021, in prep.). Based on the GeORG and Hessen 3D models, a simplified fault model containing about a dozen of the largest faults in the northern URG region was furthermore developed. For the areas outside the URG that are not located in Hesse, information on horizon depths was extracted from the models of Freymark et al. (2015) and Freymark et al. (2020). Due to the lower density of the input data there, the model resolution is also lower but still acceptable, since the main focus was not on the graben shoulders where outcrops provide sufficient details on the crystalline basement. Additionally, the depth of the Moho and lower crust from the Freymark et al. (2020) model was used to calculate a regional gravity field (see section 3.2.1 for more details).

Apart from the mentioned modelling results, geological contacts and outcrops of large fault zones at the surface were digitized from various geological maps. To validate the initial model and the inversion result, especially with regard to the basement lithology, a database provided by the Hessian State Agency for Nature Conservation, Environment and Geology (HLNUG) containing about 170 boreholes deeper than 70 m was used. However, most of the wells are located in the Odenwald or on the Sprendlinger Horst outside the URG. Therefore, information on crystalline rocks beneath the Permo-Triassic and Cenozoic graben infill is very sparse. A summary of the deep crystalline basement wells in the northern URG is given in Table 1.

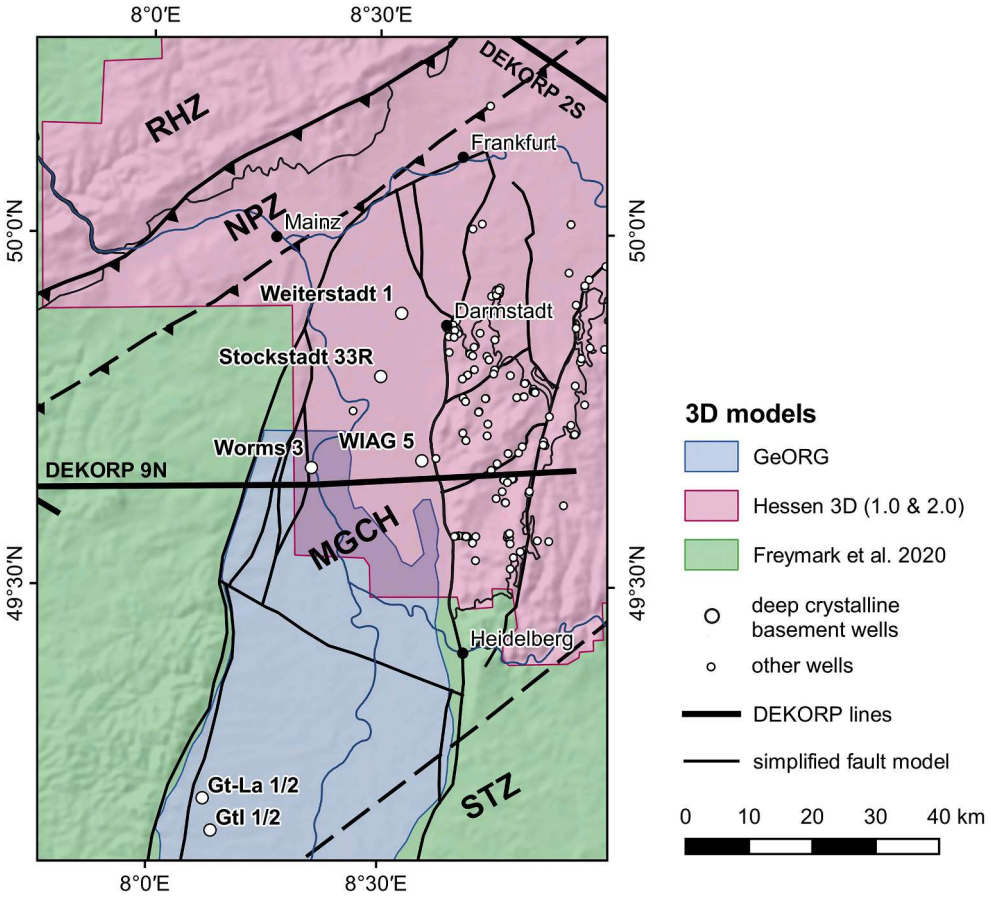

Fig. 3. Overview of the structural input data for the 3D modelling of the northern URG. RHZ = Rhenohercynian Zone, NPZ = Northern Phyllite Zone, MGCH = Mid-German Crystalline High, STZ = Saxothuringian Zone, URG = Upper Rhine Graben.

Table 1
Summary the deep wells in the northern URG reaching the crystalline basement.

Well name	Depth to top basement [m]	Basement lithology	Petrophysical data available
Insheim GTI 1/2	3418, 3338 TVD	granite	–
Landau GtLa 1/2	2487, 2550 TVD	granite	–
Stockstadt 33R	2245 MD	granodiorit	Frey et al. (2020), Weinert et al. (2020a)
Weiterstadt 1	2505 MD	granite, amphibolite	Frey et al. (2020), Weinert et al. (2020a)
WIAG Hessen 5	2180 MD	granite, amphibolites	–
Worms 3	2204 MD	fractured gneiss	Frey et al. (2020), Weinert et al. (2020a)

3.1.2. Gravity and magnetic data

For the gravity modelling, a compilation of terrestrial point measurements provided by the Leibniz Institute for Applied Geophysics (LIAG), the Hessian Administration for Soil Management and Geoinformation (HVBG) and the State Agency for Surveying and Geo Base Information Rhineland-Palatinate (LVermGeo) was used. In the study area, the combined dataset consists of more than 7000 stations with a distance between a few hundred meters and about 2 km. Consequently, the resolution of the observed gravity anomalies varies considerably across the northern URG and the adjacent areas. A complete Bouguer correction has been carried out with a reference density of 2.67 g/cm^3. From this point data, a Bouguer anomaly grid with a nominal resolution of 500 m was calculated by applying a minimum curvature approach (Fig. 4A).

The values of the gravity anomalies range from about −40 to +20 mGal. The inner part of the URG is characterized by a distinct negative anomaly that can to a large extent be explained by the relatively light sedimentary infill. The largest anomaly highs represent rather local features and are located at the mafic Frankenstein Complex and the Mainz Basin. There are moreover some broader highs, for example in the Kraichgau and the Palatinate.

The total magnetic field anomaly grid shown in Fig. 4B is a compiled dataset of several surface and aero-geophysical surveys that have been carried out since the 1960s (Gabriel et al., 2011). Airborne measurements have been performed by PRAKLA-SEISMOS between 1965 and 1971 with a line-spacing of 2200 m and a point distance of approximately 65 m. Besides, the LIAG and predecessor institutes conducted supplementary magnetic surveys. As for the gravity field, there are therefore lateral variations of the resolution.

The anomalies vary from about −150 nT to more than 300 nT in the northern URG. The magnetic field in the northern URG is dominated by SW-NE striking features which are most likely caused by the Variscan units. Their pronunciation possibly results from the steeply dipping foliation of the basement units, as observed, for example, in the Flasergranitoid Zone. In addition, a laterally heterogeneous upper crust is indicated by the abundant local variations. The strongest magnetic high coincides with the above-mentioned gravity anomaly at the Frankenstein Complex. This anomaly extends to the SW underneath the graben infill and might be furthermore associated with the magnetic high at the southeastern Palatinate. Another broad positive anomaly is located in the area of the southern Odenwald plutons. Magnetic anomaly lows are mostly concentrated in an SW-NE trending belt at the northern and western margin of the MGCH. Another distinct negative anomaly is connected to the Flasergranitoid Zone and the Böllstein Odenwald.

The post-Varican deposits can generally be considered magnetically transparent due to their low magnetic susceptibility (Table 2; Frey et al., 2020). Excluded from this assumption are the Permo-Carboniferous volcanic-sedimentary horizons and the scattered tertiary volcanics (Vogelsberg, Roßdorf, Otzberg, Messel). Especially in the Saar-Nahe Basin, at the Vogelsberg and at the northern margin of the URG, these volcanics are source for strong and short wavelength magnetic anomalies, which are also partly linked to positive gravity anomalies (e.g. Mainz Basin).

3.1.3. Petrophysical data

Comprehensive data on the rock density and magnetic susceptibility of the common lithologies in the northern URG were collected in order to attribute realistic petrophysical properties to the geological units in the gravity and magnetic models. Density measurements have been conducted in several previous studies and the results were compiled in the P^3 database (Bär et al., 2020). A summary of the petrophysical parameters of the MGCH is additionally given in the database of Weinert et al. (2020a, 2020b). The density distribution of the Cenozoic sediments was inferred from borehole logs of the five deep wells Eich 22, Eich 27, Eich H1, Weiterstadt 1 and Worms 3 in the northern URG. Besides, measurements of the magnetic susceptibility were done with the SM-30 handheld device from GeoResults. In total about 430 samples of various geological units provided by the Institute for Rock Conservation (IfS) in Mainz were analyzed (Frey et al., 2020). Figs. 4C and D show the distribution of all density and susceptibility measurements in the study area. In case, very little or no information was available, e.g. in the Saxothuringian or Rhenohercynian Zones, values from the models of Freymark et al. (2015) and Edel and Schulmann (2009) were adopted.

Table 2 summarizes petrophysical parameters for the main rock types. Because the model units (Table 3) are lithologically heterogeneous, a volumetric approach to calculate the model parameters was applied. This means that the parameters from Table 2 were weighted by the area fraction of the rock type in the respective unit. For the Permo-Carboniferous, Mesozoic and Cenozoic sediments, density-depth gradients were defined to account for the compaction caused by the increasing load.

For all basement units, a parameter optimization was performed before inversion to achieve a good initial fit between the forward modelled and observed potential fields. An optimization is required because, apart from the Odenwald and Saar-Nahe Basin, only very few outcrops of the crystalline basement are available, thus the distribution of density and magnetic susceptibility is not sufficiently constrained. Moreover, samples from quarries and natural outcrops are not necessarily representative for the entire model unit due to e.g. weathering and exhumation effects. A summary of the initial, optimized and inverted properties is given in Table 4.

3.2. Methods

3.2.1. 3D geological forward modelling

The 3D structural modelling of the northern URG was performed with the commercial platform GeoModeller (Calcagno et al., 2008; Guillen et al., 2008; Lajaunie et al., 1997), which enables the development of complex geological models based on different input data and allows the integration and inversion of geophysical measurements. The software uses the principles of potential field interpolation and considers both structural data and stratigraphic rules to construct the model (Calcagno et al., 2008; Lajaunie et al., 1997). Geological contacts are considered as isopotential surfaces and the orientation of a horizon corresponds to the gradient of the field. This ensures that a consistent and smooth model is created in agreement with defined geological rules, e.g. chronology and relations between the geological events.

The model domain has a size of 90 km in E-W and 130 km in N-S

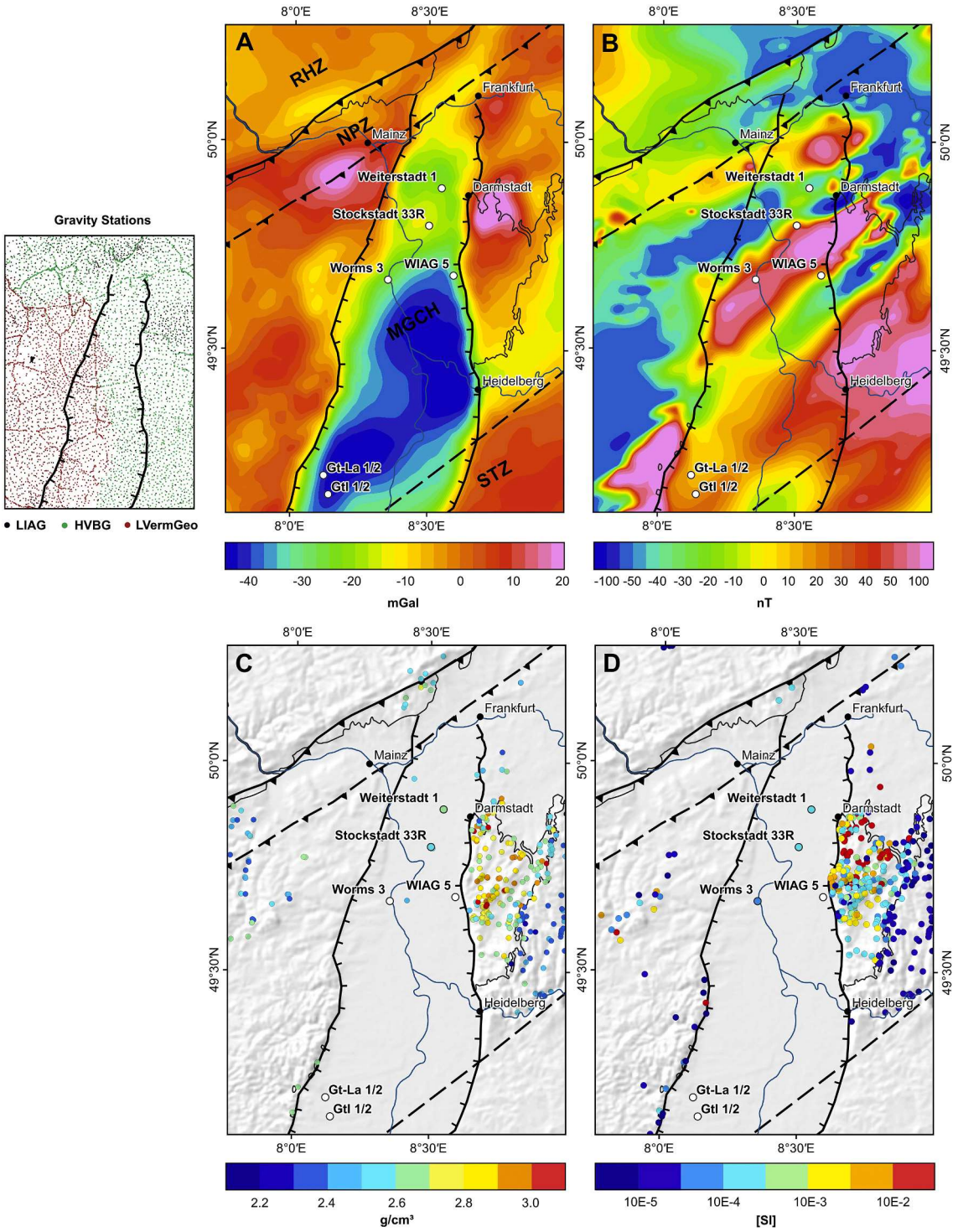

Fig. 4. Overview of the geophysical and petrophysical input data: (A) Bouguer anomalies in the northern URG region including map of the used gravity stations; (B) magnetic anomalies; (C) sample locations of bulk density measurements; (D) sample locations of magnetic susceptibility measurements. RHZ = Rhenohercynian Zone, NPZ = Northern Phyllite Zone, MGCH = Mid-German Crystalline High, STZ = Saxothuringian Zone, URG = Upper Rhine Graben. (Data Basis and Copyright of the gravity and magnetic data: Leibniz Institut für Angewandte Geophysik, Hannover; Hessische Verwaltung für Bodenmanagement und Geoinformation; Geobasisinformationen der Vermessungs- und Katasterverwaltung Rheinland-Pfalz).

direction (see Fig. 1). It covers a large part of the graben shoulders, since the main outcrops of the crystalline basement are located here. The top surface of the model is the DEM given by the Shuttle Radar Topography Mission (SRTM) (van Zyl, 2001) with an original resolution of one arc second and was resampled to a cell size of 500 m to reduce the computational effort.

To separate the different sources of the gravity field, three distinct forward models, a regional, a sedimentary and a basement model of the northern URG were developed that cover different depth intervals of the lithosphere. A summary of all model units is given in Table 3. The individual gravitational effects of the regional and sedimentary model were forward calculated and subtracted from the observed field. This

Table 2
Petrophysical properties of the main lithologies from the northern URG region that were measured on rock samples.

Rock type	Mean density [g/cm^3]	Mean magnetic susceptibility [SI]
Granite	2.65 ± 0.028	0.0020 ± 0.0043
Granodiorite	2.72 ± 0.062	0.0017 ± 0.0020
Diorite	2.80 ± 0.052	0.0062 ± 0.0094
Gabbro	2.90 ± 0.068	0.0221 ± 0.0284
Low-grade metasediments	2.73 ± 0.088	–
Gneiss	2.65 ± 0.055	0.0012 ± 0.0041
Amphibolite	2.91 ± 0.125	0.0089 ± 0.0114
Permian and Cenozoic volcanics	2.72 ± 0.147	0.0065 ± 0.0089
Permian and Triassic sandstones	2.46 ± 0.116	1.9*E*-5 ± 2.2E-5
Cenozoic sandstones	2.25 ± 0.104	–

approach, also known as stripping (e.g. Hammer, 1963), results in a residual map of the Bouguer anomalies (Fig. 7) that provides direct insight into the density distribution of the crystalline basement. Based on this product as well as the magnetic anomalies and structural data, the initial basement model was created.

The basement model consists of 10 units, whereby the MGCH was divided into 7 subunits (Fig. 5). According to the surface outcrops, the 4 units Frankenstein Complex, Flasergranitoid Zone, Southern Odenwald and Böllstein Odenwald were defined. To explain the positive gravity and magnetic anomaly in the Southeast Palatinate, an additional body with similar properties as the Frankenstein Complex was introduced, referred to as the Southwestern Magnetic Body in the following. The northwestern part of the MGCH was modelled as a separate body, which is characterized by a high density and low susceptibility, analogously to the Saxothuringian Zone. However, due to the scarcity of wells and outcrops, little information is available about this zone's composition. Finally, a granitoid body of reduced density was defined north of the Frankenstein Complex, which explains the local gravity low and is evidenced by small outcrops and boreholes at the Sprendlinger Horst.

In areas where the geological contacts are not exposed, the model geometry is based on the magnetic and gravity anomalies or on existing interpretations (e.g. Franke, 2000; Will et al., 2015). The boundaries between the main tectonic units were modelled as southeastwards dipping thrusts according to the DEKORP 2S and 9 N lines (Behr and Heinrichs, 1987; Jodocy and Stober, 2010; Oncken, 1998). The interfaces between the plutonic bodies of the MGCH are generally assumed to be steeply dipping.

3.2.2. 3D joint-inversion

A structure-coupled joint inversion of gravity and magnetic data has been carried out to improve the developed basement forward model and to gain detailed insights about the spatial distribution of petrophysical properties. In contrast to the separate inversion of the two potential fields, this approach reduces the non-uniqueness of the modelling result. A stochastic inversion algorithm based on a Monte-Carlo simulation is implemented in GeoModeller. The inversion explores a large number of variations of the structural and petrophysical models. Those realizations which reduce the inconsistencies between the calculated and observed anomalies are selected and allow a statistical evaluation of the inversion results. A detailed description of the inversion scheme is given in Guillen et al. (2008). In the following and in Fig. 6, the specific workflow applied in this study is summarized:

1. A priori model
   The basement forward model served as the a priori information for the inversion. The parametrization of the individual units is constrained by the petrophysical data and the optimized densities and magnetic susceptibilities shown in Table 4 were used as starting values. The parameters of the sediments and the lower crust were set to constant reference values (density = 2.67 g/cm^3 and magnetic susceptibility = 0) as their effect was already considered during the forward modelling.
2. Model discretization
   For the inversion, the continuous horizons were converted into a discrete cuboid voxel model. The cell size has to be small enough to represent the geological structures adequately. It should be noted, however, that the computational effort increases of course with a growing number of voxels. Therefore, a uniform cell size of 1 × 1 km was used in the horizontal plane. In vertical direction, a varying cell size was defined. To take into account the topographic effects, a relatively small cell height of 50 m was used above the mean sea level. Below, the cell height increases gradually from 500 m to about 1500 m towards the base. Consequently, the model consists in total of about 540,000 voxels.
3. Calculation of gravity and magnetic anomalies
   The geophysical response of the initial density and susceptibility model is calculated by summing the effect of each voxel. The calculation was done on a constant height of 1000 m a.s.l. to minimize model artifacts, for example, due to the discretization.
4. Disturbing the model
   During each iteration, either petrophysical properties or the lithology of one cell are randomly changed according to the defined probability density functions. The magnitude of lithology changes is

Table 3
Summary of the three forward models including the modelled units and their main lithology.

Model	Horizon	Main lithology
Sedimentary model	Cenozoic	sandstones, claystones, marl, subordinate carbonates and evaporites
	Keuper	sandstones, claystones, subordinate evaporites
	Muschelkalk	limestones, dolostones
	Buntsandstein	sandstones, subordinate claystones
	Permo-Carboniferous	sandstones, conglomerate, subordinate claystones, felsic to mafic volcanic rocks
Regional model	Lower Crust	mafic and metamorphic rocks
	Lithospheric Mantle	ultrasmafic rocks
Basement model	Rhenohercynian Zone	low-grade metasediments
	Northern Phyllite Zone	metasediments, metavolcanics
	Mid-German Crystalline High	
	Frankenstein Complex	gabbros, amphibolites, gneiss, subordinate granitoids
	Flasergranitoid Zone	granitoids, diorites, amphibolite, gneiss
	Southern Plutons	granitoids, subordinate gneiss and amphibolites
	Böllstein Odenwald	orthogneiss, subordinate paragneiss and granitoids
	Northern Granitoids	granitoids
	Southwestern Magnetic Body	very uncertain, similar to Frankenstein Complex
	Northwestern MGCH	gneiss, metasediments
	Saxothuringian Zone	gneiss, metasediments

Table 4
Summary of petrophysical model parameters. Magnetic properties were only considered in the basement model. The properties of the basement units were derived from the available petrophysical databases (initial values) and then optimized (optimized values; see Section 3.1.3 for more details). During the joint inversion, the anomaly misfit is further reduced by adjusting the property distribution.

Model	Horizon	Initial density [g/cm^3]	Opt. density [g/cm^3]	Inverted density [g/cm^3]	Initial mag. susc. [SI]	Opt. mag. susc. [SI]	Inverted mag. susc. [SI]
Sedimentary model	Cenozoic	2.0–2.63	–	–	–	–	–
	Keuper	2.45–2.65	–	–	–	–	–
	Muschelkalk	2.70	–	–	–	–	–
	Buntsandstein	2.40–2.65	–	–	–	–	–
	Permo-Carboniferous	2.48–2.65	–	–	–	–	–
Regional model	Lower Crust	2900	–	–	–	–	–
	Lithospheric Mantle	3300	–	–	–	–	–
Basement model	Rhenohercynian Zone	2.715	2.71	2.706 ± 0.027	0.0001	0.0001	0.0003 ± 0.0004
	Northern Phyllite Zone	2.74	2.74	2.742 ± 0.030	0.0001	0.0001	0.0003 ± 0.0006
	Mid-German Crystalline High						
	Frankenstein Complex	2.80	2.76	2.752 ± 0.026	0.0082	0.01	0.0167 ± 0.0242
	Flasergranitoid Zone	2.71	2.68	2.685 ± 0.022	0.0032	0.001	0.0022 ± 0.0030
	Southern Plutons	2.695	2.69	2.687 ± 0.019	0.0022	0.004	0.0107 ± 0.0127
	Böllstein Odenwald	2.66	2.68	2.676 ± 0.017	0.0014	0.003	0.0071 ± 0.0081
	Northern Granitoids	2.685	2.685	2.672 ± 0.023	0.001	0.0007	0.0012 ± 0.0025
	Southwestern Magnetic Body	2.74	2.73	2.736 ± 0.022	0.01	0.01	0.0130 ± 0.0166
	Northwestern MGCH	2.735	2.75	2.747 ± 0.030	0.001	0.0005	0.0013 ± 0.0019
	Saxothuringian Zone	2.80	2.795	2.798 ± 0.021	0.001	0.0003	0.0011 ± 0.0013

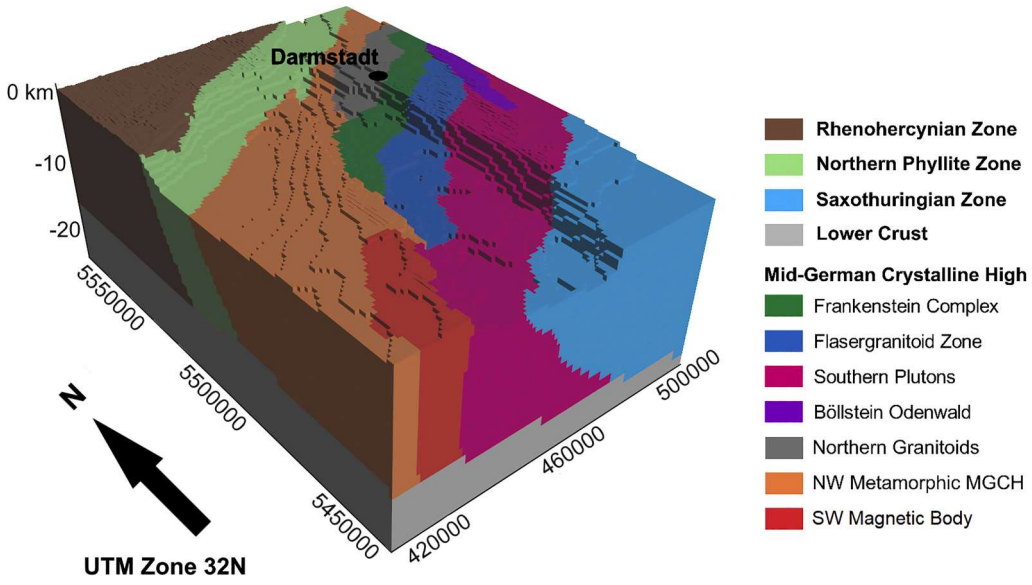

Fig. 5. Illustration of the 3D forward model of the crystalline basement in the northern URG region.

controlled by the parameters shape ratio, volume ratio and communality, which were set to moderate values according to the documentation of GeoModeller (Intrepid Intrepid Geophysics, 2017). Moreover, the top of the basement and lower crust were fixed so that only the units within the upper crystalline crust could be modified.

5. Recalculation of the geophysical effect
   Based on the disturbed model, gravity and magnetic anomalies are recalculated.
6. Likelihood of the disturbed model
   The likelihood of the disturbed model $L(m_{dis})$ is calculated as a function of the misfit with the observed data and compared to the likelihood of the current model $L(m_{cur})$. If $L(m_{dis}) > L(m_{cur})$, m_{dis} is accepted and becomes m_{cur} in the next iteration. If $L(m_{dis}) \leq L(m_{cur})$, m_{dis} might still be accepted, depending on a randomly sampled number, to ensure that the inversion does not get stuck in local minima. All accepted models are stored in a separate file.
7. Iteration and computing inversion result
   The algorithm starts over with step 4 until 500 million iterations have been calculated. This high number of realizations is required to visit every cell several times. Afterwards, all accepted models are combined to a summary model that contains information about the mean density and susceptibility, the standard deviation, and the most probable model unit of a cell.

4. Results

4.1. Residual gravity anomalies

A residual Bouguer Anomaly map of the northern URG was generated by stripping the sedimentary and regional gravity effect from the

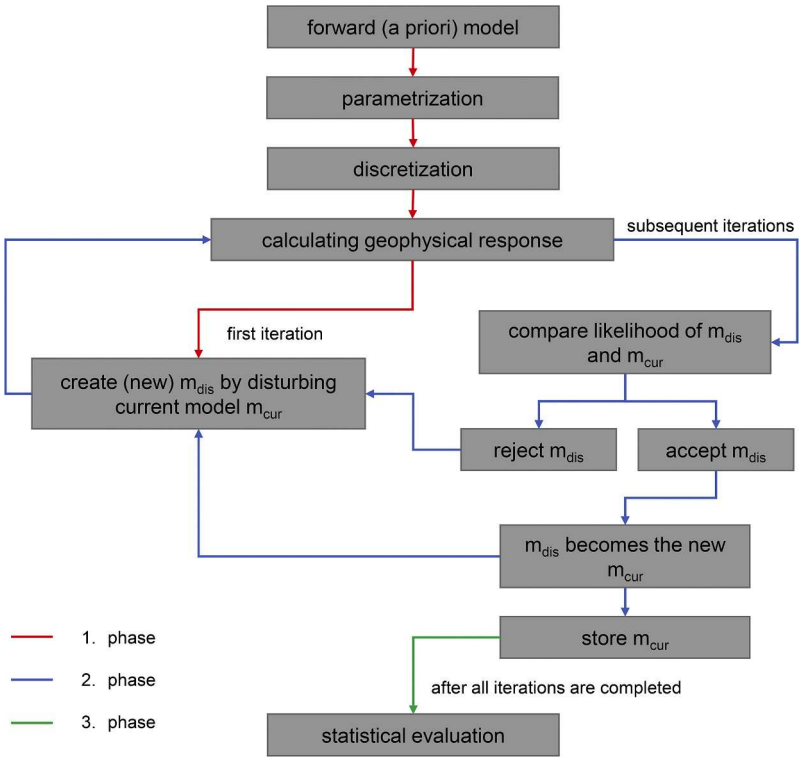

Fig. 6. Generalized workflow of the stochastic joint inversion of gravity and magnetic data.

observed data (Fig. 7). As a result, the field is no longer dominated by the distinct negative anomaly along the graben created by the Cenozoic infill. Instead, this product mainly represents features of the crystalline basement. As with the magnetic data, NE-SW striking features can be traced across the URG that are caused by the Variscan belt.

The strongest high of the residual anomalies is now located in the Saxothuringian Zone, which consists of a dense metamorphic crust and is clearly distinguishable from the granitoids of the southern MGCH. Another broad high extends over the northern/northwestern MGCH and parts of the Northern Phyllite Zone, which are covered by the thick Permo-Carboniferous deposits of the Saar-Nahe Basin. Further local anomaly highs are found at the Frankenstein Complex and at the southeastern Palatinate, both of which can be explained by the presence of mafic rocks. The most pronounced gravity low is located in the granites/granodiorites area of the southern Odenwald and along the SW extension of the Flasergranitoid Zone.

A comparison of the residual Bouguer anomalies with the pole-reduced magnetic anomalies shows that there are partly strong correlations between these two potential fields, which is a prerequisite for the joint inversion. This is particularly evident in the Odenwald: positive correlation in the Frankenstein complex and the Böllstein Odenwald, negative correlation in the southern Odenwald. A negative correlation occurs furthermore in the northwestern MGCH and the Saxothuringian Zones, where gravity highs coincide with magnetic lows. In contrast, a clear relationship exists not everywhere in the inner part of the URG. The separation of the Flasergranitoid Zone and southern Granitoids is thus subject to larger uncertainties.

4.2. Inverse model

Fig. 8 shows a comparison of the 3D basement forward model with the most probable model of the northern URG derived from the joint inversion of gravity and magnetic data. After the inversion, the interfaces are locally shifted by up to 10 km. Particularly large changes occur at the boundary between MGCH and the Northern Phyllite Zone. The tectonic contact is located further north and appears more irregular than presumed. Note, however, that the very similar petrophysical properties of these two units (Table 4) make a separation with the inversion approach difficult. The associated uncertainties are emphasized by the reduced probability of the inversion result in this area (Fig. 8C & F). Along Profile PP' (Fig. 8D & E), the main features of the inverted model correspond broadly to the forward model. As in the map view, the reduced thickness of the Northern Phyllite Zone is apparent. The interfaces of the inverse model are in general irregularly shaped, which might be related to the random character of the Monte Carlo simulation. Again, the probability of inversion results reveals uncertainties of locally several kilometers at the unit boundaries.

The mean density and susceptibility distributions at the top of the basement are illustrated in Fig. 9A & B. Local clusters of these properties are present within and across individual model units, indicating lithological variations in the respective area. In the Odenwald, the inverted density directly corresponds with the mapped lithologies: high density for mafic rocks of the Frankenstein Complex, intermediate densities in the dioritic domains of the Flasergranitoid Zone and relatively low densities in the predominantly felsic areas of the southern Odenwald. In contrast, the susceptibility varies over more than four orders of magnitude in the study area, making a correlation with the lithology more difficult. Particularly high values are found at the Frankenstein Complex and the Southwestern Magnetic Body, but also in the southern Odenwald. Another highly magnetized body is located at the northern margin of the MGCH, which is also characterized by a relatively high density, indicating the presence of intermediate to mafic magmatic rocks. The metasedimentary units, in particular the Rhenohercynian, the Northern Phyllite and the Saxothuringian Zone, generally exhibit very low susceptibilities. Fig. 9C & D show the standard deviations of the inverted density and susceptibility calculated for each cell of the model. Increased values occur at the model unit boundaries and in the areas of high susceptibility, but are still very small relative to the mean. Consequently, a high level of confidence in the inverted petrophysical models can be assumed.

A comparison of the initial, optimized and inverted model parameters is given in Table 4 for the basement units. For the rock density, only

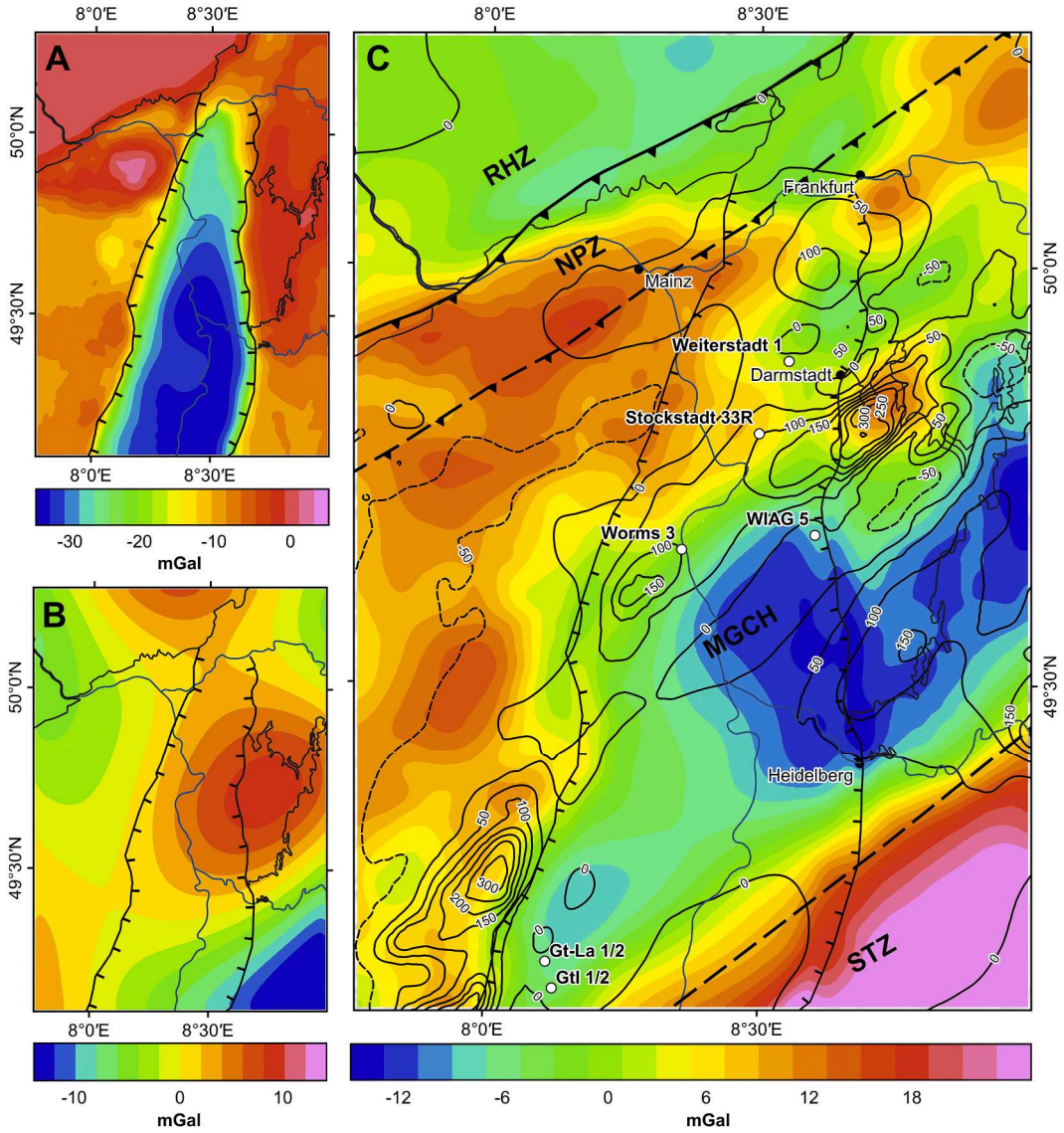

Fig. 7. Separation of the gravity anomalies: (A) forward calculated gravitational effect of the sediments in the northern URG region; (B) forward calculated regional gravity field; (C) residual Bouguer anomalies. The isolines represent the magnetic anomalies after a reduction to the magnetic pole. RHZ = Rhenohercynian Zone, NPZ = Northern Phyllite Zone, MGCH = Mid-German Crystalline High, STZ = Saxothuringian Zone.

small differences can be observed between the values derived from the petrophysical data and the final values. Thus, these existing databases provide already a representative image of the density distribution, at least in the MGCH. By contrast, the magnetic susceptibility shows significantly stronger differences between initial and inverted parameters, e.g., in the Böllstein Odenwald or the Southern Plutons. These, however, are still within the natural variations of the susceptibility, which were measured on the outcrop samples (Table 2).

4.3. Model misfit

Fig. 10 shows the misfits between the observed and forward modelled respectively inverted potential fields. The forward model is able to describe the main features of the Bouguer anomalies and parts of the magnetic anomalies, but the RMS misfit is still relatively high with 5.3 mGal and 42.1 nT. Particularly large differences can be observed at the transition from the MGCH to the Northern Phyllite Zone. Moreover, the magnitude of the magnetic anomalies is usually underestimated. After the inversion, the RMS misfit is with 0.6 mGal and 11.0 nT reduced by 90% and 75%, respectively. The largest deviations of the Bouguer anomalies are still found in the northwestern MGCH and the Northern Phyllite Zone as well as along the main border faults, but the differences between the observation and the model are now relatively small (±4 mGal). In addition, the modelled magnetic anomalies are significantly improved, especially in the inner part of the URG. Larger differences still exist in the north, possibly due to the influence of the volcanic rocks of the Vogelsberg and Permo-Carboniferous, which were not considered during inversion.

5. Discussion

5.1. Uncertainties of applied methods

A detailed 3D basement model of the northern URG was developed by integrating available structural information as well as gravity and magnetic data. Especially the stripping of the sedimentary and regional gravity field (Fig. 7) was helpful as the residual Bouguer anomalies provide key insights on the composition of the crystalline upper crust. However, it should be noted that this approach is affected by various uncertainties. First of all, the horizon depths in the sediment model are

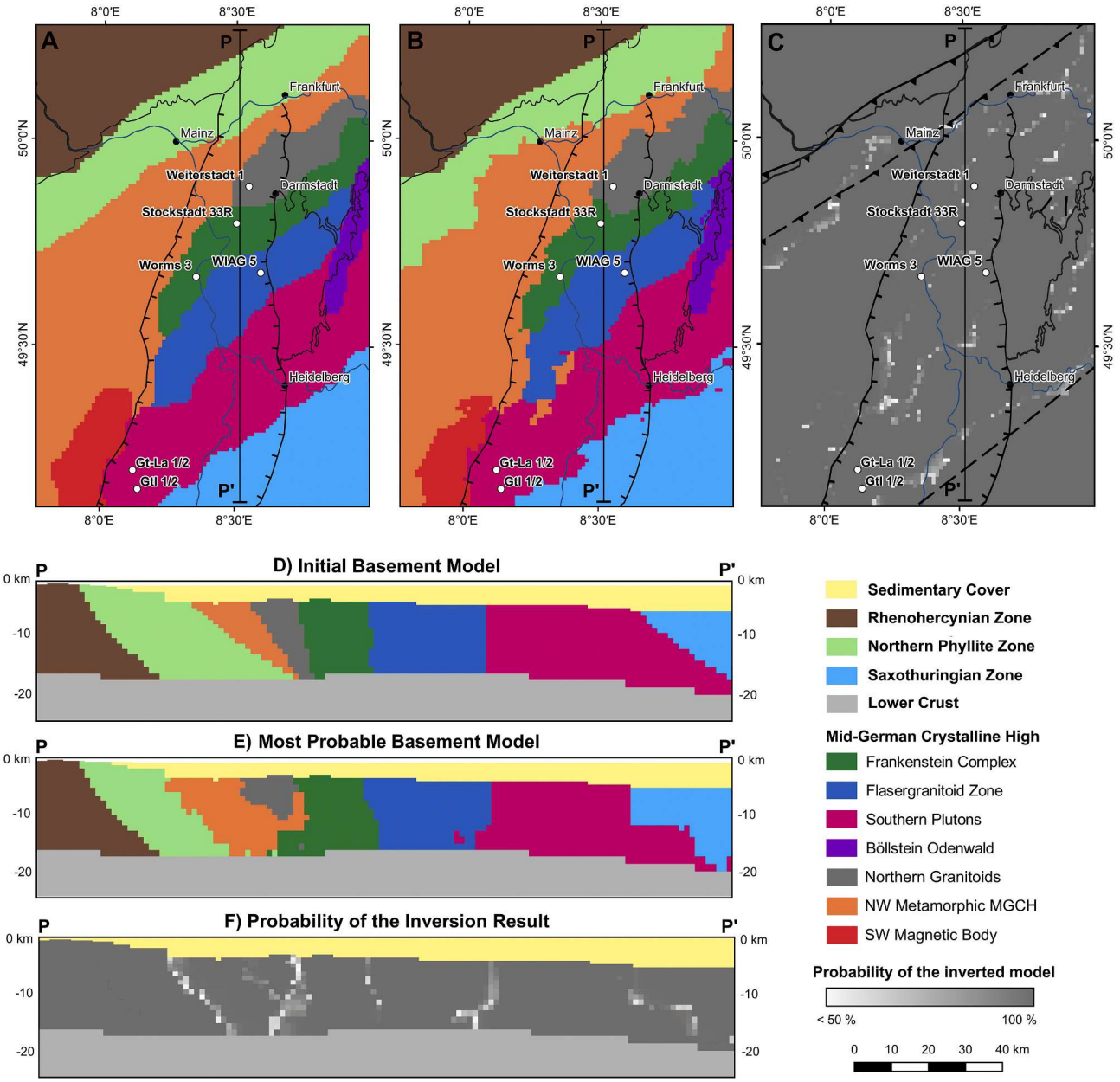

Fig. 8. Summary of the joint inversion results: (A) forward model at the top basement; (B) most probable model after inversion at the top basement; (C) probability of the inverted model at the top basement; (D) forward model along profile PP'; (E) most probable model after inversion along profile PP'; (F) probability of the inverted model along profile PP'.

subject to errors that have an impact on the calculated gravity field of several mGal. Likewise, the defined density distribution at depth is uncertain since it is only supported by a few data points. A laterally homogeneous density gradient was assumed, which may not reflect the actual variations within the sediments. Particularly large uncertainties exist in connection with the Permo-Carboniferous volcanic formations. They are typically characterized by a variable thickness and composition, with the density ranging from 2.6 to more than 3.0 g/cm^3, thus causing the gravity effect to vary considerably. In the Mainz Basin, these volcanic horizons have a significant but hardly quantifiable impact on the gravity anomalies, which makes the separation of the underlying MGCH and the Northern Phyllite Zone challenging.

For the modelling of the magnetic anomalies, the susceptibility of all post-Variscan deposits was set to 0 [SI]. This assumption is roughly valid for the clastic and carbonate sediments, but Permo-Carboniferous and Cenozoic volcanic deposits show in general higher susceptibilities. They might be sources of stronger magnetic anomalies in the Saar-Nahe Basin, on the Sprendlinger Horst and in the northernmost URG. Ignoring their effect leads most likely to the increased anomaly misfits in these areas (Fig. 10) and can partly corrupt the inversion result. An improved sediment model including the volcanic intercalations and better knowledge about the petrophysical properties would consequently result in a more accurate calculation of the gravity and magnetic anomalies. This, however, would require an extension of the petrophysical database and an in-depth analysis of the existing well logs.

Moreover, also the regional gravity model is affected by some uncertainty. On the one hand, the seismic profiles and receiver function data on which the depth of the lower crust and the Moho are based are very sparse. On the other hand, this data can be subject to errors of several kilometers. This can easily lead to variations in the calculated gravity effect of up to 10 mGal. But these uncertainties influence the inversion only to a limited extent because the wavelength is generally

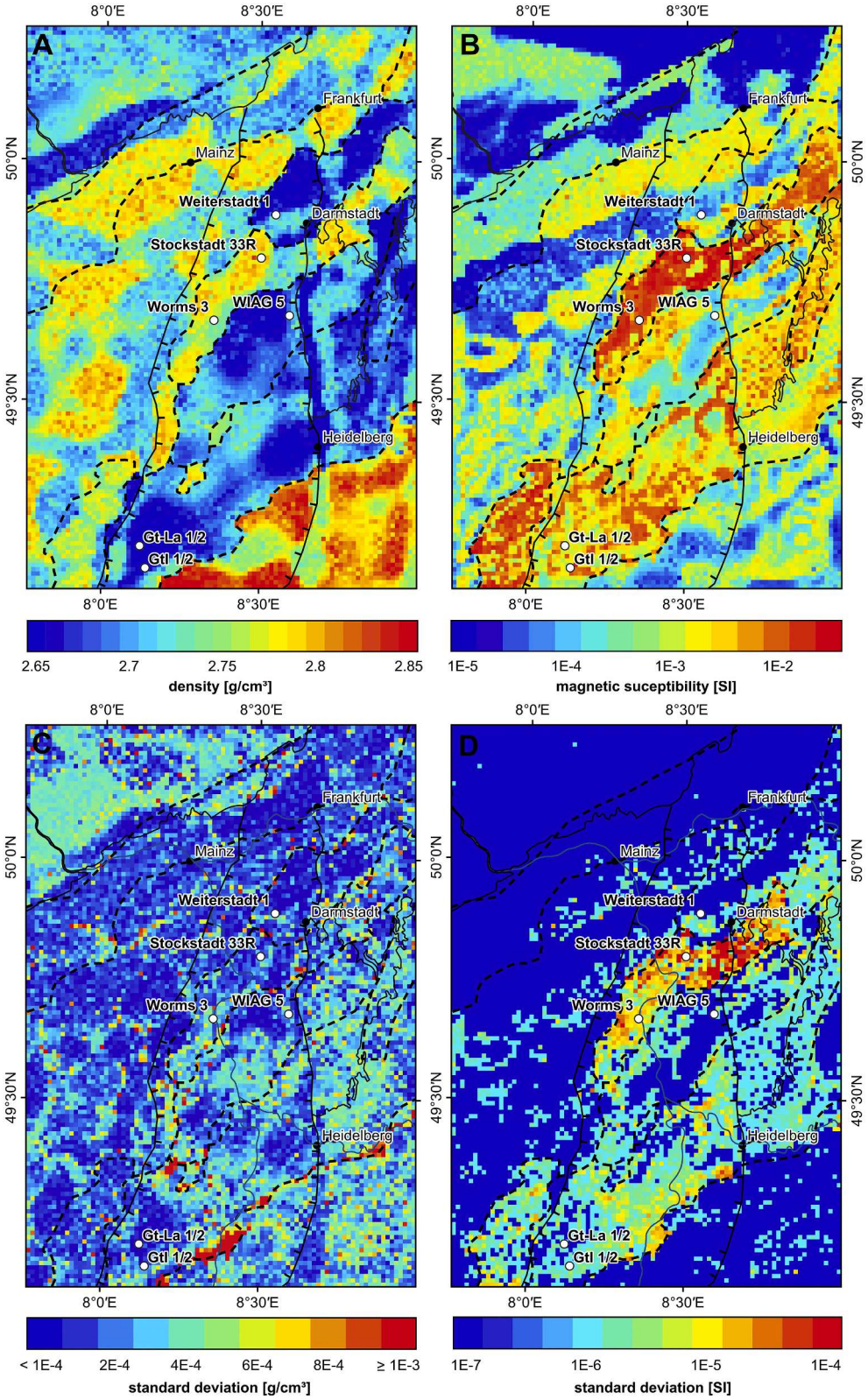

Fig. 9. Overview of the inverted petrophysical properties at the top of the basement: (A) mean density, (B) mean susceptibility; (C) & (D) standard deviation of the inverted properties for each cell. The dashed lines represent the interfaces of the inverted model units.

very long.

The basement model resulting from the joint inversion is able to describe the gravity and magnetic anomalies very well (Figs. 10B & D). It can therefore be assumed, that the final density and susceptibility distributions are realistic representations of the crystalline basement. Nevertheless, due to the random character of the Monte Carlo simulation also geologically implausible features might be generated, making a thorough plausibility check of the inversion result necessary.

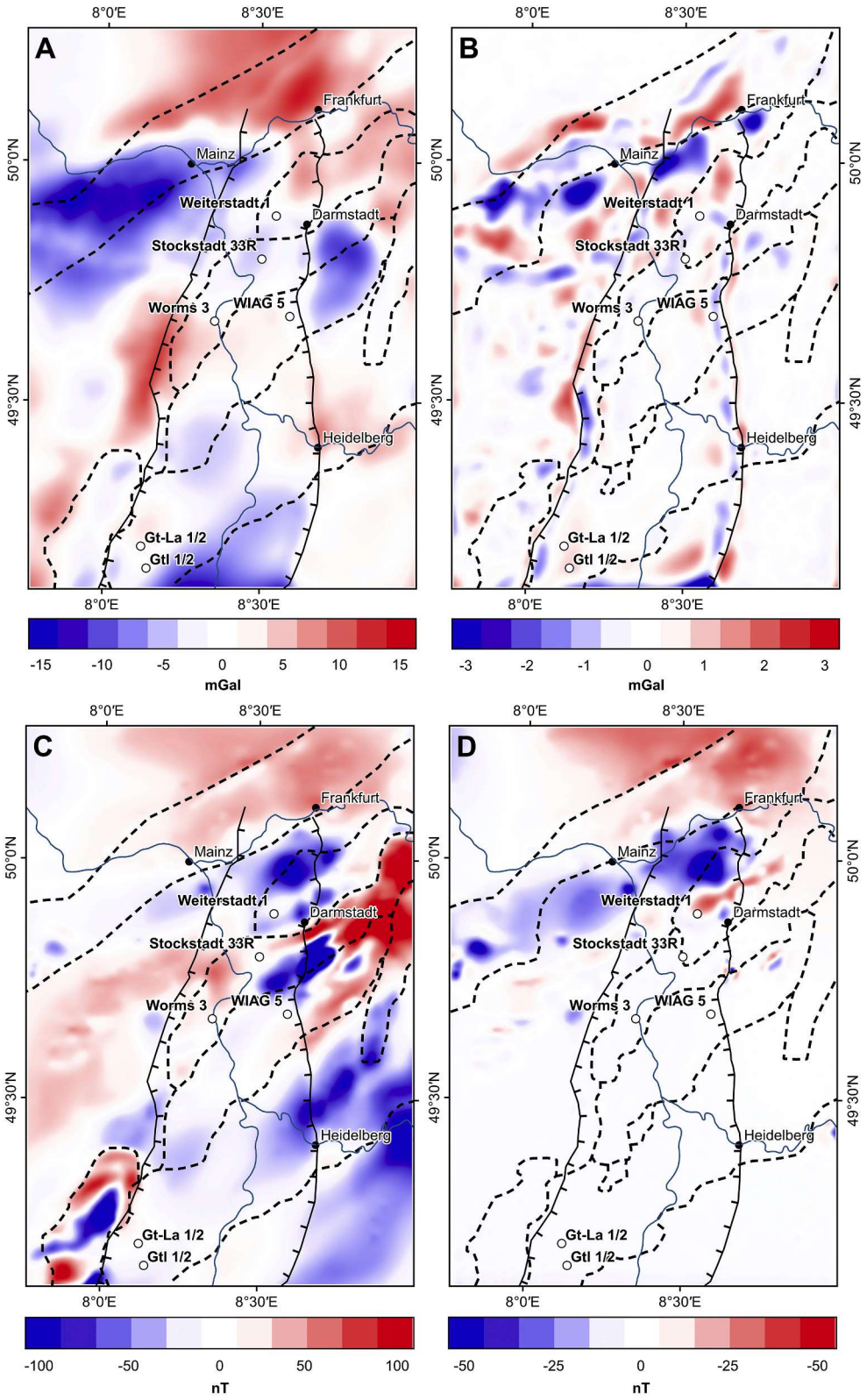

Fig. 10. Misfit between modelled and observed anomalies: (A) misfit of the forward modelled residual Bouguer anomalies; (B) misfit of the inverted residual Bouguer anomalies; (C) misfit of the forward calculated magnetic anomalies; (D) misfit of the inverted magnetic anomalies. The dashed lines represent the interfaces of the initial (A & C) respectively inverted model units (B & D).

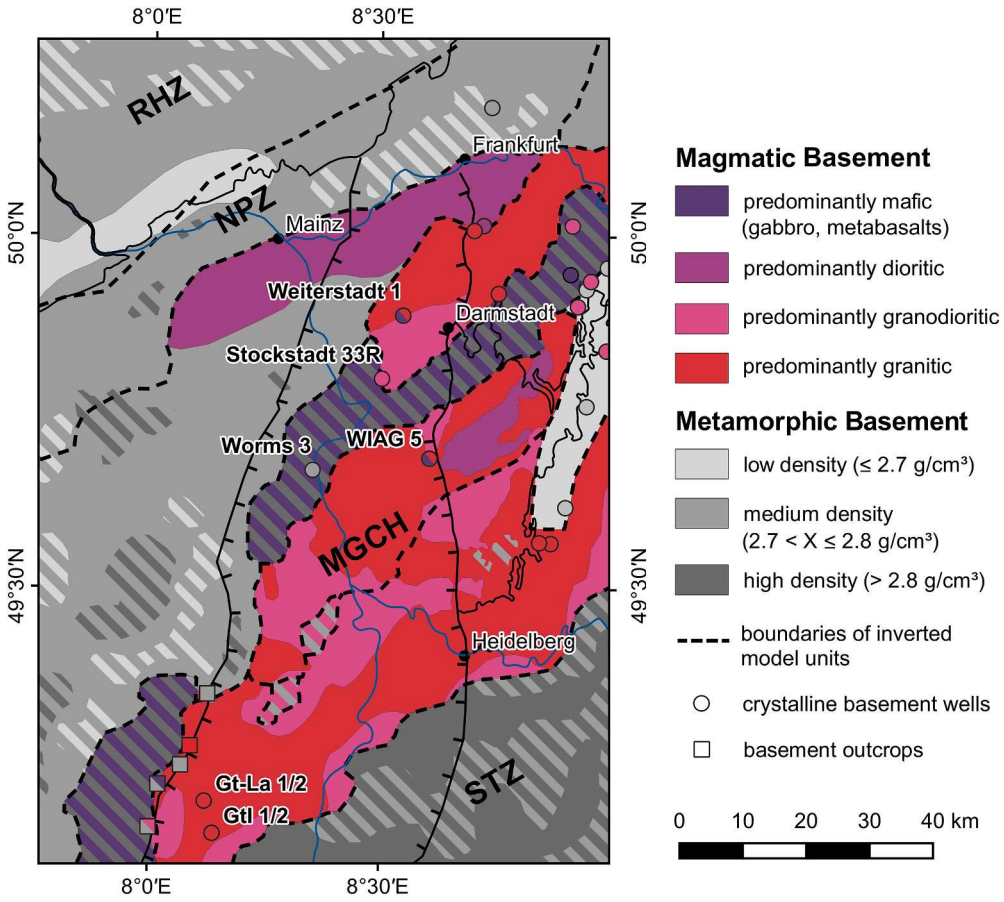

Fig. 11. Interpretative map of the lithologies at the top basement based on the results of the joint gravity and magnetic inversion. Available crystalline basement wells and outcrops at the graben shoulders are largely consistent with the interpretation. RHZ = Rhenohercynian Zone, NPZ = Northern Phyllite Zone, MGCH = Mid-German Crystalline High, STZ = Saxothuringian Zone, URG = Upper Rhine Graben.

Furthermore, the inversion result depends to a large extent on the inversion parameters and the starting model, but the general agreement with the crystalline outcrops at the graben shoulders and the wells in the northern URG shows that the selected initial conditions are reasonable. Indications of model uncertainties are provided by the probabilities of the inverted 3D structures (Fig. 8C & F).

5.2. Basement structure and composition

The petrophysical analysis revealed that the rock density and magnetic susceptibility are strongly depending on the lithology (Table 2). Conversely, information on the distribution of the main lithologies in the crystalline basement of the northern URG can be deduced from the inverted parameter models (Fig. 9). Based on the outcrops at the graben margins, the deep crystalline wells in the URG, and the density and susceptibility models, an interpretive geologic map of the basement beneath the sedimentary cover was generated. (Fig. 11). Areas with comparatively low magnetic susceptibility ($< 10^{-3}$ [SI]) are interpreted as being predominantly metamorphic. This assumption can be confirmed in the Northern Phyllite Zone, the Rhenohercynian Zone, and the Saxothuringian Zone, whose composition is relatively well known from outcrops. It is also suggested that metamorphic rocks are dominant in the northwestern MGCH, which is supported by exposed early Paleozoic metasediments in the Palatinate and the petrophysical similarities to the Saxothuringian and Northern Phyllite Zone. The transition between the metamorphic MGCH to the Northern Phyllite Zone is not marked by a sharp discontinuity in the residual gravity signal, indicating major lithological parallels and a paired evolution of these units in a volcanic arc respectively fore-arc setting (Krohe, 1991).

Large parts of the northern URG basement and the area east of it are presumably dominated by plutonic rocks given the high magnetic susceptibility. The distinction between different magmatic rocks is primarily based on the rock density (Table 2). According to this, granites and granodiorites occur mainly in the southwestern extension of the Flasergranitoid Zone and in the southern Bergsträßer Odenwald. The boundary between these two units cannot be clearly traced in the density model, but the Flasergranitoid Zone is generally characterized by lower susceptibility or, alternatively, increased remanent magnetization. Mafic rocks are concentrated in a NNE-SSW trending band that includes the Southwestern Magnetic Body and the Frankenstein Complex. Intermediate rocks may be present along the northern margin of the MGCH, supported by the two wells Neuhof 1 and 2 encountering diorite.

The interpretation covers only the larger geological bodies, small-scale lithological variations cannot be resolved with the applied method so far. Examples for this are the narrow amphibolite-gneiss complexes, the so-called Schieferzüge, in the Bergsträßer Odenwald, which are most likely continuous towards the southwest. Their location in the northern URG can only be estimated by assuming a constant strike direction. Furthermore, the natural variations of the petrophysical parameters as well as the partial overlap of the parameter distributions of different rock types imply considerable uncertainties in the separation of individual lithologies. Also, in addition to the main rock type, density and magnetic susceptibility depend on several aspects such as fracture porosity, hydrothermal alteration or mineral alteration (Airo, 2002; Ladygin et al., 2000; Ündül, 2016), which cannot be quantified here in detail due to the lack of comprehensive well data.

Despite the significant uncertainties, the presented investigations

provide an important basis for geothermal potential assessments in the northern URG. As mentioned above, especially thermal but also hydraulic parameters are strongly affected by the lithology (Stober and Bucher, 2007). Granitoids, which are the crystalline rocks with the most favorable properties for geothermal exploitation, represent more than 50% of the basement in the northern URG. In comparison, the less suitable mafic and metamorphic rocks occupy a rather subordinate area. Additionally, Weinert et al. (2020a) found a direct relationship between bulk density and thermal conductivity for the rock samples of the MGCH. The petrophysical models can therefore be used to infer the spatial distribution of thermal properties in the basement, allowing again more realistic potential estimates and heat flow simulations.

5.3. Geodynamic interpretation

The MGCH is traditionally regarded as a volcanic arc or active continental margin, which was formed in the Late Devonian and Carboniferous by the southward subduction of the Rheic and Rhenohercynian Oceans and later continental collision (Franke, 2000; Kroner et al., 2008; Zeh and Gerdes, 2010). Due to contrasting geodynamic conditions along the strike direction, a zone of variable composition and structure has formed. Especially on the opposite sides of the URG, there are significant differences, mainly due to oblique convergence (Flöttmann and Oncken, 1992; Oncken, 1997). Accordingly, the MGCH is probably dominated by a metamorphic basement in the west, which can be interpreted as the relic of a Paleozoic fore-arc. East of the URG, the convergence rates during the main orogeny phase were much higher, therefore the fore-arc is not preserved in this area. Instead, subduction-related plutons and metamorphic rocks with pressure-dominated overprint are present here.

The Frankenstein Complex and Southwestern Magnetic Body are likely the remains of a volcanic island arc (e.g. Altherr et al., 1999), which was formed in an early phase of the marine basin closure. Whereas the basement is largely exposed in the Odenwald, it is covered by Carboniferous to Triassic (meta-)sediments in the Palatinate. It appears that these two units are separated by a 15 to 20 km sinistral offset near the western graben boundary fault. This observation might be attributed to the sinistral strike-slip movements in the URG, which are particularly evident in the central and southern rift valley. Alternatively, this setting might still represent the primary geometry of the Variscan orogen with a changing trend from NE-SW in the Odenwald to NNE-SSW in the Palatinate and Vosges.

6. Conclusions and outlook

All publicly available structural and petrophysical data on the crystalline basement in the northern URG were compiled into one comprehensive model. By integrating gravity and magnetic data, a detailed geological 3D model of the region was developed. From the investigations described above, the following conclusions can be drawn:

- Residual Bouguer and magnetic anomalies exhibit NE-SW oriented features that depict the main Variscan basement structures. The metamorphic units are usually recognized by gravity highs and magnetic lows, whereas the magmatic complexes are often associated with magnetic highs and varying gravity anomalies.
- Joint inversion modelling allowed to obtain a density and susceptibility model of the crystalline basement in the northern URG region which provides a good match with the observed gravity and magnetic data
- The petrophysical analysis demonstrated that the main rock types are characterized by specific property ranges. The inversion results can therefore be used to draw up an interpretative map of the basement lithology in the northern URG, which is also consistent with outcrops and wells.
- Major parts of the northern URG basement are dominated by granitoid intrusions that offer suitable properties for deep geothermal utilization. Metamorphic and mafic rocks are concentrated in a relatively narrow band and along the western graben border. However, it must be mentioned that this interpretation remains speculative due to the non-uniqueness of potential fields studies. Besides, only larger connected bodies can be resolved; investigation of small-scale lithologic variations is not possible based on the currently available data.

In future studies, efforts will be focused on using the developed 3D model to perform a most realistic estimation of the geothermal potential in the northern URG. The spatial distribution of thermal properties can be derived from the inverted density model. Furthermore, comprehensive structural geological information will be integrated, mainly from the Odenwald, to assess the hydraulic properties of the basement.

To reduce the uncertainties related to the Permo-Carboniferous and Cenozoic volcanics, a detailed analysis of well data from the northernmost URG, the Saar-Nahe Basin and the Sprendlinger Horst is necessary. In particular, the incorporation of all existing well logs would improve the understanding of the location, thickness and properties of these horizons. In addition, the joint inversion of gravitational and magnetic data is also promising on a smaller scale, since a higher resolution of the discretized model would allow mapping the properties of large fault zones, which represent the main target for geothermal projects in the URG. For this purpose, the integration of existing 3D seismic data sets, that enable precise modelling of the geological structures, seems promising. This would minimize the uncertainties of the forward model considerably and the inversion could provide more reliable results.

Data availability statement

Datasets containing petrophysical properties of the crystalline basement in the URG region including density and magnetic susceptibility measurements can be found at doi:https://doi.org/10.5194/essd-12-2485-2020 (Bär et al., 2020), doi:10.25534/tudatalib-278 (Weinert et al., 2020b) and doi:10.48328/tudatalib-393 (Frey et al., 2020). Gravity and magnetic data can be requested individually from the Leibniz Institute for Applied Geophysics (LIAG), the Hessian Administration for Soil Management and Geoinformation (HVBG) and the State Agency for Surveying and Geo Base Information Rhineland-Palatinate (LVermGeo). Finally, the 3D model of the northern URG crystalline basement is publicly available at doi:10.48328/tudatalib-417.2 (Frey et al., 2021).

Funding

This study was funded by the Interreg NWE Program through the Roll-out of Deep Geothermal Energy in North-West Europe (DGE-ROLLOUT) Project (www.nweurope.eu/DGE-Rollout). The Interreg NWE Program is part of the European Cohesion Policy and is financed by the European Regional Development Fund (ERDF).

Declaration of Competing Interest

The authors declare that they have no known competing financial interests or personal relationships that could have appeared to influence the work reported in this paper.

Acknowledgements

We thank all researchers and involved institutions (TUDa, GFZ, HLNUG, LGRB-BW, LGB-RP) of the Hessen 3D (1.0 and 2.0) and GeORG projects, whose activities were essential for this study. We are furthermore grateful that the Institut für Steinkonservierung Mainz e.V. provided the rock samples of the URG region for our petrophysical

investigations. We thank Prof. Dr. Eva Schill for the helpful discussions on the analysis and interpretation of the geophysical data. Additionally, we thank Dr. Jens Grimmer and one anonymous reviewer for their critical but constructive reviews and comments which helped to improve the manuscript considerably.

References

Agemar, T., Schellschmidt, R., Schulz, R., 2012. Subsurface temperature distribution of Germany. Geothermics 44, 65–77. https://doi.org/10.1016/j.geothermics.2012.07.002.

Airo, M.-L., 2002. Aeromagnetic and aeroradiometric response to hydrothermal alteration. Surv. Geophys. 23, 273–302. https://doi.org/10.1023/A:1015556614694.

Altenberger, U., Besch, T., 1993. The Bllstein Odenwald: evidence for pre- to early Variscan plate convergence in the Central European variscides. Int. J. Earth Sci. 82 (3), 475–488. https://doi.org/10.1007/BF00212411.

Altherr, R., Henes-Klaiber, U., Hegner, E., Satir, M., Langer, C., 1999. Plutonism in the Variscan Odenwald (Germany): from subduction to collision. Int. J. Earth Sci. 88, 422–443. https://doi.org/10.1007/s005310050276.

Anderle, H.-J., Franke, W., Schwab, M., 1995. III.C.1 Stratigraphy. In: Dallmeyer, R.D., Franke, W., Weber, K. (Eds.), Pre-Permian Geology of Central and Eastern Europe. Springer Berlin Heidelberg, Berlin, Heidelberg, pp. 99–107.

Anthes, G., Reischmann, T., 1997. New 207Pb/206Pb single zircon evaporation ages from the central part of the Mid German Crystalline Rise. Terra Nostra 97 (5), 10. https://doi.org/10.1016/j.jseaes.2007.04.004.

Aretz, A., Bär, K., Götz, A.E., Sass, I., 2016. Outcrop analogue study of Permocarboniferous geothermal sandstone reservoir formations (northern Upper Rhine Graben, Germany): impact of mineral content, depositional environment and diagenesis on petrophysical properties. Int. J. Earth Sci. 105 (5), 1431–1452. https://doi.org/10.1007/s00531-015-1263-2.

Arndt, D., 2012. Geologische Strukturmodellierung von Hessen zur Bestimmung von Geopotenzialen. Dissertation. Technical University of Darmstadt, p. 116.

Bächler, D., Kohl, T., Rybach, L., 2003. Impact of graben-parallel faults on hydrothermal convection—Rhine Graben case study. Phys. Chem. Earth Parts A/B/C 28, 431–441. https://doi.org/10.1016/S1474-7065(03)00063-9.

Backhaus, E., 1974. Limnische und fluviatile Sedimentation im südwestdeutschen Buntsandstein. Int. J. Earth Sci. 63 (3), 925–942. https://doi.org/10.1007/BF01821318.

Backhaus, E., 1975. Der Buntsandstein im Odenwald. In: Amstutz, G.C., Meisl, S., Nickel, E. (Eds.), Mineralien und Gesteine im Odenwald. Heidelberg, pp. 299–320.

Backhaus, E., Heim, D., 1995. Die fluvio-lakustrine Fazies des Übergangsbereichs Plattensandstein/Rötquarzit (Oberer Buntsandstein) im mittleren Odenwald unter besonderer Berücksichtigung der Violetten Zone. Geol. Jb. Hessen 123, 49–68.

Backhaus, E., Schwarz, S., 2003. Ein Sammelprofil des Buntsandsteins und Zechsteins im mittleren Odenwald anhand von Bohrungen und Gamma-Logs. Geol. Jb. Hessen 130, 91–107.

Baillieux, P., Schill, E., Edel, J.-B., Mauri, G., 2013. Localization of temperature anomalies in the Upper Rhine Graben: insights from geophysics and neotectonic activity. Int. Geol. Rev. 55 (14), 1744–1762. https://doi.org/10.1080/00206814.2013.794914.

Bär, K.M., 2012. Untersuchung der tiefengeothermischen Potenziale von Hessen. Dissertation. Technical University of Darmstadt, p. 268.

Bär, K., Hintze, M., Weinert, S., Sippel, J., Freymark, J., Scheck-Wenderoth, M., Sass, I., 2016. Das Verbundprojekt Hessen 3D 2.0. Geothermische Energie 3 (85), 24–25.

Bär, K., Reinsch, T., Bott, J., 2020. The PetroPhysical Property Database (P^3) – A global compilation of lab-measured rock properties. Earth Syst. Sci. Data 12 (4), 2485–2515. https://doi.org/10.5194/essd-12-2485-2020.

Bär, K., Homuth, B., Stiller, M., Weinert, S., Bott, J., Oncken, O., Franke, W., Henke, A., 2021. New Interpretation of a reprocessed Crustal Scale Seismic Profile across the Mid German Crystalline High and the Northern Upper Rhine Graben, Germany. In: In preparation for Geochemistry, Geophysics, Geosystems, AGU Advancing Earth and Space Science Journal. In Prep.

Behr, H.J., Heinrichs, T., 1987. Geological interpretation of DEKORP 2-S: a deep seismic reflection profile across the Saxothuringian and possible implications for the late Variscan structural evolution of Central Europe. Tectonophysics 142 (2–4), 173–202. https://doi.org/10.1016/0040-1951(87)90122-3.

Behr, H.-J., Engel, W., Franke, W., Giese, P., Weber, K., 1984. The Variscan Belt in Central Europe: Main structures, geodynamic implications, open questions. Tectonophysics 109 (1–2), 15–40. https://doi.org/10.1016/0040-1951(84)90168-9.

Behrmann, J.H., Hermann, O., Horstmann, M., Tanner, D.C., Bertrand, G., 2003. Anatomy and kinematics of oblique continental rifting revealed: a three-dimensional case study of the southeast Upper Rhine graben (Germany). Bulletin 87 (7), 1105–1121. https://doi.org/10.1306/02180300153.

Böcker, J., 2015. Petroleum System and Thermal History of the Upper Rhine Graben - Implications from Organic Geochemical Analyses, Oil-Source Rock Correlations and Numerical Modelling. Dissertation. RWTH Aachen, p. 154.

Boigk, H., 1981. Erdöl und Erdölgas in der Bundesrepublik Deutschland. Schweizerbart, Stuttgart, p. 330.

Boigk, H., Schöneich, H., 1974. The Rhinegraben: geologic history and neotectonic activity – Perm, Trias und älterer Jura im Bereich der südlichen Mittelmeer-Mjösen-Zone und des Rheingrabens. In: Illies, J.H., Fuchs, K. (Eds.), Approaches to Taphrogenesis. Schweizerbart, Stuttgart, pp. 60–72.

Bosch, M., McGaughey, J., 2001. Joint inversion of gravity and magnetic data under lithologic constraints. Lead. Edge 20 (8), 877–881. https://doi.org/10.1190/1.1487299.

Bosch, M., Meza, R., Jiménez, R., Hönig, A., 2006. Joint gravity and magnetic inversion in 3D using Monte Carlo methods. GEOPHYSICS 71 (4), G153–G156. https://doi.org/10.1190/1.2209952.

Brun, J.P., Gutscher, M.-A., teams, 1992. Deep crustal structure of the Rhine Graben from dekorp-ecors seismic reflection data: a summary. Tectonophysics 208 (1–3), 139–147. https://doi.org/10.1016/0040-1951(92)90340-C.

Buchmann, T.J., Connolly, P.T., 2007. Contemporary kinematics of the Upper Rhine Graben: a 3D finite element approach. Glob. Planet. Chang. 58, 287–309. https://doi.org/10.1016/j.gloplacha.2007.02.012.

Buchner, F., 1981. Rhinegraben: Horizontal stylolites indicating stress regimes of earlier stages of rifting. Tectonophysics 73 (1–3), 113–118. https://doi.org/10.1016/0040-1951(81)90178-5.

Calcagno, P., Chilès, J.P., Courrioux, G., Guillen, A., 2008. Geological modelling from field data and geological knowledge, part I – Modelling method coupling 3D potential-field interpolation and geological rules. Phys. Earth Planet. Inter. 171 (1–4), 147–157. https://doi.org/10.1016/j.pepi.2008.06.013.

Crowley, Q.G., Floyd, P.A., Winchester, J.A., Franke, W., Holland, J.G., 2000. Early Palaeozoic rift-related magmatism in Variscan Europe: fragmentation of the Armorican Terrane Assemblage. Terra Nova 12 (4), 171–180. https://doi.org/10.1046/j.1365-3121.2000.00290.x.

Dachroth, W., 1988. Genese des linksrheinischen Buntsandsteins und Beziehungen zwischen Ablagerungsbedingungen und Stratigraphie. Jahresber. Mitt. Oberrhein Geol. Ver. 70, 267–333. https://doi.org/10.1127/jmogv/70/1988/267.

Dallmeyer, R.D., Franke, W., Weber, K. (Eds.), 1995. Pre-Permian Geology of Central and Eastern Europe. Springer Berlin Heidelberg, Berlin, Heidelberg, p. 593.

Dezayes, C., Lerouge, C., Innocent, C., Lach, P., 2021. Structural control on fluid circulation in a graben system: constraints from the Saint Pierre Bois quarry (Vosges, France). J. Struct. Geol. 146, 104323. https://doi.org/10.1016/j.jsg.2021.104323.

Dèzes, P., Schmid, S.M., Ziegler, P.A., 2004. Evolution of the European Cenozoic Rift System: interaction of the Alpine and Pyrenean orogens with their foreland lithosphere. Tectonophysics 389 (1–2), 1–33. https://doi.org/10.1016/j.tecto.2004.06.011.

Doebl, F., 1967. The Tertiary and Pleistocene sediments of the northern and central part of the Upper Rhinegraben. Abhandlungen des Geologischen Landesamtes Baden-Württemberg 6, 48–54.

Doebl, F., Olbrecht, W., 1974. An isobath map of the Tertiary base in the Rhinegraben. In: Illies, J.H., Fuchs, K. (Eds.), Approaches to Taphrogenesis. Schweizerbart, Stuttgart, pp. 71–72.

Edel, J.B., Fluck, P., 1989. The upper Rhenish Shield basement (Vosges, Upper Rhinegraben and Schwarzwald): main structural features deduced from magnetic, gravimetric and geological data. Tectonophysics 169 (4), 303–316. https://doi.org/10.1016/0040-1951(89)90093-0.

Edel, J., Schulmann, K., 2009. Geophysical constraints and model of the "Saxothuringian and Rhenohercynian subductions - magmatic arc system" in NE France and SW Germany. Bull. De La Societe Geologique De France - BULL SOC GEOL FR 180, 545–558. https://doi.org/10.2113/gssgfbull.180.6.545.

Edel, J.B., Weber, K., 1995. Cadomian terranes, wrench faulting and thrusting in the central Europe Variscides: geophysical and geological evidence. Int. J. Earth Sci. 84 https://doi.org/10.1007/BF00260450.

Edel, J.-B., Schulmann, K., Rotstein, Y., 2007. The Variscan tectonic inheritance of the Upper Rhine Graben: evidence of reactivations in the Lias, Late Eocene–Oligocene up to the recent. Int. J. Earth Sci. 96, 305–325. https://doi.org/10.1007/s00531-006-0092-8.

Edel, J.B., Maurer, V., Dalmais, E., Genter, A., Richard, A., Letourneau, O., Hehn, R., 2018. Structure and nature of the Palaeozoic basement based on magnetic, gravimetric and seismic investigations in the central Upper Rhinegraben. Geotherm. Energy 6 (1), 13. https://doi.org/10.1186/s40517-018-0099-y.

Feist-Burkhardt, S., Götz, A., Szulc, J., Borkhataria, R., Geluk, M., Haas, J., Hornung, J., Jordan, P., Kempf, O., Jozef, M., Nawrocki, J., Reinhardt, L., Ricken, W., Röhling, H.-G., Rüffer, T., Török, Á., Zuehlke, R., 2008. Triassic. In: McCann, T. (Ed.), The Geology of Central Europe: Volume 2: Mesozoic and Cenozoic. Geological Society of London, London, pp. 749–821.

Flöttmann, T., Oncken, O., 1992. Contraints on the evolution of the Mid German Crystalline Rise - A study of outcrops west of the river Rhine. Geol. Rundsch. 82 (2), 515–543.

Franke, W., 2000. The mid-European segment of the Variscides: tectonostratigraphic units, terrane boundaries and plate tectonic evolution. Geol. Soc. Lond., Spec. Publ. 179, 35–61. https://doi.org/10.1144/GSL.SP.2000.179.01.05.

Franke, W., Cocks, L.R.M., Torsvik, T.H., 2017. The Palaeozoic Variscan oceans revisited. Gondwana Res. 48, 257–284. https://doi.org/10.1016/j.gr.2017.03.005.

Frenzel, G., 1971. Die Mineralparagenese der Albersweiler Lamprophyre. Neues J. Mineral. Abh. 115, 164–191.

Frey, M., Ebbing, J., 2020. The deep geothermal potential of the radiogenic Løvstakken Granite in western Norway. NJG. https://doi.org/10.17850/njg100-1-4.

Frey, M., Bär, K., Sass, I., 2020. Database of the Magnetic Susceptibility of the Mid-German Crystalline High. Technical University of Darmstadt, TUdatalib doi: 10.48328/tudatalib-393.

Freymark, J., Sippel, J., Scheck-Wenderoth, M., Baer, K., Stiller, M., Kracht, M., Fritsche, J.-G., 2015. Heterogeneous crystalline crust controls the shallow thermal field – A case study of Hessen (Germany). Energy Procedia 76, 331–340. https://doi.org/10.1016/j.egypro.2015.07.837.

Freymark, J., Sippel, J., Scheck-Wenderoth, M., Bär, K., Stiller, M., Fritsche, J.-G., Kracht, M., 2017. The deep thermal field of the Upper Rhine Graben. Tectonophysics 694, 114–129. https://doi.org/10.1016/j.tecto.2016.11.013.

Freymark, J., Bott, J., Scheck-Wenderoth, M., Bär, K., Stiller, M., Fritsche, J.-G., Kracht, M., Gomez Dacal, M.L., 2020. 3D-URG: 3D gravity constrained structural model of the Upper Rhine Graben. GFZ Data Services. https://doi.org/10.5880/GFZ.4.5.2020.004.

Gabriel, G., Vogel, D., Scheibe, R., Lindner, H., Pucher, R., Wonik, T., Krawczyk, C.M., 2011. Anomalies of the Earth's total magnetic field in Germany – the first complete homogenous data set reveals new opportunities for multiscale geoscientific studies. Geophys. J. Int. 184 (3), 1113–1118. https://doi.org/10.1111/j.1365-246X.2010.04924.x.

Gallardo, L.A., Thebaud, N., 2012. New insights into Archean granite-greenstone architecture through joint gravity and magnetic inversion. Geology 40 (3), 215–218. https://doi.org/10.1130/G32817.1.

Geyer, O.F., Gwinner, M.P., Simon, T., 2011. Geologie von Baden-Württemberg, 5th ed. Schweizerbart, Stuttgart, p. 627.

Giese, P., 1995. Main features of geophysical structures in Central Europe. In: Dallmeyer, R.D., Franke, W., Weber, K. (Eds.), Pre-Permian Geology of Central and Eastern Europe. Springer Berlin Heidelberg, Berlin, Heidelberg, pp. 7–25.

Grimmer, J.C., Ritter, J.R.R., Eisbacher, G.H., Fielitz, W., 2017. The late Variscan control on the location and asymmetry of the Upper Rhine Graben. Int. J. Earth Sci. 106 (3), 827–853. https://doi.org/10.1007/s00531-016-1336-x.

Guillen, A., Calcagno, P., Courrioux, G., Joly, A., Ledru, P., 2008. Geological modelling from field data and geological knowledge, Part II, Modelling validation using gravity and magnetic data inversion. Phys. Earth Planet. Inter. 171 (1–4), 158–169. https://doi.org/10.1016/j.pepi.2008.06.014.

Hammer, S., 1963. Deep Gravity Interpretation by Stripping. GEOPHYSICS 28 (3), 369–378. https://doi.org/10.1190/1.1439186.

Henk, A., 1992. Mächtigkeit und Alter der erodierten Sedimente im Saar-Nahe-Becken (SW-Deutschland). Int. J. Earth Sci. 81 (2), 323–331. https://doi.org/10.1007/BF01828601.

Henk, A., 1993a. Late orogenic Basin evolution in the Variscan internides: the Saar-Nahe Basin, southwest Germany. Tectonophysics 223 (3–4), 273–290. https://doi.org/10.1016/0040-1951(93)90141-6.

Henk, A., 1993b. Subsidenz und tektonik des Saar-Nahe-Beckens (SW-Deutschland). Int. J. Earth Sci. 82 (1), 3–19. https://doi.org/10.1007/BF00563266.

Hertle, M., 2003. Numerische Simulation der geologischen Entwicklungsgeschichte des permokarbonen Saar-Nahe-Beckens. Dissertation. RWTH Aachen, p. 166.

Hirschmann, G., 1995. IV.B lithological characteristics. In: Dallmeyer, R.D., Franke, W., Weber, K. (Eds.), Pre-Permian Geology of Central and Eastern Europe. Springer Berlin Heidelberg, Berlin, Heidelberg, pp. 155–163.

Homuth, B., Rümpker, G., Deckert, H., Kracht, M., 2014. Seismicity of the northern Upper Rhine Graben — Constraints on the present-day stress field from focal mechanisms. Tectonophysics 632, 8–20. https://doi.org/10.1016/j.tecto.2014.05.037.

Intrepid Geophysics, 2017. GeoModeller User Manual: Tutorial C (Forward & Inverse Modelling of Potential Fields).

Illies, J.H., Greiner, G., 1979. Holocene Movements and State of Stress in the Rhinegraben Rift System, Vol. 13, pp. 349–359. https://doi.org/10.1016/B978-0-444-41783-1.50057-X.

Jain, C., Vogt, C., Clauser, C., 2015. Maximum potential for geothermal power in Germany based on engineered geothermal systems. Geotherm. Energ 3 (1). https://doi.org/10.1186/s40517-015-0033-5.

Jaupart, C., Mareschal, J.-C., Iarotsky, L., 2016. Radiogenic heat production in the continental crust. Lithos 262, 398–427. https://doi.org/10.1016/j.lithos.2016.07.017.

Jodocy, M., Stober, I., 2010. Geologisch-geothermische Tiefenprofile für den südlichen Teil des Oberrheingrabens in Baden-Württemberg. Z. Geol. Wiss. 38 (1), 3–25.

Kamm, J., Lundin, I.A., Bastani, M., Sadeghi, M., Pedersen, L.B., 2015. Joint inversion of gravity, magnetic, and petrophysical data — A case study from a gabbro intrusion in Boden, Sweden. GEOPHYSICS 80 (5), B131–B152. https://doi.org/10.1190/geo2014-0122.1.

Kemnitz, H., Romer, R.L., Oncken, O., 2002. Gondwana break-up and the northern margin of the Saxothuringian belt (Variscides of Central Europe). Int. J. Earth Sci. 91 (2), 246–259. https://doi.org/10.1007/s005310100209.

Kirsch, H., Kober, B., Lippolt, H.J., 1988. Age of intrusion and rapid cooling of the Frankenstein gabbro (Odenwald, SW-Germany) evidenced by40Ar/39Ar and single-zircon207Pb/206Pb measurements. Int. J. Earth Sci. 77 (3), 693–711. https://doi.org/10.1007/BF01830178.

Klügel, T., 1997. Geometrie und Kinematik einer variszischen Plattengrenze: der Südrand des Rhenoherzynikums im Taunus. Hessisches Landesamt für Bodenforschung, p. 215.

Kossmat, F., 1927. Gliederung des varistischen Gebirgsbaues: Abhandlungen Sächsischen Geologischen Landesamts, Vol. 1.

Kreuzer, H., Harre, W., 1975. K/Ar-Altersbestimmungen an Hornblenden und Biotiten des Kristallinen Odenwalds. In: Amstutz, G.C., Meisl, S., Nickel, E. (Eds.), Mineralien und Gesteine im Odenwald. Heidelberg, pp. 70–78.

Krohe, A., 1991. Emplacement of synkinematic plutons in the Variscan Odenwald (Germany) controlled by transtensional tectonics. Int. J. Earth Sci. 80 (2), 391–409. https://doi.org/10.1007/BF01829373.

Krohe, A., 1992. Structural evolution of intermediate-crustal rocks in a strike-slip and extensional setting (Variscan Odenwald, SW Germany): differential upward transport of metamorphic complexes and changing deformation mechanisms. Tectonophysics 205 (4), 357–386. https://doi.org/10.1016/0040-1951(92)90443-A.

Krohe, A., Willner, A.P., 1995. IV.C.2 the Odenwald Crystalline complex. In: Dallmeyer, R.D., Franke, W., Weber, K. (Eds.), Pre-Permian Geology of Central and Eastern Europe. Springer Berlin Heidelberg, Berlin, Heidelberg, pp. 182–185.

Kroner, U., Mansy, J.L., Mazur, S., Aleksandrowski, P., Hann, H.P., Huckriede, H., 2008. Variscan tectonics. In: McCann, T. (Ed.), The Geology of Central Europe: Volume 1: Precambrian and Palaeozoic. Geological Society of London, London, pp. 599–664.

Lachenbruch, A.H., 1970. Crustal temperature and heat production: Implications of the linear heat-flow relation. J. Geophys. Res. 75 (17), 3291–3300. https://doi.org/10.1029/JB075i017p03291.

Ladygin, V., Frolova, J., Rychagov, S., 2000. Formation of composition and petrophysical properties of hydrothermally altered rocks in geothermal reservoir. In: Proc. WGC, pp. 2695–2699.

Lajaunie, C., Courrioux, G., Manuel, L., 1997. Foliation fields and 3D cartography in geology: principles of a method based on potential interpolation. Math. Geol. 29 (4), 571–584. https://doi.org/10.1007/BF02775087.

Laue, S., Reischmann, T., 1994. Petrographie und Geochemie variszischer Intrusiva der westlichen Rheingrabenschulter. Mitt Pollichia 81, 195–214.

Laue, S., Reischmann, T., Emmermann, K.H., 1990. Geochemical variation of granitoid rocks from the NW margin of the Rhinegraben. In: Ber Dsch Mineral Ges Eur J Mineral 2 (Beih 1), p. 156.

Li, Y., Oldenburg, D.W., 1996. 3-D inversion of magnetic data. GEOPHYSICS 61 (2), 394–408. https://doi.org/10.1190/1.1443968.

Li, Y., Oldenburg, D.W., 1998. 3-D inversion of gravity data. GEOPHYSICS 63 (1), 109–119. https://doi.org/10.1190/1.1444302.

Marell, D., 1989. Das Rotliegende zwischen Odenwald und Taunus. Geologische Abhandlungen Hessen, Wiesbaden.

Mareschal, J.-C., Jaupart, C., 2013. Radiogenic heat production, thermal regime and evolution of continental crust. Tectonophysics 609, 524–534. https://doi.org/10.1016/j.tecto.2012.12.001.

Martha, S.O., Zulauf, G., Dörr, W., Nesbor, H.-D., Petschick, R., Prinz-Grimm, P., Gerdes, A., 2014. The Saxothuringian-Rhenohercynian boundary underneath the Vogelsberg volcanic field: evidence from basement xenoliths and U-Pb zircon data of trachyte. Zdgg 165, 373–394. https://doi.org/10.1127/1860-1804/2014/0079.

McCann, T. (Ed.), 2008a. The Geology of Central Europe: Volume 1: Precambrian and Palaeozoic. Geological Society of London, London, p. 748.

McCann, T. (Ed.), 2008b. The Geology of Central Europe: Volume 2: Mesozoic and Cenozoic. Geological Society of London, London, p. 752.

McCann, T., Skompski, S., Poty, E., Dusar, M., Vozarova, A., Schneider, J., Wetzel, A., Krainer, K., 2008. Carboniferous. In: McCann, T. (Ed.), The Geology of Central Europe: Volume 1: Precambrian and Palaeozoic. Geological Society of London, London, pp. 410–530.

Meier, L., Eisbacher, G.H., 1991. Crustal kinematics and deep structure of the northern Rhine Graben, Germany. Tectonics 10 (3), 621–630. https://doi.org/10.1029/91TC00142.

Meissner, R., Bortfeld, R.K. (Eds.), 1990. DEKORP-Atlas: Results of Deutsches Kontinentales Reflexionsseismisches Programm, 1st ed. Springer, Berlin.

Molenaar, N., Felder, M., Bär, K., Götz, A.E., 2015. What classic greywacke (litharenite) can reveal about feldspar diagenesis: an example from Permian Rotliegend sandstone in Hessen, Germany. Sediment. Geol. 326, 79–93. https://doi.org/10.1016/j.sedgeo.2015.07.002.

Mosegaard, K., Tarantola, A., 1995. Monte Carlo sampling of solutions to inverse problems. J. Geophys. Res. 100 (B7), 12431–12447. https://doi.org/10.1029/94JB03097.

Müller, H., 1996. Das Permokarbon im nördlichen Oberrheingraben: Paläogeographische und strukturelle Entwicklung des permokarbonen Saar-Nahe-Beckens im nördlichen Oberrheingraben. Hess. Landesamt für Bodenforschung, Wiesbaden, p. 85.

Okrusch, M., 1995. Metamorphic Evolution. In: Dallmeyer, R.D., Franke, W., Weber, K. (Eds.), Pre-Permian Geology of Central and Eastern Europe. Springer Berlin Heidelberg, Berlin, Heidelberg, pp. 201–213.

Okrusch, M., Schubert, W., Nasir, S., 1995. IV.D Igneous activity (Pre- to Early Variscan Magmatism). In: Dallmeyer, R.D., Franke, W., Weber, K. (Eds.), Pre-Permian Geology of Central and Eastern Europe. Springer Berlin Heidelberg, Berlin, Heidelberg, pp. 190–200.

Oncken, O., 1995. III.B.2 Structure. In: Dallmeyer, R.D., Franke, W., Weber, K. (Eds.), Pre-Permian Geology of Central and Eastern Europe. Springer Berlin Heidelberg, Berlin, Heidelberg, pp. 50–58.

Oncken, O., 1997. Transformation of a magmatic arc and an orogenic root during oblique collision and its consequences for the evolution of the European Variscides (Mid-German Crystalline rise). Geol. Rundsch. 86 (1), 2–20. https://doi.org/10.1007/s005310050118.

Oncken, O., 1998. Orogenic mass transfer and reflection seismic patterns — Evidence from DEKORP sections across the European Variscides (central Germany). Tectonophysics 286, 47–61. https://doi.org/10.1016/S0040-1951(97)00254-0.

Oncken, O., von Winterfeld, C., Dittmar, U., 1999. Accretion of a rifted passive margin: the Late Paleozoic Rhenohercynian fold and thrust belt (Middle European Variscides). Tectonics 18 (1), 75–91. https://doi.org/10.1029/98TC02763.

Reinhold, C., Schwarz, M., Bruss, D., Heesbeen, B., Perner, M., Suana, M., 2016. The Northern Upper Rhine Graben: re-dawn of a mature petroleum province? Swiss Bull angew. Geol. 21, 35–56. https://doi.org/10.5169/seals-658196.

Reischmann, T., Anthes, G., Jaeckel, P., Altenberger, U., 2001. Age and origin of the Böllsteiner Odenwald. Mineral. Petrol. 72 (1–3), 29–44. https://doi.org/10.1007/s007100170025.

Rotstein, Y., Schaming, M., 2011. The Upper Rhine Graben (URG) revisited: Miocene transtension and transpression account for the observed first-order structures. Tectonics 30, 1–14. https://doi.org/10.1029/2010TC002767.

Rotstein, Y., Edel, J.-B., Gabriel, G., Boulanger, D., Schaming, M., Munschy, M., 2006. Insight into the structure of the Upper Rhine Graben and its basement from a new compilation of Bouguer Gravity. Tectonophysics 425, 55–70. https://doi.org/10.1016/j.tecto.2006.07.002.

Rousset, D., Bayer, R., Guillon, D., Edel, J.B., 1993. Structure of the southern Rhine Graben from gravity and reflection seismic data (ecors-dekorp program). Tectonophysics 221 (2), 135–153. https://doi.org/10.1016/0040-1951(93)90329-I.

Schäfer, A., 1989. Variscan molasse in the Saar-Nahe Basin (W-Germany), Upper Carboniferous and Lower Permian. Int. J. Earth Sci. 78 (2), 499–524. https://doi.org/10.1007/BF01776188.

Schäfer, A., 2011. Tectonics and sedimentation in the continental strike-slip Saar-Nahe Basin (Carboniferous-Permian, West Germany). Zdgg 162 (2), 127–155. https://doi.org/10.1127/1860-1804/2011/0162-0127.

Scheck-Wenderoth, M., Krzywiec, P., Zühlke, R., Maystrenko, Y., Froitzheim, N., 2008. Permian to cretaceous tectonics of Central Europe. In: McCann, T. (Ed.), The Geology of Central Europe: Volume 1: Precambrian and Palaeozoic. Geological Society of London, London, pp. 999–1030.

Schumacher, M.E., 2002. Upper Rhine Graben: role of preexisting structures during rift evolution. Tectonics 21 (1), 6-1–6-17. https://doi.org/10.1029/2001TC900022.

Sissingh, W., 1998. Comparative Tertiary stratigraphy of the Rhine Graben, Bresse Graben and Molasse Basin: correlation of Alpine foreland events. Tectonophysics 300 (1–4), 249–284. https://doi.org/10.1016/S0040-1951(98)00243-1.

Sittler, C., 1969. The sedimentary trough of the Rhine graben. Tectonophysics 8, 543–560.

Sittler, C., 1992. Illustration de l'histoire géologique du Fossé rhénan et de l'Alsace. Neues Jahrb. Geol. Palaontol. Abh. 186 (3), 255–282.

Skrzypek, E., Schulmann, K., Tabaud, A.-S., Edel, J.-B., 2014. Palaeozoic evolution of the Variscan Vosges Mountains. Geol. Soc. Lond., Spec. Publ. 405 (1), 45–75. https://doi.org/10.1144/SP405.8.

Sokol, G., Nitsch, E., Anders, B., Beccaletto, L., Capar, L., Mermy, D.C., Dezayes, C., Dresmann, H., Elsass, P., Fehn, C., Fischer, G., Franz, M., Haneke, J., Huggenberger, P., Kärcher, T., Krzyzanowski, J., Oliviero, G., Prestel, R., Rodat, C., Rupf, I., Schuff, J., Siemon, S., Storz, R., Tesch, J., Urban, S., Weidenfeller, M., Wielandt-Schuster, U., Wirsing, G., Zumsprekel, H., 2013. Geopotenziale des tieferen Untergrundes im Oberrheingraben: Fachlich-Technischer Abschlussbericht des INTERREG-Projekts GeORG. In: Teil 1: Ziele und Ergebnisse des Projekts (Zusammenfassung). Freiburg i.Br./Mainz/Strasbourg/Basel.

Stein, E., 2001. The geology of the Odenwald Crystalline complex. Mineral. Petrol. 72 (1–3), 7–28. https://doi.org/10.1007/s007100170024.

Stellrecht, R., 1971. Geologisch-tektonische Entwicklung im Raum Albersweiler/Pfalz. jber_oberrh 53, 239–262. https://doi.org/10.1127/jmogv/53/1971/239.

Stober, I., Bucher, K., 2007. Hydraulic properties of the crystalline basement. Hydrogeol. J. 15, 213–224. https://doi.org/10.1007/s10040-006-0094-4.

Stollhofen, H., 1998. Facies architecture variations and seismogenic structures in the Carboniferous–Permian Saar–Nahe Basin (SW Germany): evidence for extension-related transfer fault activity. Sediment. Geol. 119 (1–2), 47–83. https://doi.org/10.1016/S0037-0738(98)00040-2.

Suess, F.E., 1926. Intrusion-und Wandertektonik im variszischen Grundgebirge. Gebr. Bornträger, Berlin, p. 286.

Timmermann, Martin, 2008. Palaeozoic magmatism. In: McCann, T. (Ed.), The Geology of Central Europe: Volume 2: Mesozoic and Cenozoic. Geological Society of London, London.

Ündül, Ö., 2016. Assessment of mineralogical and petrographic factors affecting petrophysical properties, strength and cracking processes of volcanic rocks. Eng. Geol. 210, 10–22. https://doi.org/10.1016/j.enggeo.2016.06.001.

van Zyl, J.J., 2001. The shuttle Radar Topography Mission (SRTM): a breakthrough in remote sensing of topography. Acta Astronautica 48 (5–12), 559–565. https://doi.org/10.1016/S0094-5765(01)00020-0.

Vilà, M., Fernández, M., Jiménez-Munt, I., 2010. Radiogenic heat production variability of some common lithological groups and its significance to lithospheric thermal modeling. Tectonophysics 490 (3–4), 152–164. https://doi.org/10.1016/j.tecto.2010.05.003.

Villemin, T., Bergerat, F., 1987. L'evolution structurale du fosse rhenan au cours du Cenozoique; un bilan de la deformation et des effets thermiques de l'extension. Bulletin de la Société Géologique de France III 245–255. https://doi.org/10.2113/gssgfbull.III.2.245.

Villemin, T., Alvarez, F., Angelier, J., 1986. The Rhinegraben: Extension, subsidence and shoulder uplift. Tectonophysics 128 (1–2), 47–59. https://doi.org/10.1016/0040-1951(86)90307-0.

von Seckendorff, V., Arz, C., Lorenz, V., 2004. Magmatism of the late Variscan intermontane Saar-Nahe Basin (Germany): a review. Geol. Soc. Lond., Spec. Publ. 223 (1), 361–391. https://doi.org/10.1144/GSL.SP.2004.223.01.16.

Weber, K., 1995a. IV.C.3 the Saar-Nahe Basin. In: Dallmeyer, R.D., Franke, W., Weber, K. (Eds.), Pre-Permian Geology of Central and Eastern Europe. Springer Berlin Heidelberg, Berlin, Heidelberg, pp. 182–185.

Weber, K., 1995b. IV.C.4 Structural Relationship between Saar-Nahe Basin, Odenwald, and Spessart Mts. In: Dallmeyer, R.D., Franke, W., Weber, K. (Eds.), Pre-Permian Geology of Central and Eastern Europe. Springer Berlin Heidelberg, Berlin, Heidelberg, pp. 186–189.

Weinert, S., Bär, K., Sass, I., 2020a. Database of Petrophysical Properties of the Mid-German Crystalline High. In review. Earth Syst. Sci. Data Discuss.. https://doi.org/10.5194/essd-2020-211.

Weinert, S., Bär, K., Sass, I., 2020b. Petrophysical Properties of the Mid-German Crystalline High: A Database for Bavarian, Hessian, Rhineland-Palatinate and Thuringian Outcrops. Technical University of Darmstadt, TUdatalib doi:10.25534/tudatalib-278.

Weinert, S., Bär, K., Sass, I., 2021. A Geological 3D-Structural Model of the Hessian Mid-German Basement. TUdatalib. In Prep.

Welsch, B., Bär, K., Rühaak, W., Sass, I., 2014. An Outcrop Analogue Study on the Suitability of Crystalline Rocks as Heat Storage Media. In: Röhling, H.G., Zulauf, G. (Eds.), GeoFrankfurt 2014 - Dynamik des Systems Erde/Earth Systems Dynamics, Abstract Volume. Schweizerbart Science Publishers, Stuttgart, p. 546.

Will, T.M., Lee, S.-H., Schmädicke, E., Frimmel, H.E., Okrusch, M., 2015. Variscan terrane boundaries in the Odenwald–Spessart basement, Mid-German Crystalline Zone: New evidence from ocean ridge, intraplate and arc-derived metabasaltic rocks. Lithos 220-223, 23–42. https://doi.org/10.1016/j.lithos.2015.01.018.

Zeh, A., Gerdes, A., 2010. Baltica- and Gondwana-derived sediments in the Mid-German Crystalline rise (Central Europe): Implications for the closure of the Rheic Ocean. Gondwana Res. 17 (2–3), 254–263. https://doi.org/10.1016/j.gr.2009.08.004.

Ziegler, P.A., 1990. Geological Atlas of Western and Central Europe 1990, 2nd ed. Shell Internationale Petroleum Maatschappij BV, The Hague, p. 239.

Ziegler, P.A., 1992. European Cenozoic rift system. Tectonophysics 208 (1–3), 91–111. https://doi.org/10.1016/0040-1951(92)90338-7.

Ziegler, P.A., Dèzes, P., 2005. Evolution of the lithosphere in the area of the Rhine Rift System. Int. J. Earth Sci. 94 (4), 594–614. https://doi.org/10.1007/s00531-005-0474-3.

4. Techno-Economic Assessment of Geothermal Resources in the Variscan Basement of the Northern Upper Rhine Graben

This chapter includes the peer-reviewed research article with same title that was published in the journal Natural Resources Research (Springer Nature) on the 09 December 2022. The content is unchanged.

A quantitative resource assessment for the basement in the northern Upper Rhine Graben based on the inversion results and additional datasets is presented. Emphasis was placed on the potentials linked to large-scale fault zones, which are generally considered as fluid conduits in the basement. Model uncertainties were quantified through Monte Carlo simulation. A sensitivity analysis was subsequently used to examine the impact of selected factors on the levelized costs of energy as well as geothermal reserves. By comparing the calculated resources with the socio-economic-environmental potential at the surface, favorable sites for geothermal drilling were indicated. The combination of geological, technical, economic and societal aspects of geothermal exploitation in the applied approach provides stakeholders with a useful basis for decision-making.

Reference:

Frey, M., van der Vaart, J., Bär, K., Bossennec, Calcagno, P., Dezayes, C., & Sass, I. (2023). Techno-Economic Assessment of Geothermal Resources in the Variscan Basement of the Northern Upper Rhine Graben. Natural Resources Research, 32. https://doi.org/10.1007/s11053-022-10138-4.

Natural Resources Research, Vol. 32, No. 1, February 2023 (© 2022)
https://doi.org/10.1007/s11053-022-10138-4

Original Paper

Techno-Economic Assessment of Geothermal Resources in the Variscan Basement of the Northern Upper Rhine Graben

Matthis Frey,[1,5] Jeroen van derVaart,[1] Kristian Bär,[2] Claire Bossennec,[1] Philippe Calcagno,[3] Chrystel Dezayes,[3] and Ingo Sass[1,4]

Received 7 July 2022; accepted 26 October 2022
Published online: 9 December 2022

Deep geothermal energy represents an essential component of the future energy supply because the resources greatly exceed the demand, and the base load capability can compensate for temporal fluctuations in wind and solar power. By far, the largest amount of heat is contained in the crystalline basement, accessible almost everywhere through deep drilling. An interdisciplinary approach for a techno-economic resource assessment was applied to provide stakeholders with a more reliable basis for decision-making in the Northern Upper Rhine Graben. This approach incorporated data from various sources such as boreholes, outcrops, geophysical surveys, geomechanical models, and operating geothermal power plants. Emphasis was placed on resources tied to large-scale fault zones, exhibiting preferential hydraulic properties. Uncertainties in the calculations were quantified using Monte Carlo simulations. The resource base in the basement of the Northern Upper Rhine Graben is about 830 PWh_{th}, of which about 8.2–16.1 PWh_{th} could potentially be extracted with current technologies in enhanced geothermal systems. A comprehensive sensitivity analysis was carried out, examining the economic influence of nine parameters. Considering the reference power plant and the energy prices before the Ukraine war began in February 2022, the geothermal reserves are about 65% of the resources. However, given the massive recent increase in heat and electricity prices, a higher percentage is also possible. Finally, a socio-economic-environmental assessment shows that in the Northern Upper Rhine Graben, geothermal resources largely coincide with favorable conditions at the surface, making the region a preferred target for geothermal utilization.

KEY WORDS: Crystalline basement, Geothermal energy, Techno-economic resource assessment, Monte Carlo simulation, Sensitivity analysis.

INTRODUCTION

A rapid reduction in greenhouse gas emissions is essential to mitigate the global effects of man-made climate change. To achieve this aim, major parts of the energy supply need to be shifted from fossil fuels to renewable sources in the coming years (IPCC, 2022). Up to now, German governments and investors have focused primarily on wind and solar

[1]Department of Geothermal Science and Technology, Institute of Applied Geosciences, Technical University of Darmstadt, Schnittspahnstraße 9, 64287 Darmstadt, Germany.
[2]GeoThermal Engineering GmbH, An der Raumfabrik 33C, 76227 Karlsruhe, Germany.
[3]BRGM, 3 Avenue Claude Guillemin, BP 36009 45060 Orléans Cedex, France.
[4]GFZ German Research Centre for Geosciences, Section 4.8: Geoenergy, Telegrafenberg, 14473 Potsdam, Germany.
[5]To whom correspondence should be addressed; e-mail: frey@geo.tu-darmstadt.de

power. However, the significant discrepancy between energy supply and demand throughout the year makes the construction of large energy storages necessary (Bär et al., 2015; Bussar et al., 2016; Welsch et al., 2018). In comparison, geothermal energy enables a base-load capable energy supply such that peak loads can be compensated effectively (Tester et al., 2006; Huenges et al., 2013; Stober & Bucher, 2021). In particular for heat supply, where the dependency on fossil energy sources is still very high both in the residential and commercial sectors, there is a considerable need to expand renewables (BMWi, 2021), much of which can be covered by deep geothermal power plants (Moeck, 2022). At present, geothermal energy accounts for only a small share of the energy mix in Germany, but the expansion of this technology is essential for a successfull energy transition (Bracke & Huenges, 2022). The Upper Rhine Graben (URG) is an ideal region for geothermal utilization due to the significantly increased temperature gradient and several potential reservoir horizons (Pribnow & Schellschmidt, 2000; Sass et al., 2011; Stober & Bucher, 2015; Freymark et al., 2017). Here, enhanced/engineered geothermal systems (EGS) are generally developed where the permeability of the fractured reservoir is improved by hydro-mechanical and/or hydrochemical stimulation. The reservoir volume is constrained by the hydraulically active fracture network during operation and can be mapped using, e.g., induced seismicity. In total, 17 deep geothermal projects have been implemented in the URG since the late 1970s, seven of which are currently in operation (Bruchsal, Insheim, Landau, Riehen, Rittershoffen, Soultz-sous-Forêts, Weinheim), providing 50 MW_{th} of heat and 10 MW_{el} of electricity (Frey et al., 2022a). Thus, only a small portion of the total geothermal resources are currently being utilized (e.g., Kock & Kaltschmitt, 2012).

While aquifers are the preferred targets of geothermal drilling, such hydrothermal reservoirs hold only about 1% of the total resources (Paschen et al., 2003). In contrast, by far the largest amount of heat is contained in the Variscan basement, which is characterized by very high temperatures and an increased density of fractures and faults in the URG (Genter & Traineau, 1996; Sausse & Genter, 2005; Dezayes et al., 2010; Glaas et al., 2021; Bossennec et al., 2022; Frey et al., 2022b). The fault and fracture network may have reasonable natural permeability or has the potential to be enhanced by stimulation. However, exploration has been subject to significant uncertainties due to the small number of wells that penetrate the entire sedimentary cover and reach the basement. Moreover, the depth resolution or overall quality of most 2D seismic lines is insufficient to image basement structures accurately.

In the past 2 decades, several studies have been conducted to quantify geothermal resources in the URG basement, but their strong geologic simplification of the basement usually allows only for regional considerations (Paschen et al., 2003; Sass et al., 2011; Kock & Kaltschmitt, 2012; GeORG Projektteam, 2013; Jain et al., 2015). In the framework of the Hessen 3D 2.0 (Bär et al., 2021b) and DGE rollout projects (www.nweurope.eu/dge-roll out), gravity and magnetic data were additionally integrated to develop the most detailed 3D model of the crystalline crust in the Northern URG to date (Frey et al., 2021). These results are combined with comprehensive thermal, petrophysical, geomechanical, and financial information to obtain a refined techno-economic resource assessment. This model provides stakeholders with a valuable basis for decision-making during site and reservoir selection for geothermal drilling. The deep geothermal resources of the sedimentary reservoir horizons in the Northern URG will be covered in a subsequent publication by van der Vaart et al. (in prep.).

GEOLOGICAL FRAMEWORK

The URG is a passive continental rift system that developed from the Eocene onwards due to the changing lithospheric stress field in the alpine foreland (e.g., Ziegler et al., 1995). Both location and orientation of the URG are governed by the reactivation of large fault and shear zones in the basement that formed since the Paleozoic (Schumacher, 2002; Edel et al., 2007; Grimmer et al., 2017). The complex multiphase Cenozoic rift evolution caused a distinct asymmetry both parallel and perpendicular to the strike direction, evident in the significant variations in sediment thickness throughout the URG (e.g., Doebl & Olbrecht, 1974). In the first main rifting phase, crustal extension was dominant, dividing the crust into numerous isolated fault blocks, bounded by large-scale normal faults. During the Miocene, a counterclockwise rotation of σ_{Hmax} led to the reactivation of these faults in a strike-slip or oblique sense (Buchner, 1981; Behrmann et al., 2003; Dèzes et al., 2004). The URG represents a convection-dominated geothermal play system,

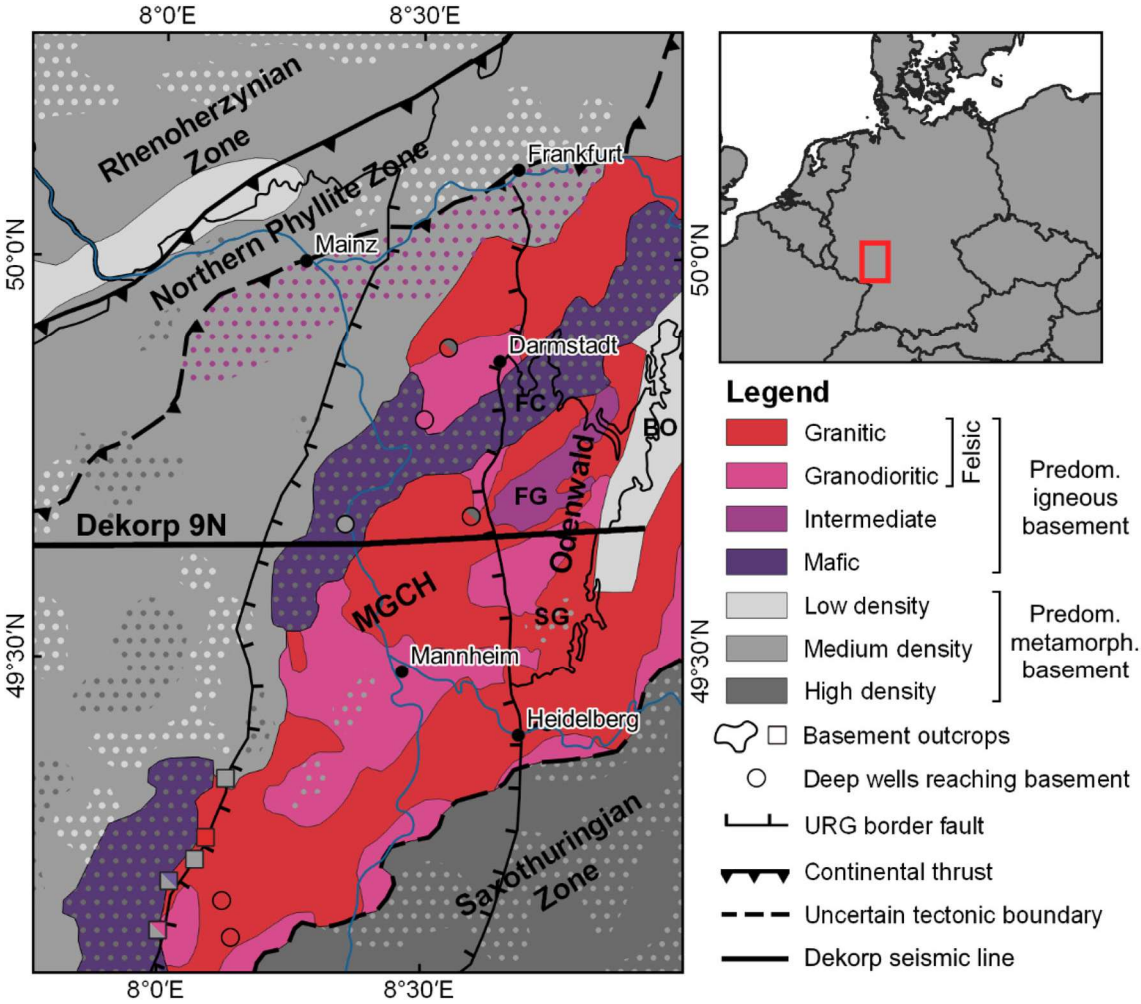

Figure 1. Predictive subcrop map of the Northern URG crystalline basement based on the joint gravity and magnetic inversion of Frey et al. (2021). Dotted signature indicates areas of heterogeneous composition and uncertain interpretation. A detailed image of the fault network in the Northern URG is given in Figure 2. *BO* Böllsteiner Odenwald, *FC* Frankenstein complex, *FG* Flasergranitoid zone, *SG* Flasergranitoid zone.

where local thermal anomalies mainly result from the upwelling of deep groundwaters along fault zones with increased fracture permeability in the fault damage zones (Moeck, 2014).

The basement architecture in the URG region was mainly established during the Variscan orogeny (Kossmat, 1927; Behr et al., 1984), involving the juxtaposition of Laurussia, Gondwana and several micro-terranes (Armorican Terrane Assemblage) with the main collisional phase during the Carboniferous (e.g., Kroner et al., 2008). In the Northern URG, the Mid-German Crystalline High (MGCH) makes up most of the basement (Fig. 1), which is interpreted as a former active continental margin in the north of Armorican Terrane Assemblage (Franke, 2000; Zeh & Gerdes, 2010). The crystalline Odenwald at the northeastern margin of the URG is the largest outcrop of the MGCH and reveals substantial lateral heterogeneity in composition and structure (Krohe & Willner, 1995; Stein, 2001). In the western (Bergsträßer) Odenwald, subduction-related igneous rocks predominate that intruded into meta-volcano and meta-sedimentary host rocks (Krohe, 1991; Altherr et al., 1999). From north (Frankenstein Complex) to south (Southern Plutons) a transition from predominantly mafic to felsic plutonic rocks can be observed. Similarly, the age of the intrusives decreases from about 360 Ma to about 325–330 Ma toward the south (Kreuzer & Harre, 1975; Kirsch et al., 1988; Anthes & Reis-

chmann, 2001). Only a few basement outcrops exist in isolated quarries along the western rift margin, and less than 10 deep wells in the URG reached the basement so far (Fig. 1). However, additional information is provided by gravity and magnetic data, which were used to trace distinct lithologic units hidden beneath the sedimentary cover (for details see Frey et al., 2021).

The MGCH is separated from the Northern Phyllite Zone (NPZ) to the north by a major continental thrust zone (Blundell et al., 1992; Brun et al., 1992), whose location is not precisely known yet. The NPZ, exposed in the southern Taunus and Hunsrück, comprised a tectonic mélange of greenschist-facies meta-sediments and meta-volcanics (Klügel, 1997). To the south, the MGCH merges into the Saxothuringian Zone, which consists of a metamorphic early Paleozoic shelf sequence overlying Neoproterozoic gneiss (Falk et al., 1995).

MATERIAL AND METHODS

3D Model and Parametrization

The resource assessment approach of this study is based on a plausible 3D model of the crystalline basement in the Northern URG. The software Petrel was used to merge existing models, mainly from the GeORG, Hesse 3D and DGE Rollout projects (Sass et al., 2011; GeORG Projektteam, 2013; Bär et al., 2021b; Frey et al., 2021; van der Vaart et al., 2021). Furthermore, additional borehole data and seismic profiles, e.g., the reprocessed DEKORP 9 N line (Homuth et al., 2021), were included. The final model spans over 110 km from north to south, 60 km from east to west, and extends to a depth of 6 km. In previous geothermal potential studies (Paschen et al. 2003; Tester et al, 2006), 10 km was often assumed as the maximum depth of technically feasible utilization, which leads to far too optimistic estimates. In fact, almost no geological data are available below 6 km, preventing any reliable statements about the hydraulic, thermal and geomechanical conditions in this depth range. The 3D model was converted into an irregular grid with a cell size of typically $500 \times 500 \times 500$ m^3. At the top of the basement, the cell height varies to handle the anticipated subsurface topography (Fig. 2a) as accurately as possible.

Supplementary to the structural model of the basement, information on the subsurface temperature distribution is essential. Therefore, the Germany-wide temperature model of Agemar et al. (2012) was used (Fig. 2b), which covers both the sedimentary horizons and the basement with a spatial resolution of 2×2 km. The model used data from approximately 10,500 wells of varying quality. A 3D universal kriging approach was applied to calculate the temperature model, providing indications of the measurement and kriging uncertainties. In the basement, where almost no temperature information is available in the model (mostly below 4–5 km depth), a constant temperature increase of 30 °C/km was assumed to extrapolate temperature values. This value agrees with observed geothermal gradients below the convection-dominated depth interval, e.g., in Soultz-sous-Forêts (Genter et al., 2010). It should be noted that local convection cells, lithological changes, or fault zones are poorly resolved in this purely interpolative model. However, the measured regional-scale thermal anomalies are well represented. Temperature models with a higher resolution exist for specific parts of the URG (Bär et al., 2021b), but because they do not cover the entire model domain, they were not considered further here. The reference temperature was set to the mean surface temperature issued by the German Weather Service for 1991–2020 (DWD, 2021) (about 11 °C in the Northern URG). Additionally, information about the inverted rock density was taken from Frey et al. (2021) (Fig. 2c). Petrophysical data, mainly the specific heat capacity, were adapted from the databases of Bär et al. (2020) and Weinert et al. (2020). Information on the 3D stress tensor in the Northern URG, provided by Ahlers et al. (2021), was used to determine the reactivation potential of fault zones (see details below).

Technical Assessment

The volumetric ('heat in place') approach, proposed by Muffler and Cataldi (1978), was adopted in this study and further refined to quantify the geothermal resources of the basement. This rather simplistic method involves a limited number of parameters, allowing the uncertainties to be reasonably quantified. In comparison, assessment schemes based on numerical simulation require several assumptions about the reservoir (properties, pore pressure, temperature, etc.), the well comple-

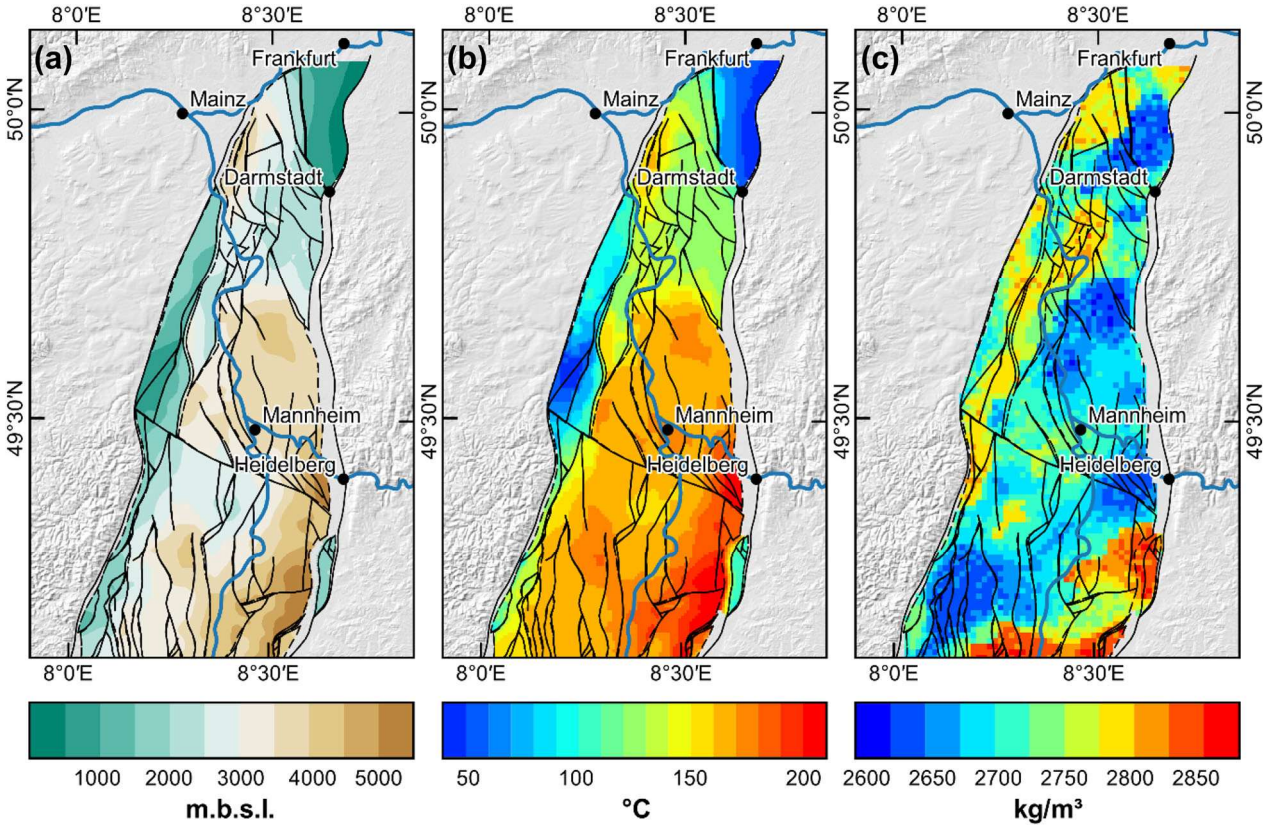

Figure 2. Input data for the geothermal resource assessment: (**a**) depth of the crystalline basement top including all modeled faults; (**b**) reservoir temperature at the basement top (based on the temperature model of Agemar et al., 2012); (**c**) inverted bulk density at the basement top (adapted from Frey et al., 2021).

tion design, the pumping rate, and the operational parameters of the power plant (e.g., Jain et al., 2015). However, especially the hydraulic properties can vary over several orders of magnitude in the basement (Manning & Ingebritsen, 1999; Stober & Bucher, 2007; Achtziger-Zupančič et al., 2017). This makes any simulation result hardly reliable if either the fracture network properties or the local hydraulic parameters are not known from borehole geophysics or hydraulic well testing.

The resource base Q_{total} (J or Wh), also referred to as heat in place or theoretical potential, describes the total amount of thermal energy stored in the Earth's crust (in this case, down to 6 km depth) relative to the ambient surface temperature T_0 (°C). Q_{total} of the individual model cells is calculated as:

$$Q_{\text{total}} = V_{\text{total}} \cdot \rho \cdot c(T_{\text{r}} - T_0) \tag{1}$$

where V_{total} is the volume (m^3) of each model cell, ρ is the rock density (kg/m^3), c is the specific heat capacity (J/kg/K) and T_{r} is the reservoir temperature (°C). Due to the fundamentally low porosity of the crystalline basement, the thermal properties of the pore fluid are not regarded.

The geothermal resources Q_{rec} (J or Wh), also known as recoverable heat or technical potential (Muffler and Cataldi, 1978), are defined as the share of the total thermal energy stored in the reservoir that can be extracted considering the current technologies, thus:

$$Q_{\text{rec}} = Q_{\text{total}} \cdot R \tag{2}$$

Consequently, the thermal recovery factor R (unitless) is one of the key factors that influence the potential productivity of geothermal projects. It depends on various parameters, such as the geometry of the reservoir, permeability, reinjection and abandonment temperature (temperature drop in the reservoir at which operation becomes uneconomical), flow rate, and well design (Garg & Combs, 2015; Agemar et al., 2018). The most reliable infor-

mation on the recovery factor is derived from production data of existing geothermal projects. Accordingly, the recovery factor can be as high as 25% for hydrothermal systems (Tester et al., 2006). In fractured reservoirs, R is generally smaller due to the lower permeability. In active geothermal fields in the USA, such as The Geysers, Coso, and Dixie Valley, the recovery factor ranges from about 5–20% (Williams, 2007). In contrast, Grant (2016) reported recovery factors of only 0.2–2% for the research EGS sites Fenton Hill (USA), Rosemanowes (United Kingdom), Hijori (Japan), and Cooper Basin (Australia). Recovery factors from EGS plants in the URG are currently not publicly available. In the present study, a range of R from 0 to 2% is therefore assumed for the base case, i.e., without the influence of large-scale fault zones. The possibility of zero recovery is included in the assessment to account for the risk of too low productivity.

Fault zones in the crystalline basement are generally considered to be effective fluid conduits (Caine et al., 1996; Evans et al., 1997; Bense et al., 2013). A two to three order of magnitude increase in permeability compared to the host rock is primarily observed in the damage zone, which can be several hundred meters wide depending on the displacement. Consequently, an improved heat recovery is expected when targeting major fault zones (e.g., Jolie et al., 2015). Here, a maximum recovery factor of up to 20% was assumed, which is considered the upper limit for fracture-dominated systems (Tester et al., 2006; Williams et al., 2008). Furthermore, the relative location of the fault planes within the regional stress field was taken as a proxy for maximum heat recovery (Agemar et al., 2017). For this purpose, the slip and dilation tendency were calculated for each modeled fault (Morris et al., 1996; Ferrill & Morris, 2003), which were then used as linear weightings for the recovery factor. The slip tendency T_s (Fig. 3a) describes the ratio of the shear stress τ to the normal stress σ_n on a surface (stress components are given in N/m^2), thus:

$$T_s = \frac{\tau}{\sigma_n} \tag{3}$$

The dilations tendency T_d (Fig. 3b) is calculated from the normal stress as well as the largest and smallest principal stresses σ_1 and σ_3, thus:

$$T_d = \frac{\sigma_1 - \sigma_n}{\sigma_1 - \sigma_3} \tag{4}$$

In addition, e.g., Stober and Bucher (2007) showed that the permeability of the basement is strongly dependent on the lithology. They reported results from hydraulic tests in the Black Forest showing that permeability in gneiss can be up to two orders of magnitude lower than in granite under comparable stress conditions. The geomechanical behavior of the foliated metamorphic rocks during reservoir stimulation and production is more complex to predict than for igneous rocks. There is an increased tendency of re-closing fractures, which are formed primarily along the foliation. To account for this, the recovery factor of the metamorphic basement was downweighed by a factor of 0.1 based on the inversion results and interpretations of Frey et al. (2021).

The potential amount of electricity E (J or Wh) that could be generated in the model area is then obtained by multiplying Q_{rec} with the unitless electrical system efficiency η (Beardsmore et al., 2010). A distinction needs to be made between gross and net system efficiency to consider the parasitic electricity consumption of the pumps, thus:

$$E_{gross/net} = \eta_{gross/net} \cdot Q_{rec} \tag{5}$$

According to Eyerer et al. (2020), η_{gross} and η_{net} can be described as a function of the fluid temperature T_{fl} (°C), thus:

$$\eta_{gross} = 13.59 \cdot \ln(T_{fl}) - 62.38 \tag{6}$$

$$\eta_{net} = 13.20 \cdot \ln(T_{fl}) - 57.60 \tag{7}$$

The mean electrical power output P_{el} (W) of a power plant is calculated by dividing the total gross electricity produced by the project lifetime T_{life} (years) and the annual full load hours h_{full}, thus:

$$P_{el,gross/net} = \frac{E_{gross/net}}{T_{life} \cdot h_{full}} \tag{8}$$

Monte Carlo Simulation

The resource assessment described above involves several parameters subject to varying degrees of uncertainty. Probability density functions (PDF) can be derived directly from the data basis for some parameters, such as temperature, density, or specific heat capacity. For the recovery factor, ranges of possible values have to be assumed since only a limited database is available (see assumed ranges

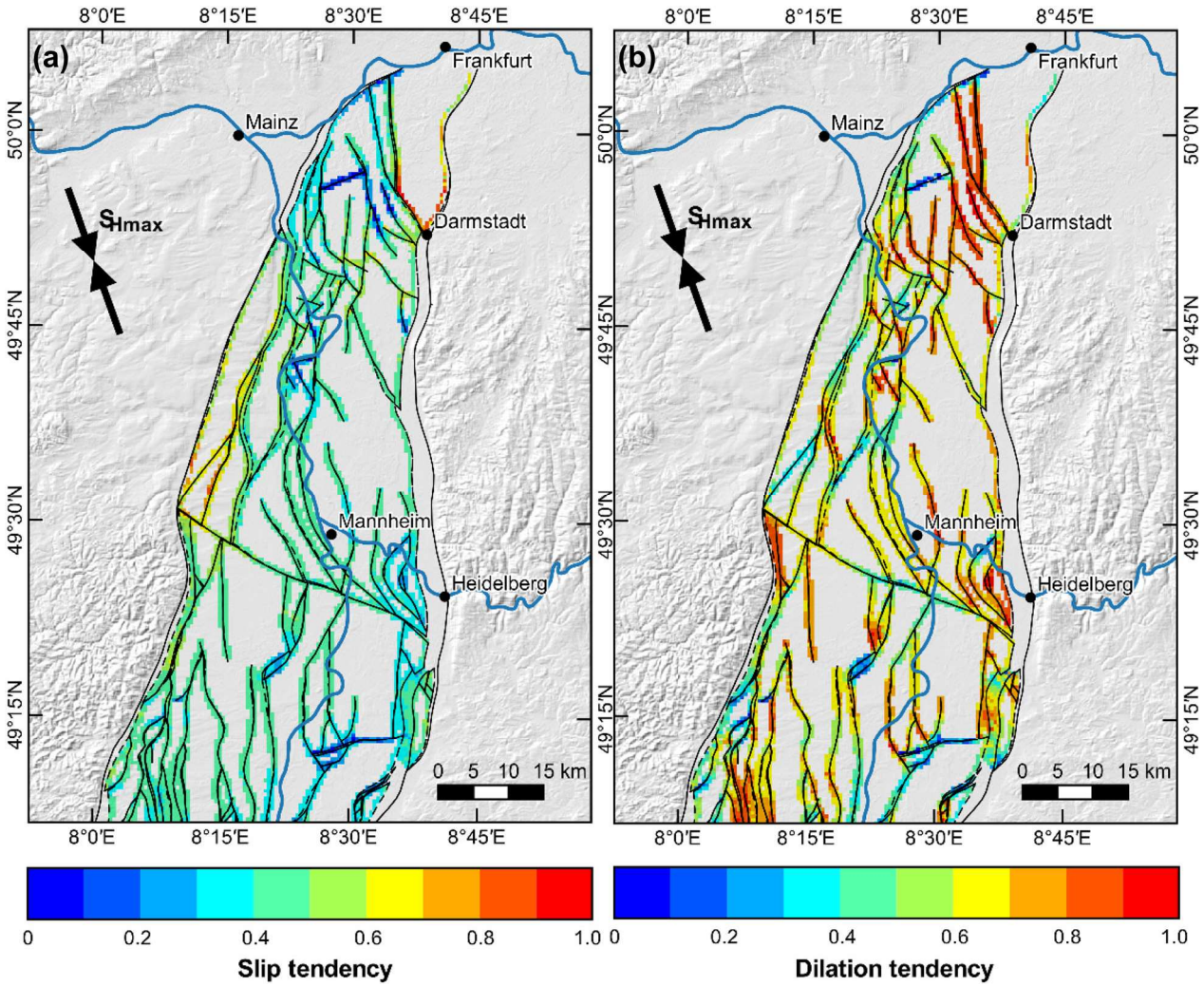

Figure 3. Reactivation potential of fault zones: (**a**) slip tendency, (**b**) dilation tendency of modeled faults at the top of the crystalline basement in the Northern URG. Uncertainties of the stress model were not considered.

above). The associated data publication of this study (Frey et al., 2022d) contains the parameterized model used for the calculations, including the standard deviations or ranges of the parameters.

To quantify the risks of geothermal exploration, it is important to combine the individual uncertainties of the input data into a cumulative uncertainty of the target variable. For this purpose, a Monte Carlo simulation was implemented, which is widely used in geosciences (Sambridge & Mosegaard, 2002; Garg & Combs, 2010; Caers, 2011). The basic principle is that random samples of the input parameters are drawn from the previously defined PDFs. The generated values are then used to perform the above-described calculations. This process is repeated 100,000 times to obtain a significant distribution, which can then be analyzed statistically.

Economical Assessment

The share of geothermal resources that can be exploited economically at present is referred to as geothermal reserves. These can be determined by comparing the levelized costs of energy (LCOE) with the average revenues earned from the sale of electricity and heat. LCOE describes the ratio of the power plant's net present value (NPV), including the total investment c_{invest}, the operation and maintenance costs $c_{\text{O\&M}}$, and the potential revenues r, to

Table 1. Compilation of economic parameters und costs components of geothermal power plants in the URG. Please note that all costs and revenues refer to the conditions before the war in Ukraine and the corresponding energy price increases. In addition, some of the consulted literature sources are significantly older than 2022, thus it is indicated for which year the prices are valid (€$_{year}$). For the conversion of prices as of January 2022, the Producer Price Index was used

Item	Costs	Comments	References
Investment costs			
Exploration	1,500,000	In €$_{2022}$	
Drill site	1,000,000	In €$_{2022}$	
Drilling	$1.198 \cdot e^{0.0004354 \bullet z_{md}}$	In €$_{2014}$ per well, Measured depth in m	Schlagermann (2014)
Reservoir stimulation	1,500,000	In €$_{2022}$	
Hydraulic Tests	1,000,000	In €$_{2022}$	
Well Logging	65 z_{md}	In €$_{2014}$ per well, Measured depth in m	Schlagermann (2014)
Submersible pump	1,000,000	In €$_{2022}$	
ORC plant	$\begin{cases} 3000 \cdot P_{el} : P_{el} < 3\,\text{MW} \\ 2000 \cdot P_{el} : P_{el} \geq 3\,\text{MW} \end{cases}$	In €$_{2022}$, electrical power In kW	
Combined heat and power generation	Additional 25% of plant costs	In €$_{2022}$	
Seismic monitoring network	1,500,000	In €$_{2014}$	Schlagermann (2014)
Public relations	500,000	In €$_{2022}$	
Engineering, project management	12% of total investment costs		Adams et al. (2021)
Discount rate	8.25	In %	
Operation and monitoring	3% of investment costs per year		Eyerer et al. (2020)
Revenues			
Feed-in tariff for electricity	0.252 €/kWh	First 20 years of operation	
Market price for electricity	0.071 €/kWh	After 20 years of operation	AEE (2013), Eyerer et al.(2020)
Market price for heat	0.03 €/kWh		Eyerer et al. (2020)

the NPV of the net electricity generated over the project lifetime (Short et al., 1995), thus:

$$\mathrm{LCOE} = \frac{\sum_t (c_{\mathrm{invest},t} + c_{\mathrm{O\&M},t} + r_t) \cdot (1+d)^{-t}}{\sum_t E_{\mathrm{net}} \cdot (1+d)^{-t}} \quad (9)$$

where t is the time step (years) and d the annual effective discount rate (%). Due to the comparatively high risk of geothermal projects, 8.25% was assumed (e.g., Eyerer et al., 2020).

Compilations of the investment costs of geothermal power plants are provided by various sources (Stefánsson, 2002; Sanyal, 2004; Beckers et al., 2014; Limberger et al., 2014; Schlagermann, 2014; Adams et al., 2021). The cost components described therein are in some cases site- and power plant-specific and therefore not directly applicable for each region. To compare data from different years, the Producer Price Index was used to convert prices to be valid for January 2022 (Destatis, 2022b). After consulting with German industry experts (e.g., Menzel 2022), a generalized cost overview was compiled (Table 1). Accordingly, the total investments consist of the costs for the exploration, the drilling including stimulation, hydraulic tests and geophysical logs, the submersible pump, the power plant at the surface, the management, engineering, planning, and public relations work, the seismological monitoring network, and the insurance of exploration risks. In the following, the major cost elements are discussed in more detail.

Drilling and well completion are the largest cost figures and can reach up to 70% of the total investment for EGS projects. Empirical well cost equations, e.g., published by Legarth (2003), Bloomfield and Laney (2005), Tester et al. (2006), Lukawski et al. (2014) and Schlagermann (2014), generally show an exponential or quadratic increase in cost with depth. For this study, the empirical equation of Schlagermann (2014) was used (Table 1), which focuses on the German market. A simple doublet system with one production well and one injection well was assumed, as this is until now still the standard for EGS projects in the URG. Geothermal wells are usually drilled from one plat-

Table 2. Summary of economic and technical parameter investigated in the sensitivity analysis. Assumed properties of the reference combined heat and power plant are based on operating EGS installations in the URG and worldwide

Parameter	Reference value
Maximum well depth	5 km (TVD)
Lateral reservoir extent	2 km
Recovery factor	Specific for each model cell (see sub-section technical assessment)
Project lifetime	25 years
Full load hours	8000 h/year (electrical), 2000 h/year (thermal)
Investment costs	Specific for each site (see Table 1)
Discount rate	8.25%
Mean heat revenue	0.03 €/kWh
Mean electricity revenue	0.216 €/kWh

form and thus need to be deviated to develop a sufficiently large reservoir volume. The resulting measured depth z_{md} (m) of a well was approximated as:

$$z_{\mathrm{md}} = \sqrt{z_{\mathrm{tvd}}^2 + s^2} \tag{10}$$

where z_{tvd} is the true vertical depth and s the horizontal distance of the wells (both given in m).

Apart from borehole construction, significant costs are related to surface installations of the power plant. Because the reservoir temperatures are generally below 200 °C in the URG, only binary plants based on the Organic Rankine Cycle (ORC) or Kalina Cycle are applicable. Literature data on the specific costs of binary power plants display a wide range, from about 1000 €/kW to over 5000 €/kW (Rettig et al., 2011; Quoilin et al., 2013; Franco & Vaccaro, 2014; Heberle & Brüggemann, 2015; Lemmens, 2015; Tartière & Astolfi, 2017). However, high values are mainly associated with small ORCs (<< 1000 kW), and costs are expected to decrease with increasing electrical power. A step function was defined accordingly (Table 1). In analogy to the power plant in Landau, an electricity-driven combined heat and power (CHP) process with a power to heat ratio of 0.5 was assumed, in which the residual heat from the ORC can be fed into a district heating network. Such a system additionally requires a heat exchanger and piping. These investments can vary greatly depending on the plant specifications. Thus, additional costs of 25% were estimated for simplification.

While capital expenditures are considered overnight expenses, operation and maintenance costs are recurring annually. They include the costs of personnel, well and surface facility maintenance, seismic monitoring, and insurance. These amount to about 3% of the total investment costs for EGS projects. Potential revenues arise from the sale of heat from CHP operations.

Sensitivity Analysis

The LCOE and thus the geothermal reserves are influenced by various technical and economic factors. To quantify the respective effect, a comprehensive sensitivity study was conducted. For this purpose, nine parameters were selected and were assumed to have significant impact on the LCOE (Table 2). Based on the experience of existing geothermal projects, values for a reference power plant were defined. These parameters were then varied systematically in equal steps (- 40%, - 20%, + 20%, + 40%). Excluded from this are the well depth and the lateral reservoir extent, as the variation of these parameters is predetermined by the fixed model discretization.

RESULTS

Geothermal Resource Base and Resources

Figure 4a illustrates the total geothermal resource base in the crystalline basement of the Northern URG to a depth of 6 km. The combined heat in place is approximately 830 PWh, with significant spatial variations. While the resource base exceeds 100 TWh per 500 × 500 m^2 raster cell at the western and northeastern rift margin, it only ranges from 20 to 40 TWh south of Heidelberg. These variations can be explained primarily by differences

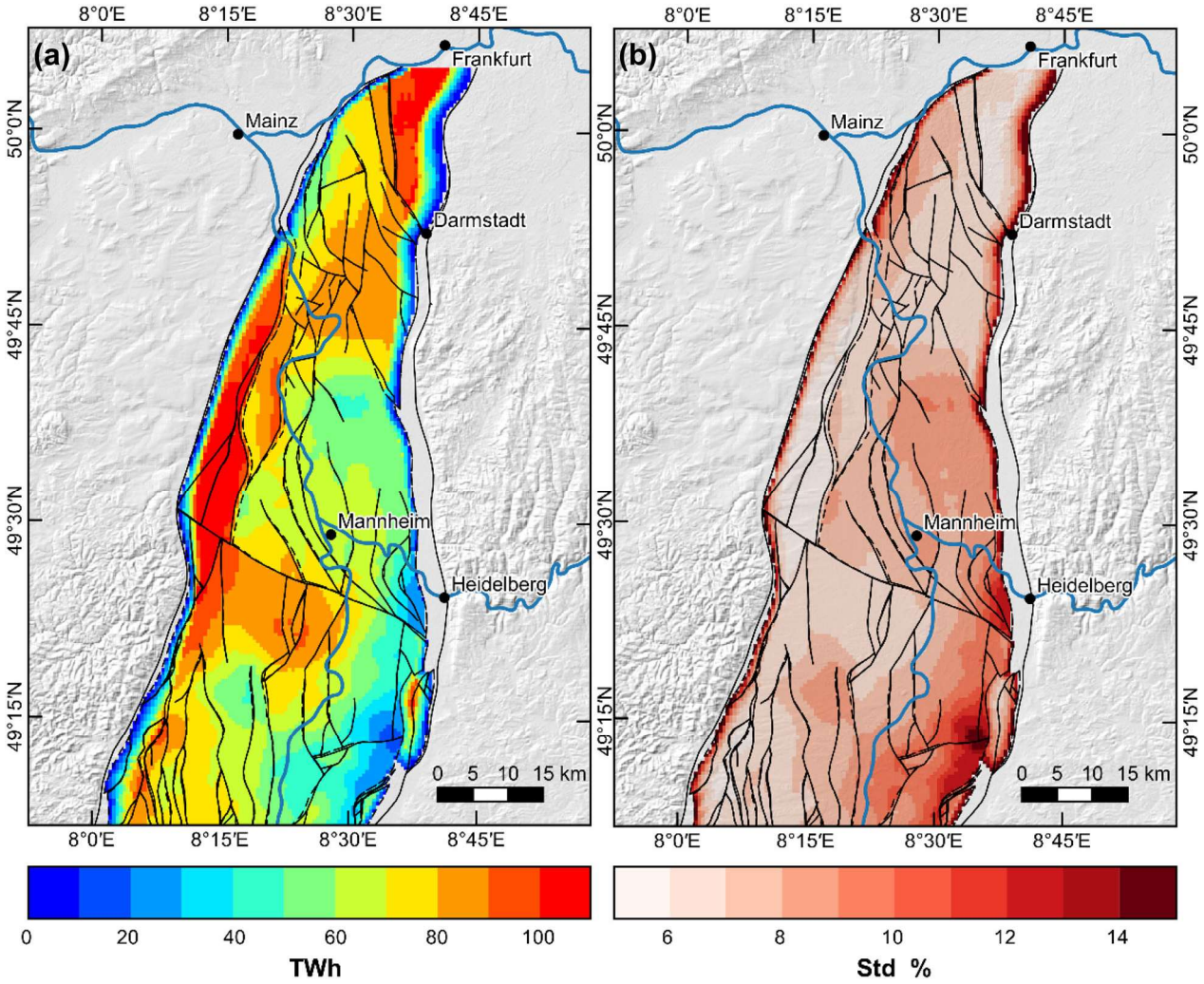

Figure 4. (**a**) Total geothermal resource base (heat in place) in the crystalline basement down to 6 km depth in the Northern URG (heat per 500 × 500 m^2 raster cell). (**b**) Relative standard deviation of the resource base. Note that the geothermal resources of the overlying sedimentary reservoirs are not included.

in the depth to the basement. Accordingly, the thickness of the basement wedge ranges from less than 1 km to more than 5 km within the asymmetric URG (cf. Fig. 2a). The calculation uncertainties are shown as relative standard deviations in Figure 4b. With more than 14%, they are largest at the southeastern margin of the URG. Here, the greater depth of the basement leads to higher standard deviations of the input parameters and thus also of the calculation result.

To avoid the dominating effect of the varying basement thickness down to 6 km depth, three distinct depth slices (3–4 km, 4–5 km, and 5–6 km) of the geothermal resource base were extracted from the model (Fig. 5). The heat in place shown therein is primarily dependent on the distribution of temperature and petrophysical properties. In general, the heat content increases with depth as the temperature also increases. Between 3 and 4 km depth, the resource base is very heterogeneously distributed, mainly because the basement is not yet reached or only partially reached at this depth interval in the eastern URG (see Fig. 2). Between 4–5 km and 5–6 km depth, the resource base varies by about ± 10% from the average. Consistently high heat in place values are present in the area southwest of Mannheim due to the local positive temperature anomaly.

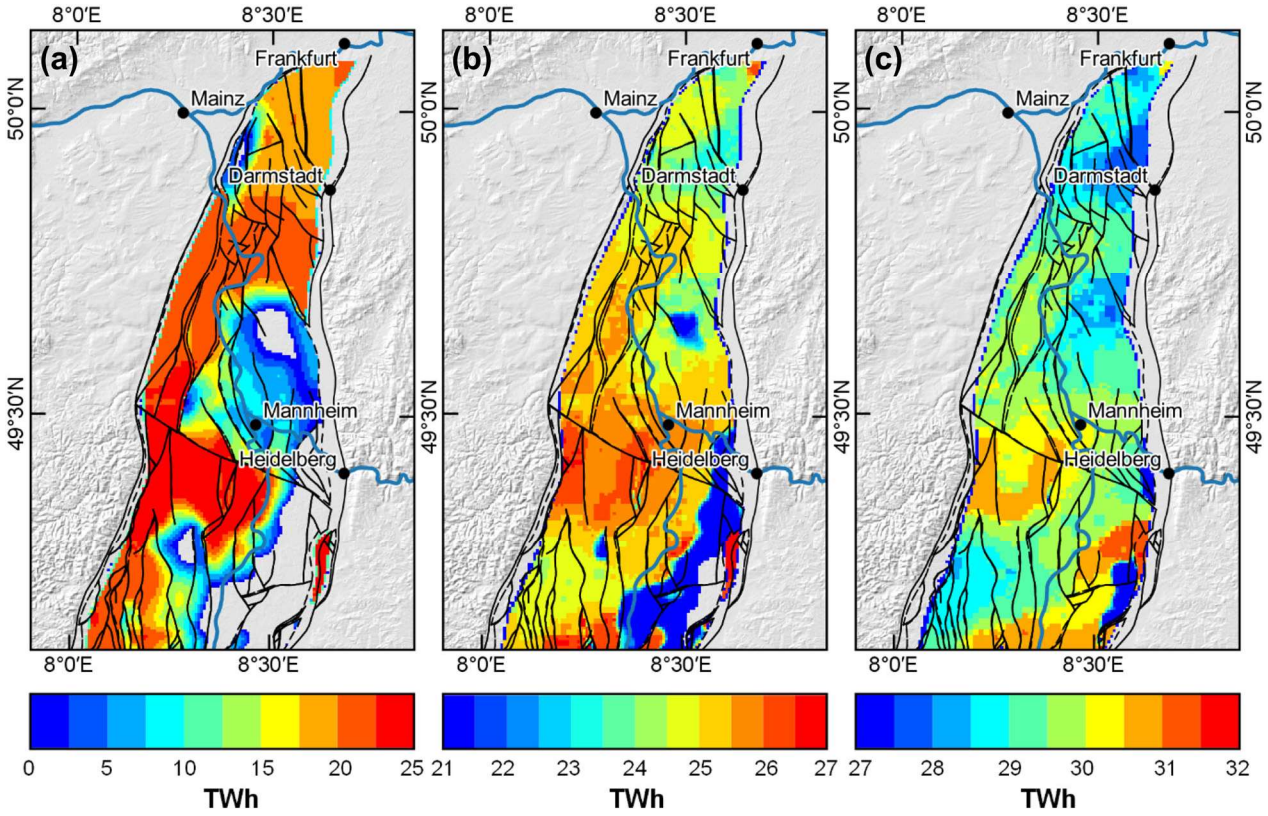

Figure 5. Depth slices of the geothermal resource base (heat in place) in the crystalline basement (heat per 500 × 500 m^2 raster cell): (**a**) between 3 and 4 km depth; (**b**) between 4 and 5 km depth; and (**c**) between 5 and 6 km depth.

Figure 6 shows three alternative scenarios of potentially recoverable geothermal resources considering the currently available EGS technologies. Scenario A (Fig. 6a) describes the base case, where a maximum R of 2% is assumed for the entire basement, as observed in EGS projects worldwide. The combined resources, in this case, are about 8.2 PWh_{th}, allowing a net electricity generation of 0.7 PWh_{el}. The highest values of up to 2 TWh_{th} per 500 × 500 m^2 are again located at the western and northeastern edges of the Northern URG. Scenario B (Fig. 6b) integrates the influence of large-scale fault zones and the regional stress field into the calculation. As a result, the resources amount to about 16.1 PWh_{th}, with a potential electricity production of 1.3 PWh_{el}. The highest values of up to 5 TWh per 500 × 500 m^2 are reached along favorably oriented faults and at fault intersections. The area along the southwestern rift margin exhibits particularly high resources due to the increased fault density and the positive local temperature anomaly. In addition, there are significant geothermal resources around Mannheim and west of Darmstadt. Scenario C (Fig. 6c) also considered the basement lithology. It was assumed that less favorable hydrogeological conditions characterize the predominantly metamorphic and mafic basement compared to the granitoid basement (Stober & Bucher, 2007). Accordingly, the northwestern and southwestern rift margins are less suitable for deep geothermal exploitation. In this case, the total combined resources are about 9.8 PWh_{th}, corresponding to a net electricity production of 0.8 PWh_{el}. The uncertainties are shown as relative standard deviations in Figure 6d–f. The general pattern is similar to Figure 4b, but the standard deviation is substantially higher, ranging from 20 to 60% of the resources. For scenario B, the standard deviation is additionally increased along the modeled fault zones and for scenario C along the boundaries of the major basement units.

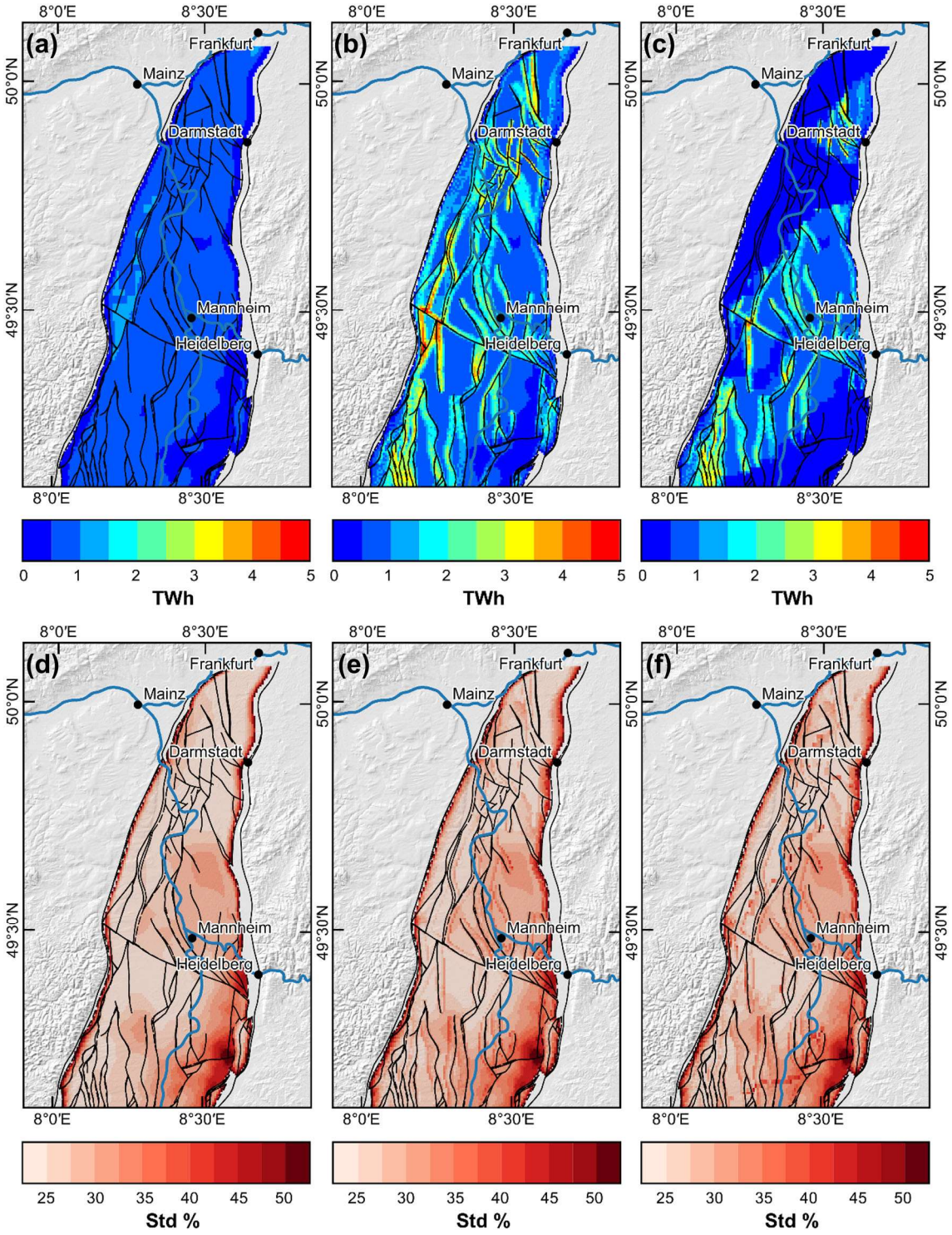

Figure 6. Recoverable geothermal resources in the Northern URG crystalline basement (per 500 × 500 m^2 raster cell). (**a**) Scenario A: base case. (**b**) Scenario B: including the influence of fault zones. (**c**) Scenario C: including the influence of the basement lithology on hydrogeological properties. (**d**–**f**) relative standard deviations of the results.

LCOE and Geothermal Reserves

An economic evaluation was performed based on the calculated recoverable geothermal resources as displayed in Figure 6c and the properties of the reference power plant in Table 2. From this, the cost-supply diagram in Figure 7a is obtained, where the LCOE is plotted against the respective cumulative net electricity production. The curve approaches the geothermal resources for large LCOE. The economically exploitable fraction is obtained by comparing the LCOE with the mean revenues for electricity. Assuming a project lifetime of 25 years (Eyerer et al., 2020), these amount to about 21.6 ct/kWh_{el}, as the feed-in tariff of 25.2 ct/kWh_{el} is paid for 20 years, and afterward a market revenue of about 7.1 ct/kWh_{el} can be expected (AEE, 2013). Accordingly, the geothermal reserves for the reference case amount to about 300 TWh_{el} or 65% of the resources. Note that these assumed revenues are valid for the situation prior to the energy crisis resulting from the Ukraine war. In the first months of 2022, a significant increase in energy prices occurred, but due to the extreme volatility of the market, no reliable forecast of prices can currently be made.

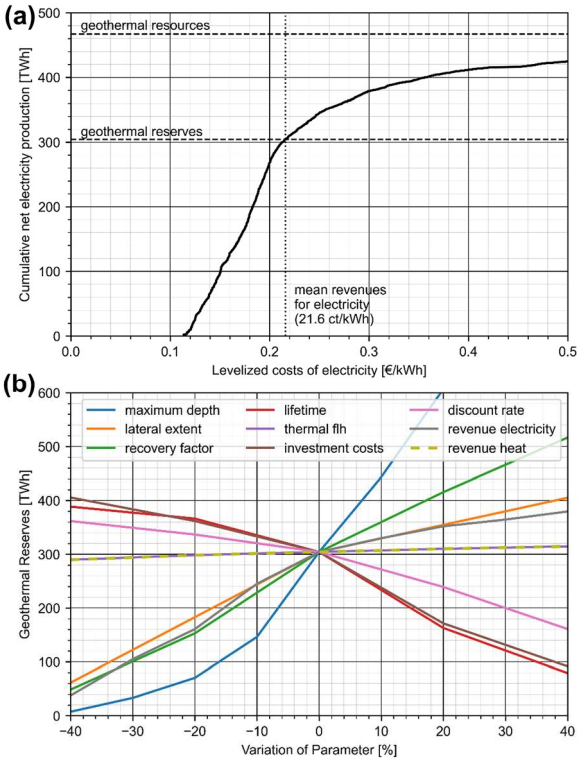

Figure 7. (**a**) Cost-supply diagram for the reference power plant. (**b**) Sensitivity analysis of nine factors affecting the total geothermal reserves in the Northern URG crystalline basement. See Table 2 for details of these parameters..

The technical and the economic-financial framework may differ considerably from the reference configuration for specific projects. For this reason, the influence of nine parameters on the LCOE and geothermal reserves was systematically investigated in a sensitivity analysis (Fig. 7b). Detailed cost-supply diagrams for each parameter are given in Figure 8. In general, there is a high degree of agreement with the results of Eyerer et al. (2020), who conducted a similar analysis for hydrothermal reservoirs in Germany.

The maximum drilling depth has the highest positive effect on the total available geothermal resources. It is considered that with deeper wells, also the open hole section becomes longer and therefore more heat can be produced from the reservoir. Furthermore, the fluid temperature increases with depth and thus also the heat content. If the basement is developed to a depth of 6 km instead of 5 km in the entire Northern URG, the reserves are about 110% higher. However, while drilling costs, risk, and technical challenges increase exponentially with depth, the permeability of the basement decreases, making wells deeper than 5 km still rather unlikely in the near future. Recovery factor and the lateral extent of the reservoir, which essentially determine the total amount of heat that a doublet can potentially produce, also positively influence the reserves. They strongly depend, among other factors, on the hydro-mechanical properties of the fracture network, well design, and stimulation effectiveness. A higher recovery factor primarily increases the available recoverable resources and decreases the LCOE, leading to an improved ratio of reserves to resources. The extent of the reservoir does not affect the overall amount of recoverable heat, but with larger reservoir volume, the ratio of reserves to resources increases. Accordingly, geothermal reserves can be significantly increased in the future with improved reservoir enhancement technologies or customized well design patterns with more wells than just the standard doublet and multilaterals in the reservoir section.

Average electricity revenues during the project period are particularly sensitive to political changes in the energy market. Feed-in tariffs are regularly reassessed, hence reductions are possible in the coming years. Conversely, energy prices are generally very volatile, so electricity revenues can fall or

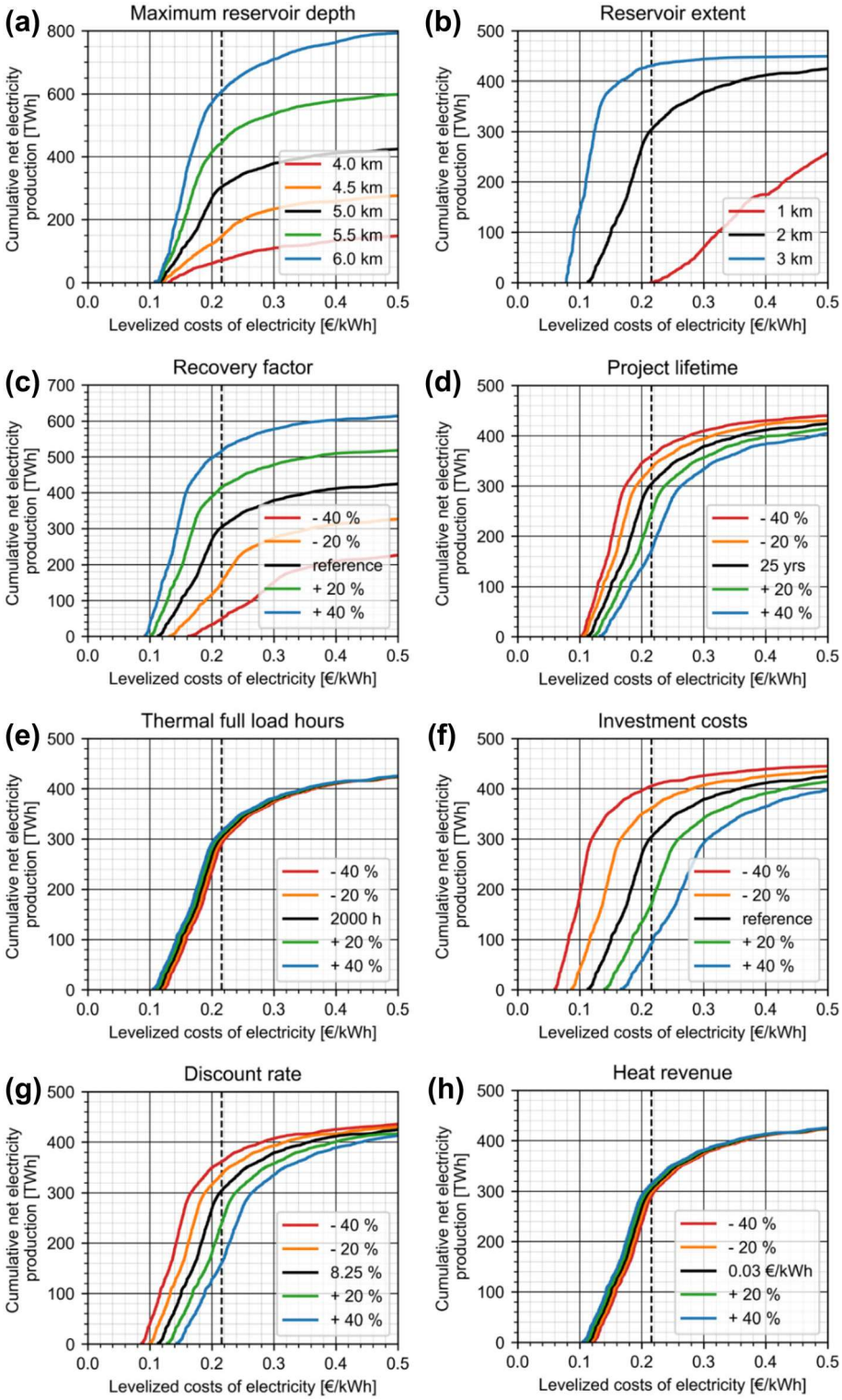

Figure 8. Detailed cost-supply diagrams for eight parameters affecting the electricity production costs and geothermal reserves. The black lines correspond to the reference power plant. The dotted black lines indicate the mean revenue for electricity over the project lifetime of 25 years. No explicit reference values are given for the recovery factor and the investment costs, as they are site-specific.

rise steeply on the free energy market. An increase in average revenues of about 20% would result in about 15% higher reserves, while a 20% decrease would result in 50% lower reserves. In addition, the impact of investment costs is significant. A 20% increase in costs means halving the reserves compared to the reference case. Potentials for cost reductions exist for the ORC and Kalina technologies on the one hand and drilling costs on the other hand.

Interestingly, project lifetime seems to have a similar impact on reserves as investment costs. The reason for this is that with increasing time, the average revenues decrease since feed-in tariffs are only paid for a fixed period. Therefore, from an economic point of view, limiting the project lifetime to 20 years is recommended. The discount rate reflects the risk assessment of geothermal projects. As more power plants are successfully built, this rate may decrease, resulting in lower power production costs and higher reserves. The thermal full load hours and thermal revenues for the assumed power-to-heat ratio of 0.5 only slightly affect the reserves.

DISCUSSION

Limitations of the Volumetric Approach

For the first time, a techno-economic assessment of geothermal resources was carried out for the Variscan basement in the Northern URG, which produced a high-resolution map (500×500 m^2 cell size) of the resources including uncertainties (Fig. 6). That said, it is important to note that the approach still significantly simplifies the geothermal system. The purely static model neglects all temporal changes in the reservoir during operation, as they are difficult to quantify on the regional scale. This includes the temperature decline during production, the replenishment of the resource by conduction, convection and radiogenic heat production, as well as changes in permeability due to mineral scaling or thermal contraction of the host rock. As a result, the recovery factor is not constant over the project lifetime (Grant, 2018), but reliable data on the temporal behavior in EGS are still rare.

Furthermore, the fracture network properties are excluded from the regional model, which greatly impact the flow rate in geothermal wells and thus affect the profitability of the power plant. A simplified well design was assumed, but depending on the local structural framework, the actual well path and completion may vary significantly. Finally, the cost components and other properties for deep geothermal power plants compiled in Tables 1 and 2 are also subject to large variations. A sensitivity analysis therefore compared the individual influence on the LCOE and geothermal reserves.

Consequently, the results presented are mainly indicative of areas with high potential for geothermal use and cannot replace a detailed site-specific investigation prior to drilling. The resource maps are an important basis for a first site selection and the planning of tailored exploration measures. In this context, the integration of 3D seismic datasets is crucial to locate all potentially permeable faults by tracing them from sedimentary horizons down into the basement. Additional information for the reservoir characterization can be provided, for example, by electromagnetic and gravity surveys as well as thermal and hydrochemical monitoring (Bär et al., 2021a). Based on a detailed local 3D model, the temporal thermo-hydro-mechanical (THM) processes relevant for the reservoir stimulation and sustainable operation of the geothermal doublet should then be simulated by high-resolution coupled numerical models. Thereby, the petrophysical rock properties can be derived from comprehensive laboratory investigations and corrected for reservoir conditions (e.g., Bär et al., 2020). Hydrogeological properties of the reservoir may be approximated by combining the few hydraulic test data in the crystalline basement with discrete fracture network models (e.g., Koike et al., 2015; Mahmoodpour et al., 2021). Information on the fracture network properties is provided by sparse boreholes (Afshari et al., 2019; Glaas et al., 2021) but more importantly by analog studies (Bossennec et al., 2021; Bossennec et al., 2022; Frey et al., 2022b). Of particular interest is the influence of the fault damage zone thickness and permeability on the productivity of a geothermal doublet, which can be systematically investigated in high-resolution local models. With a better understanding of the hydraulic reservoir characteristics, it is then possible to estimate the time period over which geothermal heat production can potentially be sustained.

Implications for Geothermal Exploration and Utilization

The presented resource assessment demonstrated that the crystalline basement in the Northern

URG is an attractive reservoir for deep geothermal exploitation due to the vast resource base of 830 PWh_{th}. However, only a fraction (8.2–16.1 PWh_{th}) of it is presumably recoverable with currently available technologies. As expected, the largest resources are associated with major fault zones with a high reactivation potential. Note that in some cases, even fault zones with intermediate slip and dilation tendency may exhibit comparatively high permeabilities, as for example, in Bruchsal. Additional indicators for the potential permeability of fault zones are listed by Agemar et al. (2017) but were not further integrated in the regional-scale study. However, these indicators might be of greater use for local exploration when defining potential drilling targets.

Depending on the hydraulic far-field connectivity, reservoir depletion usually progresses faster than heat resupply through pure conduction and radiogenic heat production. Therefore, after the project lifetime, a rest period is required to recharge the geothermal resources for sustainable utilization of the basement. Conservative estimates suggest a period of about 1000 years (Paschen et al., 2003; Eyerer et al., 2020), which would correspond to a maximum annual heat production of about 8–16 TWh_{th}/year. For comparison, the total annual heat demand in the Northern URG is about 30.6 TWh_{th}/year (Strozyk et al., 2021). Pritchett (1998), on the other hand, reports that 90% of the heat will be renewed after three times the production period. Thus, with a 25-year lifetime, an annual heat production of about 80–160 TWh_{th}/year would be possible. Tester et al. (2006) argue that production can be considered renewable if less than 10% of the heat is extracted annually. This corresponds to a maximum heat production of 0.8–1.6 PWh_{th}/year. More precise insights about the sustainability of geothermal energy will only be provided by long-term experience from commercial EGS projects, but the experiences so far show that the reservoirs in the URG are very well connected to the far-field and can thus be quickly recharged by natural brine circulation on a large scale.

The LCOE analysis has shown that about 65% of the geothermal resources in the Northern URG basement could be exploited economically in the reference case (considering the energy price increase in 2022, the percentage is likely to be even higher). This assessment depends on both the reservoir characteristics and specific investments of the power plants. Drilling is the largest cost factor in EGS projects. The more wells are drilled, the more proven the technologies are and the better the subsurface is explored, resulting in lower risk and shorter drilling times. Therefore, e.g., Limberger et al. (2014) assume that these costs will decrease significantly in the next decades, which is, however, hardly quantifiable. Another way to reduce drilling costs is to drill multiple wells from one drill pad to take advantage of economies of scale. This is particularly useful if a single doublet proves the resources.

Moreover, the effective stimulation of the reservoir plays an essential role. It essentially controls the reservoir volume, the connectivity of the fracture network, and the recovery factor (e.g., Schulte et al., 2010). In this context, the development of novel stimulation methods is required to minimize the induced seismicity (e.g., Amann et al., 2018). In situ experiments addressing these objectives are to be conducted at the planned GeoLaB underground geoscience laboratory on the eastern margin of the URG (Schätzler et al., 2020).

This study investigates an exclusive geothermal utilization of the basement. Additionally, several sedimentary formations in the Northern URG are suitable for deep geothermal exploitation, namely the Permo-Carboniferous, Buntsandstein, Muschelkalk, and Tertiary sandstones. In particular in the eastern rift area, where the resource base in the basement is low (see Fig. 4), these horizons represent the preferred exploration targets. However, their geothermal potential is not further quantified herein but will be the subject of a subsequent publication (van der Vaart et al., in prep.). Some geothermal projects in the URG pursue a multi-reservoir approach, for example, in Insheim, Landau and Rittershoffen, where both sedimentary horizons and the basement are exploited together. This reduces the exploration risk, and a higher flow rate as well as a higher heat production can be achieved at the same drilling depth. Co-production of heat and electricity currently provides the most economic benefit, as the feed-in tariff for electricity is relatively high, and the sale of heat provides an additional revenue stream. For direct use of heat from the basement, the LCOH usually exceed 0.03 €/kWh_{th}, which was higher than average prices in the Northern URG before the Ukraine war. However, as mentioned above, energy prices have increased by up to 90% in the first months of 2022 (Destatis, 2022a), making the direct use of heat from th basement an economically viable solution as of now.

In addition to conventional EGS projects, interest in closed-loop geothermal systems (CLGS)

has increased in recent years, where heat transfer from the reservoir to the working fluid is based solely on conduction (Beckers et al., 2022). Various designs exist in this regard, including coaxial pipes or large subsurface heat exchangers consisting of multiple lateral horizontal wells (Winsloe et al., 2021). These approaches include several advantages in that they are independent of subsurface hydraulic properties, no stimulation is required, less corrosion and scaling occur, and plants can be scaled as required. CLGS can also be retrofitted into existing geothermal, oil, and gas wells. Disadvantages include high drilling costs and comparatively rapid temperature decline during operation. The companies Eavor and GreenFire Energy have already realized initial demonstration projects in North America (Higgins et al., 2019; Toews et al., 2020). Nevertheless, the technical and economic feasibility on a full industrial scale has yet to be proven. In the URG, there is no direct competition to the classical EGS projects since the CLGS target mostly undisturbed rock units, which are not the primary drill sites for open systems.

Socio-economic-environmental Potential

Apart from the geological, technical and financial parameters, the conditions at the surface must always be considered when developing geothermal power plants, as these can have both positive and negative effects on the feasibility of such projects. Frey et al. (2022c) mapped the socio-economic-environmental potential for deep geothermal energy in the URG. The three considered dimensions consist in total of nine individual indicators. The social dimension includes the population-related aspects of population density, heat demand, social level, and acceptance of renewable energy forms. The economic dimension comprises the gross domestic product, the existing district heating network infrastructure and the public debt rate. Finally, the environmental dimension examines the aspects of land access and greenhouse gas emissions. The different quantifiable components were first normalized and then joined into a composite index via an unweighted generalized mean (for a detailed description of the approach see Frey et al., 2022c).

In the Northern URG, the socio-economic-environmental index exhibits a wide distribution (Fig. 9), with a clear trend between urban and rural areas. The highest potential is found in the large cities and their peripheral districts, which can be attributed to the concentration of population and industry as well as the extensive heat supply infrastructure (e.g., district heating networks of Frankfurt, Darmstadt, Mannheim and Heidelberg). Here, natural and landscape conservation areas can be limiting factors that make access to geothermal resources difficult or in rare cases completely impossible, since drilling below these areas is still possible by deviated wells at sufficient depth. These are mainly concentrated along the Rhine. The more sparsely populated and agriculturally dominated areas west of the Rhine have the lowest overall socio-economic-environmental potential.

The comparison of the recoverable resources and mean LCOE (Fig. 9a, b) with the socio-economic-environmental index (Fig. 9c) reveals a high degree of correlation. In particular in the Rhine-Neckar area, favorable conditions in the subsurface and on the surface are combined. Likewise, the areas along the southwestern margin of the Northern URG and around Darmstadt are positively rated. Although the socio-economic conditions are good in the Frankfurt metropolitan region, the crystalline basement is less suitable for geothermal utilization.

Again, this regional evaluation is mostly indicative for locations with an overall high potential. In particular, the social acceptance of geothermal plants can vary considerably at the local level and depends primarily on the quality of communication and the integration of the population by the project developers. The specific decision-making for a drill site represents a multidimensional problem that has to be solved via analytical hierarchical processes (Raos et al., 2022). This involves carefully weighing the conditions in the subsurface against the conditions at the surface.

CONCLUSIONS

A detailed techno-economic resource assessment was conducted for the crystalline basement in the Northern URG. The following conclusions are drawn from these investigations:

- The Northern URG basement exhibits a vast geothermal resource base of approximately 830 PWh_{th}, of which between 8.2 and 16.1 PWh_{th} are potentially recoverable with current technologies. Geothermal reserves amount to at least

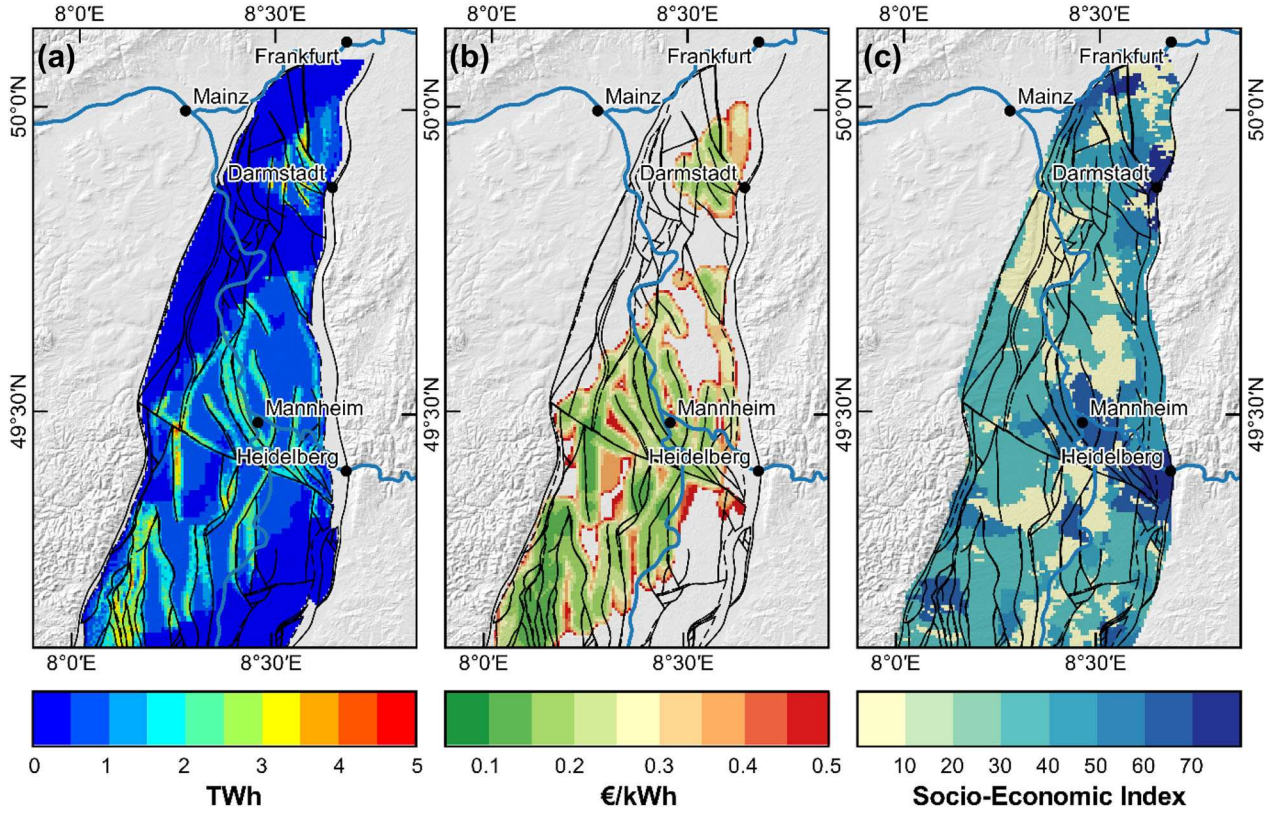

Figure 9. Comparison of (**a**) the recoverable geothermal resources (per 500 × 500 m^2 raster cell, Scenario C, see Fig. 6), (**b**) the LCEO for the reference power plant (see. Table 2) and (**c**) the socio-economical-environmental potential in the Northern URG. The unitless index ranges from 0 (worst conditions) to 100 (ideal conditions).

65% of the resources. The substantial energy price increases at the beginning of 2022 result in an even higher share of resources that could be used economically. However, due to the energy market volatility, it is currently impossible to make a reliable forecast of price developments.

- The geothermal resources are mainly tied to fault zones with high slip and dilation tendencies located in predominantly granitoid basement units. The largest uncertainties are found along the eastern rift margin, where the top of basement is deepest.
- The impact of various CHP plant properties on the LCOE was investigated using a sensitivity analysis. Significant influences were found for the maximum drilling depth, the recovery factor, the reservoir development, the investment costs, the project lifetime, the discount rate and the average revenue for electricity. In contrast, the thermal full load hours and the average revenue from the sale of heat have a lower significance.
- The socio-economic-environmental potential for deep geothermal energy reveals a clear urban–rural trend. A comparison with the resources shows a high degree of agreement in the Rhine-Main area, west of Darmstadt, the southeastern areas around Mannheim, and the southwestern rift margin close to Landau
- The techno-economic and socio-economic-environmental analyses are primarily indicative of areas with high potential. They are not a substitute for local targeted exploration activities and multidimensional decision-making processes.
- In-depth studies of the dynamic behavior of reservoir properties during production need to be carried out using local coupled THM models

ACKNOWLEDGMENTS

We thank the three anonymous reviewers for their very helpful comments on this manuscript. The

research was funded by the Interreg NWE Program through the Roll-out of Deep Geothermal Energy in North-West Europe (DGE-ROLLOUT Project, w ww.nweurope.eu/DGE-Rollout). The Interreg NWE Program is part of the European Cohesion Policy and is financed by the European Regional Development Fund (ERDF). We acknowledge support by the Deutsche Forschungsgemeinschaft (DFG—German Research Foundation) and the Open Access Publishing Fund of Technical University of Darmstadt, through the DEAL project. Petrel was kindly provided by Schlumberger for this research.

FUNDING

Open Access funding enabled and organized by Projekt DEAL.

DATA AVAILABILITY

The discretized and parameterized model used for the geothermal resource assessment can be found in the TUDatalib repository, https://doi.org/10.48328/tudatalib-898.

DECLARATIONS

Conflict of Interest The authors have no relevant financial or non-financial interests to disclose.

OPEN ACCESS

REFERENCES

Achtziger-Zupančič, P., Loew, S., & Mariéthoz, G. (2017). A new global database to improve predictions of permeability distribution in crystalline rocks at site scale. *Journal of Geophysical Research: Solid Earth, 122*(5), 3513–3539.

Adams, B., Ogland-Hand, J., Bielicki, J. M., Schädle, P., & Saar, M. (2021). *Estimating the geothermal electricity generation potential of sedimentary basins using genGEO (the generalizable GEOthermal techno-economic simulator)*. Retrieved 27 June 2022, from https://doi.org/10.26434/chemrxiv.13514440.

AEE. (2013). *Studienvergleich: Entwicklung der Stromgroßhandels-und der CO2—Zertifikatspreise. Forschungsradar Erneuerbare Energien*. Agentur für Erneuerbare Energien.

Afshari, M., Valley, B., & Evans, K. (2019). Scaling of fracture patterns in three deep boreholes and implications for constraining fractal discrete fracture network models. *Rock Mechanics and Rock Engineering, 52*(6), 1723–1743.

Agemar, T., Hese, F., Moeck, I., & Stober, I. (2017). Kriterienkatalog für die Erfassung tiefreichender Störungen und ihrer geothermischen Nutzbarkeit in Deutschland. *ZDGG, 168*(2), 285–300.

Agemar, T., Schellschmidt, R., & Schulz, R. (2012). Subsurface temperature distribution of Germany. *Geothermics, 44*, 65–77. https://doi.org/10.1016/j.geothermics.2012.07.002.

Agemar, T., Weber, J., & Moeck, I. (2018). Assessment and public reporting of geothermal resources in Germany: Review and outlook. *Energies, 11*(2), 332. https://doi.org/10.3390/en11020332.

Ahlers, S., Henk, A., Hergert, T., Reiter, K., Müller, B., Röckel, L., Heidbach, O., Morawietz, S., Scheck-Wenderoth, M., & Anikiev, D. (2021). 3D crustal stress state of Germany according to a data-calibrated geomechanical model. *Solid Earth, 12*(8), 1777–1799.

Altherr, R., Henes-Klaiber, U., Hegner, E., Satir, M., & Langer, C. (1999). Plutonism in the Variscan Odenwald (Germany): From subduction to collision. *International Journal of Earth Sciences, 88*(3), 422–443.

Amann, F., Gischig, V., Evans, K., Doetsch, J., Jalali, R., Valley, B., Krietsch, H., Dutler, N., Villiger, L., Brixel, B., Klepikova, M., Kittilä, A., Madonna, C., Wiemer, S., Saar, M. O., Loew, S., Driesner, T., Maurer, H., & Giardini, D. (2018). The seismo-hydromechanical behavior during deep geothermal reservoir stimulations: Open questions tackled in a decameter-scale in situ stimulation experiment. *Solid Earth, 9*(1), 115–137.

Anthes, G., & Reischmann, T. (2001). Timing of granitoid magmatism in the eastern mid-German crystalline rise. *Journal of Geodynamics, 31*(2), 119–143.

Bär, K., Reinecker, J., Bott, J., Cacace, M., Frey, M., van der Vaart, J., Scheck-Wenderoth, M., Ritter, O., Homuth, B., Fritsche, J.-G., Spath, F., & Sass, I. (2021a). Integrated exploration strategy 'ConvEx' to detect hydrothermal convection in the subsurface. In *Proceedings of the world geothermal congress 2020*. Reykjavik, Iceland.

Bär, K., Reinsch, T., & Bott, J. (2020). The petrophysical property database (P^3)—A global compilation of lab-measured rock properties. *Earth System Science Data, 12*(4), 2485–2515.

Bär, K., Rühaak, W., Welsch, B., Schulte, D., Homuth, S., & Sass, I. (2015). Seasonal high temperature heat storage with medium deep borehole heat exchangers. *Energy Procedia, 76*, 351–360.

Bär, K., Schäffer, R., Weinert, S., & Sass, I. (2021b). *Schlussbericht Verbundprojekt "Hessen 3D 2.0": 3D-modell der geothermischen Tiefenpotenziale von Hessen*. Technical University of Darmstadt.

Beardsmore, G. R., Rybach, L., Blackwell, D., & Baron, C. (2010). A protocol for estimating and mapping global EGS potential. *GRC Transactions, 34*, 301–312.

Beckers, K. F., Lukawski, M. Z., Anderson, B. J., Moore, M. C., & Tester, J. W. (2014). Levelized costs of electricity and direct-use heat from enhanced geothermal systems. *Journal of Renewable and Sustainable Energy, 6*(1), 13141.

Beckers, K. F., Rangel-Jurado, N., Chandrasekar, H., Hawkins, A. J., Fulton, P. M., & Tester, J. W. (2022). Techno-economic performance of closed-loop geothermal systems for heat production and electricity generation. *Geothermics, 100*, 102318.

Behr, H.-J., Engel, W., Franke, W., Giese, P., & Weber, K. (1984). The Variscan Belt in Central Europe: Main structures, geodynamic implications, open questions. *Tectonophysics, 109*(1–2), 15–40.

Behrmann, J. H., Hermann, O., Horstmann, M., Tanner, D. C., & Bertrand, G. (2003). Anatomy and kinematics of oblique continental rifting revealed: A three-dimensional case study of the southeast Upper Rhine graben (Germany). *Bulletin, 87*(7), 1105–1121.

Bense, V. F., Gleeson, T., Loveless, S. E., Bour, O., & Scibek, J. (2013). Fault zone hydrogeology. *Earth-Science Reviews, 127*, 171–192.

Bloomfield, K. K., & Laney, P. T. (2005). *Estimating well costs for enhanced geothermal system applications*. Idaho Falls: Idaho National Lab (INL).

Blundell, D. J., Freeman, R., Mueller, S., & Button, S. (1992). *A continent revealed: The European geotraverse, structure and dynamic evolution*. Cambridge University Press.

BMWi. (2021). *Zahlen und Fakten: Energiedaten: Nationale und Internationale Entwicklung*. Bundesministerium für Wirtschaft und Energie.

Bossennec, C., Frey, M., Seib, L., Bär, K., & Sass, I. (2021). Multiscale characterisation of fracture patterns of a crystalline reservoir analogue. *Geosciences, 11*(9), 371.

Bossennec, C., Seib, L., Frey, M., van der Vaart, J., & Sass, I. (2022). Structural architecture and permeability patterns of crystalline reservoir rocks in the Northern Upper Rhine Graben: Insights from surface analogues of the Odenwald. *Energies, 15*(4), 1310.

Bracke, R., & Huenges, E. (2022). *Roadmap Tiefengeothermie für Deutschland: Handlungsempfehlungen für Politik*. GFZ Potsdam, Frauenhofer IEG.

Brun, J. P., Gutscher, M.-A., Teams. (1992). Deep crustal structure of the Rhine Graben from dekorp-ecors seismic reflection data: A summary. *Tectonophysics, 208*(1–3), 139–147.

Buchner, F. (1981). Rhinegraben: Horizontal stylolites indicating stress regimes of earlier stages of rifting. *Tectonophysics, 73*(1–3), 113–118.

Bussar, C., Stöcker, P., Cai, Z., Moraes, L., Jr., Magnor, D., Wiernes, P., van Bracht, N., Moser, A., & Sauer, D. U. (2016). Large-scale integration of renewable energies and impact on storage demand in a European renewable power system of 2050—Sensitivity study. *Journal of Energy Storage, 6*, 1–10.

Caers, J. (2011). *Modeling uncertainty in the earth sciences*. Wiley.

Caine, J. S., Evans, J. P., & Forster, C. B. (1996). Fault zone architecture and permeability structure. *Geology, 24*(11), 1025–1028.

Destatis. (2022a). *Daten zur Energiepreisentwicklung—Lange Reihen bis April 2022a.* Statistisches Bundesamt. Retrieved 15 June 2022a, from https://www.destatis.de/DE/Themen/Wirtschaft/Preise/Publikationen/Energiepreise/energiepreisentwicklung-pdf-5619001.html.

Destatis. (2022b). *Erzeugerpreisindex gewerblicher Produkte.* Statistische Bundesamt. Retrieved 10 Feb 2022b, from https://www.destatis.de/DE/Themen/Wirtschaft/Preise/Erzeugerpreisindex-gewerbliche-Produkte/_inhalt.html.

Dezayes, C., Genter, A., & Valley, B. (2010). Structure of the low permeable naturally fractured geothermal reservoir at Soultz. *Comptes Rendus Geoscience, 342*(7–8), 517–530.

Dèzes, P., Schmid, S. M., & Ziegler, P. A. (2004). Evolution of the European Cenozoic Rift System: Interaction of the Alpine and Pyrenean orogens with their foreland lithosphere. *Tectonophysics, 389*(1–2), 1–33.

Doebl, F., & Olbrecht, W. (1974). An isobath map of the Tertiary base in the Rhinegraben. In J. H. Illies & K. Fuchs (Eds.), *Approaches to taphrogenesis* (pp. 71–72). Schweizerbart.

DWD. (2021). *Mean air temperature in Germany between 1991 and 2020*. Deutscher Wetterdienst. Retrieved 27 June 2022, from https://opendata.dwd.de/climate_environment/CDC/grids_germany/multi_annual/air_temperature_mean/.

Edel, J. B., Schulmann, K., & Rotstein, Y. (2007). The Variscan tectonic inheritance of the Upper Rhine Graben: Evidence of reactivations in the Lias, Late Eocene-Oligocene up to the recent. *International Journal of Earth Sciences, 96*(2), 305–325.

Evans, J. P., Forster, C. B., & Goddard, J. V. (1997). Permeability of fault-related rocks, and implications for hydraulic structure of fault zones. *Journal of structural Geology, 19*(11), 1393–1404.

Eyerer, S., Schifflechner, C., Hofbauer, S., Bauer, W., Wieland, C., & Spliethoff, H. (2020). Combined heat and power from hydrothermal geothermal resources in Germany: An assessment of the potential. *Renewable and Sustainable Energy Reviews, 120*, 109661.

Falk, F., Franke, W., & Kurze, M. (1995). Stratigraphy. In R. D. Dallmeyer, W. Franke, & K. Weber (Eds.), *Pre-Permian geology of central and eastern Europe* (pp. 221–234). Springer.

Ferrill, D. A., & Morris, A. P. (2003). Dilational normal faults. *Journal of Structural Geology, 25*(2), 183–196.

Franco, A., & Vaccaro, M. (2014). A combined energetic and economic approach for the sustainable design of geothermal plants. *Energy Conversion and Management, 87*, 735–745.

Franke, W. (2000). The mid-European segment of the Variscides: Tectonostratigraphic units, terrane boundaries and plate tectonic evolution. *Geological Society, London, Special Publications, 179*, 35–61.

Frey, M., Bär, K., Stober, I., Reinecker, J., van der Vaart, J., & Sass, I. (2022a). Assessment of deep geothermal research and development in the Upper Rhine Graben. *Geothermal Energy, 10*(18), 1–67.

Frey, M., Bossennec, C., Seib, L., Bär, K., Schill, E., & Sass, I. (2022b). Interdisciplinary fracture network characterization in the crystalline basement: A case study from the Southern Odenwald, SW Germany. *Solid Earth, 13*(6), 935–955.

Frey, M., van der Vaart, J., Bär, K. (2022c). *Socio-economic potential mapping for deep geothermal energy in the Upper Rhine Graben*: *Report WP T1—2.3: DGE-rollout project.* TU Darmstadt.

Frey, M., van der Vaart, J., Bär, K., Bossennec, C., Calcagno, P., Dezayes, C., & Sass, I. (2022d). *Geothermal resource model of the northern Upper Rhine Graben crystalline basement*. TUdatalib. Retrieved 27 June 2022c, from https://doi.org/10.48328/tudatalib-898.

Frey, M., Weinert, S., Bär, K., van der Vaart, J., Dezayes, C., Calcagno, P., & Sass, I. (2021). Integrated 3D geological modelling of the northern Upper Rhine Graben by joint inversion of gravimetry and magnetic data. *Tectonophysics, 813*, 228927.

Freymark, J., Sippel, J., Scheck-Wenderoth, M., Bär, K., Stiller, M., Fritsche, J.-G., & Kracht, M. (2017). The deep thermal field of the Upper Rhine Graben. *Tectonophysics, 694*, 114–129.

Garg, S. K., & Combs, J. (2010). Appropriate use of USGS vulometric "heat in place" method and Monte Carlo calcu-

lations. In *Proceedings of the thirty-fourth workshop on geothermal reservoir engineering*. Stanford, California.
Garg, S. K., & Combs, J. (2015). A reformulation of USGS volumetric ''heat in place'' resource estimation method. *Geothermics, 55*, 150–158. https://doi.org/10.1016/j.geothermics.2015.02.004.
Genter, A., Evans, K., Cuenot, N., Fritsch, D., & Sanjuan, B. (2010). Contribution of the exploration of deep crystalline fractured reservoir of Soultz to the knowledge of enhanced geothermal systems (EGS). *Comptes Rendus Geoscience, 342*(7–8), 502–516.
Genter, A., & Traineau, H. (1996). Analysis of macroscopic fractures in granite in the HDR geothermal well EPS-1, Soultz-sous-Forêts, France. *Journal of Volcanology and Geothermal Research, 72*(1–2), 121–141.
GeORG Projektteam. (2013). *Geopotenziale des tieferen Untergrundes im Oberrheingraben: Fachlich-Technischer Abschlussbericht des INTERREG-Projekts GeORG*. Freiburg i.Br./Mainz/Strasbourg/Basel.
Glaas, C., Vidal, J., & Genter, A. (2021). Structural characterization of naturally fractured geothermal reservoirs in the central Upper Rhine Graben. *Journal of Structural Geology, 148*, 104370.
Grant, M. A. (2016). Physical performance indicators for HDR/EGS projects. *Geothermics, 63*, 2–4.
Grant, M. A. (2018). Integrated exploration strategy 'ConvEx' to detect hydrothermal convection in the subsurface. In *Proceedings of the 43rd workshop on geothermal reservoir engineering Stanford University*. Stanford, California.
Grimmer, J. C., Ritter, J. R. R., Eisbacher, G. H., & Fielitz, W. (2017). The Late Variscan control on the location and asymmetry of the Upper Rhine Graben. *International Journal of Earth Sciences, 106*(3), 827–853.
Heberle, F., & Brüggemann, D. (2015). Thermo-economic evaluation of organic Rankine cycles for geothermal power generation using zeotropic mixtures. *Energies, 8*(3), 2097–2124.
Higgins, B., Muir, J., Scherer, J., & Amaya, A. (2019). GreenFire energy closed-loop geothermal demonstration at the Coso geothermal field. *GRC Transactions, 43*, 434–448.
Homuth, B., Bär, K., Weinert, S., & Sass, I. (2021). Reprocessing of the hessian DEKORP seismic profiles. In *Tagungsband des 81. Jahrestagung der Deutschen Geophysikalischen Gesellschaft*, Kiel.
Huenges, E., Kohl, T., Kolditz, O., Bremer, J., Scheck-Wenderoth, M., & Vienken, T. (2013). Geothermal energy systems: Research perspective for domestic energy provision. *Environmental Earth Sciences, 70*(8), 3927–3933.
IPCC. (2022). *Working Group III contribution to the IPCC sixth assessment report (AR6-WG3)*.
Jain, C., Vogt, C., & Clauser, C. (2015). Maximum potential for geothermal power in Germany based on engineered geothermal systems. *Geotherm Energy, 3*(1), 1–20.
Jolie, E., Moeck, I., & Faulds, J. E. (2015). Quantitative structural–geological exploration of fault-controlled geothermal systems—A case study from the Basin-and-Range Province, Nevada (USA). *Geothermics, 54*, 54–67.
Kirsch, H., Kober, B., & Lippolt, H. J. (1988). Age of intrusion and rapid cooling of the Frankenstein gabbro (Odenwald, SW-Germany) evidenced by40Ar/39Ar and single-zircon207Pb/206Pb measurements. *International Journal of Earth Sciences, 77*(3), 693–711.
Klügel, T. (1997). *Geometrie und Kinematik einer variszischen Plattengrenze: der Südrand des Rhenoherzynikums im Taunus*. Hessisches Landesamt für Bodenforschung.
Kock, N., & Kaltschmitt, M. (2012). Geothermisch erschließbare Niedertemperaturwärmesenken in Deutschland—Identifikation und Quantifizierung. *Zeitschrift für Energiewirtschaft, 36*(3), 191–203.
Koike, K., Kubo, T., Liu, C., Masoud, A., Amano, K., Kurihara, A., Matsuoka, T., & Lanyon, B. (2015). 3D geostatistical modeling of fracture system in a granitic massif to characterize hydraulic properties and fracture distribution. *Tectonophysics, 660*, 1–16.
Kossmat, F. (1927). Gliederung des varistischen Gebirgsbaues. *Abhandlungen Sächsischen Geologischen Landesamts, 1*, 1–39.
Kreuzer, H., & Harre, W. (1975). K/Ar-altersbestimmungen an hornblenden und biotiten des kristallinen Odenwalds. In G. C. Amstutz, S. Meisl, & E. Nickel (Eds.), *Mineralien und gesteine im Odenwald* (pp. 70–78). Heidelberg.
Krohe, A. (1991). Emplacement of synkinematic plutons in the Variscan Odenwald (Germany) controlled by transtensional tectonics. *International Journal of Earth Sciences, 80*(2), 391–409.
Krohe, A., & Willner, A. P. (1995). IV.C.2 the Odenwald crystalline complex. In R. D. Dallmeyer, W. Franke, & K. Weber (Eds.), *Pre-permian geology of central and eastern Europe* (pp. 182–185). Berlin Heidelberg: Springer.
Kroner, U., Mansy, J. L., Mazur, S., Aleksandrowski, P., Hann, H. P., & Huckriede, H. (2008). Variscan tectonics. In T. McCann (Ed.), *The geology of central Europe: Volume 1: Precambrian and palaeozoic* (pp. 599–664). Geological Society of London.
Legarth, B. A. (2003). *Erschließung sedimentärer Speichergesteine für eine geothermische Stromerzeugung: Scientific technical report STR03/09*. GFZ German Research Centre for Geosciences.
Lemmens, S. (2015). A perspective on costs and cost estimation techniques for organic rankine cycle systems. In *Proceedings of the 3rd international seminar on ORC power systems (ASME ORC 2015)*, Brussels, Belgium.
Limberger, J., Calcagno, P., Manzella, A., Trumpy, E., Boxem, T., Pluymaekers, M. P. D., & van Wees, J.-D. (2014). Assessing the prospective resource base for enhanced geothermal systems in Europe. *Geothermal Energy Science, 2*(1), 55–71.
Lukawski, M. Z., Anderson, B. J., Augustine, C., Capuano, L. E., Beckers, K. F., Livesay, B., & Tester, J. W. (2014). Cost analysis of oil, gas, and geothermal well drilling. *Journal of Petroleum Science and Engineering, 118*, 1–14.
Mahmoodpour, S., Singh, M., Turan, A., Bär, K., & Sass, I. (2021). Hydro-thermal modeling for geothermal energy extraction from Soultz-sous-Forêts, France. *Geosciences, 11*(11), 464.
Manning, C. E., & Ingebritsen, S. E. (1999). Permeability of the continental crust: Implications of geothermal data and metamorphic systems. *Reviews of Geophysics, 37*(1), 127–150.
Moeck, I. (2022). *Metastudie zur nationalen Erdwärmestrategie: Ersatz fossiler Brennstoffe im Bereich Raumwärme und Warmwasser durch Geothermie als unverzichtbarer Bestandteil im Energiesektor Ökowärme bis 2045*. Leibniz-Institut für Angewandte Geophysik, Hannover.
Moeck, I. S. (2014). Catalog of geothermal play types based on geologic controls. *Renewable and Sustainable Energy Reviews, 37*, 867–882.
Morris, A., Ferrill, D. A., & Brent Henderson, D. (1996). Slip-tendency analysis and fault reactivation. *Geology, 24*(3), 275.
Muffler, P., & Cataldi, R. (1978). Methods for regional assessment of geothermal resources. *Geothermics, 7*(2–4), 53–89.
Paschen, H., Ortel, D., & Grünwald, R. (2003). *Möglichkeiten geothermischer* Stromerzeugung in Deutschland: Sachstandsbericht. Büro für Technikfolgen-Abschätzung beim Deutschen Bundestag.
Pribnow, D., & Schellschmidt, R. (2000). Thermal tracking of upper crustal fluid flow in the Rhine Graben. *Geophysical Research Letters, 27*(13), 1957–1960.
Pritchett, J. W. (1998). Modeling post-abandonment electrical capacity recovery for a two-phase geothermal reservoir. *Geothermal Resources Council Transaction, 22*, 521–528.

Quoilin, S., van den Broek, M., Declaye, S., Dewallef, P., & Lemort, V. (2013). Techno-economic survey of Organic Rankine Cycle (ORC) systems. *Renewable and Sustainable Energy Reviews, 22*, 168–186.

Raos, S., Hranić, J., Rajšl, I., & Bär, K. (2022). An extended methodology for multi-criteria decision-making process focused on enhanced geothermal systems. *Energy Conversion and Management, 258*, 115253.

Rettig, A., Lagler, M., Lamare, T., Li, S., Mahadea, V., McCallion, S., & Chernushevich, J. (2011). Application of organic Rankine cycles (ORC). In *Proceedings of the world engineer's convention*. Geneva, Switzerland.

Sambridge, M., & Mosegaard, K. (2002). Monte Carlo Methods in geophysical inverse problems. *Reviews of Geophysics, 40*(3), 1–29.

Sanyal, S.K. (2004). Cost of geothermal power and factors that affect it. In *Proceedings of the Twenty-Ninth Workshop on Geothermal Reservoir Engineering*, Stanford, California. 26.-28. January.

Sass, I., Hoppe, A., Arndt, D., & Bär, K. (2011). *Forschungs-und Entwicklungsprojekt 3D Modell der Geothermischen Tiefenpotenziale von Hessen: Abschlussbericht*. TU Darmstadt.

Sausse, J., & Genter, A. (2005). Types of permeable fractures in granite. *Geological Society, London, Special Publications, 240*(1), 1–14.

Schätzler, K., Bremer, J., Schill, E., Kohl, T., Kühn, M., Kolditz, O., Sass, I. (2020). GeoLaB – Das geowissenschaftliche Zukunftsprojekt für Deutschland. Mining Report Glückauf. https://mining-report.de/geolab-das-geowissenschaftliche-zukunftsprojekt-fuer-deutschland/.

Schlagermann, P. (2014). *Exergoökonomische analyse geothermischer strombereitstellung am beispiel des oberrheingrabens*. PhD Thesis. TU München.

Schulte, T., Zimmermann, G., Vuataz, F., Portier, S., Tischner, T., Junker, R., Jatho, R., & Huenges, E. (2010). Enhancing geothermal reservoirs. In E. Huenges (Ed.), *Geothermal energy systems* (pp. 173–243). Wiley.

Schumacher, M. E. (2002). Upper Rhine Graben: Role of preexisting structures during rift evolution. *Tectonics, 21*(1), 1–17.

Short, W., Packey, D. J., & Holt, T. (1995). *A manual for the economic evaluation of energy efficiency and renewable energy technologies*. National Renewable Energy Lab (NREL).

Stefánsson, V. (2002). Investment cost for geothermal power plants. *Geothermics, 31*(2), 263–272.

Stein, E. (2001). The geology of the Odenwald crystalline complex. *Mineralogy and Petrology, 72*(1–3), 7–28.

Stober, I., & Bucher, K. (2007). Hydraulic properties of the crystalline basement. *Hydrogeology Journal, 15*(2), 213–224.

Stober, I., & Bucher, K. (2015). Hydraulic and hydrochemical properties of deep sedimentary reservoirs of the Upper Rhine Graben, Europe. *Geofluids, 15*(3), 464–482.

Stober, I., & Bucher, K. (2021). *Geothermal energy: From theoretical models to exploration and development*. Springer.

Strozyk, F., Herbst, E., & Khashfe, E. (2021). *Map of the spatial distribution of the heat demand at the surface*: *Report WP T1—2.1: DGE-Rollout Project*. Fraunhofer IEG.

Tartière, T., & Astolfi, M. (2017). A world overview of the organic Rankine cycle market. *Energy Procedia, 129*, 2–9. https://doi.org/10.1016/j.egypro.2017.09.159.

Tester, J. W., Anderson, B. J., Batchelor, A. S., Blackwell, D. D., DiPippo, R., Drake, E. M., Garnish, J., Livesay, B., Moore, M. C., Nichols, K., Petty, S., Toksöz, M. N., & Veatch, R. W. (2006). *The future of geothermal energy: Impact of enhanced geothermal systems (EGS) on the United States in the 21st Century*. MIT.

Toews, M., Riddell, D., Vany, J., & Schwarz, B. (2020). Case study of a multilateral closed-loop geothermal system. In *Proceedings of the world geothermal congress 2020*, Reykjavik, Iceland.

van der Vaart, J., Bär, K., Frey, M., Reinecker, J., & Sass, I. (2021). Quantifying model uncertainty of a geothermal 3D model of the Cenozoic deposits in the northern Upper Rhine Graben, Germany. *Journal of Applied and Regional Geology. Zeitschrift der Deutschen Gesellschaft für Geowissenschaften, 172*(3), 365–379.

Weinert, S., Bär, K., & Sass, I. (2020). *Petrophysical properties of the mid-german crystalline high: A database for Bavarian, Hessian, Rhineland-Palatinate and Thuringian Outcrops*. TUdatalib. Retrieved 27 June 2022, from https://doi.org/10.25534/tudatalib-278.

Welsch, B., Göllner-Völker, L., Schulte, D. O., Bär, K., Sass, I., & Schebek, L. (2018). Environmental and economic assessment of borehole thermal energy storage in district heating systems. *Applied Energy, 216*, 73–90.

Williams, C. F. (2007). Updated methods for estimating recovery factors for geothermal resources. In *Proceedings of the thirty-second workshop on geothermal reservoir engineering*. Stanford, California.

Williams, C. F., Reed, M. F., & Mariner, R. H. (2008). *A review of methods applied by the U.S. geological survey in the assessment of identified geothermal resources: Open-file report 2008–1296*. USGS.

Winsloe, R., Richter, A., & Vany, J. (2021). The emerging (and proven) technologies that could finally make geothermal scalable. In *Proceedings of the world geothermal congress 2020*, Reykjavik, Iceland.

Zeh, A., & Gerdes, A. (2010). Baltica- and Gondwana-derived sediments in the Mid-German Crystalline Rise (Central Europe): Implications for the closure of the Rheic ocean. *Gondwana Research, 17*(2–3), 254–263.

Ziegler, P. A., Cloetingh, S., & van Wees, J.-D. (1995). Dynamics of intra-plate compressional deformation: The Alpine foreland and other examples. *Tectonophysics, 252*(1–4), 7–59.

5. Interdisciplinary Fracture Network Characterization in the Crystalline Basement: A Case Study from the Southern Odenwald, SW Germany

This chapter includes the peer-reviewed research article with same title that was published in the journal Solid Earth (Copernicus) on the 6 May 2022. The content is unchanged.

The chapter comprises an interdisciplinary, outcrop analog study of the fracture network in the basement in the southern Odenwald. The gained insights into the structural framework of the basement helped to overcome the lack of data from deep wells in the Upper Rhine Graben. Lidar surveys of quarry walls were combined with lineament analysis to obtain a multiscale description of the fracture network. This information was direct input for a Discrete Fracture Network (DFN) modelling, with the purpose to estimate the basement permeability under reservoir conditions. A refined mapping and characterization of potentially permeable fractures and faults was furthermore carried out by measuring gravity and radon anomalies. Based on the findings, recommendations for reservoir development in the northern Upper Rhine Graben are presented.

Reference:

Frey, M., Bossennec, C., Seib, L., Bär, K., Schill, E., & Sass, I. (2022). Interdisciplinary fracture network characterization in the crystalline basement: a case study from the Southern Odenwald, SW Germany. Solid Earth, 13(6), 935-955. https://doi.org/10.5194/se-13-935-2022.

Solid Earth, 13, 935–955, 2022
https://doi.org/10.5194/se-13-935-2022

Solid Earth Open Access EGU

Interdisciplinary fracture network characterization in the crystalline basement: a case study from the Southern Odenwald, SW Germany

Matthis Frey[1], **Claire Bossennec**[1], **Lukas Seib**[1], **Kristian Bär**[2], **Eva Schill**[1,3], **and Ingo Sass**[1,4]

[1]Technical University of Darmstadt, Institute of Applied Geosciences, Department of Geothermal Science and Technology, Schnittspahnstraße 9, 64287 Darmstadt, Germany
[2]GeoThermal Engineering GmbH, An der Raumfabrik 33c, 76227 Karlsruhe, Germany
[3]Karlsruher Institut für Technologie, Hermann-von-Helmholtz-Platz 1, 76344 Eggenstein-Leopoldshafen, Germany
[4]GFZ German Research Centre for Geosciences, Section 4.8: Geoenergy, Telegrafenberg, 14473 Potsdam, Germany

Correspondence: Matthis Frey (frey@geo.tu-darmstadt.de)

Received: 21 September 2021 – Discussion started: 26 October 2021
Revised: 6 May 2022 – Accepted: 6 May 2022 – Published: 2 June 2022

Abstract. The crystalline basement is considered a ubiquitous and almost inexhaustible source of geothermal energy in the Upper Rhine Graben (URG) and other regions worldwide. The hydraulic properties of the basement, which are one of the key factors in the productivity of geothermal power plants, are primarily controlled by hydraulically active faults and fractures. While the most accurate in situ information about the general fracture network is obtained from image logs of deep boreholes, such data are generally sparse and costly and thus often not openly accessible. To circumvent this problem, an outcrop analogue study was conducted with interdisciplinary geoscientific methods in the Tromm Granite, located in the southern Odenwald at the northeastern margin of the URG. Using light detection and ranging (lidar) scanning, the key characteristics of the fracture network were extracted in a total of five outcrops; these were additionally complemented by lineament analysis of two different digital elevation models (DEMs). Based on this, discrete fracture network (DFN) models were developed to calculate equivalent permeability tensors under assumed reservoir conditions. The influences of different parameters, such as fracture orientation, density, aperture and mineralization, were investigated. In addition, extensive gravity and radon measurements were carried out in the study area, allowing fault zones with naturally increased porosity and permeability to be mapped. Gravity anomalies served as input data for a stochastic density inversion, through which areas of potentially increased open porosity were identified. A laterally heterogeneous fracture network characterizes the Tromm Granite, with the highest natural permeabilities expected at the pluton margin, due to the influence of large shear and fault zones.

1 Introduction

The Upper Rhine Graben (URG) represents a region with a high potential for deep geothermal projects in Central Europe due to a significantly increased geothermal gradient of more than 100 °C km^{-1} locally (e.g., Agemar et al., 2014). Often based on knowledge gained from hydrocarbon production, the exploration of geothermally relevant depths began in the 1980s, allowing decades of experience to be built upon (Dezayes et al., 2005b; Cuenot et al., 2008; Genter et al., 2010). Convective heat transport along active large-scale fault zones has been identified as the main reason for the elevated temperatures at shallow depths (Bächler et al., 2003; Baillieux et al., 2013; Guillou-Frottier et al., 2013; Duwiquet et al., 2021). The resulting thermal anomalies are also supported by graben-wide radiogenic heat production, increased heat flux from the mantle and the thermal blanketing effect resulting from the low thermal conductivity of the thick sedimentary cover (Freymark et al., 2017). When exploiting the resulting vast potential, reservoirs with suffi-

cient natural permeability are aimed at to ensure economically viable fluid production. In this context, the top of the crystalline basement in the URG presents an attractive target. In this part of the basement, the abundance of fractures and faults often enables substantial natural fluid flow (Sausse and Genter, 2005; Vidal et al., 2017; Dezayes et al., 2021; Glaas et al., 2021). Examples of successful geothermal production from the crystalline basement in the URG are the EGS (enhanced geothermal system) projects in Insheim, Landau, Rittershoffen and Soultz-sous-Forêts (Schill et al., 2017; Vidal and Genter, 2018).

Fluid flow in fractured reservoirs depends on a multitude of parameters and processes, such as the density, orientation, length, opening and roughness of fractures, stress conditions or the influence of mineralization (Stober and Bucher, 2007; Ledésert et al., 2010; Bisdom et al., 2017; Meller and Ledésert, 2017). Consequently, it is essential to characterize and quantify the properties of the fracture network. The most reliable discrete fracture network (DFN) models have been obtained from geophysical logs in combination with vertical seismic profiling (Genter and Traineau, 1996; Genter et al., 1997; Dezayes et al., 2010; Sausse et al., 2010; Schill et al., 2017; Afshari et al., 2019; Glaas et al., 2021). However, drillings in the crystalline basement of the URG are generally sparse. Furthermore, models of fracture networks from wells and vertical seismic profiling (VSP) lack information – particularly for small-sized fractures – on the fracture length, the aperture and the fracture mineralization. Thus, as the distances to deep boreholes increase, the uncertainty related to the organization and properties of the fracture network also increases. New insights and especially a better spatial and multi-scale understanding of the fracture network characteristics can be gained by investigating the exposed crystalline rocks at the graben shoulders as an outcrop analogue for the URG basement (e.g., Weinert et al., 2020; Bossennec et al., 2021; Dezayes et al., 2021). The greenfield case study presented here focuses on the Tromm Granite in the southern Odenwald (Fig. 1). This highly fractured granitic pluton is relatively homogeneous with respect to lithology and representative of the predominantly granitoid basement in the northern URG (Frey et al., 2021b). Furthermore, the Tromm Granite is a promising site for the geothermal underground research laboratory GeoLaB (Schill et al., 2016), where thermal–hydraulic–mechanical–chemical processes in fractures will be investigated in the future to minimize the risk to future enhanced geothermal systems.

The characterization of fracture networks in the Tromm Granite was performed using a combination of established techniques at multiple scales. Outcrops distributed over the entire pluton were analyzed using the light detection and ranging (lidar) technique (Fisher et al., 2014; Biber et al., 2018; Zeng et al., 2018). Visible fractures were identified and the relevant structural parameters were extracted. This dataset was supplemented by the examination of lineaments in two digital elevation models (DEMs) with 1 m and 1 arcsec resolutions, following the approaches of Pickering et al. (1995), Guerriero et al. (2011), Bertrand et al. (2015) and Meixner et al. (2018). Based on this dataset, DFN models were developed from which the effects of various fracture network parameters on the hydraulic properties of the crystalline basement could be inferred. Because major faults are not outcropping in the area, fault zones were characterized by surface gravity measurements, as shown by Guglielmetti et al. (2013), Altwegg et al. (2015) and Deckert et al. (2017). The stochastic inversion of these gravity data allowed the porosity in the granite to be estimated (e.g., Li and Oldenburg, 1998). Moreover, permeable fault zones were indicated by radon measurements (King et al., 1996; Ioannides et al., 2003; Jolie et al., 2015). As a result, a comprehensive multidisciplinary dataset was obtained that is unique to a crystalline outcrop analogue. This integrated approach provides insights into the permeability structure of the basement that are partially transferable to reservoirs of comparable lithology and structural configuration in the URG.

2 Geological framework

The crystalline Odenwald at the northeastern margin of the URG is the largest outcrop of the Mid-German Crystalline High (MGCH), extending over 50 km from Heidelberg to Darmstadt (Fig. 1). This complex is usually subdivided into two petrogenetic units, the Bergsträßer Odenwald and the Böllsteiner Odenwald, which are separated by a large-scale sinistral shear zone called the Otzberg Shear Zone (Amstutz et al., 1975; Schälicke, 1975; Stein, 2001). The older Böllsteiner Odenwald, located in the east, consists mainly of dome-shaped granitoid orthogneisses whose protoliths were emplaced during the Lower Devonian (Altenberger and Besch, 1993; Reischmann et al., 2001).

In comparison, the Bergsträßer Odenwald is dominated by Variscan plutonic rocks intruded into a metamorphic volcanic–sedimentary series (Altherr et al., 1999). The relics of these host rocks, commonly referred to as Schieferzüge (shale and gneiss bands), comprise gneisses, mica schists, amphibolites and (scarcely) marble (Okrusch et al., 1975). From north to south, the exposed basement rocks show a gradual transition from a primitive island arc regime to a collisional setting (Okrusch et al., 1995; Altherr et al., 1999). While the older northern Frankenstein Complex (intrusion ages 362±7 Ma) (Todt et al., 1995) exhibits a primarily mafic composition, the southern plutons are predominantly felsic. For the latter, hornblende and biotite ages of between 326 and 336 Ma and an intrusion depth of 15 to 19 km were determined (Kreuzer and Harre, 1975). The emplacement of granitoids in the Carboniferous occurred during a syn-orogenic phase in an overall transtensional to extensional setting, as evidenced by large-scale strike-slip and normal faults, separating the individual magmatic and metamorphic units (Krohe, 1991; Krohe and Willner, 1995). These con-

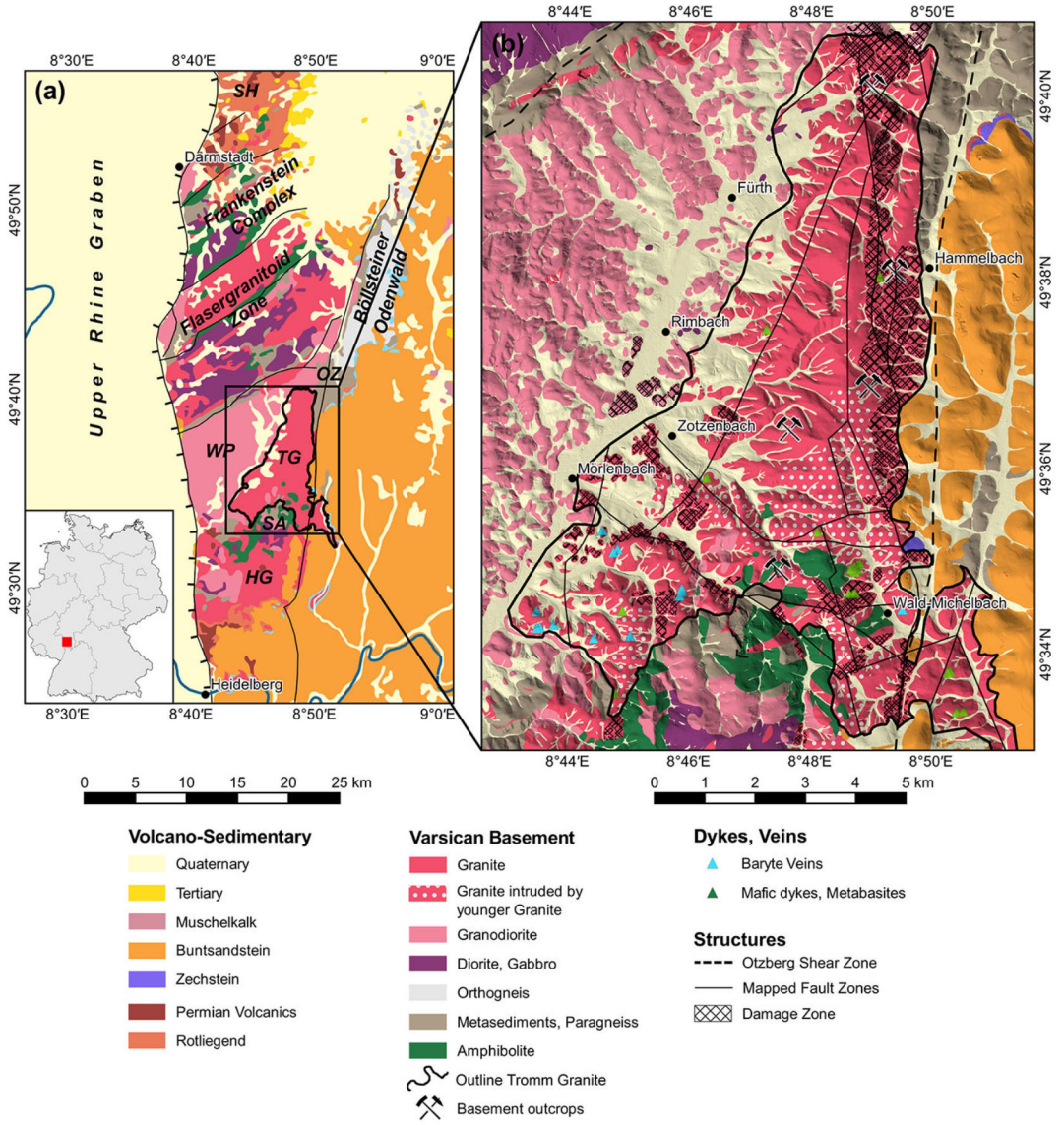

Figure 1. Overview of the study area: **(a)** geological map of the Odenwald (modified after HLUG, 2007); **(b)** geological map of the Tromm Granite in the southern Odenwald (Klemm, 1900, 1928, 1929, 1933). The fault zone map was compiled from various geological maps. HG = Heidelberg Granite, OZ = Otzberg Shear Zone, SA = Schollenagglomerat, SH = Sprendlinger Horst, TG = Tromm Granite, WP = Weschnitz Pluton.

ditions are likely related to oblique subduction of the Rheic or Rhenohercynian basins and associated back-arc spreading. Mineral alignment within the plutonic rocks indicates plastic deformation during crystallization (Krohe, 1992). With progressive cooling, the increasingly brittle deformation was concentrated in large fault zones (Hess and Schmidt, 1989).

The Tromm Granite forms a ca. 60 km^2 large wedge between the Weschnitz Pluton to the west and the metamorphic Böllsteiner Odenwald to the east. The Tromm Granite is a medium- to coarse-grained, orthoclase-rich, biotite-bearing and often reddish granite containing large potassium feldspar inclusions (Maggetti, 1975). Locally, the rock gradually merges into granodiorite, and mixed specimens can be observed. The southern part between Zotzenbach and Wald-Michelbach exhibits a fine-grained variety of the Tromm Granite of a similar mineralogical composition to and a younger age than the coarser variety. In several locations, the granite is intruded by different generations of granitic, aplitic or pegmatitic dykes and veins (Klemm, 1933).

While an interlocking of the two plutons characterizes the contact between the Tromm Granite with the Weschnitz Granodiorite, the eastern boundary constitutes a 1–2 km wide heterogeneous westward-dipping mylonitization and cataclasic zone along the Otzberg Fault (Schälicke, 1975; Hess and Schmidt, 1989). In the southeast, parts of this zone are overlain by Buntsandstein. To the south, the pluton is bounded

by the so-called Schollenagglomerat (Nickel, 1975). This is presumably a former Schieferzug that was dismantled into separate blocks by shear movements along the Otzberg Shear Zone and by the intrusion of the Tromm Granite (Schälicke, 1975). The remaining amphibolite-facies-overprinted rocks are often strongly intruded and assimilated by granitic dykes. The amphibolites are derived from mafic volcanic rocks or tuffs, whereas the gneisses and mica schists are of paragenic origin (Todt et al., 1995; Poller et al., 2001; Schubert et al., 2001).

Most of the mapped and interpreted faults strike NNE–SSW to NNW–SS, which approximately corresponds to the measured orientation of s_{Hmax} (130 to 165°) in the northern URG (Reiter et al., 2016). A secondary direction is present at WNW–ESE. Lamprophyric dykes in the mylonites of the Otzberg Shear Zone are dated at 330 Ma, suggesting that most of the shearing along this zone occurred shortly after the emplacement of the Tromm Granite (Hess and Schmidt, 1989). Later reactivations during Permian rifting or the opening of the URG in the Cenozoic are likely, as indicated by the vertical offset of post-Variscan sediments at the eastern margin of the Tromm Granite, which locally reaches several hundred meters (Klemm, 1933). It is generally difficult to assess the age of the faults where no sediments are preserved for correlation and mineralizations within the faults are not dated.

3 Material and methods

The interdisciplinary and multi-scale fracture network characterization was carried out using the following methods. The first part focuses on structural geological investigations and DFN modelling. The second part presents the applied geophysical acquisition techniques in detail. A summary of all investigations into the Tromm Granite is given in Fig. 2.

3.1 Structural investigations

3.1.1 Lineament analysis

Two DEMs of the Tromm Granite were examined with respect to the density, length and orientation of lineaments. The high-resolution DEM with a cell size of 1 m allowed detailed structural investigations. In addition, the satellite-based Shuttle Radar Topography Mission (SRTM) model with a resolution of 1 arcsec was used to identify regional structural features.

Lineaments are natural, rectilinear surface features that are uniquely identifiable and likely reflect subsurface structures, i.e., faults, discontinuities, or weakness zones. It should be noted that shallow dipping faults may not appear as linear structures and thus may be underrepresented, especially in areas of strong relief. However, most faults in the Tromm Granite are assumed to be rather steeply dipping.

The methodology of lineament analysis is described in previous studies, e.g., in Bertrand et al. (2015), Meixner et al. (2018) and Bossennec et al. (2021). The software QGis was used to generate hill shade maps from the DEMs, which were then visually inspected for lineaments. To avoid misinterpretation, four different illumination azimuths of the hill shade maps (90, 135, 180 and 225°) were compared and the results were checked for anthropogenic structures such as roads or other buildings. The digitized lineaments were used to calculate the lineament density P20 (number of fractures per unit area) and intensity P21 (total length of fractures per unit area) (Sanderson and Nixon, 2018).

3.1.2 Outcrop analysis

Five abandoned quarries located across the Tromm Granite were selected for detailed structural analysis of the fracture network (Fig. 2). As also described in Bossennec et al. (2021), the RIEGL VG 400 lidar instrument was used to generate high-resolution point clouds (point spacing ≤ 1 cm) of the outcrop walls. Compared to classical scanlines, this approach allows for relatively quick acquisition of large structural datasets. At the same time, the statistical bias is reduced as all visible fractures are detected, not only those that cross a 1D line. For an in-depth discussion of the reliability of lidar for outcrop analysis, see Fisher et al. (2014), Vazaios et al. (2017), Biber et al. (2018) or Zeng et al. (2018).

The raw lidar data were first imported into RiSCAN PRO to merge individual scans. Further analysis of the point clouds was performed using the open-source software CloudCompare and QGis. The point cloud was resampled to less than 2 million points to reduce the computational effort of the following steps. Afterwards, the orientations of the surface normals were calculated by triangulating between the points, and these normals were converted to the dip and dip directions. Based on this, the Ransac shape detection plugin was applied to automatically extract the orientations of continuous fracture planes (e.g., Drews et al., 2018). The following parameters were chosen for this step: maximum distance to plane = 5 cm, scanning distance = 20 cm, maximum normal deviation = 10°. Each detected plane was visually inspected and removed if it did not represent natural fractures.

Besides automatic plane recognition, the lidar data were also manually interpreted in QGis to investigate the fracture length, density and connectivity (Fig. 3). For this purpose, side projections of the point clouds were rasterized and hill shade maps were again generated. Visible fractures were then digitized to compute the fracture areal density P20 and intensity P21. Additionally, the linear fracture frequency P10 was extracted along virtual horizontal scanlines for each outcrop. Furthermore, the topology of the fractures was studied to characterize the connectivity of the network. For this, the tips of all fracture branches were classified into three groups: isolated (I), abutting (Y) and crossing (X) nodes. The aver-

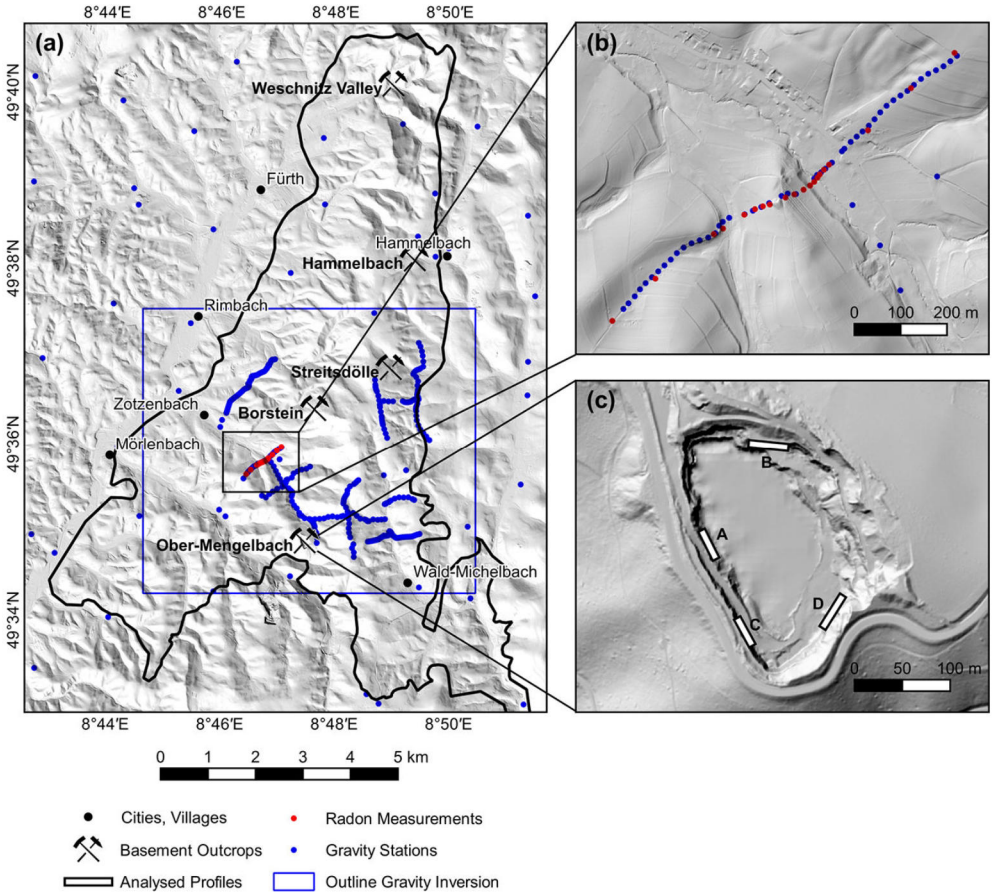

Figure 2. Overview map of the surveys conducted in the Tromm Granite: **(a)** locations of structural and geophysical data acquisitions; **(b)** detailed view of the combined gravity and radon profile; **(c)** detailed view of the quarry in Ober-Mengelbach with the locations of 2D profiles, which have been manually interpreted. The digital elevation model was provided by the HVBG (Hessische Verwaltung für Bodenmanagement und Geoinformation).

age number of connections per line c_L was calculated from the number of nodes per type (Sanderson and Nixon, 2018).

The results of the lineament and outcrop analyses were finally summarized in a normalized trace length cumulative-frequency plot with a power law fitted to the data, which describes the relationship between the frequency and the cumulative distribution of fracture lengths (Pickering et al., 1995; Marrett et al., 1999).

3.1.3 DFN modeling

DFN models were generated with the software FracMan to quantitatively model the hydraulic properties of the fractured crystalline basement based on the structural parameters acquired in the field. Fracture orientations were implemented by performing a cluster analysis of the dip directions and dip angles extracted from the lidar data. The fracture density was defined along a virtual horizontal borehole using the calculated P10 values. The fracture length distribution was set according to the computed power law. A lower cutoff of 70 cm was applied, as significant censoring, i.e., underrepresentation of short fractures, occurs below this length. The effective fracture aperture largely governs the hydraulic conductivity of fractures. Due to exhumation and weathering processes, measured aperture values at near-surface outcrops are usually not reliable (Place et al., 2016). Instead, an exponential distribution of the apertures and – following Sausse and Genter (2005) – three possible mean values (10, 50 and 100 µm) were assumed. A more accurate approach would be to relate the aperture to the normal stress on the fracture plane (Bisdom et al., 2017), but as the local stress magnitudes are largely unconstrained in the Tromm Granite, this was not pursued further. Additionally, previous studies showed that a major fraction of the naturally occurring fractures in the crystalline basement are mineralized at reservoir depth, and therefore only a small share of the fractures allow fluid flow (Genter and Traineau, 1996; McCaffrey et al., 1999; Evans et al., 2005). For this reason, three different scenarios for the proportion of hydraulically active fractures in the DFN model were defined (1 %, 10 % and 100 %).

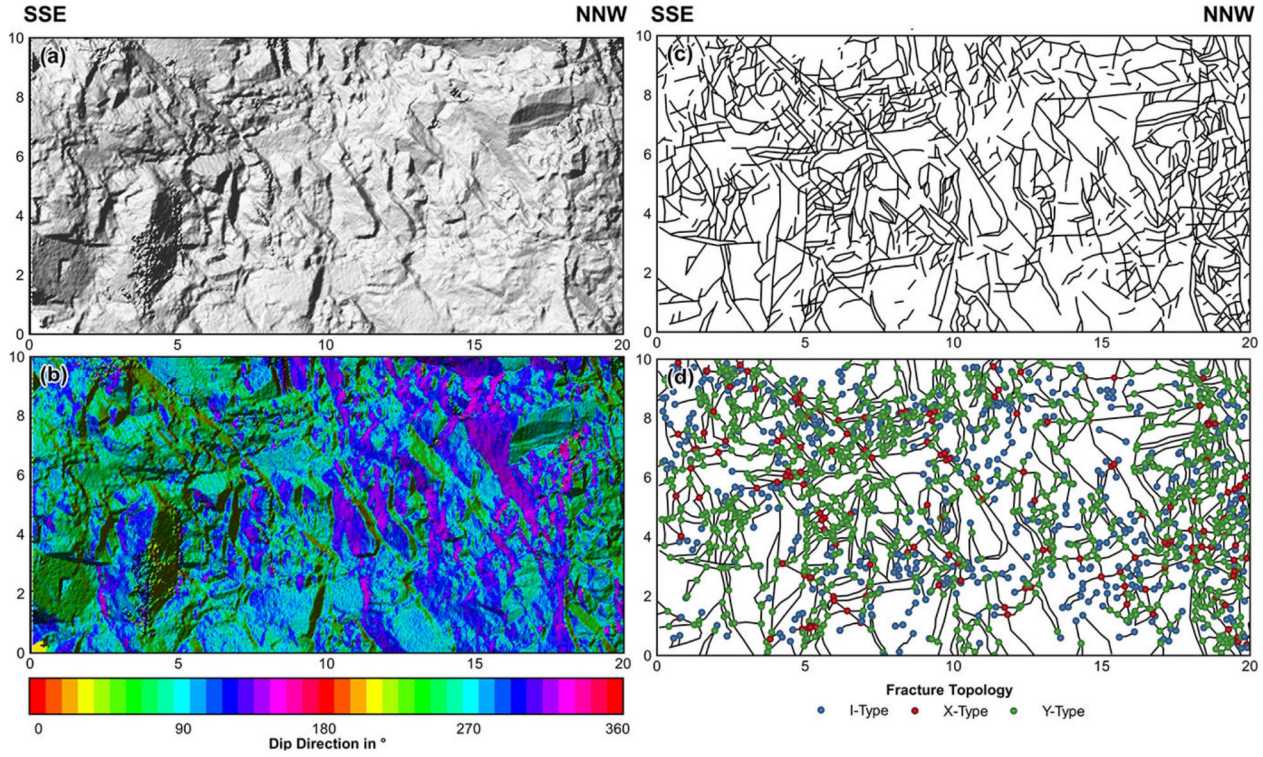

Figure 3. Interpretation of a scanned outcrop wall from the quarry in Ober-Mengelbach (Profile A in Fig. 2): **(a)** rasterized side view; **(b)** calculated dip direction; **(c)** manually interpreted fracture traces; **(d)** topology of the fracture nodes.

For a sufficient number of discontinuities, the fractured basement behaves like an anisotropic porous medium. The equivalent porous medium (EPM) permeability tensor can thus be calculated for a DFN model by, e.g., the approach of Oda (1985). The undisturbed rock matrix is considered impermeable (Jing and Stephansson, 2007; Weinert et al., 2020), implying that fluid flow occurs exclusively through connected fractures. The directional permeability is related to the size, orientation, opening and connectivity of the fractures. One key factor is the relationship between the fluid flow along a fracture and the aperture, which is described by a cubic law (Snow, 1965). This relationship is based on the assumption of laminar flow between two parallel surfaces, which is often not the case due to the irregular surfaces and apertures of the fractures and can therefore lead to errors. The permeability tensors were computed along a regularly spaced grid with a cell size of 10 m to reduce the computational effort, and then mean values were calculated for the entire DFN model. Different cell sizes between 1 and 20 m were tested, revealing no significant differences in the resulting mean permeability tensor.

3.2 Geophysical surveys

3.2.1 Gravity data acquisition

During two surveys in summer 2020 and spring 2021, gravity measurements at 431 stations along 11 profiles were conducted in the Tromm Granite (Fig. 2). Since a differential GPS was used to determine the position, the campaigns were restricted to the southern, less densely forested part. The GPS data were corrected against known fix points, resulting in ca. 10 to 20 cm vertical accuracy. Gravity measurements were performed using the Scintrex® CG-6 Autograv gravimeter with an average station spacing of 100 m or 20 to 25 m close to presumed fault zones. Base measurements were taken 3 times per day at a fixed station to record the instrument drift. Measurements with a standard deviation greater than 0.05 mGal were excluded. A complete Bouguer anomaly was calculated for all gravity stations by applying the standard correction density of 2670 kg m^{-3}, which corresponds approximately to the mean rock density of the Tromm Granite (Weinert et al., 2020), as also confirmed by Nettleton analysis (Nettleton, 1939). Particular focus was directed at the topographic correction, which reached up to 2 mGal along some profiles due to the steep terrain. The calculation was performed with the software GSolve (McCubbine et al., 2018) in three separate zones (Zone 1: 0 to 2.1 km, DEM 10 m; Zone 2: 2.1 to 81 km, DEM 100 m; Zone 3: 81

to 167 km, DEM 1 km). Taking into account all uncertainties in the data acquisition and processing, especially the height error and the standard deviation of the measurement, a cumulative error in the Bouguer anomaly of less than 0.1 mGal was determined.

For the regional gravity signal analysis, ca. 5300 additional data points provided by the Leibniz Institute for Applied Geophysics (LIAG) and the Hessian Administration for Land Management and Geoinformation (HVGB) were used within a radius of 50 km around the survey area. Together with the newly acquired data, a Bouguer anomaly map with a nominal resolution of 20 m was calculated using the minimum curvature interpolation method. A series of high-pass filters with cutoff wavelengths of 10, 5, and 2 km were then applied to subtract the regional gravity field.

3.2.2 Inversion of the gravity data

A stochastic 3D inversion of the high-pass filter Bouguer anomaly (10 km cutoff wavelength) was performed to infer the density distribution and the porosity in the subsurface. The commercial platform GeoModeller (Intrepid Geophysics), which employs a Monte Carlo Markov chain algorithm to invert geophysical data, was used for this purpose. A detailed discussion of the methodology is available in Guillen et al. (2008). The model domain has extensions of 7 km in the E–W direction and 6 km in the N–S direction and a depth of 2 km. The upper boundary is defined by the 10 m DEM. Given the relative homogeneity of the pluton with respect to the matrix density and the lack of structural input data, an unconstrained inversion was performed. The continuous model was converted into a discrete cuboid voxel model with a cell size of $50 \times 50 \times 50$ m. Further decreasing the cell size potentially resolves more details but exponentially increases the computational time of the inversion. A mean density of the Tromm Granite of $2670 \pm 50\,\mathrm{kg\,m^{-3}}$ was defined as the starting value for the rock density (Weinert et al., 2020).

The algorithm first calculates the geophysical effect of the starting model, in this case a homogeneous half-space, and then uses a Bayesian approach to determine the likelihood of the model. In subsequent iterations, random variations of the model are generated according to the probability distribution of the rock density. Models that lead to a reduction in the deviation between the calculated and measured gravity anomalies have a higher likelihood and are stored. After 250 million iterations, a large collection of possible models have been generated, allowing statistic evaluation. Finally, the porosity is estimated, assuming the abovementioned homogeneity of the Tromm granite, using

$$\Phi = \frac{\rho_{\mathrm{bulk}} - \rho_{\mathrm{matrix}}}{\rho_{\mathrm{fluid}} - \rho_{\mathrm{matrix}}}, \quad (1)$$

where ρ_{bulk} is the bulk density, ρ_{fluid} is the fluid density (ca. $1000\,\mathrm{kg\,m^{-3}}$), ρ_{matrix} is the matrix density and Φ is the porosity. Note that this equation cannot be simply applied in the southernmost Tromm Granite, where significant lithological heterogeneity is observed, resulting in variations of the bulk density without the influence of increased fracture porosity.

3.2.3 Radon measurements

Radon is a naturally occurring radioactive gas that is concentrated in the soil air. The most abundant Rn isotope, with a proportion of ca. 90 %, is Rn-222, with a half-life of 3.82 d, which is formed in the decay series of U-238. Permeable fault zones may provide migration pathways where Rn-222 transport to the surface is enhanced. Consequently, elevated radon concentrations are expected in the close vicinity of hydraulically active faults (Ioannides et al., 2003; Baskaran, 2016; Jolie et al., 2016; Vazaios et al., 2017).

Measurements of the activity concentration [$\mathrm{Beq\,m^{-3}}$] of Rn-222 were carried out with the Saphymo AlphaGUARD 2000Pro at 20 points on one profile that crosses two presumed fault zones (Fig. 2b). Soil air was sampled using a hollow probe driven 1 m deep into the subsurface. A pump connected to this probe flooded the ionization chamber of the radon monitor. The activity concentration was measured at 1 min intervals. After 15 min, the air in the chamber was completely exchanged. The pump was then switched off, and the chamber was short-circuited for an additional 10 min. During this time interval, most of the very short-lived thoron (Rn-220, $t_{1/2} = 55.6$ s) decayed, so the final reading corresponded only to the Rn-222 concentration. Furthermore, soil samples were taken with a slotted probe at all stations to determine the soil type. Repeated measurements were performed at a base station to quantify the temporal variability of the concentration measurements.

4 Results

4.1 Fracture network properties

4.1.1 Lineament distribution

Figure 4 and Table 1 compare the faults that were determined by geological mapping in the Tromm Granite area with the geologically significant lineaments extracted from the SRTM model and the DEM with 1 m resolution. A total of 30 faults with a characteristic length (arithmetic mean of the fracture length) of ca. 2900 m were extracted from geological maps (modified after Klemm, 1900, 1928, 1929, 1933; HLUG, 2007), corresponding to a P21 value of $0.0014\,\mathrm{m\,m^{-2}}$. The total number of elements that were identified with the lineament analyses is significantly higher: 177 for SRTM and 471 for the 1 m DEM. Their characteristic lengths of 1187 and 680 m, respectively, are smaller and decrease with increasing resolution. The P21 is $0.0034\,\mathrm{m\,m^{-2}}$ for the SRTM lineaments and $0.0051\,\mathrm{m\,m^{-2}}$ for the lineaments of the high-

resolution DEM. In all datasets, a heterogeneous spatial distribution of the faults or lineaments can be observed. The element density is highest in the eastern part of the Tromm Granite, i.e., in the area influenced by the Otzberg Shear Zone. The density is significantly lower in the west, especially for the mapped faults and the SRTM lineaments.

The main strike of the mapped faults ranges from 160 to 170°, which corresponds approximately to the direction of maximum horizontal stress s_{Hmax} (Reiter et al., 2016). In contrast, the main set of SRTM lineaments strikes with $090 \pm 30°$. The strike directions of lineaments from the high-resolution DEM show nearly a uniform distribution, with a slight accumulation of lineaments at 100°.

4.1.2 Fracture networks in outcrops

In total, five outcrops of varying size, distributed over the entire Tromm Granite area and hence representing the heterogeneity of the pluton, were investigated using lidar (Figs. 1 and 2). Outcrop walls are generally vertical. Borstein and Streitsdölle, the two abandoned quarries in the central part of the study area, are dominated by the typical medium- to coarse-grained Tromm Granite. Remnants or intrusions of other rock species are scarce, but veins of younger granites can frequently be observed. These two outcrops have the lowest areal fracture intensity, with a P21 of 2.43 and $2.83\,\mathrm{m\,m^{-2}}$, respectively (Table 1). Conversely, the fracture characteristic length is the longest here, reaching 1.28 and 1.62 m, respectively. The main set of fractures dips steeply and strikes $160 \pm 20°$, which corresponds to the main direction of the geologically mapped faults in the Tromm Granite (Fig. 4). A second, subordinate set of steeply dipping conjugate fractures strikes $060 \pm 10°$. Shallow dipping fractures are very rare.

The most extended outcrop examined is an abandoned quarry with dimensions of ca. 150×250 m close to the village of Ober-Mengelbach at the southern border of the Tromm Granite (Fig. 2). In contrast to Borstein and Streitsdölle, the lithological conditions found here are more heterogeneous. Meter-wide to 10 m wide amphibolite zones that are highly deformed and intruded by granite or granodiorite were observed throughout the quarry. The magmatic contacts are usually not abrupt but rather characterized by mixed forms of amphibolite and granitoids. Again, several generations of granite intrusions can be distinguished. The distribution of fractures was investigated along four 2D profiles with lengths between 20 and 30 m and a height of 10 m (see Fig. 2 for location). The P21 ranges from 3.60 to $5.87\,\mathrm{m\,m^{-2}}$ and is thus about twice as high as in the central Tromm Granite. The extraction of fracture orientations using the Ransac filter was carried out for all outcrop walls to obtain the most comprehensive dataset possible. Again, the primary set of fractures strikes $160 \pm 20°$ and a secondary set strikes $070 \pm 10°$ (Fig. 5).

The two smaller outcrops in Hammelbach and Weschnitz Valley are located at the northeastern border of the Tromm Granite. Here, a fine- to medium-grained cataclastic granite is predominant, which was considerably affected by the adjacent Otzberg Shear Zone. Consequently, the P21 is highest here: 10.82 and $9.07\,\mathrm{m\,m^{-2}}$, respectively. The fracture orientation also differs significantly from the other three locations. In Hammelbach, the fractures strike almost exclusively $100 \pm 20°$. In the Weschnitz Valley at the northern margin of the Tromm Granite, two fracture sets were found, striking 050 ± 10 and $130 \pm 20°$, respectively. These directions correlate well with the orientation of the close-by lineaments.

4.1.3 Length distribution and fracture connectivity

Figure 6a provides a compilation of all identified faults and geologically significant lineaments from the Tromm Granite, with the length plotted against the cumulative number of fractures normalized to the analyzed surface area. Length values range from 0.02 m to 9 km, hence covering about 6 orders of magnitude. The data points follow a power-law distribution with an exponent of -1.96, which represents a typical value for fracture networks in the crystalline and especially granitic basement, as shown in previous studies (Bertrand et al., 2015; Bossennec et al., 2021; Chabani et al., 2021). Deviations of the lineament and fracture data from this law can be explained by censoring and truncation effects. While not all small-sized fractures can be identified due to the limited resolution of the lidar point clouds, the full lengths of long fractures are often truncated at the edges of the visible outcrop walls. To obtain the best power-law fit, shorter cutoff lengths of 70 cm for the outcrop fractures and 500 m for the lineaments were therefore selected.

The IXY topology was examined to quantify the connectivity of the encountered fracture networks; this is expressed as the average number of connections per line, c_{L}. An interpretation was made for the fractures at the outcrop scale and the lineaments at the regional scale (Fig. 6b). All datasets appear in the lower-left corner of the IXY diagram, showing a dominance of Y-nodes. The proportions of I- and X-nodes range from 5 % to 15 %, respectively. This node topology results in a c_{L} of ca. 3 to 5, indicating generally high connectivity of the fractures. A correlation between fracture intensity and connectivity can also be seen. The lowest c_{L} (2.96) was determined for the Borstein outcrop, where P21 is also the smallest (2.43). In Hammelbach and in the Weschnitz Valley, the highest P21 (ca. $9–11\,\mathrm{m\,m^{-2}}$) and c_{L} (ca. 4) values were found. Another striking feature is the high connectivity of the mapped faults; they exhibit almost no isolated ends, which might result from a bias of the mapping geologist.

4.1.4 Results of DFN modeling

DFN models were created for the two outcrops in Borstein and Weschnitz Valley, which represent the end members of

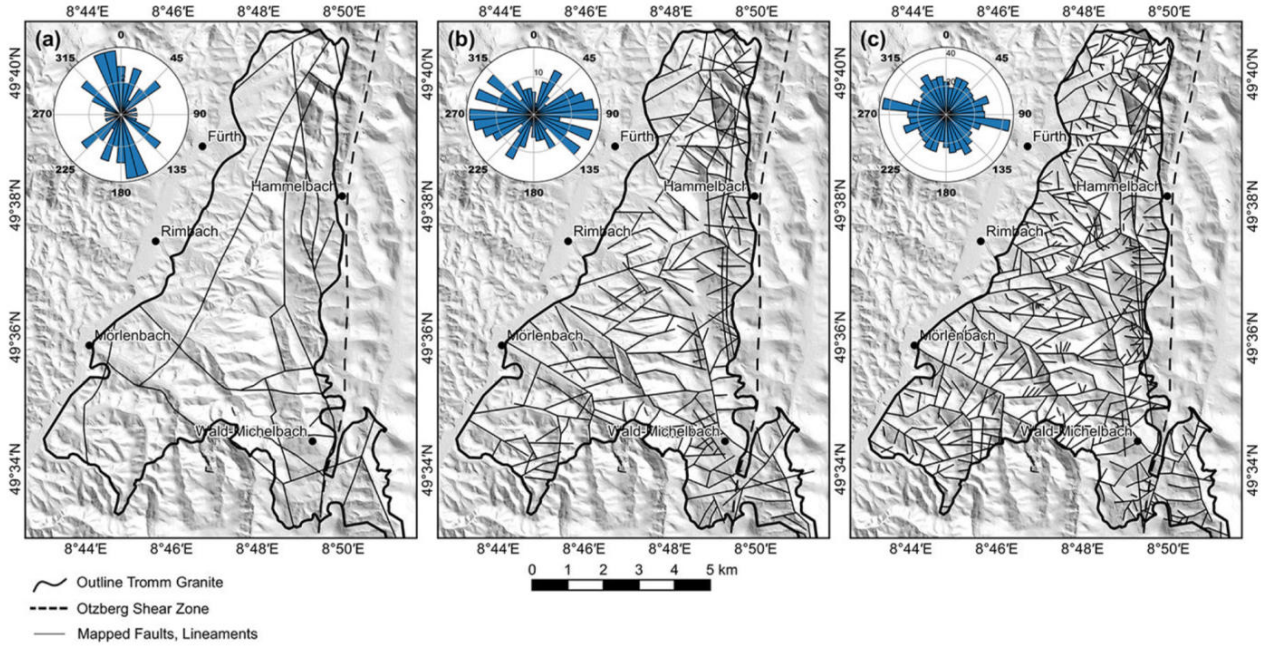

Figure 4. Summary of the lineament analysis in the Tromm Granite area: **(a)** compilation of mapped faults from various geological maps (modified after Klemm, 1900, 1928, 1929, 1933; HLUG, 2007); **(b)** regional analysis using SRTM data with 1 arcsec resolution (van Zyl, 2001); **(c)** local analysis using the 1 m DEM provided by the HVBG.

Table 1. Summary of fracture network properties for all outcrops analyzed in the Tromm Granite area.

Object	Area [m^2]	No. fractures	Min. length [m]	Max. length [m]	Char. length [m]	P10 [frac. m^{-1}]	P10 > 70 cm [frac. m^{-1}]	P20 [frac. m^{-2}]	P21] [frac. m^{-2}]	c_L
Faults and lineaments										
Fault compilation	62.7×10^6	30	195	9369	2899	–	–	4.79×10^{-7}	0.0014	–
SRTM (1 arcsec)	62.7×10^6	177	238	4624	1187	–	–	2.84×10^{-6}	0.0034	–
DEM 1 m	62.7×10^6	471	74	9001	680	–	–	7.53×10^{-6}	0.0051	–
Outcrops										
Borstein	475	903	0.1	11.22	1.28	1.62	1.31	1.9	2.43	2.96
Hammelbach	67	1351	0.03	3.91	0.54	6.95	2.27	20.16	10.82	3.94
Streitsdölle	288	521	0.06	12.96	1.57	1.9	1.61	1.81	2.83	3.44
Weschnitz Valley	119	1332	0.03	7.57	0.81	7.05	4.25	11.19	9.07	4.09
OMB total	1050	5778	0.02	10.28	0.83	2.66	1.69	5.5	4.54	3.23
OMB Profile A	200	767	0.05	7.27	0.98	2.73	1.84	3.84	3.78	3.02
OMB Profile B	300	1647	0.06	6.24	0.89	3.17	2.07	5.49	4.89	3.11
OMB Profile C	250	2383	0.02	7.74	0.62	3.42	1.65	9.53	5.87	3.3
OMB Profile D	300	981	0.06	10.28	1.1	2.34	1.59	3.27	3.6	3.43

OMB = Ober-Mengelbach.

the Tromm Granite in terms of fracture density (Fig. 7). The estimated EPM permeabilities in the x (E–W), y (N–S) and z directions are summarized in Fig. 8. The fracture mean aperture has the largest influence on the permeability, as these two parameters are related via a cubic law. Practically speaking, this means that increasing the aperture by 1 order of magnitude leads to an increase in the permeability of 3 orders of magnitude. The proportion of open fractures, in contrast, is linearly related to the permeability, i.e., a 10-fold increase also increases permeability by a factor of 10. Furthermore, the orientation of the fracture sets has a significant effect on the permeability of the basement. At Borstein, the permeability in the main direction of the fractures (k_{yy}) is almost 1 order of magnitude higher than the permeability perpen-

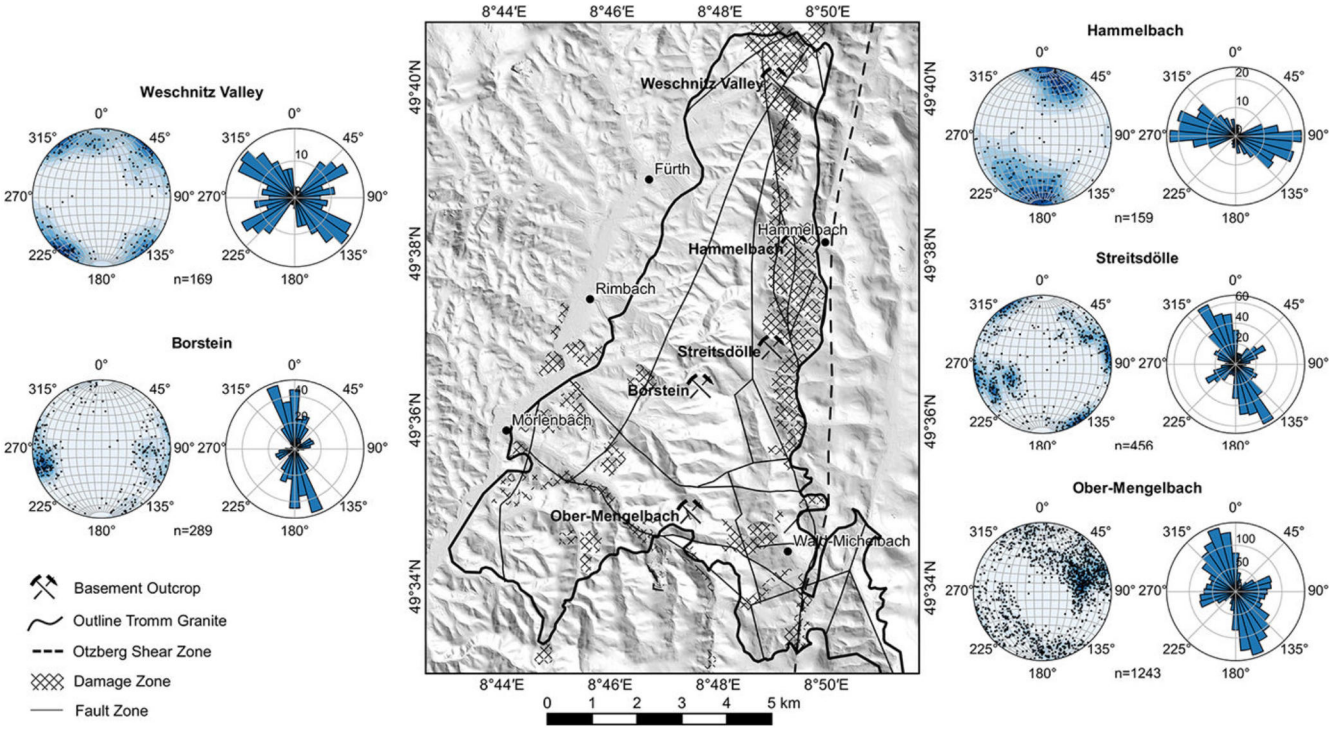

Figure 5. Summary of the outcrop analysis in the Tromm Granite area (faults and outline of the Tromm Granite from Klemm, 1900, 1928, 1929, 1933 and HLUG, 2007).

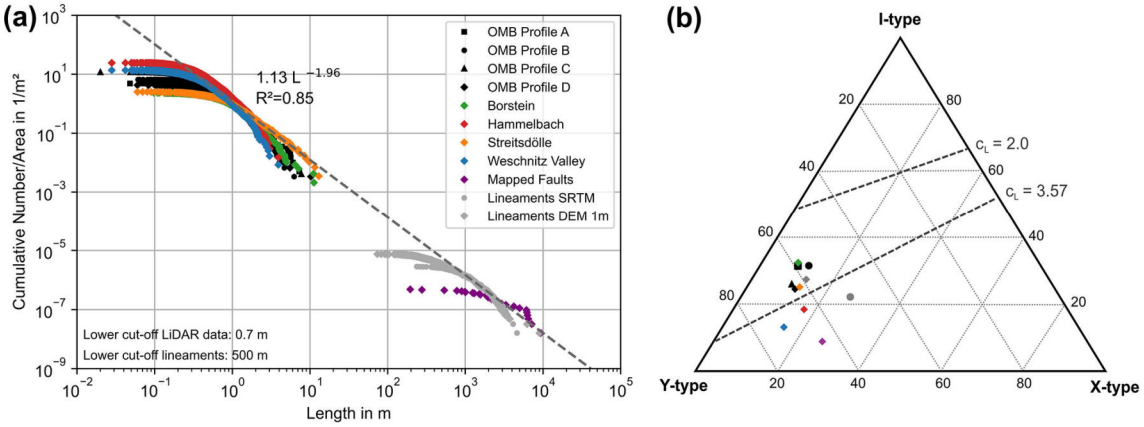

Figure 6. **(a)** Area-normalized trace length cumulative-frequency plot; **(b)** triangular plot of the proportions of I-, X- and Y-nodes of the analyzed outcrops.

dicular to it (k_{xx}). Finally, the difference between Borstein and Weschnitz Valley again reaches 1 order of magnitude, depending on the direction, for the same aperture and proportion of open fractures. This variability is mainly due to the approximately 4 times higher fracture density in the second outcrop (Fig. 8).

To test the transferability of the results to crystalline reservoirs in the URG, a comparison with hydrogeological data, e.g., from Soultz-sous-Forêts, is useful. Here, the mean permeabilities of the fractured granitic basement range from 1×10^{-16} to 1×10^{-14} m^2 at a reservoir depth of 3 to 5 km (Vogt et al., 2012; Baujard et al., 2017; Egert et al., 2020). Accordingly, realistic permeabilities result for (1) a mean aperture of 10 µm and (2) for 50 µm when 1 % to 10 % of the fractures are open. For 100 µm, the calculated permeabilities are too high in all cases and would represent permeabilities of single large-scale fractures or faults instead, while the smaller-scale fractures would have smaller fracture apertures.

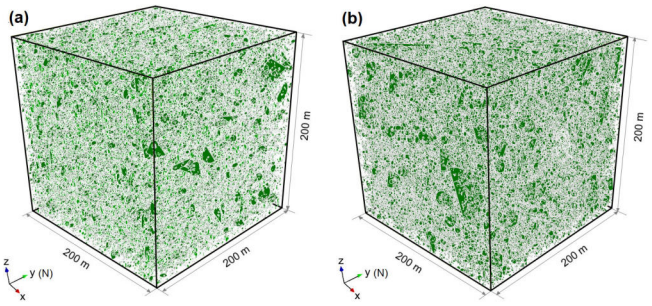

Figure 7. Illustration of DFN models with 1 % open fractures for **(a)** the Borstein quarry ($n = 214\,287$) and **(b)** the Weschnitz Valley quarry ($n = 279\,787$).

		Borstein			Weschnitz Valley		
		mean aperture			mean aperture		
	m²	10 µm	50 µm	100 µm	10 µm	50 µm	100 µm
100 % open	k_{xx}	5.0E-16	6.3E-14	5.0E-13	3.8E-15	5.1E-13	4.1E-12
	k_{yy}	2.1E-15	2.5E-13	1.9E-12	1.7E-15	2.2E-13	1.7E-12
	k_{zz}	2.2E-15	2.6E-13	2.0E-12	4.5E-15	6.0E-13	4.7E-12
10 % open	k_{xx}	4.8E-17	6.2E-15	4.9E-14	4.0E-16	5.6E-14	3.4E-13
	k_{yy}	2.0E-16	2.5E-14	1.9E-13	1.7E-16	2.3E-14	1.5E-13
	k_{zz}	2.1E-16	2.6E-14	2.0E-13	4.7E-16	6.5E-14	4.0E-13
1 % open	k_{xx}	7.6E-18	1.9E-15	1.1E-14	5.2E-17	1.2E-14	5.7E-14
	k_{yy}	2.6E-17	3.2E-15	5.1E-14	2.6E-17	5.2E-15	2.5E-14
	k_{zz}	2.7E-17	4.4E-15	5.1E-14	6.6E-17	1.4E-14	6.7E-14

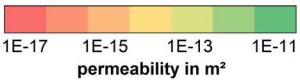

Figure 8. Summary of the DFN modeling. The Oda permeabilities in the x, y and z directions were calculated as a function of the fracture density, orientation, aperture and proportion of open fractures.

It should be noted that the hydraulic properties of fractured reservoirs are subject to strong spatial variations. For example, permeability can be increased by several orders of magnitudes close to active faults. In contrast, at larger distances from these faults or large-scale fractures, the mean permeability of the basement is of the order of 1×10^{-18} to $1 \times 10^{-17}\,\mathrm{m}^2$.

4.2 Gravity and radon anomalies

4.2.1 Bouguer anomalies

Figure 9 integrates the results of the two gravity surveys into the existing datasets (© Leibniz-Institut für Angewandte Geophysik, © Hessische Verwaltung für Bodenmanagement und Geoinformation). Within the Tromm Granite, Bouguer anomalies range from ca. −10 to −5 mGal and are uncorrelated with the topography. The gravity field in this area is dominated by a NW–SE-oriented regional trend (Fig. 9b) that was obtained by applying a low-pass filter with a cutoff wavelength of 10 km. Residual anomalies involving presumably lower depth ranges were obtained by applying high-pass filters with cutoff wavelengths decreasing from 10 to 2 km (Fig. 9c–e). The residual field exhibits distinct positive and negative anomalies. However, especially in the central part of the Tromm Granite, the lack of data points leads to considerable uncertainties.

The strongest positive anomaly of 1 to 1.5 mGal is located north of Wald-Michelbach and coincides with a major lineament. Similarly, a positive anomaly of 0.5 to 1 mGal can be observed along the presumed fault zone between Zotzenbach and Wald-Michelbach. The strongest negative anomaly, with an amplitude of ca. −0.5 to −1 mGal, extends over several kilometers from SSW to NNE at the western boundary of the Tromm Granite to the Weschnitz Granodiorite. Note that this area is covered by Quaternary sediments that are locally more than 20 m thick but generally less than 10 m thick. However, the anomaly increases and persists with increasing cutoff wavelength. Another negative anomaly of ca. −0.4 mGal is located at the eastern boundary of the pluton, southeast of the village of Tromm. Here, the granite is highly fractured due to the proximity to the Otzberg Shear Zone, which is also indicated by the high concentration of local lineaments. However, a direct correlation between Bouguer anomalies and individual faults or lineaments is usually not observed.

Besides these larger anomalies, short-wavelength variations of the gravity signal in the range of −0.3 to 0.3 mGal occur on individual profiles, which is still significantly higher than the cumulative uncertainty of the Bouguer anomaly.

4.2.2 Inversion results

Results of the stochastic gravity inversion are shown as differences from the homogeneous density of $2670 \pm 50\,\mathrm{kg\,m^{-3}}$ of the starting model in Fig. 10. The inverted mean densities range from 2520 to $2840\,\mathrm{kg\,m^{-3}}$, with a mean standard deviation of $2.5\,\mathrm{kg\,m^{-3}}$. Near the surface, the density distribution largely resembles the observed Bouguer anomalies. The most significant density decrease of ca. $100\,\mathrm{kg\,m^{-3}}$ is found at the western boundary of the Tromm Granite and may be partly related to the Quaternary cover. This difference decreases to about 50–75 $\mathrm{kg\,m^{-3}}$ below a depth of about 200 m. In addition, smaller density decreases in the range of 30 to $100\,\mathrm{kg\,m^{-3}}$ occur at the eastern boundary near the Otzberg Shear Zone. This area has been geologically mapped and attributed to the damage zone of the Otzberg Shear Zone. Assuming lithological homogeneity of the Tromm Granite, this decrease would result in a fracture porosity of ca. 2 % to 6 %. Increased densities are mainly found in the area of the granodioritic Weschnitz Pluton and along the assumed fault in Gadern, north of Wald-Michelbach. Also, very small-scale density variations are present in the south, which can be attributed to the lithological heterogeneity at the transition from Tromm Granite to the Schollenagglomerat Zone.

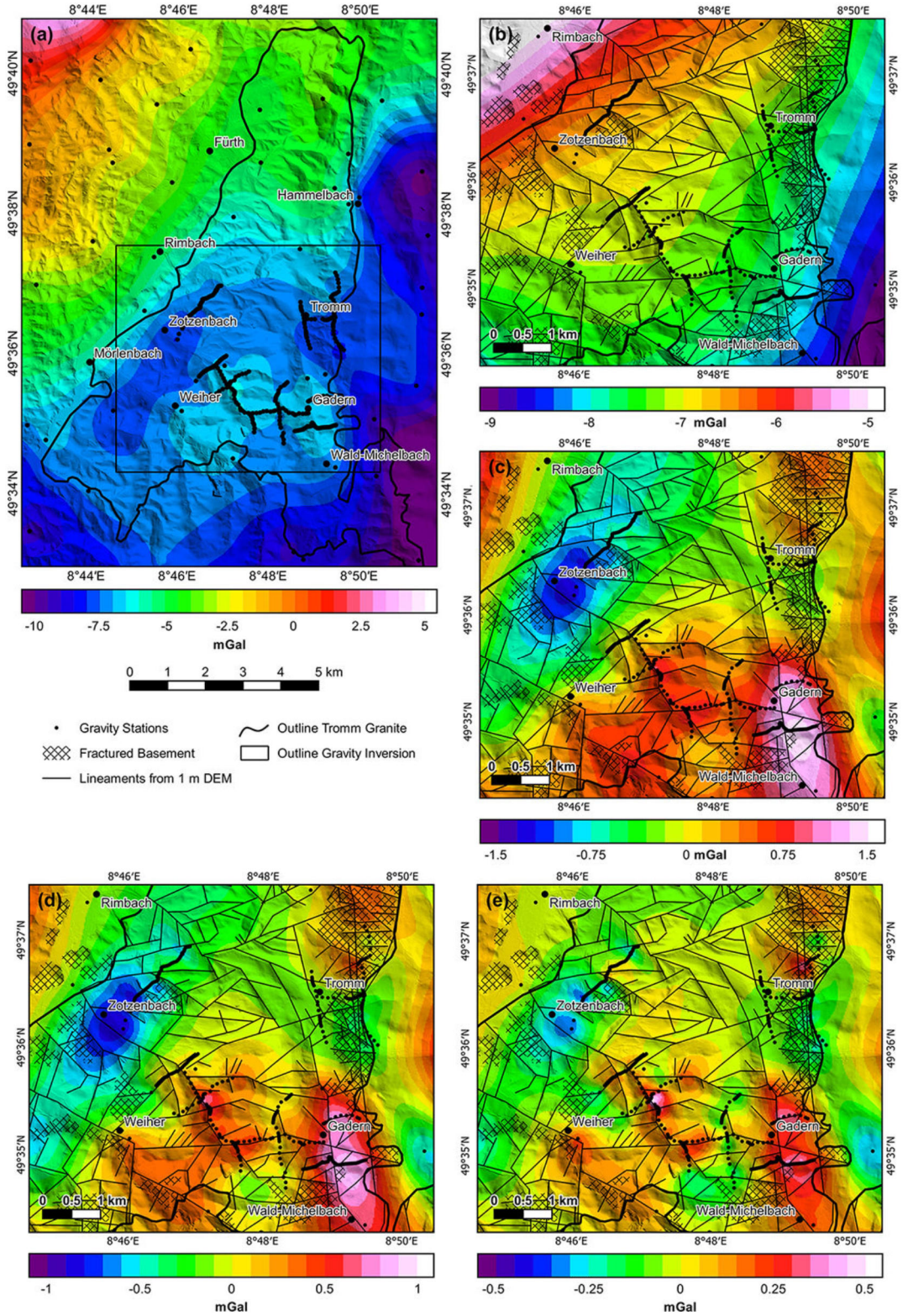

Figure 9. Results of the gravity survey: **(a)** complete Bouguer anomaly map for the Tromm Granite (© Leibniz-Institut für Angewandte Geophysik, © Hessische Verwaltung für Bodenmanagement und Geoinformation); **(b)** low-pass-filtered Bouguer anomaly with 10 km cutoff wavelength; **(c)** high-pass-filtered Bouguer anomaly with 10 km cutoff; **(d)** high-pass-filtered Bouguer anomaly with 5 km cutoff; **(e)** high-pass-filtered Bouguer anomaly with 2 km cutoff.

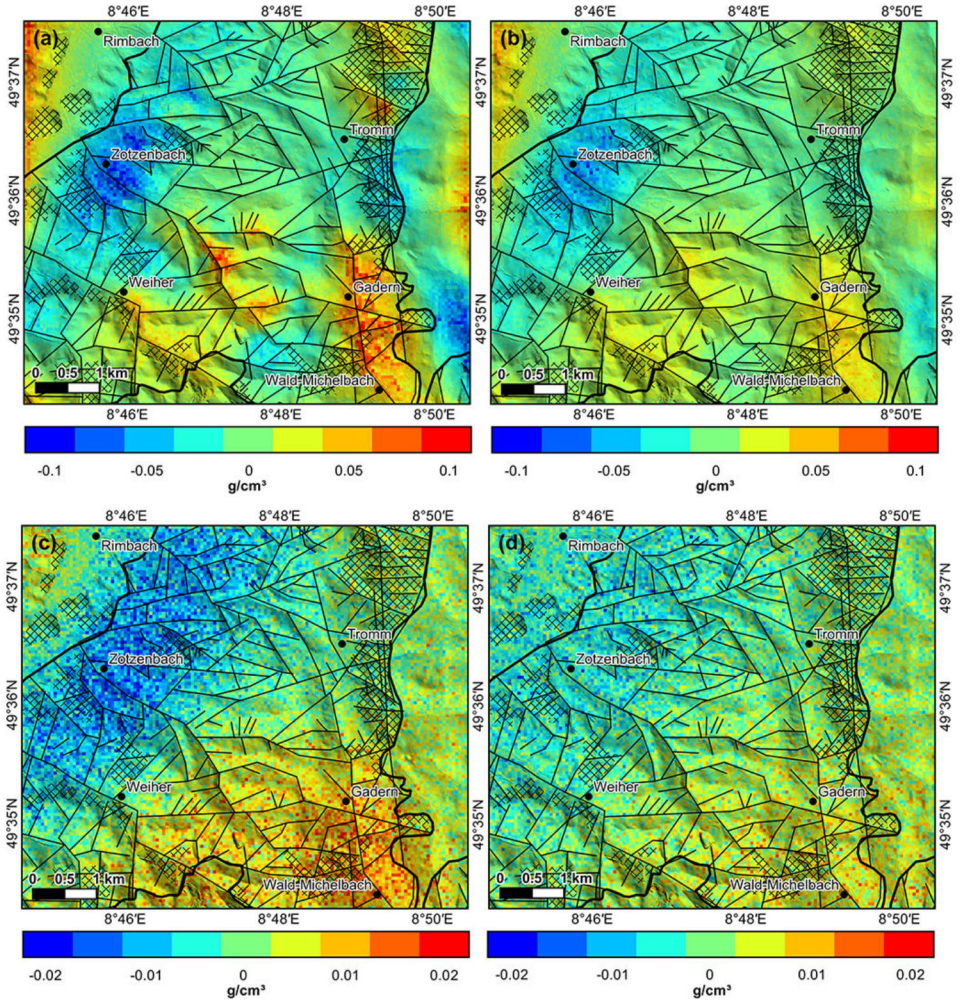

Figure 10. Results of the gravity inversion. Difference between the inverted density and the initial density of $2670 \pm 50\,\mathrm{kg\,m^{-3}}$ at **(a)** the top of the basement, **(b)** 0 m a.s.l., **(c)** 1000 m b.s.l. and **(d)** 2000 m b.s.l. Note the different color scales for **(a)** and **(b)** vs. **(c)** and **(d)**.

At greater depths, the inverted density model becomes more diffuse and the density variations are generally smaller. At 0 m a.s.l., the negative anomaly in the west and the positive anomaly in Gadern can still be clearly recognized. In contrast, the density reduction at the eastern edge is very weak. At 1000 m b.s.l., the variations have a very long wavelength and range between only -30 and $30\,\mathrm{kg\,m^{-3}}$. At the model base at 2000 m b.s.l., the density is almost homogeneously distributed.

4.2.3 Comparison of gravity and radon measurements

A comparison of the radon activity concentration in soil air with the corresponding Bouguer anomalies is shown in Fig. 11 (see Fig. 2 for the locations of the stations). A background activity of ca. $25\,\mathrm{kBeq\,m^{-3}}$ was determined. Furthermore, the repeated base measurements revealed a standard deviation of $5\,\mathrm{kBeq\,m^{-3}}$. Near the two assumed fault zones, a significant increase in the activity concentration can be observed, with two pronounced peaks of 5 to 7 times the background value. The highest radon activity was measured in the zone between the two presumed faults (center of Fig. 11), which coincides with a local negative Bouguer anomaly of ca. -0.1 mGal, indicating an increase in fracture intensity and open porosity. The second peak is located close to the northeastern fault zone, but here, as with the southwestern fault, a positive Bouguer anomaly is present. Thus, there is only a partial correlation between the two datasets.

5 Discussion

5.1 Fracture network characteristics

Based on the extensive structural geological investigations at the five outcrops and the lineament analysis, a more comprehensive description of the fracture network in the Tromm Granite has been obtained. Scale independence of the frac-

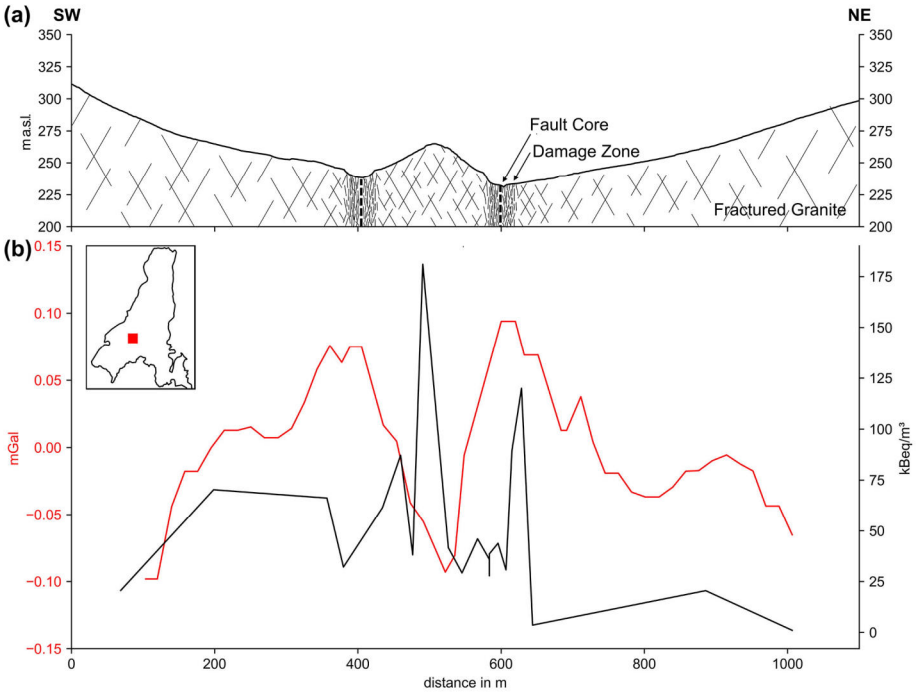

Figure 11. **(a)** Schematic cross-section of the investigated profile; **(b)** comparison of the high-pass-filtered Bouguer anomalies (red line) and the measured radon concentration in the soil air (black line). The small map shows the location of the profile within the Tromm Granite (see also Fig. 2).

ture length distribution was demonstrated with a power-law exponent of ca. −2. The length distribution is thus similar to those in other granitoid bodies in the URG region and other regions worldwide (Bertrand et al., 2015; Chabani et al., 2021).

Like the fracture length, the connectivity of the fracture network seems to be independent of scale or location. All outcrops and lineament maps indicate a dominance of Y-nodes, which is in clear contrast to the northern Odenwald, where I- and X-nodes represent the largest share (Bossennec et al., 2021). This can be attributed to different regional tectonic conditions during the intrusion, cooling and exhumation, or to overprinting under variable stress conditions.

Compared to fracture length and connectivity, the orientation of the fracture sets shows some scale-dependent and spatial variations. In the outcrops Ober-Mengelbach, Borstein and Streitsdölle, the fracture orientations are controlled by the main fault direction of $160 \pm 20°$ in the Tromm Granite. In contrast, the fracture sets of the two outcrops of Hammelbach and Weschnitz Valley are more influenced by local fault zones, as indicated by the lineament analysis (Fig. 4). Furthermore, the N–S trend of the mapped faults is difficult to find in the two lineament maps. Instead, elements perpendicular to it, i.e., oriented E–W, are dominant here.

Similar to the fracture orientation, the fracture density is subject to considerable lateral changes, which can be attributed to the influence of large-scale tectonic structures, especially at the pluton margins. In the eastern part of the Tromm Granite, the basement is deformed by the nearby Otzerg Shear Zone. As a result, there is an evident accumulation of lineaments, and the outcrops show by far the highest fracture density. Medium fracture densities were found in Ober-Mengelbach, in the southern part of the pluton, i.e., at the border with the Schollenagglomerat. Although this area lacks pronounced long fault zones, the lithological heterogeneities led to more intense granite deformation than in the central Tromm Granite. Accordingly, the lowest fracture density was found in the Borstein and Streitsdölle outcrops.

In summary, the Tromm Granite is likely not characterized by a complete fractal fracture network, which is consistent with, e.g., studies from the western rift shoulder (Bertrand et al., 2018). Although fracture length and connectivity seem to be independent of scale and location, orientation and fracture density show variations with location. This fact must be considered when evaluating and modeling the basement, as varying the fracture orientation and density can increase or decrease permeability by up to 1 order of magnitude depending on the assumed mean apertures (Fig. 8).

5.2 Interpretation of gravity and radon anomalies

The measured gravity anomalies provide insights into the subsurface density distribution of the Tromm Granite (Figs. 9 and 10). Negative anomalies of up to 1 mGal are concentrated at the western and eastern boundaries of the pluton, where the basement is strongly deformed and fractured. Comparable re-

sults in the Argentera Massif (NW Italy) were linked to a fracture porosity of a few percent (Guglielmetti et al., 2013). However, a layer of low-density Quaternary sediments several tens of meters thick or a thick basement weathering horizon could also lead to negative gravity anomalies. Borehole data from the HLNUG suggest that Quaternary sediment thicknesses typically do not exceed 10 to 15 m, accounting for a maximum of −0.2 mGal of the signal. Nevertheless, it is known that the weathering zone in the granite is locally 20 to 40 m thick, which could account for a gravity anomaly of up to −0.5 mGal.

In general, individual faults can rarely be accurately traced with the gravity data acquired for the Tromm Granite, as the influence of fracture porosity on bulk density is too small. Instead, areas can be identified where a high density of faults and fractures leads to increased porosity and thus to a significant density reduction. Accordingly, the Tromm Granite is potentially structurally weakened at the contact with the Weschnitz Pluton in the western part of the study area. Unfortunately, there are neither larger outcrops nor available well data, leaving this assumption speculative. The slightly smaller negative anomaly at the eastern boundary with the Buntsandstein can be explained by the proximity to the Otzberg Shear Zone. Here, the pluton is presumably characterized by similar structural properties to those in the Hammelbach and Weschnitztal outcrops, which means that the fracture density and thus the porosity are increased. Interestingly, the anomaly does not extend over the entire damage zone at the eastern margin of the Tromm Granite, but is concentrated in a limited area with a high density of intersecting lineaments. A possible explanation is that the fractures are partially mineralized with, e.g., barite (e.g., Tranter et al., 2021), resulting in increased bulk density.

Positive gravity anomalies of up to 1.5 mGal can be observed at the southern Tromm Granite along two fault zones. In Gadern, several lamphropyric intrusions were mapped and, as in the quarry of Ober-Mengelbach, localized amphibolitic zones are present. These mafic rocks have a considerably higher density (2700–3100 kg m^{-3}) than the Tromm Granite, which explains the gravity high. Due to the lithological heterogeneity in the southern Tromm Granite, quantification of the fracture porosity using the gravity data is difficult here.

Radon measurements were carried out along just one profile due to the high time consumption of this method. Accordingly, a regional interpretation of the results is only possible to a limited extent. Nevertheless, the determined radon anomalies give helpful indications about the architecture of the analyzed fault zones. Two distinct radon peaks indicate localized permeable fracture zones in the granite. The highest activity correlates with a negative Bouguer anomaly, which further supports this assumption. Interestingly, the peaks are not located directly above the assumed positions of the faults, but in the damage zone a few meters to tens of meters to the sides, suggesting low permeability in the fault core (Caine et al., 1996). A comparison of gravity, radon and structural data illustrates the complex architecture of fault zones in the crystalline basement (Faulkner et al., 2010; Bossennec et al., 2021, 2022), consisting of several adjacent permeable and impermeable zones, which may also be influenced by clay mineralization. By combining gravity and radon measurements, it is thus possible to on the one hand study the dimensions of the fracture network, and on the other hand to evaluate its behavior (sealed or open).

5.3 Implication for deep geothermal exploration and GeoLaB

The Tromm Granite represents a suitable site for the planned geothermal underground research laboratory (GeoLaB), as the main criteria proposed by Schill et al. (2016) are met. Firstly, except for the southern part, the pluton exhibits low geological complexity, with a rather homogeneous crystalline matrix. The high fracture density of 1.62 to 6.95 m^{-1} and good connectivity ensures sufficient hydraulic fracture permeability for the experiments. As required, the Tromm Granite is located in a normal faulting to strike-slip regime. In addition, the primarily NNW–SSE-oriented fractures have a high reactivation potential in the ambient stress system. There is no extensive drainage in the area due to historical mining activities in adits, resulting in controllable hydraulic boundary conditions. Finally, the topography in the central part of the Tromm Granite can be described as plateau-like, allowing an overburden above the tunnel ranging between 300 and 400 m, which assures undisturbed stress conditions. The interdisciplinary dataset described herein will serve as an important basis for the planning of further exploration activities in the area as well as the final site selection.

Furthermore, the Tromm Granite is a well-suited outcrop analogue for the crystalline basement in the URG. The granitic body has a similar mineralogical composition to the reservoir rocks, e.g., in Soultz-sous-Forêts or Rittershoffen (Traineau et al., 1991; Dezayes et al., 2005a; Vidal et al., 2018). Granitoids are dominant in the northern URG, as inferred from the joint inversion of gravity and magnetic data (Baillieux et al., 2013; Frey et al., 2021b). Moreover, the Tromm Granite was intruded in the same tectonic setting and overprinted under comparable conditions to the granites of the URG. Nevertheless, a direct transfer to deep geothermal reservoirs, where in situ hydrothermal alteration and mineralization as well as complex geomechanical processes occur, is challenging considering that weathering and exhumation significantly affect the near-surface fracture network. Unfortunately, no major fault zone is exposed in the study area, making it virtually impossible to evaluate the true nature of the mineralization and fluid circulation patterns. The applied gravity and radon surveys help to overcome this lack of outcrops and provide insights into the basement's permeability structure.

A DFN parameter study was carried out to estimate the hydraulic properties of the Tromm Granite under assumed reservoir conditions (Fig. 8). The calculated permeabilities show a range of several orders of magnitude, indicating the uncertainties of this approach. Direct transfer of the hydrogeological properties to the reservoirs is therefore only possible to a limited extent, but the effects of individual parameters can be followed well. The fracture aperture primarily determines the permeability of the basement, which is in agreement with detailed sensitivity studies, e.g., performed by Niven and Deutsch (2009) or Mahmoodpour et al. (2022). The degree of mineralization (here considered the proportion of open fractures), the fracture density and the fracture orientation also influence the Oda permeability but have smaller effects. DFN modeling suggests that only a small proportion of the total fracture network is contributing to the flow. With an average aperture of 10 to 50 µm, probably only 1 % to 10 % of the fractures allow fluid flow, which fits well with observations from Soultz-sous-Forets (Sausse et al., 2010; Egert et al., 2020). It should also be noted that k_{xx} and k_{yy} show a difference of up to 1 order of magnitude (e.g., Mahmoodpour et al., 2021), which is particularly relevant when planning the well path trajectories of geothermal doublets and the experiments in GeoLaB. Accordingly, a geothermal doublet oriented approximately in a direction such that the open-hole sections intersect a high number of N–S-oriented fractures probably yields the highest production rates, which is consistent with observations from, e.g., Rittershoffen.

Minimizing induced seismicity during stimulation and operation represents a major challenge for deep geothermal exploitation of the crystalline basement (Zhang et al., 2013; Meller and Ledésert, 2017; Rathnaweera et al., 2020) and will be addressed experimentally in GeoLaB. Stimulation is generally more feasible in reservoirs with naturally elevated permeability, because lower injection pressures are required. The highest permeability is expected near large-scale fault zones with well-developed damage zones and hydrothermal overprinting. However, the structural geological investigations in the Tromm Granite show that, in certain areas, sufficient permeability may also occur in the outer damage zones of large faults, i.e., at distances of several hundred meters to kilometers from the fault core.

Apart from hydrogeological properties, the temperature of the reservoir is an important parameter for any geothermal prospection. The thermal field in the URG has been extensively studied in the past (e.g., Pribnow and Schellschmidt, 2000; Bächler et al., 2003; Baillieux et al., 2013). Accordingly, temperature anomalies are mainly linked to hydrothermal convection zones, which cannot be localized very precisely using classical exploration methods as yet. Bär et al. (2021) therefore propose an integrated approach that combines 3D seismic, electromagnetic and gravity data with geothermal gradients from medium-depth boreholes, enabling more accurate mapping of ascending hot brines.

In addition to deep EGS projects, underground heat storage will significantly contribute to reducing emissions in the future energy supply. Thereby, the seasonal fluctuations of other renewable energy sources such as solar and wind energy can be compensated for. It is expected that medium-depth borehole heat exchangers (MD-BHE) in the crystalline basement have the highest efficiency among comparable technologies and can be applied almost anywhere that the basement is situated near the surface (Welsch et al., 2016). Again, a detailed characterization of the fracture network is essential since open fractures can act as potential fluid conduits that reduce the heat recoverability. In this respect, the presented data can serve as input for thermal–hydraulic–mechanical simulations of MD-BHE to be built in the extended URG region.

6 Conclusions

The fracture network characterization of the Tromm Granite has led us to the following conclusions:

- Combining outcrop and lineament analysis allows for a more comprehensive description of the main fracture network characteristics.

- While fracture length distribution and connectivity are mostly scale independent, fracture orientation and density vary significantly across the Tromm Granite. The latter two parameters are heavily affected by the crustal-scale Otzberg Shear Zone.

- Hydraulic properties of the fractured basement under reservoir conditions can be estimated with DFN models and validated by hydraulic test data from deep boreholes. However, the calculated permeabilities are associated with large uncertainties, as the stress conditions and therefore the fracture aperture are highly unconstrained.

- Gravity and radon measurements enable more advanced mapping of potentially permeable zones. The fracture porosity can be inferred from the inverted density model, where homogeneous subsurface conditions are present. Lithological variations and mineralization prevent exact porosity quantification.

- Structural investigations and gravity anomalies show that the most suitable hydraulic properties are expected at the margin of the granitic pluton, where regional-scale fault zones influence the fracture network. Moreover, during the cooling of a granitic pluton, the margins were more affected by the circulation of residual fluids and are therefore more altered than the center, allowing the creation of preferential hydraulic pathways.

– The Tromm granite is a suitable site for GeoLaB, as the composition is generally homogeneous and representative of the reservoirs of the URG, high fracture density and connectivity were observed, the stress conditions and fracture orientation are favorable for reactivation, the hydraulic boundary conditions are controllable, and a sufficient overburden is ensured.

Data availability. The presented research data can be found at https://doi.org/10.48328/tudatalib-632 (Frey et al., 2021a).

Author contributions. The conceptualization of the study and the choice of methodology were made by MF, CB, and ES. The field investigations were conducted by MF, CB, and LS. Data preparation, formal analysis, and validation visualization were performed by MF. Acquisition of funding and project management were in the hands of KB and IS. The work was supervised by KB and IS. Resources were provided by IS and ES. MF wrote the original draft. All co-authors reviewed and edited the manuscript and approved the final version.

Competing interests. The contact author has declared that neither they nor their co-authors have any competing interests.

Disclaimer. Publisher's note: Copernicus Publications remains neutral with regard to jurisdictional claims in published maps and institutional affiliations.

Acknowledgements. First of all, we would like to thank Cäcilia Boller for conducting one part of the gravity measurements. We are grateful that the HLNUG, LIAG and HVGB provided the borehole, gravity and digital elevation data. We thank Sebastian Schröder and the municipalities of Wald-Michelbach and Rimbach for giving us access to the quarries in the Tromm Granite.

Financial support. The research was funded by the Interreg NWE program (grant no. NWE892) through the Roll-out of Deep Geothermal Energy in North-West Europe (DGE-ROLLOUT) project https://www.nweurope.eu/DGE-Rollout, last access: 23 May 2022). The Interreg NWE program is part of the European Cohesion Policy and is financed by the European Regional Development Fund (ERDF). We were supported by the Deutsche Forschungsgemeinschaft (DFG – German Research Foundation) and the Open Access Publishing Fund of the Technical University of Darmstadt.

Review statement. This paper was edited by Virginia Toy and reviewed by two anonymous referees.

References

Afshari, M., Valley, B., and Evans, K.: Scaling of Fracture Patterns in Three Deep Boreholes and Implications for Constraining Fractal Discrete Fracture Network Models, Rock Mech. Rock Eng., 52, 1723–1743, https://doi.org/10.1007/s00603-019-1739-7, 2019.

Agemar, T., Alten, J.-A., Ganz, B., Kuder, J., Kühne, K., Schumacher, S., and Schulz, R.: The Geothermal Information System for Germany – GeotIS, Z. Dtsch. Ges. Geowiss., 165, 129–144, https://doi.org/10.1127/1860-1804/2014/0060, 2014.

Altenberger, U. and Besch, T.: The Böllstein Odenwald: evidence for pre- to early Variscan plate convergence in the Central European variscides, Int. J. Earth Sci., 82, 475–488, https://doi.org/10.1007/BF00212411, 1993.

Altherr, R., Henes-Klaiber, U., Hegner, E., Satir, M., and Langer, C.: Plutonism in the Variscan Odenwald (Germany): from subduction to collision, Int. J. Earth Sci., 88, 422–443, https://doi.org/10.1007/s005310050276, 1999.

Altwegg, P., Schill, E., Abdelfettah, Y., Radogna, P. V., and Mauri, G.: Toward fracture porosity assessment by gravity forward modeling for geothermal exploration (Sankt Gallen, Switzerland), Geothermics, 57, 26–38, https://doi.org/10.1016/j.geothermics.2015.05.006, 2015.

Amstutz, G. C., Meisl, S., and Nickel, E. (Eds.): Mineralien und Gesteine im Odenwald, Heidelberg, VFMG, https://hdl.handle.net/10013/epic.42772 (last access: 23 May 2022), 1975.

Bächler, D., Kohl, T., and Rybach, L.: Impact of graben-parallel faults on hydrothermal convection – Rhine Graben case study, Phys. Chem. Earth, 28, 431–441, https://doi.org/10.1016/S1474-7065(03)00063-9, 2003.

Baillieux, P., Schill, E., Edel, J. B., and Mauri, G.: Localization of temperature anomalies in the Upper Rhine Graben: insights from geophysics and neotectonic activity, Int. Geol. Rev., 55, 1744–1762, https://doi.org/10.1080/00206814.2013.794914, 2013.

Bär, K., Reinecker, J., Bott, J., Cacace, M., Frey, M., van der Vaart, J., Scheck-Wenderoth, M., Ritter, O., Homuth, B., Fritsche, J.-G., Spath, F., and Sass, I.: Integrated Exploration Strategy "ConvEx" to detect Hydrothermal Convection in the Subsurface, in: Proceedings of the World Geothermal Congress 2020+1, WGC, https://www.geothermal-energy.org/cpdb/record_detail.php?id=32926 (last access: 23 May 2022), 2021.

Baskaran, M. (Ed.): Radon: A Tracer for Geological, Geophysical and Geochemical Studies, Springer International Publishing, https://doi.org/10.1007/978-3-319-21329-3, 2016.

Baujard, C., Genter, A., Dalmais, E., Maurer, V., Hehn, R., Rosillette, R., Vidal, J., and Schmittbuhl, J.: Hydrothermal characterization of wells GRT-1 and GRT-2 in Rittershoffen, France: Implications on the understanding of natural flow systems in the rhine graben, Geothermics, 65, 255–268, https://doi.org/10.1016/j.geothermics.2016.11.001, 2017.

Bertrand, L., Géraud, Y., Le Garzic, E., Place, J., Diraison, M., Walter, B., and Haffen, S.: A multiscale analysis of a fracture pattern in granite: A case study of the Tamariu granite, Catalunya, Spain, J. Struct. Geol., 78, 52–66, https://doi.org/10.1016/j.jsg.2015.05.013, 2015.

Bertrand, L., Jusseaume, J., Géraud, Y., Diraison, M., Damy, P.-C., Navelot, V., and Haffen, S.: Structural heritage, reactivation and distribution of fault and fracture network in

a rifting context: Case study of the western shoulder of the Upper Rhine Graben, J. Struct. Geol., 108, 243–255, https://doi.org/10.1016/j.jsg.2017.09.006, 2018.

Biber, K., Khan, S. D., Seers, T. D., Sarmiento, S., and Lakshmikantha, M. R.: Quantitative characterization of a naturally fractured reservoir analog using a hybrid lidar-gigapixel imaging approach, Geosphere, 14, 710–730, https://doi.org/10.1130/GES01449.1, 2018.

Bisdom, K., Nick, H. M., and Bertotti, G.: An integrated workflow for stress and flow modelling using outcrop-derived discrete fracture networks, Comput. Geosci., 103, 21–35, https://doi.org/10.1016/j.cageo.2017.02.019, 2017.

Bossennec, C., Frey, M., Seib, L., Bär, K., and Sass, I.: Multiscale Characterisation of Fracture Patterns of a Crystalline Reservoir Analogue, Geosciences, 11, 371, https://doi.org/10.3390/geosciences11090371, 2021.

Bossennec, C., Seib, L., Frey, M., van der Vaart, J., and Sass, I.: Structural Architecture and Permeability Patterns of Crystalline Reservoir Rocks in the Northern Upper Rhine Graben: Insights from Surface Analogues of the Odenwald, Energies, 15, 1310, https://doi.org/10.3390/en15041310, 2022.

Caine, J. S., Evans, J. P., and Forster, C. B.: Fault zone architecture and permeability structure, Geology, 24, 1025, https://doi.org/10.1130/0091-7613(1996)024<1025:FZAAPS>2.3.CO;2, 1996.

Chabani, A., Trullenque, G., L., B. A., and Klee, J.: Multiscale Characterization of Fracture Patterns: A Case Study of the Noble Hills Range (Death Valley, CA, USA), Application to Geothermal Reservoirs, Geosciences, 11, 280, https://doi.org/10.3390/geosciences11070280, 2021.

Cuenot, N., Faucher, J.-P., Fritsch, D., Genter, A., and Szablinski, D.: The European EGS project at Soultz-sous-Forêts: From extensive exploration to power production, in: Conversion and delivery of electrical energy in the 21st century, 1–8, IEEE, Pittsburgh, Pa., https://doi.org/10.1109/PES.2008.4596680, 2008.

Deckert, H., Bauer, W., Abe, S., Horowitz, F., and Schneider, U.: Geophysical greenfield exploration in the permocarboniferous Saar–Nahe basin – The Wiesbaden Geothermal Project, Germany, Geophys. Prospect., 66, 144–160, https://doi.org/10.1111/1365-2478.12598, 2017.

Dezayes, C., Chevremont, P., Tourlière, B., Homeier, G., and Genter, A.: Geological study of the GPK4 HFR borehole and correlation with the GPK3 borehole (Soultz-sous-Forêts, France), 2005a.

Dezayes, C., Gentier, S., and Genter, A.: Deep Geothermal Energy in Western Europe: The Soultz-Project: Final Report: BRGM/RP-54227-FR, BRGM, http://infoterre.brgm.fr/rapports/RP-54227-FR.pdf (last access: 23 May 2022), 2005b.

Dezayes, C., Genter, A., and Valley, B.: Structure of the low permeable naturally fractured geothermal reservoir at Soultz, C.R. Geosci., 342, 517–530, https://doi.org/10.1016/j.crte.2009.10.002, 2010.

Dezayes, C., Lerouge, C., Innocent, C., and Lach, P.: Structural control on fluid circulation in a graben system: Constraints from the Saint Pierre Bois quarry (Vosges, France), J. Struct. Geol., 146, 104323, https://doi.org/10.1016/j.jsg.2021.104323, 2021.

Drews, T., Miernik, G., Anders, K., Höfle, B., Profe, J., Emmerich, A., and Bechstädt, T.: Validation of fracture data recognition in rock masses by automated plane detection in 3D point clouds, Int. J. Rock Mech. Min., 109, 19–31, https://doi.org/10.1016/j.ijrmms.2018.06.023, 2018.

Duwiquet, H., Guillou-Frottier, L., Arbaret, L., Bellanger, M., Guillon, T., and Heap, M. J.: Crustal Fault Zones (CFZ) as Geothermal Power Systems: A Preliminary 3D THM Model Constrained by a Multidisciplinary Approach, Geofluids, 2021, 1–24, https://doi.org/10.1155/2021/8855632, 2021.

Egert, R., Korzani, M. G., Held, S., and Kohl, T.: Implications on large-scale flow of the fractured EGS reservoir Soultz inferred from hydraulic data and tracer experiments, Geothermics, 84, 101749, https://doi.org/10.1016/j.geothermics.2019.101749, 2020.

Evans, K. F., Genter, A., and Sausse, J.: Permeability creation and damage due to massive fluid injections into granite at 3.5 km at Soultz: 1. Borehole observations, J. Geophys. Res.-Sol. Ea., 110, B04203, https://doi.org/10.1029/2004JB003168, 2005.

Faulkner, D. R., Jackson, C., Lunn, R. J., Schlische, R. W., Shipton, Z. K., Wibberley, C., and Withjack, M. O.: A review of recent developments concerning the structure, mechanics and fluid flow properties of fault zones, J. Struct. Geol., 32, 1557–1575, https://doi.org/10.1016/j.jsg.2010.06.009, 2010.

Fisher, J. E., Shakoor, A., and Watts, C. F.: Comparing discontinuity orientation data collected by terrestrial LiDAR and transit compass methods, Eng. Geol., 181, 78–92, https://doi.org/10.1016/j.enggeo.2014.08.014, 2014.

Frey, M., Bossennec, C., Seib, L., Bär, K., and Sass, I.: Interdisciplinary Dataset on the Fracture Network of the Tromm Granite, Southern Odenwald, SW Germany, TU datalib [data set], https://doi.org/10.48328/TUDATALIB-632, 2021a.

Frey, M., Weinert, S., Bär, K., van der Vaart, J., Dezayes, C., Calcagno, P., and Sass, I.: Integrated 3D geological modelling of the northern Upper Rhine Graben by joint inversion of gravimetry and magnetic data, Tectonophysics, 813, 228927, https://doi.org/10.1016/j.tecto.2021.228927, 2021b.

Freymark, J., Sippel, J., Scheck-Wenderoth, M., Bär, K., Stiller, M., Fritsche, J.-G., and Kracht, M.: The deep thermal field of the Upper Rhine Graben, Tectonophysics, 694, 114–129, https://doi.org/10.1016/j.tecto.2016.11.013, 2017.

Genter, A. and Traineau, H.: Analysis of macroscopic fractures in granite in the HDR geothermal well EPS-1, Soultz-sous-Forets, France, J. Volcanol. Geoth. Res., 72, 121–141, https://doi.org/10.1016/0377-0273(95)00070-4, 1996.

Genter, A., Castaing, C., Dezayes, C., Tenzer, H., Traineau, H., and Villemin, T.: Comparative analysis of direct (core) and indirect (borehole imaging tools) collection of fracture data in the Hot Dry Rock Soultz reservoir (France), J. Geophys. Res.-Sol. Ea., 102, 15419–15431, https://doi.org/10.1029/97JB00626, 1997.

Genter, A., Evans, K., Cuenot, N., Fritsch, D., and Sanjuan, B.: Contribution of the exploration of deep crystalline fractured reservoir of Soultz to the knowledge of enhanced geothermal systems (EGS), C.R. Geosci., 342, 502–516, https://doi.org/10.1016/j.crte.2010.01.006, 2010.

Glaas, C., Vidal, J., and Genter, A.: Structural characterization of naturally fractured geothermal reservoirs in the central Upper Rhine Graben, J. Struct. Geol., 148, 104370, https://doi.org/10.1016/j.jsg.2021.104370, 2021.

Guerriero, V., Vitale, S., Ciarcia, S., and Mazzoli, S.: Improved statistical multi-scale analysis of fractured

reservoir analogues, Tectonophysics, 504, 14–24, https://doi.org/10.1016/j.tecto.2011.01.003, 2011.

Guglielmetti, L., Comina, C., Abdelfettah, Y., Schill, E., and Mandrone, G.: Integration of 3D geological modeling and gravity surveys for geothermal prospection in an Alpine region, Tectonophysics, 608, 1025–1036, https://doi.org/10.1016/j.tecto.2013.07.012, 2013.

Guillou-Frottier, L., Carrè, C., Bourgine, B., Bouchot, V., and Genter, A.: Structure of hydrothermal convection in the Upper Rhine Graben as inferred from corrected temperature data and basin-scale numerical models, J. Volcanol. Geoth. Res., 256, 29–49, https://doi.org/10.1016/j.jvolgeores.2013.02.008, 2013.

Hess, J. C. and Schmidt, G.: Zur Altersstellung der Kataklasite im Bereich der Otzberg-Zone, Odenwald, Geol. Jb. Hessen, 117, 69–77, 1989.

HLUG: Geologische Karte von Hessen, Hessisches Landesamt für Umwelt und Geologie, https://www.hlnug.de/fileadmin/dokumente/geologie/geologie/guek300.pdf (last access: 23 May 2022), 2007.

Ioannides, K., Papachristodoulou, C., Stamoulis, K., Karamanis, D., Pavlides, S., Chatzipetros, A., and Karakala, E.: Soil gas radon: a tool for exploring active fault zones, Appl. Radiat. Isotopes, 59, 205–213, https://doi.org/10.1016/S0969-8043(03)00164-7, 2003.

Jing, L. and Stephansson, O. (Eds.): Fundamentals of discrete element methods for rock engineering: theory and applications, Elsevier, https://doi.org/10.1016/j.ijrmms.2008.04.003, 2007.

Jolie, E., Klinkmueller, M., and Moeck, I.: Diffuse surface emanations as indicator of structural permeability in fault-controlled geothermal systems, J. Volcanol. Geoth. Res., 290, 97–113, https://doi.org/10.1016/j.jvolgeores.2014.11.003, 2015.

Jolie, E., Klinkmueller, M., Moeck, I., and Bruhn, D.: Linking gas fluxes at Earth's surface with fracture zones in an active geothermal field, Geology, 44, 187–190, https://doi.org/10.1130/G37412.1, 2016.

King, C.-Y., King, B.-S., Evans, W. C., and Zhang, W.: Spatial radon anomalies on active faults in California, Appl. Geochem., 11, 497–510, https://doi.org/10.1016/0883-2927(96)00003-0, 1996.

Klemm, G.: Geologische Karte des Großherzogtums Hessen – Blatt 6419 Beerfelden, Hessisches Landesamt für Bodenforschung, 1900.

Klemm, G.: Geologische Karte von Hessen – Blatt 6319 Erbach, Hessische Geologische Landesanstalt, 1928.

Klemm, G.: Geologische Karte von Hessen – Blatt 6418 Birkenau (Weinheim), Hessische Geologische Landesanstalt, 1929.

Klemm, G.: Geologische Karte von Hessen – Blatt 6318 Lindenfels, Hessische Geologische Landesanstalt, 1933.

Kreuzer, H. and Harre, W.: K/Ar-Altersbestimmungen an Hornblenden und Biotiten des Kristallinen Odenwalds, in: Mineralien und Gesteine im Odenwald, edited by: Amstutz, G. C., Meisl, S., and Nickel, E., 70–78, Heidelberg, VFMG, https://hdl.handle.net/10013/epic.42772, 1975.

Krohe, A.: Emplacement of synkinematic plutons in the Variscan Odenwald (Germany) controlled by transtensional tectonics, Int. J. Earth Sci., 80, 391–409, https://doi.org/10.1007/BF01829373, 1991.

Krohe, A.: Structural evolution of intermediate-crustal rocks in a strike-slip and extensional setting (Variscan Odenwald, SW Germany): differential upward transport of metamorphic complexes and changing deformation mechanisms, Tectonophysics, 205, 357–386, https://doi.org/10.1016/0040-1951(92)90443-A, 1992.

Krohe, A. and Willner, A. P.: IV.C.2 The Odenwald Crystalline Complex, in: Pre-Permian Geology of Central and Eastern Europe, edited by: Dallmeyer, R. D., Franke, W., and Weber, K., 182–185, Springer Berlin Heidelberg, Berlin, Heidelberg, https://doi.org/10.1007/978-3-642-77518-5, 1995.

Ledésert, B., Hebert, R., Genter, A., Bartier, D., Clauer, N., and Grall, C.: Fractures, hydrothermal alterations and permeability in the Soultz Enhanced Geothermal System, C.R. Geosci., 342, 607–615, https://doi.org/10.1016/j.crte.2009.09.011, 2010.

Li, Y. and Oldenburg, D. W.: 3-D inversion of gravity data, Geophysics, 63, 109–119, 1998.

Maggetti, M.: Die Tiefengesteine des Bergsträßer Odenwaldes, in: Mineralien und Gesteine im Odenwald, edited by: Amstutz, G. C., Meisl, S., and Nickel, E., 87–109, Heidelberg, VFMG, https://hdl.handle.net/10013/epic.42772, 1975.

Mahmoodpour, S., Singh, M., Turan, A., Bär, K., and Sass, I.: Hydro-Thermal Modeling for Geothermal Energy Extraction from Soultz-sous-Forêts, France, Geosciences, 11, 464, https://doi.org/10.3390/geosciences11110464, 2021.

Mahmoodpour, S., Singh, M., Turan, A., Bär, K., and Sass, I.: Simulations and global sensitivity analysis of the thermo-hydraulic-mechanical processes in a fractured geothermal reservoir, Energy, 247, 123511, https://doi.org/10.1016/j.energy.2022.123511, 2022.

Marrett, R., Ortega, O. J., and Kelsey, C. M.: Extent of power-law scaling for natural fractures in rock, Geology, 27, 799, https://doi.org/10.1130/0091-7613(1999)027<0799:EOPLSF>2.3.CO;2, 1999.

McCaffrey, K., Lonergan, L., and Wilkinson, J. (Eds.): Fractures, fluid flow and mineralization, Geological Society of London, https://doi.org/10.1144/GSL.SP.1999.155.01.22, 1999.

McCubbine, J., Tontini, F. C., Stagpoole, V., Smith, E., and O'Brien, G.: Gsolve, a Python computer program with a graphical user interface to transform relative gravity survey measurements to absolute gravity values and gravity anomalies, SoftwareX, 7, 129–137, https://doi.org/10.1016/j.softx.2018.04.003, 2018.

Meixner, J., Grimmer, J. C., Becker, A., Schill, E., and Kohl, T.: Comparison of different digital elevation models and satellite imagery for lineament analysis: Implications for identification and spatial arrangement of fault zones in crystalline basement rocks of the southern Black Forest (Germany), J. Struct. Geol., 108, 256–268, https://doi.org/10.1016/j.jsg.2017.11.006, 2018.

Meller, C. and Ledésert, B.: Is There a Link Between Mineralogy, Petrophysics, and the Hydraulic and Seismic Behaviors of the Soultz-sous-Forêts Granite During Stimulation? A Review and Reinterpretation of Petro-Hydromechanical Data Toward a Better Understanding of Induced Seismicity, J. Geophys. Res.-Sol. Ea., 122, 9755–9774, https://doi.org/10.1002/2017JB014648, 2017.

Nettleton, L. L.: Determination of Density for Reduction of Gravimeter Observations*, Geophysics, 4, 176–183, https://doi.org/10.1190/1.0403176, 1939.

Nickel, E.: Geologische Position und Petrogenese des kristallinen Odenwaldes, in: Mineralien und Gesteine im Odenwald, edited by: Amstutz, G. C., Meisl, S., and Nickel, E., 1–25, Heidelberg, VFMG, https://hdl.handle.net/10013/epic.42772, 1975.

Niven, E. B. and Deutsch, C. V.: A sensitivity analysis for equivalent permeability tensors calculated from 2D discrete fracture networks, CCG Ann. Rep., 11, 1–8, 2009.

Oda, M.: Permeability tensor for discontinuous rock masses, Géotechnique, 35, 483–495, https://doi.org/10.1680/geot.1985.35.4.483, 1985.

Okrusch, M., von Raumer, J., Matthes, S., and Schubert, W.: Mineralfazies und Stellung der Metamorphite im kristallinen Odenwald, in: Mineralien und Gesteine im Odenwald, edited by: Amstutz, G. C., Meisl, S., and Nickel, E., 109–134, Heidelberg, VFMG, https://hdl.handle.net/10013/epic.42772, 1975.

Okrusch, M., Schubert, W., and Nasir, S.: IV.D Igneous Activity (Pre- to Early Variscan Magmatism), in: Pre-Permian Geology of Central and Eastern Europe, edited by: Dallmeyer, R. D., Franke, W., and Weber, K., 190–200, Springer Berlin Heidelberg, Berlin, Heidelberg, https://doi.org/10.1007/978-3-642-77518-5, 1995.

Pickering, G., Bull, J. M., and Sanderson, D. J.: Sampling power-law distributions, Tectonophysics, 248, 1–20, https://doi.org/10.1016/0040-1951(95)00030-Q, 1995.

Place, J., Géraud, Y., Diraison, M., Herquel, G., Edel, J. B., Bano, M., Le Garzic, E., and Walter, B.: Structural control of weathering processes within exhumed granitoids: Compartmentalisation of geophysical properties by faults and fractures, J. Struct. Geol., 84, 102–119, https://doi.org/10.1016/j.jsg.2015.11.011, 2016.

Poller, U., Altenberger, U., and Schubert, W.: Geochemical investigations of the Bergsträsser Odenwald amphibolites – implicationsfor back-arc magmatism, Miner. Petrol., 72, 63–76, https://doi.org/10.1007/s007100170027, 2001.

Pribnow, D. and Schellschmidt, R.: Thermal tracking of upper crustal fluid flow in the Rhine graben, Geophys. Res. Lett., 27, 1957–1960, https://doi.org/10.1029/2000GL008494, 2000.

Rathnaweera, T. D., Wu, W., Ji, Y., and Gamage, R. P.: Understanding injection-induced seismicity in enhanced geothermal systems: From the coupled thermo-hydro-mechanical-chemical process to anthropogenic earthquake prediction, Earth-Sci. Rev., 205, 103182, https://doi.org/10.1016/j.earscirev.2020.103182, 2020.

Reischmann, T., Anthes, G., Jaeckel, P., and Altenberger, U.: Age and origin of the Böllsteiner Odenwald, Miner. Petrol., 72, 29–44, https://doi.org/10.1007/s007100170025, 2001.

Reiter, K., Heidbach, O., Müller, B., Reinecker, J., and Röckl, T.: Stress Map Germany 2016, WSM [data set], https://doi.org/10.5880/WSM.Germany2016_en, 2016.

Sanderson, D. J. and Nixon, C. W.: Topology, connectivity and percolation in fracture networks, J. Struct. Geol., 115, 167–177, https://doi.org/10.1016/j.jsg.2018.07.011, 2018.

Sausse, J. and Genter, A.: Types of permeable fractures in granite, Geol. Soc. Lond. Spec. Publ., 240, 1–14, https://doi.org/10.1144/GSL.SP.2005.240.01.01, 2005.

Sausse, J., Dezayes, C., Dorbath, L., Genter, A., and Place, J.: 3D model of fracture zones at Soultz-sous-Forêts based on geological data, image logs, induced microseismicity and vertical seismic profiles, C.R. Geosci., 342, 531–545, https://doi.org/10.1016/j.crte.2010.01.011, 2010.

Schälicke, W.: Die Otzberg-Zone, in: Mineralien und Gesteine im Odenwald, edited by: Amstutz, G. C., Meisl, S., and Nickel, E., 47–59, Heidelberg, VFMG, https://hdl.handle.net/10013/epic.42772, 1975.

Schill, E., Meixner, J., Meller, C., Grimm, M., Grimmer, J. C., Stober, I., and Kohl, T.: Criteria and geological setting for the generic geothermal underground research laboratory, GEOLAB, Geothermal Energy, 4, 7, https://doi.org/10.1186/s40517-016-0049-5, 2016.

Schill, E., Genter, A., Cuenot, N., and Kohl, T.: Hydraulic performance history at the Soultz EGS reservoirs from stimulation and long-term circulation tests, Geothermics, 70, 110–124, https://doi.org/10.1016/j.geothermics.2017.06.003, 2017.

Schubert, W., Lippolt, H. J., and Schwarz, W.: Early to Middle Carboniferous hornblende $^{40}Ar/^{39}Ar$ ages of amphibolites and gabbros from the Bergsträsser Odenwald, Miner. Petrol., 72, 113–132, https://doi.org/10.1007/s007100170029, 2001.

Snow, D. T.: A parallel plate model of fractured permeable media, PhD thesis, University of California, Berkeley, https://www.nrc.gov/docs/ML0319/ML031910452.pdf (last access: 25 May 2022), 1965.

Stein, E.: The geology of the Odenwald Crystalline Complex, Miner. Petrol., 72, 7–28, https://doi.org/10.1007/s007100170024, 2001.

Stober, I. and Bucher, K.: Hydraulic properties of the crystalline basement, Hydrogeol. J., 15, 213–224, https://doi.org/10.1007/s10040-006-0094-4, 2007.

Todt, W. A., Altenberger, U., and von Raumer, J. F.: U-Pb data on zircons for the thermal peak of metamorphism in the Variscan Odenwald, Germany, Geol. Rundsch., 84, 466–472, https://doi.org/10.1007/BF00284514, 1995.

Traineau, H., Genter, A., Cautru, J. P., Fabriol, H., and Chèvremont, P.: Petrography of the granite massif from drill cutting analysis and well log interpretation in the geothermal HDR borehole GPK1 (Soultz, Alsace, France), Geothermal Science and Technology, 3, 1–29, 1991.

Tranter, M., de Lucia, M., and Kühn, M.: Numerical investigation of barite scaling kinetics in fractures, Geothermics, 91, 102027, https://doi.org/10.1016/j.geothermics.2020.102027, 2021.

van Zyl, J. J.: The Shuttle Radar Topography Mission (SRTM): a breakthrough in remote sensing of topography, Acta Astronaut., 48, 559–565, https://doi.org/10.1016/S0094-5765(01)00020-0, 2001.

Vazaios, I., Vlachopoulos, N., and Diederichs, M. S.: Integration of Lidar-Based Structural Input and Discrete Fracture Network Generation for Underground Applications, Geotechnical and Geological Engineering, 35, 2227–2251, https://doi.org/10.1007/s10706-017-0240-x, 2017.

Vidal, J. and Genter, A.: Overview of naturally permeable fractured reservoirs in the central and southern Upper Rhine Graben: Insights from geothermal wells, Geothermics, 74, 57–73, https://doi.org/10.1016/j.geothermics.2018.02.003, 2018.

Vidal, J., Genter, A., and Chopin, F.: Permeable fracture zones in the hard rocks of the geothermal reservoir at Rittershoffen, France, J. Geophys. Res.-Sol. Ea., 122, 4864–4887, https://doi.org/10.1002/2017JB014331, 2017.

Vidal, J., Patrier, P., Genter, A., Beaufort, D., Dezayes, C., Glaas, C., Lerouge, C., and Sanjuan, B.: Clay minerals related to the circulation of geothermal fluids in boreholes at Rittershoffen (Alsace, France), J. Volcanol. Geoth. Res., 349, 192–204, https://doi.org/10.1016/j.jvolgeores.2017.10.019, 2018.

Vogt, C., Marquart, G., Kosack, C., Wolf, A., and Clauser, C.: Estimating the permeability distribution and its uncertainty

at the EGS demonstration reservoir Soultz-sous-Forêts using the ensemble Kalman filter, Water Resour. Res., 48, W08517, https://doi.org/10.1029/2011WR011673, 2012.

Weinert, S., Bär, K., and Sass, I.: Petrophysical Properties of the Mid-German Crystalline High: A Database for Bavarian, Hessian, Rhineland-Palatinate and Thuringian Outcrops, TU datalib [data set], https://doi.org/10.25534/tudatalib-278, 2020.

Welsch, B., Rühaak, W., Schulte, D. O., Bär, K., and Sass, I.: Characteristics of medium deep borehole thermal energy storage, Int. J. Energ. Res., 40, 1855–1868, https://doi.org/10.1002/er.3570, 2016.

Zeng, Q., Lu, W., Zhang, R., Zhao, J., Ren, P., and Wang, B.: LIDAR-based fracture characterization and controlling factors analysis: An outcrop case from Kuqa Depression, NW China, J. Petrol. Sci. Eng., 161, 445–457, https://doi.org/10.1016/j.petrol.2017.12.002, 2018.

Zhang, Y., Person, M., Rupp, J., Ellett, K., Celia, M. A., Gable, C. W., Bowen, B., Evans, J., Bandilla, K., Mozley, P., Dewers, T., and Elliot, T.: Hydrogeologic controls on induced seismicity in crystalline basement rocks due to fluid injection into basal reservoirs, Ground Water, 51, 525–538, https://doi.org/10.1111/gwat.12071, 2013.

6. Mapping Buried Fault Zones in a Granitic Pluton using Aeromagnetic Data

This chapter is based on the research article with same title, that was published in the Journal Pure and Applied Geophysics on the 31 March 2023. The content is unchanged.

This chapter is the follow-up of the interdisciplinary outcrop analog study in chapter 5, with a stronger focus on the exploration for GeoLaB. The results of a drone-based aeromagnetic survey in the southern Odenwald are presented. Different signal filters were compared using a synthetic model and were then applied to the field data. The filtered anomalies reveal a large number of magnetic lineaments, which are interpreted as faults and whose distribution partially correlates with the reactivation potential. The aeromagnetic data consequently provides a high-resolution map of potentially permeable faults in the study area.

Reference:

Frey, M., Bossennec, C., & Sass, I. (2023). Mapping buried fault zones in a granitic pluton using aeromagnetic data. Pure and Applied Geophysics, 180, 2241–2255. https://doi.org/10.1007/s00024-023-03258-2.

6.1. Introduction

Climate change and the current energy crisis related to the war in Ukraine, urged the need to reduce the consumption of fossil fuels and increase renewable energy sources (IPCC 2022b). In this context, deep geothermal energy plays a key role as its base-load capability can effectively compensate for weather-dependent fluctuations of other renewable energy forms. The overall largest geothermal resources are found in the crystalline basement (Tester et al. 2006; Paschen et al. 2003), accessible by deep drillings in many regions worldwide. This study focuses on the Upper Rhine Graben (URG), where the geothermal resources have already been exploited for power and heat supply as well as for balenological purposes in the past (Frey et al. 2022c).

As the natural permeability of the crystalline basement is usually very low ($<10^{-16}$ m²), so-called Enhanced Geothermal Systems (EGS) need to be developed in order to make the geothermal resources usable (Huenges 2010). They represent artificial reservoirs created by hydraulic, thermal or chemical stimulation. Depending on the applied technology and the subsurface conditions, existing fractures or new fractures are opened, resulting in a permeability increase of several orders of magnitude. Successful development of EGS is based on a comprehensive understanding of the natural fracture and fault network as well as fluid-rock interactions. However, first-order questions remain regarding the hydro-thermo-mechanical-chemical processes during stimulation and operation of the power plant. To make EGS feasible on a broad scale, these issues will be addressed in the upcoming GeoLaB (Geothermal Laboratory in the Mine) project (KIT 2022). GeoLaB will consist of a newly constructed subsurface laboratory at the eastern margin of the URG, where high-flowrate in situ experiments on fault zones will be conducted. The selection of a suitable site is based on the criteria catalog of Schill et al. (2016). Accordingly, the location should be lithologically as homogeneous as possible, have controllable hydraulic boundary conditions (preferably no mining history), exhibit undisturbed stress conditions (several hundred meters overburden above the laboratory), and contain sufficient fractures that may potentially be reactivated in the recent stress field. Two sites have already been preselected that meet these requirements: the southern Black Forest and the Tromm Granite in the Odenwald. This study concentrates on the latter.

For the planning of the approximately 1.5 km long GeoLaB tunnel, potentially permeable faults have to be identified beforehand on which the above-described experiments can be carried out. Initial characterization of the fault and fracture network in the Tromm Granite has already been carried out by Frey et al. (2022a), locally using LIDAR surveys in outcrops and regionally by analyzing morphological lineaments in high resolution digital elevation models (DEMs). However, fault zones of hundreds of meters to several kilometers length are always buried under a meter thick sedimentary and weathering cover, preventing any direct assessment of structural and hydraulic properties. In addition, uncertainties remain as to whether the DEM lineaments indeed reflect faults in the subsurface. The characterization of the fault and fracture network therefore relies mainly on indirect geophysical measurements. Gravity data, also acquired by Frey et al. (2022a), show several hundred meters wide anomalies indicative of broad zones in which the fracture porosity may be as high as 6 %. This study presents an improved mapping of potentially porous and permeable fault or fracture zones based on a newly acquired aeromagnetic dataset.

Aeromagnetic surveying is a widely used geophysical method that allows more efficient mapping of the crustal magnetic field than ground-based methods (Isles and Rankin 2013). These measurements are particularly useful in rugged and remote areas like the Tromm Granite,

where other datasets, such as seismic or borehole data, are sparse or unavailable. Aeromagnetic datasets are further advantageous when field mapping is not possible due to a sedimentary or vegetation cover of the target structures. Applications are diverse and include geological and tectonic mapping as well as mineral and hydrocarbon prospection. Depending on the target size, the corresponding surveys are carried out at a wide range of scales, from a few hectares to several thousand km². Until a few years ago, the surveys were mostly conducted with airplanes or helicopters, but the use of UAVs (Unmanned Aerial Vehicles) has recently increased (Walter et al. 2020; Cherkasov and Kapshtan 2017; Kim 2020). UAVs enable small to medium-sized surveys to be carried out generally at a lower cost with less environmental impact.

6.2. Geological Setting

The aeromagnetic survey covers the central part of the Tromm Granite, an approximately 60 km² large intrusion in the southern Odenwald (Fig. 6.1) (Stein 2001; Amstutz et al. 1975; Krohe and Willner 1995). The study area is located at the northeastern URG margin, which is part of the Mid-German Crystalline High (MGCH), consisting of mafic to felsic plutonic rocks intruded into Paleozoic metamorphic units. The crystalline basement of this region was primarily shaped during the Variscan orogeny (Kossmat 1927), that reached its peak continental collision phase during the Carboniferous. In this context, the MGCH is commonly regarded as the exposed former active continental margin of the Armorican Terrane Assemblage (Krohe 1991; Altherr et al. 1999; Okrusch et al. 1995).

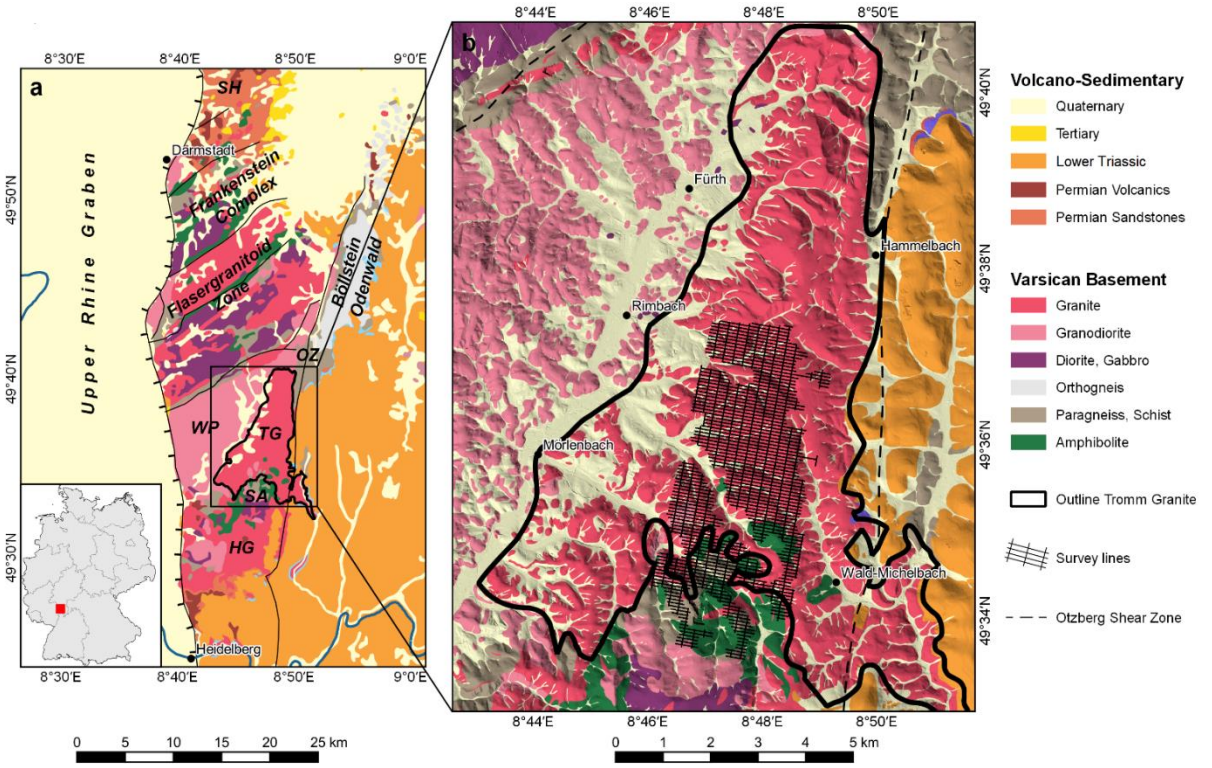

Figure 6.1: Overview of the study area: (A) geological map of the Odenwald (modified after HLUG 2007), (B) geological map of the Tromm Granite in the southern Odenwald (Klemm 1900, 1928, 1929, 1933), including in-lines and tie-lines of the aeromagnetic survey. HG = Heidelberg Granite, OZ = Otzberg Shear Zone, SA = Schollenagglomerat, SH = Sprendlinger Horst, TG = Tromm Granite, WP = Weschnitz Pluton.

The Tromm Granite consists of medium- to coarse-grained, orthoclase-rich, biotite-bearing, and often reddish granitoids characterized by large potassium feldspar inclusions (Nickel 1953; Maggetti 1975). The southern part additionally features a fine-grained variety of this granite with similar mineralogical composition but at a younger age. The granite is often intruded by aplitic or pegmatitic dykes and veins (Klemm 1933). To the east, the Tromm Granite is bounded by the 1 - 2 km wide Otzberg Fault (Schälicke 1975), a first-order crustal shear zone that has been repeatedly reactivated since the Paleozoic. In the south, the granite gradually merges into the lithologically heterogeneous "Schollenagglomerate" (Nickel 1975), which comprises gneiss, schists, amphibolites, and various magmatic rocks. In the northwest, the Tromm Granite adjoins the granodiorites of the Weschnitz Pluton. Clark (2020) reported that the Koenigsberger ratio of felsic igneous rocks is usually well below 0.5 (typically around 0.2). Accordingly, magnetization in the Tromm Granite is expected to be mainly influenced by induction, while remanent magnetization may be of minor importance.

The structural inventory of the Tromm Granite is characterized by its multiphase evolution, during which the regional stress field was repeatedly reoriented (Buchner 1981; Schumacher 2002; Behrmann et al. 2003; Dèzes et al. 2004; Bossennec et al. 2021). On the one hand, the pluton was structurally overprinted directly after its emplacement, i.e. during the final phase of the Variscan continental collision and the subsequent collapse of the orogen. At this time, deformation was especially concentrated along the Otzberg, which is documented by the extensive cataclasis and mylonitization. On the other hand, opening or reactivation of fractures and faults in the Tromm Granite occurred with the formation of the adjacent URG. The main crustal extension took place between the late Eocene and early Miocene, with the orientation of the largest horizontal stress σ_{Hmax} between NW-SE and NNE-SSW. This was followed by the still ongoing transtensive reactivation of the graben faults, with an orientation of σ_{Hmax} around NW-SE. Frey et al. (2022a) demonstrated that the orientation of fractures in the study area is largely consistent with measurements from the URG, e.g., at Soultz-sous-Forêts. This indicates that the majority of fractures are associated with the rifting. Nevertheless, the poor outcrop situation makes it difficult to draw reliable conclusions on the exact timing of fault activity in the Tromm Granite.

Direct stress measurements are not available for the southern Odenwald due to the lack of deep boreholes. Instead, stress information is derived from wells and seismic events some tens of kilometers to the west in the URG (Reiter et al. 2016). Ahlers et al. (2021) combined all available stress data into a Germany-wide stress model, and suggest that σ_{Hmax} strikes ~165° in the study area.

6.3. Material and Methods

6.3.1. Aeromagnetic Survey and Basic Data Processing

The acquisition and basic processing of the aeromagnetic dataset from the Tromm area were carried out by French company TERREMYS with their self-developed magnetic mono-sensor quadcopter. A Bartington MC03 fluxgate magnetometer was used for the magnetic measurements, which is attached to a 1 m long rigid pole and records data at 25 Hz. The survey was conducted in March 2022, covering an area of 13.3 km² during six days of measurements (Fig. 6.1). A total of 252 linear km was recorded with in-line and tie-line spacings of 70 and 210 m, respectively. The flight altitude was 70 m above ground, using a barometer for vertical

navigation. A 1 m precision GNSS was used for the horizontal positioning. Due to legal restrictions, buildings, gardens, and streets were excluded and the survey area was divided into seven sectors with separate take-off locations. An overlap of 60 m was chosen at the respective boundaries to ensure a good connection between the sectors.

The magnetic sensor was calibrated twice a day or when the take-off point was changed. This calibration enabled measurement sensitivity of about 1 nT. Additional measurements by an independent mobile base station were used to correct for diurnal variations. However, technical problems occurred after two days, which is why the corrections were based on data from the observatories Manhay (MAB) in Belgium and Fürstenfeldbruck (FUR) in Germany. The reference field IGRF-13 was subtracted to calculate the magnetic anomalies from the measured values. Subsequently, leveling correction was performed, which minimizes the anomaly differences at the crossing points of in- and tie-lines (the standard deviation is 0.1 nT after correction). A minimum curvature algorithm was applied to calculate a grid of magnetic anomalies with a cell size of 25 m, corresponding to about one third of the in-line spacing. Finally, a reduction to the magnetic north pole (RTP) was performed using the direction given by the IGRF-13 model. The RTP calculation facilitates the geologic interpretation of the data since it places the magnetic anomaly above the causative magnetic volume.

6.3.2. Anomaly Enhancement Filters

The RTP anomalies is often dominated by regional trends typically with wavelengths of several kilometers. Therefore, various filter techniques have been developed to enhance fine details and detect edges of near-surface source bodies. For this study, eight well-established algorithms were selected and compared against each other. Their mathematical principles are summarized below.

The vertical derivative (VDR) is a high-pass filters commonly calculated when interpreting magnetic anomalies. This method concentrates the anomalies above their sources in the subsurface. Expressed in a Cartesian coordinates system (x,y,z) with z being the vertical coordinate, VDR of the magnetic field component (F) is:

$$VDR = \frac{\partial F}{\partial \mathrm{z}} \tag{6.1}$$

The total horizontal gradient (THG) of the field places extreme values above the edges of the source body (Cordell 1979):

$$THG = \sqrt{\left(\frac{\partial F}{\partial \mathrm{x}}\right)^2 + \left(\frac{\partial F}{\partial \mathrm{y}}\right)^2} \tag{6.2}$$

Ma and Li (2012) proposed the normalized total horizontal gradient (NTHG), which equalizes the amplitudes within a moving window of pre-defined size:

$$NTHG_{i,j} = \frac{THG_{i,j}}{max(THG_{i-\frac{m}{2}:i+\frac{m}{2},j-\frac{n}{2}:j+\frac{n}{2}})} \tag{6.3}$$

where m and n are the width and length of the window. The analytical signal amplitude (ASA) (Roest et al. 1992) combines the gradients of the magnetic field from all three dimensions and can be used to detect the sources edges:

$$ASA = \sqrt{\left(\frac{\partial F}{\partial \mathrm{x}}\right)^2 + \left(\frac{\partial F}{\partial \mathrm{y}}\right)^2 + \left(\frac{\partial F}{\partial \mathrm{z}}\right)^2} \tag{6.4}$$

The tilt derivative (TDR), proposed by Miller and Singh (1994), normalizes the VDR using the THG. This filter enhances the short-wavelength content of the magnetic field while preserving the polarity of the anomalies. The zero crossing marks the edges, maxima and minimal are centered above the source bodies:

$$TDR = \tan^{-1}\left(\frac{VDR}{THG}\right) \tag{6.5}$$

The theta map (θ), normalizes the THG using the ASA (Wijns et al. 2005) and marks the sources edges by the signal's minima:

$$\theta = \cos^{-1}\left(\frac{THG}{ASA}\right) \tag{6.6}$$

A modified version of the tilt derivative was introduced by Cooper and Cowan (2006), which normalizes THG with the absolute value of VDR. The normalized horizontal tilt derivative TDX marks the sources edges by the signal maxima, thus yields similar results as θ:

$$TDX = tan^{-1}\left(\frac{THG}{|VDR|}\right) \tag{6.7}$$

Finally, Oksum et al. (2021) recently proposed an edge detection method based on a modified Fast Sigmoid Function FSED, which incorporates the vertical and horizontal gradients of THG. The filter provides a sharp image of the source edges:

$$FSED = \frac{R-1}{|R|+1} \tag{6.8}$$

with

$$R = \frac{\frac{\partial THG}{\partial \mathrm{z}}}{\sqrt{\left(\frac{\partial THG}{\partial \mathrm{x}}\right)^2 + \left(\frac{\partial THG}{\partial \mathrm{y}}\right)^2}} \tag{6.9}$$

6.3.3. Synthetic Model

Before being applied to the field data, the described filters were first tested on a synthetic model (Fig. 6.2) that reflects the expected subsurface structure of the Tromm Granite in a simplified way. The model was created with the software IGMAS+ (Interactive Geophysical Modelling ASistant) (Götze and Lahmeyer 1988; Schmidt et al. 2020), spanning 500 m horizontally and 200 m vertically. Three 25 m thick faults were modeled, one vertical and two dipping with 70°. An overburden of 50 m was further specified for one of the dipping faults. Different magnetic

susceptibilities were assigned to generate contrasts compared to the reference background. In addition, artificial noise was added to the synthetic field.

For an objective selection of the most appropriate filtering method, the following criteria were defined that the filtered anomalies should satisfy:

- Amplification of the short-wavelength content of the magnetic anomalies
- Correct positioning of the modelled structures without filter artifacts
- Amplification of the anomalies from buried sources
- Preservation of the polarity of the anomaly to enable the best geological interpretation
- Robustness to noise in the data (detection of magnetic sources should not be obstructed by the noise)

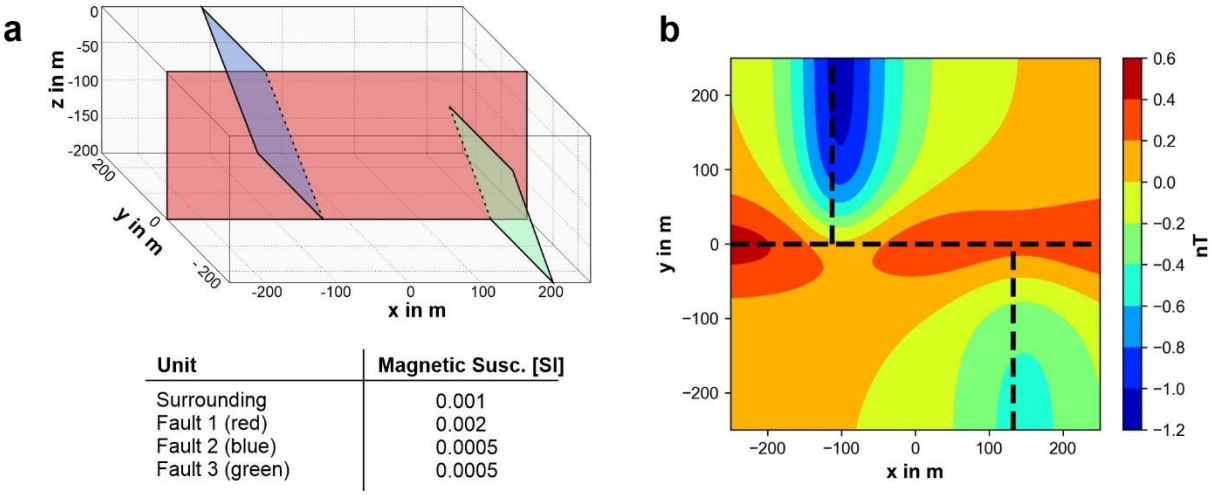

Unit	Magnetic Susc. [SI]
Surrounding	0.001
Fault 1 (red)	0.002
Fault 2 (blue)	0.0005
Fault 3 (green)	0.0005

Figure 6.2: (A) 3D model comprising three fault zones, each with a thickness of 25 m. The dip angle of the red fault is 90°, while that of the blue and green faults is 70°. The top of the green line is 50 m below the surface to represent a buried structure. The magnetic properties of the faults and surrounding rock mass are given in the table below. (B) Synthetic magnetic field calculated for this model, including the fault traces. Note that the anomalies are reduced to the magnetic north pole.

6.3.4. Assessing the Reactivation Potential

After applying the selected filter to the aeromagnetic dataset from the Tromm Granite, linear features in the filtered magnetic field with a minimum length of 250 m were then digitized and could be compared with the DEM lineament analysis performed by Frey et al. (2022a). The clustering of lineaments in specific azimuth intervals was interpreted for the recent stress conditions in the survey area based on the geomechanical modelling of Ahlers et al. (2021). For this purpose, the two parameters slip and dilation tendency were used (Morris et al. 1996; Ferrill and Morris 2003), which are measures of the reactivation potential of a fault zone. The slip tendency T_s is defined as:

$$T_s = \frac{\tau}{\sigma_n} \tag{6.10}$$

where τ is the shear stress and σ_n the normal stress acting on the fault plane. The dilation tendency T_d can be written as:

$$T_d = \frac{\sigma_1 - \sigma_n}{\sigma_1 - \sigma_3} \tag{6.11}$$

where σ_1 and σ_3 are the largest and the smallest principal stresses, respectively.

6.4. Results

6.4.1. Comparison of Different Filter Methods

6.5. Comparison of different filter methods

A comparison of the eight filter methods described above is presented for the synthetic magnetic dataset in Fig. 6.3 (without noise) and Fig. 6.4 (with noise). The visual evaluation of the filters is based on the criteria defined in the subchapter "Synthetic model". All filter methods amplify the short wavelength components of the field, concentrating the anomalies over the source volumes or their edges. VDR, ASA, TDR, θ, and TDX render the location of the modelled faults with a maximum horizontal deviation of 20 m and without producing filter artefacts. The THG filter result, in contrast, does not allow an unambiguous interpretation of the fault locations. NTHG and FSED produce significant artefacts. All filter methods can detect the buried fault zone (50 m overburden), with the best gain achieved by TDR, θ, and TDX. VDR and TDR are the only filters that preserve the original polarity of the anomalies, which is essential for the subsequent geological interpretation. Finally, the eight filters show varying sensitivity to noise in the dataset. VDR, TDR, θ, and TDX still allow detecting all modelled faults.

In summary, only VDR and TDR meet all the predefined criteria. Since TDR amplifies the signal of the buried fault more effectively, this method was selected for filtering the aeromagnetic dataset from the Tromm Granite.

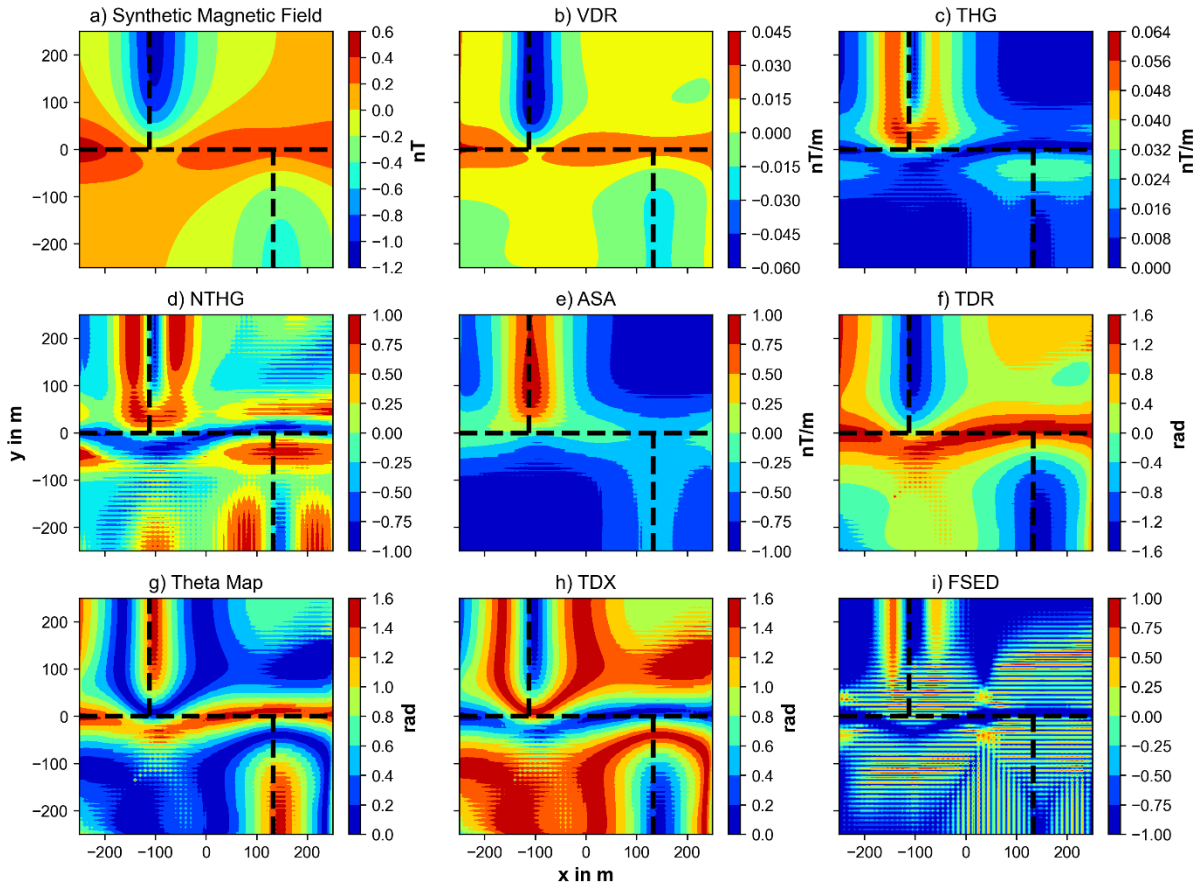
a) Synthetic Magnetic Field
b) VDR
c) THG
d) NTHG
e) ASA
f) TDR
g) Theta Map
h) TDX
i) FSED
y in m
x in m
nT
nT/m
rad

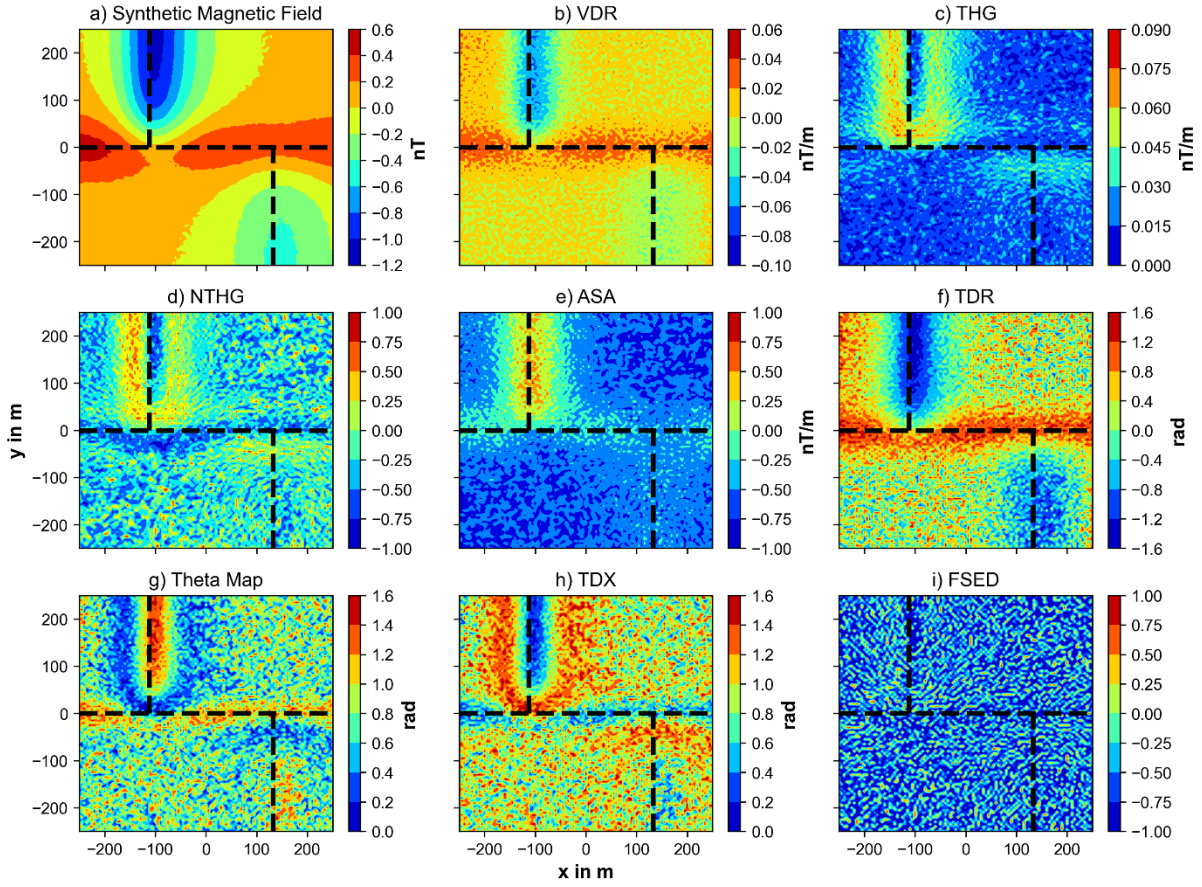
a) Synthetic Magnetic Field
b) VDR
c) THG
d) NTHG
e) ASA
f) TDR
g) Theta Map
h) TDX
i) FSED
y in m
x in m
nT
nT/m
rad

Figure 6.3: (top of previous page) Comparison of eight different enhancement filters for the magnetic data: (a) forward modeled magnetic field for the synthetic model shown in Fig. 6.2, (b) vertical derivative, (c) total horizontal gradient, (d) normalized total horizontal gradient, (e) analytical signal amplitude, (f) tilt derivative, (g) theta map, (h) normalized horizontal tilt derivative, and (i) fast sigmoid function. The dashed lines represent the fault traces in the synthetic model.

Figure 6.4: (bottom of previous page) Comparison of eight different enhancement filters for noisy magnetic data: (a) forward modeled magnetic field for the synthetic model shown in Fig. 6.2, (b) vertical derivative, (c) total horizontal gradient, (d) normalized total horizontal gradient, (e) analytical signal amplitude, (f) tilt derivative, (g) theta map, (h) normalized horizontal tilt derivative, and (i) fast sigmoid function. The dashed lines represent the fault traces in the synthetic model.

6.5.1. Magnetic Anomalies of the Tromm Granite

Fig. 6.5a illustrates the magnetic anomalies recorded in the Tromm area. The RTP anomalies range from -22.5 to 67.5 nT. Positive values of RTP are predominant at the boundary with the Schollenagglomerate in the south, which roughly coincide with mapped amphibolite bodies (Fig. 6.1). From the petrophysical investigations of rock samples from Odenwald by Frey et al. (2020) it is known that amphibolites ($\chi = 0.003 \pm 0.008$ [SI]) exhibit on average almost an order of magnitude higher magnetic susceptibility than the Tromm Granite ($\chi = 0.0007 \pm 0.001$ [SI]). This observation thus explains the concentration of positive anomalies over the amphibolite bodies. Further north, where no macroscopic changes in lithology are evident from geological mapping (Fig. 6.1), the magnetic anomalies indicate a concentric zonation of the Tromm Granite, with the magnetic maximum in the center and minima at the edges of the pluton.

The TDR filter amplifies the short wavelengths of the RTP anomalies, revealing a connected network of linear magnetic minima (Fig. 6.5b). Magnetic lineaments with a minimum length of 250 m are interpreted as potential fault zones. In total 118 lineaments, with a maximum length of 1.3 km, were extracted from the filtered anomaly map. A comparison of the magnetic with the morphological lineaments obtained by Frey et al. (2022a) from the high-resolution DEM of the Tromm Granite is shown in Fig. 6.5c. Along the prominent structures in the northern part of the aeromagnetic survey, a high level of agreement between these two independent data sets is evident. In contrast, the correlation is low in the remaining parts of the Tromm Granite.

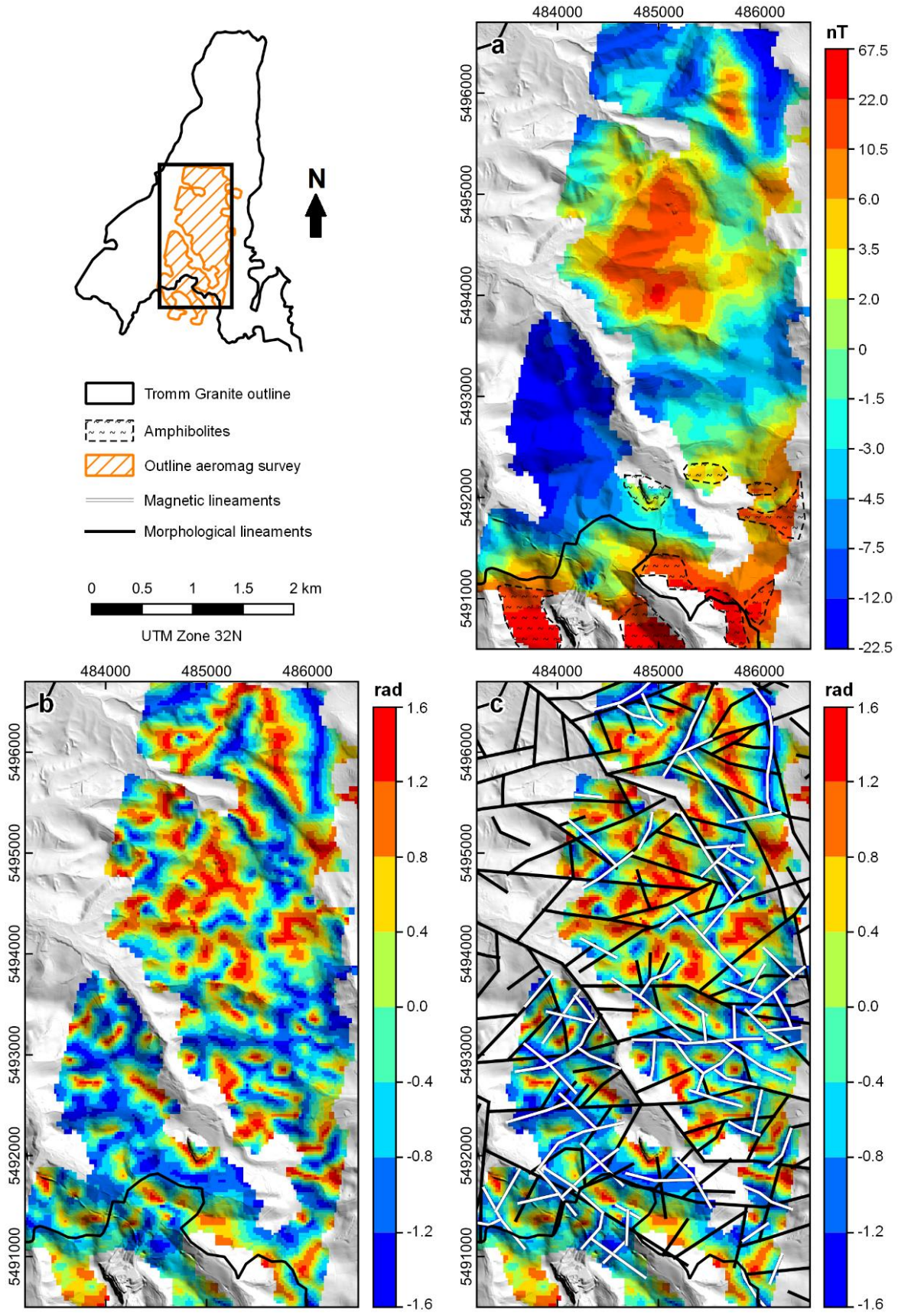

Figure 6.5: Results of the aeromagnetic survey from the Tromm Granite: (A) magnetic anomalies after reduction to the pole (RTP) at 70m above ground and with a lateral resolution 25 m, (B) Tilt derivative (TDR) of the anomalies, and (c) TDR of the anomalies with morphological and magnetic lineaments.

6.5.2. Reactivation Potential of Lineaments

Slip and dilation tendency in the current stress field were calculated for the Tromm Granite at various fault orientations (Fig. 6.6a). The dilation tendency exhibits a sinusoidal pattern with the maximum parallel to σ_{Hmax} (~165°) and the minimum parallel to σ_{hmin}. In contrast, the slip tendency is more complex, with two maxima at about 005° and 140°. For comparison, the cumulative lengths of lineaments at discrete strike intervals are given in Fig. 6.6b. Lineaments based on the DEM do not display a preferred direction, except for the cluster between 070° and 110°. No correlation with slip or dilation tendency can be detected. The magnetic lineaments are distributed more heterogeneously. Between 040° and 180°, there is a high degree of correlation with the slip tendency. The maximum cumulative length is found between 110° and 150°, coinciding with the slip tendency peak. Likewise, few magnetic lineaments were detected in the directions of minimum slip tendency. However, only a few lineaments are present between 000° and 040°, even though another maximum of the slip tendency is reached here. A correlation with the dilation tendency is not observed.

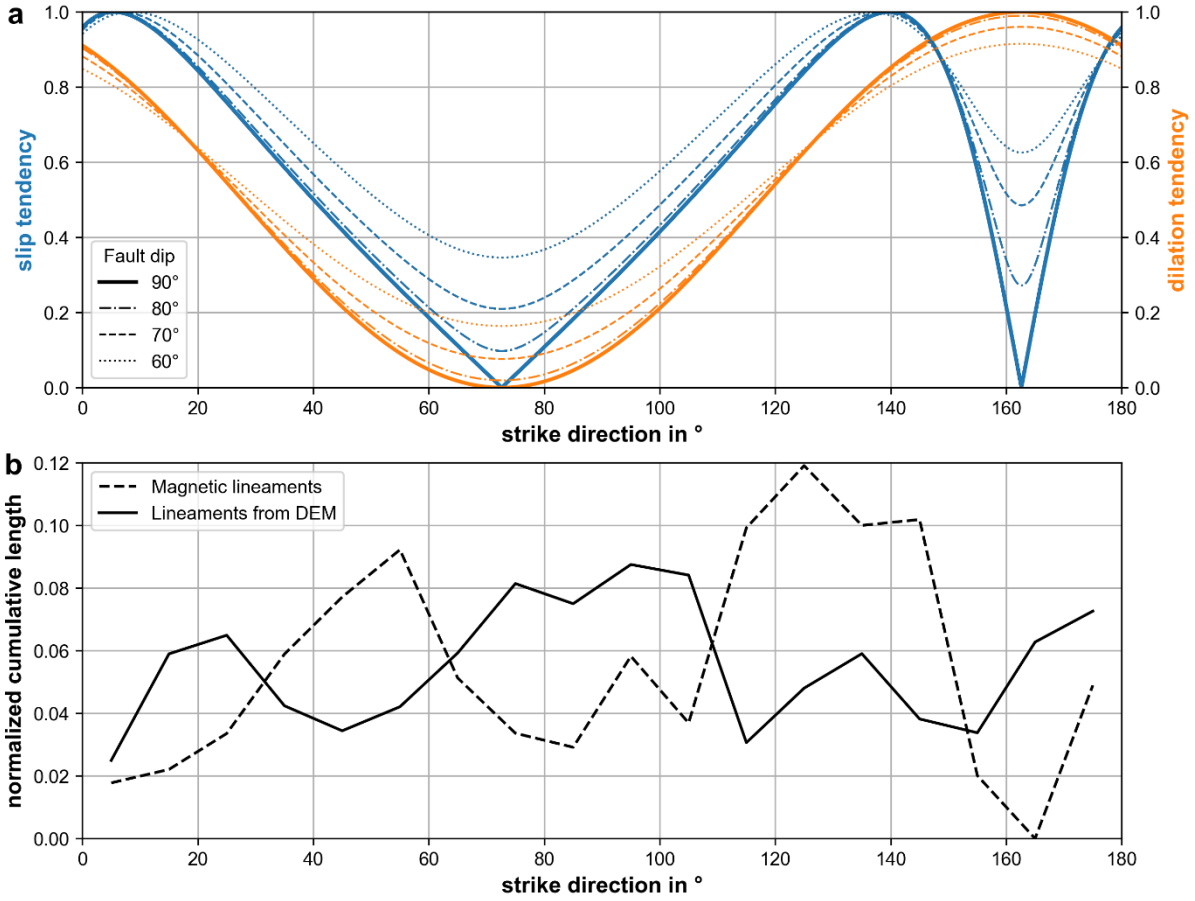

Figure 6.6: (A) Slip and dilation tendency for the Tromm Granite at various fault plane orientations, (B) normalized cumulative length of lineaments from the high-resolution digital elevation model and the enhanced aeromagnetic anomaly map.

6.6. Discussion

A high-resolution aeromagnetic survey was performed for the Tromm Granite at the northwestern URG margin. The calculated RTP anomalies indicate a concentric magnetic zonation of the pluton. Similar observations have been made for other granitoid intrusions

worldwide (Aydin et al. 2007; Gleizes et al. 1993; Antolín-Tomás et al. 2009; Benn et al. 1998). This possibly reflects the geochemical differentiation in the magma chamber during cooling and crystallization, resulting in a heterogeneous distribution of ferrimagnetic minerals (mainly magnetite) within the pluton. In addition, hydrothermal alteration and metamorphic overprinting may cause magnetic zoning.

Applying the TDR filter to the RTP anomalies reveals a network of magnetic lineaments characteristic of crystalline settings and usually interpreted as faults or fracture zones (Henkel and Guzmán 1977). The transformation of magnetite into paramagnetic minerals is considered to be the main reason for the locally reduced magnetic susceptibility. This process is accelerated in active fault zones, on the one hand, through alteration processes caused by fluid-rock interaction and, on the other hand, through the crushing of larger mineral grains as a result of tectonic deformation (Isles and Rankin 2013). In some cases, the fault core may also exhibit in increase in magnetic susceptibility compared to the surrounding undisturbed rock (Hirono et al. 2006; Tanikawa et al. 2008). Possible reasons for this include mineralogical changes caused by hydrothermal or thermo-mechanical processes in the fault zone. However, due to the lack of suitable outcrops in the Tromm Granite, this cannot be reliably assessed.

A comparison of the magnetic lineaments with lineaments from the high-resolution digital elevation model of the Tromm Granite shows that these two independent datasets are only partially correlated. Good agreement is generally found for prominent lineaments with a minimum length of 1 km. The discrepancies for the shorter lineaments might indicate that they do not necessarily represent fault zones. Alternatively, lithological variations in the pluton or magmatic veins could be responsible for the observed magnetic signal. However, the interpretation of the magnetic lineaments as fault zones is supported by the high correlation with the slip tendency under the current stress conditions. A possible explanation for this could be the repeated reactivation of favorably oriented fault planes in the Tromm Granite. The reduction of the magnetic susceptibility could be result of crushing and alteration of magnetite in these zones (Isles and Rankin 2013).

Interestingly, significantly more magnetic lineaments occur between 110° and 150° than between 000° and 040°, although a maximum of slip tendency is reached here in each case (Fig. 6.6). One possible reason could be the multiphase evolution of the crystalline basement along the URG. As described in the chapter 'Geological Setting', the regional stress field has been repeatedly reoriented since the intrusion of the Tromm Granite reoriented (Buchner 1981; Schumacher 2002; Behrmann et al. 2003; Dèzes et al. 2004; Bossennec et al. 2021). Accordingly, the seemingly abundant NW-SE striking faults may have been reactivated most frequently during the past 330 Ma, as indicated by the magnetic signal. However, a reliable reconstruction of the reactivation potential over the entire geologic history is not possible because of the large uncertainties concerning paleo-stress conditions. Alternatively, the NW-SE faults could already have been established during the Variscan orogeny. Schumacher (2002) and Edel et al. (2007), for example, reported that large-scale pre-existing Variscan structures, such as the Otzberg Zone on the eastern margin of the Tromm Granite, had a major influence on the location and geometry of the URG. Unfortunately, however, dependable statements about the timing of the formation and activation of local faults in the study area cannot be made because no suitable outcrops of such faults exist.

Bertrand et al. (2020) analyze a comparable aeromagnetic dataset consisting of two separate surveys from the western URG shoulder. Their data were acquired over a significantly larger

area (~1500 km²) than the one presented here, with a greater linespacing of 400 and 500 m, respectively (Gavazzi et al. 2020). They calculated the horizontal derivative of the RTP , which allows a delineation of the Variscan basement blocks, separated by ENE-WNW striking first-order fault zones. Furthermore, a compartmentalization of the N-S striking rift related faults is evident (Bertrand et al. 2020). However, internal structural features within homogeneous basement units are poorly resolved, most likely due to the lower resolution of the magnetic data compared to the Tromm survey.

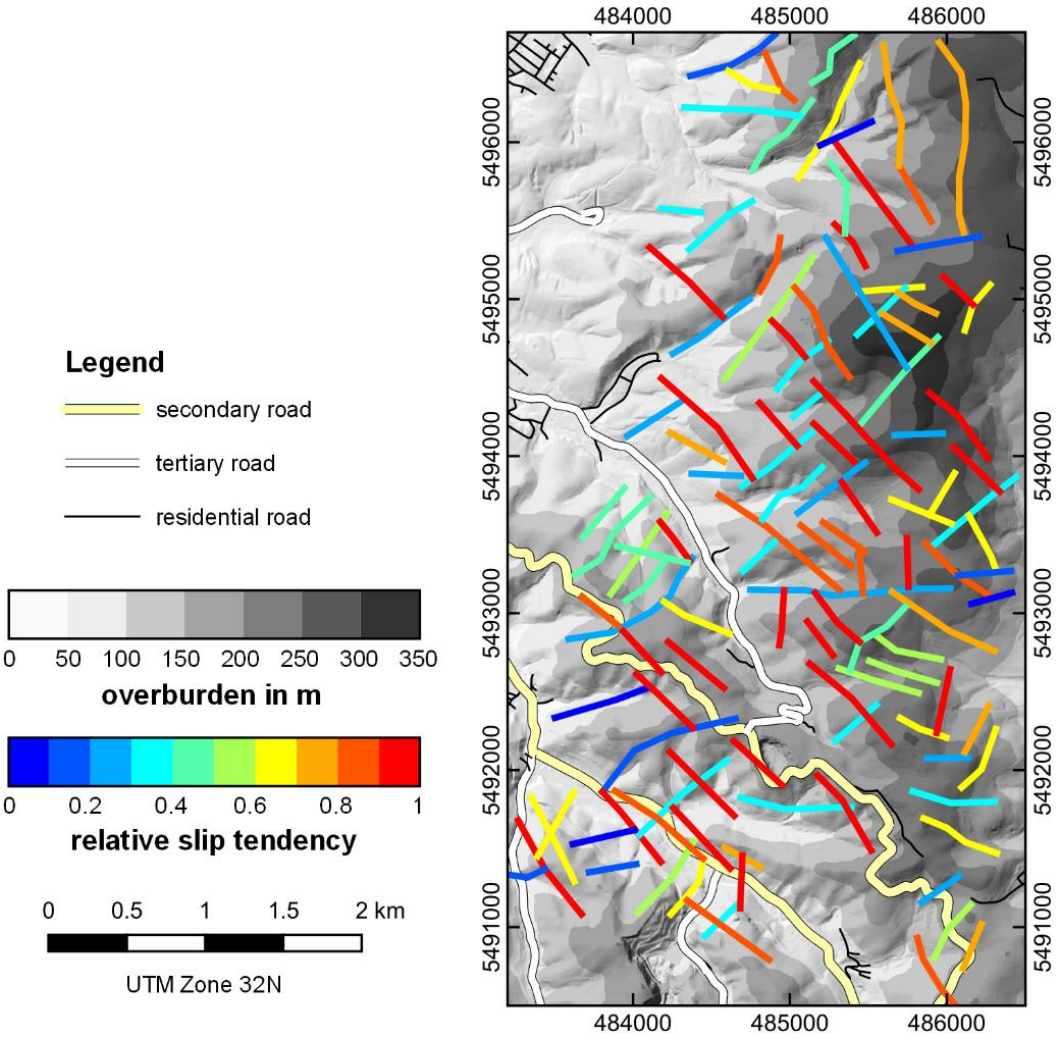

Figure 6.7: Comparison of the maximum overburden over a 1.5 km long horizontal tunnel with the magnetic lineament extracted from the TDR filtered RTP anomalies in the Tromm Granite. The relative slip tendency of the lineaments under the current stress conditions is indicated. Futhermore, the local road infrastructure is plotted on the map.

The aeromagnetic survey presented here is a cornerstone of the preliminary geological-geophysical exploration for GeoLaB. A roughly 13 km² area of the Tromm Granite, for which little structural geological data were previously available, was surveyed at high resolution. The magnetic lineaments in the TDR map (Fig. 6.5) indicate potential fault zones that serve as target structures of GeoLaB. However, in addition to permeable faults, stress conditions unaffected by topography are required, suggesting that the overburden of the approximately 1.5 km long GeoLaB tunnel should be in the range of several hundred meters. Fig. 6.7 compares this overburden with the location of magnetic lineaments. The highest overburden of up to 350 m is reached at the eastern boundary of the survey. Several lineaments are observed in this area, at least five of which have a high reactivation potential (Ts > 0.8). The TDR anomalies should

now serve as a basis for more specific geophysical investigations, for example with terrestrial gravimetry and magnetics, geoelectrics, and reflection seismics. This could provide evidence of the actual existence of faults associated with the magnetic lineaments. The final proof will be ultimately provided by exploratory drilling or the tunnel itself. Once GeoLaB is constructed, detailed susceptibility measurements across fault zones in the tunnel would be useful to verify the interpretation of the magnetic anomalies.

6.7. Conclusions

A high-resolution aeromagnetic dataset of the Tromm Granite (Odenwald, SW Germany) was acquired by drone to map and characterize the natural fault network. The following conclusions can be drawn from the investigations:

- Aeromagnetic surveys allow efficient investigations of large surface areas in rugged and remote regions, such as the Tromm Granite.
- Different filters for enhancing the shortwave magnetic signals have been reviewed and compared using a synthetic model. For the mapping of fault zones, the tilt derivative (TDR), applied after RTP, was shown to be the most reliable method.
- The unfiltered RTP anomalies from the Tromm Granite indicate a concentric zonation of the pluton, which might be associated with the differentiation of the magma chamber during its emplacement.
- The filtered RTP anomalies exhibit more than 100 magnetic lineaments that may be interpreted as potentially permeable fault and fracture zones. The clustering of these lineaments at the maximum slip tendency indicates preferential reactivation of favorably oriented fault planes.
- The TDR anomaly map provides a significant decision-making basis for the site selection process of GeoLaB
- Further exploration using geophysical methods or drilling is required to validate the results presented here.

7. General Discussion

In view of man-made climate change and the current energy crisis resulting from the Ukraine war, dependence on fossil fuels must be minimized as quickly as possible. In addition to established forms of renewable energy, such as wind, solar, biomass, or hydropower, the base-load capable deep geothermal energy will significantly contribute to the energy transition in the coming years. The URG represents a prime region for geothermal utilization, as favorable conditions in the subsurface (high geothermal gradient, high permeability) and above ground (high energy demand, well-developed heating infrastructure, etc.) are combined. Besides the hydrothermal reservoirs in the URG, the crystalline basement could provide an almost inexhaustible amount of heat by developing EGS reservoirs (Paschen et al. 2003; Kock and Kaltschmitt 2012; Bär et al. 2021). Nevertheless, investors have so far been rather hesitant towards this technology due to the high upfront costs, geological uncertainties, and risks associated with stimulation and production.

This thesis aims to advance the geothermal exploitation of crystalline reservoirs in the northern URG by comprehensively characterizing the basement and providing stakeholders with a reliable database for decision making. To overcome the lack of wells and seismic data, a multi-scale, interdisciplinary approach was adopted to explore and model the basement. The investigations carried out can be grouped into two main topics: (A) regional-scale reservoir characterization, modelling, and resource assessment (Chapters 2 – 4), and (B) outcrop-scale fracture and fault network analysis (Chapters 5 & 6). The respective methods and results are discussed below.

7.1. Regional-Scale Modelling and Resource Assessment

The regional 3D basement model was developed by integrating all publicly accessible structural data in the northern URG, with the existing GeORG and Hesse 3D models providing particularly important input (Sass et al. 2011; GeORG Projektteam 2013; Bär et al. 2021). Where these models overlap, the basement top may deviate vertically by several hundred meters, which highlights the large structural uncertainties associated with this horizon. A harmonized depth map was obtained by incorporating the reprocessed Dekorp 9N line (Homuth et al. 2021). Additional valuable insights about the basement structure and composition was derived from potential field data, which are available in high resolution over the whole study area. Regional gravity and magnetic anomalies have already been successfully used in the past to delineate the Variscan belt in the URG (Rotstein et al. 2006; Edel and Schulmann 2009; Edel et al. 2018). The novelty of this thesis lies in the joint stochastic inversion of these datasets (Chapter 3), which significantly reduces the ambiguity of the individual potential fields. This resulted in the most detailed model of the basement to date, although the unit boundaries are still subject to uncertainties of up to 2 or 3 km. Consequently, the model is rather suitable for regional than for local considerations. Uncertainties might be locally reduced by integrating 3D seismic surveys. However, such datasets were not available in the northern URG during the PhD project.

In addition to the 3D geometry of model units, the inversion also yielded information about the distribution of petrophysical properties. By comparing the inverted densities and magnetic susceptibilities with laboratory measurements on rock samples from the MGCH, an interpretative map of the basement lithology beneath the sedimentary cover was generated (Chapter 3, Fig. 11), supported further by outcrops and the few wells. Separation of the predominantly igneous from the predominantly metamorphic basement areas is crucial for

geothermal applications because, as described in Chapter 1.2, permeability may vary by several orders of magnitude depending on the lithology. But it should also be noted that gravity and magnetic anomalies can hardly resolve small-scale lithologic variations at several kilometers depth, like those observed throughout the Odenwald. Thus, the inversion primarily provides regional-scale indications about the lithology, but the actual composition of the basement can ultimately only be determined by drilling.

The inversion results were subsequently integrated into the techno-economic resource assessment for the URG basement (Chapter 4). The volumetric "heat-in-place" method, which has been widely used for more than four decades (Muffler and Cataldi 1978; Tester et al. 2006; Garg and Combs 2015), was applied and further improved. This approach involves a limited number of parameters, allowing the uncertainties to be reasonably quantified using Monte Carlo simulation. It must be noted, however, that the geothermal system is considerably simplified, for example, by disregarding all dynamic processes within the reservoir. Numerical models can theoretically provide more realistic resource estimates, but only if the geological, thermal, hydraulic, and mechanical conditions in the subsurface are accurately known. This is not the case for the basement in the northern URG, meaning that numerical models easily over or underestimate the potential heat production. While some regional numerical models already exist for the URG (Jain et al. 2015; Freymark et al. 2017; Koltzer et al. 2019), they also involve strongly simplified geologic assumptions, making the results not more reliable than those obtained by the heat-in-place method presented here.

The recovery factor R is the most important parameter for calculating the useful geothermal resources and is at the same time subject to the largest uncertainties. Data from a few EGS plants worldwide have been included in the assessment, but unfortunately no R values for geothermal reservoirs on the European mainland have been published so far. At least for Soultz-sous-Forêts, the recovery factor should be determined based on the comprehensive hydraulic data, which would improve future resource estimates in the URG. Major fault zones were proven to be hydraulic conduits in many places (Caine et al. 1996; Evans et al. 1997; Bense et al. 2013), making them the primary targets of all operating geothermal plants in the URG. Recent reactivation and a preferred orientation in the ambient stress field further increases the likelihood of enhanced permeability. Therefore, it is justified to use the reactivation potential (slip and dilation tendency) as additional weights of R. While this approach represents an important step forward in defining suitable exploration targets, it is still a simplification of the actual structural and hydraulic architecture of the fault zones. In fact, Grant (2018) reports a temporal variability of R as a result of temperature decline during extraction, resource replenishment, mineral scaling in fractures, or thermal contraction of the host rock. The R values used in this thesis represent thus broadly estimated averages over the entire power plant lifetime.

The conducted geothermal assessment showed that the resource base in the basement of the northern URG alone exceeds the annual energy demand of Germany by two orders of magnitude. Although only a fraction of this is technically usable, it still amounts to up to 16 PWh. Even by conservative estimates, a large part of the energy supply in the region could therefore be sustainably ensured by geothermal power plants. Under the market conditions in January 2022, geothermal reserves amounted to about 65 % of the resources. In view of the recent massive increases in energy prices, it is likely that even a significantly higher percentage could be utilized with a profit, but at the same time also the investment costs have increased.

The most important controlling factors for the economic operation of geothermal power plants were investigated using a sensitivity analysis. Drilling represents the largest cost driver and accounts for of up to 70 % of the total investments in EGS projects. The development of more efficient drilling methods would therefore considerably advance the expansion of geothermal energy. It is equally important to develop a large and well-connected reservoir to ensure sustained high heat production. For this purpose, suitable drilling targets with elevated initial permeability and temperature must be identified, which is facilitated by this thesis. Second, effective yet safe stimulation measures are critical to the success of the project, but considerable research in this field is still needed.

In the economic assessment, an electricity-driven combined heat and power (CHP) process was assumed, as for example installed in Landau. The business case is relatively simple in this scenario, as the largest revenues are derived from electricity sales, and electricity prices are tied to feed-in tariffs over long time periods. Nevertheless, the interest of municipal energy suppliers in direct use of heat without an intermediary power plant has recently increased significantly. This type of application provides much higher heat output than CHP plants. In addition, lower temperature levels are required, offering considerable potential for saving drilling costs. It should be noted, however, that direct heat use is only viable in areas with high heat demand and existing heat distribution infrastructure. Transporting heat over long distances through newly constructed pipelines will rarely be economical. In this respect, the northern URG offers ideal conditions as an economically strong and densely populated region in which all major cities operate district heating networks. In contrast to electricity generation, prices for heat can be subject to large fluctuations during the project period, often depending on fossil fuel prices. This may pose greater challenges to the economic design of direct heat use than electricity generation.

Apart from the geological, technological, and economic uncertainties, bureaucratic hurdles are hampering the expansion of geothermal energy and other renewables. For a rapid energy transition, approval procedures must be accelerated and simplified immediately. Equally important are increased government investments in geothermal pilot projects, which will encourage more private companies to invest in this sector. Another major concern is the insufficient accessibility of geological data in Germany, even though the Geological Data Act (Geologiedatengesetz) from 2021 stipulates that data should be made available by the state geological surveys after a maximum period of 10 years. Yet, data requests often remain fruitless or take several months to be processed, partly due to a lack of funding for the surveys. A common platform for public data sharing, like in the Netherlands (NLOG 2022), would save enormous time and financial resources during project planning.

7.2. Outcrop-Scale Fault and Fracture Network Characterization

As described above, there is a critical lack of reliable fracture network data from boreholes in the northern URG. Yet, this information is crucial for a reasonable design of the well path and reservoir stimulation as well as predictions of the heat production. To enhance the data availability, a structural characterization of the crystalline basement in the adjacent Odenwald was undertaken as part of this thesis (Fig.7.1). Previously, comprehensive petrophysical analyses were conducted on rock samples from the same area (Weinert et al. 2020). Particularly detailed structural investigations were carried out in the Tromm Granite (Chapter 5), which

presents itself as a well-suited outcrop analog for the granitic reservoirs in the URG (An overview of the structural inventory in the entire Odenwald is provided by Bossennec et al. (2022)). Fracture network properties were determined in five abandoned quarries using lidar scanning, complemented by lineament analysis on a high-resolution DEM. A densely fractured basement with high connectivity of fractures was generally encountered, enabling the development of permeable EGS reservoirs. The dominance of approximately N-S striking fractures is consistent with observations from geothermal reservoirs in the URG (Glaas et al. 2021). However, the influence of larger fault and shear zones such as the Otzberg Zone leads to pronounced lateral variations in both the density and orientation of fractures.

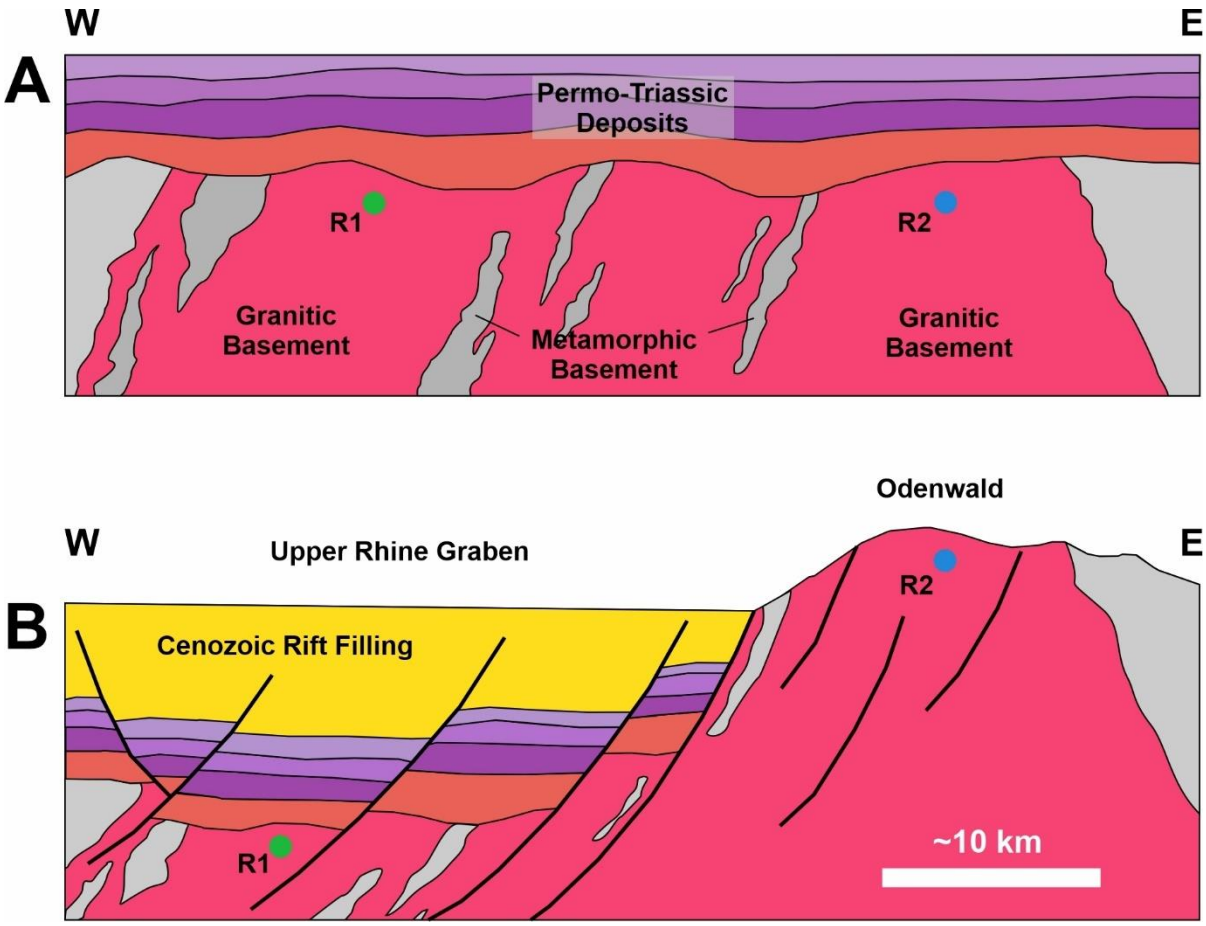

Figure 7.1: Schematic cross-sections through the URG: (A) Pre-rift stage. Reservoirs R1 and R2 are located at approximately the same depth and have comparable lithologic, structural, and hydraulic properties. (B) Post-rift stage. R1 has subsided by several kilometers, while R2 is exhumed at surface. The outcrops of R2 can be used to characterize R1. However, it should be noted that direct transfer of the analogous study of the outcrop to the deep reservoir is not trivial because of the different stress conditions, hydrothermal alteration, and weathering processes.

The investigated quarries in the Tromm Granite provide only selective insights into the fracture network. Most major fault zones in the Odenwald are furthermore buried under Cenozoic sediments, so classical structural geological methods cannot be applied to determine their architecture and hydraulic properties. Additional geophysical surveys were therefore conducted to obtain an area-wide picture of the fracture network and to identify potentially permeable faults. Again, potential field methods (gravimetric and magnetic surveys) were used, because they are comparatively inexpensive, non-invasive, and applicable in rough terrain. Especially through drone-based aeromagnetic measurements, a large, poorly accessible area could be mapped within a few days. Seismic methods would barely be applicable here and it is

questionable whether helpful results could be obtained considering that steeply dipping fractures dominate the structural inventory of the Tromm Granite. Alternatively, the basement could be imaged using electromagnetic methods, but these are costlier and have a poorer lateral resolution than the aeromagnetic data.

The measured gravity anomalies indicate rather wide zones with potentially increased fracture porosity, which are mainly related to the pluton margins and first-order shear zones (Otzberg Zone). Such structures may also be preferred targets for geothermal drilling in the URG, provided they can be identified by geophysical exploration. In lithologically heterogenic areas, gravity data are difficult to interpret in terms of fracture properties, as the two gravity effects of varying matrix density and porosity are virtually inseparable. In comparison, the filtered aeromagnetic survey reveals a better resolved picture of the fracture network within the Tromm pluton (Chapter 6). The observed linear magnetic minima can be interpreted as repeatedly reactivated and possibly hydrothermally altered fracture zones that may exhibit increased permeabilities. Interestingly, the slip tendency correlates well with the distribution of these magnetic lineaments, while there is no correlation with the lineaments extracted from DEMs. This supports the assumption made in the regional resource assessment (Chapter 4) that the reactivation potential is a useful indicator of the fault permeability. Nevertheless, the architecture of fault zones in the basement can be complex and not generalizable, as shown by the measured radon activity concentration (Chapter 5).

The biggest challenge in outcrop analog studies is the upscaling and translation to deep reservoir conditions. Reason for this is that the near-surface fracture network has been significantly overprinted by exhumation and weathering. Furthermore, there is a lack of hydraulic test data from both deep and shallow crystalline reservoirs in the northern URG region, meaning that the structural investigations cannot be validated at the moment. The fracture aperture, which largely controls the permeability, has been particularly affected by these processes. Direct measurements of the parameter in the outcrop are thus of little value. Instead, the presented estimate of reservoir permeability using DFN modelling relies on literature data of fracture aperture mainly based on numerical simulations (Mahmoodpour et al. 2021). The aperture may alternatively be constrained using the local stress tensor (Bisdom et al. 2017). The DFN models show, on the one hand, a wide spread and, on the other hand, a pronounced anisotropy of the basement permeability. Due to the increased density of N-S-directed fractures, the permeability in this direction is at least one order of magnitude higher than in E-W direction. In addition, the N-S fractures have the greatest tendency to remain open in the ambient stress field of the URG. Geothermal wells should consequently be designed in such a way that as many of these hydraulically active fractures as possible are penetrated by the open-hole section. Since the fractures are primarily steeply dipping, the use of horizontal wells parallel to σ_{hmin} is recommended. During stimulation, a steep ellipsoidal reservoir will form that is oriented parallel to σ_{Hmax} (Stober et al. 2016).

7.3. Outlook

The applied joint inversion generally proved suitable for modelling the basement in the northern URG. It is therefore desirable to extend the methodology to the central and southern URG, which would provide more consistent insights into the basement's internal structure and allow quantification of resources throughout the region. In addition to the presented inversion workflow, the influence of individual inversion parameters on the data fit should be examined in more detail by a sensitivity analysis. Gravity and magnetic data are available for the whole

URG, but with widely varying quality and resolution. For this reason, careful reprocessing and harmonizing the datasets would be necessary. In contrast to the Odenwald, few petrophysical data exist for the Black Forest and the Vosges. Adequate parameterization of the model would thus require further sampling and laboratory analyses. Once the model is extended to the South, potential applications of closed loop systems or seasonal underground thermal energy storage (UTES) will need to be evaluated in addition to EGS resources. This ensures that the entire utilization potential of the crystalline basement is explored, which will be essential for a successful energy transition.

The presented geothermal model provides a primarily regional overview of the EGS resources in the northern URG basement. This is useful for an initial site selection and early-stage planning of geothermal wells but cannot replace site-specific exploration efforts. In this context, local numerical models are crucial to simulate the coupled thermo-hydraulic-chemical-mechanical processes in the basement. By considering the dynamic variations of the reservoir, more accurate predictions of the temperature, hydraulic yield and potential heat production rates is feasible. Similarly, different well path designs or the characteristics of the targeted fault zones could be systematically investigated. The reliability of the simulation results depends strongly on the quality of the input data. The regional model could serve as a starting point but should be improved by integrating 3D seismic data. Model parameterization, especially concerning hydraulic properties, could be based on the outcrop analog studies in the Odenwald. However, when transferring the fracture network characteristics to reservoir conditions, care must be taken. Ideally, one or more low-cost exploration wells are drilled in the concession area, which would allow an analysis of the in situ structural and hydraulic properties and thereby significantly reduce the geological uncertainties and advance the numerical simulations.

The upcoming GeoLaB (Geothermal Laboratory in the Mine) project marks a milestone towards the large-scale utilization of geothermal resources in the crystalline basement (KIT 2022). It represents the world's first underground laboratory designed and built exclusively for geothermal investigations. It will be constructed at the eastern edge of the URG under the lead of the Karlsruhe Institute of Technology KIT, the German Research Center for Geosciences GFZ, and the Helmholtz Centre for Environmental Research UFZ. The unique research infrastructure will consist of a new, about 1.5 km long gallery 500 m below surface, from which several caverns will be excavated (Fig. 8.1). In these caverns, high flowrate experiments will be carried out on selected fault zones, leading to a significantly improved understanding of geothermal transport processes under in situ conditions. The project focuses on the development of advanced stimulation procedures, aiming to reduce the risk of severe induced seismicity. Additional aspects of reservoir technology, such as tunnel and wellbore stability, will furthermore be addressed. The Tromm Granite, which was extensively analyzed in this thesis, presents a well-suited site for GeoLaB according to the criteria catalogue of Schill et al. (2016). The structural and geophysical investigations (chapters 5 & 6) presented herein will thus be an important basis for the site selection and gallery planning. Based on the lineament analysis, aeromagnetic survey, and gravity measurements, potentially permeable fault zones may be identified, which should be further characterized by additional exploration measures, such as 2D and 3D seismic, geoelectrical, and electromagnetic surveying, prior to the construction phase. Once GeoLaB is established, the DFN modelling (chapter 5) can be validated with hydraulic in situ test data. Likewise, the interpretation of the aeromagnetic data could be verified by systematically measuring the magnetic susceptibility across fault zones cut by the tunnel. One of the major scientific challenges GeoLaB faces is that test results at 500 m depth

are not directly representative of conditions in the deeper URG. In this regard, the multi-scale dataset presented in this thesis will be very valuable in projecting the findings from the stimulation experiments to reservoir depth.

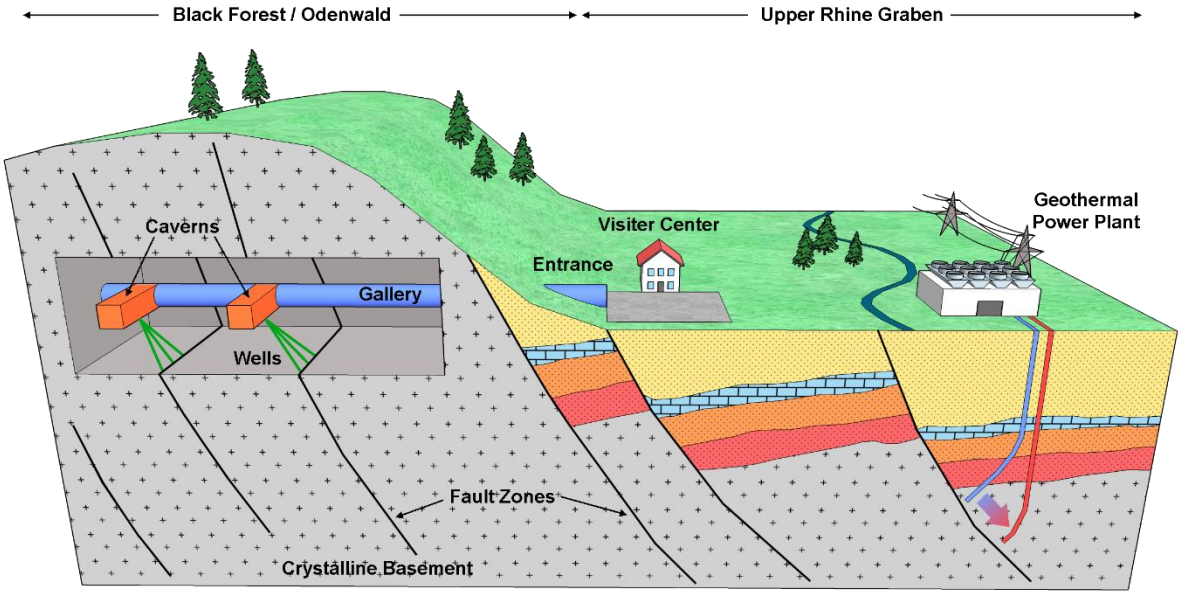

Figure 7.2: Schematic illustration of the planned GeoLaB research infrastructure in the Black Forest or Odenwald (adapted from Schätzler et al. 2020).

8. Conclusions

The expansion of deep geothermal energy is essential for a successful energy transition and for achieving the binding climate protection goals. Although it has been known for decades that the crystalline basement holds by far the largest geothermal resources, the focus of geothermal research and utilization has so far been on shallower hydrothermal systems, where geological uncertainties and project risks are usually lower. To overcome the lack of borehole and 3D seismic datasets in the basement, this thesis applied an interdisciplinary and multiscale workflow to characterize the reservoir, with the northern URG as example (Fig. 8.1). For the first time, a joint inversion of gravity and magnetics data for regional 3D modeling was performed for this region. With this newly developed model, a significantly refined resource assessment was done, allowing the selection of potentially attractive drill targets. Nevertheless, significant uncertainties remain, necessitating additional site-specific exploration efforts (3D seismic, electromagnetic methods, high-resolution gravity and magnetics surveys). The fracture network properties were analyzed in a detailed outcrop analog study. A novel approach was designed, combining structural geological and geophysical methods. By integrating the different datasets, potentially permeable fault zones could be identified. Thus, the investigations are highly beneficial for the site selection of GeoLaB and the subsequent evaluation of the stimulation experiments.

The key findings of this thesis are again summarized in the following:

- The URG offers excellent opportunities for deep geothermal exploitation, with the extensive knowledge of the subsurface, the high geothermal gradient, and several potential exploitation horizons. At the same time, the region is characterized by a high socio-economic-environmental potential. In particular, the surface energy demand is high, and the district heating infrastructure is well developed.
- Gravity and magnetics data proved valuable for characterizing the crystalline basement on both regional and local scales. Joint inversion of these datasets provided new insights into the structure and composition of the basement and indicated remaining uncertainties. Accordingly, the northern URG is most likely dominated by granitoids, which are the preferred targets of EGS projects.
- Potentially exploitable geothermal resources in the crystalline basement of the northern URG range from 8.2 to 16.1 PWh_{th}, greatly exceeding the region's heating demand. The highest doublet productivity is expected along major, recently reactivated fault zones. Slip and dilation tendency are appropriate indicators of the reactivation potential and thus fault permeability.
- More than half of the resources are likely to be economically recoverable, but this is highly sensitive to site-specific conditions and current market demand. The economic assessment is therefore strongly time-dependent.
- By integrating structural geology and geophysics, the basement's permeability structure in the outcrop could be analyzed in detail. Aeromagnetics appeared to be the most suitable method for mapping potentially permeable zones. Accordingly, high-resolution magnetic datasets could also be used in the URG for reservoir characterization as a cost-effective alternative to 3D seismic and exploration wells.
- The result transfer from the outcrop analog study to the deep reservoirs in the URG is not trivial, due to the inherently different stress regimes and alteration processes. DFN models are useful to assess hydraulic properties under assumed reservoir conditions.

These models should be validated with hydraulic test data as soon as such data become available in the northern URG.

- Finally, induced seismicity remains a major challenge in the development and operation of EGS reservoirs. This thesis applied a set of methods for locating areas of naturally elevated permeability that should be preferred as drilling targets. In these locations, lower injection pressures may be required to achieve adequate flow rates, reducing the risk of large induced seismic events. However, safe soft stimulation methods still need to be developed for the widespread use of the EGS technology. Great hopes are therefore placed on the GeoLaB project and its associated scientific program.

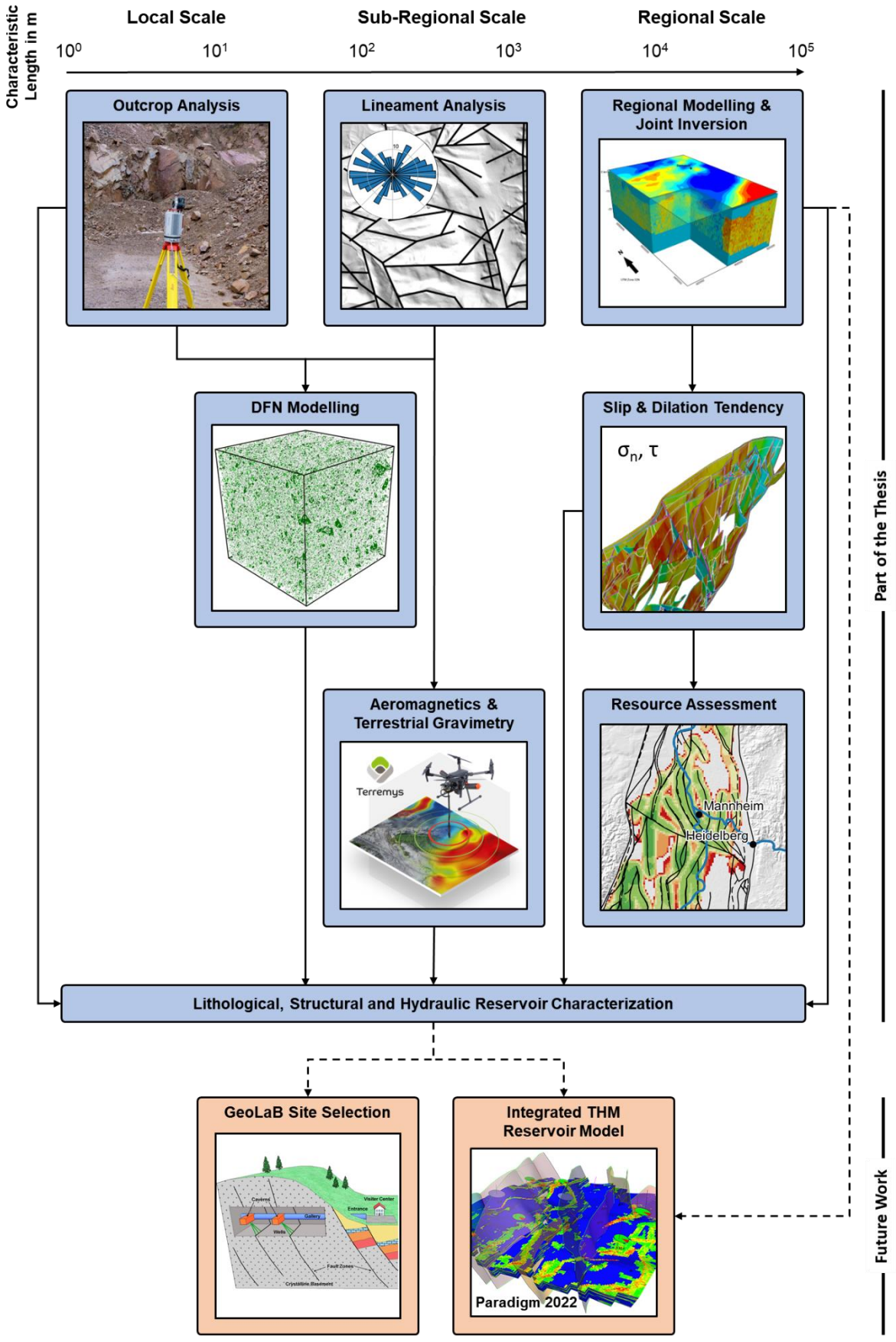

Figure 8.1: Summary and connection of the main work packages of this thesis (blue boxes). The scale of the individual investigations is indicated in each case. Orange boxes show future work packages that were not yet part of the thesis.

9. References

Achtziger-Zupančič, P.; Loew, S.; Mariéthoz, G. (2017): A new global database to improve predictions of permeability distribution in crystalline rocks at site scale. In *J. Geophys. Res.* 122 (5), pp. 3513–3539. DOI: 10.1002/2017JB014106.

AEE (2020): Anteile Erneuerbarer Energien an Strom, Wärme und Verkehr in Deutschland 1990-2020. Agentur für Erneuerbare Energien. Available online at https://www.unendlich-viel-energie.de/mediathek/grafiken/anteile-der-erneuerbaren-energien-in-den-sektoren, checked on 8/5/2022.

AEE (2022): Grafiken. Agentur für Erneuerbare Energien. Available online at https://www.unendlich-viel-energie.de/mediathek/grafiken?page=2, checked on 8/31/2022.

Agemar, Thorsten; Alten, Jessica-Aileen; Ganz, B.; Kuder, J.; Kühne, K.; Schumacher, S.; Schulz, R. (2010): GeotIS–das Geothermische Informationssystem für Deutschland. In *Der Geothermiekongress*.

Agemar, Thorsten; Schellschmidt, Rüdiger; Schulz, Rüdiger (2012): Subsurface Temperature Distribution of Germany. In *Geothermics* 44, pp. 65–77. DOI: 10.1016/j.geothermics.2012.07.002.

Ahlers, Steffen; Henk, Andreas; Hergert, Tobias; Reiter, Karsten; Müller, Birgit; Röckel, Luisa et al. (2021): 3D crustal stress state of Germany according to a data-calibrated geomechanical model. In *Solid Earth* 12 (8), pp. 1777–1799. DOI: 10.5194/se-12-1777-2021.

Altherr, R.; Henes-Klaiber, U.; Hegner, E.; Satir, M.; Langer, C. (1999): Plutonism in the Variscan Odenwald (Germany): from subduction to collision. In *International Journal of Earth Sciences* 88 (3), pp. 422–443. DOI: 10.1007/s005310050276.

Amstutz, G. C.; Meisl, S.; Nickel, E. (Eds.) (1975): Mineralien und Gesteine im Odenwald. Heidelberg.

Annoni, P.; Bolsi, P. (2020): The regional dimension of social progress in Europe: Presenting the new EU Social Progress Index. In *European Union Regional Policy Working Papers, WP 06/2020*.

Antolín-Tomás, B.; Román-Berdiel, T.; Casas-Sainz, A.; Gil-Peña, I.; Oliva, B.; Soto, R. (2009): Structural and magnetic fabric study of the Marimanha granite (Axial Zone of the Pyrenees). In *International Journal of Earth Sciences* 98 (2), pp. 427–441. DOI: 10.1007/s00531-007-0248-1.

Aydin, Ali; Ferré, Eric C.; Aslan, Zafer (2007): The magnetic susceptibility of granitic rocks as a proxy for geochemical composition: Example from the Saruhan granitoids, NE Turkey. In *Tectonophysics* 441 (1-4), pp. 85–95. DOI: 10.1016/j.tecto.2007.04.009.

Baisch, Stefan; Vörös, Robert; Rothert, Elmar; Stang, Henrik; Jung, Reinhard; Schellschmidt, Rüdiger (2010): A numerical model for fluid injection induced seismicity at Soultz-sous-Forêts. In *International Journal of Rock Mechanics and Mining Sciences* 47 (3), pp. 405–413. DOI: 10.1016/j.ijrmms.2009.10.001.

Bär, K. (2012): Assessment of the deep geothermal potentials of Hessen (Untersuchung der tiefengeothermischen Potenziale von Hessen). PhD thesis. Technische Universität Darmstadt.

Bär, K.; Reinsch, T.; Bott, J. (2020): The PetroPhysical Property Database (P^3) – a global compilation of lab-measured rock properties. In *Earth Syst. Sci. Data* 12 (4), pp. 2485–2515. DOI: 10.5194/essd-12-2485-2020.

Bär, K.; Schäffer, Rafael; Weinert, S.; Sass, I. (2021): Schlussbericht Verbundprojekt „Hessen 3D 2.0“. 3D-Modell der geothermischen Tiefenpotenziale von Hessen. Technical University Of Darmstadt.

Bär, Kristian; Rühaak, Wolfram; Welsch, Bastian; Schulte, Daniel; Homuth, Sebastian; Sass, Ingo (2015): Seasonal High Temperature Heat Storage with Medium Deep Borehole Heat Exchangers. In *Energy Procedia* 76, pp. 351–360. DOI: 10.1016/j.egypro.2015.07.841.

Barati, Reza; Liang, Jenn-Tai (2014): A review of fracturing fluid systems used for hydraulic fracturing of oil and gas wells. In *J. Appl. Polym. Sci.* 131 (16), n/a-n/a. DOI: 10.1002/app.40735.

Barton, Colleen A.; Zoback, Mark D.; Moos, Daniel (1995): Fluid flow along potentially active faults in crystalline rock. In *Geology* 23 (8), p. 683. DOI: 10.1130/0091-7613(1995)023<0683:FFAPAF>2.3.CO;2.

Bauer, Mathias Jürgen (Ed.) (2014): Handbuch Tiefe Geothermie. Prospektion, Exploration, Realisierung, Nutzung. Berlin, Heidelberg: Springer Spektrum.

Baujard, C.; Genter, A.; Dalmais, E.; Maurer, V.; Hehn, R.; Rosillette, R. et al. (2017): Hydrothermal characterization of wells GRT-1 and GRT-2 in Rittershoffen, France: Implications on the understanding of natural flow systems in the rhine graben. In *Geothermics* 65, pp. 255–268. DOI: 10.1016/j.geothermics.2016.11.001.

Baumgärtner, J.; Kölbel, T.; Mergner, H.; Schlagermann, Pascal; Hettkamp, T.; Teza, D.; Lerch, C. (2013a): Betriebserfahrungen mit den Geothermiekraftwerken Landau, Insheim und Bruchsal. In *BBR Fachmagazine fur Brunnen und Leitungsbau*, pp. 48–57.

Baumgärtner, J.; Teza, D.; Wahl, G. (2013b): Gewinnung geothermischer Energie durch Entwicklung und Zirkulation eines Störungssystems im Kristallin und deren mikroseismische Überwachung am Beispiel des Geothermieprojektes Insheim (Internal Report No. 0325158). Bestec GmbH. Landau, Germany.

Behrmann, Jan H.; Hermann, Oliver; Horstmann, Mathias; Tanner, David C.; Bertrand, Guillaume (2003): Anatomy and kinematics of oblique continental rifting revealed: A three-dimensional case study of the southeast Upper Rhine graben (Germany). In *Bulletin* 87 (7), pp. 1105–1121. DOI: 10.1306/02180300153.

Benn, Keith; Ham and, Natalie M.; Pignotta, Geoffrey S.; Bleeker, Wouter (1998): Emplacement and deformation of granites during transpression: magnetic fabrics of the Archean Sparrow pluton, Slave Province, Canada. In *Journal of Structural Geology* 20 (9-10), pp. 1247–1259. DOI: 10.1016/S0191-8141(98)00065-0.

Bense, V. F.; Gleeson, T.; Loveless, S. E.; Bour, O.; Scibek, J. (2013): Fault zone hydrogeology. In *Earth-Science Reviews* 127, pp. 171–192. DOI: 10.1016/j.earscirev.2013.09.008.

Benson, S. M.; Cole, D. R. (2008): CO2 Sequestration in Deep Sedimentary Formations. In *Elements* 4 (5), pp. 325–331. DOI: 10.2113/gselements.4.5.325.

Bertleff, B.; Joachim, H.; Koziorowski, G.; Leiber, J.; Ohmert, W.; Prestel, R. et al. (1988): Ergebnisse der Hydrogeothermiebohrungen in Baden-Württemberg. In *Jh Geol Landesamt Baden-Württemb* 30, pp. 27–116.

Bertrand, L.; Gavazzi, B.; Mercier de Lépinay, J.; Diraison, M.; Géraud, Y.; Munschy, M. (2020): On the Use of Aeromagnetism for Geological Interpretation: 2. A Case Study on Structural and Lithological Features in the Northern Vosges. In *J. Geophys. Res.* 125 (5). DOI: 10.1029/2019JB017688.

BGR (2016): Geologische Karte der Bundesrepublik Deutschland 1 : 1 000 000 (GK1000).

Biermann, F.; Boas, I. (2008): Protecting Climate Refugees: The Case for a Global Protocol. In *Environment: Science and Policy for Sustainable Development* 50 (6), pp. 8–17. DOI: 10.3200/ENVT.50.6.8-17.

Bisdom, K.; Nick, H. M.; Bertotti, G. (2017): An integrated workflow for stress and flow modelling using outcrop-derived discrete fracture networks. In *Computers & Geosciences* 103, pp. 21–35. DOI: 10.1016/j.cageo.2017.02.019.

Bloomfield, K. K.; Laney, P. T. (2005): Estimating well costs for enhanced geothermal system applications. Idaho National Lab.(INL), Idaho Falls, ID (United States).

BMU (2016): Klimaschutzplan 2050. Klimaschutzpolitische Grundsätze und Ziele der Bundesregierung. Bundesministerium für Umwelt, Naturschutz und nukleare Sicherheit. Berlin. Available online at https://www.bmuv.de/fileadmin/Daten_BMU/Download_PDF/Klimaschutz/klimaschutzplan_2050_bf.pdf, checked on 8/5/2022.

Boissavy, C.; Henry, L.; Genter, A.; Pomart, A.; Rocher, P.; Schmidlé-Bloch, V. (2019): Geothermal Energy Use, Country Update for France. In : Proceedings. European Geothermal Congress. Den Haag, 11.-14. June.

Bossennec, Claire; Géraud, Yves; Böcker, Johannes; Klug, Bernd; Mattioni, Luca; Bertrand, Lionel; Moretti, Isabelle (2021): Characterisation of fluid flow conditions and paths in the Buntsandstein Gp. sandstones reservoirs, Upper Rhine Graben. In *Bulletin de la Société Géologique de France* 192, p. 35. DOI: 10.1051/bsgf/2021027.

Bossennec, Claire; Seib, Lukas; Frey, Matthis; van der Vaart, Jeroen; Sass, Ingo (2022): Structural Architecture and Permeability Patterns of Crystalline Reservoir Rocks in the Northern Upper Rhine Graben: Insights from Surface Analogues of the Odenwald. In *Energies* 15 (4), p. 1310. DOI: 10.3390/en15041310.

Breede, Katrin; Dzebisashvili, Khatia; Liu, Xiaolei; Falcone, Gioia (2013): A systematic review of enhanced (or engineered) geothermal systems: past, present and future. In *Geothermal Energy* Geothermal Energy 2013, 1:4. DOI: 10.1186/2195-9706-1-4.

Brown, D. (1997): Review of Fenton Hill HDR test results. In : Proceedings. New Energy and Industrial Technology Development Organization (NEDO) geothermal and HRD conference. Sendai, Japan, 10.-17. March.

Buchner, Frank (1981): Rhinegraben: Horizontal stylolites indicating stress regimes of earlier stages of rifting. In *Tectonophysics* 73 (1-3), pp. 113–118. DOI: 10.1016/0040-1951(81)90178-5.

Bundesregierung (2021a): Klimaschutzgesetz 2021: Generationenvertrag für das Klima. Available online at https://www.bundesregierung.de/breg-de/themen/klimaschutz/klimaschutzgesetz-2021-1913672, checked on 8/5/2022.

Bundesregierung (2021b): Mehr Fortschritt wagen. Bündnis für mehr Freiheit, Gerechtigkeit und Nachhaltigkeit. Koalitionsvertrag zwischen SPD, BÜNDNIS 90/DIE GRÜNEN und FDP. Available online at https://www.bundesregierung.de/breg-de/service/gesetzesvorhaben/koalitionsvertrag-2021-1990800, checked on 8/8/2022.

Bundesverband Geothermie (2022): Liste der Geothermieanlagen Tiefe Geothermie 2022. Available online at https://www.geothermie.de/geothermie/geothermie-in-zahlen.html, checked on 8/5/2022.

Caine, Jonathan Saul; Evans, James P.; Forster, Craig B. (1996): Fault zone architecture and permeability structure. In *Geology* 24 (11), p. 1025. DOI: 10.1130/0091-7613(1996)024<1025:FZAAPS>2.3.CO;2.

Chamorro, César R.; García-Cuesta, José L.; Mondéjar, María E.; Pérez-Madrazo, Alfonso (2014): Enhanced geothermal systems in Europe: An estimation and comparison of the technical and sustainable potentials. In *Energy* 65, pp. 250–263. DOI: 10.1016/j.energy.2013.11.078.

Cherkasov, Sergey; Kapshtan, Dmitry (2017): Unmanned Aerial Systems for Magnetic Survey. In George Dekoulis (Ed.): Drones - Applications: InTech.

Clark, David A. (2020): Don Emerson's best of Exploration Geophysics. In *Preview* 2020 (205), pp. 43–68. DOI: 10.1080/14432471.2020.1751793.

Cooper, G.R.J.; Cowan, D. R. (2006): Enhancing potential field data using filters based on the local phase. In *Computers & Geosciences* 32 (10), pp. 1585–1591. DOI: 10.1016/j.cageo.2006.02.016.

Cordell, L. (1979): Gravimetric expression of graben faulting in Santa Fe country and the Espanola Basin, New Mexico. In R. V. Ingersoll, L. A. Woodward, H. L. James (Eds.): New Mexico Geological Society 30th Annual Fall Field Conference Guidebook, pp. 59–64.

Cornet, F. H.; Helm, J.; Poitrenaud, H.; Etchecopar, A. (1997): Seismic and Aseismic Slips Induced by Large-scale Fluid Injections. In *Pure appl. geophys.* 150, pp. 563–583. DOI: 10.1007/978-3-0348-8814-1_12.

Cuenot, N.; Faucher, J.-P.; Fritsch, D.; Genter, A.; Szablinski, D. (2008): The European EGS project at Soultz-sous-Forêts: From extensive exploration to power production. In : Conversion and delivery of electrical energy in the 21st century. 2008 IEEE Power and Energy Society general meeting ; 20 - 24 July 2008, Pittsburgh, Pennsylvania. 2008 IEEE Power & Energy Society General Meeting. Pittsburgh, PA, 7/20/2008 - 7/24/2008. IEEE Power Engineering Society; IEEE Power and Energy Society general meeting; PES general meeting. Pittsburgh, Pa.: IEEE, pp. 1–8.

Cummings, R. G.; Morris, G. E. (1979): Economic modeling of electricity production from hot dry rock geothermal reservoirs: methodology and analyses. Final Report. Research Project 1017 LASL (LA-7888-HDR).

Decancq, Koen; Lugo, María Ana (2013): Weights in Multidimensional Indices of Wellbeing: An Overview. In *Econometric Reviews* 32 (1), pp. 7–34. DOI: 10.1080/07474938.2012.690641.

Deichmann, N.; Giardini, D. (2009): Earthquakes Induced by the Stimulation of an Enhanced Geothermal System below Basel (Switzerland). In *Seismological Research Letters* 80 (5), pp. 784–798. DOI: 10.1785/gssrl.80.5.784.

Destatis (2022a): Daten zur Energiepreisentwicklung. Statistische Bundesamt. Available online at https://www.destatis.de/DE/Themen/Wirtschaft/Preise/Publikationen/Energiepreise/energiepreisentwicklung-pdf-5619001.pdf?__blob=publicationFile, checked on 8/8/2022.

Destatis (2022b): Stromerzeugung im 1. Quartal 2022: Kohle weiter wichtigster Energieträger. Statistische Bundesamt. Available online at https://www.destatis.de/DE/Presse/Pressemitteilungen/2022/06/PD22_233_43312.html, checked on 8/5/2022.

Destatis (2022c): Verbraucherpreisindex und Inflationsrate. Statistische Bundesamt. Available online at https://www.destatis.de/DE/Themen/Wirtschaft/Preise/Verbraucherpreisindex/_inhalt.html, checked on 8/5/2022.

Dezayes, C.; Gentier, S.; Genter, A. (2005): Deep Geothermal Energy in Western Europe: The Soultz-Project. Final Report. BRGM/RP-54227-FR. BRGM.

Dèzes, P.; Schmid, S. M.; Ziegler, P. A. (2004): Evolution of the European Cenozoic Rift System: interaction of the Alpine and Pyrenean orogens with their foreland lithosphere. In *Tectonophysics* 389 (1-2), pp. 1–33. DOI: 10.1016/j.tecto.2004.06.011.

DIE ZEIT (2023): Energiemonitor. Die wichtigsten Daten zur Energieversorgung – täglich aktualisiert. Available online at https://www.zeit.de/wirtschaft/energiemonitor-deutschland-gaspreis-spritpreis-energieversorgung, checked on 1/15/2023.

Dorbath, Louis; Evans, Keith; Cuenot, Nicolas; Valley, Benoît; Charléty, Jean; Frogneux, Michel (2010): The stress field at Soultz-sous-Forêts from focal mechanisms of induced seismic events: Cases of the wells GPK2 and GPK3. In *Comptes Rendus Geoscience* 342 (7-8), pp. 600–606. DOI: 10.1016/j.crte.2009.12.003.

Dornstadter, J.; Kappelmeyer, O.; Welter, M. (1999): The geothermal potential in the Upper Rhine Graben valley. In : Proceedings of the. European Geothermal Conference Basel 1999. Basel, Switzerland, 28.-30. September.

Duringer, Philippe; Aichholzer, Coralie; Orciani, Sergio; Genter, Albert (2019): The complete lithostratigraphic section of the geothermal wells in Rittershoffen (Upper Rhine Graben, eastern France): a key for future geothermal wells. In *Bulletin de la Société Géologique de France* 190, p. 13. DOI: 10.1051/bsgf/2019012.

Edel, J. B.; Maurer, V.; Dalmais, E.; Genter, A.; Richard, A.; Letourneau, O.; Hehn, R. (2018): Structure and nature of the Palaeozoic basement based on magnetic, gravimetric and seismic investigations in the central Upper Rhinegraben. In *Geothermal Energy* 6 (1), p. 13. DOI: 10.1186/s40517-018-0099-y.

Edel, J. B.; Schulmann, K. (2009): Geophysical constraints and model of the "Saxothuringian and Rhenohercynian subductions - magmatic arc system" in NE France and SW Germany. In *Bulletin De La Societe Geologique De France - BULL SOC GEOL FR* 180, pp. 545–558. DOI: 10.2113/gssgfbull.180.6.545.

Edel, J. B.; Schulmann, K.; Rotstein, Y. (2007): The Variscan tectonic inheritance of the Upper Rhine Graben: evidence of reactivations in the Lias, Late Eocene–Oligocene up to the recent. In *International Journal of Earth Sciences* 96 (2), pp. 305–325. DOI: 10.1007/s00531-006-0092-8.

Ellsworth, William L.; Giardini, Domenico; Townend, John; Ge, Shemin; Shimamoto, Toshihiko (2019): Triggering of the Pohang, Korea, Earthquake (Mw 5.5) by Enhanced Geothermal System Stimulation. In *Seismological Research Letters* 90 (5), pp. 1844–1858. DOI: 10.1785/0220190102.

Evans, James P.; Forster, Craig B.; Goddard, James V. (1997): Permeability of fault-related rocks, and implications for hydraulic structure of fault zones. In *Journal of Structural Geology* 19 (11), pp. 1393–1404. DOI: 10.1016/S0191-8141(97)00057-6.

Evans, Keith; Zappone, Alba; Kraft, Toni; Deichmann, Nicolas; Moia, Fabio (2012): A survey of the induced seismic responses to fluid injection in geothermal and CO2 reservoirs in Europe. In *Geothermics* 41, pp. 30–54. DOI: 10.1016/j.geothermics.2011.08.002.

Fäh, Donat; Gisler, Monika; Jaggi, Bernard; Kästli, Philipp; Lutz, Thomas; Masciadri, Virgilio et al. (2009): The 1356 Basel earthquake: an interdisciplinary revision. In *Geophys J Int* 178 (1), pp. 351–374. DOI: 10.1111/j.1365-246X.2009.04130.x.

Farbotko, Carol; Lazrus, Heather (2012): The first climate refugees? Contesting global narratives of climate change in Tuvalu. In *Global Environmental Change* 22 (2), pp. 382–390. DOI: 10.1016/j.gloenvcha.2011.11.014.

Faulkner, D. R.; Jackson, C.A.L.; Lunn, R. J.; Schlische, R. W.; Shipton, Z. K.; Wibberley, C.A.J.; Withjack, M. O. (2010): A review of recent developments concerning the structure, mechanics and fluid flow properties of fault zones. In *Journal of Structural Geology* 32 (11), pp. 1557–1575. DOI: 10.1016/j.jsg.2010.06.009.

Ferrill, David A.; Morris, Alan P. (2003): Dilational normal faults. In *Journal of Structural Geology* 25 (2), pp. 183–196. DOI: 10.1016/S0191-8141(02)00029-9.

Fletcher, John M.; Teran, Orlando J.; Rockwell, Thomas K.; Oskin, Michael E.; Hudnut, Kenneth W.; Spelz, Ronald M. et al. (2020): An analysis of the factors that control fault zone architecture and the importance of fault orientation relative to regional stress. In *GSA Bulletin* 132 (9-10), pp. 2084–2104. DOI: 10.1130/B35308.1.

Fossen, Haakon (2016): Structural geology. Second edition. Cambridge: Cambridge University Press.

Frey, M.; Bär, K.; Sass, I. (2020): Magnetic Susceptibility of Rock Samples of the Northern Upper Rhine Graben Region and Adjacent Areas. Technical University Of Darmstadt.

Frey, M.; Bossennec, C.; Seib, L.; Bär, K.; Schill, E.; Sass, I. (2022a): Interdisciplinary fracture network characterization in the crystalline basement: a case study from the Southern Odenwald, SW Germany. In *Solid Earth* 13 (6), pp. 935–955. DOI: 10.5194/se-13-935-2022.

Frey, M.; van der Vaart, J.; Bär, K. (2022b): Socio-Economic Potential Mapping for Deep Geothermal Energy in the Upper Rhine Graben. Report WP T1 - 2.3: DGE-Rollout Project.

Frey, Matthis; Bär, Kristian; Stober, Ingrid; Reinecker, John; van der Vaart, Jeroen; Sass, Ingo (2022c): Assessment of deep geothermal research and development in the Upper Rhine Graben. In *Geotherm Energy* 10 (1). DOI: 10.1186/s40517-022-00226-2.

Freymark, Jessica; Sippel, Judith; Scheck-Wenderoth, Magdalena; Bär, K.; Stiller, Manfred; Fritsche, Johann-Gerhard; Kracht, Matthias (2017): The deep thermal field of the Upper Rhine Graben. In *Tectonophysics* 694, pp. 114–129. DOI: 10.1016/j.tecto.2016.11.013.

Garg, Sabodh K.; Combs, Jim (2015): A reformulation of USGS volumetric "heat in place" resource estimation method. In *Geothermics* 55, pp. 150–158. DOI: 10.1016/j.geothermics.2015.02.004.

Gavazzi, B.; Bertrand, L.; Munschy, M.; Mercier de Lépinay, J.; Diraison, M.; Géraud, Y. (2020): On the Use of Aeromagnetism for Geological Interpretation: 1. Comparison of Scalar and Vector Magnetometers for Aeromagnetic Surveys and an Equivalent Source Interpolator for Combining, Gridding, and Transforming Fixed Altitude and Draping Data Sets. In *J. Geophys. Res.* 125 (5). DOI: 10.1029/2019JB018870.

Genter, A.; Traineau, H. (1996): Analysis of macroscopic fractures in granite in the HDR geothermal well EPS-1, Soultz-sous-Foreˆts, France. In *Journal of Volcanology and Geothermal Research* 72 (1-2), pp. 121–141. DOI: 10.1016/0377-0273(95)00070-4.

Genter, Albert; Evans, Keith; Cuenot, Nicolas; Fritsch, Daniel; Sanjuan, Bernard (2010): Contribution of the exploration of deep crystalline fractured reservoir of Soultz to the knowledge of enhanced geothermal systems (EGS). In *Comptes Rendus Geoscience* 342 (7-8), pp. 502–516. DOI: 10.1016/j.crte.2010.01.006.

GeORG Projektteam (2013): Geopotenziale des tieferen Untergrundes im Oberrheingraben. Fachlich-Technischer Abschlussbericht des INTERREG-Projekts GeORG. Teil 1: Ziele und Ergebnisse des Projekts (Zusammenfassung). With assistance of G. Sokol, E. Nitsch, B. Anders, L. Beccaletto, L. Capar, D. C. Mermy et al. Edited by LGRB / BRGM / LGB / AUG. Freiburg i.Br. / Mainz / Strasbourg / Basel.

Gérard, A.; Kappelmeyer, O. (1987): The Soultz-sous-Forêts project. In *Geothermics* 16 (4), pp. 393–399. DOI: 10.1016/0375-6505(87)90018-6.

Ghassemi, A.; Tarasovs, S.; Cheng, A.H.-D. (2007): A 3-D study of the effects of thermomechanical loads on fracture slip in enhanced geothermal reservoirs. In *International Journal of Rock Mechanics and Mining Sciences* 44 (8), pp. 1132–1148. DOI: 10.1016/j.ijrmms.2007.07.016.

Gischig, V. S.; Preisig, G. (2015): Hydro-Fracturing Versus Hydro-Shearing: A Critical Assessment of Two Distinct Reservoir Stimulation Mechanisms. In ISRM (Ed.): Proceedings. 13th ISRM International Congress of Rock Mechanics. Montreal, Canada, May 2015.

Glaas, C.; Vidal, J.; Genter, A. (2021): Structural characterization of naturally fractured geothermal reservoirs in the central Upper Rhine Graben. In *Journal of Structural Geology* 148, p. 104370. DOI: 10.1016/j.jsg.2021.104370.

Gleizes, Gérard; Nédélec, Anne; Bouchez, Jean-Luc; Autran, Albert; Rochette, Pierre (1993): Magnetic susceptibility of the Mont-Louis andorra ilmenite-type granite (Pyrenees): A new tool for the petrographic characterization and regional mapping of zoned granite plutons. In *J. Geophys. Res.* 98 (B3), pp. 4317–4331. DOI: 10.1029/92JB01590.

Götze, H. -J.; Lahmeyer, Bernd (1988): Application of three-dimensional interactive modeling in gravity and magnetics. In *Geophysics* 53 (8), pp. 1096–1108. DOI: 10.1190/1.1442546.

Grant, M.; Clearwater, J.; Quinao, J.; Bixley, P. F.; Le Brun, M. (2013): Thermal stimulation of geothermal wells: a review of field data. In Stanford University (Ed.): Proceedings. Thirty-Eighth Workshop on Geothermal Reservoir Engineering. Stanford, California, 11.-13. February.

Grimm, M. C. (2005): Beiträge zur Lithostratigraphie des Paläogens und Neogens im Oberrheingebiet (Oberrheingraben, Mainzer Becken, Hanauer Becken). In *Geol. Jb. Hessen* 132, pp. 79–112.

Grimm, Matthias C.; Wielandt-Schuster, Ulrike; Hottenrott, Martin; Radtke, Gudrun; Berger, Jean-Pierre; Ellwanger, Dietrich et al. (2011): Oberrheingraben (Tertiär des Oberrheingrabens). In *sdgg* 75, pp. 57–132. DOI: 10.1127/sdgg/75/2011/57.

Grimmer, J. C.; Ritter, J. R. R.; Eisbacher, G. H.; Fielitz, W. (2017): The Late Variscan control on the location and asymmetry of the Upper Rhine Graben. In *International Journal of Earth Sciences* 106 (3), pp. 827–853. DOI: 10.1007/s00531-016-1336-x.

Grünthal, Gottfried (2014): Induced seismicity related to geothermal projects versus natural tectonic earthquakes and other types of induced seismic events in Central Europe. In *Geothermics* 52, pp. 22–35. DOI: 10.1016/j.geothermics.2013.09.009.

Häring, Markus O.; Schanz, Ulrich; Ladner, Florentin; Dyer, Ben C. (2008): Characterisation of the Basel 1 enhanced geothermal system. In *Geothermics* 37 (5), pp. 469–495. DOI: 10.1016/j.geothermics.2008.06.002.

Heimlich, Christine; Gourmelen, Noël; Masson, Frédéric; Schmittbuhl, Jean; Kim, Sang-Wan; Azzola, Jérôme (2015): Uplift around the geothermal power plant of Landau (Germany) as observed by InSAR monitoring. In *Geotherm Energy* 3 (1). DOI: 10.1186/s40517-014-0024-y.

Henkel, H.; Guzmán, M. (1977): Magnetic features of fracture zones. In *Geoexploration* 15 (3), pp. 173–181. DOI: 10.1016/0016-7142(77)90024-2.

Hirono, Tetsuro; Lin, Weiren; Yeh, En-Chao; Soh, Wonn; Hashimoto, Yoshitaka; Sone, Hiroki et al. (2006): High magnetic susceptibility of fault gouge within Taiwan Chelungpu fault: Nondestructive continuous measurements of physical and chemical properties in fault rocks recovered from Hole B, TCDP. In *Geophys. Res. Lett.* 33 (15). DOI: 10.1029/2006GL026133.

HLUG (2007): Geologische Karte von Hessen: Hessisches Landesamt für Umwelt und Geologie.

Hofmann, Hannes; Zimmermann, Günter; Huenges, Ernst; Regenspurg, Simona; Aldaz, Santiago; Milkereit, Claus et al. (2021): Soft stimulation treatment of geothermal well RV-43 to meet the growing heat demand of Reykjavik. In *Geothermics* 96, p. 102146. DOI: 10.1016/j.geothermics.2021.102146.

Homuth, Benjamin; Stiller, Manfred; Schmidt, Bernd (2021): Reprocessed deep seismic reflection profile DEKORP 1988-9N across the Northern Upper Rhine Graben, Southwest Germany. DOI: 10.5880/GFZ.DEKORP-9N.002.

Huenges, E. (2016): Enhanced geothermal systems: Review and status of research and development. In Ronald DiPippo (Ed.): Geothermal Power Generation: Elsevier, pp. 743–761.

Huenges, Ernst (Ed.) (2010): Geothermal Energy Systems: Wiley.

Huenges, Ernst; Kohl, Thomas; Kolditz, Olaf; Bremer, Judith; Scheck-Wenderoth, Magdalena; Vienken, Thomas (2013): Geothermal energy systems: research perspective for domestic energy provision. In *Environ Earth Sci* 70 (8), pp. 3927–3933. DOI: 10.1007/s12665-013-2881-2.

Illies, J. H. (1978): Two Stages Rheingraben Rifting. In I. B. Ramberg, E. R. Neumann (Eds.): Tectonics and geophysics of continental rifts. Dordrecht: D. Reidel Publ. Comp., pp. 63–71.

IPCC (2022a): Climate Change 2022: Impacts, Adaptation, and Vulnerability. Contribution of Working Group II to the Sixth Assessment Report of the Intergovernmental Panel on Climate Change: Cambridge University Press.

IPCC (2022b): Working Group III contribution to the IPCC Sixth Assessment Report (AR6-WG3).

Isles, David J.; Rankin, Leigh R. (2013): Geological Interpretation of Aeromagnetic Data: Society of Exploration Geophysicists and Australian Society of Exploration Geophysicists.

Ito, Hisatoshi (2003): Inferred role of natural fractures, veins, and breccias in development of the artificial geothermal reservoir at the Ogachi Hot Dry Rock site, Japan. In *J. Geophys. Res.* 108 (B9). DOI: 10.1029/2001JB001671.

Jain, Charitra; Vogt, Christian; Clauser, Christoph (2015): Maximum potential for geothermal power in Germany based on engineered geothermal systems. In *Geotherm Energy* 3 (1). DOI: 10.1186/s40517-015-0033-5.

Jeffrey, R.; Zhang, X.; Bunger, A. P. (2010): Hydraulic Fracturing of Naturally Fractured Reservoirs. In Stanford University (Ed.): Proceedings. Thirty-Fourth Workshop on Geothermal Reservoir Engineering. Stanford, California, 1.-3. February.

Jung, Reinhard (2013): EGS — Goodbye or Back to the Future 95. In R. Jeffrey, J. McLennan, A. P. Bunger (Eds.): Effective and Sustainable Hydraulic Fracturing. International Conference for Effective and Sustainable Hydraulic Fracturing (HF2013). Brisbane, Australia, 20-22. May 2013: IntechOpen.

Kim, B. (2020): Aeromagnetic Exploration using Unmanned Aerial Vehicles: Current and Future Trends. In *Geophysics and Geophysical Exploration* 23 (3), pp. 178–191. DOI: 10.7582/GGE.2020.23.3.00178.

Kim, Kwang-Hee; Ree, Jin-Han; Kim, YoungHee; Kim, Sungshil; Kang, Su Young; Seo, Wooseok (2018): Assessing whether the 2017 Mw 5.4 Pohang earthquake in South Korea was an induced event. In *Science (New York, N.Y.)* 360 (6392), pp. 1007–1009. DOI: 10.1126/science.aat6081.

KIT (2022): GeoLaB: Zukunft mit Geothermie. Heidelberger, M. Available online at https://www.kit.edu/kit/pi_2022_056_geolab-zukunft-mit-geothermie.php, checked on 8/30/2022.

Klemm, G. (1900): Geologische Karte des Großherzogtums Hessen - Blatt 6419 Beerfelden. Darmstadt.

Klemm, G. (1928): Geologische Karte von Hessen - Blatt 6319 Erbach. Darmstadt: Hessischer Staatsverlag.

Klemm, G. (1929): Geologische Karte von Hessen - Blatt 6418 Birkenau (Weinheim). Darmstadt: Hessischer Staatsverlag.

Klemm, G. (1933): Geologische Karte von Hessen - Blatt 6318 Lindenfels. Darmstadt: Hessischer Staatsverlag.

Kock, Nils; Kaltschmitt, Martin (2012): Geothermisch erschließbare Niedertemperaturwärmesenken in Deutschland – Identifikation und Quantifizierung. In *Z Energiewirtsch* 36 (3), pp. 191–203. DOI: 10.1007/s12398-012-0079-z.

Koltzer, Nora; Scheck-Wenderoth, Magdalena; Bott, Judith; Cacace, Mauro; Frick, Maximilian; Sass, Ingo et al. (2019): The Effects of Regional Fluid Flow on Deep Temperatures (Hesse, Germany). In *Energies* 12 (11), p. 2081. DOI: 10.3390/en12112081.

Kossmat, F. (1927): Gliederung des varistischen Gebirgsbaues. In *Abhandlungen Sächsischen Geologischen Landesamts* 1, pp. 1–39.

Koudina, N.; Gonzalez Garcia, R.; Thovert, J.-F.; Adler, P. M. (1998): Permeability of three-dimensional fracture networks. In *Phys. Rev. E* 57 (4), pp. 4466–4479. DOI: 10.1103/PhysRevE.57.4466.

Krohe, A. (1991): Emplacement of synkinematic plutons in the Variscan Odenwald (Germany) controlled by transtensional tectonics. In *International Journal of Earth Sciences* 80 (2), pp. 391–409. DOI: 10.1007/BF01829373.

Krohe, A.; Willner, A. P. (1995): IV.C.2 The Odenwald Crystalline Complex. In R. D. Dallmeyer, W. Franke, K. Weber (Eds.): Pre-Permian Geology of Central and Eastern Europe. Berlin, Heidelberg: Springer Berlin Heidelberg, pp. 182–185.

Kruseman, G. P.; Ridder, N. A. de (1990): Analysis and evaluation of pumping test data. 2. ed. (completely revised). Wageningen: ILRI Publication (47).

Kruszewski, Michał; Śliwa, Tomasz; Þórhallsson, Sverrir; Assadi, Mohsen (2017): Slimhole well casing design for high-temperature geothermal exploration and reservoir assessment. In *drill* 34 (2), p. 465. DOI: 10.7494/drill.2017.34.2.465.

Ladner, F.; Schanz, U.; Häring, M. O. (2008): Deep-Heat-Mining-Projekt Basel–Erste Erkenntnisse bei der Entwicklung eines Enhanced Geothermal System (EGS). In *Bulletin für angewandte Geologie* 13, pp. 41–54. DOI: 10.5169/seals-226675.

Ledésert, B.; Hebert, R.; Genter, A.; Bartier, D.; Clauer, N.; Grall, C. (2010): Fractures, hydrothermal alterations and permeability in the Soultz Enhanced Geothermal System. In *Comptes Rendus Geoscience* 342 (7-8), pp. 607–615. DOI: 10.1016/j.crte.2009.09.011.

Li, S.; Wang, S.; Tang, H. (2022): Stimulation mechanism and design of enhanced geothermal systems: A comprehensive review. In *Renewable and Sustainable Energy Reviews* 155, p. 111914. DOI: 10.1016/j.rser.2021.111914.

Lister, Matthew (2014): Climate change refugees. In *Critical Review of International Social and Political Philosophy* 17 (5), pp. 618–634. DOI: 10.1080/13698230.2014.919059.

Liutak, O.; Baula, O.; Poruchnyk, A.; Stoliarchuk, Ya.; Kravchuk, P.; Kostynets, Iu. (2021): The Development Of Renewable Energy In The Context Of Formation Of Innovative Economy And Energy Independence As The Geopolitical Priorities Of The State. In *IOP Conference Series: Earth and Environmental Science* 628. DOI: 10.1088/1755-1315/628/1/012012.

Long, Jane C. S.; Witherspoon, Paul A. (1985): The relationship of the degree of interconnection to permeability in fracture networks. In *J. Geophys. Res.* 90 (B4), p. 3087. DOI: 10.1029/JB090iB04p03087.

Lukawski, Maciej Z.; Anderson, Brian J.; Augustine, Chad; Capuano, Louis E.; Beckers, Koenraad F.; Livesay, Bill; Tester, Jefferson W. (2014): Cost analysis of oil, gas, and geothermal well drilling. In *Journal of Petroleum Science and Engineering* 118, pp. 1–14. DOI: 10.1016/j.petrol.2014.03.012.

Lund, H.; Münster, E. (2003): Management of surplus electricity-production from a fluctuating renewable-energy source. In *Applied Energy* 76 (1-3), pp. 65–74. DOI: 10.1016/S0306-2619(03)00048-5.

Lustig, Nora (2011): Multidimensional indices of achievements and poverty: what do we gain and what do we lose? An introduction to JOEI Forum on multidimensional poverty. In *J Econ Inequal* 9 (2), pp. 227–234. DOI: 10.1007/s10888-011-9186-z.

Ma, Guoqing; Li, Lili (2012): Edge detection in potential fields with the normalized total horizontal derivative. In *Computers & Geosciences* 41, pp. 83–87. DOI: 10.1016/j.cageo.2011.08.016.

Maggetti, M. (1975): Die Tiefengesteine des Bergsträßer Odenwaldes. In G. C. Amstutz, S. Meisl, E. Nickel (Eds.): Mineralien und Gesteine im Odenwald. Heidelberg, pp. 87–109.

Mahmoodpour, Saeed; Singh, Mrityunjay; Turan, Aysegul; Bär, Kristian; Sass, Ingo (2021): Hydro-Thermal Modeling for Geothermal Energy Extraction from Soultz-sous-Forêts, France. In *Geosciences* 11 (11), p. 464. DOI: 10.3390/geosciences11110464.

Mahmoodpour, Saeed; Singh, Mrityunjay; Turan, Aysegul; Bär, Kristian; Sass, Ingo (2022): Simulations and global sensitivity analysis of the thermo-hydraulic-mechanical processes in a fractured geothermal reservoir. In *Energy* 247, p. 123511. DOI: 10.1016/j.energy.2022.123511.

Majer, Ernest L.; Baria, Roy; Stark, Mitch; Oates, Stephen; Bommer, Julian; Smith, Bill; Asanuma, Hiroshi (2007): Induced seismicity associated with Enhanced Geothermal Systems. In *Geothermics* 36 (3), pp. 185–222. DOI: 10.1016/j.geothermics.2007.03.003.

Manning, C. E.; Ingebritsen, S. E. (1999): Permeability of the continental crust: Implications of geothermal data and metamorphic systems. In *Rev. Geophys.* 37 (1), pp. 127–150. DOI: 10.1029/1998RG900002.

Maurer, Vincent; Gaucher, Emmanuel; Grunberg, Marc; Koepke, Rike; Pestourie, Romain; Cuenot, Nicolas (2020): Seismicity induced during the development of the Rittershoffen geothermal field, France. In *Geotherm Energy* 8 (1). DOI: 10.1186/s40517-020-0155-2.

McClure, Mark W.; Horne, Roland N. (2014): An investigation of stimulation mechanisms in Enhanced Geothermal Systems. In *International Journal of Rock Mechanics and Mining Sciences* 72, pp. 242–260. DOI: 10.1016/j.ijrmms.2014.07.011.

Mégel, Thomas; Kohl, Thomas; Hopkirk, Robert J. (2006): The potential of the use of dense fluids for initiating hydraulic stimulation. In *Geothermics* 35 (5-6), pp. 589–599. DOI: 10.1016/j.geothermics.2006.11.003.

Mignan, A.; Broccardo, M.; Wiemer, S.; Giardini, D. (2017): Induced seismicity closed-form traffic light system for actuarial decision-making during deep fluid injections. In *Scientific reports* 7 (1), p. 13607. DOI: 10.1038/s41598-017-13585-9.

Miller, Hugh G.; Singh, Vijay (1994): Potential field tilt—a new concept for location of potential field sources. In *Journal of Applied Geophysics* 32 (2-3), pp. 213–217. DOI: 10.1016/0926-9851(94)90022-1.

Moeck, Inga; Bendall, B.; Minning, C.; Manzella, A.; Yasukawa, K. (2020): Geothermal Play Typing – Current Development and Future Trends of a Modern Concept for Geothermal Resources Assessment. In : Proceedings. World Geothermal Congress 2020. Reykjavik, Iceland, April - October 2021.

Moeck, Inga S. (2014): Catalog of geothermal play types based on geologic controls. In *Renewable and Sustainable Energy Reviews* 37, pp. 867–882. DOI: 10.1016/j.rser.2014.05.032.

Morris, Alan; Ferrill, David A.; Brent Henderson, D.Brent (1996): Slip-tendency analysis and fault reactivation. In *Geology* 24 (3), p. 275. DOI: 10.1130/0091-7613(1996)024<0275:STAAFR>2.3.CO;2.

Morris, C. W.; Verity, R. V.; Dasie, W. (1984): Chemical stimulation treatment of a well in the Beowawe geothermal field. In *GRC Transactions* 8, pp. 269–274.

Mouchot, J.; Genter, A.; Cuenot, N.; Scheiber, Julia; Seibel, Olivier; Bosia, Clio; Ravier, Guillaume (2018): First Year of Operation from EGS geothermal Plants in Alsace, France: Scaling Issues. In Stanford University (Ed.): Proceedings. 43rd Workshop on Geothermal Reservoir Engineering. Stanford, California, 12.-14. February.

Muffler, P.; Cataldi, R. (1978): Methods for regional assessment of geothermal resources. In *Geothermics* 7 (2-4), pp. 53–89. DOI: 10.1016/0375-6505(78)90002-0.

Nickel, E. (1953): Die petrogenetische Stellung der Tromm zwischen Bergsträßer und Böllsteiner Odenwald (Beiträge zur Petrographie des Odenwaldes VI.): Die petrogenetische Stellung der Tromm zwischen Bergsträßer und Böllsteiner Odenwald: Springer-Verlag.

Nickel, E. (1975): Geologische Position und Petrogenese des kristallinen Odenwaldes. In G. C. Amstutz, S. Meisl, E. Nickel (Eds.): Mineralien und Gesteine im Odenwald. Heidelberg, pp. 1–25.

NLOG (2022): NLOG - Dutch Oil and Gas portal. Available online at https://www.nlog.nl/en/welcome-nlog, checked on 8/30/2022.

Oda, M. (1985): Permeability tensor for discontinuous rock masses. In *Géotechnique* 35 (4), pp. 483–495. DOI: 10.1680/geot.1985.35.4.483.

Okrusch, M.; Schubert, W.; Nasir, S. (1995): IV.D Igneous Activity (Pre- to Early Variscan Magmatism). In R. D. Dallmeyer, W. Franke, K. Weber (Eds.): Pre-Permian Geology of Central and Eastern Europe. Berlin, Heidelberg: Springer Berlin Heidelberg, pp. 190–200.

Oksum, E.; Le, D. V.; Vu, M. D.; Nguyen, T.-H.T.; Pham, L. T. (2021): A novel approach based on the fast sigmoid function for interpretation of potential field data. In *Bulletin of Geophysics and Oceanography* 62 (3), pp. 543–556. DOI: 10.4430/bgta0348.

Olasolo, P.; Juárez, M. C.; Morales, M. P.; D´Amico, Sebastiano; Liarte, I. A. (2016): Enhanced geothermal systems (EGS): A review. In *Renewable and Sustainable Energy Reviews* 56, pp. 133–144. DOI: 10.1016/j.rser.2015.11.031.

Paschen, H.; Ortel, D.; Grünwald, R. (2003): Möglichkeiten geothermischer Stromerzeugung in Deutschland. Sachstandsbericht. Büro für Technikfolgen-Abschätzung beim Deutschen Bundestag (TAB).

Portier, S.; André, L.; & Vuataz, F. D. (2007): Review on chemical stimulation techniques in oil industry and applications to geothermal systems. Technical report. Centre de Recherche en Géothermie, Neuchâtel.

Portier, Sandrine; Vuataz, François-David; Nami, Patrick; Sanjuan, Bernard; Gérard, André (2009): Chemical stimulation techniques for geothermal wells: experiments on the three-well EGS system at Soultz-sous-Forêts, France. In *Geothermics* 38 (4), pp. 349–359. DOI: 10.1016/j.geothermics.2009.07.001.

Potter, R.; Robinson, E.; Smith, M. (1974): Method of extracting heat from dry geothermal reservoirs on 1974. Patent no. 3786858.

Reiter, K.; Heidbach, O.; Müller, B.; Reinecker, J.; Röckl, T.; Reiter, Karsten et al. (2016): Stress Map Germany 2016. DOI: 10.5880/WSM.Germany2016_en.

Ren21 (2018): Renewables 2018. Global Status Report. Renewable Energy Policy Network for the 21st Century. Available online at https://www.ren21.net/wp-content/uploads/2019/05/GSR2018_Full-Report_English.pdf, checked on 8/10/2022.

Roest, Walter R.; Verhoef, Jacob; Pilkington, Mark (1992): Magnetic interpretation using the 3-D analytic signal. In *Geophysics* 57 (1), pp. 116–125. DOI: 10.1190/1.1443174.

Rose, P.; Xu, T.; Kovac, K.; Mella, M.; Pruess, K. (2007): Chemical stimulation in near- Chemical stimulation in near-wellbore geothermal formations: silica dissolution in the presence of calcite at high temperature and high pH. In Stanford University (Ed.): Proceedings. Thirty-Second Workshop on Geothermal Reservoir Engineering. Stanford, California, 22.-24. January.

Rotstein, Y.; Edel, J. B.; Gabriel, G.; Boulanger, D.; Schaming, M.; Munschy, M. (2006): Insight into the structure of the Upper Rhine Graben and its basement from a new compilation of Bouguer Gravity. In *Tectonophysics* 425 (1-4), pp. 55–70. DOI: 10.1016/j.tecto.2006.07.002.

Rutledge, James T.; Phillips, W. Scott (2003): Hydraulic stimulation of natural fractures as revealed by induced microearthquakes, Carthage Cotton Valley gas field, east Texas. In *Geophysics* 68 (2), pp. 441–452. DOI: 10.1190/1.1567214.

Saevarsdottir, Gudrun; Tao, Pai-chun; Stefansson, Hlynur; Harvey, William (2014): Potential use of geothermal energy sources for the production of lithium-ion batteries. In *Renewable Energy* 61, pp. 17–22. DOI: 10.1016/j.renene.2012.04.028.

Sanner, Burkhard; Karytsas, Constantine; Mendrinos, Dimitrios; Rybach, Ladislaus (2003): Current status of ground source heat pumps and underground thermal energy storage in Europe. In *Geothermics* 32 (4-6), pp. 579–588. DOI: 10.1016/S0375-6505(03)00060-9.

Sass, Ingo; Hoppe, A.; Arndt, D.; Bär, Kristian (2011): Forschungs-und Entwicklungsprojekt 3D Modell der Geothermischen Tiefenpotenziale von Hessen. Abschlussbericht. TU Darmstadt.

Sauer, K.; Munck, F. (1979): Geothermische Synthese des Oberrheingrabens (Bestandsaufnahme). Geologisches Landesamt Baden-Württemberg. Freiburg i. Br.

Sausse, J.; Genter, A. (2005): Types of permeable fractures in granite. In *Geological Society, London, Special Publications* 240 (1), pp. 1–14. DOI: 10.1144/GSL.SP.2005.240.01.01.

Schälicke, W. (1975): Die Otzberg-Zone. In G. C. Amstutz, S. Meisl, E. Nickel (Eds.): Mineralien und Gesteine im Odenwald. Heidelberg, pp. 47–59.

Schätzler, K.; Bremer, J.; Schill, E.; Kohl, T.; Kühn, M.; Kolditz, O.; Sass, I. (2020): GeoLaB – Das geowissenschaftliche Zukunftsprojekt für Deutschland. In *GeoLaB – Das geowissenschaftliche Zukunftsprojekt für Deutschland* 156 (6).

Schellschmidt, R.; Clauser, C. (1996): The thermal regime of the Upper Rhine Graben and the anomaly at Soultz. In *Zeitschrift für Angewandte Geologie* 42 (1), pp. 40–44.

Schill, E.; Genter, A.; Cuenot, N.; Kohl, T. (2017): Hydraulic performance history at the Soultz EGS reservoirs from stimulation and long-term circulation tests. In *Geothermics* 70, pp. 110–124. DOI: 10.1016/j.geothermics.2017.06.003.

Schill, Eva; Meixner, Jörg; Meller, Carola; Grimm, Manuel; Grimmer, Jens C.; Stober, Ingrid; Kohl, Thomas (2016): Criteria and geological setting for the generic geothermal underground research laboratory, GEOLAB. In *Geotherm Energy* 4 (1). DOI: 10.1186/s40517-016-0049-5.

Schmidt, Sabine; Anikiev, Denis; Götze, Hans-Jürgen; Gomez Garcia, Àngela; Gomez Dacal, Maria Laura; Meeßen, Christian et al. (2020): IGMAS+ - a tool for interdisciplinary 3D potential field modelling of complex geological structures. In EGU (Ed.): Proceedings of the EGU General Assembly 2020. EGU General Assembly. online, 4–8 May.

Schmittbuhl, J.; Lambotte, S.; Lengliné, O.; Grunberg, M.; Jund, H.; Vergne, J. et al. (2021): Induced and triggered seismicity below the city of Strasbourg, France from November 2019 to January 2021. In *Comptes Rendus. Géoscience* 353 (S1), pp. 1–24. DOI: 10.5802/crgeos.71.

Schulte, Thomas; Zimmermann, Günter; Vuataz, Francois; Portier, Sandrine; Tischner, Torsten; Junker, Ralf et al. (2010): Enhancing Geothermal Reservoirs. In Ernst Huenges (Ed.): Geothermal Energy Systems: Wiley, pp. 173–243.

Schulz, Katja E.; Bär, Kristian; Sass, Ingo (2022): Lab-Scale Permeability Enhancement by Chemical Treatment in Fractured Granite (Cornubian Batholith) for the United Downs Deep Geothermal Power Project, Cornwall (UK). In *Geosciences* 12 (1), p. 35. DOI: 10.3390/geosciences12010035.

Schumacher, Markus E. (2002): Upper Rhine Graben: Role of preexisting structures during rift evolution. In *Tectonics* 21 (1), 6-1-6-17. DOI: 10.1029/2001TC900022.

Scibek, Jacek (2020): Multidisciplinary database of permeability of fault zones and surrounding protolith rocks at world-wide sites. In *Scientific data* 7 (1), p. 95. DOI: 10.1038/s41597-020-0435-5.

Shmonov, V. M.; Vitiovtova, V. M.; Zharikov, A.V; Grafchikov, A. A. (2003): Permeability of the continental crust: implications of experimental data. In *Journal of Geochemical Exploration* 78-79, pp. 697–699. DOI: 10.1016/S0375-6742(03)00129-8.

Sibson, R. H. (1977): Fault rocks and fault mechanisms. In *Journal of the Geological Society* 133 (3), pp. 191–213. DOI: 10.1144/gsjgs.133.3.0191.

Siratovich, Paul A.; Sass, Ingo; Homuth, Sebastian; Bjornsson, Axel (2011): Thermal Stimulation of Geothermal Reservoirs and Laboratory Investigation of Thermally Induced Fractures. In *GRC Transactions* 35, pp. 1529–1535. Available online at https://www.geothermal-library.org/index.php?mode=pubs&action=view&record=1029450, checked on 8/12/2022.

Spiecker, Stephan; Weber, Christoph (2014): The future of the European electricity system and the impact of fluctuating renewable energy – A scenario analysis. In *Energy Policy* 65, pp. 185–197. DOI: 10.1016/j.enpol.2013.10.032.

Stein, E. (2001): The geology of the Odenwald Crystalline Complex. In *Mineralogy and Petrology* 72 (1-3), pp. 7–28. DOI: 10.1007/s007100170024.

Stober, Ingrid; Bucher, Kurt (1999): Deep groundwater in the crystalline basement of the Black Forest region. In *Applied Geochemistry* 14 (2), pp. 237–254. DOI: 10.1016/S0883-2927(98)00045-6.

Stober, Ingrid; Bucher, Kurt (2007): Hydraulic properties of the crystalline basement. In *Hydrogeol J* 15 (2), pp. 213–224. DOI: 10.1007/s10040-006-0094-4.

Stober, Ingrid; Fritzer, Thomas; Obst, Karsten; Agemar, Thorsten; Schulz, Rüdiger (2016): Tiefe Geothermie: Grundlagen und Nutzungsmöglichkeiten in Deutschland. Hannover: Leibniz-Institut für Angewandte Geophysik (LIAG).

Stober, Ingrid; Jodocy, Marco (2009): Characteristics of geothermal reservoirs in the Upper Rhine Graben of Baden-Württemberg and France. In *Grundwasser* 14 (2), pp. 127–137.

Strozyk, F.; Herbst, E.; Khashfe, E. (2021): Map of the spatial distribution of the heat demand at the surface. Report WP T1 – 2.1. DGE-Rollout Project. Fraunhofer IEG.

Tani, Abdallah; Camara, Mamadou Bailo; Dakyo, Brayima (2014): Energy Management in the Decentralized Generation Systems Based on Renewable Energy—Ultracapacitors and Battery to Compensate the Wind/Load Power Fluctuations. In *IEEE Trans. on Ind. Applicat.* 51 (2), pp. 1817–1827. DOI: 10.1109/TIA.2014.2354737.

Tanikawa, Wataru; Mishima, Toshiaki; Hirono, Tetsuro; Soh, Wonn; Song, Sheng-Rong (2008): High magnetic susceptibility produced by thermal decomposition of core samples from the Chelungpu fault in Taiwan. In *Earth and Planetary Science Letters* 272 (1-2), pp. 372–381. DOI: 10.1016/j.epsl.2008.05.002.

Tarkowski, Radoslaw (2019): Underground hydrogen storage: Characteristics and prospects. In *Renewable and Sustainable Energy Reviews* 105, pp. 86–94. DOI: 10.1016/j.rser.2019.01.051.

Tester, J. W.; Brown, D. W.; Potter, R. M. (1989): Hot Dry Rock geothermal energy - A new energy agenda for the twenty-first century. Los Alamos National Laboratory report LA-11514-MS. US Department of Energy. Washington D.C.

Tester, Jefferson W.; Anderson, Brian J.; Batchelor, A. S.; Blackwell, D. D.; DiPippo, Ronald; Drake, E. M. et al. (2006): The future of geothermal energy. Impact of Enhanced Geothermal Systems (EGS) on the United States in the 21st Century. MIT.

Teza, D.; Menzel, H.; Baumgärtner, J. (2008): Multihorizontansatz zur Erschließung ökonomisch relevanter Fließraten am Beispiel des Geothermieprojektes Landau. Schlussbericht.

Tian, Y.; Zhao, C. Y. (2013): A review of solar collectors and thermal energy storage in solar thermal applications. In *Applied Energy* 104, pp. 538–553. DOI: 10.1016/j.apenergy.2012.11.051.

Torabi, Anita; Berg, Silje Støren (2011): Scaling of fault attributes: A review. In *Marine and Petroleum Geology* 28 (8), pp. 1444–1460. DOI: 10.1016/j.marpetgeo.2011.04.003.

Trenczek, J.; Lühr, O.; Eiserbeck, L.; Sandhövel, M., Leuschner, V. (2022): Übersicht vergangener Extremwetterschäden in Deutschland. Methodik und Erstellung einer Schadensübersicht. Projektbericht „Kosten durch Klimawandelfolgen“.

Tulinius, H.; Correia, H.; Sigurdsson, O. (2000): Stimulating A High Enthalpy Well By Thermal Cracking. In : Proceedings. World Geothermal Congress 2000. Kyushu - Tohoku, Japan, 28. May - 10. June, pp. 1883–1888.

UBA (2022a): Erneuerbare Energien in Zahlen. Umweltbundesamt. Available online at https://www.umweltbundesamt.de/themen/klima-energie/erneuerbare-energien/erneuerbare-energien-in-zahlen#uberblick, updated on 8/8/2022.

UBA (2022b): Treibhausgas-Emissionen in Deutschland. Umweltbundesamt. Available online at https://www.umweltbundesamt.de/daten/klima/treibhausgas-emissionen-in-deutschland#emissionsentwicklung, checked on 8/5/2022.

Umweltamt Wiesbaden (2011): Der Schatz aus der Tiefe. Ein Spaziergang zu den Thermalquellen in Wiesbaden. Available online at https://www.wiesbaden.de/medien-zentral/dok/leben/umwelt-naturschutz/UA_ThermalquellenBro_A4_111213_Endfassung.pdf, checked on 8/4/2022.

United Nations (Ed.) (2015): Paris Agreement. Conference of the Parties to the United Nations Framework Convention on Climate Change (21st Session, 2015: Paris). Paris.

van Horn, Andrew; Amaya, Alvaro; Higgins, Brian; Muir, John; Scherer, Joe; Pilko, Robert; Ross, Malcolm (2020): New Opportunities and Applications for Closed-Loop Geothermal Energy Systems. In *GRC Transactions* 44, pp. 1123–1143.

Vermilye, Jan M.; Scholz, Christopher H. (1995): Relation between vein length and aperture. In *Journal of Structural Geology* 17 (3), pp. 423–434. DOI: 10.1016/0191-8141(94)00058-8.

Villemin, T.; Coletta, B. (1990): Subsidence in the Rhine Graben: a new compilation of borehole data. In : Symposium on Rhine-Rhone Rift System. ICL-WG-3. Symp.

Villemin, Thierry; Alvarez, Francis; Angelier, Jacques (1986): The Rhinegraben: Extension, subsidence and shoulder uplift. In *Tectonophysics* 128 (1-2), pp. 47–59. DOI: 10.1016/0040-1951(86)90307-0.

Walter, C.; Braun, A.; Fotopoulos, G. (2020): High-resolution unmanned aerial vehicle aeromagnetic surveys for mineral exploration targets. In *Geophysical Prospecting* 68 (1), pp. 334–349. DOI: 10.1111/1365-2478.12914.

Weinert, S.; Bär, K.; Sass, I. (2020): Petrophysical Properties of the Mid-German Crystalline High: A Database for Bavarian, Hessian, Rhineland-Palatinate and Thuringian Outcrops. Edited by Technical University Of Darmstadt.

Wiemer, S.; Tormann, T.; Herrmann, M.; Karvounis, D. C.; Kraft, T.; & Marti, M. (2017): Induzierte Erdbeben im Nachgang des eingestellten Geothermieprojekts in Basel. ETH Zurich. Available online at https://www.research-collection.ethz.ch/bitstream/handle/20.500.11850/254199/1/Induzierte-Erdbeben-im-Nachgang-des-eingestellen-Geothermieprojekts-in-Basel.pdf, checked on 8/12/2022.

Xie, X.; Weiss, W. W.; Tong, Z.; Morrow, N. R. (2005): Improved Oil Recovery From Carbonate Reservoirs by Chemical Stimulation. In *SPE Journal* 10 (03), pp. 276–285. DOI: 10.2118/89424-PA.

Yakeley, S.; Foster, T.; Laflin, W. (2007): Swellable Packers for Well Fracturing and Stimulation. In : Proceedings. SPE Annual Technical Conference and Exhibition. Anaheim, California, November 2007.

Zang, Arno; Oye, Volker; Jousset, Philippe; Deichmann, Nicholas; Gritto, Roland; McGarr, Art et al. (2014): Analysis of induced seismicity in geothermal reservoirs – An overview. In *Geothermics* 52, pp. 6–21. DOI: 10.1016/j.geothermics.2014.06.005.

Zang, Arno; Yoon, Jeoung Seok; Stephansson, Ove; Heidbach, Oliver (2013): Fatigue hydraulic fracturing by cyclic reservoir treatment enhances permeability and reduces induced seismicity. In *Geophys J Int* 195 (2), pp. 1282–1287. DOI: 10.1093/gji/ggt301.

Zhou, X. X.; Ghassemi, A.; Cheng, A. H.-D. (2009): A three-dimensional integral equation model for calculating poro- and thermoelastic stresses induced by cold water injection into a geothermal reservoir. In *Int. J. Numer. Anal. Meth. Geomech.* 33 (14), pp. 1613–1640. DOI: 10.1002/nag.780.

Ziagos, J.; Phillips, B. R.; Boyd, L.; Jelacic, A.; Stillman, G.; Hass, E. (2013): A Technological Roadmap for Strategic Development of Enhanced Geothermal Systems. In Stanford University (Ed.): Proceedings. Thirty-Eighth Workshop on Geothermal Reservoir Engineering. Stanford, California, 11.-13. February.

Ziegler, P. A. (1994): Cenozoic rift system of Western and Central-Europe-an overview. In *Geologie en Mijnbouw* 73 (2-4), pp. 99–127.

Ziegler, P. A.; Dèzes, P. (2005): Evolution of the lithosphere in the area of the Rhine Rift System. In *International Journal of Earth Sciences* 94 (4), pp. 594–614. DOI: 10.1007/s00531-005-0474-3.

Ziegler, Peter A. (1992): European Cenozoic rift system. In *Tectonophysics* 208 (1-3), pp. 91–111. DOI: 10.1016/0040-1951(92)90338-7.

Ziegler, Peter A.; Cloetingh, Sierd; van Wees, Jan-Diederik (1995): Dynamics of intra-plate compressional deformation: the Alpine foreland and other examples. In *Tectonophysics* 252 (1-4), pp. 7–59. DOI: 10.1016/0040-1951(95)00102-6.

Appendix A - Socio-Economic-Environmental Potential Mapping

Appendix A is largely based on the scientific report "Socio-Economic Potential Mapping for Deep Geothermal Energy in the Upper Rhine Graben" (Frey et al. 2022b), prepared as part of the DGE-Rollout Project. Parts of the analysis were updated, as new datasets became available. A comparison of the socio-economic-environmental potential with the calculated geothermal resources related to the Variscan basement in the northern URG is given in chapter 4.

The basis for developing any geothermal project is a comprehensive geological exploration of the subsurface, which allows quantification of the resources and identification of the risks. Ideally, the selected drill site should combine the highest possible heat recovery with the lowest possible risk. However, the efficiency and economic viability of geothermal utilization depend just as much on the conditions above ground, for example the heat demand, infrastructure, or land access. Urban areas are preferred accordingly, even though the temperature and productivity of the reservoir may be somewhat lower here. In remote areas, significant investments are required to build the power plant and distribute the energy due to often inadequate infrastructure. The associated additional costs can quickly make the operation uneconomical. Likewise, interference with natural habitats can conflict with the claim of geothermal energy to protect the environment and climate. Moreover, political and public acceptance toward renewable energies are not to be neglected, as they strongly steer the success of a geothermal project. Moeck et al. (2020) therefore suggest that the decision-making process for the most appropriate drill site should be based on a progressive and multiscale analysis of both subsurface and surface conditions.

A.1 Material and Methods

Relevant information on the socio-economic-environmental potential for the URG was collected to provide stakeholders with a reliable decision-making basis. Nine indicators (Tab. A.1) were jointly selected for all DGE-Rollout project areas to obtain a harmonized dataset for the entire Interreg region. Only publicly available data were compiled from online sources, which ensures the reproducibility of the analysis.

Table A.1: Selected indicators for the socio-economic-environmental potential mapping

Dimension	Indicator	Data source
Social	Population density	BKG Germany | Population of Municipalities INSEE France | Population of Municipalities
	Social progress index	European Commission | Social Progress Index
	Public acceptance of geothermal energy	data.gouv.fr | 2022 Legislative Election Results Bundeswahlleiter | 2021 Fedel Election Results
	Surface heat demand	https://www.nweurope.eu/DGE-ROLLOUT
Economic	Infrastructure (available district heating grids)	HAWK | Fernwärmeatlas EU | Pan-Euopean Thermal Atlas
	Gross domestic product	Eurostat | Gross Domestic Product
	Public debt	Statistics BW | Debt of Municipalities Statistics Hessen | Debt of Municipalities Statistics RLP | Debt of Municipalities France | Debt of Municipalities
Environmental	Land access (protected areas)	European Environmental Agency | Protected Areas
	Greenhouse gas emissions	Environmental Research | Carbon Footprint EU

The URG is a European cross-border region, mainly divided between Germany and France. To the south, a comparatively small area extents additionally into northern Switzerland. In German, the URG is divided among the three states of Baden-Württemberg, Hesse, and Rhineland-Palatinate. The French URG belongs mainly to the region Grand Est (European Collectivity of Alsace) and to the region Bourgogne-Franche-Compté (Départements Doubs and Territoire de Belfort). Due to this multitude of different administrative units, the collection of uniform datasets is not trivial. Information varies in date and spatial resolution (from municipality to country level) depending on the topic, with preference usually given to datasets with the highest resolution. When available, international sources, e.g., the European Statistical Commission, are preferred over national sources because usually the data is already harmonized and allow a better comparison between German and French areas.

After data collection, the nine components of the socio-economic-environmental potential were joined into a composite index. Detailed discussions of aggregating various indicators is given e.g. in Lustig (2011), Decancq and Lugo (2013), and Annoni and Bolsi (2020). Accordingly, a simplistic approach was applied, which calculated the composite index via an unweighted generalized mean:

$$I = \left(\frac{1}{n} \sum_{i=1}^{n} x_i^{\beta} \right)^{\frac{1}{\beta}} \tag{A.1}$$

Where n is the total number of components, x_i is the i-th component of the potential, and the constant β describes the compensability between the individual components. If β equals 1, the generalized mean corresponds to the arithmetic mean. Following Annoni und Bolsi (2020), a β of 0.5 was used such that the result falls between the arithmetic and geometric means.

Normalization is required to scale the indicators between 0 and 100 (this is already the case for the social progress index and the public acceptance). Therefore, a min-max transformation was carried out on the continuous parameters:

$$x_{norm} = \frac{100 * (x - x_{min})}{(x_{max} - x_{min})} \tag{A.2}$$

The minimum value x_{min} was defined as 0 in all cases and the maximum values x_{max} are derived from the respective datasets. Public debt was inverted prior to normalization, as high debt is associated with low potential for geothermal development. The infrastructure and land access datasets consist of categorical variables, thus the normalization described above cannot be applied. Instead, the infrastructure indicator was set to 100 in areas with district heating networks and 0 in areas without them. No further distinction was made based on the capacity of the networks. Since geothermal drilling will most likely not be approved in nature reserves, the total socio-economic-environmental index was set to 0 in all protected areas.

A.2 Individual Indicators

A compilation of the nine indicators of the socio-economic-environmental potential of deep geothermal utilization in the URG is shown in Fig. A.1. In the following, each parameter is described in detail.

A.2.1 Social Dimension

Population Density

Population density per municipality (Fig. A.1a) is a straightforward indicator of the surface heat and power demand. The URG is one of the most densely populated regions in Europe, with a total of about 6 million inhabitants. However, the population is quite heterogeneously distributed, with a clear contrast between urban and rural areas and a north-south trend. The Northern URG includes the Rhine-Main and Rhine-Neckar metropolitan regions with the major cities of Frankfurt, Darmstadt, Ludwigshafen, Mannheim, and Heidelberg. Population density here is well above 1000 ppl/km² in the cities and still above 500 ppl/km² in most rural municipalities. Towards the south and especially in the French URG, population density gradually decreases to about 100 to 200 ppl/km² in the countryside. Exceptions to this trend are the cities of Karlsruhe, Strasbourg, Freiburg im Breisgau, Mulhouse and Basel.

Social Progress Index

It can be assumed that high social progress favors the expansion of geothermal energy. In the last decades, various indices have been developed to measure the average social level in a region, such as the Human Development Index (HDI). The HDI considers basic indicators such as health, education, and income, while neglecting other factors that have gained importance especially in recent years. The European Social Progress Index (EU-SPI), first published in 2016, develops the approach further by including the three dimensions basic human needs, the foundations of well-being, and opportunity, each consisting of four components (Annoni and Bolsi 2020). EU-SPI describes the "capacity of a society to meet the basic human needs of its citizens, establish the building blocks that allow peoples and communities to enhance and sustain the quality of their lives, and create the conditions for all individuals to reach their full potential". Fig. A.1b shows the EU-SPI in 2020 for the NUTS 2 regions in the URG. In all regions, the index is above the EU average of 67. The lateral variability of the EU-SPI is extremely low, with the lowest value of 71.03 found for the administrative district of Darmstadt and the highest value of 72.68 found for the Alsace. For some of the subcategories (access to advanced education, personal freedom and choice, environmental quality, and personal security), however, significant differences are observed, but these largely balance each other out.

Public Acceptance

Public acceptance of geothermal energy is a crucial aspect for the success of power plant projects. Opinions and knowledge about this form of energy as well as perceptions of risks vary greatly from location to location, making any quantification at the regional level challenging. As a simple indicator for the political views of the population, the results of the recent parliamentary elections in Germany (2021) and France (2022) were considered. In Germany, all major parties except the AfD support the expansion of renewable energy. In France, nuclear power is traditionally more popular, which is why several parties and alliances oppose

renewables (RN, LR, REC, DVD, UDI). Public acceptance is derived from the relative vote share of parties in favor of renewables. It should be noted that elections are always snapshots that depend on the current national and world political situation. Furthermore, the comparability of the data is limited due to the widely differing party and electoral systems in Germany and France.

Fig. A.1c illustrates the derived acceptance indicator. In the German URG, acceptance is consistently high (> 80 %), with the highest value in Frankfurt at around 95 %. In France, acceptance is generally lower and shows strong spatial heterogeneity. The values range from around 34 % in the southern Bas-Rhin to around 84 % in Strasbourg.

Surface Heat Demand

Space heating for residential and commercial buildings accounts for about one third of the total energy consumption in Germany, a large part of which could be met by geothermal energy. The heat demand throughout northwestern Europe was quantified in the DGE-ROLLOUT report "WP T1 - 2.1 Map of spatial distribution of surface heat demand" (Strozyk et al. 2021). The resulting map has a spatial resolution of 100 x 100 m² (Fig. A.1d). The total heat demand in the URG is about 63 TWh/year, of which 51.4% comes from the residential sector and 48.6% from the commercial sector. Essentially, heat demand follows the population density, with the highest values in the metropolitan regions of the northern URG and the lowest values in the French countryside.

A.2.2 Economic Dimension

Infrastructure

District heating networks (DHNs) are inevitable to distribute the heat produced in geothermal power plants to the communities. Municipalities with existing DHNs should always be favored when choosing a drill site, as a completely new construction is seldom financially feasible. Existing DHNs in the URG were compiled from the German District Heating Atlas and the Pan-European Thermal Atlas (Fig. A.1e). According to these, slightly less than 10% of the municipalities in the URG are connected to DHNs. The infrastructure is particularly well developed in the large cities and their suburbs. No further differentiation was made regarding the grid length or capacity.

Gross Domestic Product

Gross domestic product (GDP) is a common measure of a region's economic performance that summarizes the total value of goods and services produced domestically after subtracting the inputs consumed in their production. GDP per capita allows for comparison of economic units of different sizes and thus quantification of a region's material wealth, which influences potential investments in geothermal energy. Harmonized information on GDP per capita for the European NUTS 3 regions was provided by the European Statistical Office for the year 2019 (Fig. A.1f). The values range from around 20,300 € in Rhein-Pfalz-Kreis to 96,600€ in Frankfurt am Main (EU average: €31,000). Especially in the northern URG, a clear urban-rural trend can be observed, reflecting a concentration of industry in major cities. Moreover, GDP per capita is generally lower in the French URG than in the German part.

Public Debt

Development of geothermal energy often depends to a significant extent on public investment. Accordingly, a high level of municipal debt can be an obstacle to such investments. For each municipality in the URG, information of the debt per capita were compiled (fig. A.1g). Again, there is a clear urban-rural trend, with high debt levels found in medium-sized and large cities in Germany. Ludwigshafen ranks highest in terms of debt, at €7140 per capita. In the French URG, public debt is generally lower.

A.2.3 Environmental Dimension

Land Access

Despite favorable geological and socio-economic conditions, access to the geothermal resource may be limited at the preferred site. Especially in nature and landscape protection areas, the construction of geothermal power plants is not possible at all or only under considerable restrictions. Information on the location of the naturally protected areas was obtained from the European Environmental Agency (Fig. A.1h). Nature reserves account for about 7% and landscape reserves for about 19% of the total area of the URG. Larger contiguous protected areas are mainly located in the central and northern URG along the Rhine river.

Greenhouse Gas Emissions

To meet the binding climate protection targets defined in the Paris Agreement, a rapid reduction in greenhouse gas emissions (GHG) is urgently needed. In this context, the expansion of geothermal energy can contribute significantly to the replacement of fossil fuels. The higher a region's carbon footprint, the more intensive its energy transition efforts must be. A harmonized dataset of greenhouse gas emissions for the European NUTS 2 regions was derived by Ivanova et al. (2017). The average household carbon footprint exhibits significant spatial heterogeneity in the URG (Fig. A.1i). Due to the dominance of nuclear power in France, average emissions are lowest here at 10.5 tCO2e/cap. In the German energy mix, the share of coal, oil and gas is higher, resulting in a higher carbon footprint (14 tCO2e/cap in Hesse). Besides, also the GDP, household size, urban-rural typology, education level, spending patterns, temperature, and resource availability have an impact on emissions.

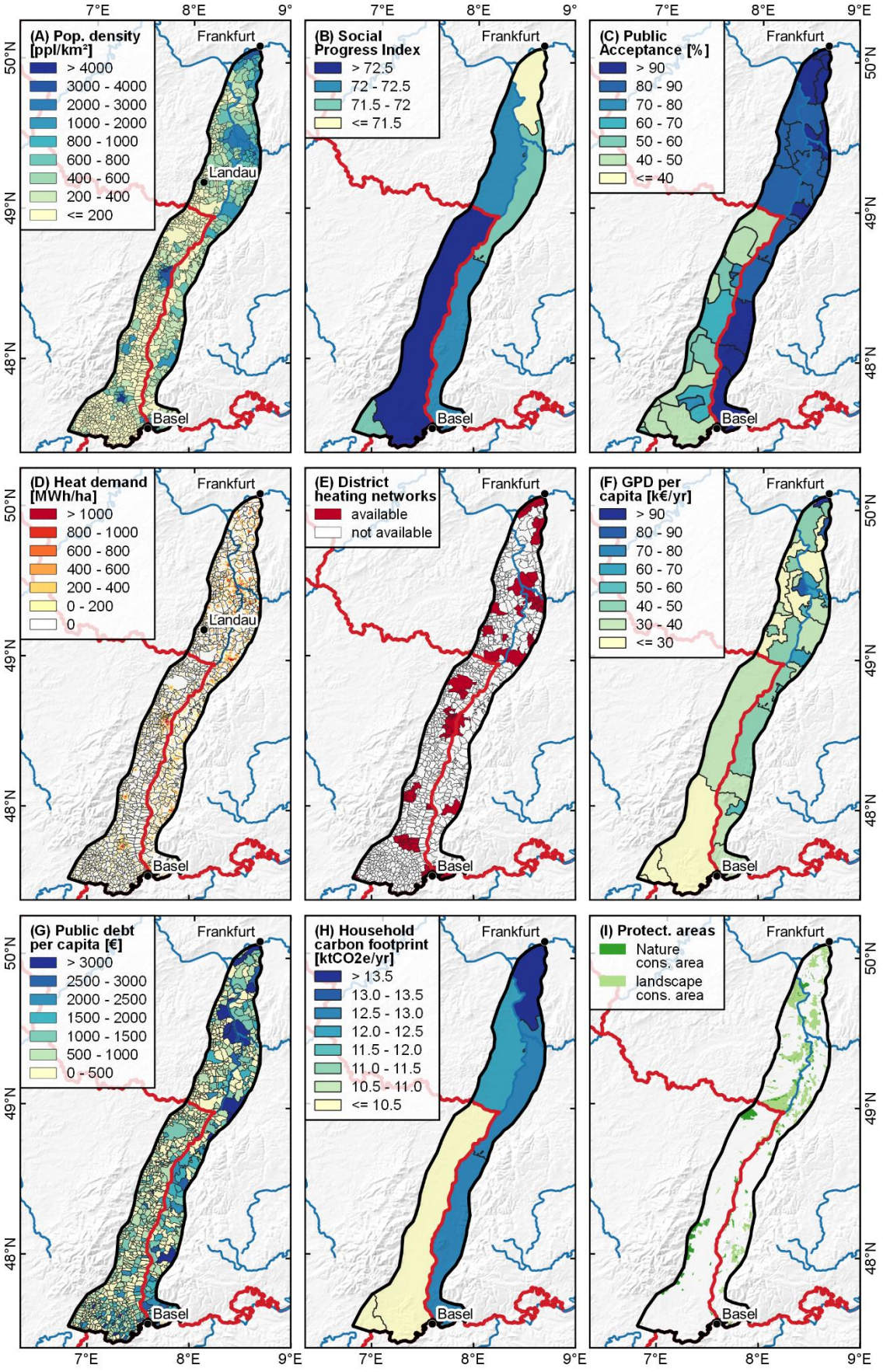

Figure A.1: Compilation of the nine indicators that were used to calculate the socio-economic-environmental potential for the development of geothermal energy in the URG.

A.3 Composite Index

Based on the indicators described above, a composite index for the socio-economic-environmental potential of deep geothermal utilization in the URG was calculated (Fig. A.2). The values range from 0 in the nature reserves to about 75 in Frankfurt. However, this map should be used mainly for qualitative interpretation, as the absolute values may vary substantially depending on the applied calculation algorithm and the parameters included. As expected, urban areas are characterized by the highest index, while the rural areas in the French URG have the lowest potential. A detailed view of the index is given in Fig. A.2 for the northern URG. This area generally exhibits medium to high potential due to its high population density, high acceptance of renewable energy among the population, high economic performance, and well-developed heat supply infrastructure. But access to geothermal resources is more often restricted here than in the rest of the URG due to a large number of nature conservation areas, which results in a overall low socio-economic-environmental potential along the Rhine.

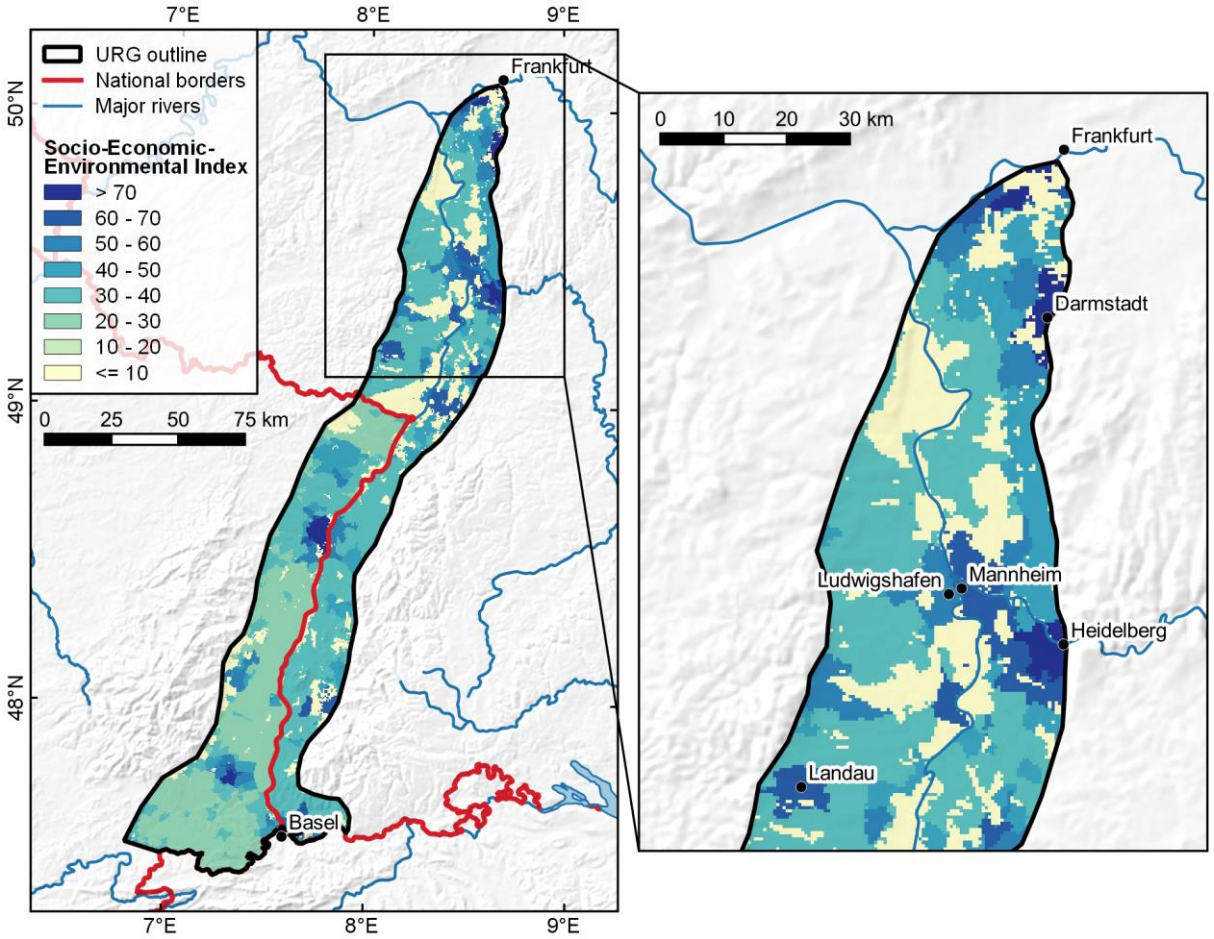

Figure A.2: Socio-economic-environmental potential for geothermal utilization based on nine individual indicators in the entire URG (left) and the northern URG (right).

Appendix B – Compilation of Data Publications

To ensure reproducibility of the presented results, all data generated during the PhD project were made publicly available in the TUdatalib repository of the Technical University of Darmstadt. An overview of all data publications is given in Table B.1.

Table B.1: Compilation of all data publications produced in the course of this thesis.

Reference	Comment
Frey, M., Bär, K., & Sass, I. (2020). Magnetic Susceptibility of Rock Samples of the Northern Upper Rhine Graben Region and Adjacent Areas. https://doi.org/10.48328/tudatalib-393.	Associated with chapter 3
Frey, M., Weinert, S., Bär, K., van der Vaart, J., Dezayes, C., Calcagno, P., & Sass, I. (2021). 3D Geological Model of the Crystalline Basement in the Northern Upper Rhine Graben Region. https://doi.org/10.48328/tudatalib-417.2.	Associated with chapter 3
Frey, M., van der Vaart, J., Bär, K., Bossennec, C., Calcagno, P., Dezayes, C., & Sass, I. (2022). Geothermal Resource Model of the Northern Upper Rhine Graben Crystalline Basement.	Associated with chapter 4
Frey, M., Bossennec, C., Seib, L., Bär, K., & Sass, I. (2021). Interdisciplinary Dataset on the Fracture Network of the Tromm Granite, Southern Odenwald, SW Germany. https://doi.org/10.48328/tudatalib-632.	Associated with chapter 5
Frey, M., Bossennec, C., & Sass, I. (2022). Aeromagnetic dataset from the Tromm Granite in the southern Odenwald. https://doi.org/10.48328/tudatalib-962.	Associated with chapter 6

Matthis Frey

Education

since Jan. 2020	**PhD student** Technical University of Darmstadt, Institute of Applied Geosciences, Department of Geothermal Science and Technology
Oct. 2017 – Dec. 2019	**Master of Geophysics** Christian-Albrecht University of Kiel, final grade: 1.0
Aug. 2018 – Dec. 2018	**Erasmus exchange semester** University of Bergen
Oct. 2014 – Nov. 2017	**Bachelor of Geosciences** Christian-Albrecht University of Kiel, final grade: 1.1
Oct. 2013 – Jul. 2014	**Bachelor of Chemical Engineering** University of Paderborn, without degree
Jul. 2013	**Abitur** KGS Altentreptow, final grade: 1.0

Work Experience

since Jan. 2020	**Research associate** Technical University of Darmstadt, Institute of Applied Geosciences, Department of Geothermal Science and Technology
Apr. 2015 – Apr. 2019 (with interruptions)	**Student research assistant** Christian-Albrecht University of Kiel, Institute of Geosciences
Sep. 2017	**Internship** H.S.W. Rostock, geotechnics and shallow geothermal systems
Mar. 2017	**Internship** Finanzamt Neubrandenburg, Bodenschätzung

Prizes and Awards

2020	Price for the best master thesis, Verein der Freunde und Förderer der Geophysik Kiel
2016 – 2019	Deutschlandstipendium